16th edition National Technical-Scientific Conference

Modern Technologies for the 3rd Millennium

March 23-24, 2017 - Oradea (Romania)

Editors

Sorin Nistor, Gabriela A. Popoviciu

EDlearning

Printed in June 2017 by Editografica • Bologna (Italy)

ISBN 978-88-87729-41-2

Contents

Geodesy and Cadastre

Construction and Architecture

Geodesy and Cadastre

The Achievement of a GIS Application Afferent to the Introduction of Sewerage Network in the Nadlac City, Arad County

Begov Ungur A.[1], Bogdan A.[2]

[1, 2] *"1 Decembrie 1918" University of Alba Iulia (ROMANIA)*
E-mail: andreeaungur@yahoo.com

Abstract

Due to the rapid pace of development of human settlements, utility networks, infrastructure, etc., results a large volume of graphic and descriptive information which need to be managed as efficiently as possible, and creating such a relational database is required. Using GIS technology can be viewed the results of high complexity analysis, that by classical methods are more difficult to achieve.

In this paper, using ArcGIS software, it was created a GIS application afferent to the introduction of sewerage network in the Nadlac city, Arad County. The introduction of water and sewerage networks in Nădlac is part of the project "Expansion and modernization of water and wastewater infrastructure in Arad", financed by the Cohesion Fund, through the Sectoral Operational Programme "Environment". This GIS application was made at the request of „SC Compania de Apă Arad SA", contributing to develop a modern sistem, according with European regulations, while also improving the services provided by „SC Compania de Apă Arad SA".

In conclusion, from the content of this paper, result that GIS application created in the present paper constitutes a fundamental element for query, storage, handling and analyzing information, because the limit of data analysis depends only on the imagination of the user.

Keywords: GIS, database, thematic map.

1 Introduction

The most important feature of a GIS consists in its capacity to make spatial analyses, which means to process the spatial data (geographical data) with the purpose to obtain information (reports) regarding the studied area [1]. For this reason, this paper is important because the achievement of this kind of GIS applications constitutes a fundamental element in the sight of query, storage, handling and analyzing information, because the limit of data analysis depends only on the imagination of the user.

Using GIS application the planning may be carried out through various local development projects (buildings, roads, water and sewerage networks, etc.), the lands on which the future investments will be placed may be studied and determined, also the following may be monitored: the progress of the modernisation works, the land records and rehabilitation of strategic objectives of interest and of the touristic ones, the health care facilities, the food-processing markets, the green spaces and recreational areas, the spaces intended for sale or concession, etc [2].

In this paper, using ArcGIS software, it was created a database afferent to the introduction of sewerage network in the Nadlac city, Arad County. The introduction of water and sewerage networks in Nădlac is part of the project "Expansion and modernization of water and wastewater infrastructure in Arad", financed by the Cohesion Fund, through the Sectoral Operational Programme "Environment". This GIS application was made at the request of „SC Compania de Apă Arad SA", contributing to develop a modern sistem, according with European regulations, while also improving the services provided by „SC Compania de Apă Arad SA".

To answer customer requirements, we chose to create a relational database by using GEODATABASE format because the Geodatabase format is a characteristic for data banks of large dimensions, both spatially and structurally, with a large number of layers and layers collections, as it is the case of present work.

The achievement of this kind of GIS applications constitutes a fundamental element in the sight of query, storage, handling and analyzing information, because the limit of data analysis depends only on the imagination of the user [3].

2 Case study

In order to accomplish this paper, in the area of interest, were carried out topographic measurements, namely on the street Ludovit Boor, Gheorghe Doja, George Coşuc, Stejarului, Abatorului, Lacului and the data storage will be made in GIS.

The topographic measurements were carried out with a total station Leica TS 06. Dates were downloaded from total station and saved in *.txt format. Information processing, respectively dates compensation was done with Toposys program. The dates obtained after compensation were exported in ASCII format. For dates processing in GIS were followed the next steps:

2.1 The file convert from *.txt format to *.dbf format

This conversion was possible using Microsoft Excel program. The *.txt file, exported from Toposys, was imported in the Microsoft Excel program, resulting four columns representing: Point name, coordinate X, coordinate Y, respectively quotas Z. At the end, the file was saved with the DBF IV (dbase4) extension (fig. 1).

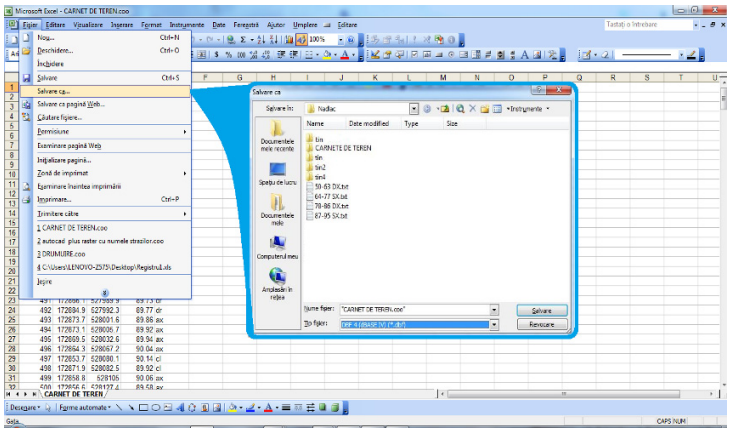

*Fig. 1. The file convert from *.txt format to *.dbf format*

2.2 The importing of *dbf file in ArcMap program

In ArcMap, by pressing ADD DATA , from toolbar, has imported the *.dbf file. After data importing, proceed to establish the coordinate system (fig. 2).

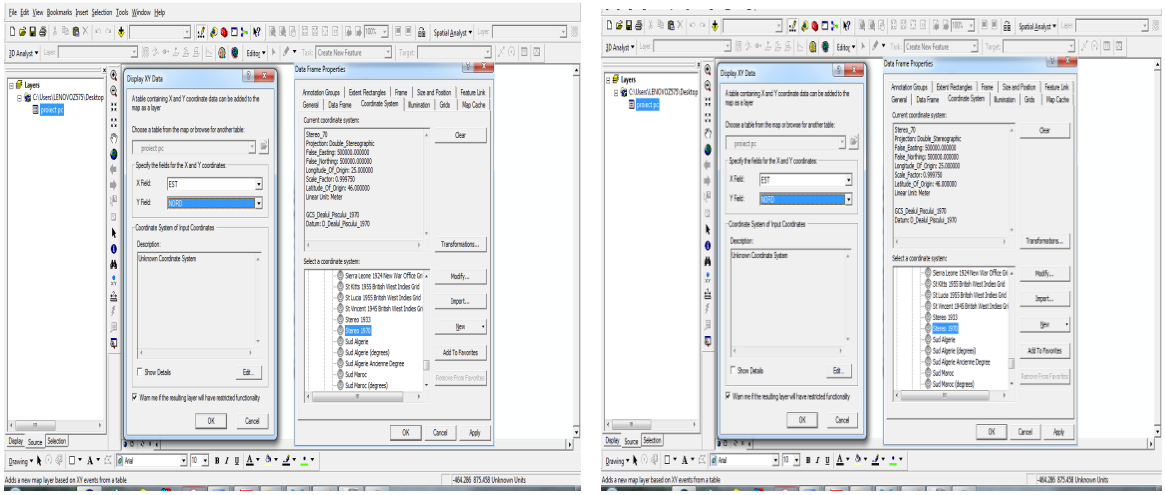

*Fig. 2. The importing of *.dbf file in ArcMap and establishing the coordinate system*

After importing data into ArcMap program it was passed to their transformation in shapefile of "point type" using command: Right-click on the layer that contains the points dates > Data > Export data.

From this moment points could be viewed in ArcMap graphic window (fig. 3) and we passed to editing the situation plan.

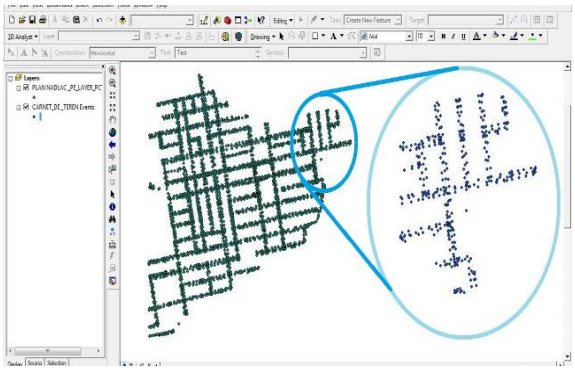

Fig. 3. ArcMap graphic window

2.3 The creating of database and data importing into database

It launches ArcCatalog application to create a new geodatabase, and then it selects the folder where these will be saved. For this is accessed the command New> Personal Geodatabase> is named the database> ENTER. Next, is add a "Feature date set", titled "Nădlac", then sets the projection system, "Stereo 1970", respectively the reference system "Black Sea 1975" (fig. 4).

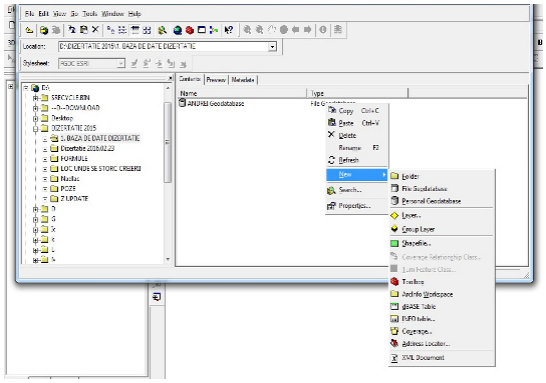

Fig. 4. The creating of database

Further, it will import the existing data: Right click > Import > Feature Class (Single) and then it will be selected those data which database will contain (fig. 5).

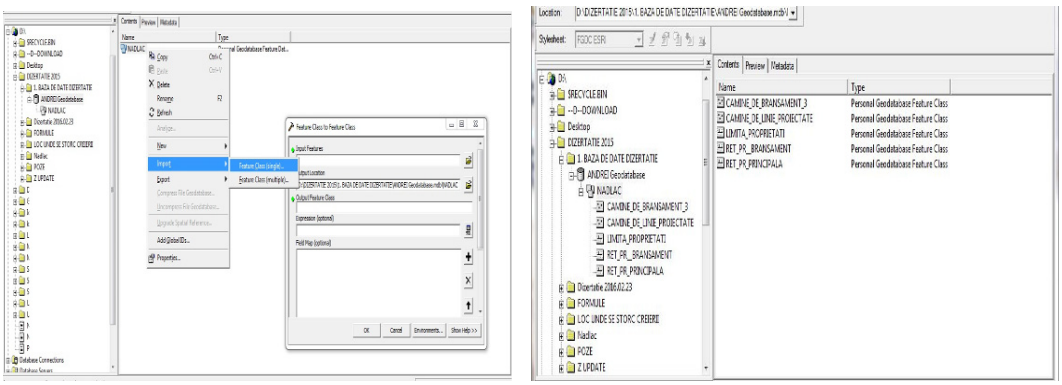

Fig. 5. Importing data into database

The completing of "Feature Class" box is done as follows: Input feature: Main design network; Output loction: file save address; Output feature: the name that shapefilul will have in Geodatabase.

2.4 The importing of tables in ArcMap

The data importing, existing in tabular form, is made only after creating of "Shapefile" files in ArcMap.

Next will be imported the tables from Excel program (fig. 6).

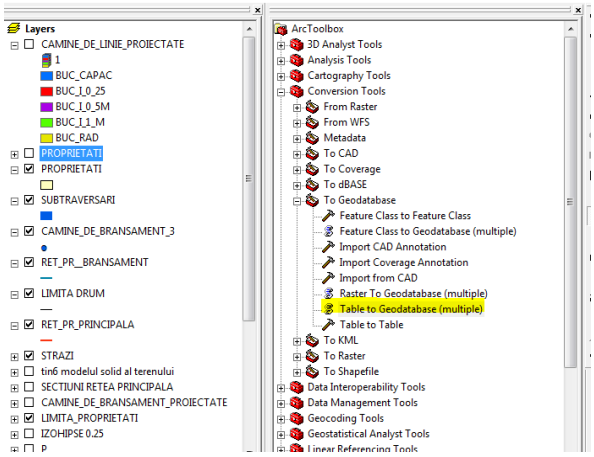

Fig. 6. The importing of tables in ArcMap

For tables conversion in ArcCatalog, from the menu toolbox, is accessed ArcToolbox > Conversion Tools > To Geodatabase > Talbe to Geodatabase (multiple) > then the table is selected.

2.5 The creating of digital terrain model

The digital terrain model was obtained accessing, from Tools toolbar, select the command 3D Analist > Create/Modify > Create TIN from feature (fig. 7).

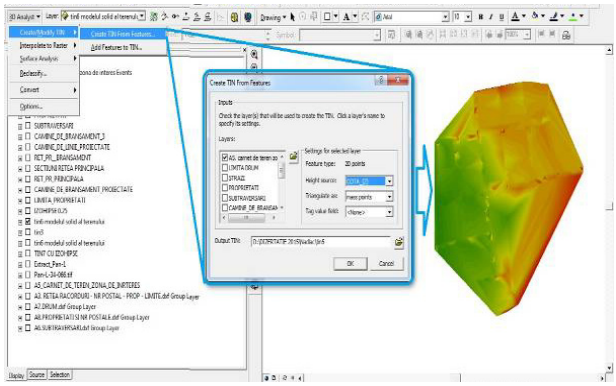

Fig. 7. Creating digital terrain model

2.6 Reports generation

The reports generated in ArcGIS, allowing rapid visualization of data series, depending on user requirements. For reports generation from Tools toolbar select the command Tools > Reports > Create (fig. 8).

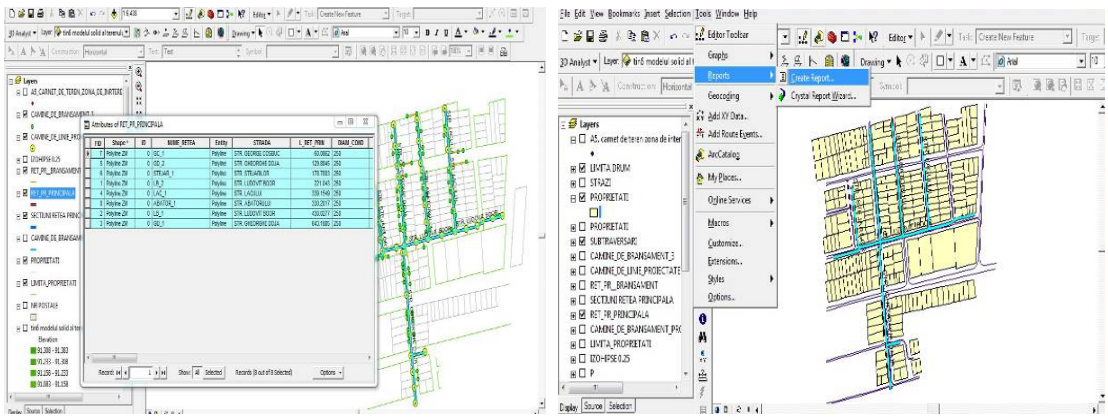

Fig. 8. Creating reports

2.7 Creating thematic maps

Vectored graphics data have attached attribute data that will help us to create different thematic maps. By switching to "Layout View" and by adding the report we create the thematic map (fig. 9). Also, we can create a legend of the map for a better view of the results of thematic map.

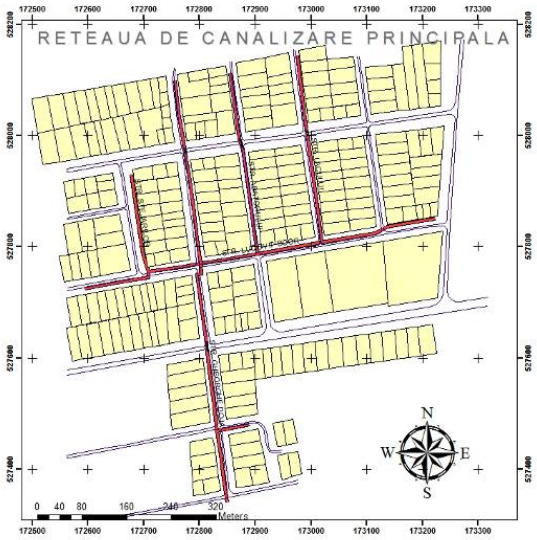

RAPORT GENERAL PRIVIND CONTINUTUL RETELEI DE CANALIZARE PRINCIPALE

STRADA	CAM_LINIE	L_RET_PRIN	DIAM_COND
STR. GHEORGHE DOJA	14	643.1885	250
STR. LUDOVIT BOOR	9	430.0277	250
STR. LACULUI	6	339.1549	250
STR. ABATORULUI	7	330.2017	250
STR. LUDOVIT BOOR	5	221.043	250
STR. STEJARILOR	4	178.7803	250
STR. GHEORGHE DOJA	3	129.8845	250
STR. GEORGE COSBUC	2	60.0862	250

CAM_LINIE Sum
50
LUNGIME_RE Sum
2332.3668

Fig. 9. Creating thematic maps

2.8 Creating graphs

Creating graphs is performed similarly to that of the reports, by accessing command Tools > Graphs > Creat, select the graphs type Vertical Bar. After selecting the "Finish" button the resulting graph can be edited, saved in various extensions or printed.

By choosing RET_PR_PRINCIPALA Layer, Value field L_RET_PRIN, respectively L_RET_RACORD a new function is added to display the cumulative length of both networks (fig. 10).

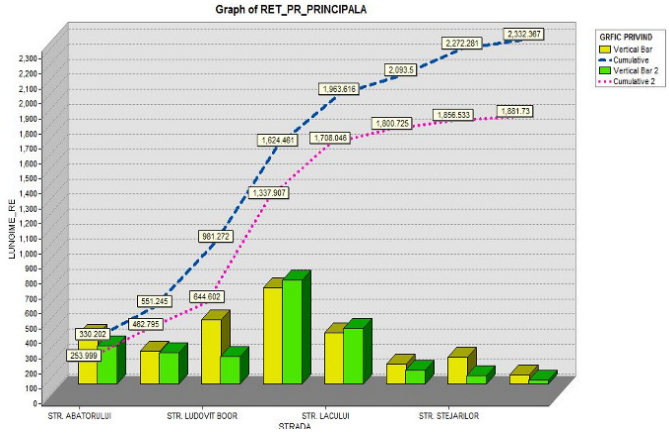

Fig. 10. Graph which shows the total length of main line respectively of branching lines

2.9 The highlighting of elements from database

The highlighting of elements from database can be done by Right click on Layer Proprieties > Symbology > Categories > Unique values, complete "Value field" with NUME_RETEA, then add the network sectors. Below is presented a highlighting of all owners connected to the network (fig. 11).

Fig. 11. The highlighting of all owners connected to the network using "Unique Value" function

The highlighting of elements can be done, also, using "Stacked" function (fig. 12).

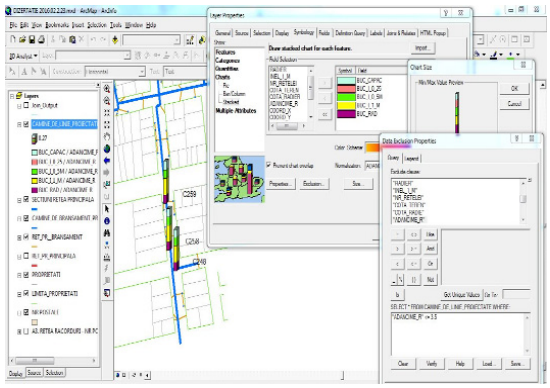

Fig. 12. The highlighting of elements using "Stacked" function

3 Conclusion

This paper presents the stages followed to create a GIS application, afferent to the introduction of sewerage network in the Nadlac city, Arad County, using ArcGIS software and how this application can help to solve various problems specific to the utility networks cadastre.

Using this technology, highly complex test results can be viewed, which by classical methods are more difficult to achiev. The achievement of this kind of GIS applications constitutes a fundamental element in the sight of query, storage, handling and analyzing information, because the limit of data analysis depends only on the imagination of the user.

The achievement and implementation of this GIS application for the Nadlac City represent a first step in the decision process regarding this area. This application can be improved with data from different fields depending on the requirements and needs of users.

REFERENCES

[1] Oncia S., Herbei M.V., Popescu C.A. (2013). Sustainable Development of the Petrosani City, the Hunedoara County Based on GIS Analysis, Journal of Environmental Protection and Ecology, Romania, Vol. 14, No. 1, pp 232.

[2] Dimen L., Borsan T., Vintan I., Gaban L. (2015). Creating and Managing a Database for Planning and Monitoring the Achievement of the Objectives of Sustainable Development in Zlatna Locality, Alba County, Journal of Environmental Protection and Ecology, Romania, Vol. 16, No 4, pp1414–1421.

[3] Begov Ungur A., Sălăgean T., Ferencz Z. (2016). Example of a GIS application afferent to the introduction of real estate cadastre in Cluj Napoca city, using AutoCAD MAP 3D, 16th International Multidisciplinary Scientific Geoconference, SGEM 2016, Book 2, Volume III, pp. 207-214.

Safety Assurance on Existing Dams. Case Study – Tungujei Dam

Boariu C., Bofu C.

Technical University Gh. Asachi Iasi, Faculty of Hydrotechnics, Geodesy and Environmental Engineering (ROMANIA)
E-mails: costelboariu@gmail.com, constantinbofu@yahoo.com

Abstract

In accordance with a Romanian legislation, dam owners or administrators are required to periodically obtain a safety operating permit. These permits are issued for a maximum of 7 years for categories A and B and 10 years for the rest. This article references the Tungujei Dam, on Sacovat River, in Iasi County. At this dam the bottom emptying conduit has a major settlement. Article details settlement calculation and propose a method to calculate inertia moment of the structure. Calculus of bottom conduit structure must estimate the interaction between deformable soil and structure. The conduit structure provided by joint have a special behavior. This method (formula) takes account of structure joint and soil characteristics.

Keywords: bottom emptying conduit; settlement; rigid structure.

1 Introduction

The Tungujei Dam is part of a vast and complex installation meant to reduce the risk of floods in the Barlad basin. This is done by the retention of roughly 11 mils.m^3 of water (equivalent to the 1% probability flood wave), thus protecting an area of about 400ha of the Barlad riverside and surrounding meadows (the unregulated Todiresti-Negresti area). The article refers to bottom emptying conduit behaviour in time.

The calculation of emptying bottom conduit may be reduced to determining reactive pressure distribution on the contact surface and this surface deformation (settlement). The most important elements that influence the pressure distribution on the surface reactive contacts are: rigidity of the structure, the degree of static indeterminacy and soil characteristics. A dam can be monitored by means of GPS technology but a proper time series analysis have to be done [2], in which a proper model of the noise have to be taken into account [3].

An accurate calculation problem is related to modeling phenomena interface between concrete structure and dam-filling body [1]. Research in recent years have shown that the ratio of pipe stiffness and soil deformability determine behavior of the structure under the action loads [4], [5], [6], [7], [8].

Concrete structure generally has a rigid body behavior embedded in the mass made up of foundation soil and the dam embankment [1], [9], [10]. Subsoil high deformability, high loads from dam earth imposed fragmentation of the concrete structure in sections of 10 m, with joints with initial openings of 2.5 cm sealed with sheets of PVC. Typically these structures joints are sealed with rubber bands or plastic [9]. The stability of the surface surrounding the dam can be monitored by using the precise point positioning (PPP) technique [12].

If not apply to such systems, as for example in the joints, then to the outer surface of the structure to be used fillers with high plasticity to ensure sealing area. Due to the complex nature of cooperation between the concrete structure and filling, the only current method capable of accurately model this phenomenon is the finite element method [1], [6]. Further calculation will be done by finite element method with Beam 2D software.

2 Bottom Emptying Conduit Behaviour

The bottom discharger is comprised, in order, of the following elements: coupling channel, control tower, access bridge, coffered pipe, energy dissipater, connector channel, riprap breakwater structure.

The coupling channel upstream connects the Sacovat River riverbed to the control tower entrance and is 18.5m long. This channel is layered with concrete slabs.

The control tower is a 19.50m high reinforced concrete structure divided into 3 compartments. The lateral sections serve the purpose of evacuating water and emptying the lake, white the central compartments is for the water intake. The bottom emptying conduit (coffered pipe) is, according to the design, at 153.10mdMN and only works under exceptional circumstances.

The coffered conduit is made up of 3 rectangular sections, each 1.75m x 2.30m wide, and servers 2 purposes: the lateral sections link to the bottom discharge and the center one if for the intake. In total, it consists of 11 pieces, each 10m long, 2 pieces that are 5m long, and one 10m piece that connect to the tower. All these pieces are linked with permanent PVC joints.

The energy dissipater has a rectangular cross section that widens from 6.05m to 8.00m along 33m. The vat like structure has 4.56m high walls, with 0.8m thick foundations and 1m thick foundation plate.

The connector channel is 62.35m long, 8 wide and has a 1‰ slope; it is trapezoidal in shape, and has a 20cm thick concrete slab revetment, resting on a downstream support.

The riprap breakwater structure is made out of rocks and is 0.8m thick on the bottom of the channel, while its thickness varies on the slopes from 0.4 to 0.8m. Its bottom width is 10m and it is 137m long. The channels widens from 8 to 10m via a 10m long flaring section. The rest of the way to the confluence with the river consists of a 50m long trapeze shaped channel dug into the ground.

According to operational regulations, ever since commissioning in 1986, settlement was noticed around the midway channel section of the dam. In 1989, a series of interventions to the joints were made in an effort to reduce ongoing infiltration. In 1996, upon inspection of the bottom discharge channel, the R6 joint was found to have widened by 1.5cm. Furthermore, various other widenings (no more than 1cm) were noticed in the water intake section. Repairs were carried out based on the measurements and the survey done at the time. In June 2005, upon further inspection, no changes from the previous state were noticed. However, according to observations made in 2015, settlement in the central part of the discharge channel is about 90cm.

Relative displacement between sections is 2cm at most - measured at joints. Some of the joints allow water to seep in which means the sealant tape has discontinuity.

3 Calculating the Settlement in the Bottom Emptying Conduit

The large bottom conduit settlement is the major cause of the joint displacement and infiltration.

The conduit has been designed as a reinforced concrete structure comprised of 3 rectangular sections, as seen in the drawing below (Fig. 2). Longitudinally, the structure has joints varying in distance from 5 to 10m. These joints are sealed with PVC tape and the reinforcing does not cross them.

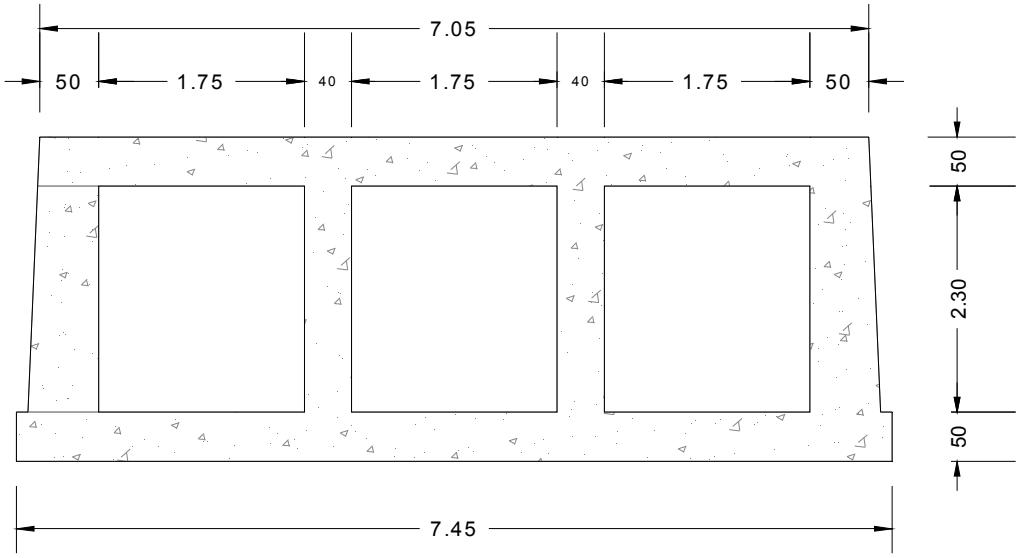

Fig. 1 Transversal section by bottom conduit

The upstream half of the conduit is horizontal by design (elevation 147.60mdMN), and the downstream section is designed with a 0.9% incline.

In June 2015, the conduit configuration due to the settlement is that which is shown below (Fig. 2). By comparison with the initial design, the maximum settlement of the conduit is measured at 92cm. Most of this occurred while the dam was being built.

Fig. 2 illustrates the following parameters: the local settlement of the conduit (in parentheses) and the still water depth in that point in front of the parentheses.

Before action is taken, a forecast of the probable evolution must be made.

Calculations that need to be done must take into account the load on the conduit and must be based of a calculation scheme.

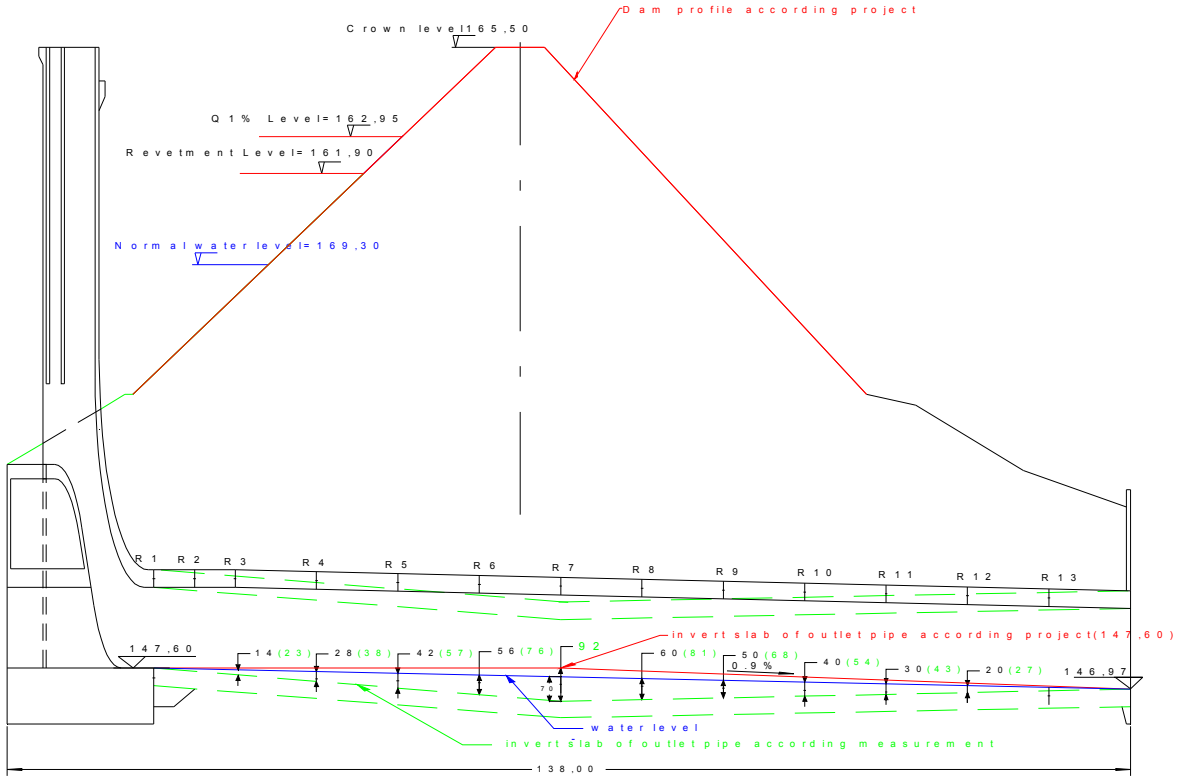

Fig. 2 Longitudinal section through outlet pipe (different scale horizontal and vertical)

The following shows the load that the dam exerts on the conduit according to Marston's theory [11] and upon Romanian standards and regulations [13], see Fig. 3.

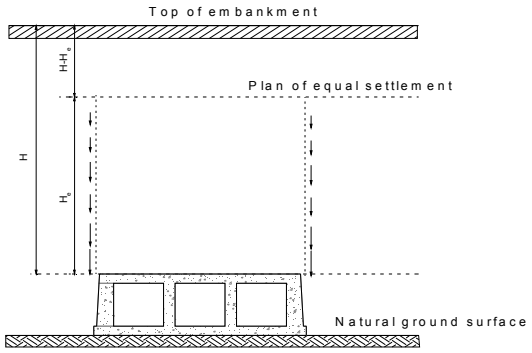

Fig. 3 Vertical loads that the earth filling exerts on the conduit

Total vertical load is: $P_v = C_e \gamma D_e^2$,

in which:

$$C_e = \frac{e^{2K\mu(H/D_e)} - 1}{2K\mu} \quad \text{or} \tag{1}$$

$$C_e = \frac{e^{2K\mu(H_e/D_e)} - 1}{2K\mu} + \left(\frac{H}{D_e} - \frac{H_e}{D_e}\right) e^{2K\mu(H_e/D_e)} \tag{2}$$

in which:

$K = tg^2(45^o - \varphi/2)$, lateral pressure coefficient Rankine,

μ = tg φ, earth friction coefficient,

H_e = position of the plane of equal settlement,

D_e = exterior pipe diameter (dimension),

H = embankment height.

Marston determined the existence of a horizontal plane above the pipe where the shearing forces are zero. This plane is called the *plane of equal settlement.* Above this plane, the interior and exterior prisms of soil settle equally. Equation (1) is valid for $H_e>H$ (the plane of equal settlement in imaginary) and equation (2) is valid for $H_e<H$. The supplementary load (apart from the weight of the soil) depends of the friction forces facing downwards that appear in the ground column above the conduit in the vertical planes tangent to the conduit.

In the case of the Tungujei Dam, the 15m filling on top of the 7.45m wide conduit, the load (per meter of conduit) is: $P_{v1} = \gamma H D_e = 19 \cdot 15 \cdot 7.45 = 2123$ kN/m; where:γ=19 kN/m^3; and Kμ=0,13 [14].

According to Marston we have (considering $H=H_e$):

$$C_e = \frac{e^{2 \cdot 0,13 \cdot 15/7,45} - 1}{2 \cdot 0,13} = 2.64$$

$$P_{v2} = C_e \gamma D_e^2 = 2.64 \cdot 19 \cdot 7.45^2 = 2784 \text{ kN/m}$$

According to Romanian standards [11], the equation for vertical pressure is:

$$P_v = C_r \gamma H D_e \text{ in which:}$$

$$C_r = \frac{e^{2K\mu \frac{H}{D_e}} - 1}{2K\mu \frac{H}{D_e}} \qquad C_r = \frac{e^{2 \cdot 0.13 \frac{15}{7.45}} - 1}{2 \cdot 0.13 \frac{15}{7.45}} = 1.31 \qquad (3)$$

Therefore: $P_v = 1.31 \cdot 19 \cdot 15 \cdot 7.45 = 2781$ kN/m.

We can observe an increase of about 30% increase in pressure on the conduit and its foundation, while the areas surrounding the structure have diminished load and can't stiffen at the same level as the rest. The calculation scheme is that for a Winkler elastic environment beam, and the software used is Beam 2D. Ground properties have been taken from the initial study done when the dam was first being designed. What is immediately noticeable is the small deformation module of the clay that the foundation was set on. The emptying conduit is consists of two 5m sections and eleven 10 m sections, each made up of reinforced concrete (Fig. 1). The sections are separated by 2.5cm joints filled with sealant tape. The conduit calculation parameters are: A=11.67 m^2; I_b=16.05 m^4; E_b=26 GPa (for C12/15 concrete).

Ground reaction was estimated by the Winkler model [15], [16]. Each node will be considered to be a spring with the following elasticity: $k_s = B \cdot l \cdot k$,

in which*:*

B = 7.45 m is the width of the conduit*; l* is the length of the finite element.

The marginal nodes will have the same coefficient of subgrade reaction as the others based recommendations by Bowles [17]. Coefficient of subgrade reaction according to Vesić and Bowles:

$$k' = 0,65 \sqrt[12]{\frac{E_p B^4}{E_b I_b}} \frac{E_p}{B(1-\mu_p^2)} \qquad k' = k \cdot B \qquad (4)$$

Ground parameters are (clay deposits):

E_p = 8 MPa; μ_p=0,35; γ_p=19 kN/m^3

$$k' = 0.65 \sqrt[12]{\frac{8 \cdot 7.45^4}{26000 \cdot 16.05}} \frac{8}{7.45(1-0.35^2)} = 4681 \text{ kN/m}^2$$

$$k_s = 4.5 \cdot 4681 = 21066 \text{ kN/m}$$

The coefficient of subgrade reaction (Winkler) according to Romanian standards (NP112) is:

$$k = k_m \frac{E_p}{\alpha(1-\mu_p^2)} \qquad (5)$$

k_m = 0,45 (from K1 table, depending upon α); α = L/B=10/7.45=1.34

Therefore: $k = 0.45\dfrac{8000}{1.34(1-0,35^2)} = 3061$ kN/m^3

The coefficient of subgrade reaction according to [15]'s equation is:

$$k \approx \frac{E_p}{B(1-\mu_p^2)} \tag{6}$$

Considering ground parameters we have: k= 1224 kN/m^3

The coefficient of subgrade reaction according determined in (6) is almost twice as large as the ones determined in (6) or (7). Subsequent calculation will use the coefficient determined by Vesić 's equation [17].

The weight of the conduit itself has been added to the calculations.

Two calculation schemes have been used for the conduit, between joints R3 and R12 (Fig. 4 and Fig. 5), as follows: The first scheme (Fig. 4) considered the 9 sections of conduit with the ends articulated. A 70cm settlement was determined:

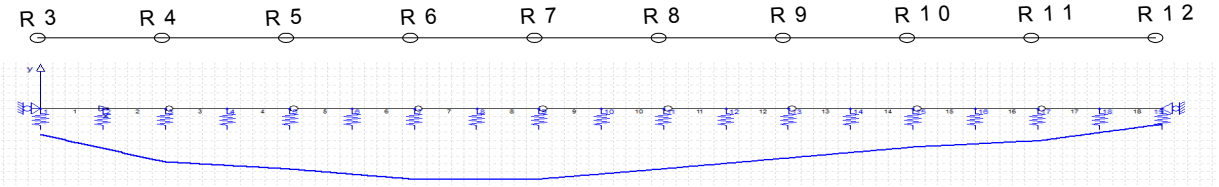

Fig. 4 Settlement calculation with hinge joint - maximum between R6-R7 is 70 cm (capture from Beam 2d)

The second scheme (Fig. 5) considered the 9 sections to be continuous, with no joints. Initial calculations reveal a 60cm settelement with a inertial momentum determined by the current section of the conduit.

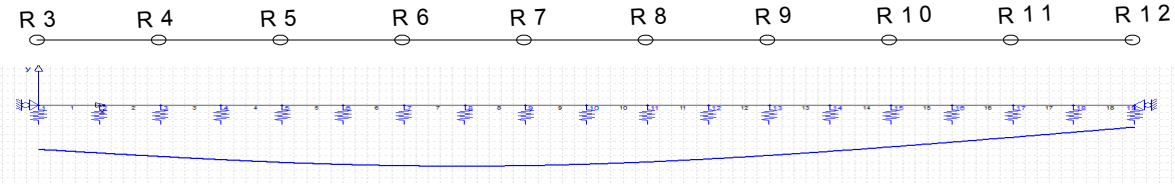

Fig. 5 Settlement calculation with rigid joint-maximum between R6-R7 is 60 cm (capture from Beam 2d)

To properly evaluate the second situation, the calculations have been extended to take into account the reasoning by Muir Wood [18] that advances the following equation for circular prefabricated block conduits:

$$I_e = I\left(\frac{4}{n}\right)^2$$

in which:

I_e=equivalent inertial momentum; I= current section inertial momentum; n = number of joints

For this structure the proposed equation is:

$$I_e = I\frac{1}{2n} \tag{7}$$

Therefore we have an equivalent momentum of: $I_e = 16.05\dfrac{1}{2\cdot 8} = 1\,\text{m}^4$

Considering this determined value, the settlement reaches 69 cm between R6 and R7:

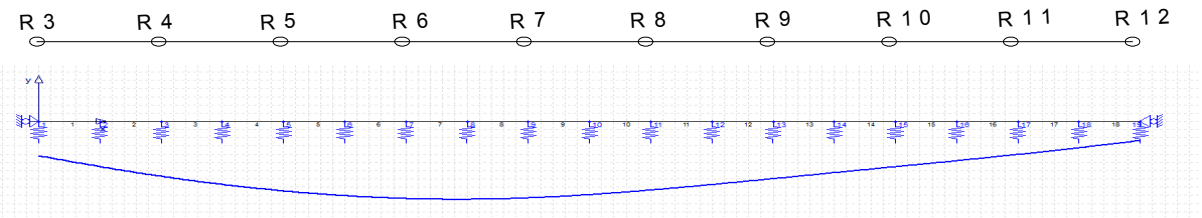

Fig. 6 Settlement calculation with equivalent momentum calculated with relation (7) - capture from Beam 2d

4 CONCLUSIONS

Considering the interventions recommended by [18] [19], in the particular case of the Tungujei Dam, the following actions are suitable:

Utilize longitudinal reinforcement across joints.—large horizontal movements often occur at randomly selected conduit joints, rather than uniformly along the conduit length. This type of concentrated movement can open gasketed conduit joints that are not designed for large horizontal movements. The use of longitudinal reinforcement across the joints and continuous welded steel pipe liners are effective in reducing concentrated openings within conduits. *In Romanian practice reinforcement at join is interrupted.*

Provide camber - A conduit that is not located on bedrock must be designed so that the amount of predicted foundation settlement does not damage the conduit or its function. A conduit constructed on a compressible foundation should be cambered to accommodate the predicted foundation settlement, to achieve a proper final grade. *For camber calculation we propose the next formula for inertia moment calculation*.

Inertia moment calculation - We use relation (7) for inertia moment calculation and with this relation maximum settlement was 69 cm, while maximum settlement considering articulated joint was 70 cm. In this way the number of joint can be related with conduit stiffness. Of the conduit stiffness depend soil structure model interaction [5], [6], [7].

REFERENCES

[1] Adrian Popovici (2002). *Baraje pentru acumulari de apa vol II* (Dams for water storage vol II), Editura Tehnica, Bucuresti.

[2] Nistor, S. and Buda, A.S (2016a). *GPS network noise analysis: a case study of data collected over an 18-month period*. Journal of Spatial Science, 61(2), 1–14. DOI:10.1080/14498596.2016.1138900

[3] Nistor, S. and Buda, A.S (2016b). *The influence of different types of noise on the velocity uncertainties in GPS time series analysis*. Acta Geodyn. Geomater., Vol. 13, No. 4 (184), 387–394, DOI: 10.13168/AGG.2016.0021.

[4] Horvath John S. (2002). *Soil-Structure Interaction Research Project;* www.engineering.manhattan.edu/civil/CGT.html.

[5] Horvath John S., Regis J. Colasanti (2011). *Practical Subgrade Model for Improved Soil-Structure Interaction Analysis: Model Development* International Journal of Geomechanics, Vol. 11, No. 1.

[6] Regis J. Colasanti, John S. Horvath (2010). *Practical Subgrade Model for Improved Soil-Structure Interaction Analysis: Software Implementation* Practice Periodical on Structural Design and Construction, Vol. 15, No. 4, November 1, 2010. ©ASCE.

[7] Boariu C. (2015). *Soil Structure Interaction Calculus, For Rigid Hydraulic Structures, Using FEM,* IOSR Journal of Mechanical and Civil Engineering (IOSR-JMCE) vol 12-2015 pag 60-68.

[8] Poulos H.G., Davis E.H., (1991) *Elastic Solutions for Soil and Rock Mechanics* Centre For Geotechnical Research University Of Sydney.

[9] USACE (2003). EM 1110-2-2400 *Structural Design and Evaluation of Outlet Works.*

[10] USACE (1998). EM 1110-2-2909 Engineering and Design *Conduits, Culverts and Pipes.*

[11] Moser A.P., S.L. Folkman (2008) *Buried pipe design, third edition,* Mc Graw Hill.

[12] Nistor, S. and Buda, A.S (2017). Evaluation of the ambiguity resolution and data products from different analysis centers on zenith wet delay using PPP method. Acta Geodyn. Geomater., Vol. 14, No. 2 (186), 205–220, DOI: 10.13168/AGG.2017.0004.

[13] NP 112-2014. *Normativ privind proiectarea fundaţiilor de suprafaţă (*Standard on the surface foundations design).

[14] D. Furis, M.E. Teodorescu, L. Sorohan (2005). *Calculul structurilor pentru transportul apei* (Calculation of structures for water transport), Conspress, Bucuresti.

[15] Teodoru I.,B., Musat V.,(2009). *Modelarea numerica a interactiunii teren structura. Grinzi de fundare* (Numerical modeling of soil structure interaction. Foundation beams), Ed. Politehnium Iasi.

[16] Stanciu A, Lungu Irina (2006). *Fundatii* (Foundations).

[17] Bowles Joseph E. (1996). Foundation Analysis and Design 5th ed, McGraw-Hill Book Co - Singapore.

[18] Muir Wood, A. M. (1975). The circular tunnel in elastic ground. Géotechnique 25, No.1, 115-117.

[19] United States Department of Agriculture, Natural Resources Conservation Service Technical Release No. 18 *Computation of Joint Extensibility Requirements* (1969).

[20] Federal Emergency Management Agency (2005) *Conduits through Embankment Dams.*

Surveying the Rural Resilience within the Oradea Hills Household Independent Cellar Landscape, Romania

Dincă I.[1], Linc R.[1], Tătar C.[1], Nistor S.[1], Staşac M.[1], Bucur L.[1]

[1]*University of Oradea, Department of Geography, Tourism and Territorial Planning (ROMANIA)*
E-mails: iulian_dinca@yahoo.co.uk, ribanalinc@yahoo.com, corina_criste_78@yahoo.com, snistor@uoradea.ro, marcu_stasac@yahoo.com, liviubucur@yahoo.com

Abstract

This research study focuses on the independent household cellar network of the Oradea Hills (Bihor County, northwestern Romania), because we intend to review the residents' and villages' resilience of these long-inhabited hills. In Bihor County there is an extensive network of cellars in various stages of evolution which represent a valuable component of the rural architectural heritage. These cellars are *independent from households* (880 units), dug into slopes at varying distances from the village hearth, but no more than 2 km away, whose age ranges from 50 to150 years. These cellars belong to 14 villages and a neighbourhood of Oradea, Bihor County seat. The study uses geographic information on the typical hilly terrain including a territory survey. The bulk of the research is dedicated to the results based on the independent household cellars' considerations on production and local rural living. Then sustainable socio-economic indicators are analyzed (e.g. the conducting of interviews, products and goods stored into the cellars). By these indicators the human and environmental capital of the Oradea Hills villages is featured, explaining how much resilience capacity there is, with a central view to the independent household cellars.

Keywords: rural landscape, rural resilience, independent household cellars, socio-economic indicators, Oradea Hills.

1 Introduction

1.1 *Geographical realities*

Even if the areas covered by grapes decreased significantly in Bihor County in the last 2-3 decades, there is a valuable rural component, in different evolution stages, materialized by a real network of cellars, located apart from households, carved into the slopes of the hills. These cellars are located in Oradea Hills abhorrent from the classical situation of the cellars, located inside the yard of the households or under the house. The carving process of these cellars was adapted to the hilly morphology, the result being different architectural, interior design and use types, which could be linked most often to different types of rural and custom living of Romanian and Hungarian communities. One would expect that these type of cellars to be found in remote, isolated areas which may explain a kind of original initiative of the inhabitants. The villages from Oradea Hills are located near Oradea, the county seat, and the main pole of social and economic attractiveness. The most remote villages having cellars are located within 50 km distance, the most villages being located under 40 km from Oradea, or a unique example, cellars located in a neighbourhood of the town. The influence of urbanization was not so strong to inhibit the appetite of the villagers for carving cellars apart from households and the capitalization of the rural tradition. Such a patrimony component, such a constructive type, not merely continues a tradition based on traditional agricultural activities but influenced grape and wine culture with very strong local features. The existence and oldness of these cellars are attributes which should increase the level of knowledge and popularity of the villages from a level mostly neglected or too less compared to the possibilities. These cellars, belonging to rural architectural patrimony, do not contribute currently either to local or regional tourism. There are premises that, with the help of these cellar apart from households, through their rehabilitation, to start the regeneration process of these villages, the increase the welfare of the inhabitants through rural tourism and ecotourism.

1.2 *The aims and objectives of the study*

The aim of the study is to analyze the resilience capacity of the inhabitants and villages from Oradea Hills. The meaning is that of increasing the occupational flexibility of the inhabitants, the development of the adaptation capacity to new demands from social, agricultural and design perspectives of the *cellars apart from households* and associated customs. In order to investigate the resilience of the inhabitants, the study follows the acquired skills by the rural communities to face the economic and social challenges of the dynamic and competitive cross-border space or among the counties within the North West Development Region. Another aim of the study refers to the analysis of the villages' resilience, studying the importance of natural and human components within the social, economic local rural sub-system, and also the importance of associated occupations related to cellars apart from households, as parts of a *positive development process and part of the building of local identity*. The results of the study could offer local actors, tourism and design specialists a glim about the generous possibilities offered by the cellars apart from households from the hilly area near Oradea, including the start of a branding process.

1.3 *References*

Resilience of rural communities refer to the adaptive capacity of a rural environment to respond to endogenous or exogenous changes and shows the ways in which a system can cope with change and mitigate its effects [1]; [2]; [3]; [4]. In the case of the rural Romanian environment, it is said to have passed through more transitional stages, given that prior to 1945, there was a private land ownership, but after 1945 till 1989, all land was taken away from individual owners and passed in the hands of the state, a process known as collectivization. This phase could also be referred to as *the tragedy of the commons* [5], a time during which all stakeholders owned the property (arable plots within/out of the village, commune, etc) at common, and each got a standardized quota of the harvest. After the 1990 the land was resituated to its former owners, some too old to manage to work it anymore, young population moving away from the village/commune by this time, leaving it quite vulnerable. From this point of view we can assert about the Romanian rural milieu that it has gone through a regime shift and the way in which it can dynamize or bounce back after such trauma is incumbent on the self-organizing capacity of the complex adaptive system of the rural community [1]. In the case of the current study, focused on the wine cellars recovery for the benefit of the local rural community, we are faced with a vulnerable declining rural community, whose past activities connected to wineyard harvesting have gradually diminished up to abandonment in many cases. A key ingredient for a resilient society is based on its social capital, namely bonding (group cohesion), bridging (ties between groups) and linking (vertical relationships) capitals [1].

These capitals can be valorised in the studied territory thanks to its resource, i.e. the wine culture and heritage which could function as a bounce back/resilient factor for the rural communities. A proposal for the community resilience would therefore be a proactive strategy triggering rejuvenation through sustainable wine tourism. Planning wine cellars for the local community benefits can be a sustainable factor for the community renewal and trace new trajectory for the community's future [6]. The diversification of activities [7] in rural communities (expansion towards tourism, wine cellar tasting) will rely on people's training, developing digital literacy skills [8] and technology. For creative rural communities and practitioners, Internet will be an indispensable tool for the economical capital valorisation as the Internet will allow to connect with peers, markets, audiences, sources of inspiration, trends and, last but not least, a tool of self-promotion [6]. Resilient rural communities manage to attract human capital back into the rural milieus, thus youth in-migration will constitute a determining challenge. Furthermore creative resilient communities build on social capital which translates in the form of trust, reciprocity, collective outlooks, values and actions; community leaders able to identify funding sources, mobilize and network the community and a collective pride in their community [6, pp 201]. According to Ungar [9], opportunities for growth in resilient communities, besides social and human capital already referred to, also rely on natural capital (land, water and wildlife), physical capital (transport, shelter and energy) and financial capital (savings, credits). Activities in the rural milieus have returned in the focus of the researcher as areas for concern in terms of agri-food system, energy security and climate change [8]. Its unpolluted physical environment relates it to recreation and leisure, certain ruralities being labelled as eco destinations for food provision and, in hilly areas where wineries are harvested, food and leisure are complemented with wine tasting, routes, trails and tours. These destinations opened towards wine tourism [10]; [11]; [12], which refers to the visiting to wineyards, wineries and wine shows for which grape and wine tastings are the main motivators and drivers for visitors. Many producers of wine involved in tourism realized that the benefits of wine tourism go beyond the wine cellar door, thus also integrating food and other leisure activities (landscape and cultural activities) alongside the wine sensorial experience [13]. This Bacchius experience seems

to be more appealing for the Y generation, as revealed by the study of Fountain and Charters [14], most tourists undertaking wine tasting being the male old generation.

According to the research of Roberts and Sparks [15] there are eight factors that provide an enhancement to the wine experience such as: authenticity of experience, value for money, service interactions, setting and surroundings, product offerings, information dissemination, learning experience and lifestyle [16]. The wine tasting experience should go beyond the wine cellar door and the interactions of tourists with wineries, thus stakeholders in the business should find inventive strategies of integrating wine tourism at a regional level with festivals, vintage car shows, wine trails and tours, food and leisure activities as in the case of many reputed countries providing this product such as France, Italy, Spain, the Switzerland, Hungary, Romania (Recaş, Dealu Mare), Greece, Australia. The importance of networking between wine cellar owners at a regional level is primordial for the business success; nonetheless some studies reveal [17] that not all farmers really want to be involved in the tourism activity, despite their harvesting wine and possessing a wine cellar, as it would divert them from their main activity, i.e. agriculture. Furthermore, nor would he/she have the skills and financial ability to become involved in the business. Based on this precept the study of Fraser and Alonso [17] revealed two groups in the wine and tourism ventures and owner expectations, namely those who perceived winery visitors as a useful adjunct to their operations and those who perceived tourism as creating a negative impact on their business. Despite there being opposite beliefs within a community, the latter's strength comes from its networking power, ability to renew itself, there needs to be synergetic and adaptive cycles within the human-environmental system [18] for a common enterprise, goal to attain sustainable development and governance in a given space; in the case of the communities herewith analyzed, wineyards and wine cellars capitalisation. Resilience in an ecological system [19] or its adaptive capacity translates in the community's continual learning for taking better decisions for the wellbeing within their environment. The physical environment of a community is inextricably linked to its resources. Nonetheless these resources need to be exploited responsibly, as an environment that is stressed by unsustainable practices might have severe outcomes in the future [18]. A currently under capitalized resource hidden within the idyllic rural landscapes of the Hills of Oradea are wine cellars. They are part of a wine harvesting heritage from a backside rural milieu [25], [26], most often economically disadvantaged [27], with an enhanced youth out-migration; therefore this wine heritage can be a great tool for local and regional regeneration [20]. Wine routes are most often also associated with aristocracy [22], as also revealed by the qualitative interviews of wine cellars' owners from the Hills of Oradea. The specific hilly relief of this space has been exploited for wine harvest ever since medieval ages, i.e. Săldăbagiu de Munte since 1371; Marghita-1422; Şişterea – 1501, which are attested as winery centres [23]; [24].

2 Location of the study area

From geographical point of view Oradiei Hills are integral part of Crisanei Hills, the last one being a subunit of the hilly area of Western Romania, drained by Crisul Repede and Barcau rivers. Oradea Hills covers an area of 393 sqkm between Crisurilor Plain (more exactly Bihariei Plain subunit) in the west and Barcaului Plain in the north, the western facade being at just 15 km from the Hungarian border. The hilly area is separated by Plopis Mountains by Fânaţelor (Ghepeşului) valley and in the southern part this hills forms the right slope of Crisul Repede River (Oradea-Borod Depression, Fig. 1). The elevation range varies between 150 and 350 meters. Oradea Hills are overlapped by eight territorial and administrative units (L.A.U., Fig. 1), with seven communes - Paleu, Cetariu, Tileagd, Lugaşu de Jos, Brusturi, Spinuş, Sârbi and fourteen villages. These administrative units are added to a neighborhood which although had all the urban facilities of a town border (it belongs to Oradea municipality) it has cellars located geographically and morphologically within Oradiei Hills. The villages are located at the periphery of the hills or within small erosional depressions (Fig. 1).

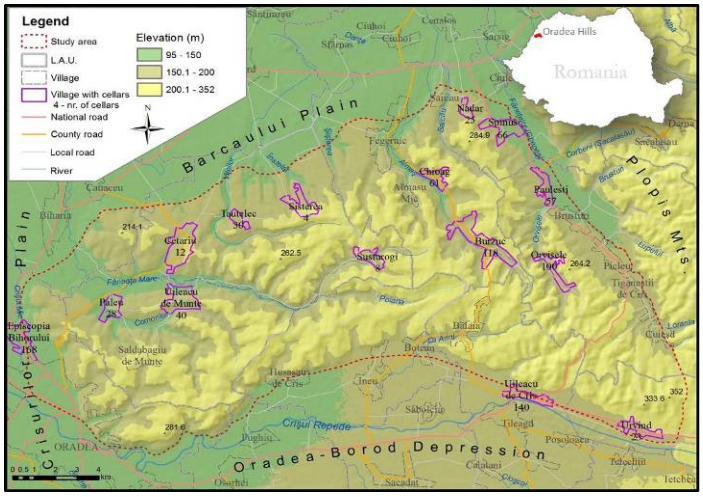

Fig. 1 Oradiei Hills. Physical map and the distribution of the cellars dug into the hills

3 Material and method

The methodology of the present study has two main components: a comprehensive analysis of the references and a field survey. The last was focused on the following items: inventory of the cellars (including the position of the cellar within the village or the street/alley); the oldness of the cellars; the identification of construction materials (separately for the vault, walls, floor, entrance doors); morphometry of the cellars (length, width, height/depth); goods and products currently stored inside the cellars.

The survey analysis was focused on few information related to: the reason why the owner built the cellar at a certain size and volume; goods and products stored inside the cellar; if they are satisfied by the functional state of the cellar (they have/have not any problem with the cellar); if the owner do other activities than agriculture; if the owner planted or has the intention to plant grape on larger parcels (or if he abandoned the viticulture); which are the wine types he store in the cellar; if they agree to introduce their cellar into a rehabilitation programme and then to use the cellar for touristic purposes (wine tasting, products selling, guided tours, local transport). The cartographic material, was used to correlate the location of the cellars to features related to physical, human, economic geography, to sociology, all material being processed using ArcGIS tools.

The resilience capacity of the inhabitants and the villages from the study area, filtered through the presence of the cellars apart from households, was analyzed using different variables which follow the local social and economic sustainability. The result of each analysis was expressed by several qualitative attributes but also by scoring each state of resilience: weak (1 point), encouraging (2 points), moderate (3 points), advanced (4 points), complete (5 points). The final result which sets the human and environmental resilience of the village is given by the average score of all variables which define the qualitative state of the certain resilience capacity.

4 Results

4.1 *Considerations upon the location of the cellars apart from households within the living and production local rural system*

The total number of cellars within Oradea Hills is 880 units.

Within the pale of rural custom and economy, the cellars apart from households (Fig. 2, Fig. 3) are a patrimony element with a very limited importance. They are appointed by villagers *cellars dug into the hill* or *cellars constructed into the hill* [28], [29], [30], [31], [32].

Fig. 2 Cellars apart from households: left (Şuşturogi village), right (Spinuş village)

Beyond the relevance of the morphological factor for the villagers from Oradea Hills or other hilly areas, we consider the term *cellars apart from households* are the most appropriate. The reasons is not only related to an agricultural use of the cellars (the storage of agricultural and processed goods in a certain place, with a constant temperature and humidity conditions) but also related to certain customs (regularly or limited use of the cellars). The choice of construction site for the cellar, at a certain distance, sometimes over 1 km, can be related to several reasons. Among these reasons one could identify some logical reasons related to the exploitations of the hill slope (as a proper place for cellar dug) and the awareness of the quality of underground environment as a storage place. Other reasons could be related to psychological, social, economic, cultural and environmental perceptions of the villagers. In turn stands some reasons: a good adaptation capacity of the villagers to the environment (they choose the hill slope for a dry cellar, abhorrent from their courtyard, partially moist); the development of strong social connections (as mutual trust among villagers that goods stored inside the cellars will not trigger stealing or robbing); the development of mutually social relations (mutual help during grape harvesting during overproduction or bad meteorological conditions); a decision of economic and agricultural efficiency meaning that it deserved constructing cellars (at sizes varying from village to village and that there will be sufficient fruit and vegetable production – mainly grapes and root vegetables). In the long run, the appearance and use of the cellars stretches from few decades to more than two centuries (in the case of few tens of cellars) and meant for the villagers the answer to the quest of present and the needs of the rural environment (self sufficiency, opening to free market).

Fig. 3 Cellars apart from households: top left (Tăutelec village), top right (Burzuc village); bottom left

(Uileacu de Criş village), bottom right (Nădar village)

4.2 *The survey interviews and results*

In order to obtain a very accurate picture about how important are these cellars apart from household for their owners, how important are from economic and social point of view and how strongly support the resilience of the study area, a set of surveys were applied. The procedure was based on direct interviews of subjects (the owners of cellars apart from households) who were found at the site but also applying the "chain selection" method (the responders name similar persons from the village in other to be interviewed). The model construction used some conceptual elements developed by [33].

A total number of 26 surveys were applied, each survey containing 8 questions. The details of each question refer to the importance of the cellar for the owner, for the community, about specific relationships for each village.

Analyzing the answers of the question related to the reason *why the cellar was built on a certain location* one could notice domination and a uniformity of arguments, the most part of the responders considering that the hills are suitable for cellar construction, meaning the optimum temperature and humidity storage conditions (65.4% from total answers). The rest of answers are divided in the following way: the reason why cellars were inherited (for cellars older than 80 years) or the parcel where the cellar is located; the fact that are bought; location of the cellar close to the grape parcel; the rock from the slope used as building material (no expense for arrangements of cellars interior); for the safety of the owners during harsh times (the longest and oldest cellars) 1. *Resilience state of the community through cellars*: 3.5 points; *Resilience state of the villages through cellars:* 4 points.

The answer at the question related to *the reason of cellar construction at a certain size*, 57.7% of answers admitted that the size is optimum for the products storage and conservation needs of the family. Other answers refer to optimum rock resistance capacity (11.5%) or to efficiency maintenance of the interior (15.3%). The rest of the answers (15.5%) are related to safety problems (for the old and very old cellars) but are also irrelevant answers. All these answers highlight the needs of the individuals and the option for intervention as a form of transformation of the built local environment capital from the hilly slope subsystem. 2. *Resilience state of the community through cellars*: 4 points; *Resilience state of the villages through cellars:* 4 points.

Just in few cases the responders established any relationship between the cellar and the nearby grape parcel. But there was a unanimous reaction about the utility of the cellars, 92.3% of the responders being satisfied or very satisfied related to the functionality of the cellars. The only discontent is related to water infiltration or vault collapse but the rate of discontent was lower for owners with cellars having 2 or 3 compartments. 3. *Resilience state of the community through cellars*: 4.5 points; *Resilience state of the villages through cellars:* 4.5 points.

The majority of the answers related to the question *which are the hosted goods and products* in the cellars, had indicated wine and tools associated to wine processing (69.2%) in all the villages from Oradea Hills. Other stored products and goods are potatoes (34.6%), vegetables (23%), fruits (19.2%). Among these one could find also other products and goods (honey, meat, pickles – 11.5%) or old traditional furniture (11.5%). The last type of items is dominantly found in the villages from the eastern part of Oradea Hills. The answers show a balanced attitude and a good knowledge of the surrounding space and environment. 4. *Resilience state of the community through cellars*: 3.5 points; *Resilience state of the villages through cellars:* 3.5 points.

Asked if they are doing *activities other than agriculture,* most responders indicated activities connected to agriculture (beekeeping, husbandry, fruit trees farming), those involved in these activities being predominantly pensioners. Non-agricultural activities are also present (15.4%) such as sewing, carpentry, driving, butchery. In few cases the viticulture is made as hobby, the owners of the cellars being employed in industry or services in the nearby Oradea (Husasăul de Cri**ş**, Tăutelec and Cetariu villages [29], Episcopia Bihorului neighbourhood). Ther answers clearly shows the dominancy of agricultural mono-specialization and a weak capacity response to present competitive everyday life. 5. *Resilience state of the community through cellars*: 2.5 points; *Resilience state of the villages through cellars:* 2 points.

The life and rural landscape regeneration process will be supported by a special attention to cellars apart from households. As most of the answers name the wine as the most important product stored in the cellars, the other two questions (*if they increased the area cultivated with grapes in the last years* and *if they intend to plant grapes*) becomes very important. All the responders admitted, to question (1), that the area cultivated with grapes decreased from 1990 (100%) and just 11.5% from responders declared that they intend to plant new parcels with grapes. The explanation is linked to the old population, unable to work, without financial or initiative support. The market for the main product of wineyards – *the wine* – is a local marker although (until the appearance of hypermarkets the inhabitants from Oradea were the main buyers of the local wine). Despite this situation, those who declared that they intent to plant new surfaces with grapes mentioned that the average area they intent to plant is about 100-200 sqm. At the first sight these surfaces seems small, without financial influence for the local

economy but one must notice that these surfaces are added to old ones. For the local tradition parcels of this size are traditional, are easy to be worked for an average family (Fig. 4). One could notice the intention of the inhabitants to replace the hybrid grape species (which are dominant) with noble grape species (in the last three years new grape species were planted, for ex. Sauvignon Blanc in Tautelec village, or Italian Riesling in Episcopia Bihor neighborhood). 6. *Resilience state of the community through cellars*: 1.5 points; *Resilience state of the villages through cellars:* 2.5 points. 7. *Resilience state of the community through cellars*: 2.5 points; *Resilience state of the villages through cellars:* 3 points.

Fig. 4 Grape parcels (left - Nădar village), with cellars (right - Uileacu de Criş village)

At the key question of the survey, *if they accept the inclusion of the cellar in a rehabilitation arrangement programme for possible touristic purpose* – the majority of the answers were positive (92.3%). The same positive attitude, together with the existence of the cellars as local wine storage places could increase the resilience of the inhabitants and the villages. 8. *Resilience state of the community through cellars*: 4.5 points; *Resilience state of the villages through cellars:* 5 points.
Mean resilience state of the community: 3.31 points, moderate to advanced (closer to moderate); *Mean resilience state of the villages*: 3.56 points, moderate to advanced (slightly closer to advanced).

4.3 *Products and goods stored into the cellars*

One could expect that the cellars are used just for wine storage. The reality is a little bit different, in case of the cellars from Oradea Hills, the importance of the wine as basic product stored in the cellars is decreasing, the wine being no longer the only product stored.

Overall, *the wine* remains the main stored product, although the quantity differs from village to village. In the villages from the northern part of the study area (Cetariu, Tăutelec, Paleu, Chioag, Spinuş) about 80-90% of the stored goods is wine. A possible explanation could be linked to the fact that these villages have extended grape surfaces, good productivity and subsequently good wine production. The cellars which store the less quantity (10-30%) are found in the isolated villages which have favorable conditions for other crops (Şuşturogi, Orvişele). The wine is stored together with plum brandy (10-20%), usually stored just for family use, in opposition with wine, which is locally sold, rarely to customers from town. Dominant are the red grape species (Othelo, Concorde, Delaware) but the white grape species are also present (Nova, Izabela, Elvira). In Paleu village Merlot wine is produced by the grapes are bought outside the study area. The wines produced from these grape species are catalogued by the producer as "home made", natural, biological wines (as hybrid grapes doesn't need any chemical treatments) but the specialists consider these wines as low quality because the alcohol content is low, the acidity is high, they are difficult to be stored (they rarely reach maturity or aging), the flavor and taste, with a higher content of methanol as noble vines [34]. Within the local context, even in the E.U. these types of wines are not agreed, the commercial capitalization using cellars dug into the hills could create a certain financial advantage for the inhabitants. In order to increase the occupational flexibility (the population from the eastern part of Oradea Hills comes from a mono-industrial economic environment based on the extraction of raw materials) this economic activity could reduce the social and economic vulnerability namely to resilience of rural communities as stability factor for a sustainable rural development. Moreover, the preservation of at least one of this hybrid grape species could contribute to the preservation of the traditional rural. *The resilience state of the community through products storage capacity:* 3.5 points; *The resilience state of the villages through products storage capacity:* 3.5 points;

An interesting feature related to storage use of cellars from Oradea Hills is given by the fact that the wine was gradually surpassed by *potatoes* as stored products (Fig. 5). The land is favorable for this crop and the

storage conditions are perfect. The majority of the owners stated that even in spring potatoes don't have sprouts, as it happens in all other storage facilities. The greatest potatoes quantities are stored in cellars of isolated villages, with an aging population whose diet, mainly in winter, is predominantly based on potatoes (80-90%, Şuşturogi, Burzuc, Chioag villages). Potatoes are added by other vegetables (in order amount: carrot, parsley, parsnip, kohlrabi, beetroot, onion, garlic) the average storage rate for these products being 10-20%, higher values being in Uileacu de Munte, Burzuc and Şuşturogi villages. The explanation is linked by culinary traditions of the Hungarian community and, by influence, of the Romanian community. *The resilience state of the community through products storage capacity:* 4.5 points; *The resilience state of the villages through products storage capacity:* 4 points;

Fig. 5 Cellars from Episcopia Bihor neighborhood where potatoes, wine and winemaking equipment are stored (left) and containers for wine storage, oak barrels, demijohns, glass barrels (right)

Quite often *fruits* (mainly apples), *honey, cereals and different canned fruits and vegetables, pickles or other foods products* (pork sausages) are stored within the cellars. Fruits, in terms of cellars capacity and frequency, are commonly stored in the villages located in the western part of the study area, where extended surfaces are covered by orchards but also many fruit trees scattered among gardens and hayfields, the percentage of storage capacity being 5-10%. *The resilience state of the community through products storage capacity:* 3.5 points; *The resilience state of the villages through products storage capacity:* 3.5 points;

Some other important set of tools, important in terms of size and diversity, are the *tools* r*elated to wine preparation and storage*. All the cellars host wood tubs, wood barrels (oak, mulberry, 60-70%), plastic or aluminium barrels, demijohns, glass barrels (Fig. 5). All adds different tools and equipment for grapes and wine processing (10-20% - grape crusher, grape squeezer, hoses) for the villages located in the eastern part of Oradea Hills and a percentage of 40-60% for the villages located in the western part. Other inventory tools hosted in the cellars are glasses for wine tasting, farming tools (hoes, shovels, rakes, axes, scythes, sickles) but also working clothes. Objects and tools from this category favours a good resilience encouraging the wood craft and a better wood use (mainly oak). *The resilience state of the community through products storage capacity:* 3.5 points; *The resilience state of the villages through products storage capacity:* 3.5 points;

The cellars with two or three compartments, in the front compartment *old furniture and objects* are stored. The furniture is usually consisted of old shelfs for storage even if, in many cases, the storage is made directly on the floor. In the front compartment there are several types of furniture, usually unused pieces from owner household. The most common pieces are tables, chairs and benches but also cabinets, shelfs and other household's items (plates, spoons, cups). An interesting situation was found in Păuleşti village, where stove and a bed were found, and, according to the owner, are used when the owners remains overnight. In Uileacu de Criş, Păuleşti, Nădar villages, the outside area of the cellar was arranged as picnic area, with open fire places, benches. The presence of these old items creates a physical comfort for the owners because they link these objects with old memories. *The resilience state of the community through products storage capacity:* 2.5 points; *The resilience state of the villages through products storage capacity:* 2 points;

Mean resilience state of the community: 3.4 points, namely moderate to advanced state; *Mean resilience state of the villages:* 3.3 points, namely moderate to advanced state.

✹

Independent household cellars prove to be not only a physically present heritage element to Oradea Hills' villages. The study results highlight at least *a good general ability of resilience* by all the analyzed socio-economic sustainability indicators. Cellars support a moderate to easily advanced general community resilience ability demonstrated by the average of 3.355 points of all profile indicators (subchapter 4.2 and 4.3). This refers to the proactive and reactive human resilience chapter (weaker, but encouraging for elderly residents, but enhanced for the adult and young adult population). Cellars also evince general moderate resilience ability in the case of villages, but lower advanced, a situation demonstrated by an average of 3.430 points of all surveyed

profile indicators. In the case of settlements' resilience demonstration leans towards the adaptive type (starting from what a competitive life involves and the inexorably modernizing rural trend), but we must accept the shifting trend for the better that the rehabilitated cellars can bring for the residents, the former acting as promoters of economic benefits both locally and individually.

5 Conclusions

The study focuses on the heritage-related importance of *independent household cellars* dug into the hilly slopes and the resilience capacity demonstration that these cellars can develop for the community and villages. Relating to the interviews' processed results, in terms of cellars' utility, 92.3% of respondents is satisfied and very satisfied with the operation and functionality of their cellars. If we refer to the hosted objects and products within cellars, wine and wine production, processing and storage associated items are the prevalent replies (69.2%) in almost all settlements of Oradea Hills. On the key question of the interview - acceptance of cellar integration in a rehabilitation program and equipment for possible tours - most interviewee were very receptive, and the responses were positive (92.3% of total answers). This positive attitude, coupled with the existence of massive cellars dug into the hillside and local wine storing help to increase the residents' and the related rural settlements resilience.

Regarding hosted products and items within cellars, overall, wine remains the main product which is found in these cellars with a majority of hybrid stored wines, unendorsed by the E.U but which allow a local recovery and a cultural advantage. An important set of items are related to the wine preparation and storage in the domestic system. The cellar contains items used for storage, wine equipment etc. The objects and the equipment in this category promote a good resilience by encouraging superior craftsmanship in wood and the upscale use of local wood (especially oak). In the case of the two or three-compartment cellars, in the first compartment (at the front) there is furniture and antiques. For the economic emancipation of the cellar owners these old objects do not seem to contribute consistently, but reality indicates the perspective concern for objects that can be converted in the case of their potential rehabilitation and equipping for rural tourism or ecotourism activities.

Local household independent cellars finally support a general community resilience ability from moderate to easily advanced, demonstrated by the 3.355 points mean of all profile indicators. And for the settlements in the Hills of Oradea, resilience leans towards the adaptive type demonstrated by the 3.430 points mean of all profile indicators, but with a predictive trend of a change for the better that rehabilitated cellars can bring to the residents as promoters of individual and community economic benefit.

REFERENCES

[1] Wilson, G.A. (2012). Community resilience, globalisation, and transitional pathways to decision-making. Geoforum 43(6), pp. 1218–1231.
[2] Mataritta-Cascante, D., Trejos, B. (2013). Community resilience in resource – dependant communities: a comparative study. Environment and Planning A 45(6), pp. 1387-1402.
[3] Skeratt S. (2013). Enhancing the Analysis of Rural Community Resilience: Evidence from Community Land Ownership. Journal of Rural Studies 31, pp. 36-46.
[4] McManus, P., Walmsley, J., Argent, N., Baum, S., Bourke, L., Martin, J., Pritchard, B., Sorensen, T. (2012). Rural Community and Rural Resilience: What Is Important to Farmers in Keeping their Country Towns Alive?, Journal of Rural Studies 28(1), pp. 20-29.
[5] Cater, C., Cater, E. (2001). Marine Environments, in Weawer D.B. The Encyclopedia of Ecotourism, CABI Publishing, Oxon, pp. 265-282.
[6] Roberts, E., Townsend, L. (2016). The Contribution of the Creative Economy to the Resilience of Rural Communities: Exploring Cultural and Digital Capital. Sociologia Ruralis 56(2), pp. 197-219.
[7] Niehof, A. (2004). The significance of diversification for rural livelihood systems. Food Policy 29(4), pp. 321-338.
[8] Roberts, E., Andersen, B.A., Skerratt, S., Farrington, J. (2016). A Review of the Rural-Digital Policy Agenda from a Community Resilience Perspective. In Press, Journal of Rural Studies. http://dx.doi.org/10.1016/j.jrurstud.2016.03.001
[9] Ungar, M. (2011). Community Resilence for Youth and Families: Facilitative Physical and Social Capital in Contexts of Adversity. Children and Youth Services Review 33(9), pp. 1742-1748.

[10] Peris-Ortiz, M., de la Cruz Del Río Rama, M., Rueda-Armengo, C. (2016). Wine and Tourism – A Strategic Segment for Sustainable Economic Development. Eds., Springer International Publishing, Switzerland.
[11] Croce, E., Perri, G. (2010). Food and Wine Tourism: Integrating Food, Travel and Territory. Cabi Tourism, Wallingford, Oxfordshire, pp. 504-505.
[12] Hall, C.M., Sharples, L., Cambourne, B., Macionis, N. (2000). Wine Tourism around the World: Development, Management and Markets. Routledge, London.
[13] Carlsen, J., Charters, S. (2006). Global wine tourism: research, management and marketing. Cabi, Oxon, Cambridge.
[14] Fountain, J., Charters, S. (2010). Generation Y as Wine Tourists: Their Expectations and Experiences at the Winery-cellar Door. In Benckendorff et al., Tourism and Generation Y, CAB International.
[15] Roberts, L., Sparks, B. (2006). Enhancing the Wine Tourism Experience: The customer's viewpoint. In Carlsen and Charters (Eds.), Global Wine Tourism: Research, Management and Marketing, pp. 47-55, UK Cabi.
[16] Carlsen, J., Boksberger, P. (2015). Enhancing Consumer Value in Wine Tourism. Journal of Hospitality & Tourism Research 39(1), pp. 132-144.
[17] Fraser, R.A, Alonso, A. (2006). Do Tourism and Wine Always Fit Together? A Consideration of Business Motivations. In Carlsen and Charters (Eds.), Global wine tourism-research, management and marketing, Cabi.
[18] Cutter, S. L., Barnes, L., Berry, M., Burton, C., Evans, E., Tate, E., Webb, J. (2008). A place-based model for understanding community resilience to natural disasters. Global Environmental Change 18(4), pp. 598-606.
[19] Robinson, G.M., Carson, D.A. (2015). Resilient Communities: Transitions, Pathways and Resourcefullness. The Geographical Journal 182(2), pp. 114-122.
[20] Novelli, M. (2004). Wine Tourism Events: Apulia, Italy. In Yeoman et al. (Eds.), Festival and Events Management – An International Arts and Culture Perspective, pp.329-345, Elsevier Butterworth-Heinemann, Oxford.
[21] Scalise, C.M. (2004). Interior Planning and Design: Projects Programs, Plans, Charetts. Thomson/Delmar Learning, New York.
[22] Szabo, A.T. (2013). Does the Countryside still feed the country? Producing and Reproducing the Rural in Transylvania. In Silva et al. (Eds.), Shaping Rural Areas in Europe, GeoJournal Library 107, pp. 165-180, Springer Netherlands.
[23] xxx (1979). Biharea 6, pp. 134, Muzeul Ţării Crişurilor, Oradea.
[24] Giurescu, C.C. (2007). Istoria Românilor. Vol. III, Partea II, Editura All, Bucureşti.
[25] Dincă, I. (2007). Le thème du paysage, entre l'éducation des goûts et le profit thématique des touristes. Exercise sur l'inventaire des paysages du Département de Bihor (Roumanie). Anuario Turismo y Sociedad 8, pp. 83-105.
[26] Dincă, I. (2009). Discovery, observation and tourism reckoning on rural space's nature through accesing common and specific features of some local landscapes. Target: the thematic backdrop of a village in Province of Crişana (Romania). Analele Universităţii din Oradea, Seria Geografie XIX, pp. 201-210.
[27] Dincă, I. (2005). Economical activity reverberations in the opinions about damaging or beautifying the rural-agricultural landscape. Case-study on the population of four villages in the central part of Bihor County (Romania). Analele Universităţii din Oradea, Seria Geografie XV, pp. 173-180.
[28] http://lege5.ro/Gratuit/g4zdmnrw/ordinul-nr-645-2005-privind-aprobarea-incadrarii-regiunilor-viticole-romanesti-in-zonele-viticole-ale-uniunii-europene-si-conditiile-aplicarii-corectiilor-de-tarie-alcoolica-si-de-aciditate-asupra-rec
[29] http://vinul.ro/editorial-vinul-de-casa.html
[30] http://riscurinaturale.blogspot.ro/2011/01/rezilienta.html
[31] HTTP://WWW.GORJEANUL.RO/REALITATEA-GORJEANA/PIVNITELE-DE-DEAL-DE-LA-VIILE-BALANESTIULUI-SI-GLODENILOR#.WB-FJI2LTIU
[32] http://vinul.ro/editorial-vinul-de-casa.html
[33] Magis, K. (2010). Community resilience: an indicator of social sustainability. Society and Natural Resources 23(5), pp. 401–416.
[34] Bakker, J., Clarke, R.J. (2012). Wine Flavour Chemistry, Second Edition, Blackwell Publishing Ltd., Chichester UK and USA.

Digital Terrain Model Draw Up Using Photogrammetry

Gridan M.-R.[1], David V.[2]

[1] *Politehnica University Timisoara, Faculty of Civil Engineering, Department of Terrestrial Communication Ways, Foundations and Cadastre (ROMANIA)*
[2] *Politehnica University Timisoara, Faculty of Civil Engineering, Department of Terrestrial Communication Ways, Foundations and Cadastre (ROMANIA)*
E-mails: roberta.gridan@upt.ro, viorica.david@upt.ro

Abstract

Earth` surface is in a continuous change, and its model have always appealed to experts in various earth sciences like geodesy, surveying, geophysics, geography and others. An important concept in representing the Earth` surface, is the digital terrain model (DTM).

The DTM made its presence known along with the development of computer systems due to its numerous advantages: has a variety of forms that can be represented (level curves, cross sections, three - dimensional representations), keeps its precision, it can be adaptable for representations in several scales and has great feasibility in the sense of automation and real-time processing.

In this paper we aim to highlight the importance of a DTM drawn up using Photogrammetric methods. The DTM, obtained in digital format through photogrammetric images correlation, can be further modified or processed for different applications like generating both level curves and orthophotoplans.

Keywords: photogrammetry, digital terrain model, stereomodel, orthoimage.

1. Introduction

If originally, terrain models were physical models, made of rubber, plastic, clay or sand, but when the computer was introduced the terrain surface modelling started to be carried out numerically or digitally. This led to digital terrain modelling and also to an accurate representation of the terrain morphology.

Digital Terrain Model (DTM) is a term commonly used interchangeably with digital elevation model (DEM). Strictly speaking a DTM refers to a model of reality which includes information relating to factors such as surface texture as well as elevation [1]. DEMs do more than improve the accuracy of satellite imagery. They bring the area of interest (AOI) to life by allowing 3D measurements and analyzes - giving a more complete picture. DEMs come in various flavours depending on customer needs:

- Digital surface models (DSMs) include buildings, trees and more. DSMs help with applications like line-of-sight analysis and signal propagation.
- Digital terrain models (DTMs) show only the 'bare earth' terrain. DTMs provide more precise results for flood models, excavation calculations, contours and orthorectification.
- Point cloud is a format that works with existing LIDAR workflows, allowing for easy editing and attribution of data.
- Vricon 3D is a fully textured 3D model that provides a truly lifelike view of the world [2].

Creating a DTM is a complex activity both by the variety of used methods for acquiring terrain data and by choosing the most appropriate approach for data processing in order to obtain a final product which combines optimal quality required for the application, with the shortest time to achieve it.

Due to the different types of applications which require a DTM and to the continuous science development there are various instruments, methods and software used for data collecting and processing in order to obtain/ to use a DTM. The digital terrain model can be obtained using different methods and technologies like:

- Topographical surveys (this method is used for small scale projects and the obtained DTM has a high precision, but it cannot be applied in the case of bumpy areas).

- Aerophotogrammetry (is used for medium and large scale projects, the obtained DTM has a high precision, depending on the terrain fragmentation and slope).
- Remote sensing (this technology is used for large scale projects and the obtained DTM has a medium or high precision, depending on the terrain fragmentation and slope).
- Contours digitization (is utilized for projects at different scales, the DTM has a medium and small precision, the method not being recommended for small areas, because on the topographic maps are not sufficient characteristic points).
- GNSS technology (is used for projects in small areas, the DTM has a medium or a high precision, the limit being the technology` performance).

Sterephotogrammetry is a complex Photogrammetric technique, through which an object tri-dimensional coordinates can be estimated. In principle, stereograms are realized by processing several images of an area, taken from different positions, with a longitudinal coverage between 60-90% so that through the composition can be gauged the area` spatial coordinates (Fig.1).

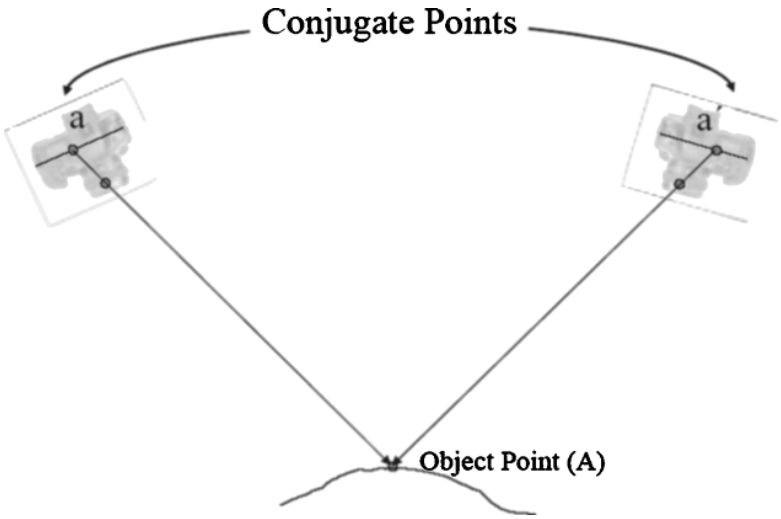

Fig. 1 Data acquiring using Stereophotogrammetry [3]

The big advantage of the digital systems in stereo photogrammetric measurements is to increase the amount of data stored during an aerial flight and the use of software that largely automates data processing, shortening in this way the processing time significantly. From the measurements is resulting a raw form of the data necessary for the DTM generation. But, to reach a usable form it requires other data editing operations, even of the initial DTM and of the intermediary ones, in order to obtain an accurate model, capable of forming a stable basis for further analysis and modelling that will be carried out.

2. Digital terrain model draw up using Photogrammetry

Creating a digital terrain model (DTM) from photogrammetric images is based on the same principle by which man creates the tri-dimensional image, i.e. the two images are observed concomitant with both eyes. Stereoscopic effect is established in the human brain, the direct stereoscopic vision conditions being fulfilled. The two images show a longitudinal coverage of at least 60%, making possible to determine and spatial play of the double coverage area. From mathematical point of view, the tri-dimensional positions of the points from the double coverage area can be determined.

Presently the term “digital terrain model” has a broader meaning, so a number of several terms which use the same representation were applied to it:

- DSM (digital surface model) which contains the surface superstructure elements z values (vegetation, buildings)
- DEM (digital elevation model) contains the height value, as measurement taken in relation with a reference level (datum) and also as absolute height [4].

Digital terrain model and digital surface model, beyond positioning information (i.e. Geographic coordinates and altitude), include general morphological information [5].

In this paper we aimed to obtain a DTM using Photogrammetric methods. Data were acquired from an aero photogrammetric flight which was conducted through the city centre of Timisoara, Romania, on the East – West direction. Due to this flight images were taken in analogue format, at the scale ≈1:3500, subsequently being converted into digital images.

A first step in obtaining a DTM is the realization of image orientation (both interior and exterior).

Into the interior orientation are determined the transformation coefficients from the camera coordinate system into the pixel-coordinate system. Basically it can be achieved in two ways:

1) By pointing the reference indexes directly by the operator (Fig. 2 our example)
2) By using image correlation techniques.

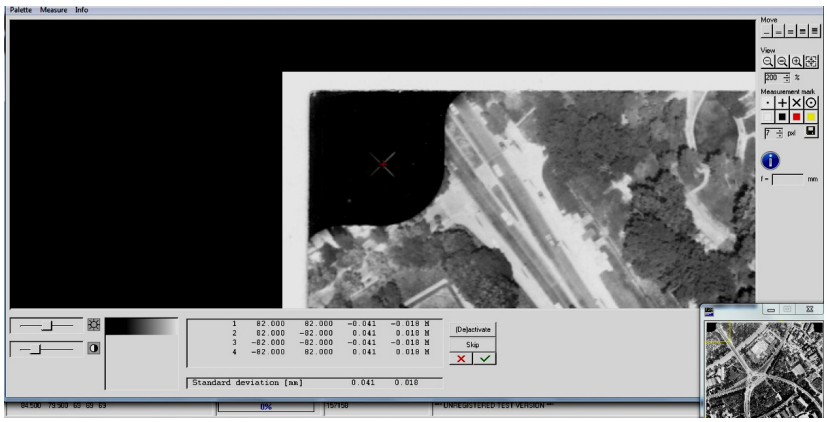

Fig. 2 Interior orientation

At the absolute orientation the correlation techniques are less used because the control points (Ground Control Points) can have different forms and can occur anywhere within the stereomodel [4]. Following the absolute orientation is carried out the transformation from the model-coordinate system into the field-coordinate system.

In our example we approached another way of achieving the orientation: for each image we realized the exterior orientation independently and manually (by measuring the control points within each image) (Fig. 3), after it following the adjacent images "connection" in order to obtain the stereomedel [6], (Fig. 4).

Fig. 3 Exterior orientation

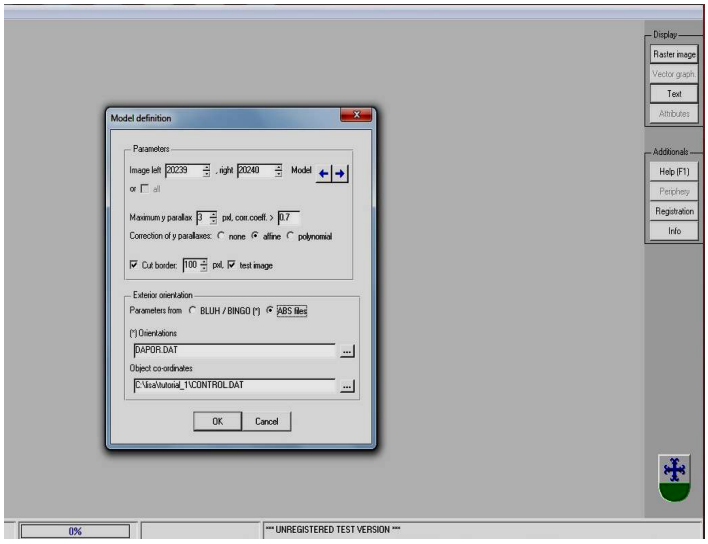

Fig. 4 Model definition

In LISA software we generated digital terrain model (Fig. 5.), which was obtained automatically by using the correlation method, in the first stage, with a correlation coefficient value ρ=0.8, and with 3 iterations (Fig. 6).

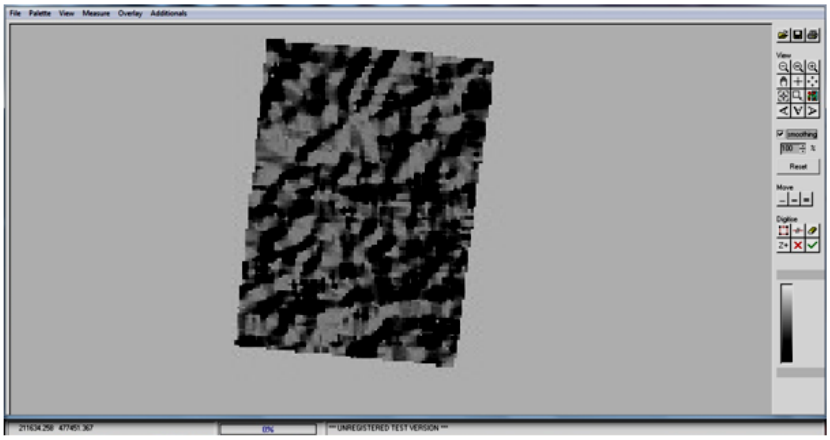

Fig. 5 Digital Terrain Model

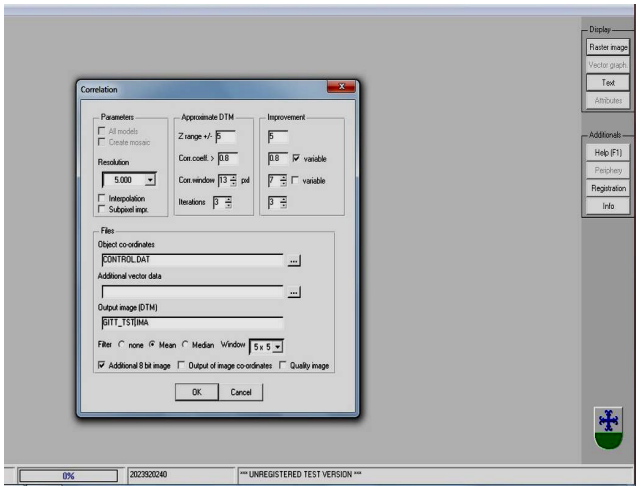

Fig. 6 The correlation parameters for DTM generating

In order to obtain several correlated points (for the DTM voids filling) we chose for a smaller value of the correlation coefficient, ρ =0.7, and for decreasing the correlation window. This was enabled by the fact that the images have a good contrast, and the terrain represented in the images is almost flat [6]. After this step, in the remained gaps we performed additional measurements of points.

Based on the obtained DTM we generated an orthoimage, which is actually the digital surface model (DSM). This digital surface model allows us to generate Orthoimages (Fig. 7).

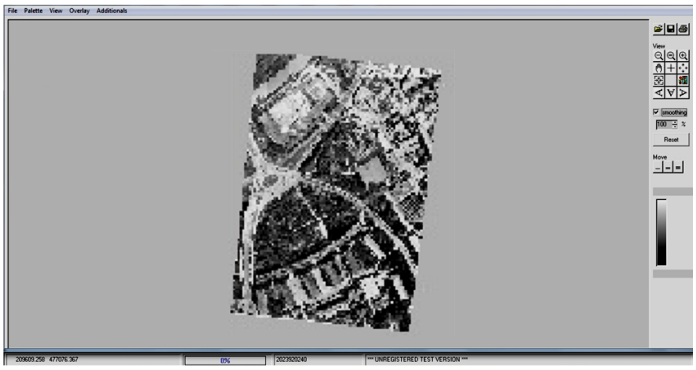

Fig. 7. Orthoimages generation

Instead for creating the contours a digital terrain model is needed, containing the Earth` physical surface altimetric information (without superstructure). So, this requires filtering the DSM in order to obtain a DTM closer to the real DTM.

After contours derivation (Fig. 8) we overlapped them over the orthoimage (Fig. 9).

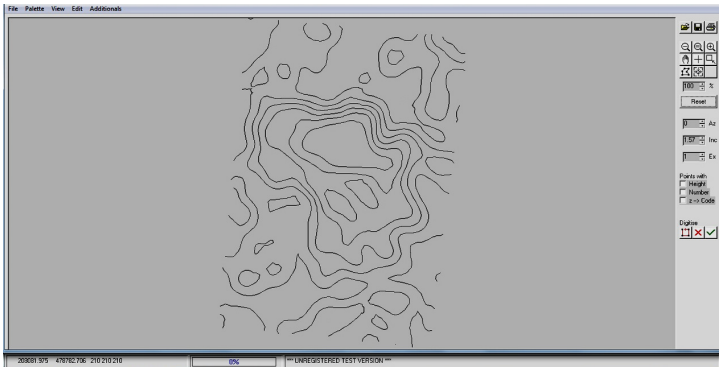

Fig. 8 Contours derivation

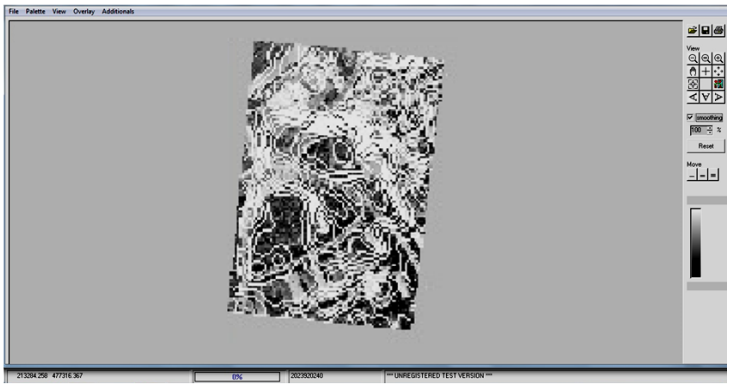

Fig. 9 Overlapping the contours over the orthoimage

Once obtained, DTM offers the possibility of further processing (by updating it), of making different measurements on details of the terrain and also its integration in various GIS applications.

3. Conclusions

Now, that scientific communities recognize the consequences of human activity on the environment the DTM is an essential tool in the effort to understand the global changes [7], its use being found increasingly necessary, the limit being set in the level of technology: both in terms of equipment for collecting and processing data and creating new methods and specialized software for each case.

Using the modern technology in order to obtain a precise DTM large data quantities can be analyzed in order to have both an accurate understanding of the terrestrial process and a human activity better management.

Stereophotogrammetry tends to become one of the main ways of data collecting in order to obtain the DTM. Through it is trying to minimize data collection effort simultaneously with increased accuracy in resulting models, presenting advantages like the possibility of eliminating redundant data when acquiring them and the data obtaining for regions where other methods can`t be applied (areas where there are topographical maps, areas where access is prohibited political or military reasons and areas with very uneven terrain).

In conclusion, the digital terrain model is a tool, an object of study, of real help for different users. Because of its digital format, it can always be used, modified or processed easily for different purposes and it represents an important tool for work efficiency in different studies which include a DTM analyze.

REFERENCES

[1] Internet Source: http://ads.ahds.ac.uk/project/goodguides/gis/sect72.html.
[2] http://blog.digitalglobe.com/2016/10/31/see-the-world-in-3d-with-digital-elevation-models/.
[3] Rita W. T. Cheng , Ayman F. Habib (2007). Stereo Photogrammetry for generating and matching facial models, Journal of Optical Engineering, Vol. 46, Issue 6, DOI:10.1117/1.2750334.
[4] I. Ionescu, (2005). Fotogrametrie Inginereasca, Ed. Matrixrom, Bucuresti, ISBN 973-685-734-4.
[5] M. Vais, Gh. Iosif, (2011). Using Lidar Measurements For Improving Or Up-Dating A Dem, Journal of Applied Engineering Sciences, Vol. 1(14), pp.123-128.
[6] W. Linder, (2009), Digital Photogrammetry, Ed. Springer, ISBN 978-3-540-92724-2, Germania.
[7] M. Sturza, A. Baciu, S. Herban (2006). Caracteristici Generale ale Modelului Digital al Terenului (DTM) şi modalităţi de utilizare ale acestuia, RevCAD, vol. 6.
[8] G. Popescu, (2010). Curs Fotogrammetrie, http://docslide.us/documents/curs-fotogrammetrie-analitica.html.

Land Market Analysis in Romania after 2014

Mancia M.S.[1], Mancia A.[1], Golea L.A.[1]

[1] *University of Oradea, Faculty of Civil Engineering, Cadastre and Architecture (ROMANIA)*
E-mails: mancia.mircea@yahoo.com, amancia@uoradea.ro, laura.golea@gmail.com

Abstract

Romania's land market suffers continuous transformations, and a law to protect the national capital was initiated without being completed. In the current global and European context it is strictly necessary to promote sustainable development of local agriculture to ensure food security and production patterns that avoid over exploitation of natural resources. Farmland in Romania are among the most fertile in Europe. The low price and quality of agricultural land are the main factors that led to the increased interest of foreigners for this natural resource called the agricultural land.

Keywords: agricultural land, development, price, purchase, transaction.

1 Introduction

Having in view the exponential growth of population on the planet, a country that has fertile land is being considered a rich country.

After World Water Vision estimates the world population will be 8.1 billion people in 2025 and 10.5 billion inhabitants in 2050, compared to 7.4 billion people existing at the end of 2016.

The contemporary relationships change and they are being structured after new models based on geopolitical, economic, social and cultural strategies. Spaces are remodeled according to the resources and natural resources, local conditions and requirements and also strategic locations.

Intensive growth of agricultural production is a requirement today, amid the growing demand for ensuring adequate food supplies for the world population.

A current problem is to manage areas of fertile land, directly productive, having in view the limited resources and environmental constraints.

2 Methodology

Romania's geographical position is favorable to agriculture; the ratio of arable land and the number of inhabitants shows that every Romanian citizen has 0.41 hectares, the EU average being of 0.212 hectares/head of the population [4].

We have the most fragmented agricultural area of EU, with 3.86 million farms in 2010, according to Eurostat.

After January 1, 2014 the land market in Romania opened, allowing citizens frm EU to buy agricultural land without restrictions.

According to DZT Equinox foreigners are interested in farmland from south and west, "where prices are lower compared to other regions of arable land. Soil type, previous crops, the existance of a system of irrigation may lead to its fragmentation, the lack of clear property documents and the lack and cadastre and tabulation." [9]

The average sizes of a farm in different EU countries are:

- Italy, 10 ha,
- France, 53.9 ha,
- Great Britain, 93.6 ha,
- Czech Republic, 133 ha,
- Greece, 5 ha,
- Romania, 3,4 ha,
- Poland, 10,2 ha.

54.4% of EU small farms are in Romania.

According to a study by the Transnational Institute in Amsterdam, which was presented in EU Parliament, "over 10% of farmland in Romania is owned by investors outside EU and 20/30% is managed by investors belonging to EU." [7]

In Romania there are no official statistics with regard to agricultural land owned by foreigners.

According to the company Agro Intelligence SISA - Information System on Food Security – "out of the total arable land owned by foreigners, 23.4% belong to Italians, 15.5% to Germans, 10% to Arabs, 8.2% to Hungarians, 6.2% to Spanish, 6.1% to Austrians and 4.5% to Danish people." [10]

The worldwide interest for farmland increases steadily and the shift to flexible global food policy towards with worldwide capital.

In 2015 European Economic and Social Committee (EESC) warned that "agricultural land market is regulated differently in EU member states." It was proposed to establish by law of an upper limit for the purchase of farmland both to individuals and to juridical ones [8].

According to studies carried out by EU specialized agencies, Romania is the country where the phenomenon of alienation of agricultural land to foreigners occurred at an "alarming" rate [5].

In 2014 the average price of arable land from România for areas up to 30 ha was 4,000 euro/ha (Ziarul Financiar).

Prices for very small lots without cadastral values had values of 1500-2500 euro/ha/ secondary market.

"Farmland in Banat are transactioned between 5,000 and 7,000 euro/ha. In Timis and Arad area many foreign investors have offered many individuals and businesses; specialized investment funds bought agricultural land they leased to local farmers for long periods – the Dutch group Rabobank or Italians from Generali" [8].

Also in 2014, in Constanta county were sold farmlands for prices up to 7,000 euro/ha. The high price of land in this area is due to the proximity of the Constanta shipping port and the possibility of trading products to values closer to the export value.

"The average rate of annual appreciation of agricultural land prices is of 40%; their price between 2002-2012 increased 25 times" after Savills House Consultancy from the UK.

In 2016 the agricultural land market has maintained its dynamism.

According to Economica.net, in 2016 were performed over 25 transactions with compacted land larger than 30 hectares. According to data posted on the website of the Ministry of Agriculture the largest areas were bought in Arges, Arad, Timis, Constanta, prices reaching up to 9,500 euro/ha.

In the area of western Romania: Timis, Arad, Bihor, prices experimented an upward trend being as attractive as in previous years (Fig. 1).

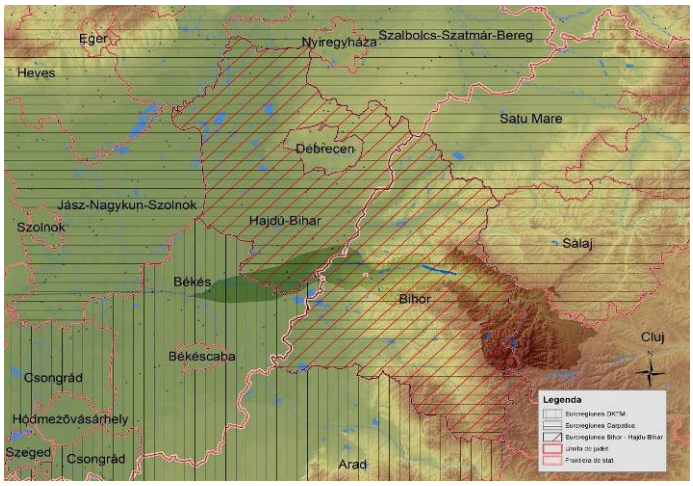

Fig. 1 Western Plain of Romania

Important factors for the sales prices (Fig. 2) are:

- Land fertility,
- The degree of consolidation,
- Cadastral situation,
- Legal position,
- Necessary logistics of modern agriculture.

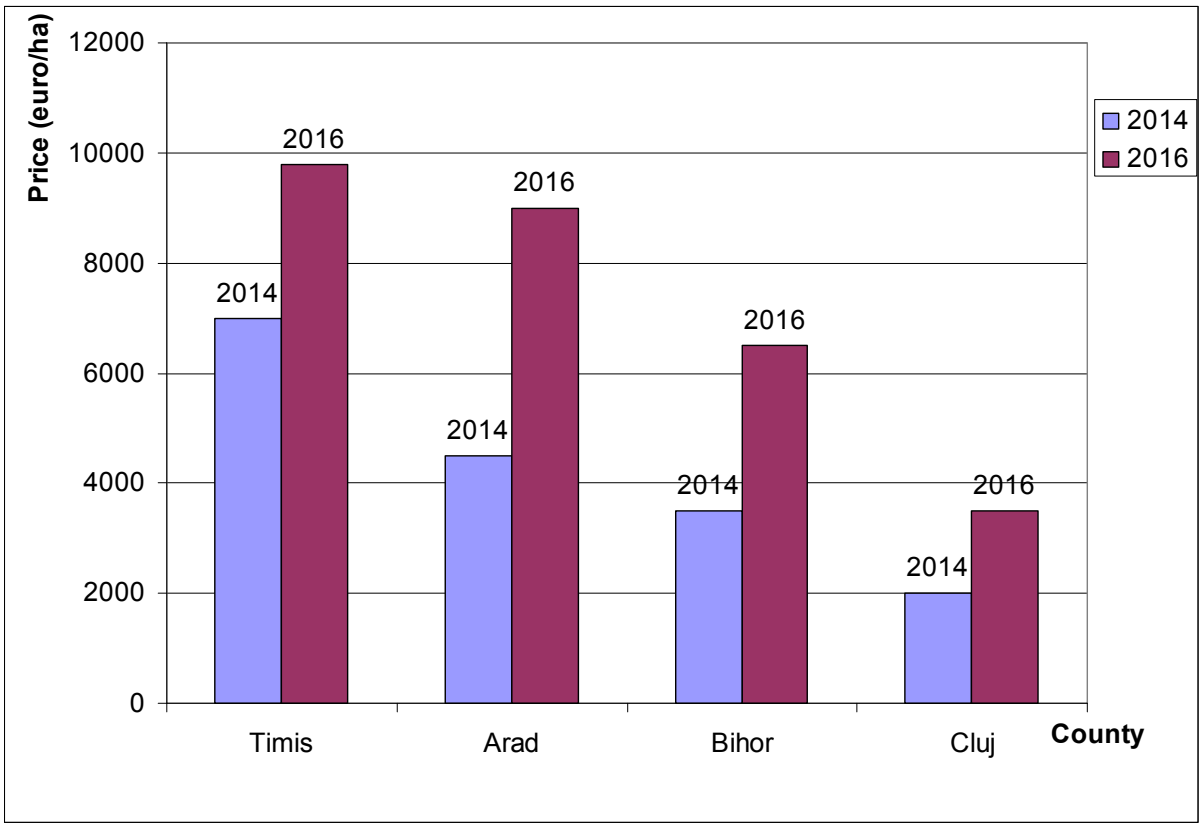

Fig. 2 Sales prices of agricultural land [6]

Unlike the the Western Plain in the prices from Transylvanian plateau are lower: the land is not so fertile, the properties are fragmented, and the fertile land is generally leasehold. The average price of pastures in Cluj County is 900-1000 Euro/ha.

Between 2012-2016, in Bihor county the land increased by up to 30%-50%.

If agricultural land was sold in 2013 with approx. 1,500 Euro/ha in localities Cefa, Diosig, Valea lui Mihai and 2,500-3,000 Euros/ha in Oşorhei, Bors, Biharia, in 2016, the same type of land was sold with 3,500-4000 Euro/ha in areas Cefa, Diosig, Valea lui Mihai; in Oşorhei the value of a hectare was 5,000 euro, 6,700 euro in Bors, Lăzăreni 4,500 euro.

Compared to Western European countries, EU member states, the agricultural land in Romania, although it has potential is traded below its value.

In Slovakia, the average price per hectare is 4,000 euros, 8,000 euros in Poland, Lithuania 1,500 euro.

In Western Europe the average trading price of the land is, according to Bloomberg Company, $ 18,521 Germany and $ 25,575 UK.

According to Proagro Capital – the economic and financial analysis, the price of agricultural land in Italy has values of 32,000-35,700 euro in the plains in the north to 14,300 euro in the lowland plains, and land in the hills has values of 18,400 euro in the north to 10,300 euro in the south [12].

3 Conclusion

"Natural resources are increasingly limited compared to the demand and, therefore, they must ensure maximum efficiency. There is fertile land it should be exploited in terms of higher productivity.

By geopolitical strategies of sustainable development the regional potential can be capitalized; it is necessary to streamline activities related to the land fund using non-polluting technologies" [13].

In an increasingly globalized market economy, establishing fair value of agricultural land – part of the national economy – is a priority that cannot be contested.

In the context of global food demand it was noted that Romania's lands are among the best to grow wheat, corn and other cereals. It is estimated that agricultural land prices will equalize with those from Central Europe – in the not too distant future.

References

[1] Declaraţie asupra mediului şi dezvoltării de la Rio de Janeiro (Environment and Development Declaration, Rio de Janeiro) (1992).
[2] Studii (2015), Comitetul Economic şi Social European CESE (Studies. European Economic and Social Committee EESC).
[3] Studii (2016) (Studies), World Water Vision.
[4] 2010-2015, Eurostat Year Book.
[5] Raport (2015), Comisia pentru Agricultură a U.E. (Report. EU Agriculture Commission)
[6] Direcţia Judeţeană pentru Agricultură – tranzacţionări terenuri agricole, Min. Agriculturii (County Department of Agriculture - Agricultural land dealings, Ministry of Agriculture.).
[7] Raport (2015) (Report), Transnational Institute, Amsterdam.
[8] www.economica.net, accesed at 16.02.2016; 15.12.2016.
[9] DZT Echinox, 27.09.2015.
[10] Raport (2014) (Report), Agro Intelligence SISA.
[11] Comitetul Economic şi Social European (CESE) (2015) (European Economic and Social Committee EESC).
[12] Proagro Capital – Analize economico-financiare (Economic and financial analysis.).
[13] Mancia M.S. (2015), Geopolitică şi planificare teritorială în bazinul Crişului Repede (Geopolitical and territorial planning in the Crisul Repede basin), Ed. Universităţii din Oradea.

Geospatial Data Acquisitions Using 3D Laser Scanning Technology in the Context of Monitoring Mines

Moscovici A.M.[1], Brebu F.M.[2], Bala A.C.[3]

[1,2,3] *Politehnica University Timisoara, Department of Overland Communication Ways, Foundations and Cadastral Survey, Traian Lalescu no.2, Timisoara, Romania*
E-mails: moscovicianca@gmail.com, floarea.brebu@upt.ro, alina.bala@upt.ro

Abstract

The data collection in geodesy have improved rapidly over recent years, smaller, more precise and the, on the other hand, they are able to collect, manage and process a large number of data within very short time.

In this sense a new concept of geospatial data acquisition has revolutionized rapid method of determining the spatial position of objects, which is based on 3D laser scanning. The advantage of a real prognosis determination is the fact that in time the investments in these types of areas can be made on time and with maximum efficiency. Practice has demonstrated that by using 3D modelling and the analysis of the movements of the areas located in mining areas, the experts in the field have better tools to perform a good prognosis in time and a good monitoring in time of the techniques used for land protection and for the protection of the existing constructions in the affected areas.

Acquisitions geospatial data, considered among the most performant methods revolutionized rapid method for determining the spatial position of objects, which is based on the 3D laser scanning. Principal advantage is determined in real time positioning and investment in these types of areas they can be made in time and with maximum efficiency. Using this method and practice, the conclusions drawn are that by using 3D modelling and analysis movements areas located in mining areas, specialists in the field have better tools to make a good prognosis whereas a good time monitoring techniques used land protection and to protect existing buildings in the affected areas.

The purpose of this paper is to highlight the importance of terrestrial laser scanning for displacements and deformations monitoring, that may occur in +210m horizon from room 22 to room 24 inclusive. The 3D scanning result in Ocnele Mari of Ramnicu Valcea County, it will contain relevant information about deformations that may occur at this horizon, if they are homogeneous or if there is a local buckling.

Keywords: 3D laser scanning, movements, deformations, mine, GIS.

1 Introduction

During the last ten years the possibilities for data acquisition in geodesy have been rapidly improved. The devices become cheaper, smaller and more accurate and, on the other hand, they are capable of gathering a large number of data within a very short time interval [1].

3D laser scanning is a quick method for measuring with great detail and accuracy. Laser scanning is one modern method which establishes a point cloud, which with millimetre precision provides a full photographic colour reproduction in 3D of the physical conditions. Scanning provides a flexible option for further modelling and visualization [2]. Whether you participate in designing a special work or the change to a project of great complexity, achieving a historic building facade, or you need reliable measurements for this type, the laser scanning works can be considered a viable solution. Laser scanning can be used for projects large and small, from laser scanning bridge to unite laser scanning of a part of a bas-relief. Here are some examples of the types of tasks, resolve laser scanning:

- Measuring facades and situations plans – interior and exterior
- Building surveying and technical installations
- Measurement of piping, tanks etc.
- Surveying for photorealistic renderings and animations
- Monitoring and deformation measuring
- Volume Measurements and calculations

Our many years of surveying experience coupled with the most advanced equipment, makes it possible to fulfil the customers wishes even under the most demanding conditions and the toughest requirements.

All mining activity produces, because of its specificity, multiple and various negative effects on the environment, exemplified by [3]:

- the landscape changes in relief, with degradation of the landscape and removals of households and the industrial objective in the exploitation areas;
- occupation of large areas of land for mining activities, storage of useful minerals substances and access routes, etc., surfaces which become totally unusable for other purposes, for a long period of time;
- land degradation, through the vertical and horizontal displacements of surface and waste dumps, challenge of serious accidents;
- contamination of flowing waters from the surface and ground waters;
- negative influences on the atmosphere, flora and fauna in the area;
- chemical pollution of the soil, which can affect its fertility properties for many years;
- noise, vibration and radiation widespread in the environment, with a strong adverse action.

These actions give rise to extremely complex phenomena and serious changes in morphology of the land due to diving and landslides occurred in the area.

In this context, the paper proposes implementation of new measurement technologies by using 3D laser scanning in monitoring these phenomena. The study case refers to the horizon of +210m situated in the mining basin Ocnele Mari of Ramnicu Valcea County.

2 Use of 3D laser scanner to monitor mine deformations

The salt deposit to Ocnele Mari is exploited to 1959 (Fig. 1) and till now through two exploitation methods, wet by dissolution kinetics (the probes) and by dry combustion.

Fig. 1 Salt deposit to Ocnele Mari in 1959

The mining works takes place in the two horizons - the horizon +226 m and the horizon +210 m and the method of operation being by small rooms and the square plateau, the current method of mining is the most modern in the world. The salt deposit from "Ocnele-Mari" is shaped like a lens elongated direction EV, measuring that effect cca.7,5 km and the NS approximatively 3,5 km in presenting a lifting axial on Ocniţei area Fig. 1, with inclinations to the N.

The salt from the deposit presents a microgranular crystal structure well developed blackish gray or white, depending on the impurities terigene intake. White salt benches of the salt alternate with darker. In the massif is distinguished the microtectonics, this phenomenon, which demonstrates the existence of small-scale tectonic disturbances that have occurred within the deposit.

The purpose of monitoring using 3D laser scanning technology in the salt mine, is to highlight the deformations that may occur over the horizon + 210m from room 22 to room 24 inclusive.

The scans at salt mine Ocnele Mari were performed using Trimble TX5 laser scanning system, manufactured by Trimble.

The 3D terrestrial laser scan results will contain relevant information where the deformations that may occur in this horizon are homogeneous or if there is a local the buckling.

3 Data analysis results after monitoring

The quality aspect of surveying using laser scanners needs careful consideration throughout the measurement and processing process. Quality starts with a full understanding of project specification. This understanding allows the correct choice of scanner, correct scan resolution, appropriate registration method and so on [4].

To study the future deformations that may occur within the 3 rooms of +210m horizon based on measurements taken can use horizontal and transverse sections, which are obtained directly from three-dimensional model when working in Trimble RealWorks software data obtained from scanning these rooms. After monitoring using 3D laser scanning in August and December 2014 were observed deformations of the ceiling of + 210m horizon in the 3 rooms (Fig. 2 and Fig. 3).

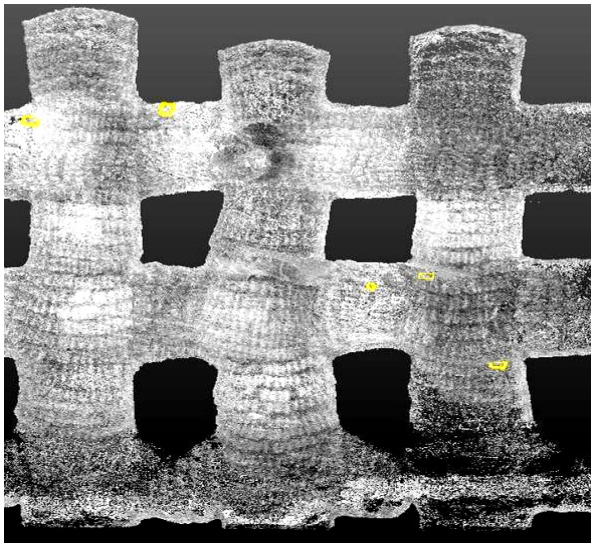

Fig. 2 Highlighting the ceiling deformations in the 3 rooms through yellow rectangles, resulting from point cloud

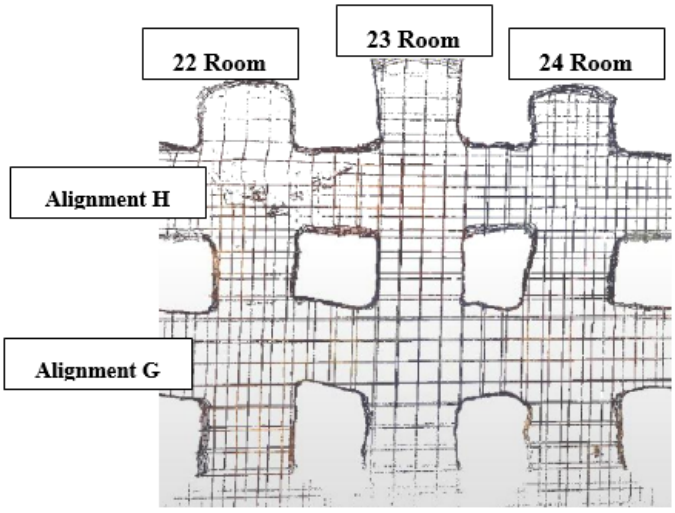

Fig. 3 Upper view of the sections point cloud

According to research conducted by tracking the deformations on alignment G and the H during the 6-month until December the movements consisted of the roof as it follows:

✓ in the 22 room was from 3.6 cm to 11 cm on 177,1cm length (Fig. 4);

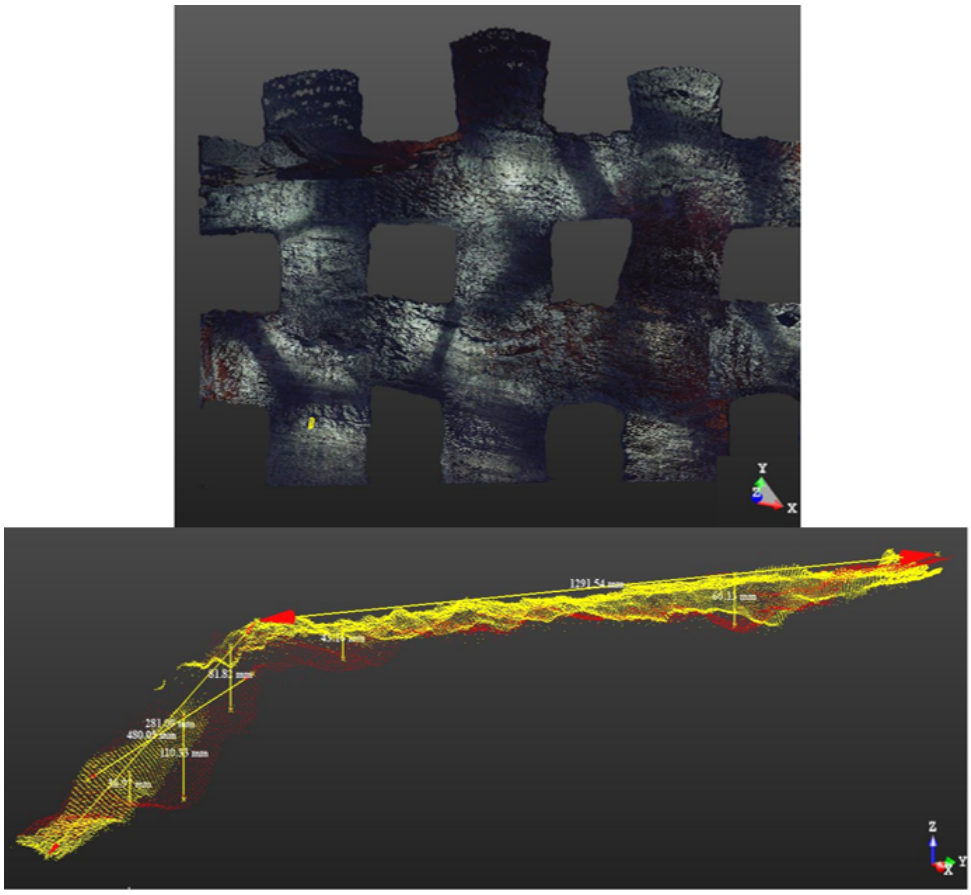

Fig. 4 Evaluation ceiling deformations of 22 room on G alignment

✓ movements in the 23 room have been from 7.7 cm to 14.10 cm (Fig. 5, Fig. 6);

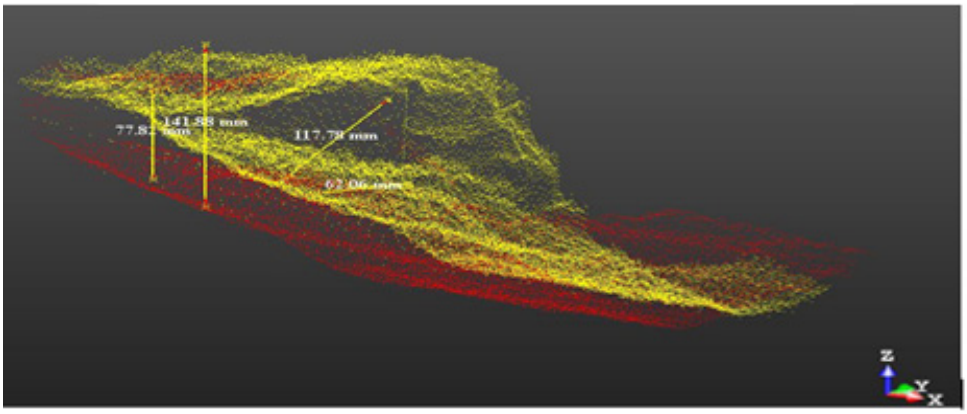

Fig. 5 Evaluation ceiling displacements from 23 room on the H alignment

✓ ceiling in 24 room not suffered deformations;

Fig. 6 Highlighting of the ceiling detaching in the rooms 22 to 24, G and H alignments

Data is captured down drift as well as from the advancing face. The survey process is conducted very quickly so there is no impact on the mining cycle. Using laser scanning for geotechnical quality control underground brings significant safety benefits, including reduced time in the drift, recording shotcrete thickness without coring and avoiding working at heights (Fig. 7). More accurate data is acquired and quickly validated. Analysing the 3D models away from active mining allows users to carefully review the information for mapping and design. [5].

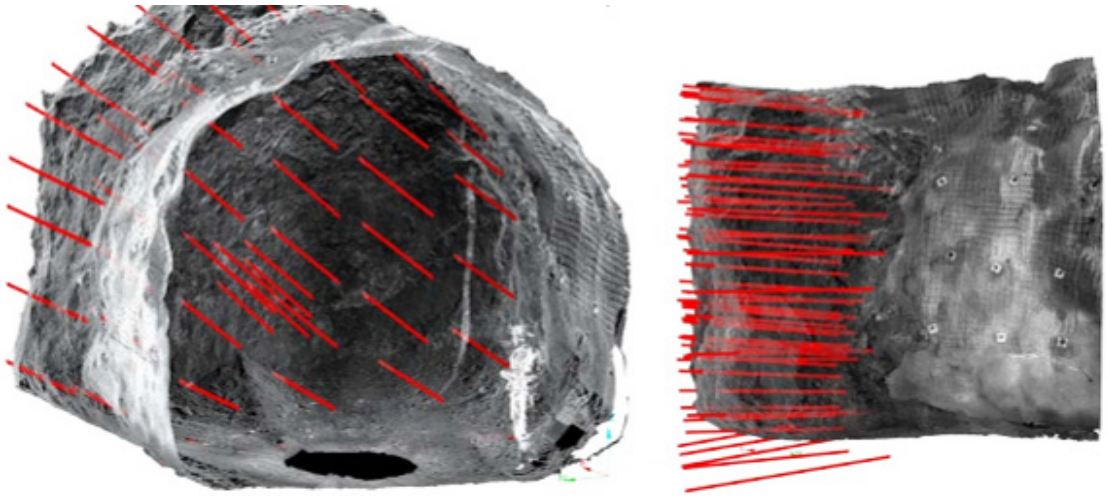

Fig. 7 Analysing the 3D models [4]

In order to carry out studies on land, to properly apply solutions and measures that prevent soil erosion, land reclamation works cooperate with a number of other disciplines such as: soil science, geology, topography, cadastre and GIS as a tool of analysis [6]. The results of GIS spatial analysis and queries are not only incomparably more effectively in the decision-making, production, inventory information process - where they already have demonstrated their capabilities, but they radically transform the perception upon surrounding reality: better and quicker understanding of the conditions and phenomena that are studied or are act upon [7].

Performing measurements in different moments for determining the quantity characteristics of one observation unit or of an entire area, the data which we obtain in this way, form a time series or a dynamic series.

This data is from the perspective of important statistics, both through values and through the order of appearance of these values [8].

4 Conclusion

3D mining scanning changes the engineering process. Engineers continue to re-think the way in which they design and measure: thus, scanner use will extend to other fields as well. However, without a texture or other information, a static image of a point cloud can be difficult to interpret, by interacting and changing the point of view, a user can understand the nature of the structure represented through points that change depending on the observation point [9].

Laser scanning technology represents a first reference for 3D modelling and data analysis, being able to be used for studies on many important directions and in various fields, such as: geophysics, mining, hydrology, environmental protection, constructions, archaeology, meteorology, etc.

References

[1] Vasiü, D., Ninkov, T., Bulatoviü, V., Sušiü, Z. and Markoviü, M.: Terrain Mapping by Applying Unmanned Aerial Vehicle and Lidar System for the Purpose of Designing in Serbia, INGEO 2014 – 6th International Conference on Engineering Surveying Prague, Czech Republic, 2014, pp.217-222;
[2] https://www.lifa.dk/3d-laser-scanning;
[3] D. FODOR: Influence of mining industry on the environment, Bulletin AGIR. 3, pp.199, (2006);
[4] Clara Beatrice VÎLCEANU, Ioan Sorin HERBAN, Carmen GRECEA, Creating 3D Models Of Heritage Objects Using Photogrammetric Image Processing, AIP Conference Proceedings 1558, 1599 (2013); pp. 1599-1602;
[5] http://www.maptek.com/pdf/i-site/case_studies/Maptek_I-Site_groundsupport_casestudy.pdf;
[6] L. Dimen, T. Borşan, C.D. Brătan - Using GIS Technology for Soil Erosion Analysis. A case study: The hydrographical Basin of "Buturoiului Valley", Jidvei, Alba County, Journal of Environmental Protection and Ecology ISSN 1311-5065, Vol. 14, 2013;
[7] Vilceanu, C. B., Herban S., Alionescu A., Using Open Source GIS for the Management of the Administrative Territorial Unit, Conference Proceedings "Modern Technologies for the 3rd Millennium", pp.73-78, 2016;
[8] Nacu V., Stoian I., Vele D., Arseni M., IT System for Monitoring Climatic Changes, Conference Proceedings "Modern Technologies for the 3rd Millennium", pp.13-16, 2016;
[9] Cuzic O.Ş. , Man T.E., Armas A., Introduction Into 3D Laser Scanning, Conference Proceedings "Modern Technologies for the 3rd Millennium", pp.13-16, 2016.

Environmental Policy in Jiu Valley Coal Mining

Munteanu R.[1], Tiuzbaian I.N.[2]

[1] *University of Petrosani (ROMANIA)*
[2] *University of Petrosani (ROMANIA)*
E-mails: rares73@yahoo.de, tiuzbaian@gmail.com

Abstract

Even if mining is on the wane, the main issues related to the environment are still up to date. They concern the soil pollution due to the sterile heaps generated by the coal exploitation and the waste waters that must be treated. Even if a large part of the areas occupied by the coal industry were rendered to the local authorities, they must be kept under control. Another major concern is the treatment of the waste waters generated by the mines that are still active.

Keywords: sterile heaps, mine waters, treatment, improving the quality of the environment.

1 Introduction

This paper refers to the mines that are part of the Energy Complex Hunedoara (Mines: Lonea, Livezeni, Vulcan and Lupeni and the treatment plant belonging to PRESTSERV Petrosani). The activity causes pollution to the water, soil, air and also produces noises and vibrations. In order to mitigate the negative effect produced by mining, some actions have been taken and are to be presented in this paper.

2 The situation of the environment and measures taken

2.1 Water

The categories of waters in the mining activity are:
- waste water (industrial)
- sewage water (household)
- water for firefighting

For the water treatment, the mines Lonea and Vulcan have SBR mechanical-biological treatment plants.

The mine in Lupeni has an intermediate plant that collects the sewage water and overflows it into the town sewage system.

The treatment of the mine waters coming from the mines Lonea, Vulcan and Lupeni is done in treatment plants. The Livezeni mine overflows the mine waters into the town sewage system.

The industrial waste waters resulted after the treatment process are directed to the settling tanks and are re-used after the settling process is finished.

In order to improve the activity of the settling ponds belonging to PRESTSERV the evacuation and valorisation of the slurry were conceded to LCC Resita Company since 2009.

The extraction of the coal slurry from both ponds is done simultaneously, but by different means, i.e.: using an excavator (down to 4.5-5 m depth) from the compartment 1A and using PNEUMA pumps installed on a barge from the compartment 1B – settling pond no. 1 and using an excavator – settling pond no. 2 (Fig. 1). Provided that the supply is continuous, the exploitation can take place normally up to a temperature of -5^0 C.
The slurry extracted form the 1B compartment of the settling pond no. 1 is overflowed either through a PVC pipe Dn= 325 mm, L= 180 m into the homogenisation and attrition (mixing) basin or directly into the basin for decreasing the kinetic energy through the metal pipes A, Dn= 325 mm and L= 250 m.

In order to obtain a dilution of 1.03-1.18 the water can be pumped from the compartment 1B using the barge pump. The material that is extracted by excavator from the pond no. 1 (compartment 1A) and pond no. 2 is transported by truck to the mixing basin having a volume of 316 m^3. The mixing basin is called "The new pond" and in this pond the attrition is realised by adding water until a dilution of 3mc/t is obtained.

The mixture from the mixing pond is pumped through a metal pipe Dn=250mm, L=40m into the basin for decreasing the kinetic energy and diluting the slurry (liquid:solid=1:3) in order to disaggregate the coal from the clay.

Fig. 1 Settling pond at Coroiesti treatment plant [1]

The slurry gets into two big hydrocyclons (D=700mm) – Fig. 2 – where the first stage of separation of particles takes place.

Fig. 2 Hydrocyclons [1]

During this stage the coal is recovered from the waste. The coal is evacuated out of the hydrocyclons on the vibrating screen and the clay and most of the water are evacuated into the tanks T1-T3 and then into the buffer tank having a volume V=47mc.

2.2 *Soil protection*

The waste resulted after the coal exploitation and preparation is dumped on sterile heaps (Fig. 3). Studies and technical projects are realised for these heaps.

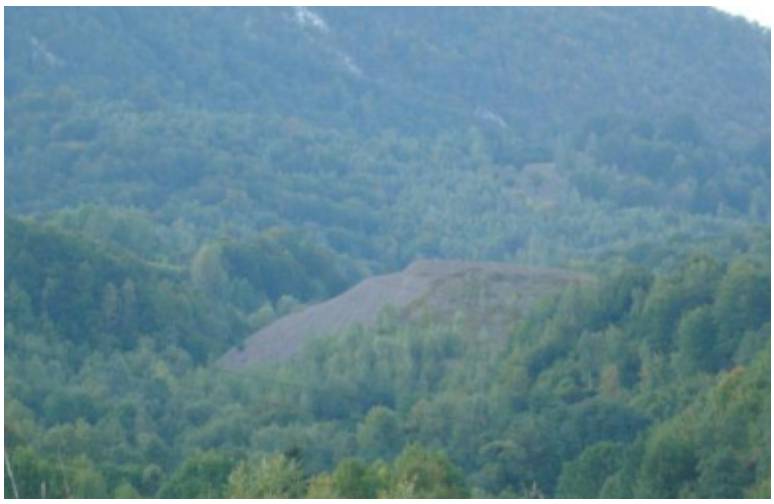

Fig. 3 Sterile heap/waste dump at Barbateni [1]

In order to monitor the waste dumps, the following actions are done:
- monthly record of the quantities of dumped waste
- daily visual inspections by the transport chief-engineer
- daily visual inspections by the environment engineer
- surveys for checking the heap geometry
- supplementary measurements in case of severe weather phenomena
- based on a yearly plan, the laboratory makes analysis of the waste from the heaps.

In order to prevent the soil pollution, the fuel, wood, storage and temporary waste storage are organised on concrete platforms. The sawdust and ashes are stored on concrete, covered platforms.

2.3 *Air protection; protection against noise and vibrations*

The air pollution sources are:
- stationary sources:
  - ventilation stations
  - heating stations
  - degassing stations
- diffuse sources:
  - loading-unloading of coal and waste
  - auto transportation
  - handling the substances from the fuel storage
  - operations for selecting the coal
  - welding
  - wood processing
  - forging

For the premises of the mines Vulcan and Lupeni, the heating is obtained by ecological heating stations that use the methane recovered from underground.

For loading-unloading and selecting the coal there are some moistening procedures that reduce the quantity of dust released into the atmosphere. The quantities of CH_4, CO and CO_2 are constantly monitored in order to control the underground conditions.

The main noise and vibration sources are the compressors and the ventilation stations. In order to reduce the noise and vibrations, new equipments replaced the old ones. The laboratory belonging to the Prestserv Petrosani is constantly monitoring the situation. The measured values respect the required parameters.

As sources for noise and vibrations coming from the preparation plant we mention:

- technological activities (hydrocyclonage, screeners, crushers, elevators bands, turbochargers, pumps)
- internal railways
- handling the materials and equipments

The measured values do not exceed the maximum allowed value of 65 dB.

In order to remove or decrease the pollution caused by the coal preparation, the preparation plant has also specific filter batteries (Fig. 4):

Fig. 4 Filter battery [1]

2.4. Preventive actions

In order to improve the quality of the environment and reduce the pollution, the Energy Company Hunedoara plans to take several actions:

1. maintenance of the surface rain draining channels and underground draining channels
2. selective waste collection and storage
3. specific works to provide stability and reduce the phenomenon of erosion for the waste dumps
4. monitoring the phenomena of subsidence
5. maintenance of the waste water treatment stations
6. maintenance of the sewage water treatment stations
7. maintenance of the rainwater sewerage network

3 Conclusions

Although mining is a polluting industry, it is necessary, because there can be no economy without mineral resources. Nevertheless, the negative effects of the coal extraction and preparation can be reduced by specific measures. The Energy Company Hunedoara (Complexul Energetic Hunedoara) took several actions and made investments in order to decrease the polluting effect on the water, soil and air. Modern equipments allow to recover the useful substances from the primary waste, as well as to release much cleaner water into the Jiu River. Also, the soil is less damaged due to a better control and maintenance of the waste dumps. Dust and noise harm mainly the air, but specific procedures and new equipments improved the situation. Of course, more actions must be taken, more investments are done and new, cleaner technologies be developed. These are concerns of the Company for the future.

References

[1] www.cenhd.ro

[2] *** (2016), Informare semestrul I 2016 pentru activitatea minieră de la Complexul Energetic Hunedoara (Report on the 1st semester of the year 2016 regarding the mining activity of the Energy Complex Hunedoara).

The Processing Workflow Needed in Order to Obtain the Main Photogrammetric Products Used in Cadastre and Topography

Nache F.[1], Stănescu R.A.[2], Păunescu C.[3]

[1] *PhD. Student, Eng., University of Bucharest, Faculty of Geology and Geophysics, Romania*
[2] *Eng., S.C. Cornel & Cornel TOPOEXIM S.R.L., Bucharest, Romania*
[3] *Prof.PhD., Eng., University of Bucharest, Faculty of Geology and Geophysics, Romania*
E-mails: nacheflorin@yahoo.ro, roxana.augustina.stanescu@gmail.com, cornelpaun@gmail.com

Abstract

This study comprises the benefits of obtaining photogrammetric products like the orthophotomosaic using images acquired with a digital non-metric camera mounted on a multirotor type of UAV (Unmaned Aerial Vehicle) or the DTM (Digital Terrain Model) obtained from the correlated point cloud. The chosen interest area is the build-up area of Santimbru village, Alba County. The importance of the orthophotomap and DTM is highlighted throughout the study, them being utilized for the realization of topographic profiles and breaklines, volume calculation, contour lines generation, extensive studies regarding the flooding risks and the optimization of general cadastral works.

Keywords: U.A.V. (Unmaned Aerial Vehicle), orthophotomosaic, Digital Terrain Model (DTM), Digital Surface Model (DSM), correlated point cloud.

1 Introduction

The orthophotoimage (*orthophotomap)* represents an aerial image or a set of aerial images, which are geometrically and radiometrically corrected, creating a representation of the terrain at a standardized scale, thus allowing the measurement of distances. The geometrical correction consists of images orthorectification, which is a process of transforming the images from a central projection into an orthogonal one. By doing so, the distorting effects caused by the motion sensor and the ones provoked by the terrain reliefs are eliminated. The radiometric corrections are necessary for straightening out the shades or the colour differences in the orthoimages, the result being a better quality and a uniformity of the shades in the group of images. The radiometric corrections are necessary especially when the images are taken in different conditions [5]. In the case of images gathered with UAV's the spatial error of orthophotos becomes more significant [3]. The solution was proposed by Amhar et al. (1998) [1] and consists in using the DSM (Digital Surface Model) instead of the DTM for generating the orthophoto.

Digital Terrain Model (DTM) is a numeric representation of the terrain surface. If what covers the terrain (constructions, vegetation, etc.) is also taken into consideration, then it is referred to as Digital Surface Model (DSM) [5].

The use of unmanned aerial systems, to collect the necessary data for the photogrammetric products, implies a reduced cost, but a longer time for collecting the data itself.

Working area is represented by the build-up area of Sântimbru, Alba County, which has a surface of 153 hectares and a moderate relief fragmentation.

2 Methodology

To obtain the orthophotomosaic and the digital terrain model it was used:

- a UAV multi-rotor system with triaxial gimbal and 18 minutes flight time;

- a Sony A7R mirrorless camera, with 50 mm focal length objective;

- ground control station which consists of: laptop with Mission Planner software, telemetry, radiocommand, OSD (On Screen Dislay) monitor and glasses;

- 2 Leica GX08 GNSS Receivers;
- One photogrammetric station.

2.1 Data acquisition

The first step has been done in the office, to establish the ground control points and the flight plan. The elements discussed will be adapted accordingly with the conditions found at the location.

The ground control points marking in the field was done with waterproof paint where the area allowed it (example: cemented platforms, asphalted roads) or plastic marks. The landmarks were distributed at a maximum distance of 300m one of each other on the entire working area – see Fig. 1.

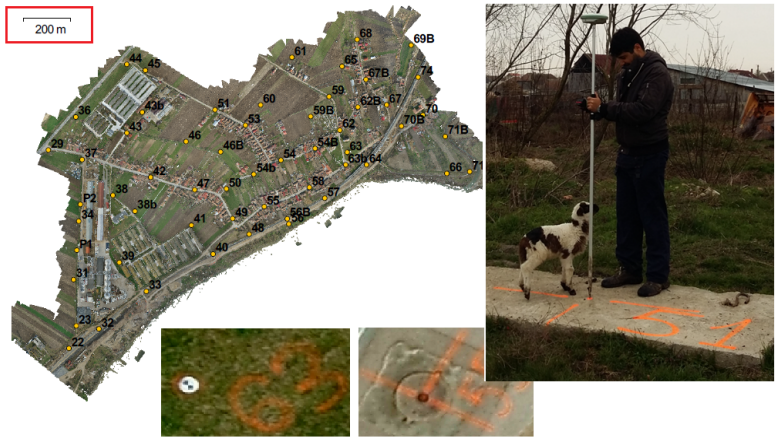

Fig. 1 Placing the Ground Control Points (GCP) on ground, materializing and determining their position

To determine the space position of the landmarks, 2 GNSS receivers were used. The measurements were done in RTK mode.

Planning the flight mission was done with the Mission Planner software – see Fig. 2, establishing the perimeter of the flight area by uploading a file with the limits of the build-up area and after, setting the parameters referring to:

- physical dimension of the sensor utilized in data acquisition (35,9 mm / 24 mm);
- the number of pixels (7360 pix / 4912 pix);
- focal lenght (50 mm);
- flight height (150 m).

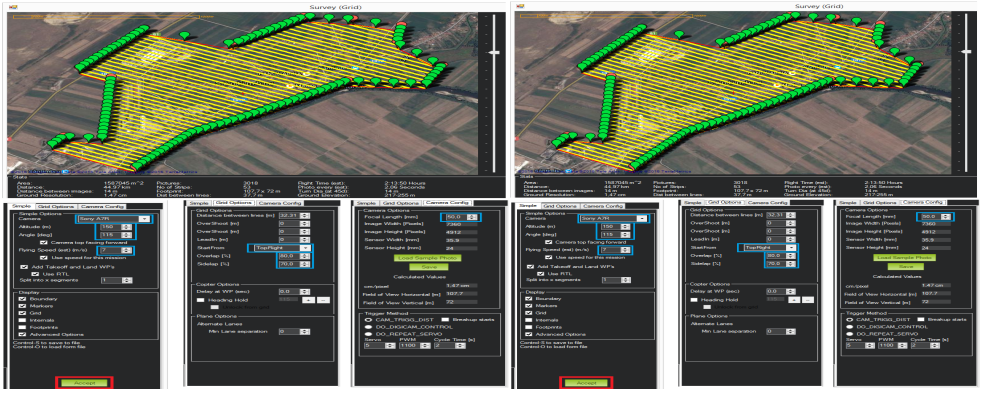

Fig. 2 Aerial photographic' mission plan

These 4 parameters are offering an estimation regarding the pixel dimension on terrain level (1, 47 cm) and also the land coverage of an image (107, 7 m / 72 m).

- overlap (80%) and sidelap (70%);
- the orientation of flight paths (115^{o});
- flight speed (7 m/s);
- mission's starting point (upper right hand side).

Throughout the aerial photographic mission, monitoring the flights is being done through the OSD screen or the OSD glasses, especially observing the retrieved image quality and the exposure time, battery's

voltage and amperage, following the flight paths, the distance from the take off point, flight height and vibration level.

2.2 Data processing

The images acquired in the aerial photographic mission (3018) will be processed with Agisoft PhotoScan. The images will be uploaded in the program and the reference system will be established (Coordinates System S-42 Romania, Stereographic Projection 1970).

After discarding the wrong images (tilted, blurred, overexposed or underexposed) the rest will be aligned, thus obtaining the parameters for the interior orientation, the relative position of the exposure points (camera position) and the tie point cloud.

Prior to the images alignment, the alignment parameters will be set. Higher accuracy settings help to obtain more accurate camera position estimates and the software works with the images of the original size, medium setting causes image downscaling by factor of 4, low by 16 and lowest by 64. If there is a good determination of the camera positions it is recommended to use the reference option for pair preselection, using generic preselection the overlapping pairs of photos are selected by matching photos using lower accuracy setting first and after the selected accuracy [2].

The next step, the 57 Ground Control Points (GCP) will be imported and each and one of them will be marked in the correspondent images. Accordingly, the control points and the check points will be established. This way, it can be established the image model's indirect georeference and estimated the accuracy of the final model – see Table 1.

Table 1 Check points' accuracy

Label	XY error [m]	Z error [m]	Error [m]	Projections	Error [pix]
P1	0.022	0.038	0.028	14	0.15
P2	0.007	0.022	0.014	9	0.18
63b	0.014	-0.020	0.017	13	0.29
56B	0.014	-0.027	0.030	11	0.23
Total	0.014	0.027	0.030		0.21

Establishing the position of the camera position with GNSS/IMU measurements it is not a precise one (±5 m), so the sensors' integrated orientation will not be realized. Instead, the indirect georeference will be done, so the aerotriangulation is made for the entire block of images.

Having the link between the image model and terrain, through the control points, the aerotriangulation can be made, thus obtaining the parameters for the exterior orientation (Table 1).

Afterwards the point cloud will be generated through automatic correlation of images, process that allows automatic correspondent points identification which are found in the overlapping area of two or more images taken from different angles and the assignment of spatial coordinates for every pixel or group of pixels – see Fig. 3.

The cases, in which the process of automatic correlation can lead to poor quality results, can be the following:

- Different perspective projections. The differences between the two images are greater according to the angle of retrieving and the roughness of the terrain (especially in mountain areas with abrupt slopes).
- Different reflectance. The radiation intensity reflected by the elements in the terrain varies in accordance to its incidence angle. Therefore, the tones of the same area can be different, so the automatic correlation algorithm can wrongly identify the points in the area. One of the causes is the light conditions which appear especially when the images are retrieved in different time spasm or different days.
- Radiometrically homogeneous areas. These are areas in which the image contrast is very low, for example – areas covered in woods, snow, lakes, etc.
- Signal/noise ratio very low. Some correlation methods allow correspondent points identification through image contrast. A low signal/noise ratio reduces the similarity between two images [4].

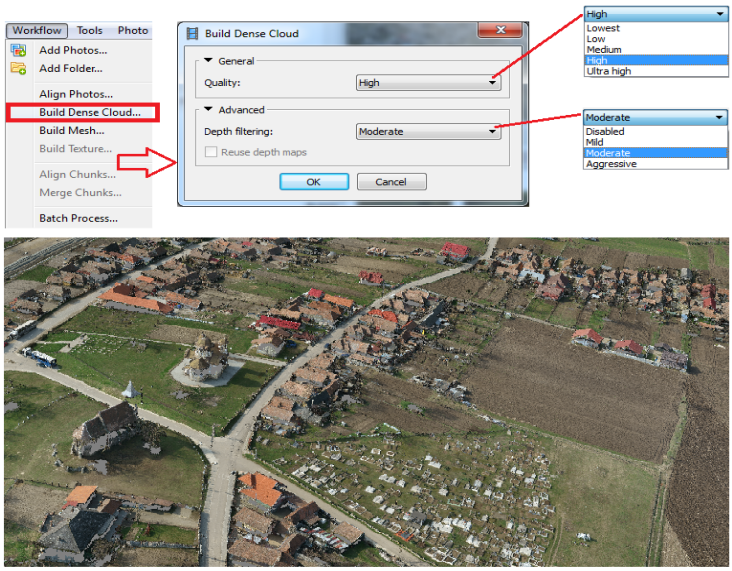

Fig. 3 Correlated point cloud

The parameters which need to be defined in the process of points cloud generation is the image compression- *Quality* → *Ultra high*, the data will be processed keeping the original image size; option *High* leads to image data processing with a reduced size factor of 4 from the initial size; *Medium* with 16, *Low* with 64 and *Lowest* with 256. For the areas with complex geometry and a significant number of details it is recommended to use the option *Mild* for *Depth Filtering* parameter, contrary it will be chosen *Aggressive* [2].

The resulting points cloud will have a 375 points on meter square density, this being the basis for the Digital Surface Model (DSM) – see Fig. 4, over which the image model will be draped, thus reducing the errors caused by the relief variation.

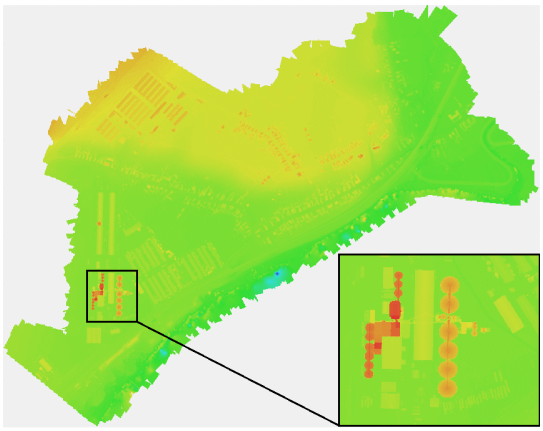

Fig. 4 Digital Surface Model (DSM)

Because of the errors from the Digital Surface Model (DSM) there can be differences of few pixels when the ortho image is inlayed. These errors can be diminished through modification of the seam lines, so the error can be spread on a bigger area- for example, the seam line to cut sidelong the roads and not transversal.

After editing the seam lines the radiometric correction is made through radiometrically correcting the entire block of images and then the orthophotomap (orthophotoimage) will be generated – see Fig. 5.

Fig. 5 Orthophotomap

To obtain the Digital Terrain Model (DTM), the unsupervised (automatic) classification will be done and then the supervised (manual) one for the correlated point cloud. This is to settle down the points which are part of the terrain class necessary for DTM generation – see Fig. 6.

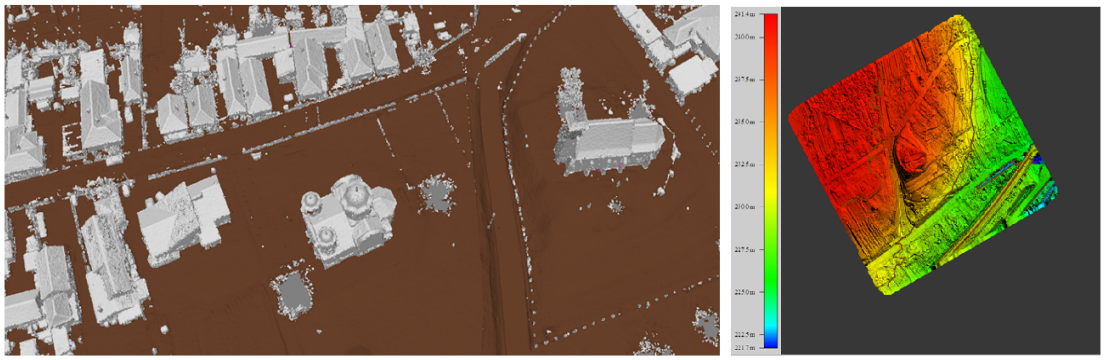

Fig. 6 Classified point cloud (left) and Digital Terrain Model (right)

3 Results and discussions

3.1 Verifying the orthophotomap and the Digital Terrain Model (DTM)

The quality verification of the orthophoto map consists of radiometric, geometric and accuracy verification.

Following visual defects are to be eliminated through radiometric and geometric verification:

- Geometrical and tone differences from the vicinity of the seam lines;
- Tone differences caused by the strong solar radiation reflexion or shadowing;
- Distorsions of some planimetrical elements, situated at a higher elevation than the terrain [4].

Accuracy verification of the orthophotomap is based on check points, different than control points used for exterior orientation of the images. To verify the accuracy it can be utilised another orthophoto map and/or terrain measurements done to determine the planimetric position of the entities that can be identified in the orthophotomap.

To test the Digital Terrain Model (DTM) accuracy the check points can be used, another digital terrain model verified and approved and/or points measured for which the altitude was also determined.

3.2 Utilizing the obtained products in topography and cadaster

Based on the obtained product it can be realised:

- Digitalisation, using the orthophotomap, of cadastral entities such as the property limit, parcel limit, etc;
- Creating a GIS application for optimizing the cadastre field work;

- Determining the construction print on ground by using the points cloud and the orthophoto map, optimum solution especially if the image data retrieving was realised also oblique and not only nadiral – see Fig. 7;
- Following the comportment in time (example: landslide study);
- Break lines obtained based on stereoscopic model;
- Contour level generation;
- Topographic profiles of the terrain;
- Determination of the volume, surface, slope, etc.

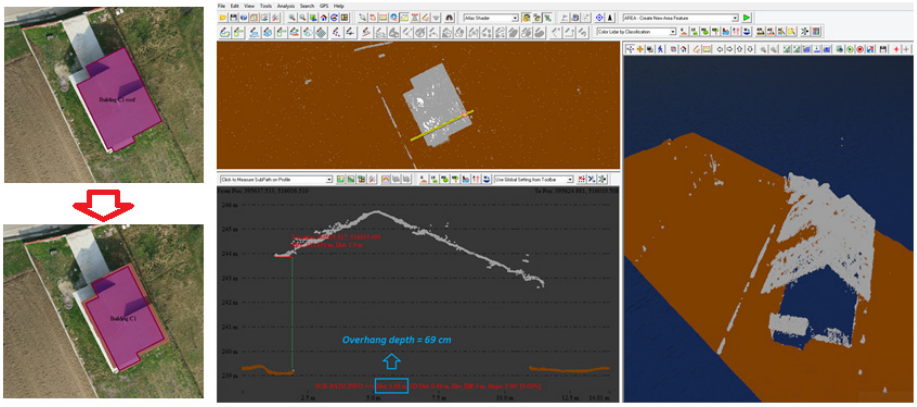

Fig. 7 Determining the construction print on ground

4 Conclusions

➢ The use of UAV in data acquisition implies a reduced cost but a longer time for collecting the data itself.

➢ The use of UAV systems in achieving photogrammetric products gives accurate results that can be successfully used especially for a moderate relief fragmentation.

➢ UAV systems are easily controlled, especially the multirotor type. The UAVs have incorporated various functions that facilitate the flight: possibility of programming the aerial photography's route, automatic maintenance of flight altitude, the return to the launching point if the radio connections are interrupted or other technical problems occur during the flight.

➢ The risks of using UAV systems are not to be ignored. It is not recommended to fly the UAV system over populated areas, because the technical problems that can lead to systems collapse can be imminent.

➢ On the other hand, specialised programs for data processing can be purchased at a low price and most of them have a high degree of automation. Also, updating ortophotomaps can be a solution when the time is not sufficient for elaborating new plans, through other methods that can take a longer time and can be more difficult.

References

[1] Amhar F., Jansa J., Ries C. (1998). The Generation of the TrueOrthophotos Using a 3D Building Model in Conjunction with a Conventional DTM. International Archives of Photogrammetry, Remote Sensing and Spatial Information Sciences, Vol. 32(4), pp.16-22.
[2] Agisoft PhotoScan User Manual, Professional Edition, Version 1.1.
[3] Eisenbeiß, H. (2009). UAV Photogrammetry, Zurich, Switzerland.
[4] Vorovencii I. (2010). *Fotogrammetrie (Photogrammetry)*, Editura Matrix Rom, Bucureşti.
[5] Zăvoianu F. (1999). *Fotogrammetria (Photogrammetry)*, Editura Tehnică, Bucureşti.

Topographic Monitoring of Landmarks Placed In the Constructions' Foundations within the Area of Influence of a Closed Salt Mine

Naş S.[1], Gâlgău R.[2], Bondrea M.[3], Poruţiu A.[4]

[1, 2, 3] Technical University of Cluj-Napoca, Faculty of Civil Engineering. 15 C Daicoviciu Street, 400020, Cluj-Napoca (ROMANIA)
[4] University of Agricultural Sciences and Veterinary Medicine Cluj-Napoca, Faculty of Horticulture, 3-5 Mănăştur Street, 400372, Cluj-Napoca (ROMANIA)
E-mail: farcasraluca19@yahoo.com

Abstract

Based on the visual and photographic findings upon constructions and land and also based on topographical measurements made on topographic landmarks placed in the field or on constructions it was sought to find a technical explanation of phenomena manifested in buildings (cracks, deterioration, displacements, etc.) and also to assess the degree of danger regarding the safety of buildings and the land in the area surrounding them.

The purpose of time tracking of land and constructions from Victoria mine area is to obtain information in order to ensure the stability of both land and buildings in the area.

Keywords: instability, monitoring, landmark, salt mining, risk reduction.

1 Introduction

The city of Slănic Prahova is located in the center of Romania, Prahova County, 45 km north of Ploieşti, situated at an altitude of 413 m (Fig. 1). This settlement became known primarily due to salt deposit exploited for over three centuries [4].

Fig. 1. Geographical location of the study site

Topographic monitoring of lands and buildings in the area of closed mines is made in order to prevent and detect possible problems that may occur after completion of closure and rehabilitation carried out in the area and can impact the environment and the population [4].

To ensure efficiency and security required in the process of exploitation of the deposits, an imperative requirement is knowledge and insurance regarding the stability of the whole underground excavation and the deposit surface in the influence area, which requires knowledge of the intensity of processes of deformation and displacement of surrounding rock, the character of redistribution and modification of the tensions and also knowledge of rheological properties of rocks (creep, relaxation etc.), properties that are changing with increasing burdens and with the passage of time [4]. The stability can be done using GNSS technology [3] and by using a proper time series analysis we can obtain reliable results [6], [7].

The Victoria mine area of influence is on a slope mostly without forests, having western exposure.

The current configuration of the slope can be considered as the result of a long term action of natural and manmade factors, which through erosion, geodynamic phenomena and human activity, manifested by the activity of extracting salt underground, led to disturbance of the equilibrium state and conferring the current morphologies, manifested by the appearance of fissures, cracks and bumps on land surface.

Regarding weather instability phenomena manifested in Victoria Mine area, it is considered that they will evolve as long as are maintained natural and anthropogenic factors of active geodynamic processes, namely:

- Unfavorable geomorphology conditions;
- Lithologic nature of the roof layers (predominantly clay with low shear fracture strength);
- Lack of appropriate protective vegetation;
- Presence of underground mine voids.

In the area of influence of mine Victoria, are monitored visually and photographically a number of 18 estates:

- 14 buildings are provided with a number of 38 operating landmarks on which were executed topographic readings shown on the records of buildings;
- 2 buildings remained with the landmarks covered due to maintenance after which, the owners refusing their replanting;
- 5 houses were tracked only visually, fitting landmarks being considered impractical because of the construction system or the seniority of the building construction.

Work on monitoring station at Victoria mine, Slănic Prahova salt mine, aims to extend, monitor, conduct land checks necessary in order to monitor and analyze development of lands and constructions by conducting quarterly topographic measurements on:

- ground terminals;
- topographic landmarks;
- topographic marks placed in the foundations of buildings.

Within monitoring projects, monitoring the behavior in time of the constructions is run throughout the entire life period of the assets, starting from the moment of execution and representing a collecting activity, interpreting the information derived from observation activity and measurements conducted to determine the position changes occurring over time, so as to ensure exploitation stability and safety [1].

2 Materials and methods

When travelling to the research spot, observations were conducted on the characteristics of existing cracks and general condition of the house, state of the pavements and the land immediately around the house. Visual observations of the land followed its deformation, such as diving, swelling, landslides, cracks, etc.

The vertical displacement of the land under the house was determined based on topographical readings made on topographic landmarks placed on the resistance structure by indicating for each item the following:

- Lifting or lowering value, in mm, for the last stage of observation, for the previous stage and the one recorded on the overall topographic observation period;
- Value of monthly average speeds, mm/month of landmarks movements on the overall topographic observation period;

– For buildings with substantially different vertical movements (in size, changing direction of displacement or lifting-lowering differential movements in the same building) was conducted a comparison regarding the monthly average travel speeds in the last two stages of observation.

Topographic measurements were performed on topographic landmarks tracking the vertical displacements, mounted on the resistance structure of the buildings and on topographic landmarks installed in the field [4].

To determine the vertical displacements of tracking landmarks, levelling measurements were performed to obtain rate (z) for each item. Landmark stability assessment, through level topographic measurements is done by comparing the level differences between the zero measurement (primary) and the current measurement.

Vertical movement represents the level change of area surface in relation to the initial level of the same areas. It is a parameter that can be determined directly by topographical levelling measurements.

Vertical displacement (ΔZ) is determined by the difference between the elevation of the current measurement and the previous measurement elevation (time immersion) or primary measurement (total immersion) [2].

1. Time immersion: $\Delta S = H_{i-1} - H_i$ [mm] (1)

where: ΔS– time immersion of the current landmark;
H_i^0 – landmark elevation on previous measurement;
H_i - landmark elevation on current measurement.

2. Total immersion: $Si = H_i^0 - H_i$ [mm] (2)

where: S_t - time immersion of the current landmark;
H_i^0 - landmark elevation on zero measurement;
H_i - landmark elevation on current measurement.

3 Results and Discussions

Maximum diving recorded during 2014-2015 was found on the slope located to the north-east compared to the Unirea shaft premises, particularly on Fundătura Crizantemelor Street, on Fulău Dumitru property and on Georgescu Dumitru property.

During December 2014 - September 2015 period, maximum recorded dives were located at the topographic landmarks, placed on Georgescu Dumitru house foundation:

– RC25 landmark, registered a -22.1 mm time immersion.
– RC26 landmark, registered a -14.7 mm time immersion.
– RC27 landmark, registered a -34.8 mm time immersion.

Comparing and analyzing the maximum diving values recorded over a longer period, July 1994 to September 201 5, they are recorded on landmarks located in Georgescu Dumitru house foundation:

– RC25 landmark, registered a total immersion of -303.3 mm.
– RC26 landmark, registered a total immersion of -407.1 mm.
– RC27 landmark, registered a total immersion of -568.0 mm.

Given the emphasized diving, read on the landmarks on Georgescu Dumitru building (RC27) and neighbouring suffusions, it is considered necessary:

- continued observation of the building;
- collecting and removing surface water accumulated in the garden s suffusions;
- topographic monitoring of the area;
- planting new landmarks.

To determine the vertical displacement (time immersion and total immersion) of topographic landmarks located in the foundations of buildings was used the relationship regarding the stability criteria of a level landmark (the difference must not eexceed $2\mu\sqrt{n}$).

$$d_{max} = \pm 2\mu\sqrt{n} \tag{3}$$

where: μ - is the square error of the share unit, different precision measurements specific error. It results the following condition:

$$n \leq \left(\frac{m}{2\mu}\right)^2 \tag{4}$$

where: m - the measurement error.

If it is considered the mean square error of the share unit to be ± 0.1 mm and the measurement error to be 0,5 mm, it is considered that the detection of mutual change of the position of two control landmarks, of 0.5 mm order, it will be possible only when $n \leq 6$ [1]. In the case of measurements related to surface mining Victoria measurement error was 0.2 mm.

4 Conclusions

The owners of the buildings subjected to tracking provided the information related to the sought phenomena, as perceived by them and who think they have a negative influence on constructions and land on private property.

Under the influence of negative phenomena that occurred in the area, the buildings have responded by cracking foundations, walls and floors accompanied by phenomena less alarming as: difficulty in closing the doors and windows, slightly tilting in vertical plane of walls, removing sidewalks from the walls of the house, local fall of wall plaster, floor elevation etc.

Vertical land deformations and land plane displacements transmit additional efforts both in the resistance structure of the building and in the non-structural elements that react with "answers by local degradation" (cracks, detachment painting, plastering, deformations, etc).

The land under the constructions influences the structural frame of constructions through foundations, causing inside it supplementary efforts and deformations. The size of the efforts and deformations of the resistance structure is dictated mainly by the magnitude of movements and not by the unevenness of these movements (lifting-lowering etc) registered at the contact point between the foundation and the ground. Deformations and displacements emphasis was found on the slope located to the north-east towards the Unirea shaft premises, particularly on Fundătura Crizantemelor Street (Fulău Georgescu) [4].

On the land belonging to Georgescu Dumitru, there are 3 areas with ponding water depressions with depth of over 2.0 m, fruit trees in the garden were inclined chaotically and in the yard, strains and bumps develop. The land behind Fulău Dumitru's garden, towards the hill slope, exhibits landslides with level breaking risk of 1-2 m wide, located mainly on the level curves, respectively numerous crater pits partially filled with water and pond vegetation type (cane) (Fig. 3, 4).

Under the influence of negative phemonena produced in the area, buildings have reacted through [4]:

- Cracks in foundations, walls and ceilings and also less alarming phenomena, such as difficulties in maneuvering doors and windows.
- Slight tilt of some vertical walls.
- Sidewalks distancing from house walls.
- Plaster falling from walls.
- Floor elevation.

Fig. 2. Foundation Crack (Construction Located on the Surface Associated to the Mine)

Fig, 3. Sidewalks Distancing from House Walls (Fulău Dumitru).

To prevent effects of socio-economic consequences in case of instability phenomena are necessary the following measures:

- Continuous pursuit of land and construction stability study of the Victoria mine area of influence because the land in this area is in an active phase of vertical displacement.
- Systematically follow through topographic measurements of subsidence phenomena occurred in Victoria mine in order to determine the factors that produce morphological manifestations of the land.
- Expansion, rehabilitation, supervision and maintenance of the topographic station by performing topographic measurements of planimetric levelling throughout Victoria mine area to prevent various natural accidents or damages by reducing and preventing environmental degradation [4].

5 References

[1] Trifan A. (2014). Contributions in the Analysis of Deformations and Displacements of Buildings and Lands, *PhD Thesis*, Bucharest.

[2] Vereş I, Farcaş R, Poruţiu A. (2014). The Topographic Monitoring of the Terrain Damaged by the Exploitation of Salt in Ocna Mureş, Romania, *14 th International Multidisciplinary Scientific Geoconference.* SGEM 2013 June 17-26, Co. Albena, Bulgaria.

[3] Nistor, S. and Buda, A.S (2017). Evaluation of the ambiguity resolution and data products from different analysis centers on zenith wet delay using PPP method. Acta Geodyn. Geomater., Vol. 14, No. 2 (186), 205–220, DOI: 10.13168/AGG.2017.0004.

[4] SĂLĂGEAN, T, RUSU,T., ONOSE, D., FARCAŞ, R., DUDA, B.,SESTRAŞ, P., The use of laser scanning technology in land monitoring of mining areas, Carpathian Journal of Earth and Environmental Sciences, August 2016, Vol. 11, No 2, p. 565 - 573
[5] SC MINESA ICPM SA. (2012). Topographic Station Monitoring Services (Extension, Surveillance, Conducting Spot Checks and Maintenance) at Mining Spot Slănic Prahova Salt Mine, Prahova County.
[6] Nistor, S. and Buda, A.S (2016a). *GPS network noise analysis: a case study of data collected over an 18-month period*. Journal of Spatial Science, 61(2), 1–14. DOI:10.1080/14498596.2016.1138900
[7] Nistor, S. and Buda, A.S (2016b). *The influence of different types of noise on the velocity uncertainties in GPS time series analysis*. Acta Geodyn. Geomater., Vol. 13, No. 4 (184), 387–394, DOI: 10.13168/AGG.2016.0021.
[8] SC MINESA ICPM SA Cluj-Napoca, (2004). [Integrated risk management to salt mines in Romania - methods, techniques and technologies for monitoring, forecasting and prevention (SALRISC) Phase II / 2004 - Identification of sites at risk of exploitation due to salt deposits].
[9] *** Http://www.ct.upt.ro/users/SorinHerban/Topografie2.pdf.

Umbra and Penumbra Impact on GPS Positioning

Nistor S.[1], Buda A.S.[1]

[1] *University of Oradea (ROMANIA)*
E-mail: sonistor@uoradea.ro, alintopoing@gmail.com

Abstract

All GPS satellite from each orbital plane due to the fact that Earth and the Sun are approximately collinear, or the orbital plane is nearly aligned with the Earth-Sun direction the so-called "eclipse" period appears. This alignment occurs twice a year and in this period, the satellite yaw attitude deviates from the nominal value. When the satellite enters into the penumbra and umbra period, perturbation caused by the solar radiation pressure, the real motion of the satellite will not follow the nominal yaw rates.

In this article we have studied the behavior of the station clock in terms of Allan variance from five GPS permanent station located in Romania. In the first stage of the processing all the data from the satellites including the penumbra and umbra period were taken into account. In the second stage the data from satellites that where in the penumbra and umbra period were excluded from processing. Also the nadir mean dependent mean phase residual by satellite were analyzed. The largest difference were for PRN 32 due to the fact that it experienced the longest period of shadowing.

Keywords: GPS, shadowing, Allan variance.

1. Introduction

The GPS satellite has two eclipse season per year for about seven weeks each [1]. When a GPS satellite experience the shadowing effect, the GPS position quality degrades. This degradation appears due to the mismodeling of the yaw attitude of the GPS affected by the eclipse season. The attitude of the navigation satellites represents the geometry and orientation of the body of the satellite. The orbit information is typically referred to the centre of mass (CoM) of the spacecraft, whereas the navigation signal emerge from the antenna at different location [2]. The position of the antenna with respect to the CoM, or the phase center offset (PCOs) and variation (PCVs) are specified in a body-fixed spacecraft coordinate system [3],[4].

The effect of "eclipsing" or "shadowing" or "penumbra and umbra" is caused by the collinearity of the Earth and Sun, resulting in a yaw attitude which deviates from the nominal. The umbra and penumbra period is presented on Fig.1.

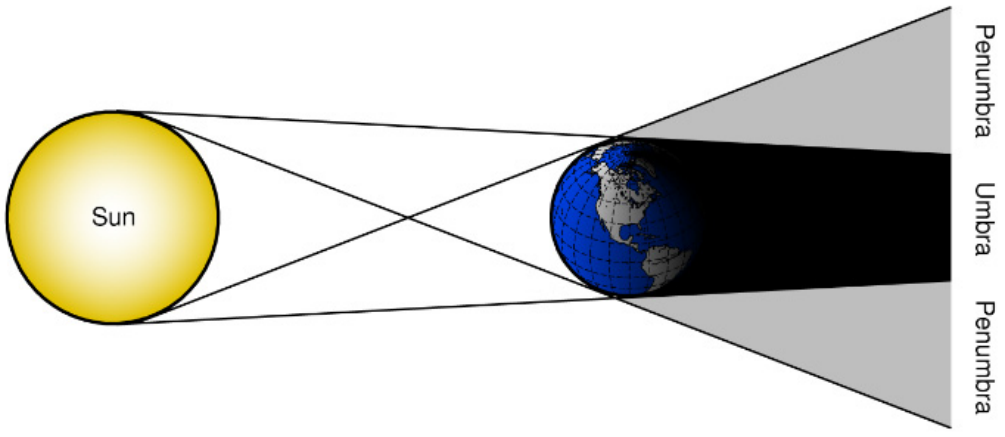

Fig. 1. The umbra and penumbra region

The acceleration of the satellite at each node is considered continuous and smooth but in the case where the satellites enters the shadow region the solar sensor of Block II/IIA satellites, are unable to control the yaw attitude, resulting in a maximum yaw rates of about $0.10\text{-}0.13^0$ /s[5]. This happens because the solar sensor had loosen sight of the Sun and it is trying to keep the solar panels towards the sun the attitude control is degraded.

The nominal yaw attitude of GPS satellites is defined as the body-fixed coordinates system with the Z -axis pointing to the Earth's centre, the Y -axis is along the solar panels and perpendicular to the Sun direction, and the X-axis points either toward the Sun for Block II, IIA or away from it for Block IIR satellites, and it completes the right-handed coordinates system [5]. The result shows that 99 % of error occurs in a long-track direction and will accumulate when crossing more shadow boundaries [6]. The satellite transmitting antenna always should point to centre of Earth and the solar panels should continuous be orientated to the Sun, where the satellite always rotate with respect to the antenna axis to maintain this orientation. This unfortunately doesn't take place when the period of collinearity or near collinearity between GPS satellites, Earth and Sun appears and the yaw attitude is not unique [7]. This is the moment when the satellite X-axis cannot orient toward or away from the Sun, which activates the noon and midnight turn maneuvers [8]. The noon turn appears when the satellite is at the closest point to the Sun, whereas the midnight turn appears when the body of the satellite is in Earth's shadow, which represents the furthest point from the Sun. A major problem is the fact that during the eclipse period the yaw attitude of the GPS satellite is highly random even 30 minutes past exiting from the eclipse season. The errors in the measurements are introduced due to the mismodelling of the transmitter phase centre and carrier phase wind-up. The resulting error can achieve 1 wavelength. The errors from the satellite dynamics are introduced due to the solar radiation pressure (SRP) force is mismodeled even after 30-minutes after exiting the shadowing period during the noon turn [9]. The solar radiation pressure is zero in the umbra period or variating in the penumbra period, thermal re-radiation force changes and the satellite temperature drops down and the solar sensor is unable to control the attitude.

2. Materials and Methods

The eclipsing yaw regimes and the duration are satellite type dependent [5]. The GPS satellite BLOCK IIR contains only the noon and midnight turn maneuvers, which can be modelled and last up to 30 minutes but for the BLOCK II/IIA satellites the eclipsing period is much more complex and it is formed by three phases: noon maneuvers, shadow crossing and finally the so-called post-shadow recovery. The yaw attitude loose of control is triggered by the solar sensor on GPS BLOCK II/IIA satellites, which is causing the X-asis of the satellites to start yawing around the Z-axis with certain rates. The necessary recovery time of the nominal yaw orientation after exiting a shadow period is around 30 minutes and the total time for both shadow crossing period and post shadow recovery can last up to almost 90 minutes [7]. This effect is explained on Fig. 2.

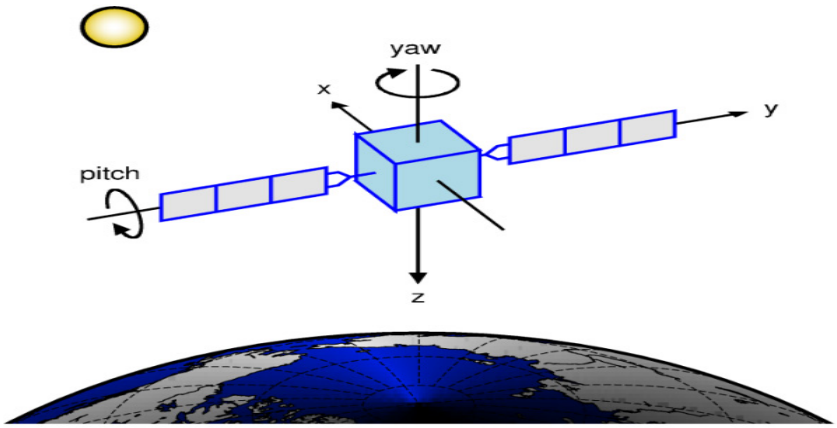

Fig. 2. Yaw rate of a satellite – source [10].

Four regimes govern the yaw attitude of a GPS satellite: nominal attitude, shadow crossing, post shadow maneuver and noon maneuver. In the period of non-eclipsing period the satellite is in the nominal attitude regime, were the post shadow maneuver starts immediately after emerging from the Earth's shadow and lasts until has regained its nominal attitude. The necessary time for this phase can last from zero to 40 minutes. When the beta angle goes below 5^0 the noon maneuver occurs and last between zero and 40 minutes [8]. The beta angle represents the angle between the Sun vector and the orbit plane. It has positive values if the Sun forms an acute angle with the orbit normal and negative otherwise. The midnight maneuver represents the yaw maneuver of the satellite which is conducted from shadow entry until it resume nominal attitude after the exit of

the shadow period. The noon maneuvers represents the maneuver of the satellite which is conducted in the vicinity of the orbit noon when the nominal yaw rate would be higher than the yaw rate of the satellite is able to maintain. This period ends when the satellite resumes nominal attitude. In Fig. 3 it is presented the above statements.

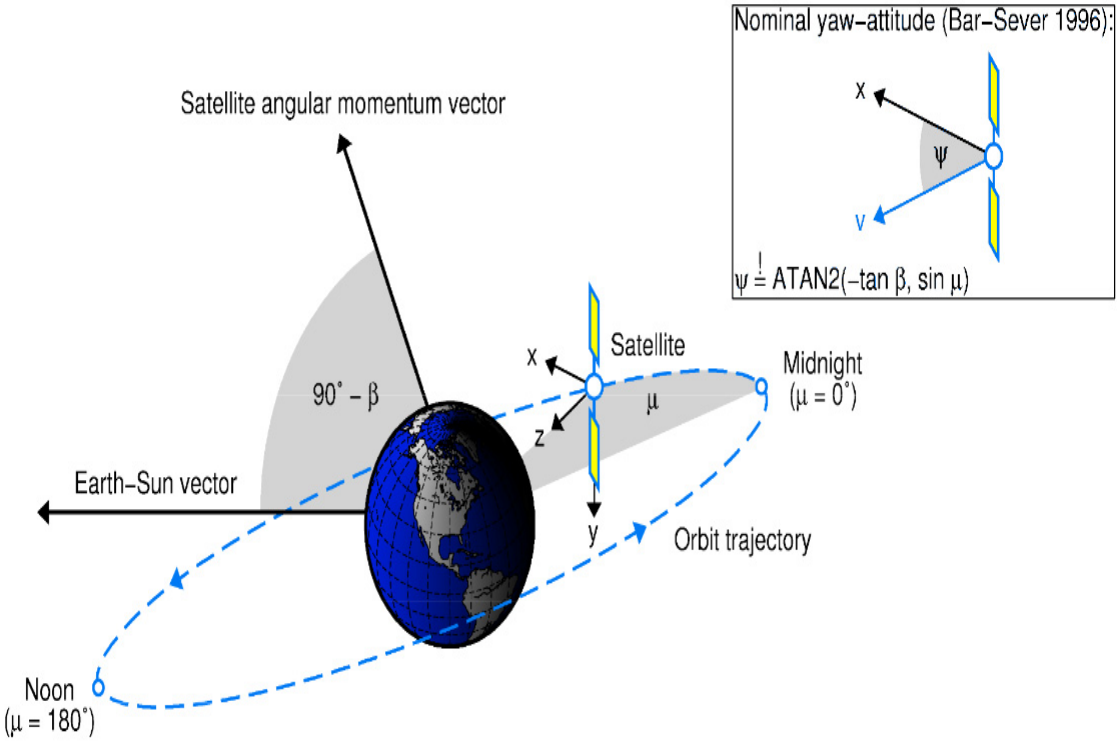

Fig. 3. Geometry of an eclipsing orbit – source [10].

The problem is that each Analysis Center (AC) adopts a specific attitude model, thus creating the effect of inconsistency [11].

Use as many sections and subsections as you need (e.g. Introduction, Methodology, Results, Conclusions, etc.) and end the paper with the list of references.

3. Results

In our study we have used the data from five GPS permanent station in Romania. The data were from 099 and 100 day of year 2015. The data was processed at 30 second interval resulting in a 23321 data for the case when the satellite from eclipse season was removed. In the case where the GPS satellites were in the eclipse season and they were taken into account a number of 23376 data had resulted. In the first stage on the analysis the data were processed without excluding the satellites that experienced the eclipse season and in the second stage the satellites that experienced eclipse season plus 30 minutes after exiting the shadow region were removed. This was done only for the BLOCK II/IIA satellites whereas the BLOCK IIR satellites that experienced the shadow season weren't removed. This was done because the BLOCK IIR satellites do not have any eccentricity in X or Y axis which represents the most significant yaw error contribution. The yaw rate for the PRN 30, 31 and 32 are presented in Fig. 4.

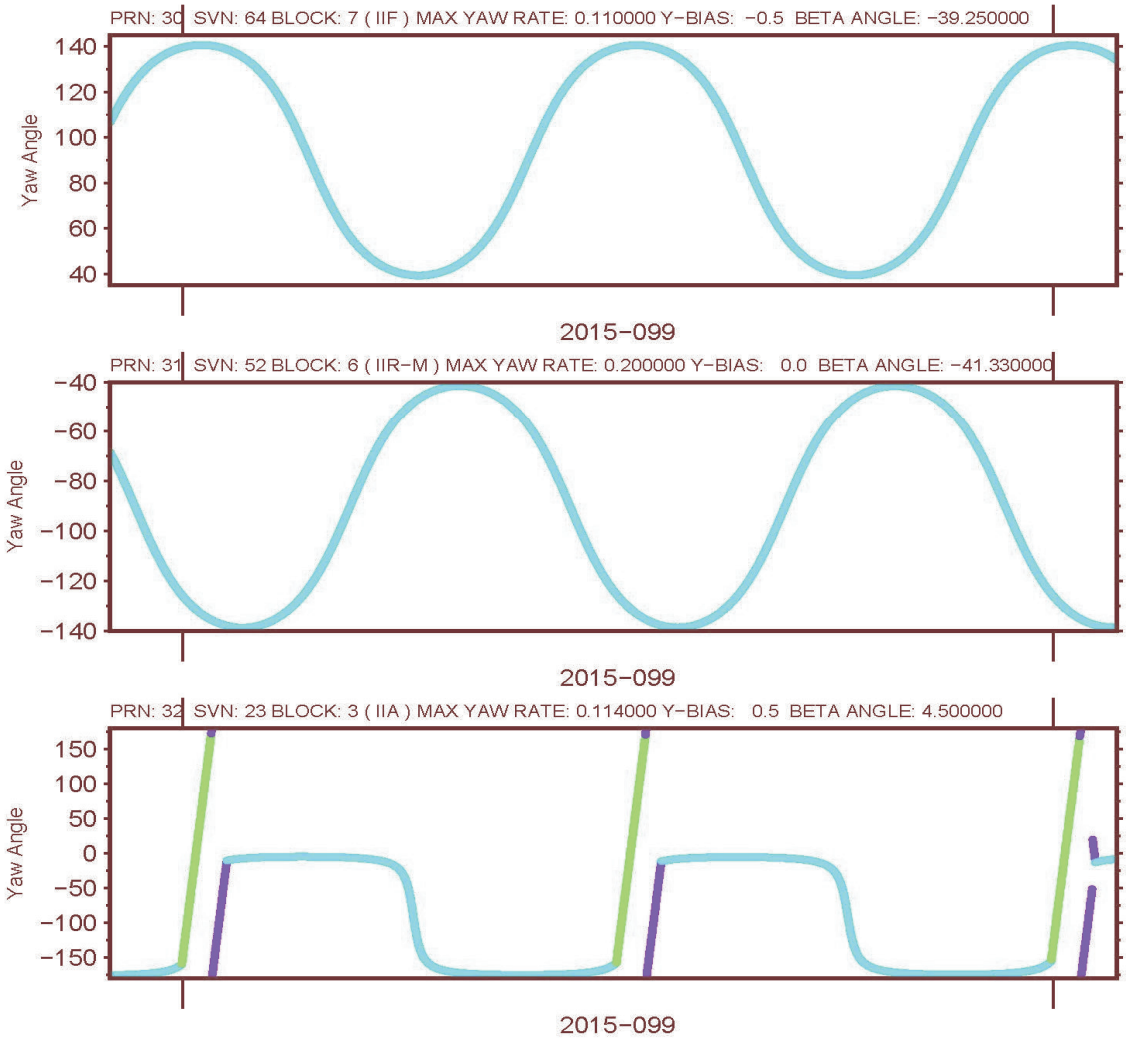

Fig. 4. The yaw rate for the PRN 30, 31 and 32

The blue continuous line represents the nominal yaw rate, where the green and purple line represents the yaw rate in the shadowing region. It can be seen that PRN 32 which is a BLOCK IIA satellite experience shadowing region and Y-bias of 0.5^0 is added. The beta angle is positive and it has a value of 4.5^0. In this case the beta angle that is formed is positive which represents the fact that the Sun forms an acute angle with the normal orbit. In the case of PRN 32, the satellite experienced an umbra and a penumbra region and the umbra and penumbra region was due to the Earth position and not of the Moon.

The mean phase residual for the PRN 32 was computed by taking into account the umbra and penumbra period and without this season is presented in Fig. 5.

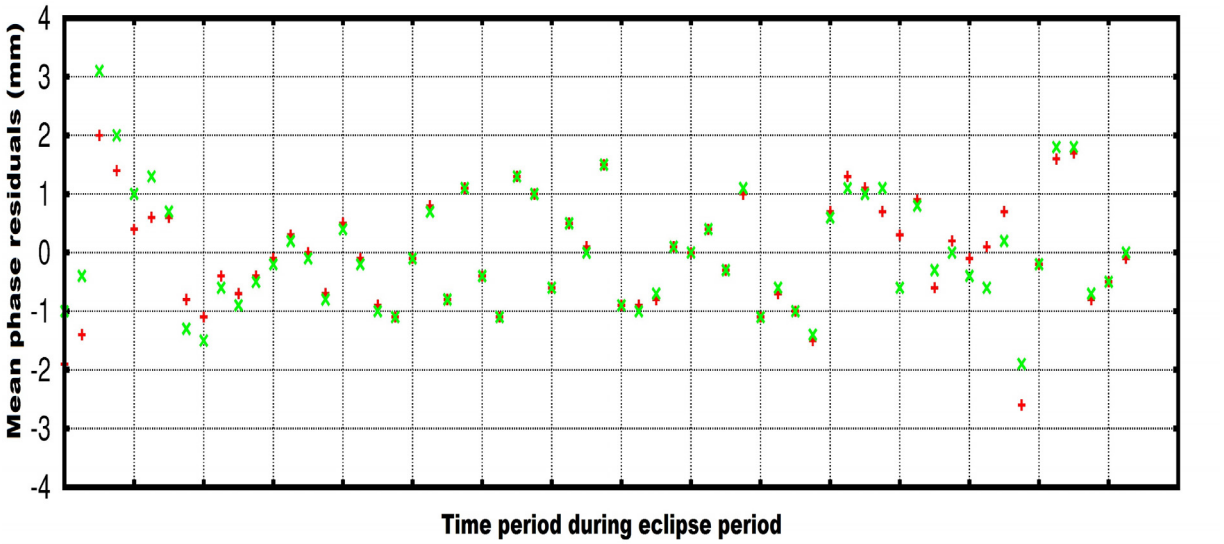

The green asterix represents the mean phase residual of the satellite PRN 32 when no yaw attitude model was taken into account. The red crosses represents the mean phase residual of the satellite PRN 32 when the yaw attitude model was taken into account for the umbra and penumbra effect. Regarding the Allan variance for the PRN 32 when the shadowing effect wasn't taken into account a value of 0.0174 ppb was obtain and when the shadowing effect was taken into account the Allan variance was 0.0100 ppb. Although this values doesn't seems to be very high this type of error affect especially the precise point positioning technique which is "sensible" to each data products from different Analysis Centers [12].

4. Conclusion

The satellite clock estimation is significant influenced by the yaw attitude model especially for the umbra and penumbra period.

An improper modelling of the yaw rate especially for the BLOCK II/IIA satellites can conduct in small errors which are absorbed into positioning estimates causing cm level fluctuation but also the tropospheric and clock solution are affected by this error. The range and clock errors can cause error for up the 15 cm. A possibility is that the satellite that "suffers" from the shadowing effect should be excluded from the processing, especially for the high-precision positioning applications. Not only for the umbra and penumbra period but also for approximately 30 minutes after exiting the eclipse. The problem appears when the satellite clock are also estimated in a global phase solution which can weaken the satellite clock solution that it is used for precise point positioning (PPP) applications. Whereas the double differencing solution can eliminate this type of error.

The BLOCK IIR satellites aren't affected so much by the mismodelling of the yaw attitude because they have nu antenna phase center eccentricity in the body X or Y axis. Also this satellites have no post shadow recovery and also the midnight and noon turns are significantly shorter than the satellites in BLOCK II/IIA.

Because of the inconsistency of the yaw attitude models used by each individual ACs for the satellite clock estimation can create problematic IGS combined clock solution, so when using the IGS data products from shadowing satellites especially for PPP application should be used with extra care.

References

[1] L. Mervart (1995). "Ambiguity resolution techniques in geodetic and geodynamic applications of the Global Positioning System.," *Geod.-Geophys. Arb. Schweiz, No. 53,* vol. 53.

[2] O. Montenbruck *et al.(*2015). "GNSS satellite geometry and attitude models," *Adv. Sp. Res.*, vol. 56, no. 6, pp. 1015–1029, 2015.

[3] R. Schmid, M. Rothacher, D. Thaller, and P. Steigenberger,(2005). "Absolute phase center corrections of satellite and receiver antennas," *GPS Solut.*, vol. 9, no. 4, pp. 283–293.

[4] R. Schmid, P. Steigenberger, G. Gendt, M. Ge, and M. Rothacher (2007). "Generation of a consistent absolute phase-center correction model for GPS receiver and satellite antennas," *J. Geod.*, vol. 81, no. 12, pp. 781–798.

[5] J. Kouba, "A simplified yaw-attitude model for eclipsing GPS satellites (2009)." *GPS Solut.*, vol. 13, no. 1, pp. 1–12, 2009.
[6] B. Duan *et al.*, "Mitigation of Orbit Integration Errors for Eclipsing Satellites (2016). " in *China Satellite Navigation Conference (CSNC) 2016 Proceedings: Volume III*, 2016, pp. 167–174.
[7] B. Zhang, J. Ou, Y. Yuan, and S. Zhong (2010). "Yaw attitude of eclipsing GPS satellites and its impact on solutions from precise point positioning," *Chinese Sci. Bull.*, vol. 55, no. 32, pp. 3687–3693.
[8] Y. E. Bar-Sever (1996) "A new model for GPS yaw attitude," *J. Geod.*, vol. 70, no. 11, pp. 714–723.
[9] Y. E. Bar-Sever (1994) *Improvement to the GPS attitude control subsystem enables predictable attitude during eclipse seasons*. IGS Central Bureau, Jet Propulsion Laboratory.
[10] F. Dilssner, T. Springer, and W. Enderle (2011). "GPS IIF yaw attitude control during eclipse season," in *AGU Fall Meeting Abstracts*, vol. 1, p. 4.
[11] G. Beutler *et al.* (1994). "Extended orbit modeling techniques at the CODE processing center of the international GPS service for geodynamics (IGS): theory and initial results.," *Manuscr. Geod.*, vol. 19, pp. 367–386.
[12] S. Nistor and A. S. Buda (2017). "Evaluation of the ambiguity resolution and data products from different analysis centers on zenith wet delay using PPP method," *Acta Geodyn. Geomater.*, vol. 14, no. 2 (186), pp. 205–220, 2017.

Accuracy Assessment of a 3D Model Reconstructed from Images Acquired with a Low-Cost UAV

Oniga N.[1], Macovei N.[2], Negrilă A.[3]

[1,2] *"Gheorghe Asachi" Technical University of Iasi,*
[3] *Technical University of Civil Engineering, Bucharest,*
E-mails: ersilia.oniga@tuiasi.ro, cardeimihaela@yahoo.com, aurel.negrila@geodezie.utcb.ro

Abstract

Nowadays, low-cost Unmanned Aerial Systems (UAS) are widely used equipments in hydrotechnical applications, providing the acquisition of a high number of images at very high resolution, in a very short time. Therefore, the accuracy of using this technology in hydrotechnical mapping must be evaluated. To achieve results a small overflow was chosen. First were determined, with high precision by GNSS technology, the coordinates of 15 points, 5 of them being artificial and 10 natural. Three of them were used as ground control points (GCP), while the remaining 12 served as check points (CP) for accuracy assessment. Then, the overflow 3D model was created as a point cloud which was automatically generated based on digital images acquired with a low-cost UAS, namely DJI Phantom 3 Standard, using the Structure from Motion (SfM) algorithm. Based on this point cloud, a mesh surface was also created automatically. In order to bring the image network results into the national reference coordinate system, the minimum number of GCPs, i.e 3 artificial points, was used. The overflow 3D model obtained by UAS technology was compared with the TLS (Terrestrial Laser Scanner) point cloud acquired with the Leica Scantation2 laser scanner. The preliminary results showed high potential for using low-cost UAVs in modelling hydrotechnical constructions.

Keywords: low-cost UAS, DJI Phantom 3, hydrotehnical 3D mapping, accuracy, assessment.

1 Introduction

Nowadays, photogrammetric mapping is the new 'trendy topic', although the concept has been around since Leonardo da Vinci's time and it has been in use in practice for over a century. Unmanned Aerial Systems (UAS) technology, offers now the possibility of data acquisition and 3D modelling to thousands of people from different areas of expertise but, from a surveying standpoint, accuracy is the key [1]. In order to build 3D models from UAS images, the Structure from Motion (SfM) algorithm is frequently used, which involves the simultaneous determination of intrinsic and extrinsic camera parameters, the result being a dense 3D point cloud obtained by matching pixel positions in images. However, any lens distortions introduce errors in this process and degrade the accuracy of the model, especially those of cameras installed on UAS systems, since these platforms can't allow the transportation of high quality navigation devices like those coupled to airborne cameras or LiDAR sensors [2]. Therefore, survey control of an UAS photogrammetric project is essential to manage these errors.

Bringing the results of a UAS photogrammetric project in a known coordinate system requires the georeferencing process, either direct using GNSS/INS data or indirect which implies using ground control points (GCPs), or a combination of both.

2 Materials and methods

For this case study, a small overflow located in Cucuteni village, Iasi County was chosen, with a surface of 1269 square meters.

The main materials for this task are the UAS images acquired with a low-cost UAS, the point cloud acquired with the Leica ScanStation 2 laser scanner and the measurements made with GNSS (Global Navigation Satellite System) surveying tools.

So, the first equipment used for this case study is the low-cost UAS platform, DJI Phantom 3 Standard, whose characteristics can be found in [3]. The second equipment used is the ScanStation2 laser scanner produced

by Leica Geosystems, which is a terrestrial scanner system used mainly in static measurement, being a scanning flexible solution which rapidly captures and measures all the details in a scene, ideal for complex environments and the third equipment is a South S82 GNSS receiver.

The GNSS measurements were transformed into "Stereographical on unique secant plan-1970" coordinate system with the TransDatRO official application of the National Agency for Cadastre and Land Registration, the UAV images were handled using "3DF Zephyr Pro" software [4], while the TLS point cloud (Fig. 1 a) was the result of a three individuals point clouds registration using the Leica Cyclone v.6.0 software. The comparison between the UAS point cloud and the TLS point cloud was made using the Hausdorff distance [5], implemented into "CloudCompare" open-source software [6].

2.1 *Ground control*

In order to obtain accurate information when using a low-cost UAS, the indirect georeferencing process must be used [2], the placing and measuring of GCPs being mandatory. For this case study, the GCPs were made by plexiglass, having the centre marked by the intersection of two black triangles and a metal bold. Five points were placed over the overflow, three of them being used as ground control points (GCP), while the remaining two as check points (CP) for accuracy assessment. Then, their coordinates along with the coordinates of 10 natural check points representing the overflow characteristic points, were measured with high accuracy using the GNSS technology.

2.2 *Image acquisition*

The flight was done in manual mode, in approximately 10 minutes. In order to assure a regular and higher overlap in the image block, the overflow was photographed all around at an altitude of approximately 18 m above the ground, 31 images being taken from 31 different camera positions distributed circularly around the overflow.

As these platforms are strongly influenced by the presence of wind piloting capabilities and GNSS/INS quality, all randomly affecting the altitude and location of the platforms during the flight [2], it is recommended to take as many images as possible with sufficient overlap.

3 Results

3.1 *Three-dimensional reconstruction process of the overflow*

3.3.1 Image processing

SfM involves the use of several images with sufficient overlap, from which the features that will be used for the 3D reconstruction of the scene will be extracted.

The property 3D reconstruction process includes a series of steps presented in [3].

For this case study, following the bundle adjustment process i.e. a non-linear optimization procedure in order to minimize an appropriate cost function [7], the "*3DF Zephyr Pro* software calculated the three-dimensional coordinates of common features identified by image matching algorithm, in a local coordinate system, the interior orientation parameters and the exterior orientation for each camera position. So, in a first step, a point cloud was automatically generated, containing a number of 378446 points (Fig. 1 b) and in a second step, a textured mesh surface was automatically created based on the point cloud, containing 756858 triangles (Fig. 1 c).

(a) (b) (c)

Fig. 1 TLS point cloud with laser reflectance information (a), the overflow 3D model represented as a point cloud (b), the overflow 3D model represented as a mesh surface and the camera positions and orientations (c)

3.3.2 Georeferencing the image network results

To perform indirect georeferencing there are basically two ways to proceed, mentioned in [4].

For this case study, a free-network approach in the bundle adjustment was applied and only at the end of the bundle adjustment a similarity (Helmert) transformation was performed in order to bring the image network results into the desired reference coordinate system, i.e "Stereographical on unique secant plane 1970". As demonstrated in [3], if no constraint is introduced in the process of bundle adjustment, increasing the GCPs number will not improve the 3D shape of the surveyed scene. So, in this situation, the minimum number of three artificial GCPs was used. This points form a triangle close to equilateral, positioned in the center of the overflow, with a surface of 15% from the total one.

3.2 *Quality assessment of the UAV point cloud by using check points*

In this section we assess the accuracy of the point cloud automatically generated based on digital images acquired with a low-cost UAS, by measuring and comparing the coordinates of the CPs with the ones determined with high accuracy using the GNSS technology.

In Fig. 2 we can see the position of three Control points 1, 2 and 3, 10 Natural Check points 1, 2 ... 10 and the two Artificial Check points 1 and 2.

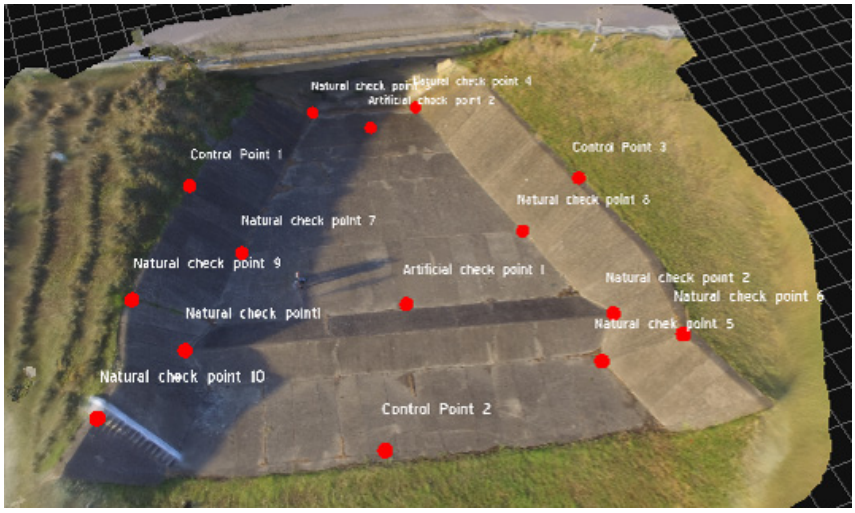

Fig. 2 The visualization of the Control Points 1, 2 and 3, the Natural Check points 1, 2 ... 10 and the Artificial Check points 1 and 2

The coordinates of the above mentioned points were measured on oriented images. Then, the differences between them and the ones measured with precision using the GNSS technology were calculated. Based on these differences, the residual was calculated, which is the Euclidian distance between the two coordinate sets for a point calculated with the distance equation [8]:

$$D = \sqrt{(X_r - X_i)^2 + (Y_r - Y_i)^2 + (Z_r - Z_i)^2}, \quad (1)$$

where:

(X_r, Y_r, Z_r) – the coordinates of a characteristic point computed after the GNSS measurements (reference),

(X_i, Y_i, Z_i) – the coordinates of a characteristic point computed based on image measurements.

The residuals of the 12 CPs coordinates after the process of indirect georeferencing using the minimum number of GCPs, i.e 3 artificial points, are listed in Table 1.

Table 1 The coordinates of the 12 check points residuals

Point no.	The point type	Differences			D [m]	Ei [m]
		$Xr-X_i$ [m]	$Yr-Y_i$ [m]	$Zr-Z_i$ [m]		
0	*1*	*2*	*3*	*4*	*5*	*6*
1	artificial	0.003	-0.003	-0.002	0.005	0.081

0	1	2	3	4	5	6
2	artificial	-0.003	0.008	-0.006	0.010	0.174
3	natural	-0.011	0.039	0.007	0.041	0.688
4	natural	-0.007	-0.014	0.014	0.021	0.350
5	natural	-0.090	-0.080	0.052	0.131	2.197
6	natural	0.029	0.044	-0.061	0.080	1.344
7	natural	-0.060	0.015	0.045	0.077	1.281
8	natural	0.048	0.039	0.055	0.082	1.376
9	natural	-0.023	0.015	-0.009	0.029	0.492
10	natural	0.008	0.010	0.011	0.017	0.284
11	natural	0.015	0.042	0.004	0.045	0.746
12	natural	0.008	-0.012	0.030	0.034	0.566
Cumulative Root Mean Square Error		0.036	0.034	0.033		

The results showed maximum RMSE of 1 cm in the case of artificial check points, a maximum RMSE of 13 cm and a minimum RMSE of 1.7 cm in the case of using natural check points.

To determine the cumulative RMS error, the following calculations were made: the X RMS error with a value of 0.036 m, the Y RMS error with a value of 0.034 m and the Z RMS error with a value of 0.033 m [8].

The cumulative root mean square error (T) calculated for the 12 check points was evaluated using the value of 0.059 m, confirming that the coordinate differences for the two survey methods are of similar precision, allowing the usage of either of them by convenience, to get similar results.

A normalized value representing each point RMS error in relation to the cumulative RMS error is given by the relation:

$$E_i = R_i / T, \tag{3}$$

where: E_i – error contribution of point "i",
R_i – the RMS error for point "i",
T – cumulative RMS error.

In the case study of the 3D modelling process, the standard errors for each analyzed point ranged between a minimum value of 0.081 m and a maximum value of 2.197 m.

3.3 *Quality assessment of the UAS point cloud by using the TLS point cloud*

In this section we assess the accuracy of the point cloud automatically generated based on digital images acquired with a low-cost UAS, by comparing the UAS point cloud with reference data, using the Hausdorff distance implemented into "CloudCompare" software [6]. For this case study we considered as reference data the TLS point cloud resulted from the scanning and manual filtering processes.

First, a mesh surface was created based on the TLS point cloud using "Mesh-Delaunay 2.5D (best fitting plane)" function from the "Edit" menu, then, the Hausdorff distances between each point and the mesh surface were calculated, using the "Distance-Cloud/Mesh Dist" function from the "Tools" menu (Fig. 3 a).

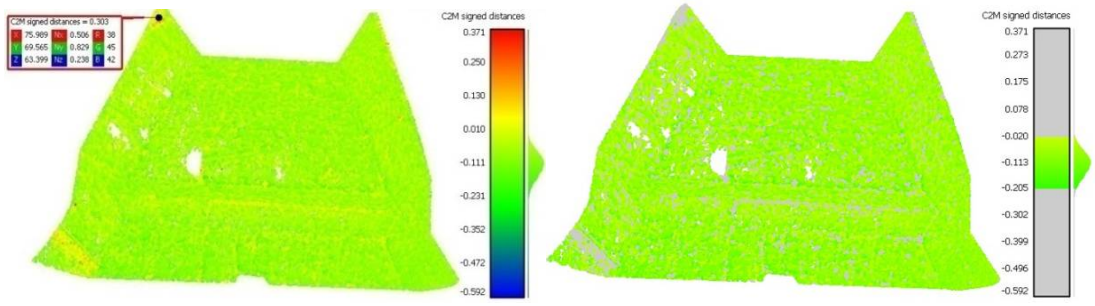

(a) (b)

Fig. 3 The differences between the UAS point cloud and the mesh surface created based on the TLS point cloud

By analysing the Hausdorff distances (differences) distribution histogram, it can be seen that the Hausdorff distances values range between -0.592 m ÷ +0.371 m, while most of them fill only a small part, namely -0.205 m ÷ +0.020 m. So, we coloured in gray the points for which the Hausdorff distances are situated outside this interval and then, analysing the points colours we can see that the gray points are mingled with the green ones (situated inside the interval), concluding that the UAV point cloud is very noisy (Fig. 3 b). If we filter the point cloud, choosing only the points situated inside the above mentioned interval, the standard deviation becomes 4.1 cm, with almost 1 cm smaller than before the filtering process, i.e. 5.3 cm, the precision not being significantly improved. Therefore, we need to find out how noisy the UAS point cloud is.

So, using the "Segment" function from the "Edit" menu, both point clouds, the UAS and the TLS one, were segmented in order to extract only the point cloud that belongs to the bottom of the overflow. Then, with the help of "Fit-Plane" function from the "Tools" menu, two best fitting plans were created for both point clouds, the RMS being 5.2 cm in the case of UAS point cloud, respectively 1.1 cm in the case of TLS point cloud (Fig. 4).

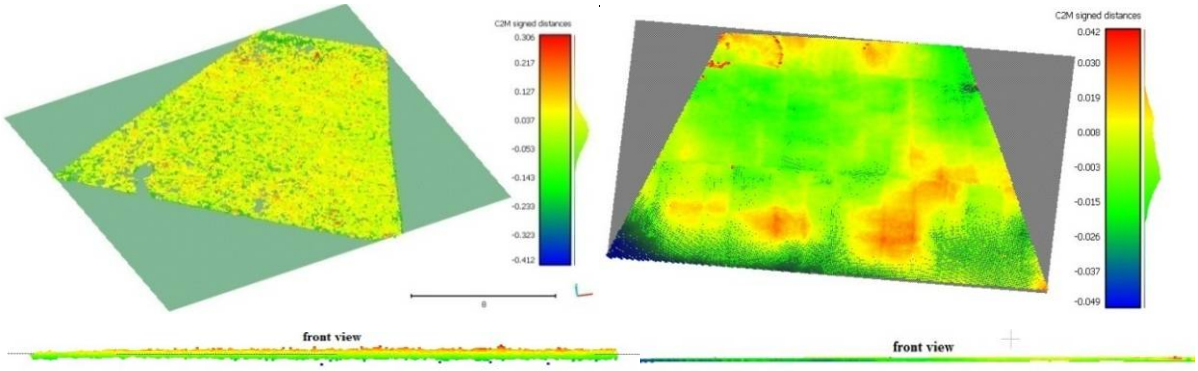

(a) (b)

Fig. 4 The best fitting plane and the Hausdorff distances between each point and the fitted plane calculated for the UAS cloud (a) and the TLS point cloud (b) (perspective view and front view)

By analysing the Hausdorff distances distribution histogram calculated based on the UAS point cloud, it can be seen that the Hausdorff distances values range between -0.412 m ÷ +0.306 m, while most of them fill only a small part, namely -0.107 m ÷ +0.105 m. Likewise, in the case of the histogram calculated based on the TLS point cloud, the Hausdorff distances values range between -0.049 m ÷ +0.042 m, while most of them fill only a small part, namely -0.021 m ÷ +0.022 m. As would be expected, it is immediately apparent that the UAS point cloud is very noisy and its accuracy, in comparison with the TLS point cloud, is approximately five times smaller.

In addition, using the "Segmentation-Cross Section" function from the "Edit" menu, two cross sections with a width of 20 cm were created in the same spatial position (Fig. 5 a) for both point clouds, the UAS (Fig. 5 b) and the TLS one (Fig. 5c), the differences between the two point clouds being visible with clear eye.

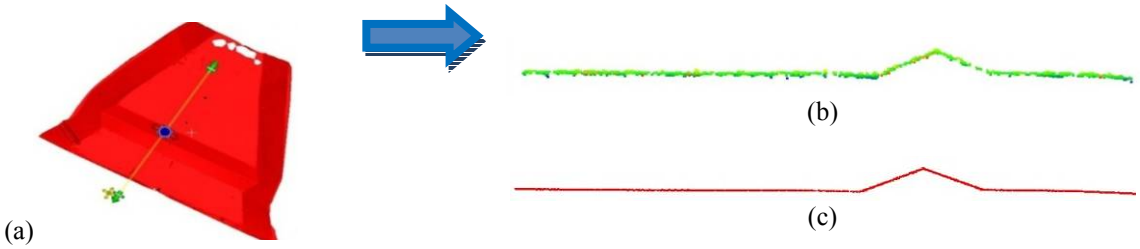

(a) (b) (c)

Fig. 5 Cross sections spatial position: (a) through the UAS point cloud (b) and the TLS point cloud (c)

Finally, the orthophoto has been generated for the study overflow using the "3DF Zephyr Pro" software, having as reference object the mesh surface, for documentation and visualization purposes. The camera altitude above ground was set at 20 m and all 5 artificial GCPs and CP were used to define a reference plane (Fig. 6 a). Then, the Digital Surface Model in raster format with a spatial resolution of 0.2 m was created for the UAS point cloud by using the "Opals" software, interpolating all points using the "movingPlanes" method, 8 neighbours and 1 m search radius (Fig. 6 b and c).

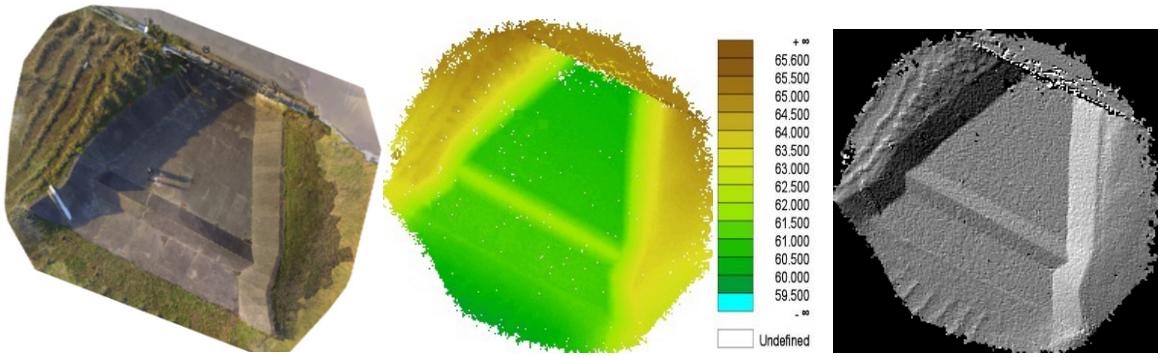

(a) (b) (c)

Fig. 6 The overflow orthophoto: (a), the Digital Surface Model of the study area represented in raster format (0.2 m cell size) using the standard colour palette (b) and hillshade (c)

Conclusions

With UASs, 'everyone's a surveyor', but good technical error management sets the professional surveyor apart from the cool visual 3D modeller [1].

The UAS method with appropriate photogrammetric evaluation methods, offers a great potential to gain information from the captured data that are useful for hydrotehnical applications. In areas where access can be difficult, UAVs offer a valuable alternative to tachymetry and GNSS technology.

By computing the RMSE of the point coordinates using the data from both surveys, a high precision was obtained for the artificial points rectangular coordinates (*X, Y, Z*). Thus, the maximum positioning errors encountered for the artificial check points was 1 cm (for the number 2 point) and the minimum positioning errors was 5 mm (for the number 1 point). In the case of natural check points, the precision is reduced comparing to the artificial points, due to the fact that the natural points are the overflow characteristic points, most of which are covered by grass or soil in reality, making their identification and measurement on images a difficult task.

By calculating the Hausdorff distances between the UAS point cloud and the mesh surface created based on TLS point cloud, a standard deviation of 5.3 cm was obtained concluding that the UAS point cloud is very noisy. After the filtering process, a standard deviation of 4.1 cm was obtained.

References

[1] Klau R. (2016). Precise UAV Camera Positioning for 3D Mapping. Available at: https://www.gim-international.com/content/news/precise-uav-camera-positioning-for-3d-mapping

[2] Nex F, Remondino F. (2013). UAV for 3D mapping applications: a review. Applied Geomatics 6(1), pp. 1-15.

[3] Oniga V. E., Chirila C., Macovei M. (2016). Low-cost unmanned aerial systems in cadastral applications, 16th International Multidisciplinary Scientific Geo Conference, SGEM 2016, Albena, Bulgaria, Book 2 Informatics, Geoinformatics and Remote Sensing, Volume II, , ISSN: 1314-2704, DOI: 10.5593/sgem2016B22, pp. 947-954.

[4] Information on http://www.3dflow.net.

[5] Aspert, N., Santa-Cruz, D., Ebrahimi, T. (2002). Mesh: measuring errors between surfaces using the Hausdorff distance. In Proc. of the IEEE International Conference in Multimedia and Expo (ICME), vol. 1, pp. 705-708, Lausanne, Elveţia, August 26-29.

[6] Girardeau-Montaut, D. – CloudCompare version 2.6.1 - user manual, (2015). On line at: http://www.danielgm.net/cc/doc/qCC/CloudCompare%20v2.6.1%20%20User%20manual.pdf.

[7] Gruen A, Beyer H A. (2001). System calibration through self-calibration. Calibration and Orientation of Cameras in Computer Vision, Gruen and Huang (Eds.), Springer Series in Information Sciences, 34, pp.163-194.

[8] Oniga V. E., Chirila C., Şutu M. (2012). Terrestrial laser scanner surveying versus total station surveying for 3D building model generation, Scientific Journal „Mathematical Modelling in Civil Engineering", Vol.8. no.4, pp. 168-177.

Land Tenure Promotion for Achieving Local Sustainability

Palamariu M.[1], Tulbure I.[2,3], Dreghici A.[2]

[1] *University of Agricultural Sciences and Veterinary Medicine Cluj-Napoca (ROMANIA)*
[2] *University "1 December 1918", Alba Iulia (ROMANIA)*
[3] *Clausthal University of Technology, Clausthal-Zellerfeld (GERMANY)*
E-mails: mpalamariu@gmail.com, ildiko.tulbure@tu-clausthal.de, alexandra.popa@hotmail.com

Abstract

Assuring the sustainability of our human society is currently representing a pretty discussed topic on technical, economic as well as on social and political level. In this context inter- and transdisciplinary approaches are required in order to succeed developing and applying proper sustainable development strategies on different levels, i.e. on national, regional as well as on local level. In the last time it came out that achieving local sustainability is among the most critically issues of the 21st century, independent if people are living in urban or rural areas. In this regard it is self-evident the importance of a proper land use planning and administration, as being the general term used for rural and urban planning including various disciplines. Land Use is one of the most visible targets of the sustainability topics and connected with it the issue of land tenure. Sustainable land use implies land tenure promotion, which supports sustainable development and creates an obvious balance of environmental preservation, commerce and liability. A comprehensive assessment regarding an efficient land use plan provides a vision for the future development possibilities for achieving sustainable regions. Gaining strategies on local level means actually developing strategies for sustainable urbanism. The vision of future sustainable cities, by taking into account regional differences, is worldwide a pretty discussed topic, also in some Eastern European countries and implies first of all the clarification of land tenure critical aspects. In this paper some concrete strategies for land tenure promotion will be discussed in order to assure an appropriate sustainable land use planning on a local level with the goal of shaping sustainable urban and rural planning.

Keywords: land tenure, local sustainability, land use planning, sustainable city, interdisciplinary approaches.

Introduction

In the worldwide debates regarding currently existing possibilities for assuring the sustainability of our human society several times has been emphasized the important role played by shaping on a local level high living standards for inhabitants. Such an attempt can be fulfilled by cost and energy friendly housing alternatives, considering not only technical and economic aspects, but also environmental, sportive and cultural ones. All these requirements are actually directed to the vision of creating in the future the necessary technical infrastructure by a proper land-use management and the appropriate mentality in order to succeed living in the so-called "sustainable city" [4, 10, 16]. Worldwide began in the last time discussions on scientific, political and social levels in order to find the best solutions for shaping Sustainable Cities, which could be applicable to several countries all over the world, but with respect to specific regional conditions especially cultural differences [1, 6, 16].

In the year 1987 the Brundtland Report was released, where for the first time the concept of sustainable development has been defined [5]. Several discussions regarding this concept followed 1992 at the Conference for Environment and Development in Rio de Janeiro, where the much debated document „Agenda 21" has been released. The need of simultaneously considering several fields became self-evident in order to succeed the successful operationalization of sustainable development on different levels, on global, national and regional as well as on a local level [6]. The vision is to find the best strategies for assuring especially the local sustainability, by taking into account the plenty of aspects concerning technological, economic and social activities together with aspects related to land tenure, land use planning, administration and management [4, 11, 15].

Strategies for Gaining Local Sustainability

The idea of elaborating appropriate *strategies for sustainable development on a local level* means actually developing strategies for *urban sustainability* in cities or for *rural sustainability* in the countryside. Nowadays a pretty discussed topic on a global level is the existing possibility of developing in the future *sustainable cities*, by taking into account regional differences [1, 4, 10]. It was recognized that the urban sustainability is among the most critically important global issues of the 21st century. It is estimated that over 50% of the world's population now lives in urban areas. Some developed scenarios for the future urban development estimate that by 2050 the proportion of the global population living in cities will rise to 70% [6]. A need *per-se* is the consideration of specific regional conditions in different countries by following the goal of achieving local sustainability in cities or villages, as it is required because of the existing situation in some Eastern European countries [4, 6, 16, 18].

The current real worldwide situation is emphasizing that the fight against climate change will be won or lost in high degree in urban settlements, so that it is crucial that the urban habitats will become more efficient, not only for themselves, but for future generations and the earth's diverse ecosystems. The big challenge is that currently the energy consumption in cities is about 75% of the world's energy consumption and the pollutants emissions in cities are around 80% of all greenhouse gas emissions [6]. In this regard gaining sustainable urban as well as rural development is a real necessity and several newly discussed strategies in this regard have at their base the concept of *Decoupling*, which is a pretty recent term in the sustainability literature [16]. It was mentioned first time by the Club of Rome, during its Conference "Governance of the Commons", that took place in September 2013 in Ottawa, Canada. This term typically refers to the ability of breaking the long held causal relationship between economic growth and growth in the consumption of natural resources. The essence of decoupling means to assure a high quality of life for all citizens in the world, but without having a rapid growth in the energy consumption, with all its impacts on the environment, and not only. Decoupling goes beyond simple price adjustments or marginal policy shifts but strikes a blow at the heart of the fundamental yet mistaken belief that economic growth and natural resources use are two sides of the same coin, joined forever in a mutually reinforcing bind. Those who advocate decoupling believe that the binding knot can, and must, be broken in order to assure the *local urban* or *rural sustainability* [16, 17].

Decoupling, as a strategy for gaining *local sustainability* on urban or rural level has to be amended by the promotion of *obvious land tenure* in order to assure the population readiness for supporting a high quality land use planning, administration and management [4, 10, 17, 18].

Regarding the concrete situation in Romania, the question is nowadays how to transform a city or a village in Romania in a regional model of sustainable development in order to get the local sustainability on urban or rural level, this means to get a *sustainable city* or a *sustainable village* [2, 4, 10]. After joining the European Union in 2007, the word "sustainability" started to be heard more frequently in Romania. New opportunities for people to explore and learn from Western European countries were suddenly opened. Small steps have been taken since then, sometimes because of bureaucracy, sometimes because of other priorities, and sometimes because of lack of knowledge and lack of financial resources in order to clarify *specific land tenure aspects* [18]. Nevertheless it has to be mentioned that in the last years some progress has been registered especially in the field of sustainable urban development [12, 17], but until now there is little guidance on what actually constitutes a sustainable form of development in the countryside, where first of all clarifying land tenure aspects plays an important role [18].

In order to emphasize the made progress in the field of sustainable urban development, the five biggest cities in Romania will be considered: Bucharest, Cluj-Napoca, Timisoara, Iasi and Constanta. In order to become sustainable cities, they all share some things in common: they want an urban regeneration, to reduce energy consumption and to use new transportation possibilities, other than cars [2]. On the other side, the Romanian Government approved 2009 a program for the rehabilitation of residential urban buildings constructed from 1950–1990. And there are plenty of those. There were four major benefits from this action plan: increasing the energy efficiency of the buildings, changing the facades, protecting the environment by reducing emissions and reducing the amount of money spent by building owners. Also the idea of constructing green buildings come very much into discussions, as for instance in Cluj-Napoca. This city has the first green school of Romania. Starting in 2013, the construction of green buildings has been encouraged by local authorities, for instance by reducing local taxes for them by 50%.

A lot of discussions have started also in the field of alternative transportation possibilities. The population in several cities did agree that bicycles will need to be used more frequently. The largest bike-sharing project in the country was launched 2010 in Bucharest, followed 2011 by Cluj-Napoca and Constanta and 2012 by Timisoara. Each city is hoping that this will help reducing their carbon footprint and sustain the development of an adequate infrastructure for cyclists, but several difficulties regarding land tenure aspects did appear and have to be clarified [2, 18].

The city Alba Iulia in Romania, having a number of inhabitants of 66,369 has a Development Strategy that aims to acknowledge the urban mechanisms as a positive force in improving the housing standards, the

equity and sustainability standards. The strategic plan is to address issues related to improving the quality of pedestrian areas and all public space areas and also to improve the accessibility in the historical part of the city, this is the Fortress Area. The environmental policy of Alba Iulia is also targeting transport issues, as the tourism activities are pretty developed in this city, and in this regard several aspects concerning land tenure have to be systematically approached [2, 18].

Aspects concerning Land Tenure Promotion

As mentioned until now in order to achieve a sustainable human settlement development and to achieve a local sustainability on urban or rural level land tenure promotion has a crucial importance and in this regard the proper clarification of land tenure aspects is strongly required. Without a lack of a proper land tenure promotion it is not possible to get an integrated sustainable land use planning, administration and management [4, 10, 18].

The situation and the evolution of Cadaster in Romania – due to the problems concerning land tenure in Romania (incomplete data, no up-to-date and sporadically registrations), at the moment there are projects developed in order to support and achieve complete systematic registration. Therefore, Romanian legislation has changed several times in a short period of time, in order to facilitate registration of land hold informally. According to CESAR data, more than 50% of land owners do not have proper legal documents. Therefore, their interest in achieving a sustainable development is decreased because of the land rights limitation [13].

The projection system used for graphical registration documents is the Stereographic 1970System, used in Romania since 1973. Basic topographic plans (1:2.000, 1:5.000, 1:10.000) as well as cadastral maps (1:50.000) use the Stereographic 1970 System. Geodetic and topographic measurements needed for national economy development should be executed in the Stereographic System 1970. All land parcels should have their limits well defined in this system, according to the existing registration graphical data [8].

The National Agency for Cadaster and Land Registry develops a strategy concerning geodetic and cartographic works for modern cadastral registration support that refers to the modernization of the national geodetic network, using GNSS technology. For national homogeneous coordinate system, ANCPI offers a free software for coordinate transformation, TransDat [3].

In order to ensure a support compatible with the INSPIRE Directive for implementing cadastral registry in solving land tenure problems, the National Agency for Cadaster and Land Registry introduces E-Terra 3. E-Terra represents an integrated informatics system in cadaster and land registry that allows ANCPI to manage cadastral registration and Land Registry in Romania. It offers support for all technical works of identification, measurement, description and land registration in cadastral documents and their representation on cadastral plans and maps [9].

All these issues are trying to be solved by national authorities. Additionally, there should be mentioned the awareness of land owners over the importance of the solving the problems concerning the land tenure, in order to achieve local sustainability.

Promoting Land Tenure for Achieving Local Sustainability

It should be mentioned from the beginning that the idea of achieving local *urban* or *rural sustainability* does represent an innovative development direction in the field of shaping sustainable settlements in the specific conditions for each considered country [4, 17]. Actually nowadays there is still no agreement regarding a general definition for a sustainable settlement, city or village, and there is no complete agreement upon paradigm for what parameters are relevant for gaining local sustainability. However, in order to get local sustainability a sustainable settlement should be able to demonstrate an efficient integrated sustainable land use planning, administration and management, as presented in Fig. 1, where a proper land tenure promotion is representing a key element in the operationalization of sustainable development [18].

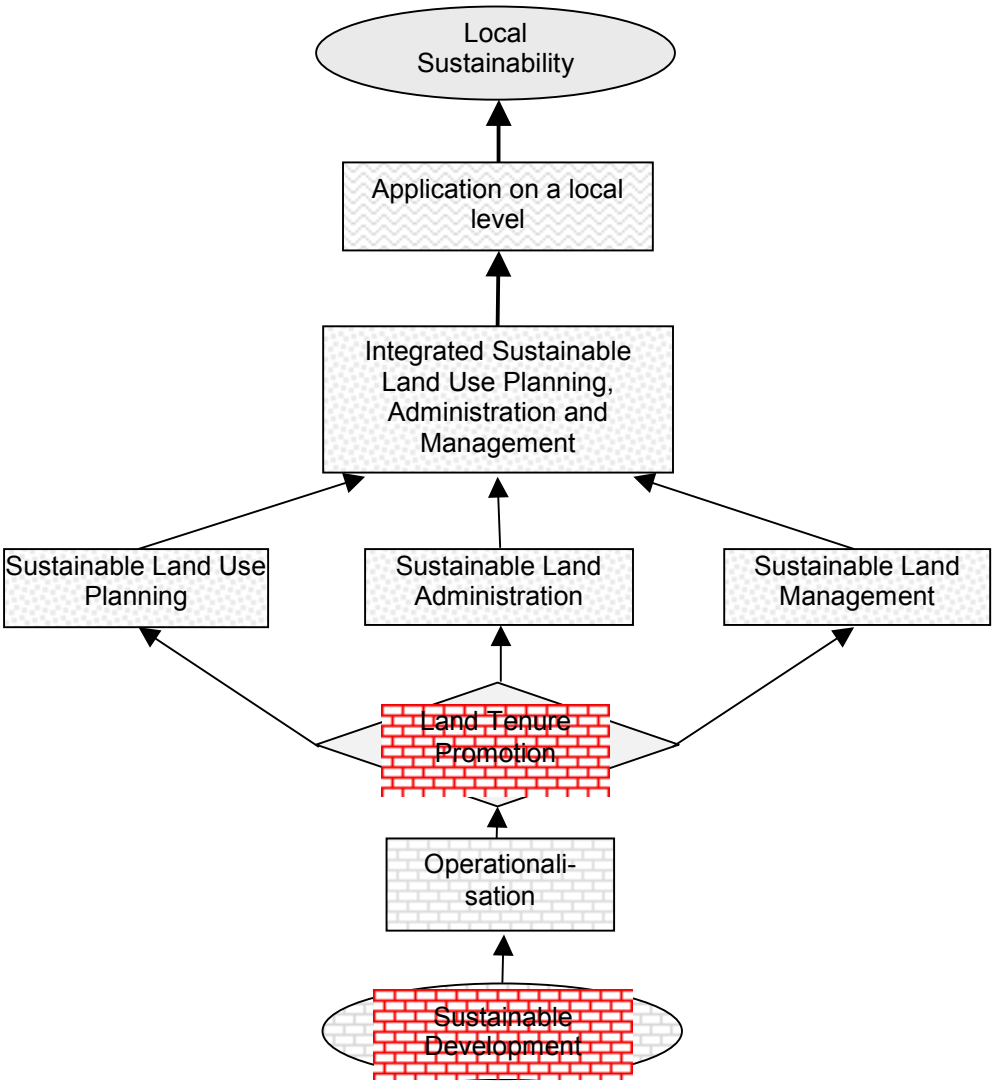

Fig. 1 The Role of Land Tenure Promotion for achieving Local Sustainability

Land Use Planning for Getting Sustainable Settlements

However, a sustainable settlement should be able to demonstrate an efficient land use planning, to feed itself with minimal reliance on the surrounding countryside, and to power itself with renewable sources of energy. For this purpose land tenure promotion is the base to further develop different strategies for local sustainability [18]. Besides technical, environmental and economic aspects, a sustainable integrated land use planning as well as a sustainable land administration and land management do represent key factors in shaping sustainable settlements, so this means in achieving local sustainability [4, 10].

Nowadays the goal is to generally promote the idea of achieving sustainable regions, not only sustainable cities, by taking into account all aspects related to this issue such as technical, economic, social and environmental aspects in the field of adequate living conditions and housing space, proper resource use, mobility, governance as well as social life. Connected to this idea, developing a kind of a ”general methodology” to be applied into the practice for real concrete situations by taking into consideration regional differences would represent a major progress in this field, just to come from the vision of sustainable settlements to the reality. The general methodology for shaping a sustainable settlement should contain aspects related to sustainable land use planning, land administration and management [4, 10].

In order to achieve the main goal of the present developments in the field of assuring a sustainable rural and urban development several aspects regarding first of all a proper land tenure promotion, followed by an

efficient land use planning, land administration and land management have to be considered. In this regard it would be useful that Romanian settlements will become partners in international networks of sustainable settlements, just to learn about experiences of other villages or cities in other countries and to cooperate in this field of shaping a sustainable rural and urban development. On the other side the desire is to find appropriate ways to establish strategies for the sustainable rural and urban development in Romania [16].

In order to assure the sustainability of our society there is a need to shape sustainable settlements and therefore there is a need to recognize all possibilities in order to assure achieving this goal. Regarding possibilities for an adequate land use planning some of the recognized strategies for shaping sustainable settlements are therefore in the field of assuring appropriate housing areas for inhabitants, of shaping suitable recreation parks, of generating adequate transportation infrastructure, including road and highway traffic, as well as railway services. Another important direction in getting sustainable settlements is represented by the possibility of shaping pedestrian zones in cities or villages as well as outside them, in order to place emphasis on walking alternatives instead of travelling by car in such inhabited regions [14].

Considering urban areas, sustainable urbanism does represent a pretty new development direction combining the creation and enhancement of pedestrian zones in the city with the need to build high-performance infrastructure and buildings. This is a new modern approach trying to integrate into the city infrastructure also pedestrian zones or bicycle paths as transportation systems along with high performance green buildings into the current developments and ongoing plans. In order to try transforming a city into a sustainable one, several local policies can be used, as mentioned below:

- Increasing sustainability through social and cultural activities;
- Integrating transportation and land use in an efficient manner;
- Creating sustainable neighborhoods with walk-to-work neighborhood centers of locally-owned businesses;
- Creating possibilities of car-sharing on every block;
- Shaping walkable neighborhoods.

In the last time it came out that sustainable urbanism is among the most critically issues of the 21st century. It is estimated that over 50% of the world's population now lives in urban areas. Some developed scenarios for the future urban development estimate that by 2050 the proportion of the global population living in cities will rise to 70%. In this regard it is self-evident the importance of an efficient land use planning, administration and management, connected with a proper land tenure promotion, as being the general term used for urban planning containing various disciplines. The idea is to order and regulate land use on the base of clear land tenure in an efficient and ethical way, thus preventing land use conflicts [2]. Land tenure is appropriate to manage the development of land use within its jurisdiction and is actually the base for further developments in this field. In doing so, the needs of a community can be assured while safeguarding natural resources [2]. To this end, it is the systematic assessment of land and water potential, alternatives for land use, and economic and social conditions in order to select and adopt the best land use options.

In this context the current and long-term availability of water should be treated as the vital starting point of any land use planning and decision based on the promotion of land tenure. Preserving sustainable water sources has to be an important point in the community planning, because it must include the provision and protection of local water supply [6].

The comprehensive program regarding the land use plan based on land tenure provides a vision for the future possibilities of development regarding achieving sustainable settlements. Gaining sustainable strategies on local level means actually developing strategies for the rural or urban sustainability. The vision of shaping in the future sustainable settlements, cities or villages is worldwide a pretty discussed topic, also in some Eastern European countries, by taking into account regional differences [16].

Conclusions

For assuring the local sustainability in the form of shaping sustainable human settlements an appropriate sustainable land use planning, administration and management on a local level is necessary to be carried out, where the role of a proper land tenure promotion is very important. The advantages of a proper land use planning based on an adequate land tenure promotion, beside land administration and management have to be used by the local decision makers in order to take the best decisions for assuring the sustainability of rural and urban development. As a conclusion, in the made presentation it has been emphasized that some of the recognized strategies regarding the land use planning based on land tenure promotion for shaping sustainable settlements are therefore in the field of assuring appropriate housing areas for city inhabitants, suitable recreation parks, generating adequate transportation infrastructure, including road and highway traffic, railway service, as well as bicycle paths. Decoupling, as a strategy for getting local sustainability on urban and rural level has to be completed by the land tenure promotion in order to assure the population support for a high quality land use

planning, administration and management. Another relevant goal in order to achieve the local sustainability is represented by shaping pedestrian zones inside the human settlements as well as outside these settlements. Rural and urban sustainability does represent a pretty new development direction combining the creation and enhancement of pedestrian zones in the human settlements with the need to build high-performance infrastructure and buildings. This is a new modern approach trying to integrate technical aspects, with economic, environmental, social and cultural ones. On the other side there is a need to take the responsibilities for inappropriate land tenure promotion and land use planning, because this can really compromise the idea of shaping sustainable human settlements.

References

[1] Banse, G., Nelson, G., Parodi, O. (Eds.) (2011). Sustainable Development - The Cultural Perspective. Edition Sigma, Berlin.

[2] City Council (2011). Sustainable Development Strategy of the Alba Region AIDA. Alba Municipality, Romania.

[3] Dragomir, P. I., Rus, T. (). Projects of The National Agency for Cadastre and Land Registry in the field of geodesy, http://www.rompos.ro/

[4] Enemark, S. (2007). Integrated Land-Use Management for Sustainable Development. International Federation of Surveyors, Copenhagen.

[5] Hauff V. (Ed) (1987). Our Common Future. The Brundtland Report of the World Commission on Environment and Development. Oxford Univ. Press, Oxford.

[6] Jischa, M. F. (2005). Herausforderung Zukunft, second edition, Elsevier, Spektrum Akademischer Verlag, Heidelberg.

[7] Ministry for Regional Development and Public Administration (2014). Strategia de dezvoltare teritorială a României – Studii de fundamentare (Romanian Land Development Strategy – Foundation Studies). http://www.sdtr.ro/ .

[8] Morosanu, B. (2007). Relative linear deformation in projection systems Stereographic 1970, Gauss-Kruger, UTM and comparison between them, http://www.geo-spatial.org/

[9] National Agency for Cadastre and Land Registry (2016). Documentation for training system E-Terra 3, http://www.ancpi.ro/

[10] Palamariu, M., Tulbure, I. (2016), Land Use Planning Strategies for Shaping a Sustainable City. In: Proceedings of the 16th International Multidisciplinary Scientific Geoconference SGEM2016, 28.06.-07.07.2016, Book3, Vol. I, "Geodesy and Cartography", pag.: 317-322, Albena, Bulgaria.

[11] Parodi, O., Banse, G., Schaffer, A. (Ed.) (2010), Wechselspiele: Kultur und Nachhaltigkeit. Annäherungen an ein Spannungsfeld. Edition Sigma, Berlin.

[12] Salvador Rueda Palenzuela (Ed), (2012). The Green Book on Urban and Local Sustainability in the Information Age. Ministry of Agriculture, Food and Environment and the Urban Ecology Agency of Barcelona, Madrid, Spain.

[13] Săvoiu I., Land Administration Domain Model: opportunities for enhancing systematic registration in Romania, RevCAD 15/2015, pp. 147-161, Romania.

[14] Tulbure, I., Palamariu, M. (2010). Environmental Assessment of Some Mining based Industrial Activities. In: Proceedings of the 10th International Multidisciplinary Scientific Geoconference SGEM2010, 20-26.06.2010, Vol. 2, pp. 237-244, Albena, Bulgaria.

[15] Tulbure I. (2013). Technology Assessment. Lecture Notes. Course at the Clausthal University of Technology. Clausthal-Zellerfeld, Germany.

[16] Tulbure, I. (2014). Sustainable City in Romania – from Vision to Reality. Proceedings of the Conference "Sustainability 2014: Future Urban Development at Different Scales", 05. - 09.05.2014, Karlsruhe, Germany.

[17] Tulbure, I. (2016). Local Sustainability Implementing Strategies. In: Proceedings of the 16th International Multidisciplinary Scientific Geoconference, SGEM2016, 30.06.-06.07.2016, Book6, Vol.II, "Green Building Technologies&Materials", pp. 621-628, Albena, Bulgaria.

[18] United Nations Food and Agriculture Organization (2015). Land tenure supports sustainable development, http://www.fao.org/home/en/

GIS in Active Monitoring of Green Spaces

Păunescu V.[1], Călin M.[1], Manea R.[1], Moscovici A.[2], Sălăgean T.[3]

[1] *University of Agronomic Sciences and Veterinary Medicine Bucharest (ROMANIA)*
[2] *University Politechnica Timisoara (ROMANIA)*
[3] *University of Agricultural Sciences and Veterinary Medicine Cluj-Napoca (ROMANIA)*
E-mail: tudor.salagean@usamvcluj.ro

Abstract

It application for green cadastre has emerged as a necessity of expanding and detailing the urban cadastre, its object being vegetation, with a dynamics of growth and development, respectively a structural change very well defined in time. The geographic information system for achieving green cadastre requires a recovery, at least periodically, to capture all the structural changes which determine the overall functionality. At national level spatial data exchange is necessary in order to avoid additional costs of generating and managing information and their integration into other databases.

Keywords: database, GIS, green cadastre.

Introduction

Green cadastre has emerged as a necessity of expanding the urban cadastre, especially for green spaces like parks, promenades etc. Using IT applications for cadastre is beneficial because it enables better data management.

The general arrangement of the territory in urban areas should ensure the coordination of multiple interests that relate to the same territory and rational use of resources to ensure its harmonious development.

Therefore is justified the need for a set of geographic data to improve the management of trees and land which has green spaces destination, aimed mainly at identifying the characteristics and condition of existing trees in the city.

Inventorization, care and management of green spaces can be complicated by the natural and social factors: insects and diseases, fire, natural events such as ice storms and wind [1]. Green spaces can contribute in direct and indirect ways for CO_2 reduction in the atmosphere, can reduce the temperature, contributing to lower pollution, water runoff and soil erosion, providing a place for recreation, education and learning [2].

Green spaces are an essential element of the human habitat. The range of green spaces is very wide, taking into account two main categories: green spaces outside the city and green spaces in the city (or urban green spaces). The term green space is entered in Law no. 24 from 15 January 2007 (Law on the regulation and management of urban green spaces) as a green area in the towns and cities, defined as a network mosaic or a system of seminatural ecosystems, whose specific is determined by vegetation (wood, tree, shrub, flowery and herbaceous) [3].

A more recent definition is: Green space is the surface with vegetation where at least 25 percent of the area is covered with perennials or any area with three or more trees where their crown of foliage provides cover at least 20 percent of area [4]. Another important feature is the identification of land bound for green spaces, currently occupied or not with green spaces, respectively the land which is degraded and that can be arranged with green spaces in the future.

It aims to automatically generate alerts and reports when, due to the development of the crown circumference and height, the trees fall on a collision course with other urban targets (aerial networks for utilities and telecommunications, road signs, traffic lights etc), based on algorithms which take into account annual growth rate of each species of tree.

Materials and Methods

In some countries, the parameters related to a single tree are used as the basis for inventory green spaces, for example: tree species, average height of a tree or volume of timber. In most countries almost all of these variables are collected manually by measuring each tree, field surveys, thus with high costs on a fairly large period of time [5].

As final products will be: the GIS digital map, the green spaces database, the list of specific classifications and the tools necessary to the operation and maintenance of the related data collections.

By making the local registry of green spaces is aimed the inventory and transposition of all green spaces and tree species from Bucharest in GIS format.

According to Mintas H. (2013), the local register of green spaces was introduced by Law No 24/2007 and represents a complex documentation regarding the track of green spaces throughout the Bucharest city, established as a GIS type information system [6].

The Association Cornel & Cornel Topoexim (2013) states that the Local Register of green areas is a result of work measurement, identification, inventory and mapping of land defined as green areas and of collecting information specific to the species of trees and existing vegetation, to determine the qualitative and quantitative indicators [7].

The difference from other databases constructed for this purpose in other projects of this kind, is the number of attributes collected and a series of extra fields. This database is not only a listing and positioning of trees with few features, but a complete base capable of generating complex analyzes made in spatial context.

If until recently the trend for database was to have specific applications for different situations or goals, we see increasingly the trend to generate more information that we can easily integrate in different environments.

To identify all the elements from the database were achieved a photogrammetric fly which led to the achievement of an orthophotomap of Bucharest with a scale of 1:500. The database was made in ArcGIS, specifically in ArcCatalog.

Were created object classes as follows: the road axis, the axis for public transport, boundaries, buildings, degraded lands, street furniture, green spaces, maps, elements of the map, comments, zip code, power lines, roads, trees, water (Fig. 1).

The attributes were collected on field and placed in application and then migrated to the corresponding database fields (Fig. 2). The fields are numerous and vary according to the characteristics of the objects. For trees we have different fields such as: species, age, class vitality, height, trunk diameter, canopy diameter, street, planting year, the level of maintenance, administrative limit and comments.

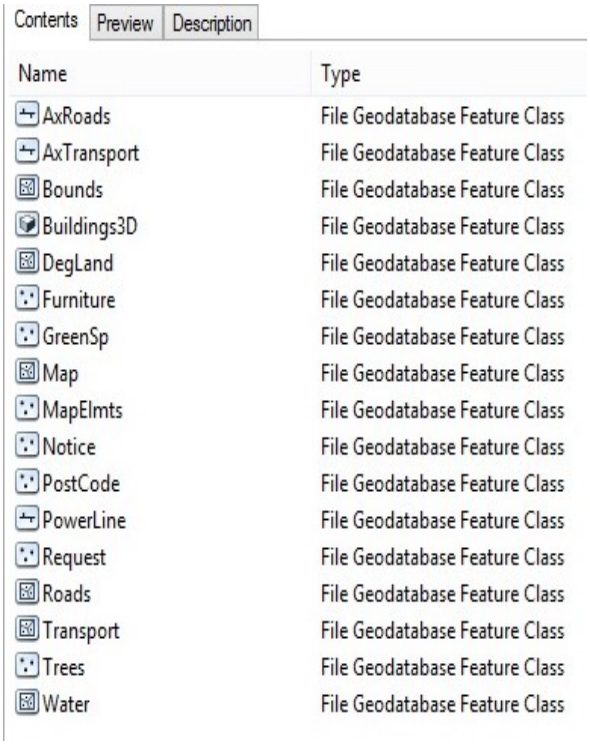

Fig. 1 Object classes

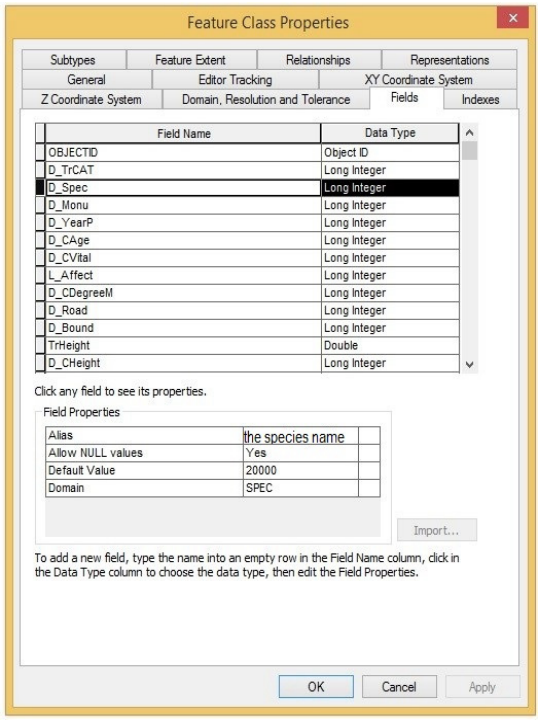

Fig. 2 Fields of the database

The database architecture was designed so that there are relationships between tables, making a logical model for query options (Fig. 3). The primary key is the electronic indicators specific for each attribute. For ease of insertion, a number of attributes are encoded with numerical identifiers.

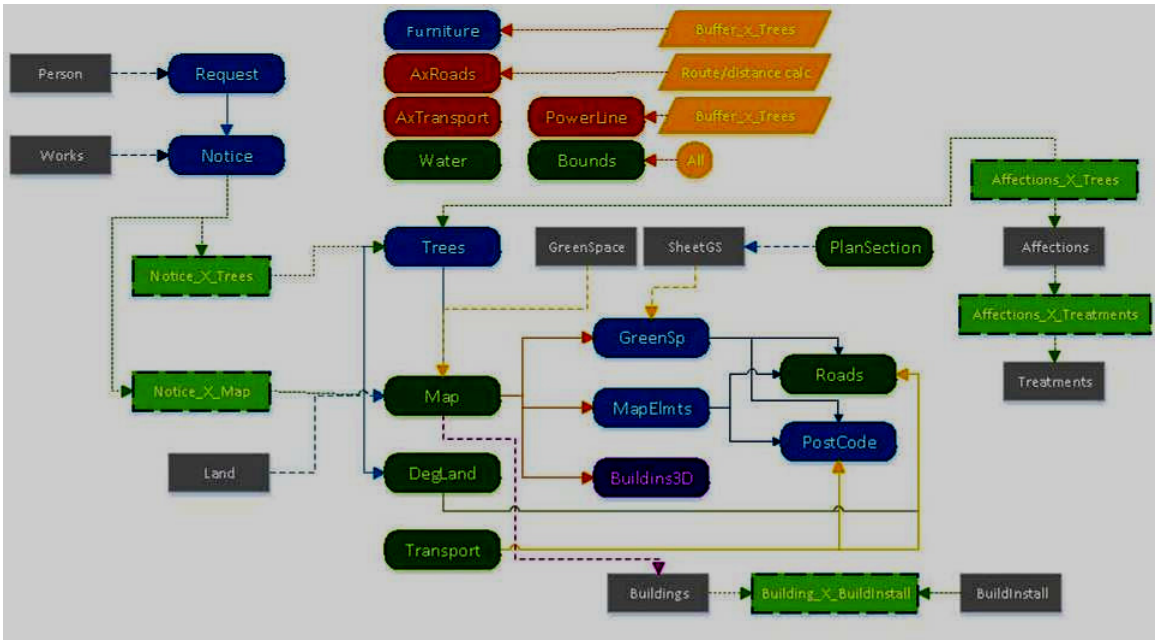

Fig. 3 The database architecture

Results and Discussions

In this paper are detailed the features of embodiment of local registry of green spaces, the inventory and transposition in GIS format of green spaces and tree species existing in Bucharest, identify problems and fix them so in 2020 to reach the current average level of the cities from European Union in terms of key indicators of sustainable development.

In GIS, object attributes are stored in the attribute table. Selecting the subject, we can view the information arranged in fields described above (Fig. 4).

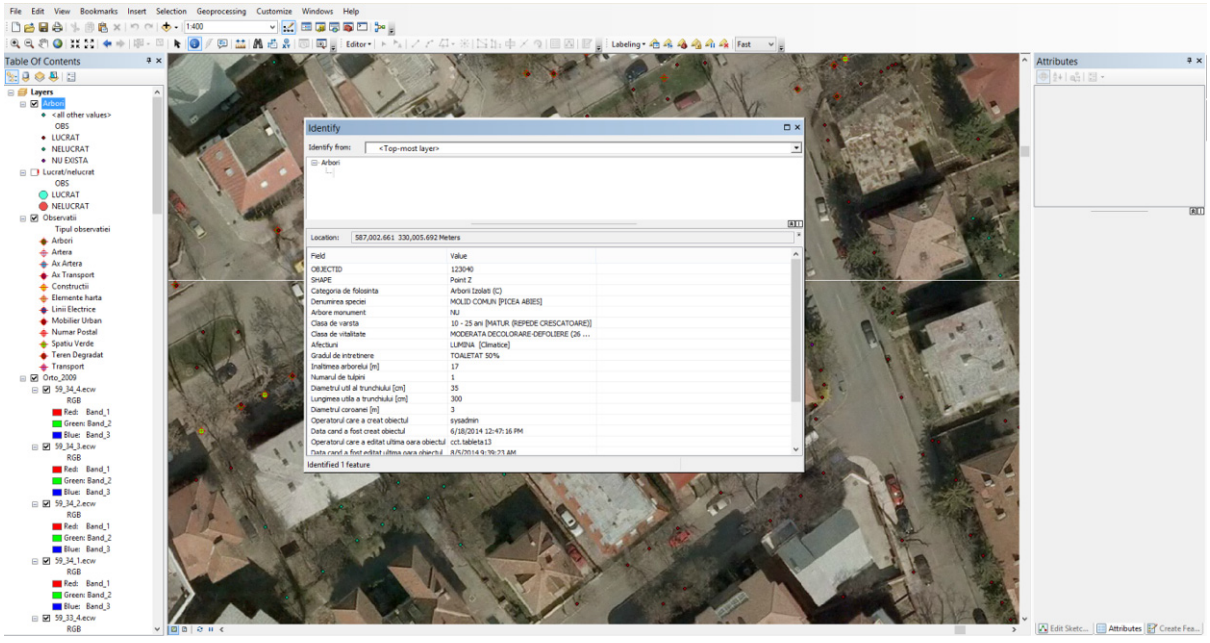

Fig. 4 Visualizing the trees attributes in GIS

Any Geographical Information System must be capable of performing a number of specific operations (Fig. 5). Queries use relationships between tables by accessing data from various fields after some selection criteria. For example if we want to select all the trees which are declared monument that are found in the database and are completely dry.

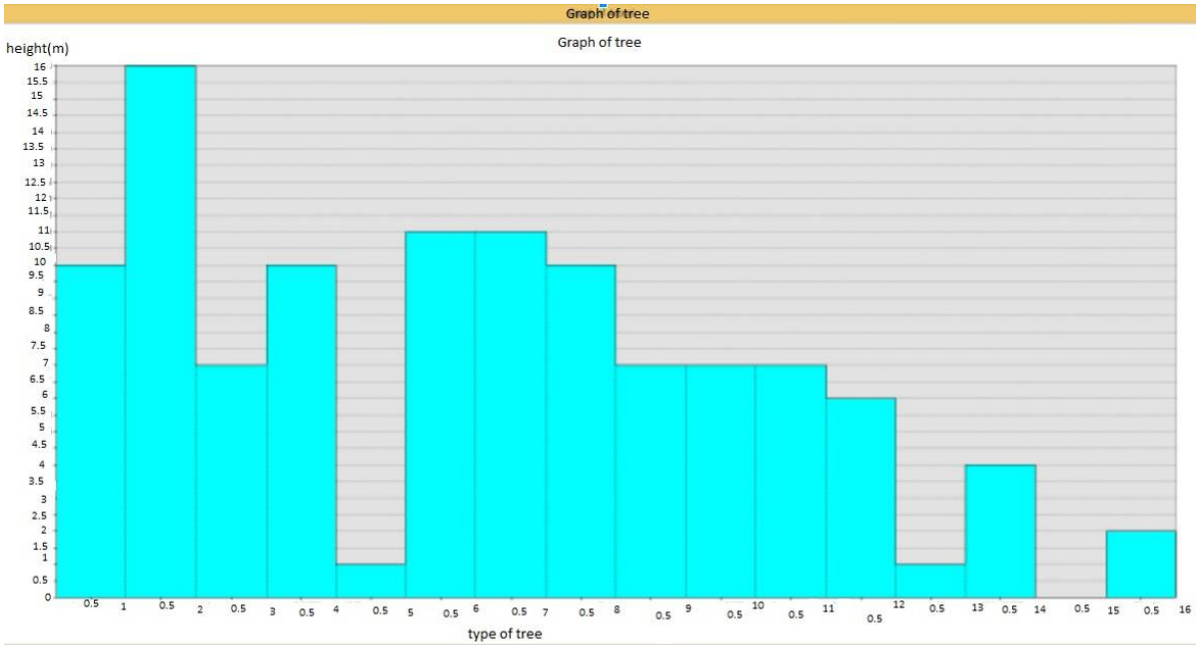

Fig. 5 Specific operations of a GIS (trees height histogram)

Another quality of a Geographic Information System is that it must be able to generate reports. Their complexity is defined by the attributes you want visualize. We can, for example, generate a report that gives us information about: use category, monument trees, diseases, level of maintenance, tree canopy diameter. Also for needs analysis and visualization can make a series of graphs. We can achieve such heights histograms to view trees from the database (Fig. 5). The heights histogram was a specific demand by the Bucharest City Hall.

Based on the collected attributes was carried out the application for the local register of green spaces in GIS (Fig. 6, 7).

Fig. 6 Visualizing in GIS

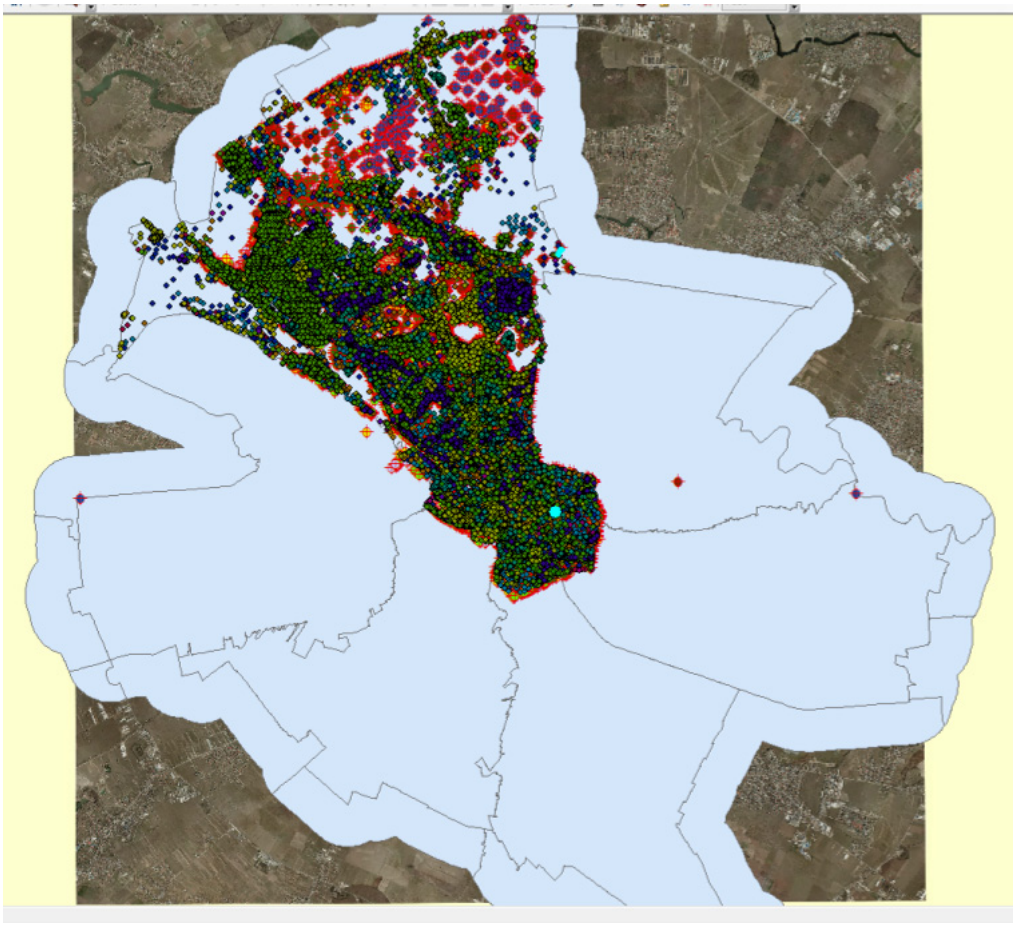

Fig. 7 The stage of the project at the time of interruption

It may achieve a series of spatial queries (Fig. 8 a). Any system of this type must be able to achieve a number of spatial queries such as trees situated at a distance from the street or in a given artery (Fig. 8b).

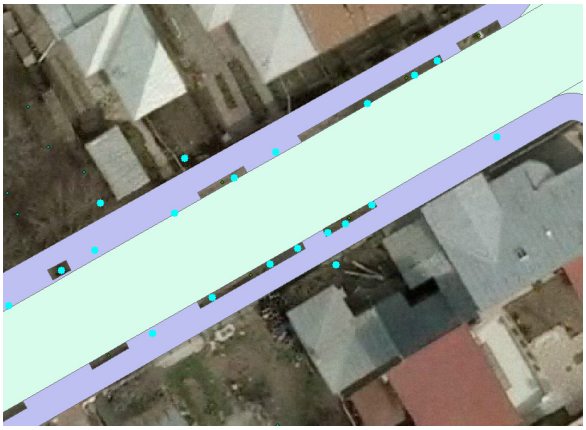

a - The trees which are near a street

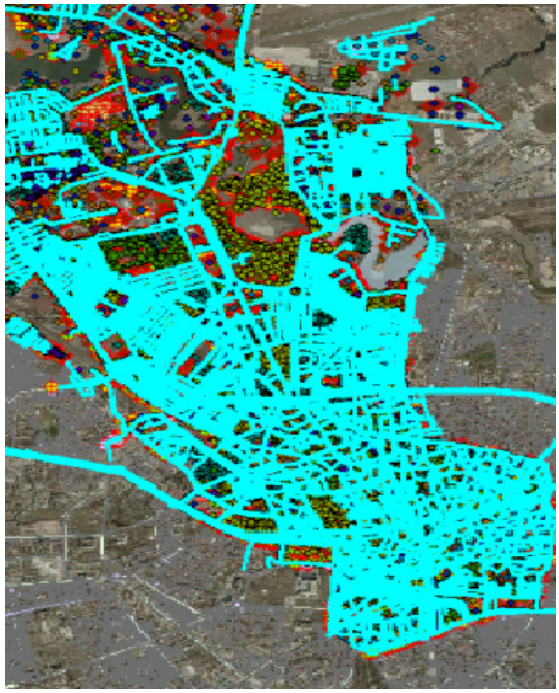

b - Arteries containing trees

Fig. 8 Selections in ArcGIS

Conclusions

The presented study doesn't refer just to trees and green spaces. It is a construction that not only provide information regarding the placement of objects and its features, but also provides a complete picture of the situation by considering all objects in connection with the project aim.

By introducing into the database the attributes related to street furniture, electrical lines, degraded lands or waterways, it gives important information on road infrastructure. Therefore the database is not a simple list of attributes related to green spaces and trees, but becomes a tool for analysis and management of existing green fund in Bucharest.

The software application is meant, in addition to providing an accurate knowledge of the entire vegetal fund of a city, to contribute to a better maintenance, management and development of green spaces because we are facing a large element of dynamism. Also the software application assists the decision-making process for planning urban parks, development zones, proper selection of trees etc., to quantify the impact on the climate [8].

The geographic information system for achieving green cadastre requires a recovery, at least periodically, to capture all the structural changes which determine the overall functionality.

The idea to connect all databases under the INSPIRE Directive aims at bringing a unified system of space data that are under the authority of the Member States from the European Union [9].

At national level spatial data exchange is necessary in order to avoid additional costs of generating and managing information and their integration into other databases.

Thereby eliminating the redundancy is desired so that the information collected can be used for various applications. The application for local register of green spaces collects a variety of different attributes of objects in connection with the main object of the paper, green spaces. This information will be integrated into adjacent applications for different purposes.

References

[1]. Nowak, D. J., Stein, S. M., Randler, P. B., Greenfield, E. J., Comas, S. J., Carr, M. A., & Alig, R. J. (2010). *Sustaining America's urban trees and forests* (Vol. 62). United States Department of Agriculture, Forest Service, Northern Research Station.

[2]. Tasoulas, E., Varras, G., Tsirogiannis, I., & Myriounis, C. (2013). Development of a GIS application for urban forestry management planning. *Procedia Technology*, *8*, 70-80.

[3]. Law 24/2007 updated and republished. The law regarding the regulation and management of green spaces in urban area, republished in Official Gazette No. 764 from 10.11.2009.

[4]. Assessment, M. S. (2016). Vegetation Inventory Report: Truganina Cemetery Grassland. State of Victoria.

[5]. Schmitt, M., Shahzad, M., & Zhu, X. X. (2015). Reconstruction of individual trees from multi-aspect TomoSAR data. *Remote Sensing of Environment*, *165*, 175-185.

[6]. Mintas Horia (2013). Specifications concerning the award of contract services covering inventory and updating of the register of private green spaces from Bucharest according to Law No 24/2007 and MDRT Order 1466/2010.

[7]. Cornel&Cornel Topoexim Association (2013). Technical proposal. Inventory of private green spaces and updating the green spaces register of Bucharest.

[8]. Varras, G., Andreopoulou, Z., Tasoulas, E., Papadimas, C., Tsirogiannis, I., Myriounis, C., & Koliouska, C. (2016). Multi-Purpose Internet-Based Information System 'Urban': Urban Tree Database and Climate Impact Evaluation. *Journal of Environmental Protection and Ecology*, *17*(1), 380-386.

[9]. Svedin, U. (2015). Urban Development and the Environmental Challenges—"Green" Systems Considerations for the EU. In *Sustainable Development, Knowledge Society and Smart Future Manufacturing Technologies* (pp. 81-112). Springer International Publishing.

Modern Methods and Techniques for Data Acquisition in Order to Obtain Photogrammetric Products Used in the Aeronautical Field

Plăvicheanu S.[1], Nache F.[2], Dragomir P.I.[3]

[1] *PhD. Student, Eng., Technical University of Civil Engineering of Bucharest, Faculty of Geodesy, (ROMANIA)*
[2] *PhD. Student, Eng., University of Bucharest, Faculty of Geology and Geophysics, Romania*
[3] *Prof. PhD. Eng., Technical University of Civil Engineering of Bucharest, Faculty of Geodesy, (ROMANIA)*
E-mails: sabina.plavicheanu@yahoo.com, nacheflorin@yahoo.ro, petreiuliu.dragomir@gmail.com

Abstract

The main aim of this study is to provide an overview of the research, aspects and analysis regarding geodetic works for airport infrastructure, using modern techniques for data acquisition and comparing the resulting products. Using aerial photogrammetry and considering the aeronautical data quality requirements, high resolution products are obtained, such as three-dimensional digital models, digital terrain model based on correlated point cloud or LiDAR point cloud and orthophoto.

Keywords: UAV, aerial photogrammetry, DSM/DTM, aeronautical survey, aeronautical data.

1 Introduction

Baia Mare International Airport, located in Tăuţii Măgherăuş, Maramureş County, Romania, is going through a comprehensive modernization process which involves extending the take-off-landing runway and improving the pavement surface, leading thus to raising the air traffic's level of safety. For the purpose of extending the take-off-landing runway with 360 m to the west extremity in the direction of the threshold 10, it was considered changing natural limits, by diverting the course of Băiţa River and also the communal road DC 97 and reconfiguration of the technological perimeter road. At the same time, works were carried out for existing land consolidation and the extension of the runway required the expropriation of urban land in Tăuţii Măgherăuş locality, afferent to the aeronautical lighting system of the pavement surface [1]. The requirements for geodetic works in aeronautical field concern the accuracy, integrity and resolution for collected aeronautical data and information [2]. Aeronautical studies conducted in accordance with ICAO and EUROCONTROL requirements for attaining aeronautical charts, electronic terrain and obstacle aerodrome mapping, lead to maintaining safety in air space and on the ground. In this regard, the obstacle clearance requirements are met, by determining the complex, virtual surfaces, described above the terrain, in vertical plane, designed from the edges of the runway's strip, surfaces that must not be intersected by any fixed obstacle in the underlying area. In urban areas, classic measurements for determining the horizontal position, elevation and height for all objects in the area of interest would be an arduous and expensive process. Thus, there is a more efficient option, faster and with a lower price, the modern methods and techniques for data acquisition to describe virtual reality in a 3D space [3, 4]. Using aerial images taken with UAV systems, three-dimensional digital models are generated: Digital Terrain Model (DTM) and Digital Surface Model (DSM), which can be used to determine the areas where the terrain may obstruct the safety of air traffic and also the obstacles penetrating the areas described above [5].

2 Methodology

Spatial data quality depends mainly on the acquisition methods, for those errors will be propagated and amplified by processing. Spatial data required for performing an aeronautical study are obtained through a combination of field measurements and photogrammetric studies. A special attention is given to capturing and identifying objects with a small diameter [4] (antennas, poles) that are projected above the Obstacle Limitation Surfaces (OLS), which shall be defined according to the aerodrome's category. Thus, the photogrammetric flight must be conducted at a lower altitude, in order to achieve a high spatial accuracy. It is proved that rational

planning of the photogrammetric flight is essential for achieving the exterior orientation of the images and obtaining high quality photogrammetric products. The pixel size is the dominant factor in choosing flight parameters, in order to ensure the fulfilment of technical requirements.

2.1 Data acquisition

The first step in collecting the spatial data consists in establishing the ground control points and marking them in the field with weatherproof paint and plastic targets. So that the minimum requirements regarding the accuracy are met [2], ground control points must be determined with a horizontal accuracy ±10cm and with a vertical accuracy ±5cm. Also, the same minimum requirements concern connecting the control network to WGS84 reference system, with a minimum accuracy ±10cm.

The area of interest has coverage of 248 ha. To have an optimum density of ground control points, for obtaining the final photogrammetric products, the orthophoto image, Digital Terrain Model and Digital Surface Model, 43 ground control points were marked, three of which were selected as check points (Fig. 1). Ground control points' position has been determined using GNSS technology, RTK method, using base-rover system.

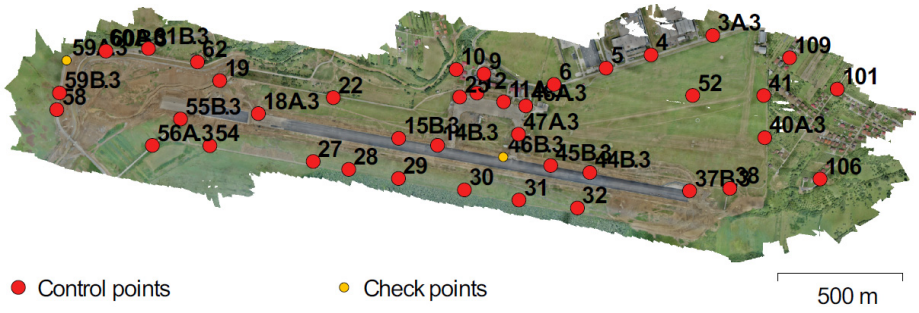

Fig. 1 Ground control points distribution

After pre-marking ground control points in the field, the flight mission is planned, using Mission Planner software, for which shall be set:

- The coverage area;
- The sensor type used for acquiring images (DSC-RX100M2 4864x3648 pix), flight height (80 m) and the focal length of the lens (10.4mm), in order to estimate the ground resolution (1.89 cm/pix);
- Longitudinal overlap (80%) of images within a strip and sidelap (60%) of images between two strips;
- The orientation of flying paths (270 °);
- Flying speed (12 m/s).

The flight mission is transmitted to the U.A.V system's control unit, XFL-X9 model, through radio connection provided by telemetry. Monitoring and flight control is accomplished using the ground control station, consisting of a laptop where Mission Planner is installed, telemetry antenna, O.S.D. (On Screen Display) monitor and radio transmitter. As a result of the flight mission, within a period of time of 3h, 3279 images have been taken, for which the estimated coordinates of the perspective centers shall not be used due to the airborne G.P.S.'s poor accuracy (±1-2 m).

2.2 Data processing

The acquired data, 3279 images and coordinates for 43 ground control points defined in S-42 datum, Stereographic 1970 projection and Black Sea 1975 vertical reference system, will be inserted in Agisoft PhotoScan software.

In order to obtain the orthophoto, the following processing steps were carried out:

- Aligning images, as a result, interior orientation parameters are obtained, relative coordinates for perspective centers and tie point cloud (Fig. 2) between images (2.895.529 points).
- Placing the markers on images and establishing control points and check points.

The control points make the connection between the image model and the terrain model. Ground control points' accuracy is shown in Table 1.

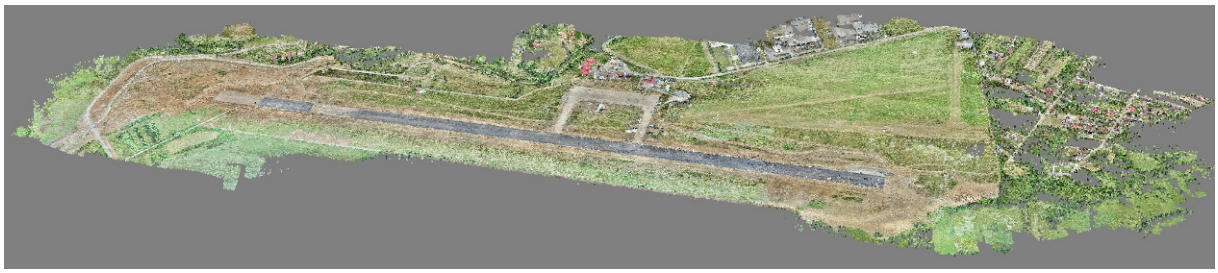

Fig. 2 Tie point cloud

Table 1 Ground control points' accuracy

Name	ΔX (cm)	ΔY (cm)	ΔZ (cm)	RMSE (cm)	Marking error (pix)
10	3.27	-3.69	0.33	4.94	0.5
101	1.96	0.46	1.33	2.41	0.45
106	3.35	0.58	1.46	3.7	0.78
109	0.79	-0.39	1.26	1.54	0.23
11A.3	-0.86	1.67	1.03	2.14	0.42
12	2.37	1.41	-0.33	2.78	0.51
14B.3	0.03	0.55	0.16	0.58	0.59
15B.3	-1.14	2.67	0.78	3.01	0.51
18A.3	-0.48	1.49	4.04	4.34	0.52
19	2.13	0.53	-2.39	3.25	0.67
22	-0.9	1.63	-4.44	4.81	0.38
25	1.33	-0.59	0.28	1.48	0.57
27	2.92	0.73	-1.94	3.58	0.48
28	2.02	-0.65	-0.68	2.23	0.37
29	0.07	-1.76	-0.34	1.79	0.37
30	0.74	-0.53	-0.55	1.07	0.23
31	0.21	0.57	-1	1.17	0.28
32	4.31	4.46	-0.53	11.32	0.5
37B.3	-4.57	-3.7	5.55	16.97	0.45
38	2.04	-4.04	-6.37	14.66	0.82
3A.3	3.43	0.52	-0.53	3.51	0.18

Name	ΔX (cm)	ΔY (cm)	ΔZ (cm)	RMSE (cm)	Marking error (pix)
4	-2.15	4.2	-1.91	5.1	0.47
40A.3	2.47	-3.06	0.86	4.02	0.13
41	0.86	3.38	1.91	3.97	0.11
44B.3	-6.3	4.16	0.89	7.6	0.24
45B.3	-0.93	3.93	-0.43	4.06	0.42
47A.3	0.88	0.4	3.42	3.56	0.42
48A.3	2.24	-0.39	0.9	2.45	0.54
5	-1.01	-1.76	3.47	4.02	0.64
52	-3.15	-0.14	-6.45	7.18	0.66
54	-0.6	0.82	-1.96	2.21	0.76
55B.3	-1.65	-4.03	4.55	6.3	0.67
56A.3	-0.86	-4.67	1.82	5.09	0.58
58	-0.95	-1.33	-7.97	8.14	0.53
59B.3	-0.6	0.73	2.97	3.12	0.24
6	-2.74	1.09	-1.77	3.44	0.47
60B.3	0.81	0.31	1.99	2.17	0.63
61B.3	1.65	-3.49	-1.56	4.16	0.5
62	-0.77	1.29	3.18	3.52	0.44
9	-0.05	1.8	0.15	1.81	0.29
Total	3.11	3.52	2.84	5.49	0.49

The check points indicate the accuracy of the final model and need to be distributed evenly within the areas of interest, but not on a narrow area. Check points' accuracy is shown in Table 2.

➢ Optimizing images alignment (aerotriangulation), achieving exterior orientation parameters, constraint made through indirect georeferencing since only the ground control points were used.

Table 2 Check points' accuracy

Name	ΔX (cm)	ΔY (cm)	ΔZ (cm)	RMSE (cm)	Marking error (pix)
46B.3	0.40	2.68	-0.77	2.82	0.26
59A.3	-2.06	-3.06	-7.96	8.77	0.51
60A.3	5.06	1.23	-0.45	5.23	0.35
Total	3.16	2.45	4.62	6.12	0.41

➢ Generating the correlated point cloud; by correlation, a set of spatial coordinates is determined for each pixel, therefore, obtaining the cloud with a number of 505.143.426 points (Fig. 3).

Fig. 3 Correlated point cloud

➢ Generating the Digital Surface Model, used as reference area for draping the image model (Fig. 4). The Digital Surface Model (DSM) is an elevation model, describing the earth surface, including the tops of vegetation, buildings, powerlines or any other objects.

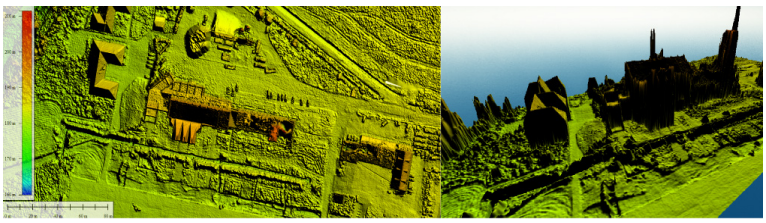

Fig. 4 Digital Surface Model

➢ Generating orthomosaic and seam line editing.
➢ Generating orthophoto (Fig. 5).

Fig. 5 Orthophoto

➢ Correlated point cloud classification, using unsupervised classification for terrain class and supervised classification, class of points on the basis of which the Digital Terrain Model is generated (Fig. 6).

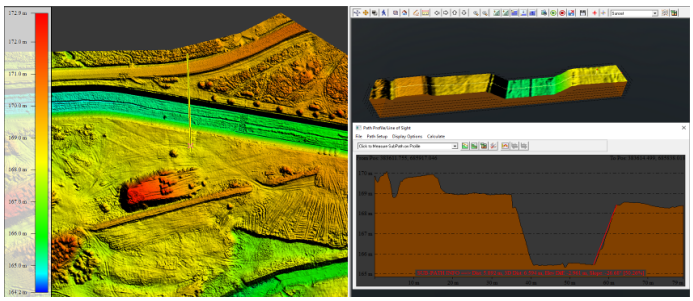

Fig. 6 Digital Terrain Model - diverting the course of Băiţa river

2.3 Comparative analysis

2.3.1 Orthophoto accuracy verification

For orthophoto verification, planimetric coordinates for 48 offshoot points were used, determined using GNSS technology, RTK method, the base-rover system. Analyzing the results, orthophoto with the surveyed points, a total error of ±3 cm has been estimated (Table 3). In addition to the orthophoto's accuracy, the radiometric accuracy and its geometry are also verified, by eliminating geometric and tonal differences at the seam line boundaries or the distortion of certain elevated planimetric elements in relation to the ground level.

Table 3 Orthophoto's accuracy

Name	X (m)	Y (m)	ΔX (cm)	ΔY (cm)	Name	X (m)	Y (m)	ΔX (cm)	ΔY (cm)
Pole	686312.960	382705.890	2.2	3.5	Antenna	685974.300	386092.900	1.2	-2.9
Pole	685638.390	382144.500	3.2	1.7	Building	685903.970	386073.730	2.7	-3.7
Building	685618.970	382170.340	3.1	3.4	Control_Tower	685749.560	385018.700	0.9	-1.6
Wind_sock	685617.010	385828.250	2.9	2.9	Pole	685743.640	384928.250	2.9	-2.5
Wind_sock	685697.200	384212.550	2.2	3	Pole	685347.220	387500.260	2.1	-2.6
Pole	685728.490	385004.390	3.5	4	Pole	685305.640	387487.720	1	-2.1
Lightning_rod	685716.460	385114.040	1.6	-3.8	Fence	685291.380	387500.300	1.2	-2.4
Building	685694.200	385152.660	1	-1.3	Pole	685292.780	387503.610	2.4	-2.1
Building	685694.200	385152.660	1.1	2.5	Pole	685227.570	387486.810	4	4.4
Building	685667.770	385207.140	3.7	-5	Pole	685204.720	387498.630	1.6	-2.1
Building	685895.100	385537.170	2.4	-3.4	Pole	685157.170	387527.400	2	2.9
Building	685856.450	385549.450	0.9	2.3	Pole	685043.930	387473.620	1.4	-2.7
Fence	685854.550	385537.500	1.1	-2.2	Building	685308.170	387537.960	2.2	-2.5
Building	685887.670	385640.920	2.7	2.9	Building	685828.730	384874.510	2.2	2.9
Fence	685912.830	385724.030	0.8	-2.6	Pole	686312.960	382705.890	1.3	4.5
Building	685950.300	385839.280	2.3	-2.2	Pole	685644.950	382120.770	1.7	1.9
Pole	686041.430	386085.860	4.2	-3.2	Pole	685595.460	382186.500	4.1	3.6
Building	686018.330	386102.020	0.7	-3	Building	685592.220	382186.940	2.7	5.6
Building	685974.300	386092.900	4.4	-1.6	Antenna	685996.550	385778.820	3.1	2.8
					Total			2.3	3

2.3.2 Digital Terrain Model (DTM) and Digital Surface Model (DSM) accuracy verification

Digital Terrain Model and Digital Surface Model verification was achieved using the spatial coordinates of 40 points, which had been surveyed with the total station, whilst the coordinates of support points have been determined using GNSS technology, static. The results obtained by comparing the digital models with measured points, have a vertical accuracy of ± 7 cm (Table 4).

Table 4 DTM/DSM's accuracy

Name	X (m)	Y (m)	Z (m)	ΔZ (cm)	Name	X (m)	Y (m)	Z (m)	ΔZ (cm)
Elevation_point1	685724.870	383484.960	167.22	-6.3	Building	685737.450	384790.180	179.49	-7.3
Elevation_point2	685714.160	383545.230	167.98	-7.1	Elevation_point11	685187.870	385762.020	177.50	5.2
Elevation_point3	685703.560	383604.890	168.80	-8.5	Elevation_point12	685407.710	385900.290	185.37	-6.6
Elevation_point4	685724.870	383484.960	167.22	5.9	Elevation_point13	685194.340	385592.960	178.17	-8.9
Elevation_point5	685714.160	383545.230	167.98	-8.1	Elevation_point14	685241.230	385597.580	181.50	-7.1
Elevation_point6	685703.560	383604.890	168.80	-7.3	Road	685350.540	387497.810	186.50	-5.4
Elevation_point7	685765.490	383259.920	166.32	-7.5	Pole	685697.348	385106.267	183.35	-7.9
Elevation_point8	685742.510	383427.220	167.51	-6.1	Pole	685707.694	385043.808	182.30	-6.8
Elevation_point9	685723.490	383423.900	168.99	5.5	Pole	685719.885	384972.019	182.11	4.9
Elevation_point10	685775.530	383204.740	166.04	-8.2	Pole	685678.132	385177.270	183.68	-7.5
					Total				6.9

3 Results and discussions

As a result of data acquisition and obtaining the photogrammetric products, Electronic Terrain and Obstacle Database (eTOD) is implemented, which incorporates sets of data relating to the terrain and the obstacles. The terrain datasets enclose a grid of points, the bare-earth model containing elevations of natural terrain features, excluding vegetation or buildings. The obstacle datasets include the representation of fixed or mobile obstacles, by points, lines (antennas, poles) or polygons (buildings). Using the Digital Terrain Model (DTM) and the Digital Surface Model (DSM), 3D modelling can be done, offering the possibility to automatically determine obstacles penetrating the Obstacle Limitation Surfaces (OLS) around the airport (Fig. 7).

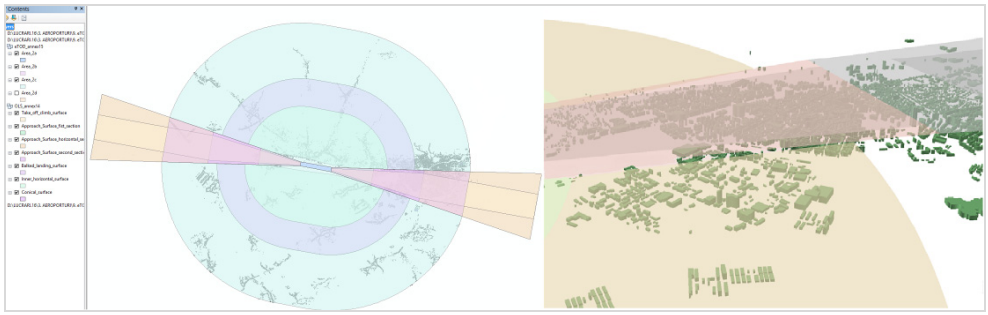

Fig. 7 Electronic and Terrain Obstacle Database (eTOD), Obstacle Limitation Surfaces (OLS)

4 Conclusions

In order to maintain the airspace free from obstacles, so as to allow operations to be conducted safely, data acquisition requirements are higher.

The primary objective of the study is locating with high accuracy the vertical objects which penetrate the obstacle limitation surfaces.

Thus, depending on the methods and techniques for data acquisition should be considered the individuality of geodetic works for airport infrastructure.

As a result of the study, the photogrammetric method is the most efficient method for acquiring spatial data considering the costs, the duration in relation to the area of interest, the accuracy of the measurements and the risk of leaving out obstacles. GNSS and classic determinations represent the ideal method for data validation.

This study reveals that certain thin objects such as antennas, poles, could not be detected.

In further studies, start from the premise that by modifying the configuration of the photogrammetric flight, either by reducing the flight altitude or increasing the number of scan lines or using a different data acquisition sensor, the purposes of the project can be achieved.

References

[1] Regia Autonomă Aeroportul Internaţional Baia Mare (2015). Caiet de sarcini pentru "Reactualizarea studiului de fezabilitate pentru investiţia Extindere şi modernizare suprafeţe aeroportuare la Aeroportul Internaţional Baia Mare" (Autonomous Regie Baia Mare International Airport (2015). Specifications for Updating the feasibility study for Expansion and modernization of airport surfaces investment for Baia Mare International Airport).

[2] European Organization for the Safety of Air Navigation (2012). EUROCONTROL Specification for the Origination of Aeronautical Data.

[3] Prado Molina, J., Quintero Pérez, J.A., Rosales Tapia, A.R., Peralta Higuera, A., Ramírez Beltrán, M.A., Zamora Jiménez, M. (2012). Elaboración de cartas aeronáuticas OACI: planos de obstáculos de aeródromo, a partir de imágenes aéreas digitales de pequeño formato, SciELO Analytics, *Investigaciones geográficas,* n.79, pp.75-96, ISSN 0188-4611.

[4] Parrish, C.E., Nowak, R.D. (2009). Improved Approach to Lidar Airport Obstruction Surveying Using Full Waveform Data, *Journal of Surveying Engineering,* Vol.135, No.2, pp.72-82, ISSN 1943-5428.

[5] Abdalla, R. (2004). Utilizing 3D web-based GIS for infrastructure protection and emergency preparedness, ISPRS Congress, Proceedings of Commission VII, Vol. XXXV, Istambul.

Individualization of Parcels and their Importance in Legal Relationships

Popoviciu G.A., Henţ E.I.

[1] *University of Oradea, Faculty of Civil Engineering, Cadastre and Architecture (ROMANIA)*
[2] *University of Oradea, Faculty of Environmental Protection (ROMANIA)*
E-mails: gpopoviciu@uoradea.ro , hentemanuela@yahoo.com

Abstract

Present paper try to shows the importance of the area of a parcel marked in cadastral documentation. This because the parcel is met mainly in the civil circuit, compared to other legal relations. A prime example is the name of the place or category of use. Thus, in convention of sale and purchase, the two parties of this convention mutually agree that the seller deliver the thing, and the buyer to ensure price over which it was agreed - stipulated in article 1313 Civil Code. According with it, in real estate, the seller is obliged to show the object to the buyer which understand to be alienated, and the extent to which wants to alienate, i.e. the area - where it relates to land, the apartment or house - when concerns construction. Also, our paper tries to show the importance of the land use category. This one, individualized by a code, it is one of the parcel's attributes (area of land situated in a territorial administrative units on a well established site, with one category of purpose and belonging to one or multiple owners, in tenancy).

Keywords: category of use, individualization, parcel's attributes.

1 Introduction

In literature and also in our reality cadastre is viewing normally a parcel which are based and up-to-date land information system which containing a record of interests in land (e.g. rights, restrictions and responsibilities). Normally it includes a geometric description of land parcels connected to other records which describing the nature of the interests, of the ownership or control of those interests. And, many time the value of the parcel and its improvements. It is established mostly for fiscal purpose (e.g. valuation and equitable taxation), legal purpose (devolution), to assist in the management of land and land use (e.g. for planning and other administrative purposes), and enables sustainable development and environmental protection [4].

The fundamental territorial unity of the cadastre is parcel; this because all information on land buildings, which summarizes the cadastre (possession, use category, area, class, cadastral net income) gather and process on the parcel.

That being established, we say that the ground surface having the same judicial nature is distinctly determined using these parcels contained inside a closed line with constructions and plantations which are actually an integral part thereof, and that one or more co-owners are in individualization exercising a property right. In other words, two neighbouring parcels may belong to one or more owners if they differ by category of use [3].

The principal characters of the parcel could be summarized as being:

- has an only category of use unit;
- it belongs to a single territory;
- it belongs to a single terrain surface;
- it has distinct and visible boundaries;
- it is registered in all cadastral works under a single number, called "topographical number.

2 Methodology

In the next lines we will talk about the main rules for making individualization of parcels. By adopting electronic data processing procedures estate parcel, as the smallest territorial ordering information, it gained more importance, and the number has topographical integrator role. In most cases the cadastral parcel is super imposed parcel of land registry, defined as a unit of rights [4].

As a person's name serves to distinguish one individual from another, so the parcels differ from each other in that number topographically. So we can say that the "name" individualization parcel is given by the topographical number, which can be used only once within a cadastral territory.

That being so, the individualization of surface soil will be done by reproducing on the map after a measurement, and by entering the following data:

- the name of cadastral territory;
- the parcel of land number;
- topographical number.

For understanding, we say that the parcel of land represents that's parcels which are numbered, so it is necessary and numbered, when will proceed to identify a plot of land.

With these data, in terms of cadastral that surface is unequivocally named; exist one condition, meaning that in case of identical names of some cadastral territories, to be no doubt about belonging to a particular territory. At the same time, these (the respective dates) have a particular importance for survey – called in specialty literature "register of civil status for buildings" –, in terms of public trust to the land register, confidence without the property can't be defence, but neither the credit cannot be guaranteed.

A special importance for survey and land registry has the topographical number, because through it, those parts of land's surface (parcels, pieces of land), delimited and formally established through measuring, appear in the civil circuit. This function of topographical number is fulfilled as long as remains unchanged in cadastral works [2].

At the root of survey was necessary took a levying integrated right and fair taxes, but that institution which has contributed most to the increase of its authority, was the Land Registry, which was "imposed" in those countries (or states or provinces) in which the society has democratized early and in which the property was democratized by the land reform and in which the people gained more rights in state.

Along with the human rights, *in rem* rights have the most important role in any society. They are rights which implying a direct and immediate power on any determined body, power which can be translated by an amount of attributes and faculties likely to be brought against any individual for it must respect of everyone. The property is the perfect real right, and between body things most important is the earth, because it is the condition of human existence, which provides them with food and housing.

On these premises, Land Registry appeared and was perfected in order to give safety to the land owners, even to those who borrow money guarantee with land.

In this system, cadastre determined by marking, measuring and mapping work body and the parcel numbering and distinguishing it nominates [2]. Thus determined, nominated and individualized is registered in the Land Registry in relation with those holders of real rights.

So, by cadastral measurements, the real estate are specified and individualized, and by numbering are nominalised absolutely necessary conditions for organization of advertising rights through land registration and thereby they are protected against all.

Regarding the importance of the parcel area marked in cadastral documentation, we find it mainly in the civil circuit, to other legal relations. A prime example is the name of the place or category of use. In sale and purchase contracts, the two parties of it mutually agree: seller to deliver the thing, and the buyer to ensure price over which they agreed – it is stipulated in article 1313of the Civil Code [6].

In real estate, the seller is obliged show to the buyer the object which he understand to be alienated, event the extent to which wants to alienate, i.e. the area - when it relates to a land or an apartment or a house - when concerns construction.

In the Land Registry matter it's always resolves the land register extract, shown in article 1315 of the Civil Code [6]. The sale of a property is based on a measurement and in this case, the buyer takes it as it is in reality, or the sale is based on an extract from the cadastre or land register, and in this case, the buyer considers true the content of these documents. Later, if he found that the surface mentioned in the contract and, implicitly in the land registry, does not correspond to reality, or according with article 1326 of the Civil Code "the seller is obligated to deliver content sold that thing in the extent determined by contract, but with the changes below shown." [6] These changes relate to the situation when the surface is smaller in reality than that's one mentioned in the contract and in this case there are two legal ways to resolve: whether the seller will lower the price proportional to the difference in surface (article 1327 / Civil Code) or the contract will be terminated (article 1020 / Civil Code). If the surface is actually greater than that shown in the contract, the buyer can complete the asking price (article 1328 / Civil Code) [6]. But if the difference between the surface declared in the contract based on data from the land registry or cadastre and that found in reality falls within the measurement tolerances allowed, the contract is valid on the surface.

Surface parcel's worth in delimited of two neighbouring territories processes, as follows:

- If by land measuring of those parts into process results that the applicant has a smaller area than the land registry, and the defendant is presumed that the boundary was violated by the latter one;

- It is possible that the real estate surface of the applicant to be lower in reality than in the cadastre register or in land register and the defendant's surface actually correspond to that of cadastre and land registry, in which case it is assumed that there had been a mistake to the original measure.

In all conflicts for delimited of two neighbouring surfaces, among other materials signs, surface (parcel) contributes in a big way to solving that's [2].

The parcel has a much importance in case of expropriation for public utility, especially when it relates to land particularly valuable, such as construction land, vineyards, for the construction and development of greenhouses, irrigated cropland etc.

In case of that's buildings affected by expropriation which are not entered into cadastre evidences and land register, its will be identified in an annex to expropriation decision with part of surface and parcel number or by any other things for identifying of them - article 6(3) [1].

According with article 7(1,2) [1], in order to clarify the legal situation of those areas affected by expropriation, the expropriator will prepare in individual way the cadastral documentation in accordance with applicable law, based on parcelled plans drawn up by sectors cadastral lots.

With other words, we must understand that an expropriation corridor must be overlapped those lots affected by expropriation plans, drawn up according to Government Decision no. 890/2005 for approving of the Regulation on procedure for formation, powers and functioning of commissions for establishing property rights on lands, of model and award of property titles and the issuance of the owners, as amended and supplemented, including site plans and demarcation of the buildings received by the National Agency for Cadastre and Land through its territorial units. In case that parcelled plans weren't prepared to start expropriation procedure, local committees for the implementation of the Land Law are obliged to take legal steps for their preparation expeditiously. In former non-cooperativized areas the overlapping is making over the land plans and land registry [1].

3 Conclusions

On the basis of the existing or expected legal situation, as main task of the cadastre, parcels are represented on a large scale map with an identifier for its. This identifier is used in the land register to indicate the legal object in a special manner. As already mentioned before, this identifier (parcel number) connects the legal part with the cartographic one.

Besides the some characteristic elements of the cadastre exists a register which contains physical attributes of the parcel (i.e. identifier, local location, area, kind of use and abstract attributes like data for land tax such as value, proprietor and/or taxpayer).

As we already said the parcel represent the most important part of cadastre. For this and in this context it is necessary to pay attention to some relevant aspects, such as:

a) Generally – whether for legal use or for ecological applications – a land parcel can be defined as a continuous area of land within which unique and homogeneous interests are recognized [5].

Such a parcel, from the legal cadastral purposes, reflects homogeneity in legal interest. From the land use purposes such a parcel reflects homogeneity in use [5].

For more understanding of this concept, these parcels are surveyed and, also, mapped by a closed line and indicated by a number (parcel identifier) on the map.

b) In relation to the parcel boundaries the question on what data can be relied on plays a role. The cadastral system sustained that this issues are mainly based on physical boundary features, man-made or natural. The precise position of the boundary within these physical features depends on the general land law of the country concerned. After entering the precise data in the land register the boundary is equally fixed for everybody and also guaranteed. Without registering of the precise survey data, these boundaries are not legally fixed.

c) Concerning the identification of any parcel is remarked that this has to be simple and easy to understand, unambiguous, reliable and flexible. There is a tendency towards using also identification by coordinates.

Finally, we will say that the importance of the surface parcel in legal relations is well known to anyone who, in everyday life, had contact with estate issues.

References

1. Norma metodologică de aplicare a Legii nr. 255/2010 privind exproprierea pentru cauză de utilitate publică, necesară realizării unor obiective de interes naţional, judeţean şi local din 19.01.2011 (The implementing rule of the Law No. 255/2010 for the expropriation proceedings on the public utility case necessary to achieve objectives, local interest from national and county, 19.01.2011).

2. Henssen, J.L.G. (1995). “Cadastre and its legal aspects" from Jo Henssen in the Lecture Material, Workshop E, "From Research to Application through Cooperation" of the Joint European Conference and Exhibition on Geographical Information in The Hague, The Netherlands, March 26-31, 1995.
3. Miclea, M. (2000). Mic lexicon de cadastru și carte funciară (Small lexicon of cadastre and land registry), Ed. All Beck, Bucureşti.
4. Silva, Maria Augusta, Stubkjær, Erik (2002), A review of methodologies used in research on cadastral development, in Computers, Environment and Urban Systems, vol. 26, issue 5, pp. 403-423, Elsevier Ltd., http://dx.doi.org/10.1016/S0198-9715(02)00011-X.
5. Stoter, Jantien E., Oosterom van P. (2006). 3D Cadastre in an International Context: Legal, Organizational, and Technological Aspects, CRC Press, Taylor and Francis Group, ISBN 0-8493-3932-4, pp. 1, 19-20.
6. Romanian Civil Code.

Rural Landscape Regeneration by the Household Independent Cellars' Geospatial Analysis and Rehabilitation

Tătar C.[1], Dincă I.[1], Linc R.[1], Nistor S.[1], Judea D.[2], Bucur L.[1], Stașac M.[1]

[1]*University of Oradea, Department of Geography, Tourism and Territorial Planning (ROMANIA)*
[2]*University of Oradea, Department of Visual Arts (ROMANIA)*
E-mails: corina_criste_78@yahoo.com, iulian_dinca@ahoo.co.uk, ribanalinc@yahoo.com, snistor@uoradea.ro, diart17@yahoo.ro, liviubucur@yahoo.com, marcu_stasac@yahoo.com

Abstract

The research paper consists of four connecting parts, namely the territorial systematization and alignment of the household independent cellars of the Oradea Hills, a direct outcome of field surveys carried out during the research. The field work and its out coming geospatial analysis allowed for the cellars' categorization, according to their basically morphometric features, into five distinct types. Their status and functionality further on allowed to make a geospatial analysis referring to the cellars use dynamics, through GIS mapping, namely which percentage of the 880 identified cellars are active, in conservation, abandoned or destroyed, all followed indicators being featured on a summative map featuring the villages of the Oradea Hills. All these analyzed items allowed for the elaboration of specific planning proposal models for each of the five identified types of cellars.

Keywords: independent household cellars, use dynamics, cellar planning proposal, rural landscape regeneration.

1 Introduction

The household independent cellars of this study are located in the central part of Bihor County (north-western part of Romania – Fig. 1). Over the last 50 years many farms from the rural area of Oradea Hills have lost their traditional function because of the great changes in the agricultural sector both at a national and European level. Thus despite the great number inventoried on the territory of the Oradea Hills of 880 underground cellars on a an area of 393 sqkm, these wine cellars have thus become redundant, most are still active, some in conservation, but some in an advanced state of decay, that is why their adequate planning with the maintenance of their aesthetic appeal and local identity features [1] comes to the forefront [2]. Nonetheless the preservation of this rural built heritage is quite expensive, a carefully planned reuse is necessary for their medium and long term survival [3]. There are certain criteria which these cellars need to respect, among which a constant temperature [4]; [5] and this passive calling potential needs to be capitalized in the continental climate [6] as the one from Romania too.

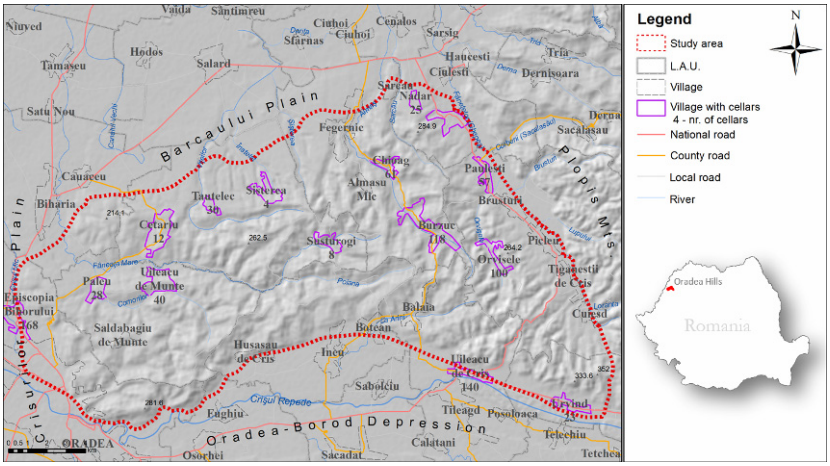

Fig. 1 Oradea Hills and the household independent cellars' location

Humans have valorized the environment in order to meet their needs; these household independent cellars are still used by farmers to store their agricultural produce, thus creating a specific heritage landscape [7]. These traditional landscapes are now shinking or disappearing due to multiple primary abiotic factors such as psyhiography, lithology and territorial typology, that is why their assessment is necessary [8], a goal met by the categorization into a typology and the analysis of the territorial structure and land arrangement, which was meant to fill the gap in the existent literature in the case of household independent cellars of Oradea Hills. In the case of the latter, the geospatial analysis helps for a better understanding of the household independent cellars disposal on the territory, their alignments and the way they have evolved across time in terms of functionality within the backdrop of a shrinking rural society, visualizing these changes by the help of geospatial technology [9] such as GIS mapping.

Each village of Oradea Hills represents a small scale environment, its complexity depends on a certain succession of biotic, abiotic and anthropic components. Its built component, mostly anthropic, can be multiplied thus contributing to a new life quality of the rural. This multiplication can be activated by the *regeneration of the local built rural environment*. This process can be supported by a built element, treated with both indifference and creativity by local, regional economic and administrative actors, namely the household independent cellars. The present study analyses the process of regeneration at two levels of intervention: the first level is that of the identification of *cellars typology* (this process is necessary because of the huge number of units and the great architectural and construction diversity which responds to local conditions), the second level is to find *design and rehabilitation/arrangement solutions for the selected cellars* which could finally be integrated in an economic circuit as a model of an eco-friendly agritourism [10]. For this purpose a number of 880 household independent cellars were inventoried form 14 villages belonging to Oradea Hills and a neighbourhood of Oradea, i.e. Episcopia. Oradea Hills spread over eight territorial and administrative units (L.A.Us), with seven communes - Paleu, Cetariu, Tileagd, Lugaşu de Jos, Brusturi, Spinuş, Sârbi and fourteen villages, covering an area of 393 sqkm with a relief elevation ranging between 150-350 meters. The remotest villages bearing cellars are 50 km away, most such villages being located within 40 km from Oradea.

These cellars, belonging to rural built-up landscape [11], [12] do not currently contribute to either local or regional tourism. There are premises that through their rehabilitation the regeneration process of these villages will start, as well as increasing the welfare of the inhabitants through rural tourism and ecotourism [13], [14], [15].

2 Methodology

The methodology of the present study has two main components: an analysis of references and a field survey. The last was focused on the following items: inventory of the 880 cellars pertaining to Oradea Hills; the oldness of the cellars; the functional state of the cellars (active, in conservation or abandoned, destroyed); the identification of construction materials; morphometry of the cellars (length, width, height/depth). Related to the rehabilitation/regeneration process as an element of the built rural landscape several design solutions were proposed, both for the interior and for the exterior, adapted furniture for the interior/exterior of the cellars, all the proposed solutions following the local traditions or adopting a modern style. The cartographic material was used to correlate the location of the cellars to features related to physical and economic geography, all material being processed using ArcGIS tools.

3 Results

3.1 *The household independent cellar territorial structure and organization as elements for the social and economical integration*

The household independent cellars of Oradea Hills have unique features from a territorial point of view. The location of the cellars is not identical; we can talk about an individual distribution and structure repartition for almost every village of Oradea Hills. The results are structures, alignments and distances which differ from village to village. Thus, a number of 880 household independent cellars belonging to the Hills of Oradea were inventoried, categorized and geospatially analyzed so as to manage to propose concrete planning models for their rehabilitation and per whole for the entire landscape regeneration.

The most frequent situation related to the cellars' place highlights their multiple locations, mostly outside the built-up area of the villages. There are villages with four cellar locations (Burzuc, Spinuş), villages with three cellar locations (Păuleşti, Uileacu de Criş, Paleu), the rest of villages having one or two cellar locations. One could notice that the villages with most cellar locations are situated in the north-eastern part of Oradea Hills. The explanation could be related to several factors: the high territorial extension of the villages; a complex process of the built-up area; each owner wanted to have a cellar as close as possible to his household;

the most suitable locations were chosen according to slope exposition; the type and resistance properties of lithology are also important. Otherwise the multiple locations cannot be considered as an economic or social disadvantage. On the contrary, it is a proof of the residents' skill in choosing the right location for the cellars and a geo-cultural advantage for the village.

The way in which the *cellars are organized within the territory* (Fig. 2) refers to the situation when the option of location is associated to an identity type (it's about a cellar or a group of cellars from a village) but also the way in which the cellars are located within the slope. The most frequent type is the linear one (the linear alignment – Fig. 2) when the cellars follows the contour lines of the slopes. Without minimizing the attractiveness of the rural landscape having this linear alignment type, the unique feature of the villages is amplified by other types of spatial distribution of cellars. Four other spatial distribution types were identified in the study area. All these situations reflect the perfect adaptation to slope morphology (rarely over 20^0) and the option of the owners who prefer the vicinity of other cellars, different from the isolated location.

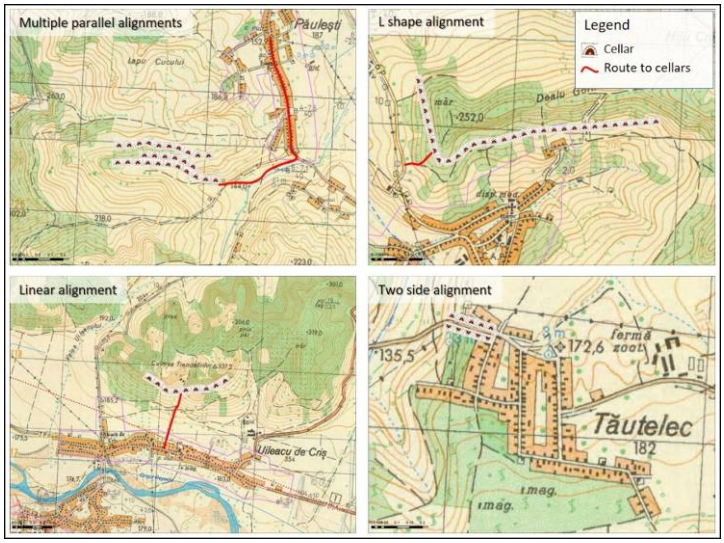

Fig. 2 Alignment types and the optimum route between built-up area and the location of the cellars

Regardless of the alignment type, it should be noted that the distance between two cellars (measured from the centre of the entrance of two consecutive cellars) differs from village to village. Those located on the eastern part of the study area have 6-8 m between two consecutive cellars (shorter cellars on smaller parcels). The villages located on the southern part have 10 to 12-meter long cellars. The explanation could be related to the more favourable lithological and morphological features of the slopes but also to the area of the parcels, the new owners using the new or old cellars for active weekend recreational activities.

The independent position of the cellars, apart from households, involves other indicators, namely the *route and distance* between the built-up area and the location of the cellars. The shorter distances which separate the center of the villages (or the end of the nearest street) to cellars are 0.1 - 0.4 km (in case of Chioag, Paleu, Tăutelec villages). Longer distances are those between 0.8 – 1.3 km, the longest distance being 2.1 km (in case of Spinuș village). The routes between a certain location (center of the village or the end of a road/path) and the cellars are relevant from two perspectives: on the one hand for the owner, who is able to reach faster to the cellar in order to store his goods and, on the other hand, for the guests (relatives, friends of the owner, future tourists).

The degree of difficulty to reach the cellars is medium to easy for the villages located in the north-eastern part of the study area (linear, direct routes or with a slight detour). The access to cellars of the other villages of the study area is very handy, the routes being linear, almost direct.

3.2 *Typology of household independent cellars*

The analysis process also led to the identification of five cellar types, grouped as such by the authors according to their morphometry, building material, goods' storage, oldness and void configuration.

Cellars Type 1 (Fig. 3), size of the cellar (length x height x width): 40m x 4-6m x 3-5m; the shape of the cavity is linear or in "L" shape (curved not as right angle), the vault is tight to large; oldness: 130-140 years (even from XVIth century but its an undocumented information); building materials for floor/walls/vault clayey compacted earth; entrance door material: wood or metal; hosted goods or products: wine or plum brandy barrels, potatoes, vegetables; other interesting features: the dimensions of the cellar represents the social status of the owner (landlords had big cellars, for ex. in Paleu, Uileacu de Munte or Spinuș villages); the access into the cellar

is by descending few steps but there are cellars where the floor is at the same level with the entrance – in case of the cellars from Spinuş village.

Cellars Type 2 (Fig. 4). Size of the cellar (length x height x width): 25-30m x 2.5-4 m x 1.5-2.5 m; the shape of the cavity is linear; oldness: 120-190 years; building materials for floor/walls/vault clayey compacted earth and consolidated sand and vaults coated with bricks; entrance door material: wood or metal, in some cases metal lattice; hosted goods or products: vine barrels, potatoes, pickles, old barrels and tools, old gas lamps, old furniture; other interesting features: the entrance is at the ground level; the cellar has two compartments (the first one, 5m long, with walls and vault made of bricks, the second compartment being made from earth); the facades are Barocoo, Secession style, with wood plates mounted above the entrance on which was carved or painted the year of construction or the name of the owner (in case of Episcopia Bihorului neighbourhood); the cellars have ventilation holes; the entrance is at the level of the ground or few steps beneath the level of the ground.

Fig. 3 Pictures from inside and outside, type of construction material and hosted object in type 1 cellars

Fig. 4. Pictures from inside and outside, type of construction materials and objects hosted by type 2 cellars

Cellars Type 3 (Fig. 5). Size of the cellar (length x height x width): 15-16m x 2-2.5 m x 2m; the shape of the cavity is linear or in "L" shape in few cases; oldness: 95-170 years; building materials for floor/walls/vault: bricks or earth (walls, vault), earth or concrete (floor); entrance door material: oak or metal lattice; hosted goods or products: vine barrels, potatoes, pickles, canned vegetables (fruits, bean, peas, peppers) stored on stands or on rude furniture, farming tools, different tools for grape processing (press, glass bottles); other interesting features: many cellars are well preserved, few are rehabilitated (with wood pillars which supports the front compartment), in some cases the vault is almost collapsing; above some cellars weekend

houses were built (Episcopia Bihorului, Uileacu de Criş, Spinuş); the floor is at the level of the ground of few steps lower.

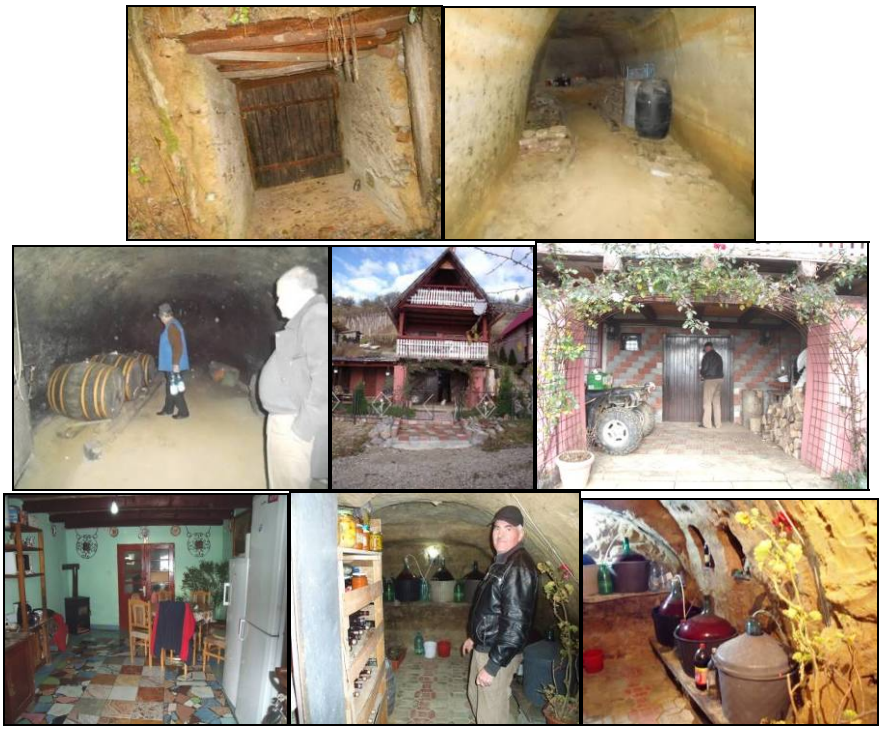

Fig. 5 Pictures from inside and outside, type of construction materials and objects hosted by type 3 cellars

Cellars Type 4 (Fig. 6). Size of the cellar (length x height x width): 10-12m x 2-3 m x 2-2.5m; oldness: 70 - 80 years; building materials for floor/walls/vault: bricks or earth (walls, vault), earth or concrete (floor); entrance door material: oak or metal (usually painted metal plates); hosted goods or products: plastic or wood vine barrels, canned vegetables or fruits, on stands flower pots, on walls braided red or white onion; other interesting features: cellars have 2-3 compartments (the first is used as a lobby, it has 9-12 sqm, the second is a narrow corridor of 1,5-3m x 1,5 m and the third is use as storage compartment at it has a size of 2-2,5m x 5-7m); in case of some cellars the first compartment is arranged as resting place for the workers during hot summer days; above some cellars were built as weekend houses (Episcopia Bihorului, Burzuc, Uileacu de Criş, Nădar); the floor is at the level of the ground of few steps lower.

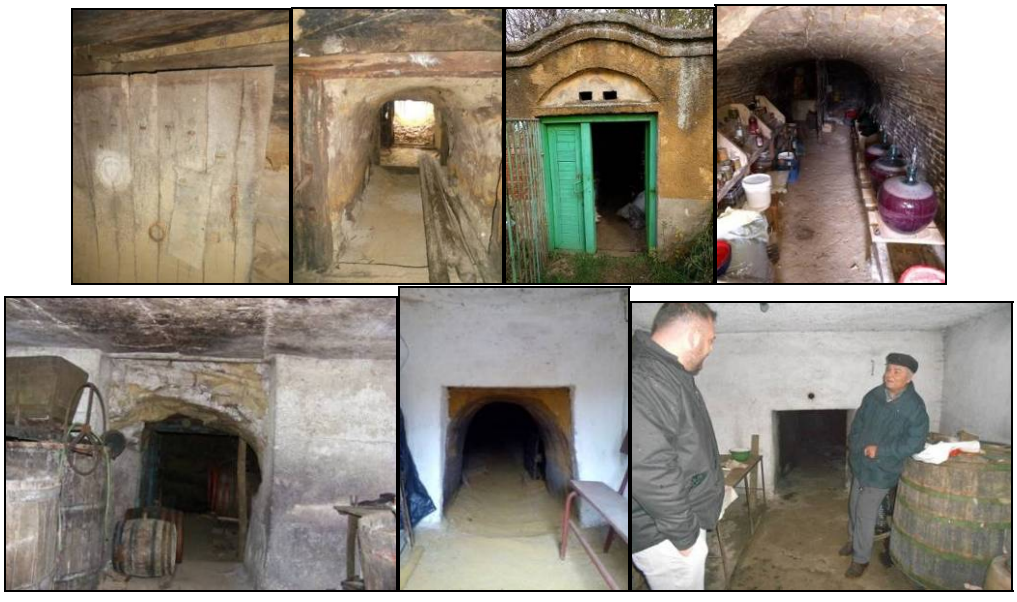

Fig. 6 Pictures from inside and outside, type of construction materials and objects hosted by type 4 cellars

Cellars Type 5 (Fig. 7). Size of the cellar (length x height x width): 5-8m x 2-2.5m x 2m; oldness: 70 - 80 years; building materials for floor/walls/vault: compacted earth for walls and vault, compacted earth for floor; compacted earth and concrete for the floor and bricks; entrance door material: oak or metal; hosted goods or products: potatoes, vine, tools for grape processing, onion, apples and other fruits stored on stands, jars with honey, plum brandy, work clothes and shoes, farming tools, barrels; other interesting features: some cellars are connected to electricity; cellars has one or two compartments; the access from the village to the cellars is along a narrow, "V' shape lane of about 12-15m long, dug into the slope, with/without table in front of cellars entrance; the floor is at the level of the ground.

Fig. 7 Pictures from inside and outside, type of construction materials and objects hosted by type 5 cellars

3.3 *Cellar use dynamics*

For the cellar use dynamics what really matters are the categories of cellars, *namely active, in conservation, abandoned* and *destroyed.* The first three categories show their simplified level of functionality, the latter being outside the circle of production and maintenance of some practices belonging to rural use.

The analysis of the results (shown in Fig. 8) clearly indicates the dominance of the *active type* of cellars in the villages of Oradea Hills. The maximum values of active cellars, by reference to the total number (i.e. 180), can be found in Uileacu de Criș, Urvind, Chioag villages but also in Episcopia Bihorului neighbourhood (Fig. 9). The explanation is linked to the solidity of these constructions, the favourable position (access also to a European road) and easy access for the owners, easy access with heavy materials necessary for maintenance/rehabilitation and construction of new ones and also the easy access to transfer goods hosted from/to cellars. The high number of active cellars counts significantly for the resilience capacity of the villages through the adjustment to modern development demands and the preservation of a life style with a remarkable rural uniqueness. A relatively important percentage of active cellars (68-92%) could also be found in the rest of the villages (ex. Burzuc, Tăutelec, Cetariu, Paleu, Șușturogi). The explanation of these relatively high values is related to the dominance of the retired owners.

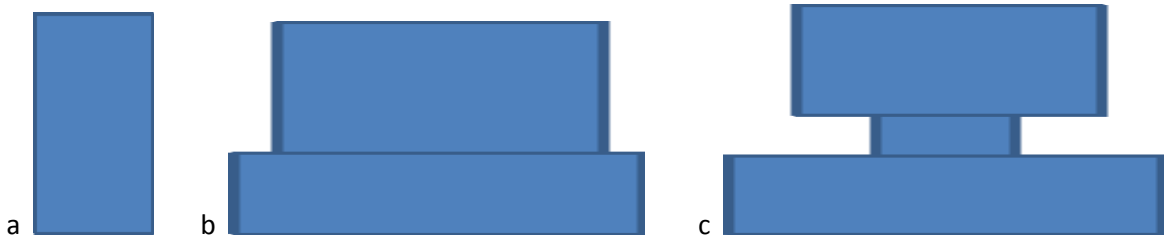

Fig. 8 Partitioning types of cellars: a. with one compartment; b. with two compartments (lobby in the left side, storage compartment in the right); c. with three compartments (a lobby and two storage compartments)

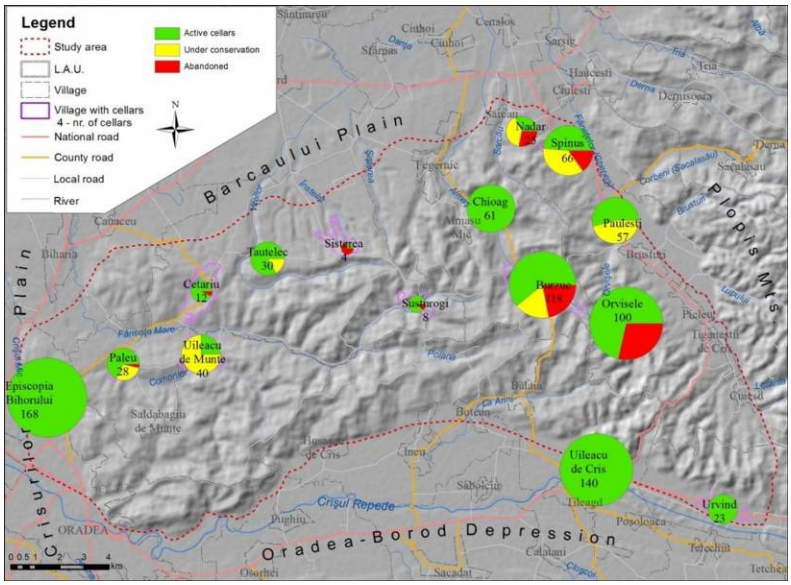

Fig. 9 Dynamic of cellars use in the villages of Oradea Hills

The cellars *in a conservation state* are dominant in the eastern part of the study area (36-46% from total number) and isolated cellars which are present in two villages in the western part of the study area. The 15-21% percentage of *abandoned cellars* could be related to the soft lithology which makes difficult the preservation of the optimum quality of cellars, to the ageing of population who are no longer attracted to work in agriculture and to preserve the cellars (for ex. the situation from Șișterea village, with a 75% percentage of abandoned cellars but reported to a very small total number of cellars). The category of *destroyed cellars* worth to be mentioned just statistically, have mostly collapsed many years ago. This category could be found in the north-eastern part of the study area (about 3-4 units/village), this average value is exceeded just in the case of Spinuș village (10 units/ village) and in Păulești village (25 units/ village).

Another used indicator is the *type of material used for the entrance doors.* The entrance doors are made from two types of materials: oak and metal (Fig. 3, Fig. 6). The wood entrance doors relate to 45-55% of the total number (are dominant in Burzuc and Șușturogi villages) and are linked to the oldest cellars, are very durable, the wood being from the nearby forests and this type of entrance doors preserves the peasant style both in villages with dominant Romanian or Hungarian population. The rest of entrance doors are made from metal (present in all villages) and are present as painted metal plates, punctured metal plates or welded metal elements. This type of material is predominantly used for the new cellars (not older than 45 years). The metal entrance doors can hardly be included in the peasant rural architectural style, in some cases, the impression is of ruggedness, rudeness but when these cellars were built, during the 6-7th decades of the last century, purchasing this type of material was very easy from communist construction sites or from building materials warehouses. *The maintenance level* of the cellars, even for those in conservation state, is good to very good, both the walls, the roof and the floor, made from natural rock, keeping the cavity intact and proper for goods and agricultural products storage (Fig. 3, Fig. 4, Fig. 5, Fig. 6).

The *oldness of cellars* is also an important element for the resilience of the villages (as an identity element of the rural culture). Most part of cellars has 70-80 years old but their state is as good as at the beginning. About a third from the total number are under 50 years old, are all active and perfectly functional. The oldness of the rest is between 120-150 years (for the cellars of Paleu, Uileacu de Munte, Spinuș villages there are is historical, undocumented information, according to which they were in use from XVI-XVII century).

The dimension of the cellars is very diverse proving a perfect adaptation between the storage capacity and the needs of each family. The portioning is adapted to the needs of each family but also adapted to the resistance of the rock in which the cellars is dug, one can identify three types of partitioning (Fig. 8), without a clear pattern for any village. For the most part of the villages the two compartment type is the dominant type.

3.4 *Rehabilitation through adapted design and arrangement of the cellars*

The second level of investigation for the regeneration of the rural landscape proposes for rehabilitation just some of the 5 types of cellars (discussed at subchapter 3.2) in order to find design and re-arrangement solutions. The final aim is to increase the value of the cellars, to increase the income of the owners after the

introduction of the cellars in a touristic/ecotouristic programme, to motivate the increase of life quality within the villages, to change the perception and to increase the motivation of the inhabitants and finally to create a local brand starting from the existence of the cellars. The owners of the rehabilitated cellars could be integrated in activities such as: local or family wine business, plum brandy, fruit soft drinks, food tasting, selling farming products or local medical plants; selling of handicraft items; associated service activities (guided tours, explanations about the cellars, the village, local transport).

The reconditioning of cellars from the aspect and construction structure point of view assumes several solutions we proposed for the interior of the five types of cellars as well as for the outside area of the cellars.
The proposed *construction materials* for the walls and vault: lining with old fashion burned clay bricks (Fig. 10, 11, 12) or with oak or acacia lumber (Fig. 13, 14). Motivation: the compartments of the cellar would have a hospitable, rustic, natural, organic atmosphere and both types of materials are very suitable for structural stability of the cellar.

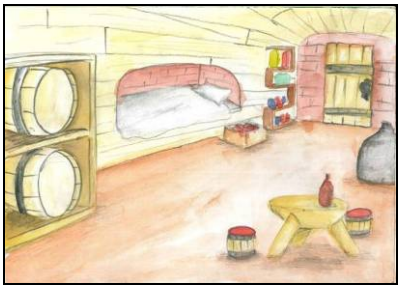

Fig. 10 Proposals of interior designs for type 1 cellars

Fig. 11 Proposals of interior designs for type 2 cellars

As far as the floor is concerned, the best solution we consider to be the compacted earth on which one could add a layer of gravel or crushed stones (Fig. 10, 12, 13, 14) or big size round stones (Fig. 11) both solutions offering a harmonious aspect of the compartment. The proposed *colours* are dominantly bright to neutral, from white, yellow, grey to brick-red and the *textures* from smooth dull to rough and very rough for the materials of the floor.

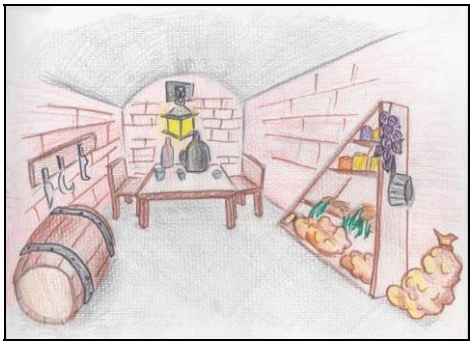

Fig. 12 Reconditioning and interior design for type 3 cellars

Fig. 13 Interior design, furniture and products for type 4 cellars

The *volumes and the functional partitioning* are maintained and take over the former spaces of the cellars. Just for the type 1 and 2 we propose the construction of some small compartments for tourists host/rest (in case of additional partitioning of the end of the cellars – Fig. 10) or of some stands, carved on the end or side walls, in order to increase the storage or exposed area of the small size cellars (Fig. 13). *The furniture* (Fig. 10, 11, 12, 13, 14) is predominantly made from wood, with a stylized design or compatible with the lines and volumes of the compartment: round (Fig. 10, 12, 13) or slightly elongated (Fig. 11, 12) for tables and chairs, in the form of barrels or cut from barrels, round edges stands (Fig. 12, 13) used for canned products' storage, supports for barrels and farming tools or for tools used for vine processing.

The position of the furniture is meant to support three types of activities: a housing/resting activity (for the long, roomy cellars, in case of its partitioning – Fig. 10) and a tasting/socialization activity (Fig. 11, 12, 14); the last activity type is assigned for storage and exhibition activities (Fig. 10, 11, 12, 13, 14). Because some of the cellars are connected to electricity we propose some solutions for lighting using rustic L.E.D chandeliers (Fig. 12, 13, 14) and for the cellars without electricity the use of rustic candles or L.E.D. lighting using batteries, the aim of the last two proposals being not to change the inner temperature conditions and to add a pleasant feeling from the combination of light and shades. To complete the rustic aspect the cellars must contain *other*

products and tools: vegetables, fruits, honey, reconditioned grape and vine processing tools, old objects of the owners, working clothes, farming tools, braided onion and garlic or medicinal plants.

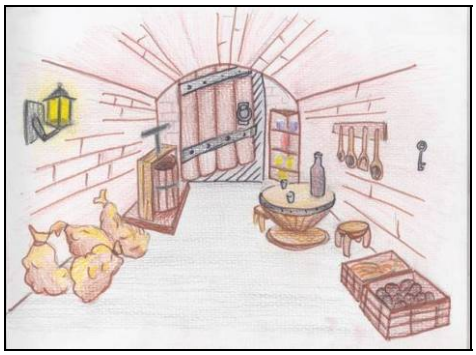

Fig. 14 Interior design and furniture for type 5 cellars

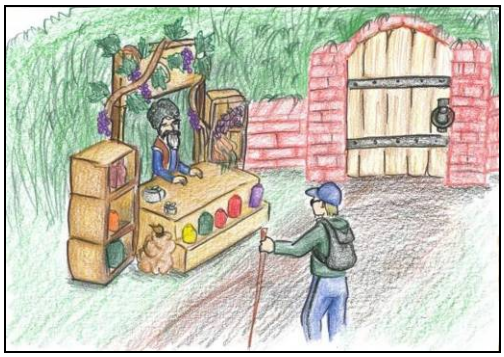

Fig. 15 Proposed sketch for exterior design and products exhibition

For the design of the exterior (Fig. 15), we propose just the reconditioning of the entrance walls, without a severe intervention which could alter the harmony between the interior and the exterior. In order to increase the income, in eventuality of selling products to tourists or visitors, and to increase the visibility of products, we propose a wood stand which will be placed in front of the entrance. This stand will be consisted of three bodies (a counter and two open cabinets) and a wood batch board with the name of the owner (optional) or, with stylized letters, the profile of the cellar.

4 Conclusions

The location of Oradea Hills household independent cellars was chosen by the villagers according to more factors, the choice being influenced by how easily they can be reached, the field study results being that their reach is from medium to easy due to their linear disposal within the rural landscape morphology. The geospatial analysis further on consisted of showing the c*ellars' use dynamics* featured by *active, in-conservation, abandoned and destroyed cellars* which illustrates the simplified situation of their functionality across time. The maximum values of active cellars percentage in relation to the total number of cellars are reported for the southern part of the area. In-conservation cellars have such status due to the owners leaving to work abroad or the owners' repositioning intentions for working the land that could provide products for cellars.

The typological identification process led to the individualization of five cellar types with their own characteristics grouped according to their morphometry, building material, goods' storage, oldness and void configuration. The village landscape regeneration proposed for rehabilitation some cellars of the five-identified types and featured the design and planning solutions in order to increase the value of this property, to increase the cellar owners' revenue, to motivate other villagers, change their mentality and look for new ways to increase life quality and create a local brand.

References

[1] Korosec-Serfaty, P. (1984). The home from attic to cellar. Journal of Environmental Psychology 4(4), pp. 303-321.
[2] Fuentes, J.M., Gallego, E., Gracia, A.I., Ayuga, F. (2010). New uses for old traditional farm buildings: The case of the underground wine cellars in Spain. Land Use Policy 27(3), pp. 738-748.
[3] Gaskell, P., Owen, P. (2006). Historic Farm Buildings: Constructing the Evidence Base. Report to English Heritage and the Countryside Agency, available on-line at: http://www.helm.org.uk
[4] Barbaresi, A., Torreggiani. D., Benni, S., Tassinari, P. (2014). Underground cellar thermal simulation: Definition of a method for modelling performance assessment based on experimental calibration. Energy and Buildings 77, pp. 363-372.
[5] Tinti, F., Barbaresi, A., Benni, S., Torreggiani, D., Bruno, R., Tassinari, P. (2014). Experimental analysis of shallow underground temperature for the assessment of energy efficiency potential of underground wine cellars. Energy and Buildings 80, pp. 451-460.
[6] Guerrero, I.C., Ocana, S.M. (2005). Study of the thermal behaviour of traditional wine cellars: the case of the area of "Tierras Sorianas del Cid" (Spain). Renewable Energy 30(1), pp. 43-55.

[7] Arias, P., Ordóñez, C., Lorenzo, H., Herraez, J., Armesto, J. (2007). Low-cost documentation of traditional agro-industrial buildings by close-range photogrammetry. Building and Environment 42(4), pp. 1817-1827.
[8] Cullotta, S., Barbera, G. (2011). Mapping traditional cultural landscapes in the Mediterranean area using a combined multidisciplinary approach: Method and application to Mount Etna (Sicily; Italy). Landscape and Urban Planning 100(1-2), pp. 98-108.
[9] D'Alessandro, F. (2016). Green Building for a Green Tourism. A New Model of Eco-friendly Agritourism. Agriculture and Agricultural Science Procedia 8, Florence "Sustainability of Well-Being International Forum". 2015: Food for Sustainability and not just food, FlorenceSWIF2015, pp. 201-210.
[10] De Montis, A., Ledda, A., Serra, V., Noce, M., Barra, M., De Montis, S. (2017). A method for analysing and planning rural built-up landscapes: The case of Sardinia, Italy. Land Use Policy 62, pp. 113-131.
[11] Jeong, J. S., García-Moruno, L. (2016). The study of building integration into the surrounding rural landscape: Focus on implementation of a Web-based MC-SDSS and its validation by two-way participation. Land Use Policy 57, pp. 719-729.
[12] Yeager, C. D., Steiger, T. (2013). Applied geography in a digital age: The case for mixed methods, Applied Geography 39, pp. 1-4.
[13] Hall, C.M. (2005). Biosecurity and Wine Tourism. Tourism Management 26(6), pp. 931-938.
[14] Cruz, T., Fernandez, M. (2016). Dimensions and outcomes of experience quality in tourism: The case of Port wine cellars. Journal of Retailing and Consumer Services 31, pp. 371-379.
[15] Novelli, M. (2004). Wine Tourism Events: Apulia, Italy. In Yeoman et al. (Eds.), Festival and Events Management – An International Arts and Culture Perspective, pp.329-345, Elsevier Butterworth-Heinemann, Oxford.

Time Structural Behaviour of Buildings Monitored by Topographic Technologies

Vîlceanu C.B.[1], Herban S.[2], Muşat C.[3]

[1,2,3] *Politehnica University Timisoara, Department of Overland Communication Ways, Foundations and Cadastral Survey, Traian Lalescu no.2, Timisoara (ROMANIA)*
E-mails: beatrice.vilceanu@upt.ro, sorin.herban@upt.ro, cosmin.musat@upt.ro

Abstract

The continuous research from the last decade concerning urban soils and foundation sites is due to their function as support for the urban infrastructure. In the context of the urban congestion, soils withstand a major impact of mechanical transformations and consistency changes due to the pollution and chemicals present in the industrial emissions and household wastes. These changes lead to consequences that influence the stability and security of constructions, such as reduction of permeability, drainage and aeration. The development of measuring techniques has permitted and created the possibility of determining and emphasizing even the most subtle of movements regarding buildings and industrial structures. Even so, the movements of some building elements are rather difficult to be quantified. The study revealed in this paper work refers to a relatively new construction built in 2009, linked to existing old buildings. In exploitation, transverse cracks could be observed in the structure of the old buildings. Following these phenomena, special monitoring was imposed upon the ensemble of buildings that serve the Faculty of Medical Bioengineering of Iaşi, because Romanian norms at force impose an accurate and precise monitoring in time for a construction to be safely exploited. Topographic-geodetic measurements were made so that the resistance of the structure's pillars of the four buildings could be studied and observed. This paper aims to emphasize the importance of the chosen surveying method which implied modern and accurate technologies, as well as to highlight the scientific input of geodetic data in the context of sustainable development.

Keywords: topographic-geodetic monitoring, foundation sites settlements, sustainable development, geometric levelling, benchmark.

1 Introduction

The continuous research from the last years concerning urban soils and foundation sites is due to their function as support for the urban infrastructure. The foundation layer stability depends on the interaction of permanent factors, namely geological, geomorphological, structural, and temporary, such as climatic, hydrological, seismic, forestry and anthropic conditions. The factors that influence the foundation soils and transform it into difficult soils are: heavy rainfall; the rise of the groundwater level, river erosion; frost action; the action of vibrations, seismic shocks, the thixotropy of rocks; anthropic activities like uncontrolled deforestation, digging, excavations, which may lead to the destabilization of slopes and landslides and therefore massive collapse of buildings or even loss of human lives. Under the influence of physical, chemical and biological elements, the soil structures suffer an extensive destruction, consisting of the reduction of porosity, increase of apparent density, acceleration of compaction due to the action of numerous compressive forces. These changes lead to other consequences that influence the stability [1] and security of constructions [2], such as reduction of permeability, drainage and aeration. Moreover, the reduction of water infiltration and gas diffusion appears like a secondary effect, which leads eventually to the disappearance of vegetation and the acceleration of soil compaction. In the context of the urban congestion, soils withstand a major impact of mechanical transformations and consistency changes also due to the pollution and chemicals present in the industrial emissions and household wastes.

1.1 *Background*

Geological and physical-geographical background place Romania in the category of countries with high potential for the production of various forms of instability. Areas with the highest potential of triggering landslides are located mostly in the Subcarpathian regions of our country. From the geological point of view

(Fig. 1), Iaşi region is located in the central-eastern part of the Moldavian Platform and totally reflects the features of the structural assembly.

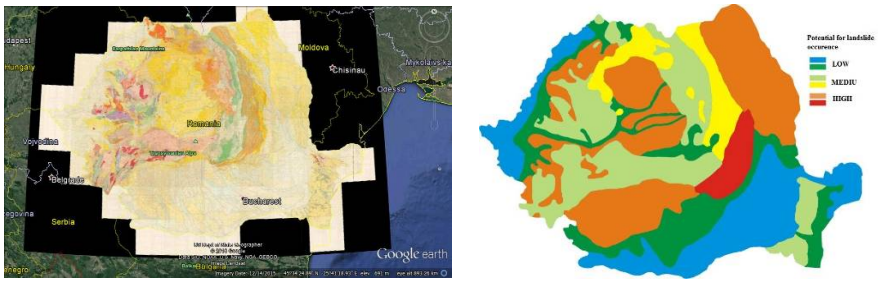

Fig. 1 Geological map of Romania

Clay-marl formations predominate, with some intercalations of sands, being a poorly wooded area. Clay soils belong to the category of dampening-sensitive soils and they are characterized by the fact that in conditions of high humidity they have large deformations under the action of external loads or even their own weight. The size and duration of the deformations depend on the nature of the load, the size and shape of the loading surface and the level of dampening of the ground. The specific particularity of clay soils consists in their sensitivity to dampening, which expresses the capacity of these soils to sharply reduce the volume of goals for a given pressure, when subjected to flooding, as a result of the destruction of their structure.

Against the background of this geological substrate, a fragmented landscape was created due to the hydrography. From the climatic point of view, it is an area with pronounced continental influences, affected by oriental air masses, characterized by heavy rainfall, particularly in the summer. Because of these aspects, floods are frequent, especially in the plain areas, which favour the occurrence of landslides and the damage of the foundation ground.

The statistics show that hazardous meteorological phenomena which occurred in Iaşi region in the last twenty years, caused temporary flooding of low areas in the Municipality of Iaşi [3], leading even to the loss of human lives and considerable material damage, which negatively affected the region both socially and economically.

2 Topographic Studies

The development of measuring techniques has permitted and created the possibility of determining and emphasizing even the most subtle of movements regarding buildings and industrial structures. Even so, characterizing the behaviour in time of buildings represents a difficult task for engineers. This is because it has to be realised in the context of coming under the three pillars of sustainable development.

The topographic-geodetic methods belong to the category of determinations of movements and deformations [4], [5]. Vertical displacements of constructions [6] occur mainly due to the compression of the soil under the action of loads transmitted to the foundation. These degradations may be due to the high or uneven compressibility of the foundation ground, the intensive dampening of the land, the influence of new constructions carried out in the vicinity, overloading of the ground with deposits placed nearby the constructions, the lowering or the raising of the groundwater level, the execution of drillings or excavations in the area, achieving of underground works in the vicinity or under the constructions.

The study revealed in this paper work refers to a relatively new construction built in 2009, linked to existing old buildings. In exploitation, transverse cracks (Fig. 2) could be observed in the structure of the old buildings, made of reinforced concrete frames and slabs.

Fig. 2 Measuring transverse cracks in the structure of the old buildings

As a result of the floods that have occurred in the Iaşi region in the last decade, the foundation layer was strongly affected. The features and configurations of the foundation soils, that consist of brown yellow powder clay, loess sensitive to dampening, were identified in the geotechnical study of 1998, providing an overall of buffers beneath the soles of the clay foundation.

Following these phenomena, topographic monitoring was imposed upon the ensemble of buildings that serve the Faculty of Medical Bioengineering, because Romanian norms at force impose an accurate and precise monitoring in time for a construction to be safely exploited.

It is known that geodetic methods actively contribute to determining and establishing the behaviour in time and the impact of the constructions upon the environment.

Topographic-geodetic measurements have been realized so that the resistance of the structure's pillars of the four buildings could be studied and observed. For achieving the topographic observations necessary for determining foundation settlements of the constructions, eighteen observation marks were mounted on the buildings and eight depth benchmarks situated outside the influence area of the buildings, disposed as shown in Fig. 3.

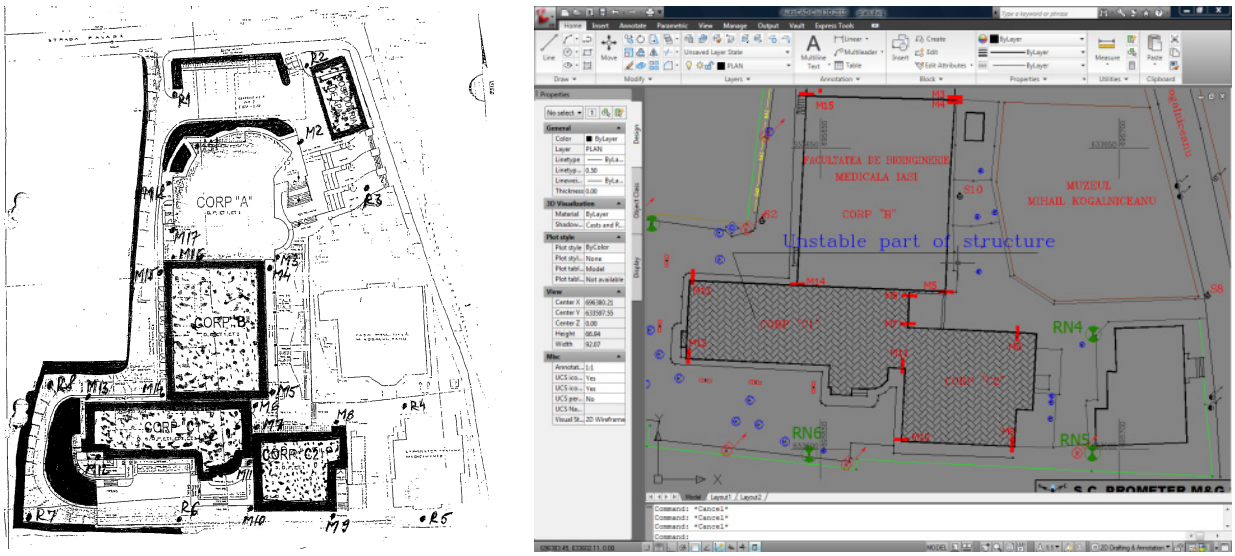

Fig. 3 The arrangement of the reference depth benchmarks and the observation marks encased in the constructions

Considering the nature of the foundation layer, yellow-brown sensitive to dampening clay loess, it was found that the most suitable for this situation the type of depth reference benchmark, indicated by the technical specification 016-097 Standard and represented in Fig. 4.

Fig. 4 The mounting of the reference depth benchmarks

For mounting the reference were carried out 10meter depth drillings. The technical specifications stating that the lower end of the benchmark should be embedded at a minimum depth of 2 meters in the plastic varta clay layer, disposed beneath the dampening-sensitive clay layer, have been taken into consideration.

This solution was chosen by taking into account the nature of foundation layer and the characteristics of the constructions, knowing the good results that can be obtained for topographic observations due to the small displacements or variations of this type of benchmarks.

Their positioning was made so as to ensure the uniform coverage of the observed perimeter, on stable ground, without running the risk to degrade over time, protected against mechanical actions [7]. Their role is to

ensure the stability of the reference horizontal plane against which the vertical displacement of the control points is determined. Their number shall provide the perception of the character of displacements and strains of the studied buildings.

The observation marks encased on the constructions meet the technical specifications of 016-097 Standards. They were mounted in horizontal position, in the resistance elements of constructions, on concrete pillars, on the inside and on the outside of the buildings, about 60 centimetres from the pavement or concrete platform, so that they are not damaged or obstructed during the construction works, as shown in Fig. 5.

Fig. 5 The observation marks, on the inside and on the outside of the buildings

The observation marks are made of steel, bar shaped, with hemispheric head made of stainless, durable metal, which can easily support the topographic rod or the optical prism. The rods were fixed with cement mortar in the holes dug into the concrete structure of the buildings. For a better preservation of their initial condition and to avoid chipping or damage, protection is achieved through special covers.

Control marks are meant to render the vertical displacements of the structure that they are fixed on with high accuracy. These observation marks encased on the building are moving along with the construction and so, through observations carried out upon them, the values of vertical displacements can be established.

Because of the fact that the movements of some building elements are rather difficult to be quantified, when choosing the measuring methods for determining vertical displacements of constructions the specialists have to consider the required accuracy, structural particularities and the nature of the foundation layer. In order to determine the settlements of these observation marks mounted in the structure of the buildings serving the Faculty of Medical Bioengineering, geometric levelling method was chosen for high accuracy of the observations, imposed by Romanian legislation for class C of constructions founded on difficult terrain. This topographical method provides the most accurate results and offers the greatest precision, taking into consideration the situation given. On site, high precision geometric levelling was effected, both ways and in closed loop, between the fundamental benchmarks R1 and R8, in order to determine their stability. From the reference benchmarks, second order geometric levelling was carried out, to the control benchmarks placed on the foundations of the buildings or on the resistance elements, inside the area of the Faculty of Bioengineering, according to the specific design theme and the plan with the location of placement.

Topographic measurements for determining the vertical variation of an element of the structure or the ensemble of buildings is always achieved in the form of observation cycles [6]. Five cycles of topographic measurements were performed using the geometric levelling method in order to determinate the building's settlements, according to the programme established through the project. Following the recommendations, the first cycle of measurements was carried out in September of 2011, approximately 15 days after mounting the benchmarks, performing three measurements within two weeks. The second cycle of measurements was performed in October of 2011, after four weeks from mounting the benchmarks and consists of two measurements. The third cycle of measurements was carried out three months after mounting the benchmarks, in December 2011, two measurements being performed. The last two cycles of observations, cycle four and cycle five, were carried out during the next year, namely in April and July of 2012. Beginning with the second cycle possible subsidence and instability of the observation marks were revealed. The results were compared to the guidance values of the displacements or deformation admitted for constructions, specified in Annex C of 3300/2-85 Standard. The representation of the results was handed over to the beneficiary both in tabular and chart form.

3 Results and discussions

Differences obtained may be reported either to the reference cycle of observations, thus expressing the total settlement, or between the intermediate cycles of measurements, thus obtaining a partial settlement of one or more observation marks. Based on data input and the processing, absolute values of the vertical movement (Table 1) were established.

Table 1 The displacements of the reference benchmarks

Benchmark	Condition	Basic measurement September 2011 (m)	October 2011 (m)	December 2011 (m)	April 2012 (m)	July 2012 (m)	Δh Sept. 2011 – July 2012 (mm)	Δh Dec. 2011 – April 2012 (mm)
R1	Good	107.8336	107.8345	107.8347	107.8354	107.8363	2.7	0.9
R2	Good	108.5841	108.5843	108.5841	108.5850	108.5835	-0.6	-1.5
R3	Good	107.2145	107.2144	107.2148	107.2155	107.2155	1.0	0
R4	Good	103.5812	103.5808	103.5801	103.5808	103.5808	-0.4	0
R5	Good	102.7300	102.7306	102.7306	102.7316	102.7316	-1.6	0
R6	Good	102.7362	102.7357	102.7359	102.7355	102.7355	-0.7	0
R7	Good	102.9430	102.9430	102.9430	102.9430	102.9430	0	0
R8	Good	103.3766	103.3775	103.3774	103.3773	103.3773	0.7	0

The values of the foundation deformations and displacements (Fig. 6) are considered to be important elements when characterizing the safety of the structure. The dynamic movement of the structure was measurement and represented both in tabular and chart form, in Fig. 6 and 7. The value of this deviation is very small, being of order of mm.

Obs. mark	Condition	September 2011 Cycle I			Cycle II October 2011		Cycle III December 2011		Cycle IV April 2012		Cycle V July 2012		April – July 2012
		H(m)	H(m)	H(m)	ΔH(mm)	H(m)	ΔH(mm)	H(m)	ΔH(mm)	H(m)	ΔH(mm)	H(m)	ΔH(mm)
M1	Good	108.0582	108.0579	108.0576	-0.1	108.0575	-1.3	108.0569	-4.1	108.0535	-4.8	108.0528	-0.7
M2	Good	108.3694	108.3730	108.3720	0.8	108.3728	-3.4	108.3728	-0.1	108.3710	-2.5	108.3695	-1.5
M3	Good	106.2769	106.2768	106.2771	-0.7	106.2764	-0.8	106.2761	-1.7	106.2754	-4.5	106.2726	-2.8
M4	Good	106.2567	106.2568	106.2569	-0.7	106.2562	-0.6	106.2561	-1.2	106.2557	-3.8	106.2531	-2.6
M5	Good	105.0699	105.0697	105.0700	0.5	105.0705	-0.7	105.0692	0.5	105.0705	-0.7	105.0693	-1.2
M6	Good	105.4276	105.4275	105.4278	0.2	105.4280	-0.4	105.4272	0.5	105.4283	-0.9	105.4269	-1.4
M7	Good	105.4536	105.4536	105.4535	0.5	105.4540	-0.4	105.4532	1.0	105.4545	0.1	105.4536	-0.9
M8	Good	104.4654	104.4655	104.4656	0.8	104.4664	-0.1	104.4653	0.7	104.4663	0.3	104.4659	-0.4
M9	Good	103.2939	103.2941	103.2936	-0.2	103.2934	-0.9	103.2930	1.7	103.2953	1.2	103.2948	-0.5
M10	Good	103.3850	103.3852	103.3847	0.7	103.3854	0.1	103.3851	1.6	103.3863	1.4	103.3861	-0.2
M11	Good	103.3826	103.3831	103.3828	0.9	103.3837	1.8	103.3844	1.2	103.3840	1.9	103.3847	0.7
M12	Good	103.4431	103.4433	103.4433	0.4	103.4437	0.7	103.4438	-0.9	103.4424	1.4	103.4447	2.3
M13	Good	103.8616	103.8617	103.8617	0.7	103.8624	0.5	103.8621	-1.2	103.8605	0	103.8617	1.2
M14	Good	105.2943	105.2941	105.2945	-0.7	105.2938	-1.1	105.2932	-3.2	105.2913	0.2	105.2947	3.4.
M15	Good	105.9062	105.9063	105.9061	0.5	105.9066	0.5	105.9067	1.2	105.9073	-1.1	105.9050	-2.3
M16	Good	108.9365	108.9366	108.9363	-0.3	108.9360	-0.3	108.9362	-0.3	108.9360	-2.2	108.9341	-1.9
M17	Good	107.6226	107.6225	107.6222	0.3	107.6225	-1.3	107.6213	-1.7	107.6205	-2.5	107.6197	-0.8
M18	Good	107.7306	107.7304	107.7303	0.2	108.7305	-1.3	107.7293	-3.3	107.7270	-3.4	107.7269	-0.1

Fig. 6 The displacements of the observation marks

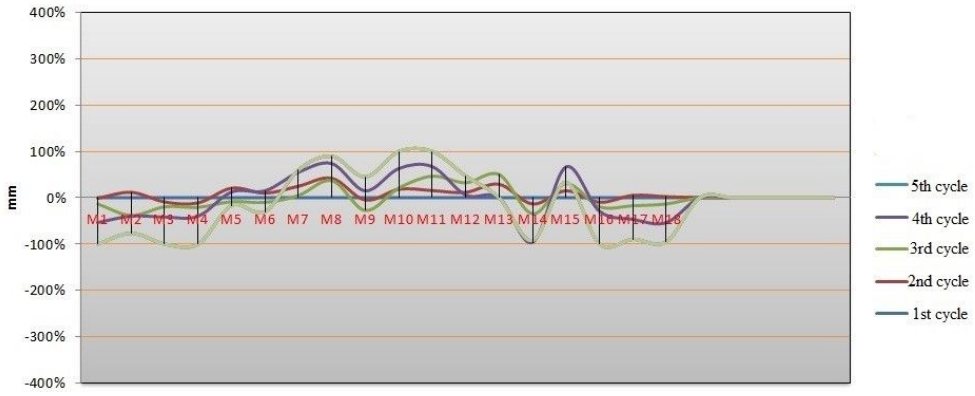

Fig. 7 The observation marks, on the inside and on the outside of the buildings

The geometrical levelling was achieved with the LEICA DNA 03 automatic electronic level and with an invar kit, having an accuracy of 0.3mm/km, working radius between 1.8meters and 110meters and a minimum focusing distance of 0.6meters. Levelling instruments used were technically checked before the execution of the measurements and found that they are in good condition. Compensation of field measurements was carried out with Leica Geoffice Combined software.

Topographic measurements were also carried out in order to achieve the horizontal plane containing the details of the studied area (Fig. 3). The measurements were effected using the LEICA TCRA 1205+ total station, having an angular precision of 5" and the distance of 2ppm, in good temperature and environment conditions.

The adjustment of the field measurements carried out on route was achieved using the least square calculation method, indirect measurements, using Leica GeoOffice Combined software [3].

The results of the measurements reveal a displacement of the reference benchmarks only for R1=0,9mm and R2=-1,5mm, which were placed closer to the new building and they must have been influenced by the works carried out in the area. The minimum displacement of the observation marks for the first three cycles was 0.1mm and the maximum of 1.3mm. The results of the measurements achieved in April and July of 2012, after seven and ten months, reveal an increase of the displacements, the values being comprised between 0 and 4.8mm, especially for M1, M2, M3 and M17, M18, observation marks encased on the new building. The data derived from measurements were processed by the client, constructor and authorized persons, the objective being the remediation of any dysfunction and the reduction of the effects caused by the degradation of the buildings and the impact on the environment.

4 Conclusions

At a larger scale, it is clear that engineers, regardless of their specialization in environmental matters, civil engineering or surveying, have a key role in ensuring sustainable development. The society should focus on the prevention of environmental problems using the development of proactive new solutions given by engineers. The difficulty in the measurement of building displacements is to find a spatial measurement technique that meets requirements such as, precision, reliability, low cost and user friendly. Some of these advantages can be obtained by using topographic-geodetic methods, but main challenge is to find one to satisfy all the conditions. In particular, from the values obtained in the five cycles of measurements, it can be concluded that the variation of displacements is framed within the tolerances admitted for Class C buildings (construction in difficult terrain), specified in Annex C to 3300/2-85 Standard, Calculation of foundation soils in case of direct foundation. Analysing the results, it was recommended that the monitoring of the constructions that serve the Faculty of Medical Bioengineering should be continued, as a measure imposed in accordance with Romanian legislation, in order to determine the effective displacements of the building using accurate surveying methods. At least two cycles of observations should be done every year, until the mitigation of these values, in order to ensure a safe exploitation.

References

[1] Moldovan, I.M., Ilieş, N.M. (2014). Stabilization of a potentialy sliding slope by building an underground house, Journal of Applied Engineering Sciences, 4(17), Issue 2, pp. 75-81.

[2] Nistor, Gh.; Nistor, I. (2011). Contributions to the Improvement of the Measuring Technology and Precision of the Cyclic Determination of the Vertical Deformation of Constructions using High Precision Geometric Leveling Measurements, RevCAD – Journal of Geodesy and Cadastre, no. 11, pp.159-168.

[3] Tudorică, M; Bob, C. (2015). The influence of foundation soils concerning the behaviour of buildings, DOI: 10.1515/jaes-2015-0026, Journal of Applied Engineering Sciences, 5(18), Issue 2, pp. 87-93.

[4] Crenganis, L; Bofu, C; Tutunaru, I; Balan, I; Corduneanu, F. (2015). Preliminary Flood Risk Assessment in the Jijia River Basin, 15th edition National Technical-Scientific Conference – Modern Technologies for the 3rd Millennium, Romania, ISBN 978-88-7587-724-8, WOS:000378314000002, pp. 7-12.

[5] Herban, IS; Musat, CC. (2012). Measuring and Determining the Dynamic Deformation of Constructions Using Modern Technologies and Techniques, Journal of Environmental Protection and Ecology, 13(2A), WOS:000310557400050, pp. 1200-1207.

[6] Nacu, V; Stoian, I; Vele, D; Arseni, M. (2015). Geodetic Methods Regarding the Crustal Movements and Earthquake Prediction, 5th edition National Technical-Scientific Conference – Modern Technologies for the 3rd Millennium, Romania, ISBN 978-88-7587-724-8, WOS:000378314000006, pp. 27-33.

[7] Naş, S; Farcaş, R; Poruţiu, A. (2015). Considerations regarding the stability of landmarks used to determine the vertical movements from a rock salt exploitation field, 15th edition National Technical-Scientific Conference – Modern Technologies for the 3rd Millennium, Romania, ISBN 978-88-7587-724-8, WOS:000378314000008, pp. 43-47.

[8] Herban, SI; Vilceanu, CB; Alionescu, A; Grecea, C. (2014). Studying the movement of buildings and developing models to determine real settlements, Journal of Environmental Protection and Ecology, 15(2), WOS:000339362500044, pp. 789-796.

Construction and Architecture

Constructed Wetlands for Wastewater Treatment

Ancas A.D.[1], Profire M.[2], Statescu F.[3]

[1] *Technical University Gh. Asachi Iasi (ROMANIA)*
[2] *Technical University Gh. Asachi Iasi (ROMANIA)*
[3] *Technical University Gh. Asachi Iasi (ROMANIA)*
E-mails: ancas05@yahoo.co, profiremihai@yahoo.com, fstatesc@yahoo.fr

Abstract

In the past decade interest has grown for use in the treatment of various wastewaters of the improvement wetland. Field applications extend from single-family residences, municipal and public facilities covered by relatively low cost and low energy consumption, operation is easy. Currently there is a lack of consensus regarding the use of different criteria guiding the design of such systems. Wetlands are designed as a simple and environmental friendly solution for the treatment of wastewater, particularly suited for small and medium sized installations. Artificial wetlands are hybrid systems consisting of water treatment facilities with underground drainage which keep the water level below the surface of another medium that is wet bed.

This paper, based on the author's own research, presents the concept of wet-type arrangement underground drainage (SF) that can provide high levels of performance by reducing C_2O_5 and TSS (Total Suspended Solids), relatively low cost of construction, maintenance and operation e.g. [1].

Keywords: wetland, hybrid systems, wastewaters, environment, sustainable development.

1 Constructed Wetlands

Constructed wetlands are natural ecosystems where wastewater is introduced for biological and physical treatment in a sand filter that has grown vegetation (Fig. 1).

Filter bed can be filled with sand or gravel and materials and will be airtight isolated (with natural soil or plastic film). Wastewater treatment is provided by the activity of bacteria in the bio-film filter substrate and has physical and absorbing effects.

To accelerate, over the surface of the sand filter plants are grown, usually cane, therefore often they are referred to as filter bed cane

Constructed wetlands were used for the first time in Germany and their use for cleaning wastewater is more than 40 years, especially in rural areas of Austria, France, Greece and other countries.

There are different types of systems but using the system prevails sub-superficial the water level remains below that surface. Depending on the embodiment of this system they can be divided into two categories - with vertical exhaust and horizontal evacuation.

In general constructed wetlands include a pre-treatment step for sedimentation of solid organic materials in order to avoid clogging.

Another model that requires no pre-treatment has been successfully developed in France for raw sewage.

Fig. 1 Local wetlands e.g. [2]

The table below (table 1) briefly presents the main advantages and disadvantages of such systems.

Table 1 Advantages and disadvantages of constructed wetlands e.g. [2]

Advantages	Disadvantages
Low or zero energy consumption (using a pump can be avoided if natural inclination is sufficient)	Require more space (less than for ponds)
Easy operation and maintenance	It can generate odour, if the system does not provide a preliminary treatment (French system)
Lack of electromechanical equipment	If the project requires a prior treatment is needed sludge disposal
Adaptable to seasonal changes	Cutting vegetation frequently (annually)
Improved pathogens removal	
Partially removing nutrients	
Framing an harmonious landscape	
The lack of noise pollution	
Possibility of raw sewage (French system)	
Minimum sludge management	
Recommended for concepts	

2 Concept of arrangement – Wet Bed type SF

Wetlands are defined as areas where surface water is close to the soil surface enough time throughout the year to maintain saturation conditions and corresponding vegetation.

Wetland designed / constructed (moist) is defined as a wet area arranged especially for pollution control and waste management, with another location than natural wetland.

There are two basic types of wetlands: wetlands with FWS and wetlands with SF.

It is estimated that SF arrangements, have some advantages over those type FWS, so if the water surface is maintained below the surface environment, the risk of odours or vector insects exposure is reduced. In addition, there is the opinion that the environment provides a surface available for treating larger than the concept FWS so that treatment response can be faster to type SF who therefore may have a smaller area than the FWS system designed in the same conditions of waste water.

SF wet landscaping concept, developed by Seidel, includes a number of layers composed of sand or gravel, which supports emergent aquatic vegetation such as bulrush, sedge / reeds.

In all cases the current direction is vertical through each element / cell to drain and then to cell / next item. They have obtained excellent performance in reduction / removal of C_2O_5, Nitrogen, Phosphorus and organic matter complex.

Pilot studies on the concept are only marginally successful and not used these years.

Reducing physical C_2O_5 occurs rapidly and fixing the material particles in voids / pores of rock.C_2O_5 is reduced by microbial culture and the environment on the surface attached to plant roots and rhizomes that penetrate the bed.

Compared with other forms of wastewater treatment, wetland systemsthe both of its SF and FWS -, C_2O_5 are unique in that the system is actually produced through the decomposition of plant litter and other organic material incidents. As a result, these systems can never achieve a complete reduction of C_2O_5, so it is typically present in the effluent of a C_2O_5 of 2-7 mg / l.

3 Model Design

The unevenness of the application complicates the development of organic waste water with the accuracy of a design model for reducing C_2O_5 in particular, it is likely that the actual reduction ratio varies along the flow and consequently C_2O_5 is produced by the decomposition of residual plant debris.

Constant flow for SF wetlands is judged as superior to other types of wetlands.

Table 2 compares the constants of three treatment concepts.

Tabel 2.The constants of three treatment concepts

The treatment process	Constant (day^{-1})
SF wetlands type	1,104
Lagoon	0,117
FWS wetlands type	0,501

The reduction of suspended solids is very effective in arranging SF wetland. The major part of the reduction occurs in the first few meters from the entrance area.

To reduce TSS (solid suspension) there is no kinetic design model available. Following studies make it clear that reducing TSS follows the same pattern as for C_2O_5.

Immediate conclusion is that when a system is designed for a specific level of reduction C_2O_5 in particular, reducing TSS will be comparable as long as they maintain groundwater flow system in bed.

Many SF wetland systems are designed to reduce only C_2O_5 and TSS. In some cases they have been reviewed requiring a reduction of ammonia but this requirement involves very large areas of land or alternative treatment methods.

4 Applications of SF Wet Systems

Mainly in most operating systems, the concept of moist is the most commonly used type of FWS. Next we will briefly examine and illustrate possibilities for these applications to use the concept SF.

In this case there is the assumption that leakage is permanent and that the waste water should not contain large amounts of inorganic matter that could lead to porous bed rapid clogging premises.

One of the applications SF wetlands can be filtering landslides. In this case the flow is relatively uniform and has a weak content of inorganic solids in suspension. Wet SF arrangements can also be used to treat drainage from mines or in agricultural runoffs.

In conclusion, the use of wet SF facilities is probably the most convenient due to hydraulic restrictions imposed for environmental wastewater treatment, relatively low concentrations and solid matter flow conditions relatively uniform and in locations where the advantages of how to drain groundwater are considered important.

5 Research Requirements

Research necessary for understanding the concept of fitting in wet priorities were ranked high, medium, low. High priorities involve the collection of additional data on the spatial response for C_2O_5 SF wet bed facilities to enable development and validation of much improved design patterns.

Research is needed to identify the requirements and sources of Oxygen in these SF systems. Particularly important in the production of Oxygen is the role of plant roots. Using other types of plants than reed, bulrush should be investigated to determine whether there are other optimal species, too.

Low average requirements that require consideration of variable flows leave the management of communities in suffering because of their high infiltration levels into sewer systems.

Conclusions

The concept of planned wetland can provide high levels of performance to reduce C_2O_5 with relatively low costs of construction, maintenance, operation. They are particularly suitable for small and medium sized installations in areas where the porous land require them and are available at a reasonable price.

C_2O_5 reduction in SF wetlands shows a linear relationship with mass loading of C_2O_5 to levels of at least 140kg / ha / day.

SF systems of all sizes must include an adjustable final output in order to control the water level in the wet bed.

Efforts should be continued to collect reliable data on the normally operated performance scale systems to confirm and complement the results of laboratory and pilot-scale research.

References

[1] Ana Diana Ancas, Mihai Profire, *Sanitaţia durabilă - o problemă a mileniului III,* A 50-a Conferinţă jubiliară de Instalaţii: Creşterea performanţei energetice a clădirilor şi instalaţiilor aferente, Sinaia 2015, vol. I, pp16-23 (Sustainable Sanitation - A Problem of the Thirs Millennium, 50th Jubilee Conference Installations: Increasing the Energy Efficiency of Cuildings and Installations, Sinaia 2015, vol. I, pp16-23

[2] Ghid Sisteme de epurare durabilă şi eficienţa a apelor reziduale din comunităţile rurale şi suburban, www.wecf.eu (Guide Sustainable Sewage Systems and Wastewater Efficiency in Rural and Suburban Communitie).

[3] www.bodenfilter viewed at 12.09.2016.

[4] at http://www.ccb.se/documets/SustainableWWTforaNewHousingArea.HowtoFindtheRightSolution.pdf. viewed at 12.09.2016.

Modern Consolidation Solutions for Buildings with Historical Value. Part I: Reinforced Concrete Structures

Apostol I.[1], Mosoarca M.[1], Stoian V.[2]

[1] *Politehnica University of Timisoara, Faculty of Architecture and Urbanism (ROMANIA)*
[2] *Politehnica University of Timisoara, Faculty of Civil Engineering (ROMANIA)*
E-mails: iasmina.apostol@student.upt.ro, marius.mosoarca@upt.ro, valeriu.stoian@upt.ro

Abstract

In western part of Romania, the end of the nineteenth and the beginning of the twentieth century were characterised by a specific way of construction, using reinforced concrete elements, such as slabs, beams, walls and framing. Despite of the reinforced concrete that was used, after earthquakes, historic buildings have recorded important damages, differentiated by the intensity and type of the earthquake. That happened because of the lack of seismic behaviour consideration, so the reinforced concrete that was used didn't work properly. In order to assure the existence of history for the next generations, we need to make sure that we understand the failure mechanisms and that we consolidate the structures based on The Chart of Venice principles. In order to do so, we decided to show some consolidation methods based on natural materials and reversible methods that were used on one reinforced concrete structure in Timisoara, Romania (case study). In Timisoara area there are a lot of similar buildings, so our case study can be used as a model for other buildings with similar problems.

Keywords: reinforced concrete, history, consolidation, reversible, natural materials

1 Introduction

In Banat area, Romania, there are a lot of historic structures made of reinforced concrete, such as dams, bridges, water towers, industrial buildings, roofs that weren't calculated or evaluated for seismic risk. Most of these structures have low bearing capacity because of low grade concrete, reinforcements without ductility that are highly damaged, low percentages of reinforcement, putting at risk the security of buildings and their historic value [1].

Vrancea and Banat are the two of the most important seismic zones in Romania. Vrancea area is characterised by intermediate deep earthquakes (150 km), with long duration and a large number of cycles. Those characteristics create significant inelastic deformations [2]. Banat area instead is characterised by shallow earthquakes, having a peak ground acceleration of 0.20g, with short periods of vibrations, pulse action with a powerful first cycle and horizontal and vertical components of the same size, as we can see in Table 1 [3]. Timisoara city is located in the Banat seismic area, so the historical buildings need to be revaluated for the capacity to face the specific seismic behaviour of the area.

Table 1 Intensities of earthquakes from Banat region on MSK scale

Seismic intensity	V	VI	VII	VII-VIII
	1889	1973	1879	1879
	1896		1859	1915
Year	1902		1900	1991
	1907		1941	
	1950		1959	

Different types of reinforcements, made without proper calculation and evaluation do not provide the necessary ductility for buildings located in the seismic zone Banat, Romania. On the other hand, interventions made properly, but based only on structural characteristics may not respect the restoration principles of The Chart of Venice, so appears the question: How can we assure the necessary strength for buildings with historical value without compromising that specific historical and cultural value? So, it is necessary to identify new and innovative methods to consolidate the reinforced concrete structure elements, using fibre-based materials. This article presents the state of degradation of one case study constructions and a modern way of strengthen this historic buildings with precisely reversible and natural solutions, that can be applied also on other similar cases.

2 Description of the building (case study) and state of degradation

The case study building is located in the historical centre of Timisoara, a city in the Banat seismic area, Romania. The buildings were made during 1934-3939, based on the specific construction types and technology of the time. The building has 10.75x19.10 m in plan, a basement level, a floor level and one story up. The main structure is based on a reinforced concrete frame, filled with masonry. Foundations are isolated as pillars, while the slab above the basement is made of reinforced concrete beams with a supplementary layer of wooden beams and reinforced concrete slab. The rest of the slabs are made of reinforced concrete beams with supplementary wooden beams and cases of wood [4].

The problems identified at the place are a lot and very different, because of the lack of interventions during time, as we can see in Fig. 1 a, b, c [4].

Fig. 1 Degradation of the building facades

The results of the experimental tests that were made on the columns and beams of the frame structure have shown a weak concrete, just C8/10 [5]. According to the technical expertise [4], the building was classified with Rs1 seismic risk, so it needed urgent interventions in order to put it in safety. Construction shows degradation, because of the lack of interventions during time. A few interventions were made, but not for the structure, with the only purpose to change interior compartmentations or interior design.

3 Modern methods for consolidation

In order to define the purpose of intervention, it was made a spatial analysis of the building using Axis Software, aiming to reduce lateral displacements and interstory drift, and increasing the stability, rigidity and bearing capacity of the main structure elements of resistance. The spatial-dynamic analysis was made first for the unconsolidated building (Fig. 2 a, b, c, d), for a q value considered 2. The values for the interstory drift are presented in Table 2 [6].

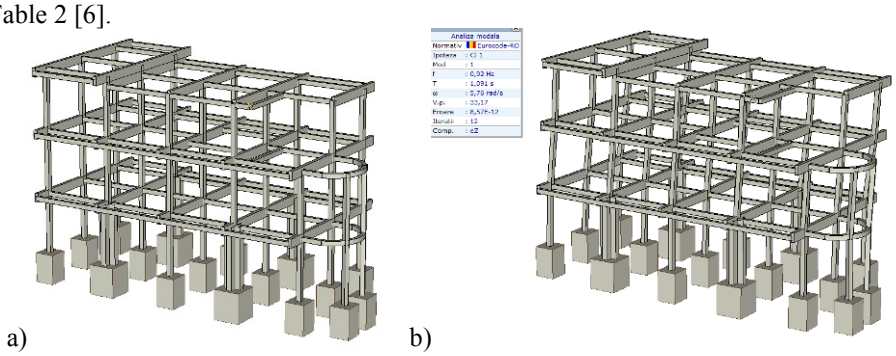

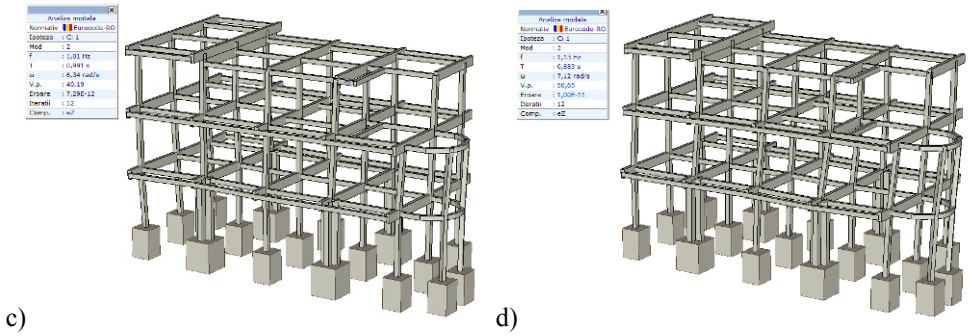

c) d)

Fig. 2 a) Undeformed shape of the building, b) Deformed shape of the building before consolidation - mode 1, period of vibration T=1.091 sec, c) Deformed shape of the building before consolidation - mode 2, period of vibration T=0.991 sec, d) Deformed shape of the building before consolidation - mode 3, period of vibration T=0.883 sec

Table 2. Interstory drift seismic action – before consolidating the building (q=2)

Level	h [mm]	ex [mm]	ey [mm]	ν	$\nu * d_{r} * q$ [mm]		0,01h [mm]	Resolution
Basement	3500	44	7	0.5	44.0	>	35	not OK
First floor	3600	51	28	0.5	51.0	>	36	not OK
Second floor	3500	24	35	0.5	35.0	>	35	not OK

To transfer forces to the foundation soil, at the basement floor level it was realized a general slab in a 30 cm thick concrete C20 / 25 reinforced bars BST 500 with diameters between ϕ16 ÷ ϕ18 / 15 cm. Transversal beams were strengthened with steel rolled L80x10. The forces transfer from the reinforced concrete floor to consolidated beams is made by welded connectors. The columns were consolidated with rolled steel L80x10 S235, a full-length that will work with existing reinforced concrete pillars by chemical anchors, at 30 cm distance between them, with supplementary stirrups type Geosteel G2000, product by Kerakoll, as we can see in Fig. 3 a, b, c and Fig. 4 a, b, c. Geosteel G200 is a fibre-based material, a balanced biaxial basalt fiber network, with special protective treatment with alkali-resistant water-free resin solvents, and of stainless steel AISI 304 microwires thermobonded between them in order to ensure a stable fabric in both directions and of easy application on site.

The main advantages of using this new material are:

- high durability thanks to the use of stainless steel AISI 304 and a high resistance to alkali basalt fiber, tested by strict environment durability tests saline and alkaline, freeze-thaw and high humidity;
- high shear, impact and abrasion guaranteed by the properties of basalt and microwires of stainless steel arranged in both directions in alongside the basalt yarn;
- excellent mechanical performance provided by special treatment with water-based resin which allows get a real network FRP
- increasing the bearing capacity of the columns without increasing the rigidity of the structure [7].

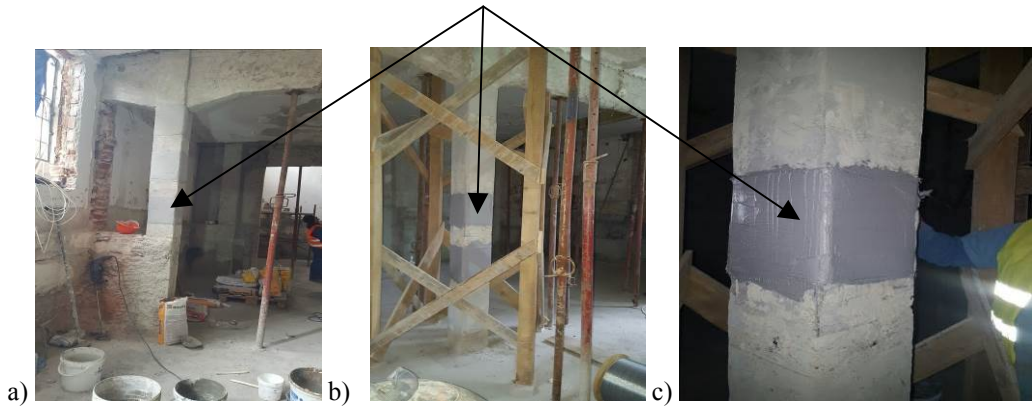

Fig. 3 Pictures of pilasters and beams consolidated with Kerakoll Geosteel 200 reversible solution

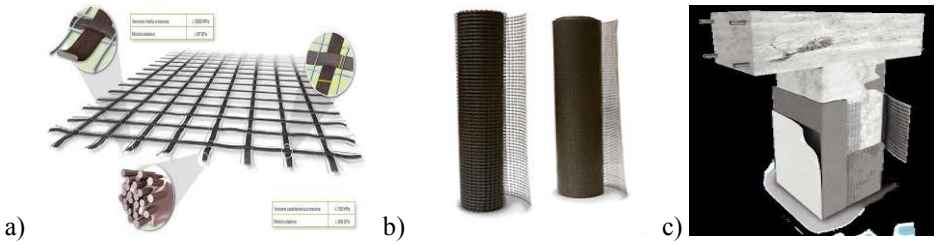

Fig. 4 Geosteel grid material

The rigidity and ductility of the structure was assured by introducing two reinforced concrete perimetral sheer walls, which didn't affect the general image of the building. The shape mode after consolidation is shown in Fig. 5 a, b, c. The values of the interstory drift after consolidation are presented in Table 3. One detail of the consolidated columns and beams is shown in Fig. 6.

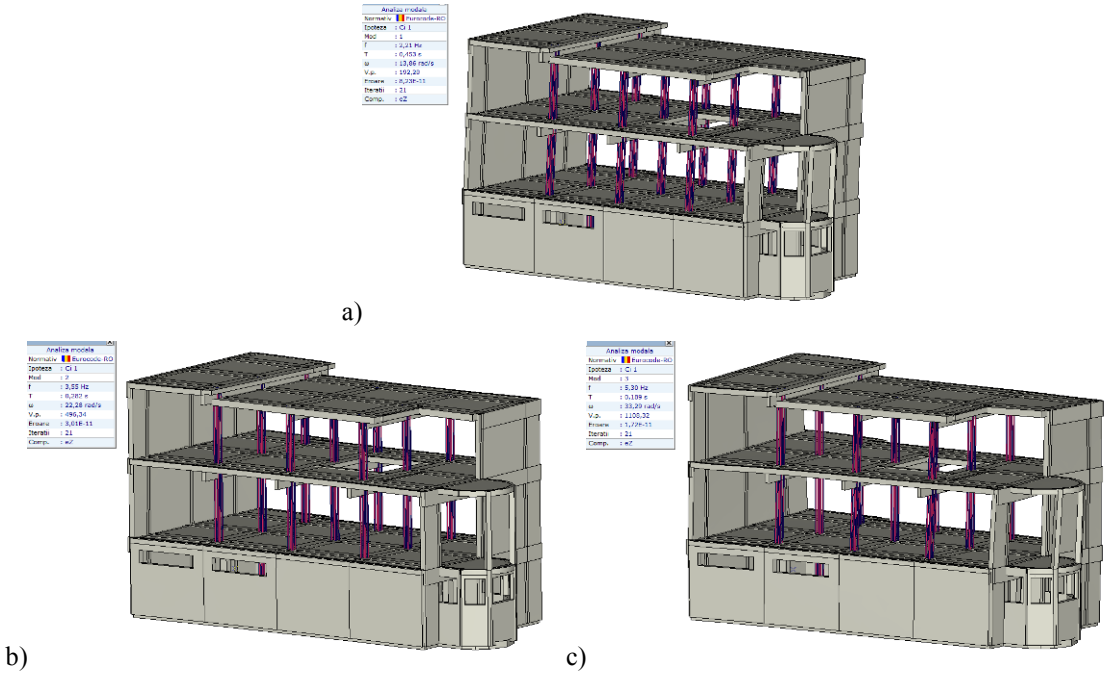

Fig. 5 a) Deformed shape of the building after consolidation - mode 1, period of vibration T=0.453 sec, b) Deformed shape of the building after consolidation - mode 2, period of vibration T=0.282 sec., c) Deformed shape of the building after consolidation - mode 3 , period of vibration T=0.189 sec.

Table 3 Interstory drift from seismic action - after consolidation of the building (q=2)

Level	h [mm]	ex [mm]	ey [mm]	ν	$\nu * d_r * q$ [mm]		0,01h [mm]	Resolution
Basement	3500	6	3	0.5	6.0	<	35	OK
First floor	3600	5	20	0.5	20.0	<	36	OK
Second floor	3600	4	17	0.5	17.0	<	36	OK

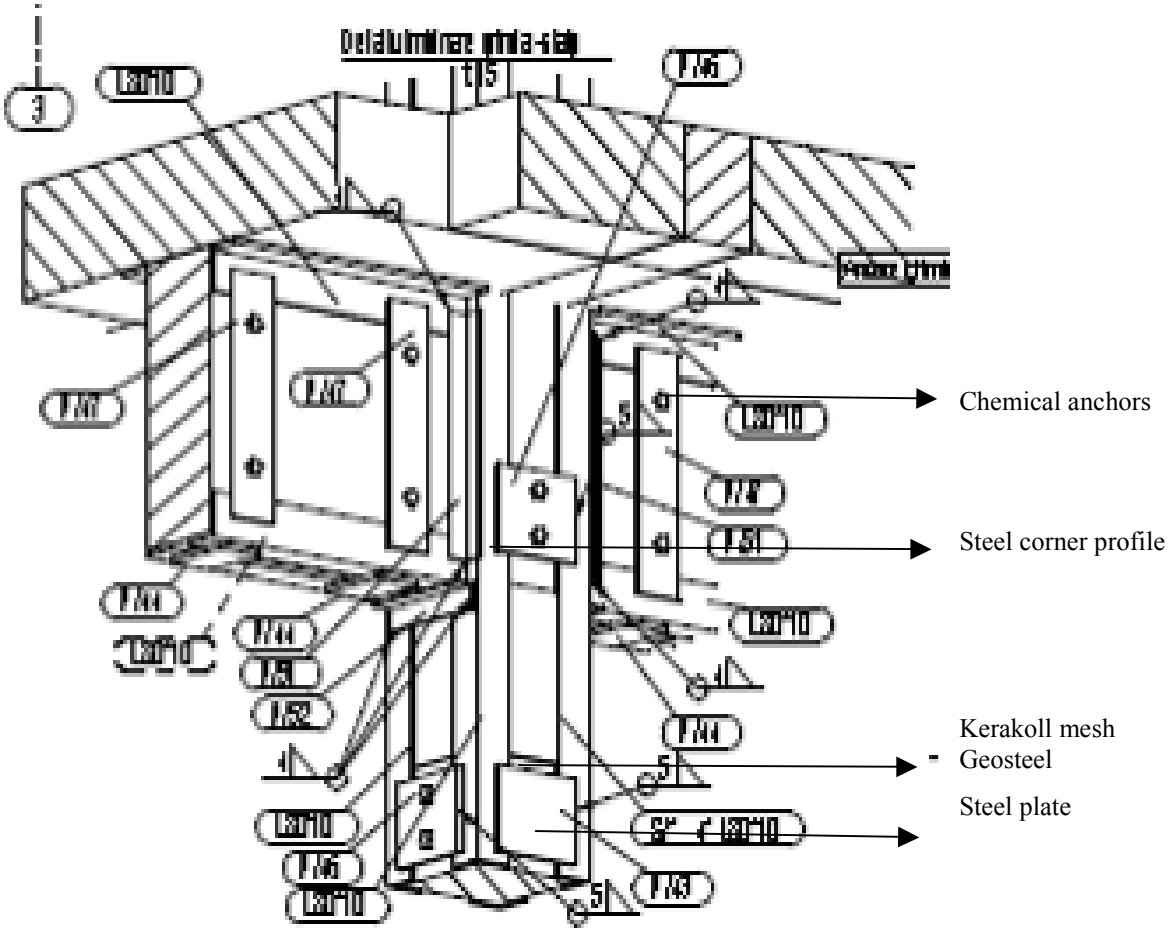

Fig. 6 Detail of consolidated columns and beams

It is very important to understand that, even if the design codes for concrete structures are in a constant change and evolution [8], historical buildings need a special approach, taking into consideration not only structural factors, but also historical and cultural ones.

4 Conclusion

This article presents a consolidation method with innovative methods and new materials for reinforced concrete columns with low bearing capacity. The consolidation proposal is reversible at any time, easy to execute and increases the bearing capacity of the reinforced concrete sections that are badly degraded and also have a small percentage of steel.

In Romania, there are normative design indications for masonry structures with historical value, but none for reinforced concrete structures with historical value. So, it is absolutely necessary to provide at least a guide for consolidation of concrete historical structures, in order to provide proper history knowledge for the next generations. Those indications should reveal proper consolidation methods for proper seismic behavior, and also should indicate materials and techniques that respect The Chart of Venice principles, so the consolidated structures can keep their historical and cultural values.

5 Acknowledgments

We would like to thanks to ing. Rares Bradean for all the technical assistance that he offered us during evaluation and structural calculation and during execution.

References

[1] Mosoarca, M., Gioncu, V. (2013). Structural safety of historical buildings made of reinforced concrete, from Banat region – Romania, Journal of Cultural Heritage, Volume 14, Issue 3, Supplement, ISSN: 1296-2074, eISSN: 1778-3674, Ed.Elsevier, pp e29-e34.

[2] Gioncu, V., Mosoarca, M. (2009). Ultimate limit state of masonry historical buildings using collapse mechanism methodology: Application for Orthodox Churches, PROHITECH 09, Taylor&Francis, London, pp 1153-1158.

[3] Mosoarca, M., Gioncu, V. (2013). Historic bearing structures. Synagogues in Timisoara. Structural degradation, 6th International Congress on Science and Technology for the Safeguard of Cultural Heritage in the Mediterranean Basin, Athens, pp 70.

[4] Marin, M. (2016). Tehnical expert's report nr. 4223/2016, unpublished.

[5] Mosoarca, M. (2016). Design project, unpublished.

[6] Incerc Institute (2016). Tehnical Report, Timisoara, unpublished.

[7] Kerakoll, The Green Building Company (2016). Guideline for the Consolidation, Structural Reinforcement and Seismic Security with New Green Technologies, p. 78-79.

[8] Chezan, C.M. (2014). Evolution of Design and Construction Practices for RC Wall Buildings in Romania, Journal of Applied Engineering Sciences, Vol.4(17), ISSUE 2/2014, pp 7-12, ISSN/ISSN-L 2247-3769/ e-ISSN2284-7197.

Determining the Optimal Dimensions of Fixed Shadowing Systems in View of Diminishing the Energy Consumption of the Buildings in Romania

Babota F.[1], Iernuţan R.[1], Moga L.M.[1], Munteanu C.[1], Tămaş F-L.[2]

[1] *Faculty of Civil Engineering, Technical University of Cluj-Napoca, 15 Constantin Daicoviciu Street, 400020 Cluj-Napoca (ROMANIA)*
[2] *Faculty of Civil Engineering, Technical University of Braşov, Braşov (ROMANIA)*
E-mail: florin.babota@ccm.utcluj.ro

Abstract

Depending upon the season, the sun light penetrating a building can have a different impact upon the building energy consumption. During winter, the sunlight reaching the southern oriented facade of the building can provide a passive solar radiation, reducing the energy consumption for building heating. However, during summer, the sun beams penetrating the building mainly through the southern orienting windows lead to an excess collection of heat. In this case, to diminish the thermal discomfort, the energy consumption increases because of the high need of cooling the area. Well designed fixed shadowing devices can diminish the cooling energy consumption during the warm season and also allow for increased energy contribution coming from solar beams. Shadowing has always been recommended as a passive manner of reducing the solar heat contribution. In order to reach this target, of diminishing energy consumption in Romanian buildings, the paper presents the calculations of the optimal dimensions of several fixed shadowing (eaves, sunblind).

Keywords: passive solar shading, solar control in buildings, shading of the building, optimal dimensions of fixed shadowing systems.

1 Introduction

Passive design is the key to sustainable building, it responds to local climate and site conditions to maximise building users' comfort and health while minimising energy use.

Using passive design can reduce temperature fluctuations, improve indoor air quality and make a home drier and more enjoyable to live in. It can also reduce energy use and environmental impacts such as greenhouse gas emissions.

Shading of house and outdoor spaces reduces summer temperatures, improves comfort and saves energy. Direct sun can generate the same heat as a single bar radiator over each square metre of a surface. Effective shading (which can include eaves, window awnings, shutters, pergolas and plantings) can block up to 90% of this heat. Shading of glass to reduce unwanted heat gain is critical, as unprotected glass is often the greatest source of heat gain in a house. However, poorly designed fixed shading can block winter sun. By calculating sun angles and considering climate and house orientation, it can be used shading to maximise thermal comfort [1].

Buildings should be designed in relation to specific climatic conditions, the changed function or the time of use or occupancy levels of internal and external spaces, and in relation to how these decisions will impact parts that remain unaltered. Landscaping can be used to improve both external and internal comfort and energy efficiency. Improvements can also be target specific, such as fitting shading devices over existing openings.

Studies of the impact of shading on annual energy use have demonstrated that shading devices reduce the cooling demand in buildings while increasing the heating loads due to loss of beneficial solar gains. Optimal shading strategies are thus climate dependent: in heating-dominated countries, fixed devices with medium to high solar transmittance and high thermal resistance or systems that can be removed in the winter are more energy efficient. Shading strategies for daylight buildings where artificial lighting is replaced by natural light through installation of dimming systems need to be investigated further [1].

The proper shadowing of a building reduces the inner temperature during summer, improves the interior comfort and saves energy. In order to perform this, it is necessary to know the position of the sun in the sky and the constructive characteristics of the building in question.

2 Position on the sun in the sky

The angle of the solar altitude γ_S [°] and the angle of solar azimuth α_S [°] represent the polar or angular coordinates defining the position of the sun in the sky relative to a reference point (observer) on the earth surface (Fig. 1) [1].

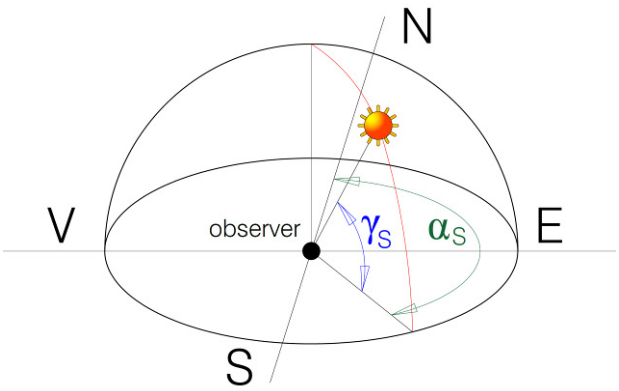

Fig. 1 The angle of the solar altitude γ_S and the angle of solar azimuth α_S [2]

The two angles are calculated with [2]:

$\gamma_S = \arcsin(\cos(\omega)\cdot\cos(\varphi)\cdot\cos(\delta) + \sin(\varphi)\cdot\sin(\delta))$
$\alpha_S = 180° \pm \arccos((\sin(\gamma S)\cdot\sin(\varphi) - \sin(\delta))/(\cos(\gamma S)\cdot\cos(\varphi)))$
$\pm$ = "+" when the solar time ST > 12:00 and "-" when the solar time ST < 12:00

With the two angles (or polar coordinates), one can draw the diagrams of the positions of the sun in the sky. The diagrams of the positions of the sun in the sky can be found for any location relative to the geographical coordinates, either with the algorithm shown here or with other calculation devices, among which a software Of the University of Oregon USA, Laboratory for monitoring solar radiation, software that can be found in the Internet [7].

Taking for Oradea the following geographical coordinates: latitude (φ=47.19°) and longitude (λ=23.06°), the sun position diagram as given by this software, shall be the one presented below (Fig.2):

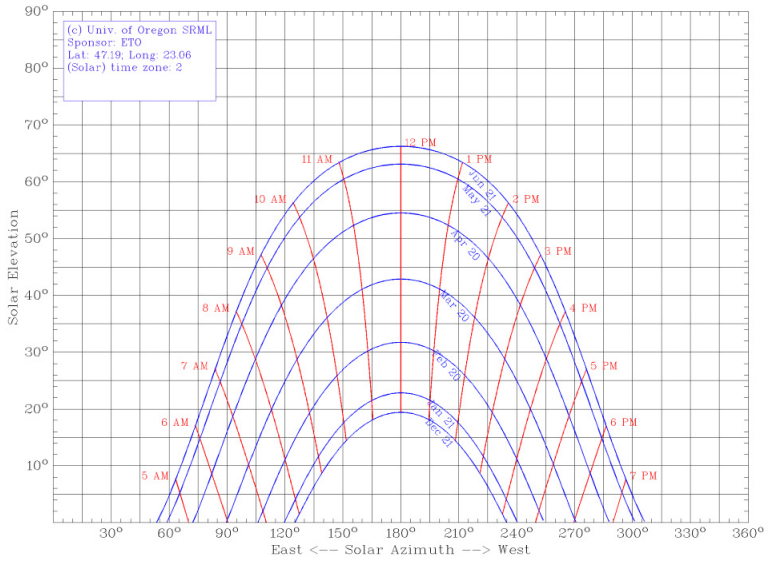

Fig. 2 The sun position diagram for Oradea

For temperate latitudes in northern hemisphere, the sun draws an arc of a circle in the sky, as follows:
- in winter: the sun rises in the south-west and sets at an azimuth angle of ± 70° (Fig. 3)
- in summer: the sun rises in the north-east and sets at an azimuth angle of ± 110° (Fig. 4).

The azimuth angle takes various values from one day to another, between the two extreme values mentioned before.

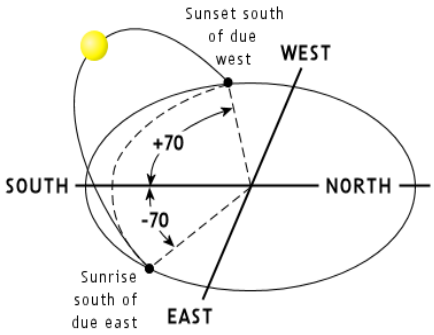

Fig. 3 Sun route during winter

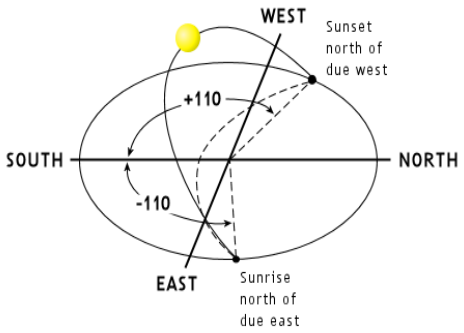

Fig. 4 Sun route during summer

During one day, the highest position of the sun above the horizon (maximum angle of solar altitude) occurs at midday (solar time 12.00). During one year, the angle of solar altitude during summer is maximum (summer solstice) and minimum during winter (winter solstice) (Fig. 5).

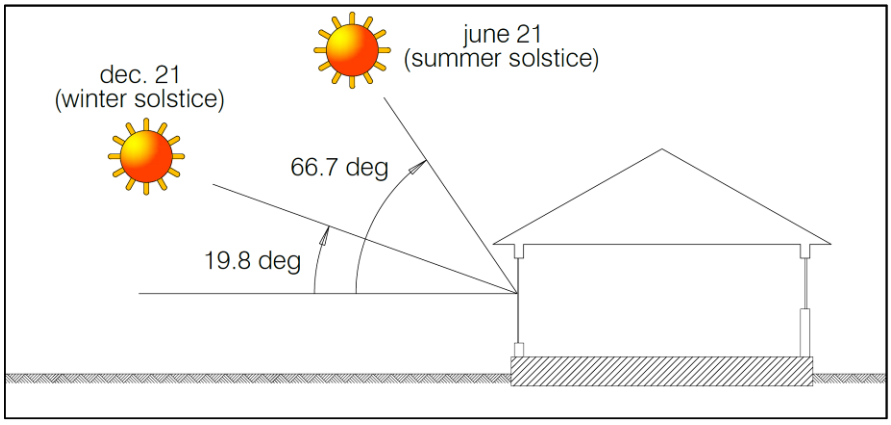

Fig. 5 Angles of solar altitude during an year (for example: Cluj-Napoca, Romania) [11]

3 Constructive principles for fixed shadowing systems

Fixed shadowing systems should be carefully designed so as to permit sun rays to fully penetrate the vitreous surfaces only during winter and stop them during summer not forgetting that the sun assumes the highest position in the sky during summer, and not also during winter.

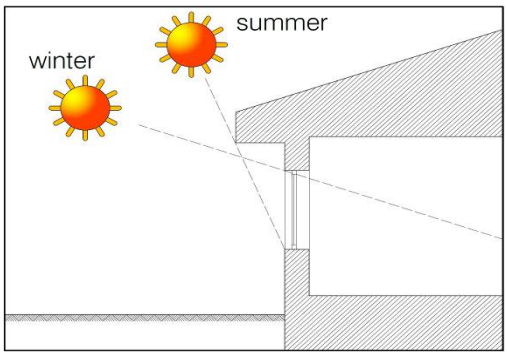

Fig. 6 Correct projection of the eaves [9]

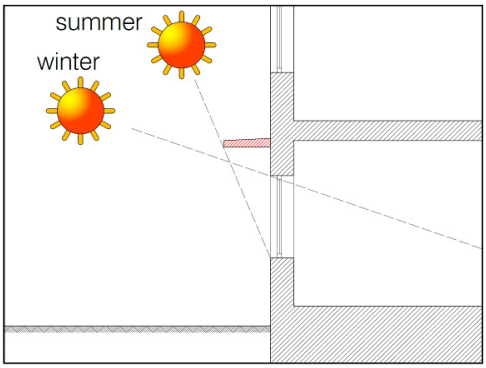

Fig. 7 Correct projection of the sunblind [9]

Shading can reduce the peakcooling load in buildings, thus reducing the size of the air conditioning equipment that will run fewer hours and consume less energy. Energy savings can range anywhere from 10%…40% [3]. Shading provides for the interception of direct solar radiation before it strikes building openings and heat absorbing materials. Interception techniques range from trees and roof overhangs to lightweight ventilated shading panels attached to walls and roofs [4]. Exterior shading devices are the most effective for creating tempered connections and transitions for indoor/outdoor spaces. The analysis suggested that solar

shading is quite useful to development of passive cooling system to maintain indoor room air temperature lower than the conventional building without shade [5].

Correctly projected eaves form, in general, the simplest and least expensive shadowing method for the southern facades in buildings with only one level or at the highest level and no other shadowing systems are required

4 Calculation of the optimal position and dimensions of the fixed shadowing systems

Shading devices should be integrated to a building's façade at an early design stage. This can be achieved using traditional design tools like solar path diagrams (Fig. 2), shading masks and special computer programs that automatically generate the optimum shading device geometry as a function of a set of input parameters [6].

In order to perform these calculations, the following hypotheses are taken:

- in the moment when sun reaches the highest point in the sky (summer solstice), the system is fully shadowed by the eaves/sunblind;
- in the moment when sun reaches the lowest point in the sky (winter solstice), solar beams shall fully pass through the vitreous surfaces.

The hypotheses are geometrically presented in Fig. 8 and mathematically, in the system of two equations below:

$$\begin{cases} tg\gamma_1 = \dfrac{h}{l} \\ tg\gamma_2 = \dfrac{h+H}{l} \end{cases} \quad (1)$$

where:

γ_1 - the angle of solar altitude, at winter solstice

γ_2 - the angle of solar altitude, at summer solstice

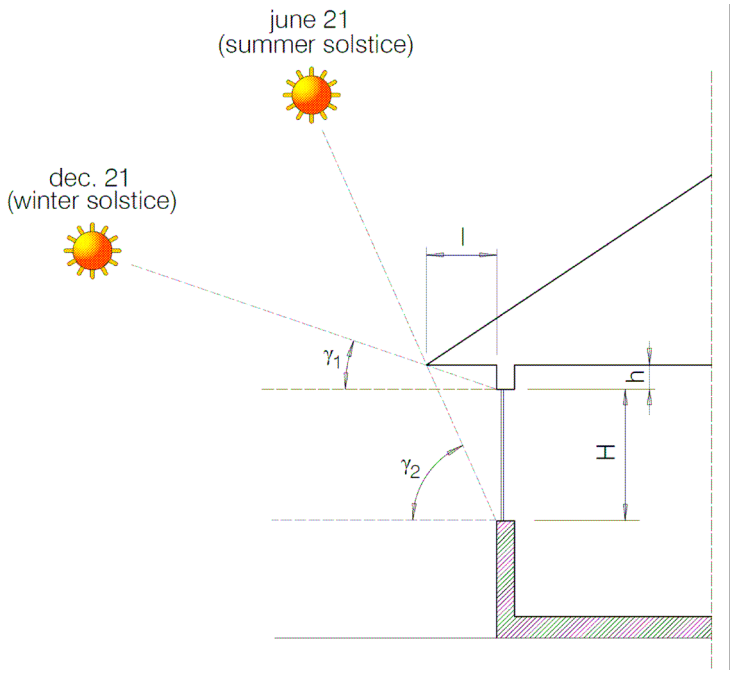

Fig. 8 Optimal position and dimensions of the eaves

The solution of the equations gives:

$$\begin{cases} l = \dfrac{h}{tg\gamma_1} \\ tg\gamma_2 = \dfrac{h+H}{\dfrac{h}{tg\gamma_1}} = \dfrac{(h+H)\cdot tg\gamma_1}{h} \end{cases} \quad (2)$$

$$\Rightarrow h \cdot tg\gamma_2 = h \cdot tg\gamma_1 + H \cdot tg\gamma_1 \Rightarrow h \cdot (tg\gamma_2 - tg\gamma_1) = H \cdot tg\gamma_1 \quad (3)$$

$$h = \frac{H \cdot tg\gamma_1}{tg\gamma_2 - tg\gamma_1} \quad (4)$$

$$l = \frac{H}{tg\gamma_2 - tg\gamma_1} \quad (5)$$

Using the two calculation formulae one can find depth "l" of the eaves or sunblind, related to the window (vitreous space) height "H" and angles of solar altitude (at summer and winter solstice). The angle of solar altitude is given by the geographical latitude of the building in question. This calculation was performed for a number of places in Romania (situated at differing geographical latitudes) using, as an example, two kinds of windows with common heights (of 1,2m and 1,5m). The results are given in Table 1 and Table 2.

Table 1 Dimension of the eaves or sun-blind in the case of a 1.2 m high window

	Place	γ_1 [°]	γ_2 [°]	H=1,2m	
				h [m]	l [m]
1	Iaşi	19,4	66,3	0,22	0,62
2	Oradea	19,6	66,4	0,22	0,62
3	Cluj-Napoca	19,8	66,7	0,22	0,61
4	Târgu-Mureş	20,1	66,9	0,22	0,61
5	Sibiu	20,8	67,6	0,22	0,59
6	Timişoara	20,9	67,7	0,22	0,58
7	Braşov	21,0	67,8	0,22	0,58
8	Brăila	21,3	68,2	0,22	0,57
9	Bucureşti	22,2	69,0	0,22	0,55
10	Constanţa	22,4	69,3	0,22	0,54

Table 2 Dimension of the eaves or sun-blind in the case of a 1.5 m high window

	Place	γ_1 [°]	γ_2 [°]	H=1,5m	
				h [m]	l [m]
1	Iaşi	19,4	66,3	0,28	0,78
2	Oradea	19,6	66,4	0,28	0,78
3	Cluj-Napoca	19,8	66,7	0,28	0,76
4	Târgu-Mureş	20,1	66,9	0,28	0,76
5	Sibiu	20,8	67,6	0,28	0,73
6	Timişoara	20,9	67,7	0,28	0,73
7	Braşov	21,0	67,8	0,28	0,73
8	Brăila	21,3	68,2	0,28	0,71
9	Bucureşti	22,2	69,0	0,28	0,68
10	Constanţa	22,4	69,3	0,28	0,67

5 Conclusions

The formulae shown and the calculations made reveal that the position of the fixed shadowing element versus the upper edge of the vitreous surface (dimension "h") does not depend upon the geographical latitude of the building, but only on the window height. Contrarily, the depth "l" of the eaves or sunblind is dependent upon both the window height "H" and the geographical latitude of the building (through the angles of the solar altitude).

The design method presented here can be used as a rule for quickly determining the optimal dimensions of a device for horizontal shadowing, related to the geographical latitude of the building and the shadowing height (the height of the vitreous surface). This kind of optimisation provides a maximum amount of heating from the solar beams during winter and a maximum efficiency in shadowing during the summer. In this way, mitigation in the building related energy costs can be achieved at minimal costs.

Utilisation of solar energy is an important part of energy efficient strategies. Solar radiation entering through transparent building components such as windows and glazed areas provides an important contribution

to heating, but can also give rise to excessive temperatures or large cooling demands. Solar protection in buildings such as special glass in windows can, when properly used, play a great part in reducing heating and cooling demands, and its use is therefore an important strategy for energy efficiency that should be evaluated at an early stage of design.

Solar shading affects energy use in a building by reducing solar gains and by modifying thermal losses through windows. Shading devices also influence daylighting levels in a room and the view to the exterior. Shading is thus closely connected with energy use in buildings for heating, cooling and lighting and with the occupants' visual and thermal comfort. Both energy use and comfort are crucial issues.

References

[1] Babota, Florin (2014). "Increase Energy Efficiency and Comfort in Homes by Incorporating Passive Solar Design Features." The Bulletin of the Polytechnic Institute of Jassy, Construction. Architecture Section 60.1, pp. 175-186.

[2] Bălan, M. C., et al. (2010). "Thermal solar collector behaviour in Romania." Polish Journal of Environmental Studies 19.1, pp. 231-241.

[3] Maleki, B. Ahmadkhani (2011). "Shading: passive cooling and energy conservation in buildings." International Journal on Technical and Physical Problems of Engineering (IJTPE) 3.4, pp. 72-79.

[4] Kamal, Mohammad Arif (2012). "An overview of passive cooling techniques in buildings: design concepts and architectural interventions." Acta Technica Napocensis: Civil Engineering & Architecture 55.1, pp. 84-97.

[5] Kumar, Rakesh, S. N. Garg, and S. C. Kaushik (2005). "Performance evaluation of multi-passive solar applications of a non air-conditioned building." International Journal of Environmental Technology and Management 5.1, pp. 60-75.

[6] Dubois, Marie-Claude (2000). "A simple chart to design shading devices considering the window solar angle dependent properties." Proceedings of the Eurosun 2000 Conference.

[7] http://solardat.uoregon.edu/SunChartProgram.html.

Energy Dissipation of retrofitted Precast Reinforced Concrete Walls subjected to seismic loading

Bindean I.A.[1], Fofiu M.[1], Stoian V.[1]

[1] *"Politehnica" University of Timisoara (ROMANIA)*
E-mails: andrei.bindean@student.upt.ro, mihai.fofiu@upt.ro, valeriu.stoian@upt

Abstract

This paper's purpose is to assess the capacity to dissipate energy of Precast Reinforced Concrete Wall Panels (PRCWP) subjected to seismic cyclic in plane loading. The authors present two specimens with different opening types; one has a door opening cut out from a window opening while the other has a large window opening. The specimens were subjected to in plane reversed cyclic loading, in order to simulate the seismic behaviour. After the specimens were tested, they were retrofitted using Carbon Fibre Reinforced Polymers (CFRP) strips mounted using the Externally Bonded Reinforcement (EBR) technique. The specimens were subjected again to the same loading procedure and the Cumulative Energy Dissipated (CED) for each cycle was computed.

Keywords: experimental test, energy dissipation, carbon fibre, seismic action.

1 Introduction

In this paper the authors investigate the capacity to dissipate energy and the difference in Cumulative Energy Dissipation (CED) of precast RC walls, subjected to seismic loading, before and after the retrofitting procedure. The goal is to observe how the retrofitting procedure affects the specimen's ability to dissipate energy, when subjected to in plane reversed cyclic loading, simulating a seismic load.

The structural system for the vast majority of apartment blocks in Romania, like in many former communist countries, is composed of Precast Reinforced Concrete Large Panels (PRCLP). A large amount of these buildings are old and in need of retrofitting. Studies have been made for different retrofitting systems for these walls [1], [2], [3], [4], [5], however, they only account for the elements maximum load bearing capacity and maximum drift, not analysing the energy dissipation capacity before and after the retrofitting strategy.

2 Experimental program

2.1 *Experimental specimens*

The elements presented in this paper are two PRCWP used in Romania for the typical five-storey residential buildings from 1970 to 1990. Two specimens were chosen for this paper, one with a large window opening (PRCWP L3) and one with a door opening cut-out from a window opening (PRCWP L1-E1), the specimens can be seen in Fig. 1. It can be seen that the top coupling beam is the most reinforced part of both specimens, while in the bottom part, below the window, there is less reinforcement. The tested specimen had the following dimensions: 2750 mm length, 2150 mm height and 100 mm thickness, while at each end a heavily reinforced T shaped boundary element was used to prevent out of plane displacement.

All features of the experimental test specimen like: dimensions, reinforcement details and material properties are taken from an existing building. Due to limitations imposed by the laboratory's dimensions and the maximum forced that could be induced by the testing gear, the element had to be scaled down by a factor of 1:1.2. It should be noted that the concrete quality of the two specimens was slightly different, although the concrete was prepared in the same concrete station respecting the same recipe. The PRCWP L3 had the concrete class C20/25 with an f_{ck}=21, 08 N/mm^2, whilst the PRCWP L1-E1 had the concrete class C16/20 with f_{ck}=17.95 N/mm^2.

For both specimens the same loading strategy was applied. Retrofitting was performed by means of Carbon Fibre Reinforced Polymers (CFRP) using Externally Bonded Reinforcement (EBR) technique for both

increasing the shear strength and to stich the cracks. The retrofitted elements are distinguished by the suffix TR which stands for element retrofitted post damage, and the T stands for element unstrengthen.

Fig. 1 Tested specimens, basic and retrofitted; left (PRCWP L1-E1), right (PRCWP L3)

2.2 *Experimental procedure*

The elements were subjected to in-plane horizontal cyclic forces induced by two hydraulic jacks supported by reaction frames. Also, the rocking effect was countered by two pseudo-constant vertical forces induced likewise by two hydraulic jacks who are visible in fig. 2. The vertical forces were kept constant at 150 kN and were increased only when the vertical displacement of the side from which the load was applied had 1mm displacement. For each mm of displacement, the load was increased by 100kN [2]. The lateral loads were applied using displacement control, the height of the wall being 2150 mm each loading step consisted of 0.1% of the height meaning 2.15mm. Hence the following load steps were implemented ±2.15mm, ±4.3mm, ±6.45mm, etc., respectively ±0.1%, ±0.2%, ±0.3%, etc. Two composite steel-reinforced concrete beams were used as load distribution systems. The remaining gap between the tested PRCWP and the beams was filled with high-strength mortar. For each load step two cycles were made and the experiment was stopped when the specimen lost 20% of its bearing capacity [2].

Ten displacement transducers and three pressure transducers were used to capture the force-displacement diagram. The test setup was designed to simulate the seismic action. This meant the test subject had to be exposed to pure shear and therefore loss of shear capacity was required as failure condition.

In this paper, the energy dissipated is calculated by using the area under the force-displacement hysteresis loops as presented in Fig. 3 and in [2], [6] and [7]. At each cycle the CED in both positive and negative direction were computed half cycle. In order to calculate the Cumulative Energy Dissipated (CED) the following incremental equation for the integration of the load displacement hysteresis loop was used:

$$CED_j = CED_{j-1} + \left(\delta_j - \delta_{j-1}\right) x \left(\frac{V_j}{2} + \frac{V_{j-1}}{2}\right)$$

where:

CED	is the Cumulative Energy Dissipated
j	is a point on the load displacement curve=a data line in the data file
δj	is the drift level
Vj	is the corresponding lateral load value

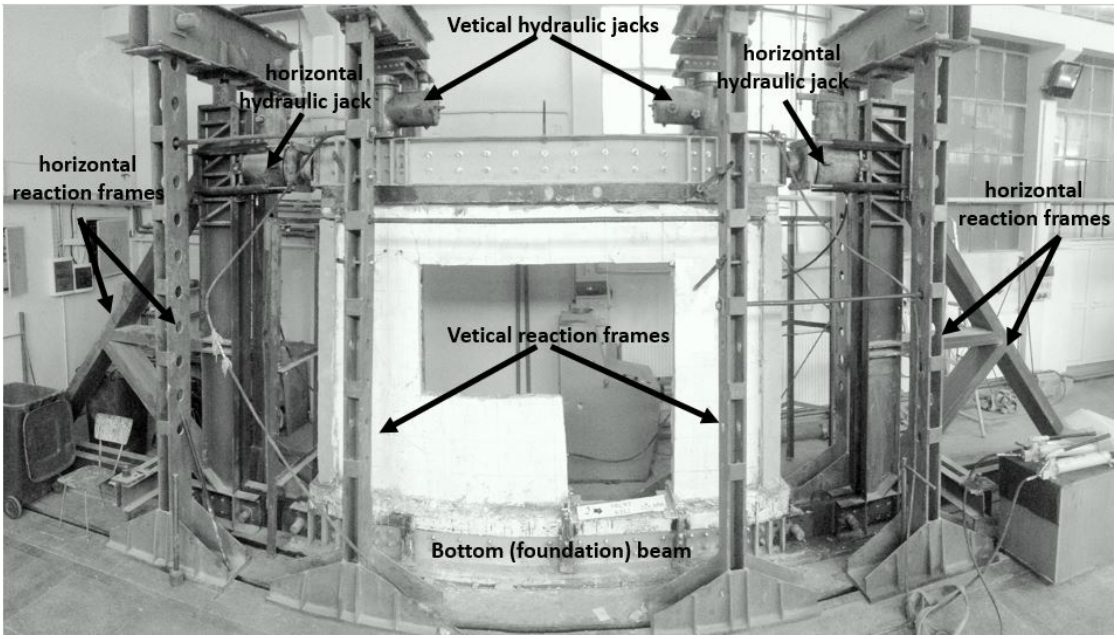

Fig. 2 Experimental stand

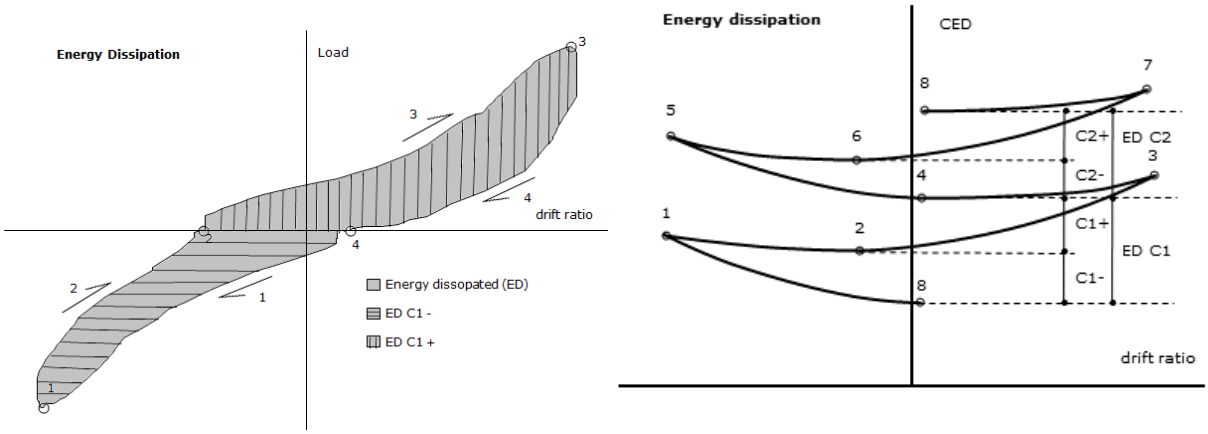

Fig. 3 Construction of energy disipation curve

3 Results and conclusions

Looking at the CED vs drift ratio diagrams presented in Fig. 4, one can observe that in both cases the retrofitted elements dissipated more energy, meaning that the retrofitting system increased the energy dissipation capabilities for the tested specimens. These results are similar to the ones obtained from literature [2], [8]. However, one should note the fact that these are only two specimens and the increase in CED for these retrofitted specimens is not enough to make a general assumption, that all PRCWP retrofitted using the above mention strategy will have larger CED compared to the unstrengthen ones. Further investigations are needed to be made on more specimens to have a definitive conclusion.

In regards to the opening type, it can be observed that the specimens with the small door opening, having a larger left pier managed to dissipate more energy, on the other hand, the concrete quality of the specimens was different, therefore the larger CED of the PRCWP L1-E1-T cannot be attributed only to the difference in the opening type.

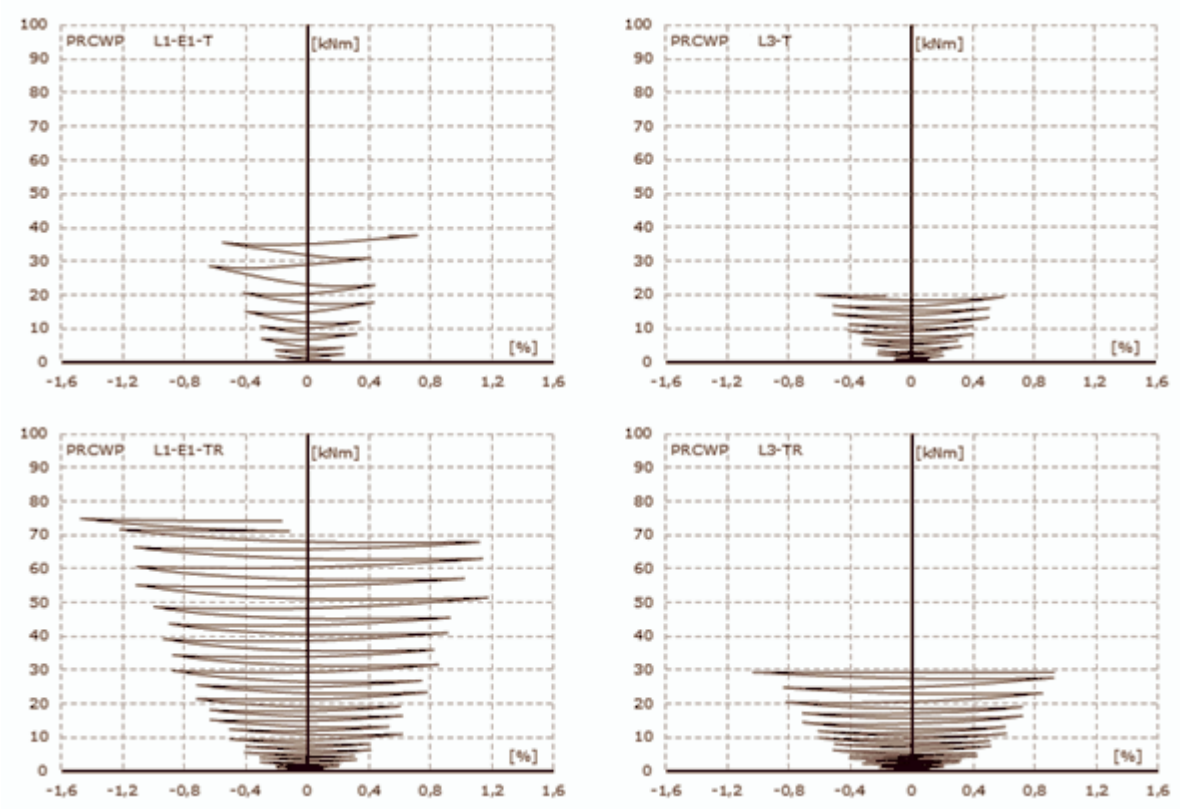

Fig. 4 Cumulative energy dissipated (CED) vs drift ratio

References

[1] Todut, C. Stoian, V., Demeter, I., (2013). Glass fiber versus carbon fiber grid used in textile reinforced mortar strengthening of precast RC walls, IACSIT International Journal of Engineering and Technology, vl.5, no.5, pp. 622-626.

[2] Demeter I. (2011). Seismic retrofit of precast RC walls by externally bonded CFRP composites. Romania: PhD Thesis, "Politehnica" University of Timisoara.

[3] Binici. B, Ozcebe, G., Ozcelik, R., (2007) Analysis and design of FRP composites for seismic retrofit of infill walls in reinforced concrete frames. Composites Part B: Engineering Volume 38(5-6), pp. 575-583.

[4] Todut, C. Dan, D., Stoian, V. (2014). Theoretical and experimental study on precast reinforced concrete wall panel subjected to shear force. Engineering Structures 80, pp. 323-328.

[5] Razaqpur, AG. Tolba, A. Contestabile, E., (2007) Blast loading response of reinforced concrete panels reinforced with externally bonded GFRP laminates, Composites Part B: Engineering Volume 38 (5-6), pp. 535-546.

[6] Hidalgo, PA. Jordan, RM., (1996). Strength and energy dissipation characteristics of reinforced concrete walls under shear failure. Proceedings of the Eleventh World Conference on Earthquake Engineering.

[7] Antoniades, KK. Salonikios, TN. Kappos, AJ. (2007). Evaluation of hysteretic response and strength of repaired R/C walls strengthened with FRPs. Engineering Structures 29(9), pp. 2158-2171.

[8] Todut C. (2015). Seismic strengthening of precast RC wall panels using FRP composites. Romania: PhD Thesis, "Politehnica" University of Timisoara.

Composite Steel Fibber Reinforced Concrete Shear Walls with Vertical Steel Encased Profiles. Experimental Study

Boita I.E.[1], Dan D.[1], Stoian V.A.[1], Florut S.C.[1], Todea V.C.[1]

[1] *Department of Civil Engineering, Politehnica University of Timisoara, 2nd T. Lalescu, 300223, Timisoara, (ROMANIA)*
ioana.boita@student.upt.ro, daniel.dan@upt.ro, valeriu.stoian@upt.ro, codrut.florut@upt.ro, viotin.todea@gmail.com

Abstract

The paper presents further results of an experimental program that was conducted at the "Politehnica" University of Timisoara, studying the behavior of composite steel-concrete shear walls (CSRCW) with partially incased profiles. Use of such shear walls represents a wide-spread solution for providing a lateral load resisting structural system, especially in the case of medium and high-rise buildings placed in seismic areas. As previous theoretical and experimental studies have proved the performance of such system, the foremost objective of the experimental program consisted in identifying innovative solutions for composite steel-concrete shear walls with enhanced performance, as steel fibber reinforced concrete which was used in order to replace traditional reinforced concrete. The program consisted in tests on 6 specimens designed as 1:3 scale steel-concrete composite elements, leading to an experimental matrix that enabled complex comparisons of various solutions. Thus a steel reinforced concrete shear wall (without any encased profiles) was used as reference, as configuration/arrangement of steel profiles and ratios of steel fibber reinforcement were varied within the other five specimens. The effective stiffness, strength and ductility are evaluated using the experimental results.

Keywords: steel fibber reinforced concrete, composite structures, seismic behaviour.

1 Introduction

During the last decade's incredible development have been made in concrete technology. One of the major progresses is Fibber Reinforced Concrete (FRC) which can be defined as a composite material consisting of simple concrete reinforced by the random dispersal of short, discontinuous, and discrete fine fibbers of specific geometry and material (steel, carbon, glass, plastic, etc.). Among all kinds of fibbers which can be used as concrete reinforcement, Steel Fibbers are the most popular ones.

Although most studies were developed on steel fibber reinforced concrete mixture and how the geometry and arrangements of steel fibbers in the concrete mixture can influence the mechanical properties of the composite material [1], there are also studies regarding the performances of small-scale elements such as beams [2] or beam-column joints [3]. This investigation implies that the use of FRC may be an alternative solution to increase the shear capacity and damage tolerance capacity. Steel fibbers, can be used in simple concrete mixture and also in ultra high performance concrete [4], [5] and self-compacting concrete mixture [6], [7] to improve the mechanical characteristics of materials, the bearing capacity of the structural elements and to reduce the amount of work in execution.

The main objective of this research project is to investigate the behavior of composite steel-concrete walls after replacing traditional field reinforcement with steel fibbers. The performances at lateral cyclic loads will be compared with those obtained from another research program that was also conducted at the University "Politehnica" in which was analyzed a series of six composite steel concrete wall structure (CSRCW - Composite Steel Concrete Reinforcement Wall) [8], [9].

2 Experimental specimens and test set-up

2.1 *Wall specimen characteristics*

The experimental program consists of six 1:3 scale Composite Steel Fibber Reinforced Concrete shear Walls (CSFRCW-1 to 6), designed using the principles from the existing codes, Eurocode 2, Eurocode 4 and Eurocode 8, [10], [11], [12], applied to composite steel-concrete elements. The results obtained from this program will be compared with the results from another research program developed also at the "Politehnica" University of Timisoara that studied 6 structural Composite Steel Reinforcement Concrete Walls (CSRCW). In order to provide an accurate comparison, the geometrical dimensions and the cross-section are similar in both studies. The only difference is that the traditional reinforcements were replaced with steel fibbers.

The experimental specimens have 3000 mm height, 1000 mm width and 100 mm in thickness, and represent a three storeys and one bay element from the base of a lateral resisting system made by shear walls. The wall panels were embedded in a heavily reinforced concrete foundation with 1500 mm length, 400 mm height and 350 mm width. The structural steel profiles were connected with the concrete web by headed shear stud connectors with d=13 mm diameter and h=75 mm length placed every 150 mm. The reinforcements from the edges of the web panel consist of 8Ø10 mm vertical bars and Ø8/75 mm horizontal stirrups. Both the steel profiles and the reinforcements were embedded into the reinforced concrete foundation block to ensure anchorage. The parameters of the steel sections used in CSFRCW specimens are presented in Table 1. The steel fibber contribution ratio is determined according to the Technical Regulation from 21/04/2003, [13]. The design details of all six types of composite steel fibber reinforced concrete walls are presented in Fig. 1. In this paper are presented some comparative results for the fourth specimen of each research program (CSFRCW-4 and CSRCW-4).

Table 1 Parameters of encased steel sections

Specimen label	Steel shape	Encasement level	bf [mm]	tf [mm]	hw [mm]	tw [mm]
CSFRCW-1	2□	fully	70	5	70	5
CSFRCW-2	2I	fully	70	7	56	7
CSFRCW-3	3I	fully	70	7	56	7
CSFRCW-4	2H	fully	70	7	56	7
CSFRCW-5	2I	partially	70	7	86	7

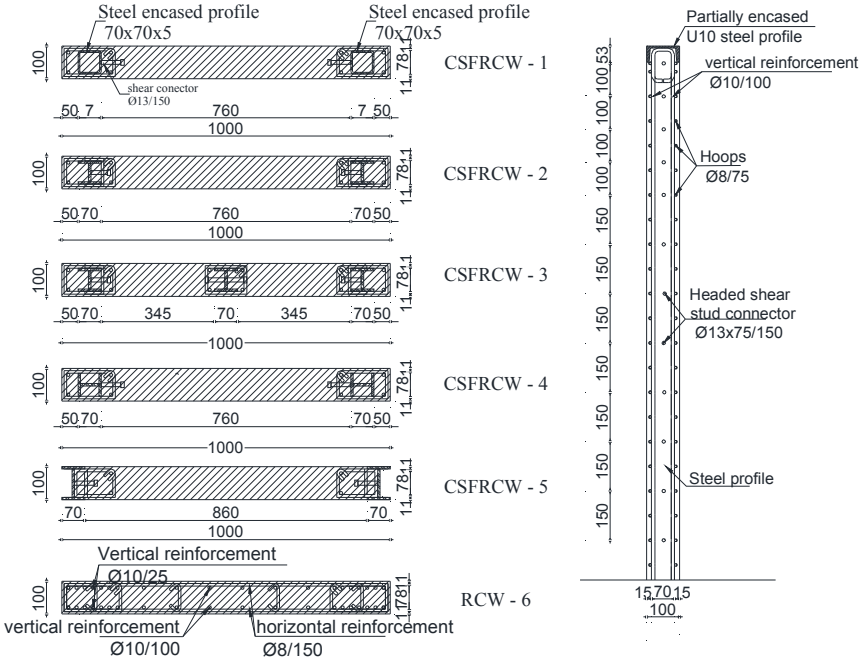

Fig. 1 Details of experimental specimens

2.2 Material properties

To determine the compressive and tensile strength of the concrete, 6 samples concrete cubes and 3 samples of prismatic elements were provided. After testing the concrete samples we obtained a strength class higher than the concrete design strength class (C20/25) used in the design process. For disperse reinforcement were used hooked steel fibbers with a tensile strength min. 1100 N/mm^2 and modulus of elasticity of 210x103 N/mm^2.

The design concrete quality was C30/37 class, the reinforcements Bst500S and the structural steel S355 JR (OL52-2k). The steel profiles were manufactured by welding the steel plates. The mixing formula of the concrete used to fabricate the specimens is the following: Cement 320 kg; Water: 170 kg/m3; Sand: 725 kg; Aggregate: 1087 kg; Filler: 70 kg; Additive: 3.5 l. The average value of cube strength at the age of 28 days is 43.06 N/mm^2, and of tension strength is 4.9 N/mm^2.

2.3 Test set-up and loading procedure

The experimental test was performed at the laboratory of Civil Engineering Department, at "Politehnica" University of Timisoara. The specimen was tested under constant vertical load and quasi-static reversed cyclic lateral loads. The lateral loads were applied alternatively from left and right. The test specimen was placed in the same plane as the loading frame, Fig.2, and was anchored with steel bolts into the laboratory reaction floor.

The loading frame consists of two steel braced frames, placed symmetrically. The lateral force was applied using two 400 kN hydraulic jacks, whereas the vertical force was induced by a 250 kN hydraulic jack. Initially, a constant vertical load of 100kN was applied to the specimen and was maintained constant during the test. The horizontal forces were applied at 400 mm below the top of the elements.

The recommended ECCS short testing procedure, [14], was used for the cyclic tests. The tests were performed in displacement control model. Minimum four cycles were performed before the elastic limit of the element was reached. After the elastic limit $\Delta y \cong 20$mm, three cycles were performed at each displacement level. The horizontal forces were applied under controlled cyclic displacements, until the strength of the specimens decreased to 85 % of the peak horizontal load. In order to monitor the behavior of the experimental specimen, pressure transducers, displacements transducers (D) and strain gauges (G) glued on the reinforcements bars and on the steel profiles, were used.

3 Experimental results

3.1 General behaviour and failure modes of fibber reinforced elements

The main objective of this research project is to investigate the possibility to replace totally or partially the traditional rebars placed in the field of composite walls with steel fibbers and to evaluate the main parameters of the behaviour stiffness, strength, ductility and make comparisons with common RC walls and Composite Shear Walls with steel encased profiles already tested in other experimental program [8, 9].

Generally, the behavior mode of a reinforced concrete wall subjected to in-plane lateral loading can be referred to as either flexural or shear. In the present experimental study, wall specimens CSFRCW-4 presented a shear mode failure with the damage of the concrete and steel profile yielding, a behaviour that is not accepted in seismic areas. The differences between the behaviour characteristics of the specimens are clearly visible by generating an envelope curve that describes the major hysteretic characteristics under cyclic loading (Fig. 3).

3.1.1 Cracking analysis

The behaviour of tested elements is presented in Fig. 3 and Table 2 for each displacement level followed by the cracking distribution during the test. For Specimen CSFRCW-4 Almost all cracks started developing at a distance of 15 cm form the edge of the wall, corresponding to the internal face of the steel profile, as the more rigid areas, the edges of the specimens reinforced with steel profile, vertical bars and stirrups, separate from the core of the wall.

The cracks appear when the tensile strength of the concrete is exceeded and the developing direction is generally perpendicular to the direction of the tension stresses. Before the elastic limit is reached only diffused cracks are formed, after this loading stage existing cracks develop towards failure, Fig. 4. For element CSFRCW-4 the first crack appeared approximately at 25 cm from the bottom line during the cycle 0.75 Δy, corresponding to a 15mm drift. During the next loading step, Δy, new horizontal cracks and the extension of the existing ones were observed. As loading cycles continue, diagonal cracks developed towards failure, in cycle $2\Delta y$.

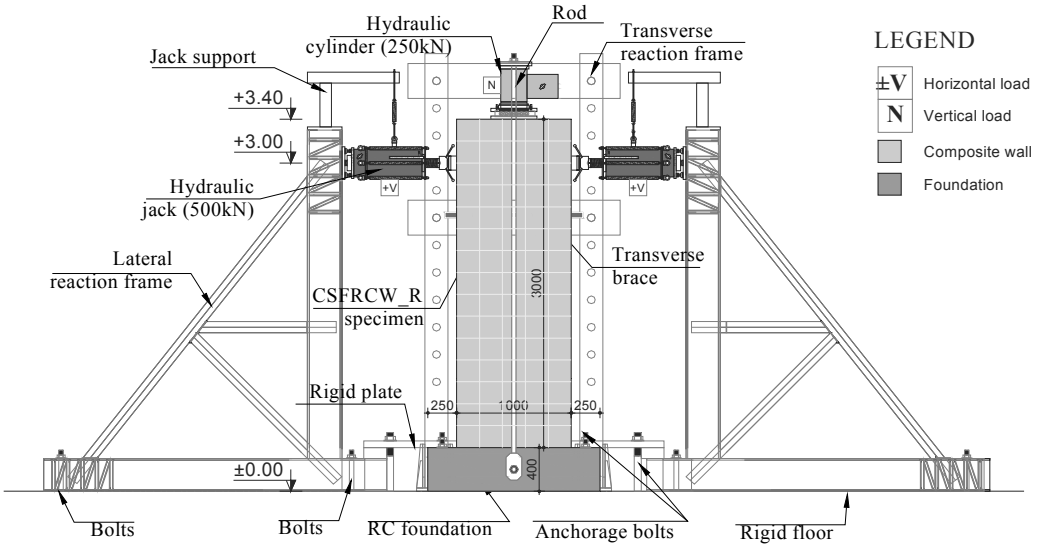

Fig. 2 General view of the test set-up

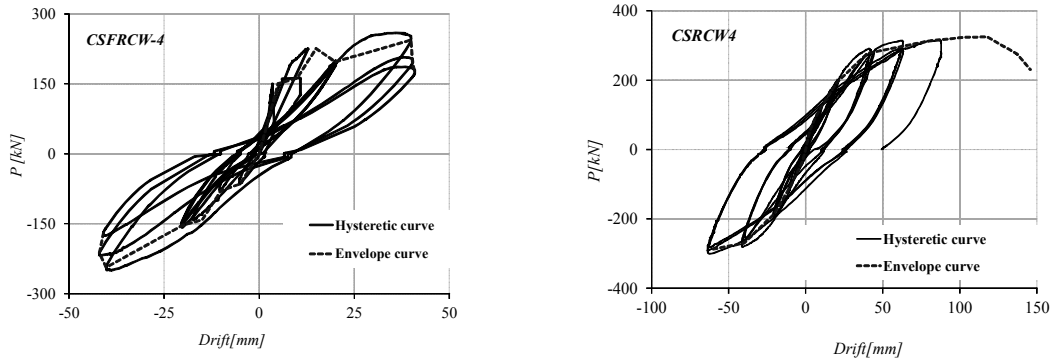

Fig. 3 Cyclic load drift envelope curves of specimens.

Table 2 Response characteristics of the specimen

Displacement stage Δ (mm)	Behavior aspects	
	CSRCW-4	CSFRCW-4
Δ < 5mm	No visible cracks appeared	
5 < Δ < 10mm	First horizontal cracks appeared	No visible cracks appeared
10 < Δ < 20mm	Horizontal cracks developed rapidly. Inclined cracks begin to develop from the horizontal ones	Diffuse inclined cracks appeared. Inclined cracks developed along element and old cracks openings increased
20 < Δ < 40mm	Inclined cracks developed along element	Failure: Cracks developed towards failure. Crushing of compressed concrete in one direction
Δ > 40mm	Failure: The horizontal and inclined cracks openings increased. The crushing of the compressed concrete produced in both directions	

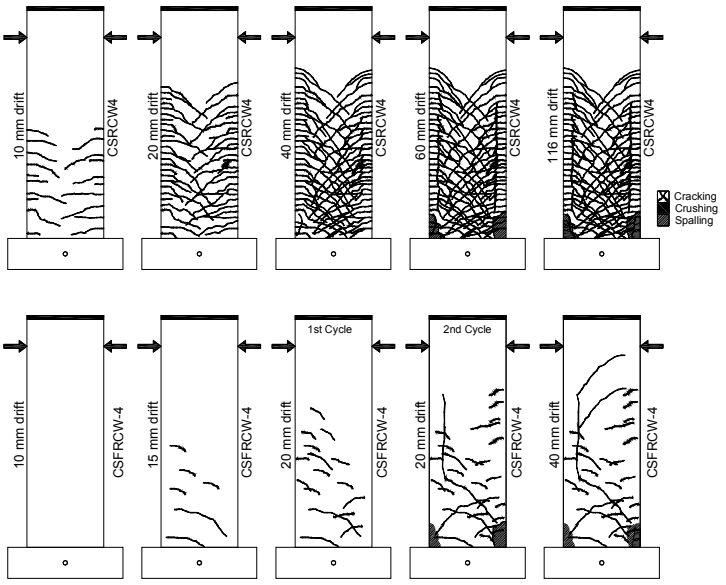

Fig. 4 Representation of crack distribution at every displacement level

3.1.2 Strength and ductility analysis

The strength of the specimens is defined in terms of load bearing capacity and represents the maximum applied horizontal force, Pmax. The absolute values of the load bearing capacity for both specimens are presented in Fig. 5. Although the values of the maximum force are closer, the failure mode is different. Element CSFRCW-4 had a shear failure at a small displacement capacity compared with element CSRCW-4 from the past research, and as it can be observed in Fig. 6 the displacement ductility is very low in the case of composite walls reinforced with steel fibbers.

The behaviour of the tested elements is characterized by the four main points denoted as: initial cracking, element yielding, limit stage and failure stage. In Table 3 are presented the correspondence between the forces and the displacements at each characteristic point from the tests. It can be observed that for the CSFRCW-4 wall initial cracking occurs at a higher force and displacement than for element CSRCW-4. It can be observed that in comparison with element CSRCW-4, until the elastic limit is reached, for element CSFRCW-4 initial cracking occurs at a higher force corresponding to a higher displacement level (Fig. 7). After the elastic limit stage, existing cracks develop leading to a brittle failure of the steel fibber reinforced concrete.

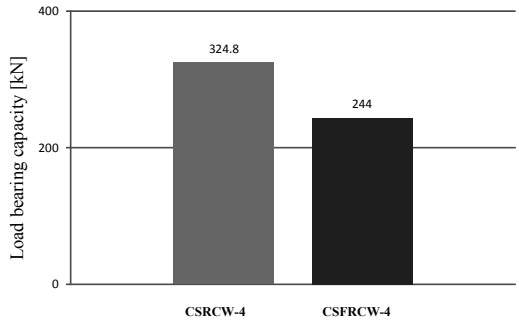

Fig. 5 The load bearing capacity of the specimens

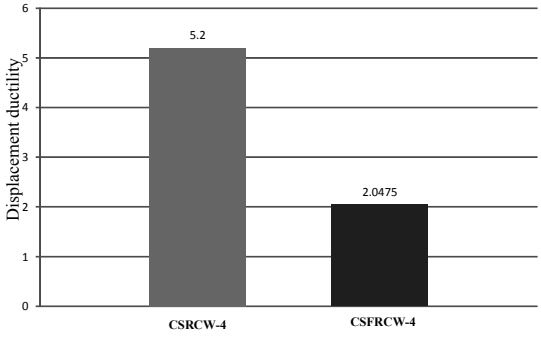

Fig. 6 Displacement ductility

Table 3 Force and displacement at different characteristic stages

Specimen	Initial cracking		Element yielding		Limit stage		Failure stage	
	Pcr [kN]	Δcr [mm]	Py [kN]	Δy [mm]	Pmax [kN]	Δmax [mm]	P85% [kN]	Δ85% [mm]
CSFRCW-4	120.5	10.02	175.07	21.84	244	39.96	174.6	40.95
CSRCW-4	94.6	7.56	238.6	26.4	324.8	117.8	275.4	137.2

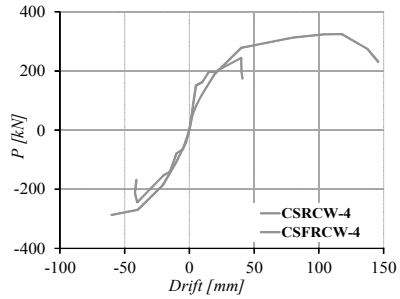

Fig. 7 Envelope curves of specimens.

4 Conclusions

Using the information presented above and the information from specific literature the following conclusions can be formulated:

1. The results shown the failure mode of the element, with a diagonal crack developing towards failure and yielding of vertical reinforcements and structural steel.
2. Comparing with CSRCW it can be observed that although the maximum load bearing capacities are quite similar, failure was brittle and occurred at a smaller displacement, the displacement ductility significantly smaller.
3. The connection between steel encased profile and reinforced concrete using welded studs behaved as full connection as was assumed in the designing process.

References

[1] Facundo Isla, Gonzalo Ruano, Bibiana Luccioni (2015). Analysis of steel fibbers pull-out. Experimental study. Construction and Building Materials 100, pp. 183-193.
[2] Halit Cenan Mertol, Eray Baran Hussain Jibril Bello (2015). Flexural behavior of lightly and heavily reinforced steel fibber concrete beams. Construction and Building Materials 98, pp. 185-193.
[3] Siva Chidambaram R., Pankaj Agarwal (2015). Seismic behaviour of hybrid fibber reinforced cementious composite beam-column joints. Materials and Design 86, pp. 771-781.
[4] Yu R., Spiesz P., Brouwers H.J.H. (2014). Mix design and properties assessment of Ultra-High Performance Fibber Reinforced Concrete (UHPFRC). Cement and Concrete Research 56, pp. 29-39.
[5] Doo-Yeol Yoo, Young-Soo Yoon (2015). Structural performance of ultra-high-performance concrete beams with different steel fibbers. Engineering Structures 102, pp. 409-423.
[6] Reza Ghavidel, Rahmat Madandoust, Malek Mohammad Ranjbar (2015). Reliability of pull-off test for steel fibber reinforced self-compacting concrete. Measurement 73, pp. 628-639.
[7] Alireza Khaloo, Elias Molaei Raisi, Payam Hosseini, Hamidreza Tahsiri (2014). Mechanical performance of self-compacting concrete reinforced with steel fibbers. Construction and Building Materials 51, pp. 179-186.
[8] Dan, D., Fabian, A. & Stoian, V. (2011). Theoretical and experimental study on composite steel–concrete shears walls with vertical steel encased profiles. Journal of Constructional Steel Research 67, pp. 800-813.
[9] Dan, D., Fabian, A. & Stoian, V. (2011). Nonlinear behaviour of composite shear walls with vertical steel encased profiles. Engineering Structures 33, pp. 2794-2804.
[10] EN 1992-1-1. Eurocode 2: Design of concrete structures, part 1-1, general rules and rules for buildings.
[11] EN 1994-1-1. Eurocode 4: Design of composite steel and concrete structures, part 1-1, general rules and rules for buildings.
[12] EN 1998-1. Eurocode 8: Design of structures for earthquake resistance.
[13] Technical Regulation “Guide to establishing the criteria for performances and composition for steel fibber reinforced concrete (in Romanian), Monitorul Oficial (Off. Monitor), 1, No.575bis, 12/08/2003.
[14] ECCS (1999). Recommended testing procedure for assessing the behaviour of structural steel elements under cyclic loads, European Convention for Constructional Steelwork.

Thermal Performances of a Ground-Air Heat Exchanger Integrated in a Mechanical Ventilation System of a Residential Building – Daily and Hourly Models

Brata S.[1], Cotorobai V.[2], Brata S.[1], Tanasa C.[1]

[1] *Politehnica University Timisoara, Department of Civil Engineering and Installations Engineering (ROMANIA)*
[2] *A"Gheorghe Asachi" University from Iasi, Department of Installations Engineering (ROMANIA)*
E-mails: silviana.brata@upt.ro, cotorobai.victoria@gmail.com, bratasorin@yahoo.com, cristina.tanasa@student.upt.ro

Abstract

Ground-air heat exchangers positioned next to or near residential buildings are used for pre-heating or pre-cooling the air needed for building ventilation. Currently, the determination of their thermal performance can be achieved by simulation tools designed for this purpose. In order to determine the heat flows taken by the air or transferred by the air to the ground, two computation models are used, a model with daily time step and a model with hourly time step. In the end, this paper presents the thermal performance of the ground-air heat exchanger based on energy transferred during the entire period of the standard climatic year and temperatures obtained at the outlet of the heat exchanger compared to inlet air temperature.

Keywords: ground-air heat exchanger, computational models.

1 Introduction

According to the amendments to Law 372/2005 republished on energy performance of buildings, by 31 December 2020 all new buildings are nearly zero-energy buildings meaning the energy consumption from conventional sources is nearly zero. The maximum allowed values for primary energy and CO_2 emissions for individual residential buildings are presented in Table 1 [1].

Table 1 Maximum allowed values for primary energy and CO2 emissions

Climatic zone	Primary energy [kWh/m^2 year]	CO_2 emissions [kg/m^2 an]
I	115	31
II	121	34
III	155	41
IV	201	51
V	229	57

The technical solutions applied to the thermal envelope and installations system of the building will contribute to the achievement of nearly zero energy consumption goals. This paper presents a study on the capability of a ground-air heat exchanger to reduce the energy consumption of the mechanical ventilation system in individual residential buildings.

Bisoniya et al. presented in [2] a synthesis on the models for one-, two- and three dimensional numerical simulations for the technical behaviour of the ground-air heat exchanger. These heat exchangers are used with the purpose of reducing the energy consumption from conventional sources. An important conclusion of the study presented in [3] is that a ground-air heat exchanger which is correctly dimensioned might reduce with 30% the electrical energy consumption of a conventional residential building. That goes without saying that the two- and three- dimensional simulation models lead to more accurate results that are likely to describe the real phenomena. The research presented in [3] shows an experimental study on the determination of the

performance coefficient of a ground-air heat exchanger used for air heating and cooling. Another study [4] develops a formula for ground-air heat exchanger design at a certain level of performance in terms of heat transfer. The soil temperature measurements that are presented in [5] are compared to the simulations performed in TRNSYS software, which uses the Kasuda formula for determining the soil temperature.

The Kasuda model was also used in [6] to determine the temperature of the soil at different depths. The results of monitoring of ground-air SC are presented in case study on an energy-efficient building [10].

2 Computational models

2.1 *General*

The comparative numerical simulation was performed using Microsoft Excel software using the specific calculation formulas for two computation models, an hourly model [8] and a daily model as presented in standard EN 15241 [9], which is part of the package of standards used for the Romanian methodology for determining the energy performance of buildings and installations Mc001. The ground-air heat exchanger studied in this paper is composed of a single plastic pipe that has the thermal and geometrical characteristics presented in Table 2.

Table 2 Thermal and geometrical parameters of the studied ground-air heat exchanger

Parameter	Value
Thermal conductivity, in W/(mK)	0.30
Exterior diameter, in m	0.200
Interior diameter, in m	0.185
Length, in m	35

The studied ground-air heat exchanger (GAHE) is common in terms of diameter and length for residential buildings that have an effective surface are between 150 m^2 and 200 m^2.

2.2 *Climatic Data*

The hourly values for the exterior air temperature that are used in the computation are given in the TRNSYS library based on METEONORM data. Fig. 1 presents the variation of the hourly outdoor air temperature during a year for the city of Timisoara.

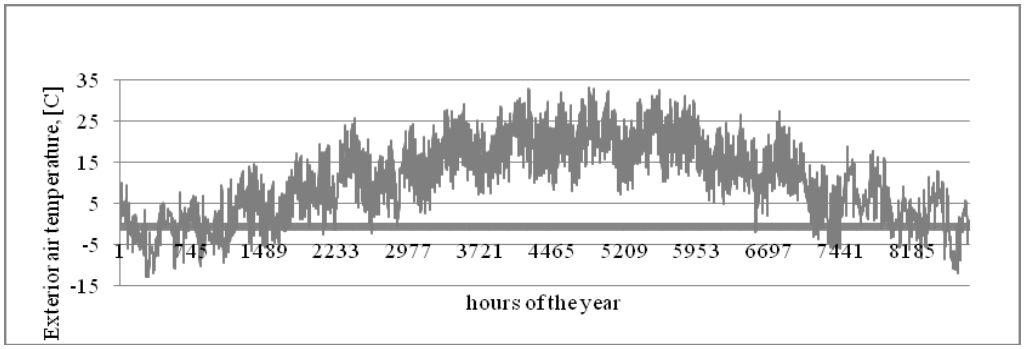

Fig. 1 Hourly exterior air temperatures for the city of Timisoara

The annual average temperature for the outdoor air is 10.6°C, the maximum average temperature is 21.3°C in July and the minimum is -1.6 ° C in January. The daily values of the outdoor air temperature used in the daily time step model were determined by calculating the corresponding arithmetical averages.

2.3 *Soil Characteristics*

In the analysis of the soil influence on the heat transfer phenomena in a ground-air heat exchanger, the thermal characteristics of soils have to be considered. The thermal conductivity of the soil depends on the mineral nature of the earths, dry bulk density and soil humidity. Since the installation depth of the heat exchanger is lower than the freezing depth, the soil freezing phenomena will not be studied. The soil type considered in this study is clay soil.

The technical parameters of the considered soil are presented in Table 3 and were established based on the characteristics presented in the C107 Romanian norm.

Table 3 Clay soils parameters according to C107

Characteristics	Interval
Soil porosity [%]	20-70
Dry bulk density [kg/m^3]	800-2200
Humidity [%]	10-40
Heat mass capacity [J/(kgK)]	1400-2600
Volumetric heat capacity [J/(m^{3}K)]	$3.0 \cdot 10^6$-$2.5 \cdot 10^6$
Thermal conductivity [W/(mK)]	1.5-2.0

There were also considered the dry bulk density, heat mass capacity and thermal conductivity values recommended for clay soils in EN 15241 [9], as seen in Table 4.

Table 4 Clay soils parameters according to EN 15421

Characteristics	Interval
Dry bulk density [kg/m^3]	1800
Heat mass capacity [J/(kgK)]	1340-1590
Thermal conductivity [W/(mK)]	1.45-2.9

The study presented in this paper was performed using the value of 1.6 W/(mK) for thermal conductivity and 2600 J/(m^{3}K) for the volumetric heat capacity.

2.4 *Soil Temperature*

The used calculation formula, the Kasuda formula, is presented in Type 77 of the TRNSYS software documentation and determines the soil temperature, t_G, for the current day of the year, t_{now}, depending on the annual evolution of the outdoor air temperature, soil type characterized by thermal diffusivity and depth from the surface of the soil. Table 5 presents the input data and the specific notations for the parameters used in the daily time step model.

Table 5 Input parameters for the dynamic simulation with daily time step

Parameters		
Name	Symbol	Value
The annual average temperature for the outdoor air, in ^{o}C	t_{mean}	10.6
Day of the year with the lowest temperature	t_{shift}	12
Depth from the surface of the soil, in m	z	1.5; 1.8; 2.0; 2.5; 3.0; 3.5
Soil temperature amplitude	t_{amp}	19.09
Soil thermal conductivity, in W/(mK)	λ	1.6
Soil thermal diffusivity, in m^2/day	α	0.05317

The graphic representations of soil temperature variation for the depths of 1.5, 2.0, 2.5, 3.0 and 3.5 m are shown in Fig. 2. The soil temperature remains constant throughout the year at a certain depth. In this case it tends to a constant value of 10.6 ° C, the annual average temperature of the outdoor air.

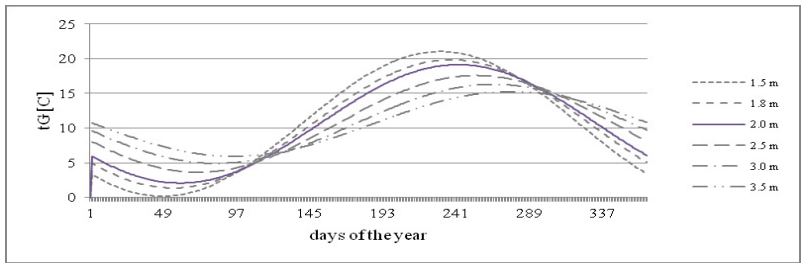

Fig. 2 Graphic representations of daily soil temperature variation depending on the depth (Kasuda formula)

By applying the hourly time step model, the soil temperature is determined with the formula presented in EN 15241 [9]. The input data and the specific notations for the parameters used in the hourly time step model are presented in Table 6.

Table 6 Input parameters for the dynamic simulation with hourly time step

Parameters		
Name	Symbol	Value
Correction factor depending on the soil type	gm	1.04
The annual average temperature for the outdoor air, in ^oC	t_{AM}	10.6
Correction factor for the amplitude	AH	variable
Annual outdoor air temperature amplitude	Δt_A	11.45
Correction factor for the soil temperature	VS	variable
Depth from the surface of the soil, in m	z	1.5…3.5

For the same installation depths for the heat exchanger 1.5, 2.0, 2.5, 3.0 and 3.5 m, as in the daily time step model, Fig. 3 show graphs of hourly soil temperature variations calculated by the hourly time step model.

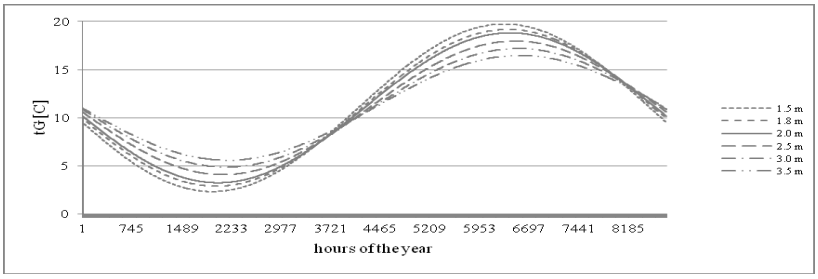

Fig. 3 Graphic representations of hourly soil temperature variation depending on the depth

Note that the models studied for the soil temperature calculation at different depths do not consider as a calculation parameter the distance location of the underground tube to the building it serves, thus, not considering the influence of the building on soil temperature.

2.5 *Building Ventilation*

The volumetric flow required by a person in case of providing domestic work is (10-15) l/s or (43-65) m^3/h for buildings integrated in the second category of buildings, respectively (6-10) l/s or (26-43) m^3/h for third category of buildings, according to the Romanian methodology for determining the energy performance of buildings Mc001. In this study it was considered that the ground-air heat exchanger serves a single family building composed of four members and the specific air flow of fresh air is 30 m^3/h/person, a value that meets the requirement for fresh air input when the concept of "passive house" is considered. The obtained total mass flow is $q_m = 0.04$ kg/s.

2.6 Air Temperature at the Exit of the Heat Exchanger

Both calculation models determine the air temperature at the exit of the ground-air heat exchanger. For this purpose the equation presented in EN 15241 is used. The equation depends on the soil temperature, air temperature at the entrance in the heat exchanger, $t_{a,i}$,, (the hourly or daily temperature of the outdoor air), the heat transfer coefficient that characterizes the soil-air or air-soil heat transfer depending on the thermal conductivity of the pipe material, inner and outer diameter of the pipe and air-inner wall of the pipe convection coefficient. The convection coefficient for air-inner wall of the pipe was determined using the Schack formula [10] and resulted close hourly values, with an annual average value of 7.44 W/(m^2K). Also, close hourly values were obtained for the heat transfer coefficient with the annual average value of 5.69 W/(m^2K). The graphic variations of the air temperature at the exit of the ground-air heat exchanger are presented only for the installation depth of 2 m, considered constant for the entire length of the heat exchanger. The results of the daily model expressed through the air temperature variation at the exit of the heat exchanger and air temperature variation at the entrance are shown graphically in Fig. 4.

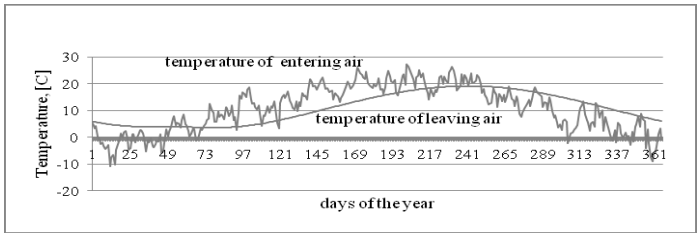

Fig. 4 Daily air temperatures at the exit of the heat exchanger

In a similar way, the air temperature variations in case of the hourly time step model were determined. The results are presented in Fig. 5.

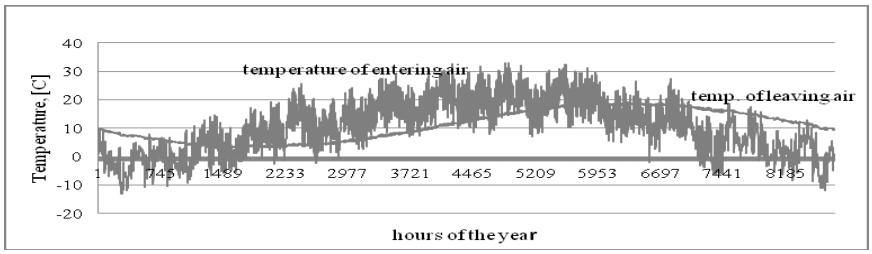

Fig. 5 Hourly air temperatures at the exit of the heat exchanger

By analysing the results obtained by applying the daily model, respectively the hourly model, several characteristics of the ground-air heat exchanger can be highlighted and are summarized in Table 7.

Table 7 Thermal characteristics of the ground-air heat exchanger

Parameter	Value	UM
Daily mode		
Heating in the coldest day of the year (day 12: from -10.97°C to 5.65 °C)	16.62	°C
Cooling in the warmest day of the year (day 231: from 26.46°C to 17.84°C)	8.62	°C
Hourly model		
Heating in the coldest day of the year (hour 273: from -13.04 °C to 7.46 °C)	20.50	°C
Cooling in the warmest day of the year (hour: 4841 from 32.98 °C to 15.32 °C)	17.66	°C

The initial thermal analysis was performed for all the installation depths presented earlier but the results presented in Table 7 are for the ground-air heat exchanger installed at a 2 m depth from the surface of the soil.

2.7 The heat transfer between ground and air

The thermal energy of the soil, used in this study for heating/cooling the fresh air in residential buildings, it is a renewable energy source with low exergy. The calculation formula used for determining heat flows transferred from the ground to air or air to the ground the situation of a ground-air heat exchanger is presented in [10]. The formula was used for both of the calculation models, hourly and daily.

The allure of the two charts representing the heat flows variations determined through the two calculation models is similar and is shown in Fig. 9 and 10. The heat flow values correspond to the heat exchanger installation depth of 2 m from the surface of the soil.

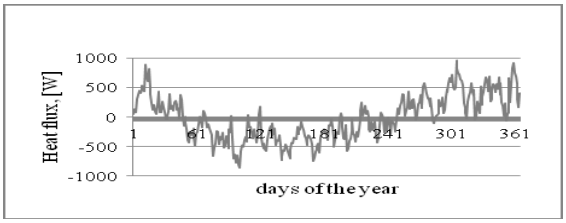

Fig. 9 Daily heat flow transferred in the ground air heat exchanger

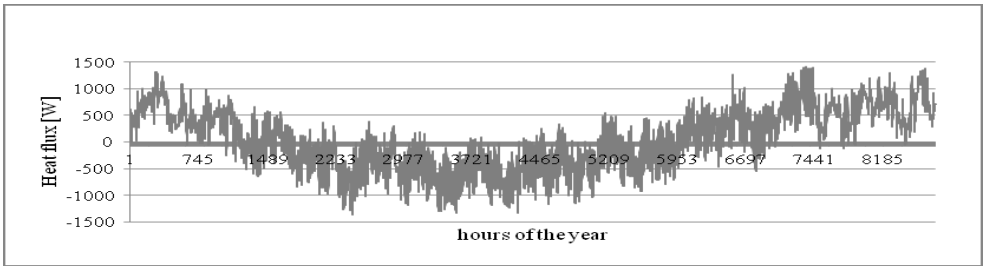

Fig.10 Hourly heat flow transferred in the ground-air heat exchanger

The energy potential of the ground-air heat exchanger for preheating the fresh air was calculated by summing all positive flows obtained by applying the daily time step model, respectively the hourly time step model, depending on the installation depth of the pipes, which is considered constant along the heat exchanger. The annual energy potential under air cooling regime was calculated by summing the negative flows. As negative heat flows also occur out of the cooling season of the building, the annual useful energy for cooling must be determined considering only the flows for the required period. The results are shown in Table 8.

Table 8 Energy potential of GAHE

Installation depth	1.5 m	1.8 m	2.0 m	2.5 m	3.0 m	3.5 m
Daily model						
Energy potential in the heating season, in kWh/an	1190	1335	1434	1665	1847	1894
Energy potential in the cooling period, in kWh/an	1219	1366	1411	1699	1883	1903
Hourly model						
Energy potential in the heating season, in kWh/an	2190	2216	2233	2277	2320	2360
Energy potential in the cooling period, in kWh/an	2000	2026	2043	2088	2131	2172

The results of this study show small differences between the heat flows taken from ground and the heat flows transferred to the ground, if different installation depths are considered (1.5…3.5 m), but big differences between the results obtained with the two models.

3 Conclusions

Analyzing simulation results performed with computational models, resulting relatively large differences, but reduces with increasing GAHE mounting depth.

As negative heat fluxes occur in outside of air cooling period, a control system on GAHE operations is required in order to reduce ventilation energy consumption. Also the GAHE operation is determined by subjective elements determined by thermal sensation of occupants.

The applied models do not consider the influence of the building in the heat transfer processes, the humidity, the potential of vapour condensation and the influence on heat transfer.

References

[1] Nearly Zero Energy Building Romania, The Romanian Ministry of Regional Development and Public Administration.
[2] Trilok Singh Bisoniya, Anil Kumar, and Prashant Baredar (2014). Study on Calculation Models of Earth-Air Heat Exchanger Systems Journal of Energy, Article ID 859286.
[3] Girja Sharan, Ratan Jadhav - Performance of Single Pass Earth-Tube Heat Exchanger: An Experimental Study, https://ideas.repec.org/p/iim/iimawp/wp00064.html.
[4] Muehleisen, R. T. (2012). Simple Design Tools for Earth-Air Heat Exchangers, Conference paper, January, doi: 10.13140/2.1.2854.5607.
[5] Georgios Florides and Soteris Kalogirou - Measurements of Ground Temperature at Various Depths,https://www.researchgate.net/publication/30500353_Annual_ground_temperature_measurements_at_various_depths
[6] G. Upadhyay, J. Kämpf and J-L. Scartezzini (2014). Ground temperature modelling: The case study of Rue des Maraichers in Geneva, Eurographics Workshop on Urban Data Modelling and Visualisation 13-18, http://infoscience.epfl.ch/record/198754/files/013-018.pdf.
[7] Trnsys 16: Energy simulation software, Documentation.
[8] Medved, Saso, UL. Ground heat exchanger for air pre-heating and cooling, IDES-EDU Energy production, Intelligent Energy Europe for a Sustainable Future.
[9] EN 15241 – Ventilations for buildings.
[10] A. Tudor, J. Pfafferott, N. Maier. Optimizing the operation of Earth-to-Air Heat Exchangers in High-Performance Ventilation Systems for Low-Energy Buildings – A Case Study www.aivc.org/sites/default/files/95.1367347897.fulll_.pdf.

Power Operating Curves Model in Wind Turbines Performance Assessment

Cătaş A.[1], Dubău C.[2]

[1] *University of Oradea, Faculty of Science, Department of Mathematics and Computer Science, 1 University St., 410087 Oradea,* (*ROMANIA*)
[2] *University of Oradea, Faculty of Environmental Protection, 26 Gen. Magheru St., 410048 Oradea,* (*ROMANIA*)
E-mails: acatas@uoradea.ro, calin_dubau@yahoo.com

Abstract

The present paper approaches the power operating curve mathematical model for a wind turbine. By making use of characteristic curves, which are very useful in processes of optimization, we can deduce the operating curves for a certain turbine. By identifying such an operating curve we are able to establish the energy performances of the wind turbine in its entire operating range. A comparative study for different values of rapidity is also presented. This study highlights the importance of certain parameters of wine turbine for different rapidity, in the process of construction and development of such aero-electrical aggregates and their optimal functioning. The results showed the accuracy of the model in wind turbines performance monitoring.

Key words: power operating curves, mathematical modeling, wind turbines.

1 Introduction

Wind energy is a renewable energy, ecological and sustainable. The optimization process of the construction of wind turbines is a continuing concern for researchers and manufacturers in the wind power field, having as finally purposes, solutions capable of performing a maximize economic efficiency of these aggregates.

In order to fulfill this desirable objective it should be identify certain way to improve the energy recovery, minimizing costs for technical solutions, high reliabilities and good maintainability. In the aero-electrical aggregates background, the component that ensures the conversion of kinetic energy of wind into mechanical energy useable to turbine shaft, through the interaction between air current and moving blade is the wine turbine. Wind turbine is composed mainly of a rotator fixed on a support shaft, comprising a hub and a moving blade consisting of one or more blades. Active body of aeolian turbines which made the quantity of converted energy is the blade. The achieving of aerodynamic performances, kinematics and energy curves of the aeolian turbines depend on the choice of certain geometry. In developing of turbine blade geometry are used improved contours (airfoil) chosen and positioned so that obtained performances for certain site-specific conditions, to be optimal. The moment of interaction between pallets assembly and fluid flow comes from the lifted aerodynamic forces and resistance produced by the outline profiles. Achieving of acceptable aerodynamic efficiency requires the use of aerodynamic performance. The performance of the wind turbine can be investigated through mathematical models and also verified by experimental measurements.

2 Material and method

Important information used in modeling of line engine is represented by the mathematical models designed for characteristic curves of different types and sizes of turbines. Highlighting the possibilities of aerodynamic optimization it can be started from the analysis of a turbine placed in a stream of air with a velocity $\vec{v}$ (upstream speed, undisturbed by introduced obstacle) which is usually identified by the two components of aerodynamic forces, namely: component on wind direction (resistance force) and perpendicular component on wind direction.

To determine the aerodynamic forces and aerodynamic moment it operates by formulas containing adimensional coefficients concretized in geometric and kinematic similarity relationships. Energy performance representation that produces a wind turbine, as a whole operating area, is materialized by the characteristic curves that are operating in the optimization process. They are of two types namely: operating (exploitation) curves, respectively adimensional curves of the type of turbine [1]. There are various types of wind turbines.

Between various types of wind turbines the rapid axial horizontal wind turbines are the most development ones. Many studies are also elaborated taking in consideration the turbines with vertical axes. Such a study was presented by the second author in a recent paper [6]. There was made a comparative analysis based on the results yielded by the calculations. There was compared: the vertical turbine V2500 [3], [4], [5] and the horizontal turbine H2500 [2].

The exploitation curves (see Fig. 1) serve the evaluations of the annual energies, which are correlated with the areas exposed to the wind and the rotations of the turbine. We can notice from the figure that the horizontal turbine in comparison with the vertical one, accomplishes power *Parb* = 3500 at speed v =10 m/s, which is a smaller value than that of the vertical turbine, where v = 12 m/s.

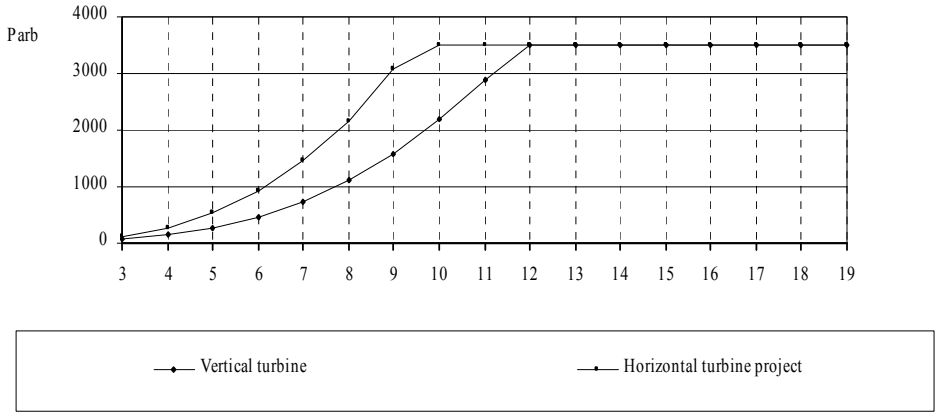

Fig. 1 Operating curves

In order to characterize the functionality of various types of turbines three adimensional coefficients are used, respectively: power coefficient, moment coefficient or torque coefficients and axial force coefficient, which have the following calculation expressions as in [1]:

$$C_P = \frac{P}{\rho \cdot \frac{v^3}{2} \cdot S}; \quad C_M = \frac{M}{\rho \cdot \frac{v^2}{2} \cdot S \cdot R}; \quad C_{F_a} = \frac{F_a}{\rho \cdot \frac{v^2}{2} \cdot S}$$

where we have used the following notations:

- S – Area swept by the turbine,
- R – Radius of the turbine,
- P – Power turbine,
- M – The moment at the engine line axis,
- F_a – Axial force,
- ρ – Mass density of air [kg/m^3],
- v – Wind speed [m/s].

The characteristic number, namely rapidity of the turbine, is defined by: $\lambda = \frac{\pi \cdot n \cdot R}{30 \cdot v}$,

where: n is the (rotation) speed turbine [rpm].

In the general analysis of wind turbines of various types we have to specify several aspects regarding the rapidity and robustness of turbine. The characteristic number associated to the turbine optimal point is denoted by λ_0 and it is called the turbine rapidity. This number characterizes the type of turbine and it represents, together with the position axis turbines, the main criteria for the characterization of the turbines. The usual field of wind turbines is $\lambda_0 = 1 \div 12$ and the turbines corresponding to the interval $\lambda_0 = 1 \div 4$ are considered "slow" in the rest of the field the turbines are considered "fast". This paper provides a mathematical simulation on the computer of the operating power curves for different wind speeds and different revolutions per minute, based on the model proposed in the work [2]. The initial values found also in this study.

3 Results and discussions

The representation of the energy performances which are performed by a wind turbine, in entire field of operating, is materialized by characteristic curves. In the optimization process it operates with these curves.

There are two kinds of such curves: the operating curves and adimensional curves (of a certain type of turbine). In order to construct the operating curves we will establish the mathematical model. In this direction, we need some characteristic parameters, namely: (v) wind speed, (n) rotation speed, (C_p) power coefficient. It follows the dependence of the power turbine (P), the dependence of the moment at the engine line axis (M) and the dependence of the axial force (F_a) as functions of rotation speed, mass density of air (ρ), the dimensions of turbine (D) – (the diameter and the exposed area) and finally the wind speed. Thus we can obtain the general form of the power operating curve: $P = f(D, \lambda_0, v, n, \rho)$ – power operating curve.For the analyzed case, the parameters (D, λ_0, ρ) is constants. The parameters (v, n) are independent variables in prescribed areas by the considered offer location and by others technical conditions of the engines line. For the graphic representations we consider v as current variable. We also use the well known relations $\lambda = u_R / v, u_R = R\omega$ and $\omega = \dfrac{\pi n\,[rpm]}{30}$. Power operating curves which result at the same point of kinematic chain (valorisation made by blading) are described below:

$$P = C_{PWT} \cdot \rho \cdot \frac{v^3}{2} \cdot S\,, \quad S = \frac{\pi D^2}{4}$$

For our applications we will use:

$$\lambda_1 = \frac{u_1}{v}, \lambda_2 = \frac{u_2}{v}$$

$u_1 = 70\,m/s$, $u_2 = 35\,m/s$, $D = 30$ m, $\lambda_0 = 7$ and mass density of air $\rho = 1,2\ kg/m^3$.

With λ the current value of the rapidity we can write:

$$C_{PWT} = C_{M_0} \cdot \lambda + a \cdot \lambda^{\alpha} - b \cdot \lambda^{\beta}\,,\ C_{PWT} = f(\lambda_0, \lambda)$$

The study of this curve, using experimental results from literature, implies the evaluation of dependence of the constants on type of turbine.

$$a = f(\lambda_0); b = f(\lambda_0); \alpha = f(\lambda_0); \beta = f(\lambda_0)$$

As a preliminary approximation it is also accepted the approximation of the torque start coefficient $C_{M_0} = \dfrac{0,2}{\lambda_0^{\,2}}$.

The above mentioned approximations resulted by specific analysis of the information existent in specialized literature. In the future these values can be corrected and adjusted using new information which occurs from improving technology. The recommended value for the constants α, β are $\alpha = 2,0$ and $\beta = 2,3$. The study can be also developed for other values of α, β but there is a condition namely $\beta > \alpha$. For our options we have $a = 0,0795, b = 0,0387$. In order to compute the power turbine values, we will use different values of the wind speed, values which depend on the rapidity of the turbine. These values were computed and are pointed in the table below (Table 1):

Table 1 The values of the power turbine

$v\,[m/s]$	$u_1 = 70\,m/s$			$u_2 = 35\,m/s$		
	λ	C_{PWT}	$P[W]$	λ	C_{PWT}	$P[W]$
7	10	0.269	39112	5	0.44	63975
8	8.75	0.443	96147	4.38	0.387	83993
9	7.77	0.510	157602	3.89	0.339	104759
10	7	0.525	222548	3.50	0.298	126322

Using Maple commands we plot (see in Fig. 2) the power operating curves of a rapid turbine for three values of the wind speed.

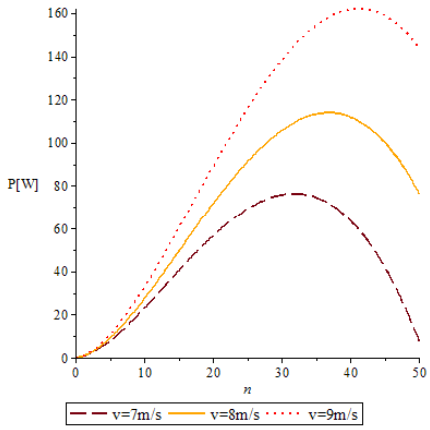

Fig. 2 Power operating curves for a rapid turbine

4 Conclusions

Based on plotted power operating curves of wine turbine we can conclude that exist a major influence of type of turbine on curves shape. Thus the above formula for the power turbine allows as a better understanding of the optimization process of energy performance of the wind turbines. They are also permitted a good management of the control and automation. The power operating curve influences the characteristics of designed technology.

References

[1] Dubău, C. (2005). Modern methods regarding the determination of the functioning characteristic curve for a pipe-line network. Analele Universităţii din Oradea, Fascicula Construcţii şi Instalaţii Hidroedilitare, vol. VIII.

[2] Dubău, C. (2007). The Utilization of Micro-Wind Assemblies within Complex Systems. Timişoara Polytechnic Press, ISBN 978-973-625-408-6, Timişoara (In romanian, Ph. D. thesis).

[3] Gyulai, F. (2000). Contributions on horizontal axis wind turbine theory. Proceedings of the 5th International Conference on Hydraulic Machinery and Hydrodynamic, Oct. 2000, Timişoara, Romania.

[4] Gyulai, F., Bej, A. (2000). State of Wind Turbines in the End of 20th Century and Proposals for Romanian Options. Scientific Bulletin of the Polytechnic University of Timişoara, Romania, Tom 45(59), ISSN 1224-6077.

[5] Gyulai, F., Bej, A., Hentea, T. (2000). Contribution to aerodynamic optimization of horizontal axis wind turbines for mountain sites. ENERGEX'2000, Proceedings of the 8th International Energy Forum and the Conference of the International Energy Foundation, Las Vegas, USA.

[6] Dubău, C. (2009). Comparative study regarding the energy of turbines with vertical and horizontal axis. Annals of DAAAM International Vienna & Proceedings, pp. 1819.

Flexural Tensile Strength Testing of Stabilized Soil Samples

Cîrcu A.P.[1], Nagy A.-Cs.[1], Moldovan D.-V.[1], Ciubotaru V.C.[2], Muntean L.E.[3]

[1] *Technical University of Cluj-Napoca, 28 Memorandumului Street, Cluj-Napoca (ROMANIA)*
[2] *University of Petroşani, 20 Universităţii street, Petroşani (ROMANIA)*
[3] *University of Agricultural Science and Veterinary Medicine, 3-5 Calea Manastur Street, Cluj-Napoca (ROMANIA)*
E-mail: alexandru.circu@mecon.utcluj.ro

Abstract

Traffic loading on a road surface causes compression in the upper layers of the structure and tension in the lower parts. These lower layers often consist of stabilized soils, for which the tensile characteristics are usually ignored. Tensile stress on the bottom of a stabilized layer should be used as a design criterion, as it is an important design parameter. For stretching tests rectangular soil cement beams were of 40x40x160 [mm] (BxHxL) size was prepared. The samples were developed in the Geotechnics laboratory of the Technical University of Cluj - Napoca. This is a first and important step of the research, as these parameters are not treated in any regulations or standards from Romania.

Keywords: stabilized soil, tensile strength, road structure.

1 Introduction

Soil on its own can be used for roadbed structures, however in some cases a form of stabilizer material is required to enhance the mechanical properties of these layers. Soil stabilization can be done by utilizing chemical additions or fiber reinforcement. The most common chemical stabilization is done by cement addition, thus creating a soil-cement admixture. Considering the fact that most of the earth structures use soil from the construction area or its vicinities, the percentage of cement needed to improve soil properties significantly has a wide range. Relying on past studies, it has been identified that the optimum amount of cement to be added in the mixture ranges from 3% to 10% by dry weight of soil, with a higher cement content tending to give greater strength to the composite. It has also been suggested that cement contents in excess of 7.5% may increase costs too much, so using a lower class concrete may be more economical [1]. Other studies show the effect of curing time on mechanical characteristics of admixture. For the cement range identified above compressive strength values obtained after 7 days of cure only reach 70% of that observed after 21 or 28 days [2]. It is therefore preferably that for soil–cement materials to be cured for at least 21 days prior to their use or testing [1, 2, 3, 4].

Traffic generated stresses are flexural in nature. Bhogal et al. [5] conducted a study to determine the dynamic modulus of rupture (MOR) for soil-cement beams with 6 and 10% content. The beam specimens were prepared in accordance with the ASTM D 1632 - 63 [6] standard test method for flexural strength of soil-cement. The samples were subjected to sinusoidal loading changing from almost zero to a load level stress, less than that which would cause failure in static mode. A frequency of 5 Hz was chosen to simulate traffic loading and the number of load repetitions was monitored on a cycle counter. It was found that the dynamic flexure mode was considerably more critical than the dynamic compression mode. The study showed that a reduction of 44% in strength can occur when soil-cement beams are subjected to dynamic flexure [5].

Whittle and Larew [7] utilized repetitive triaxial tests to investigate the fatigue behavior of cement-treated earth samples. The results presented illustrate that sample deformation, for a soil treated with 5% type III cement, increased with an increase of the ratio of applied deviator stress to the ultimate compressive stress as determined in conventional triaxial tests. It was suggested that there is a level of $\Delta\sigma_r/\Delta\sigma_s$ below which the rate of deformation for a specimen decreases as the number of repetitions increases, and above which the rate of deformation increases as the number of repetitions is increased until failure. The stress-strain curve for a soil with 5 % type III cement subjected to repeated loading indicated that for a given deviator stress, the strains observed for the repetitive triaxial tests are larger. The strains at failure, however, were reported to be essentially equal. Cement-treated soils containing type III cement exhibited higher strength and stiffness characteristics

under 100,000 applications of repeated deviator stress than cement-treated soils containing type I cement. Both cement-treated soils showed marked improvement over the unstabilized soils [7] (According to ASTM [8] there are five types of portland cement, type III having a high early strength, with slightly more C_3S in composition, suited for construction activities during the cold weather period, while type I cement being used for general purposes).

2 Materials and Methods

2.1 *Sample Preparation*

The purpose of the present study was to determine tensile strength for soil-cement beams with different percentages of cement. Lacking Romanian regulation, tests were set up according to ASTM 1635-00 [9]. The soil-cement admixture was prepared in accordance with Romanian standards. Silty clay (siCl) was used, extracted from a depth of 1 m, from a site near Cluj-Napoca. Initial geotechnical parameters of the soil were: γ_s=26.68 kN/m^3 (bulk unit weight); γ_d=17.17 kN/m^3 (dry unit weight); n=35.51% (porosity); e=0.55 (voids ratio); w=17.48% (natural water content). To determine the optimum water content for compaction a Proctor test was performed for every type of mixture tested, having different percentage of added cement. The Proctor Compaction test was made in accordance with STAS 1913-13/83, and results obtained from the test are shown in Table 1.

Table 1 Optimum water content resulted from Proctor test on the four types of mixture tested

Cement amount	2%	4%	6%	8%
Water content	21%	23%	23%	21%

The first step was drying the soil in oven at 105°C. Type II/A-LL 42,5 R Portland cement was added in amounts of 2%, 4%, 6% and 8% for 2000 g of soil, considered initial weight. The two components were mixed in dry state until a homogeneous composition was obtained. The final step of the preparation was adding water in predetermined amount (from the Proctor tests performed) and mixing manually the composition for about 30 min. The soil-cement beams were made using a mould with three chambers (Fig.1). This mould was greased with oil for a better usability. The mixture was compacted in three equal layers with an equal number of taps applied to each layer. For the compaction process a hydraulic jack was used in order to achieve a uniform pressure on each layer (Fig. 2). The size of one of the chamber's mould was 40x40x160 mm, the resulting beams having the specified dimensions. Samples were given 7 and 28 days curing time before tensile teste were performed. A total number of 8 beams were made, and stored in laboratory conditions.

Fig. 1 Mould with three chambers

Fig. 2 Hydraulic compaction jack

2.2 *Testing Procedure*

The soil-cement beams were subjected to flexural tensile strength tests, through a three-point vertical loading system, as seen in Fig. 3. Experimental tests implied putting the samples on supports placed at 10 cm distance relative to each other, and applying a concetrated load on the beams at the middle of the span. The static loading was gradually increased until the samples failed. Testing apparatus is shown in Fig. 4. A tested sample is presented in Fig. 5. ASTM 1635-00 sets standard test specimens sizes at 76x76x290 mm, but states that a similar test method may be used for testing specimens of other sizes. The modulus of rupture evaluated from ASTM D 1635-00 is calculated according to the type of beam failure. If the fracture occurs approximately in the middle of the span the MOR is calculated using:

$$R = PL/bd^2 \quad (1)$$

where: R is modulus of rupture measured in N/mm2,
P is maximum applied load in N,
L is span length = 100 mm,
b is average specimen width = 40 mm,
d is average specimen depth = 40 mm.

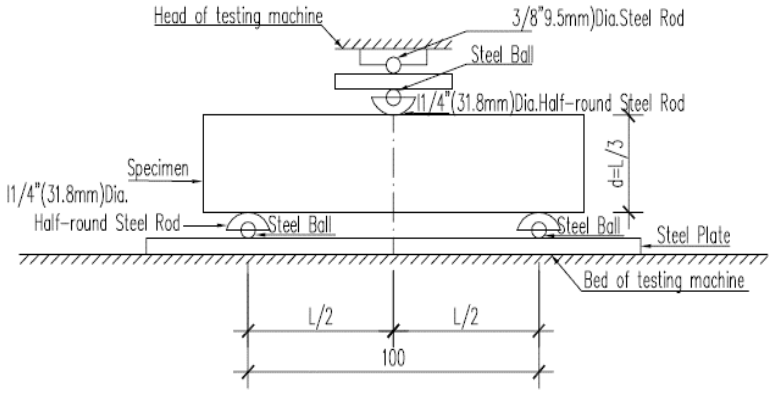

Fig. 3 View of apparatus for flexural test

Fig. 4 Flexural tensile strength testing apparatus

Fig. 5 Soil-cement testing sample

3 Results and Discussion

The results obtained on soil-cement samples after 7 and 28 days of curing time are summarized in Table 2. Graphic evolution of results is presented in Fig. 6. Although increasing exponentially with the amount of cement added in the mixture, from the economical point of view cement content above 7.5% makes the usage of lower class concrete more cost-effective [1]. By comparing the modulus of rupture obtained for different tested combinations, it was found that the 2% cement-soil mixture had an improvement of 17%, the 4% mixture had grown by 12%, as was the 6% mixture, while the 8% mixture was the most improved, having a 23.5% larger parameter after the tensile test was performed at 28 days from preparation. The results were within the margins of Bahar et al. research [2], which stated that a soil-cement admixture reaches approximately 70% of its mechanical strength after the first 7 days, additional strength being acquired after 28 days of curing.

Table 2 Modulus of rupture obtained after flexural tensile tests

Sample		Maximum applied load P* (N)	Maximum applied load P** (N)	Span length L (mm)	Specimen width b (mm)	Specimen depth d (mm)	Modulus of rupture R* (N/mm²)	Modulus of rupture R** (N/mm²)
No.	Cement content							
1	2%	190	230	100	40	40	0.297	0.359
2	4%	220	250	100	40	40	0.344	0.391
3	6%	270	310	100	40	40	0.422	0.484
4	8%	325	425	100	40	40	0.508	0.664

*after 7 days; **after 28 days

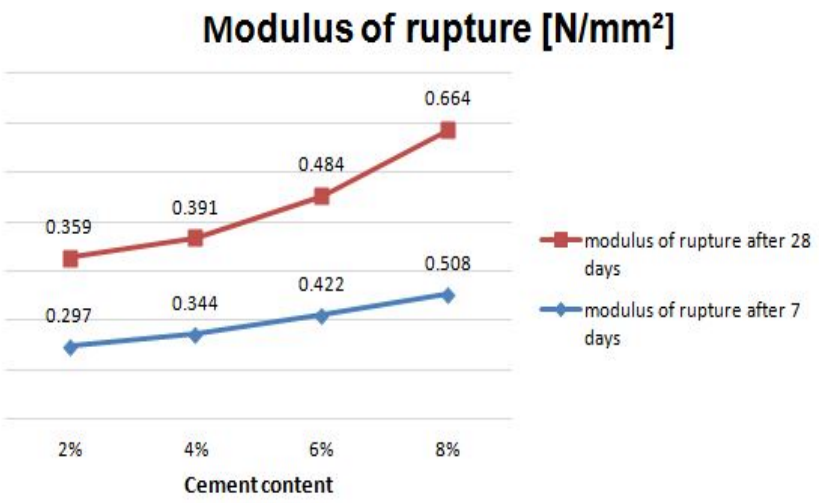

Fig. 6 Graphic evolution of the modulus of rupture at 7 and 28 days

4 Conclusion

Tensile strength of a stabilized earth layer made from soil-cement mixture is one of the least well defined properties. There are several difficulties of elaborating experimental models suitable for testing material samples for road structures. Traffic generated loads are flexural in nature, as it was modelled in this research. However, the cyclicity of traffic which gives its dynamic component was ignored at this stage. It is obvious that stabilized samples have an important tensile strength that is dependent on the amount of cement added. Considering economical criteria we suppose that further research should concentrate on 4-7% range of variation for the amount of cement. Also mechanical improvement of samples had an exponential growing towards the end of the tested range, with the highest value obtained for the 8% admixture: 23.5% bigger modulus of rupture after 28 days of curing.

References

[1] Akinmusuru, J.O. (1984). Lateritic soil–cement bricks for rural housing. The International Journal of Cement Composites and Lightweight Concrete 6(3), pp. 185–188.
[2] Bahar R., Benazzoug M., Kenai S. (2004). Performance of compacted cement-stabilised soil. Cement and Concrete Composites 26(7), pp. 811–20.
[3] Aggarwal L.K., Singh J. (1990) Effect of plant fibre extractives on properties of cement. Cement and Concrete Composites 12(2): pp. 103–8.
[4] Khazanchi A.C., Saxena M., Rao T.C. (1990). Material science of natural organic fibres reinforced composites in polymer-cement-mud matrix for construction engineering. Proceeding of the international symposium of textile composites in building construction, France, pp. 69–76.
[5] Bhogal B.S., Coupe P.S., Davies J., Fendukly L. (1995). Dynamic flexure test of soil-cement beams. Journal of Materials Science Letters 14, pp. 302-304.
[6] ASTM D 1632-63. Standard method of making and curing soil-cement compression and flexure test specimens in the laboratory.
[7] Whittle J. P., Larew H. G. (1965). Effects of Repeated Loads on Elastic Micaceous Soils Stabilized with Portland Cement. Highway Research Record No. 86, Highway Research Board, pp 28-38.
[8] ASTM C150/C150M. Standard Specification for Portland Cement.
[9] ASTM 1635-00. Standard Test Method for Flexural Strength of Soil-Cement Using Simple Beam with Third-Point Loading.

Dynamic Analysis of Internal Wind Pressure on Non-Structural Elements

Crisan A.[1], Ivan A.[1], Handabut A.[1]

[1] *Politehnica University of Timisoara, Dep. of Steel Structures and Structural Mechanics (ROMANIA)*
E-mails: andrei.crisan@upt.ro, adrian.ivan@upt.ro, andreea.handabut@student.upt.ro

Abstract

High and medium rise buildings are the new norm for urban areas as a response to high scarcity of land and ever increasing demand for business and residential space. Besides the gravitational loads (i.e. dead and live loads), these structures have to withstand horizontal loads like earthquakes and high winds. For design, a structural engineer usually considers above mentioned loadings to create the design scenarios (i.e. loading combinations). The resulting efforts are further used to evaluate the capacity demand for structural elements like beams and columns. For secondary elements (e.g. claddings, secondary walls, ceilings, etc) it is unusual to be directly exposed to loading. Counting on their inherited strength and lack of direct load, the design of secondary elements can be overlooked. Even if this approach usually stands, there are cases where the strength of secondary elements was exceeded and failure or damage occurred, causing significant money loss.

Present paper present a study that was conducted to evaluate the behavior of a plasterboard ceiling exposed to internal wind pressure. The direct exposure resulted in the collapse of entire ceiling structure, leading to significant money loss and an inhabitable apartment. The analysis was conducted in two steps using a commercially available FEA software package. The numerically obtained results were compared with in-filed observations. Further, installation and building recommendations were presented.

Keywords: plasterboard ceiling, wind pressure, dynamic analysis, failure.

1 Introduction

Wind generally represents big masses of air moving horizontally, mainly, parallel to the ground from areas of high pressure to areas of low pressure. This movement has two aspects i.e. a beneficial one and a parasitic one. The beneficial one is related to power generation, cooling of hot areas, transport of humidity, etc, while the later is related to the structural loading that it produces. Furthermore, wind is a dynamic phenomenon, with random speed and direction. The loading generated by the wind is not uniform and it is influenced by a variety of factors. For example, due to frictional forces, the mean wind speeds at the ground level are relatively low (equal to zero at ground level). Other factors include the building shape, terrain topology and neighbouring tall buildings. To evaluate wind-structure interaction, wind induced loading and air flow around structures, many researchers [1] – [8] have dedicated their efforts to describe the complex phenomenon occurring.

As a simplified approach for engineering structures with residential or business destination, the loading produced by wind can be taken as a static load proportional with the wind velocity, which increases with height and is affected by coefficients considering the above mentioned factors. Even so, it is not common practice among civil engineers to compute the wind loading on internal finishing (e.g. plaster walls, plaster ceilings, etc.) due to the fact that these systems are usually proprietary and lack standardization. Moreover, producers usually offer technical agreements and mounting details for their products guaranteeing their suitability for specified applications.

The study presented hereafter is related to an incident that leads to major money loss. Following the structure's commissioning, a tall residential building situated in Banat area, Romania, in July 2014 a storm hit the structures location. High wind speeds coupled with a series of unfortunate events (i.e. open windows and terrace's door), lead to collapse of plaster ceiling for a flat situated at the last floor of the building.

For such cases, the resident could blame the contractor for poor quality work, not using the appropriate detailing and construction materials or for not considering appropriate loading. In the same time, the contractor could blame the resident for modifying the internal space configuration of the flat without written agreement and without qualified supervision.

2 Structural System, Loading and Infield Observations

2.1 Infield situation

The study was requested following a non-structural element failure within a residential block of flats in Banat area, Romania. Following a strong wind, the plaster ceiling of a family residence collapsed, leading to high money loss and a residence not fit for living. The residential apartment is part of a high rise concrete structure. The roof was realized using corrugated sheeting with 150 mm folds and 0.88 mm thickness supported on wooden trusses. The roof slope is 4°. Underneath the corrugated sheet, a plaster ceiling was mounted. The infield situation can be observed in Fig. 1.

Fig. 1 Infield observed conditions and damages

It can be easily observed that the area is not usable for normal living conditions. The connection between the steel rods and supporting profiles has failed in multiple areas causing the collapse of the plaster ceiling in a vast area. Also, no damage was observed for the corrugated sheeting nor the connections with the steel rods.

2.2 Structural system and mounting details

To avoid any conflict of interests with producers/contactors the system is schematically presented in Fig. 2 (front and lateral view). Two plaster boards of 12.5 cm were connected to a supporting grid realized with CD60/27 aluminium profiles with 0.5 mm thickness, disposed orthogonally. The distance between the retaining C profiles varies between 750 and 850 mm on both directions, excepting near the supports, where it is limited to 450 mm.

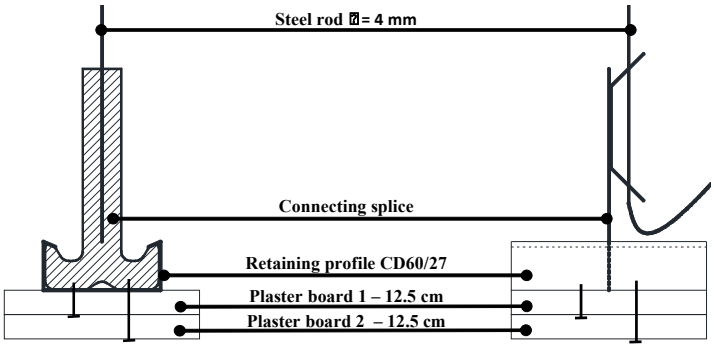

Fig. 2 Schematic details for plaster ceiling connections

On the contour, the ceiling is connected to the walls using UW30 aluminium profiles. At the intersections of the retaining profiles, the joint was detailed using special connectors, to keep the profiles in place. Inside the retaining profiles, a steel connecting splice of was introduced. The splices were fixed on steel rods, which at the top were connected to the corrugated sheet using a self-screwing bolt. On-top the supporting grid, 10 cm of mineral wool disposed to ensure thermic insulation.

2.3 Load evaluation

During its lifetime, a structure has to withstand the loads it was designed for (e.g. dead loads, live loads, environmental loads). Computed loads are used to create load combinations further used for the design of structural elements (e.g. beams, columns, slabs).

Dead load pattern includes the loads that do not vary (or vary very little) over time. This includes the self-weight of structural and non-structural elements (e.g. concrete, reinforcement, plaster, flooring system, walls, etc.). These loads are considered to have a static action following the completion of the building and are evaluated in accordance to Eurocode [9]. *Live load pattern* includes the loads imposed for the structure as well as environmental loads. While the live loads are defined by the architect, building owner and structural engineer, in according to structures' destination, the environmental loads are evaluated according to European codes and enforced by national annexes (e.g. snow load [10], wind load [11], etc.). Besides these loads, an *accidental load pattern* has to be considered during the lifetime of the structure: earthquake [12] and fire loads [13]. Since it is usual for a structure to experience more than one load at a time, to ensure the structural safety under different loading scenarios, the structural engineer has to consider various load combinations [14].

It is mandatory for the structural engineer to evaluate all loading combinations for all load bearing elements design (e.g. columns, beams, etc.), while non-structural elements are often omitted. This happens due to the fact that non-structural finishing systems are usually proprietary and producers offer technical agreements with specific mounting details. Moreover, it is usual for the general contractor to offer for future residents the option to choose the finishing, making it very difficult for the structural engineer to design a finishing system during the initial design of the structure.

In order to evaluate as accurate as possible the real loading combination for the case under discussion, the following loading patterns were considered:

a. Self-weight of supporting grid – automatically considered in accordance to defined materials, elements sections, length and gravitational pull;
b. Self-weight of plaster boards (*2 x 12.5 cm x1000 daN/m^3 =250 Pa*)
c. Self-weight of mineral wool thermal insulation (*10 cm x 40 daN/m^3=40 Pa*)
d. Wind pressure inside the structure (w_i = 460 *Pa*).

The principal focus of the present study was the wind pressure. It was necessary to evaluate the internal wind pressure to account for supplementary load on the plaster ceiling system and further to evaluate if it was the cause of collapse. The load was computed in accordance to the specifications of Romanian standard [15], accounting for infield conditions during the storm (wind speed 72 km/h @ DSNAR Arad, 1.00 PM, recorded by ANM). It can be observed that the internal wind pressure was higher than the gravitational load on the ceiling system, leading to an initial upward loading.

3 Numerical Model

For numerical simulations, the software package Abaqus/CAE [16] was used. Two numerical models were created for i) supporting rod to supporting profile connection and ii) complete assembly.

A simplified model was created to evaluate the connection capacity. For this purpose, a reference point was defined in the position of the splice to rod connection and an upward displacement was applied. To evaluate the behavior of the plaster ceiling assembly (including the support profiles and support rods), a two-step static/dynamic analysis was defined. The wind load (computed in the paragraph above) was applied in the first step as upward pressure, while in the subsequent step, the load was removed and the assembly was subjected to gravitational pull alone.

3.1 Material data, model definition and setup for connection

For present simulation, three materials were considered.

a. Aluminum (bilinear) *E= 70 GPa, v=0.35, f_y = 150 MPa, ρ = 2700 kg/m^3*
b. Steel (bilinear) *E= 210 GPa, v=0.3, f_y = 355 MPa, ρ = 8750 kg/m^3*
c. Plaster (linear) *E= 1.40 GPa, v=0.23, ρ = 1000 kg/m^3*

The aluminum profile (supporting beam), made up of a C60x25x5 profile, was defined using S4R shell elements (ABAQUS denomination) with a thickness of 0.5 mm, 0.6 mm and 0.8 mm, respectively. The connection profile (made of steel) was created using the same S4R shell elements with a thickness of 0.8 mm, 1.0 mm and 1.2 mm. These values were considered to evaluate the influence of geometric dimension onto the capacity of the conditions. The model components are presented in Fig. 3a, while Fig. 3b presents the observed failure mode.

Fig. 3

*Fig. 3*also present the failure loads for considered thicknesses. The connection splice thickness was observed to have no influence on the connection capacity, so it was omitted. It has to be mentioned that the first two considered thicknesses (e.g. 0.5 mm and 0.6 mm) were considered due to the fact that both are commercially available and they can be mistakenly interchanged by construction workers.

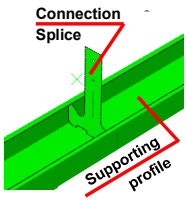

a. Connection overview

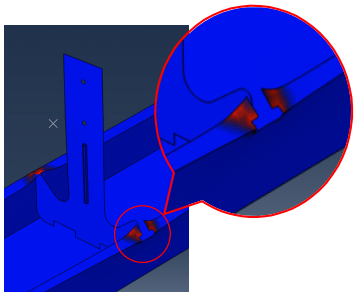

b. Obtained failure mode

Retaining profile thickness	Failure load [N]
0.5 mm	261
0.6 mm	370
0.8 mm	640

c. Connection capacity

Fig. 3 Connection overview, failure mode and capacity

It can be observed that the retaining profile thickness has a great influence on the connection capacity. It has to be mentioned that the usual profile thickness for such application is 0.5 or 0.6 mm, hence, the reference capacity for subsequent analyses will be taken accordingly.

3.2 Model definition and setup for complete assembly

The analysis was conducted in two subsequent steps: i) static step to impose the wind pressure on the plaster ceiling and ii) a dynamic/implicit step to simulate the free fall of the ceiling following the removal of the wind pressure. In Fig. 4 is presented an overview of the simulated structure together with the position of supports (i.e. walls) depicted in red.

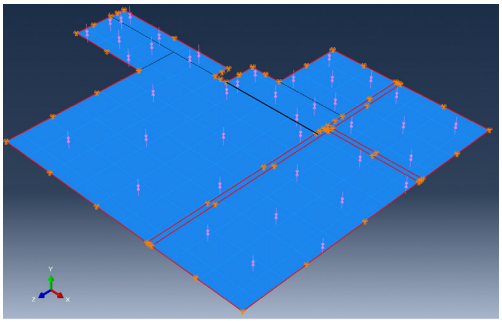

a. With intermediate wall

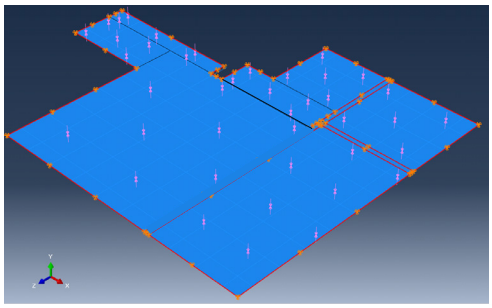

b. No intermediate wall

Fig. 4 Boundary condition details

*Fig. 5*Fig. 5 shows the position of the supporting rod and the spring element details. The plaster boards were defined as plate and discretized with S4R elements with the thickness of 25 mm. The retaining profiles were defined as beam elements with "C" section and connected with TIE constraints to the plaster boards. The connecting rods were defined as spring elements with bilinear behavior.

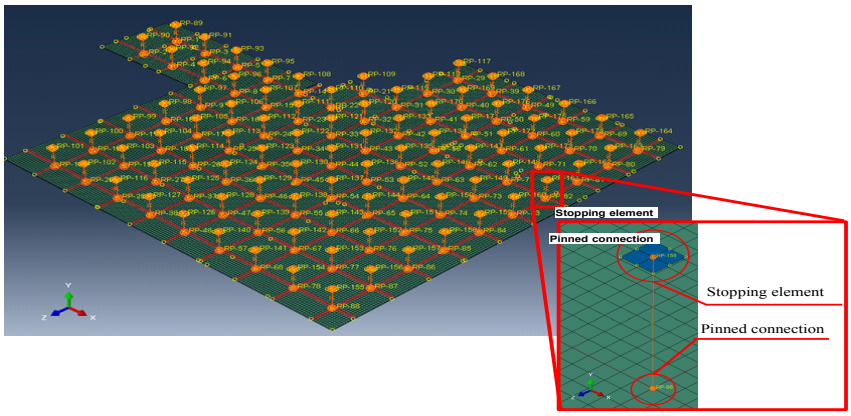

Fig. 5 Plaster ceiling overview and spring element definition detail

The stiffness in compression was assumed to be negligible (due to small cross-sectional area high length of elements), while in tension, the stiffness, K, was assumed to be proportional to the cross-sectional area, A, and the Young modulus of the material, E, and inverse proportional to the rods length, L, (K = EA/L). The elements' strength was assumed to be equal to the yield strength (i.e. $A \cdot f_y$). At the bottom of the supporting rod, the connection with the supporting profile was modelled as a pinned connection, while at the top a stopping element was connected (see Fig. 5). Further, an analytical surface was defined to simulate the roof structure. This setup allowed the upward movement of the system and the subsequent free fall, down to the predefined position. Since the main objective of the technical expertise was to determine the influence of the intermediary wall (removal), two cases were considered: i) with the intermediate wall and ii) without the intermediate wall (see Fig. 4).

The distance between the retaining C profiles was taken 750 mm on both directions (in accordance to the infield observations), excepting near the supports, where it was limited to 400 mm. On the contour, the ceiling was considered as simply supported. An initial upward deformation can be observed (see Fig. 6) due to wind pressure.

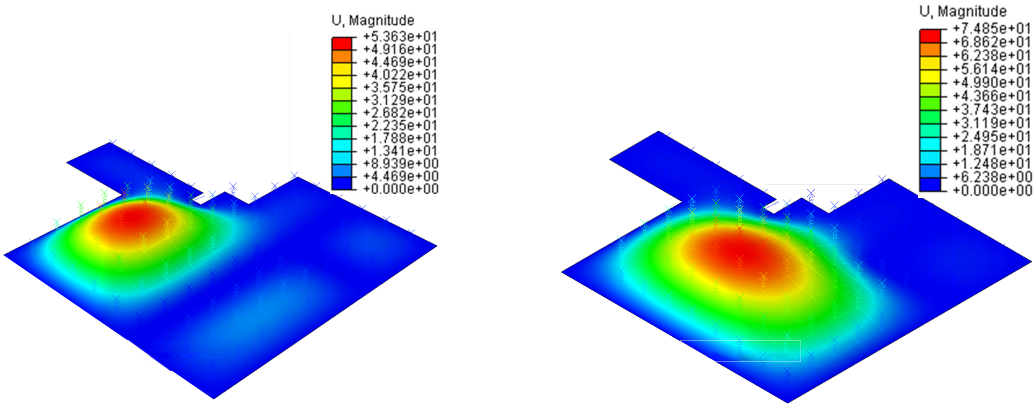

a. With intermediate wall b. No intermediate wall

Fig. 6 Deformation due to wind pressure

It can be observed that the removal of the intermediate wall increased the initial deformation induced by the wind direct pressure by about 100%. In the next step, the direct loading was removed and the ceiling was left to fall freely under the action of gravitational pull.

*Fig. 7*Fig. 7 presents the tension loads in the supporting rods following the ceiling system free fall.

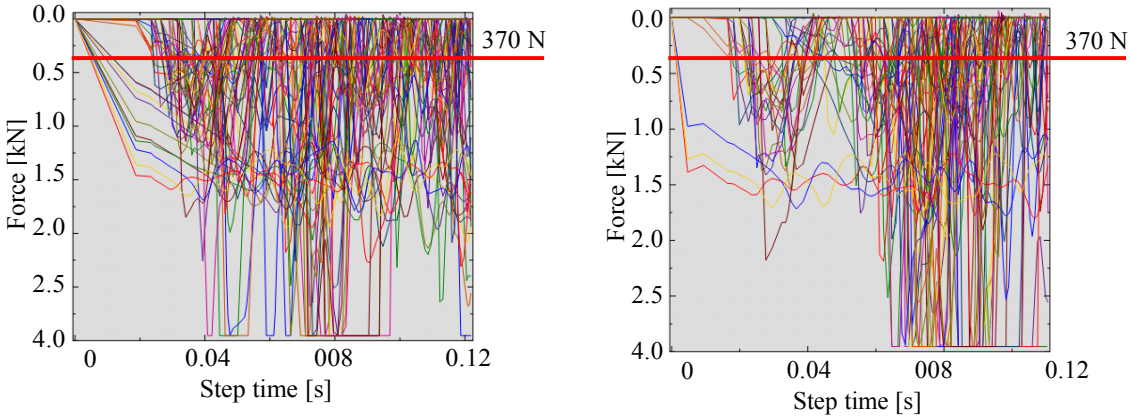

a. With intermediate wall b. No intermediate wall

Fig. 7 Forces in connection rod following the ceiling free fall

It can be easily observed that for the vast majority of the steel rods, the connection capacity was greatly exceeded. Furthermore, the axial load capacity of the steel rod was also achieved for many supporting elements due to high dynamic effects for the free falling ceiling, disregarding the fact that the intermediate wall was present or not. The influence of corrugated sheeting deformation due to wind loading was also studied. The observed difference (considering upward or downward deformation) was negligible, so, for present study, the corrugated sheeting deformation was not considered. Even if the simplified model adopted for the plaster ceiling

system cannon fully evaluate the force in supporting steel rods, a good agreement between the number of failed connections in the numerical model and the infield observations (see Fig. 1 and Fig. 7).

4 Concluding Remarks

Present paper presents the results of a dynamic analysis using FEA for a plaster ceiling system, accounting for the gravitational loads and supplementary internal wind pressure. The capacity of retaining profile connection was also evaluated by means of numerical analysis. The findings of the numerical study are in good agreement with the in-field observations.

Based on the results of the numerical analysis, it was observed that the failure of plaster ceiling was not due to the direct wind pressure, but rather due to its removal. The dynamic amplification factor following the sudden removal of upward pressure increased the gravitational loading beyond the capacity of the connections. It was also observed that the removal of the intermediary wall increased the initial upward deformation and the subsequent number of failed supporting steel rods. Even so, it can be observed that the failure of the plaster ceiling system was imminent, disregarding the intermediary wall.

In order to avoid the failure of such structures (i.e. slender plaster ceilings) the distance between the supporting elements would have to be reduced (increasing the number of supporting points). In the same time, the connection detail could be improved to limit the high shear forces created by the splice connector. On the other hand, the use of less slender supporting elements would limit the upward deformation of the ceiling limiting the amplification factor. The later solution would be preferred, but would increase the final costs. On this line, the producers and contractors should always clearly state the use conditions for internal and non-structural elements (the equivalent of a guarantee certificate). In this way, the user would be informed about the conditions of use, and that any unauthorized intervention would lead to a void guarantee. Keeping this in mind, it can be said that the correct design of slender finishing systems exposed to direct loading is important for limiting damage and possible injuries. Furthermore, FEA can provide valuable insights on the behavior of non-structural systems.

References

[1] Davenport A.G. (1961). The application of statistical concepts to the wind loading of structures, Proc. ICE, Vol. 19.

[2] Davenport A.G. (1963). *The relationship of wind structures to wind loading,* Proc. ICWE Physical Laboratory Teddington, UK.

[3] Harris R.I. (1963). *The response of structures to gusts,* Proc. ICWE Physical Lab. Teddington, UK.

[4] Kareem A. (1999). *Analysis and modelling of wind effects: Numerical techniques*, Proc. 10th Intl. Conf. Wind Eng. Copenhagen, Danmerk, Vol.1.

[5] Kareem A, Kijewski T. (2001). Probabilistic and Statistical Approaches for wind effects: Time – frequency perspectives, 5th Asia Pacific Conf. on Wind Eng. Kyoto Japan.

[6] Bos, R. Bierbooms, WAAM. Bussel, GJW van. (2015) "Importance sampling of severe wind gusts" in proceedings of EAWE 11th PhD seminar on Wind Energy in Europe, September.

[7] Yoshihide Tominaga, Bert Blocken (2016). Wind tunnel analysis of flow and dispersion in cross-ventilated isolated buildings: Impact of opening positions, Journal of Wind Engineering and Industrial Aerodynamics, Volume 155, pp. 74-88.

[8] Lukáš Pop, Zbyněk Sokol, David Hanslian (2016). *A new method for estimating maximum wind gust speed with a given return period and a high areal resolution*, Journal of Wind Engineering and Industrial Aerodynamics, Volume 158, p. 51-60.

[9] EN 1991-1-1 (2002): Eurocode 1: Actions on structures - Part 1-1: General actions - Densities, self-weight, imposed loads for buildings.

[10] EN 1991-1-3 (2005): Eurocode 1: Actions on structures Part 1-3 General actions – Snow Loads.

[11] EN 1991-1-4 (2005): Eurocode 1: Actions on structures Part 1-4: General actions - Wind actions.

[12] EN 1998-1 Eurocode 8 (2004): Design of structures for earthquake resistance – Part 1: General rules, seismic actions and rules for buildings.

[13] EN 1991-1-2: Eurocode 1 (2002): Actions on structures - Part 1-2: General actions - Actions on structures exposed to fire.

[14] EN 1990 (2002): Eurocode - Basis of structural design, 2002.

[15] Indicativ CR 1-1-4 (2012). Cod de Proiectare Evaluarea Actiunii Vântului Asupra Constructiilor (1-1-4 CR Indicative. Code of Design Assessment of wind on buildings).

[16] Abaqus CAE (2016), www.3ds.comS.

Smoke Control Design in Large Spaces

Dârmon R.[1], Suciu M.[1]

[1] *Technical University of Cluj-Napoca (ROMANIA)*
E-mails: Ruxandra.Darmon@ccm.utlcuj.ro, Mircea.Suciu@cfdp.utcluj.ro

Abstract

Over the life cycle of a building it is often the case that the initial design is modified due to changes of the building destination or occupancy, refurbishment works, maintenance, accidental factors and others. As the safety of the building users remains the priority for all the code requirements, any change of the original design must be evaluated and it should meet the minimum safety levels required by the standards. This paper presents a review of a study case for the actual smoke ventilation capacity of an atrium after the original design has been changed by the new building owners. It is investigated whether the natural or mechanical smoke control system would be appropriate in the actual conditions.

Keywords: atrium, natural ventilation, neutral plane.

Introduction

Changes of a building destination, occupancy, modernisation or refurbishment works usually bring irreversible modifications to the original design. The proposed design should have at least the same level of safety for the occupants and to not compromise the overall structural stability. Most of the fire safety building codes require the smoke layer to be maintained above the people's head height. According to the Eurocodes, the smoke layer should not drop below 2.5 m above the floor.

The smoke ventilation strategy in case of large spaces as atriums is largely influenced by the geometric dimensions and the position of the atrium into the general layout of the building [1]. The separations of the atrium from the adjacent spaces and the available openings to the ambient conditions are also critical factors affecting the final design approach.

This paper presents an assessment of the ventilation system for the atrium located in the centre of a three storey building. The atrium base, shown in Fig. 1, below, is a squared hall of 18m x 18m, designed as an exhibition place and constituting the main assembly point of the building.

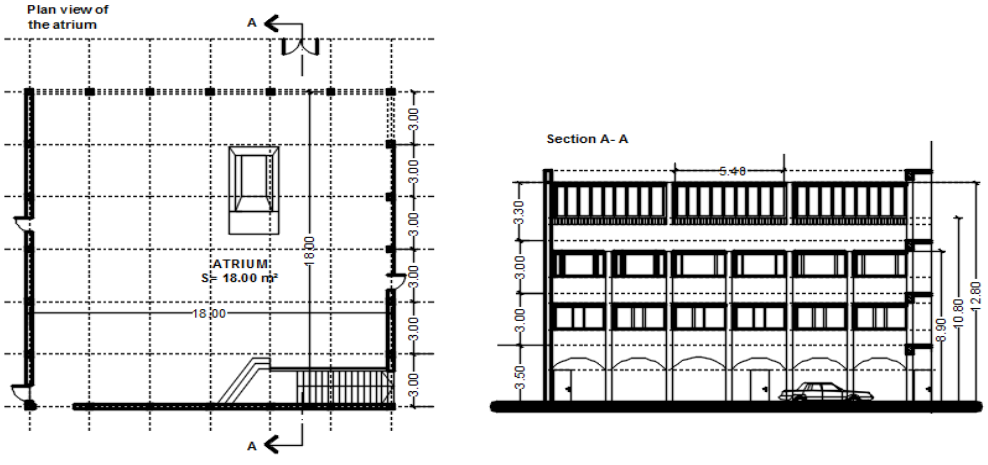

Fig. 1 Groundfloor plan and the cross section of the atrium

One side has the main entrance into the building and the other three have several doors connecting the adjacent rooms of the building. The free height of the atrium is approximately 12.8 m. At the third floor, surrounded by 2 m height glass wall, several windows were originally linked to the alarm system to open in case of fire and maintain the smoke layer above the second floor openings. Since the layout of the groundfloor has

been modified, the original natural smoke ventilation strategy should be redesigned and updated to comply with the fire safety requirements.

The intent of the new design has been to keep as much as possible from the original strategy, therefore the aim of this study is to assess whether the smoke layer can be kept above the second level windows in the atrium and what would be the total necessary outlet at the top of the atrium to maintain a natural ventilation of the smoke and heat.

1 Natural Ventilation Strategy

The smoke layer interface is imposed to remain above the second floor windows, which is about 9 m. The calculation procedure aims to estimate the necessary outlet vent area A_{out} to keep the smoke above the imposed height.

1.1 Initial assumptions

1.1.1 Openings at the lower level

At the ground floor there is only the main entrance with a surface of 5.2 m^2 that opens to outside. However, there are other 3 doors which open to adjacent rooms. In case of emergency, it has been estimated that the windows from these rooms could be automatically open and enable additional air supply. As a conservative assumption, for this study it is assumed that the door which are connected to adjacent spaces will have only half capacity of ventilation, which means a total area of 8.2 m^2 inlet at the bottom of the atrium.

The first and second floors have open balconies to the atrium. Both levels are designed as office spaces.

1.1.2 Air properties at ambient conditions

The properties of air at standard temperature and pressure are taken as:

- Density: $\rho_a = 1.204$ kg/m^3;
- Specific heat: $c_p = 1.005$ kJ/kg-K;
- Ambient temperature: $T_a = 293$ K = 20˚C.

1.1.3 Boundary conditions

The ceiling, the floor and the walls are made of concrete. The thermal properties for concrete and glass are taken as in Table 1.

Table 1 Thermal properties of the boundaries at 500˚C

Material	Conductivity k [W/mK]	Specific heat c [J/kgK]	Density ρ [kg/m³]	Thermal inertia kρc [W²s/m⁴K²]
Floor, ceiling [2]	1.13	1000	2000	2260000
Glass [3]	0.8	840	2600	1800000

1.1.4 The heat losses to boundaries

It is assumed that the boundaries are semi-infinite solids at the same temperature as the smoke and hot gases from the upper layer. The heat lost to the compartment boundaries, $\dot{q}_{loss}$, is the heat conducted from the smoke plume into the surrounding walls and ceiling surfaces, denoted A_w. This has been expressed as:

$$\dot{q}_{loss} = hA_W(T_g - T_a) \quad (1)$$

where: $h = \sqrt{\frac{k\rho\rho}{\pi t}}$ is the heat conduction coefficient for thermally thick solids.

Tg and Ta represent the smoke and ambient air temperatures, respectively and t is the time until steady state conditions are reached into the atrium. For this study it is estimated that t = 600 sec, meaning that the smoke layer interface should be constant after 10 minutes from the fire initiation.

1.1.5 Heat release rate

The amount of combustible materials at the groundfloor level is limited and controlled. However, due to the destination as an exhibition place, the thermal load is subject to variations in time. For this study, it is assumed that a car may be displayed in the centre of the atrium at a certain point in time. Based on available test data from the literature [4], a burning car could sustain a 5 MW fire.

1.2 Steady state conditions

If steady state conditions are assumed into the atrium, as shown in Fig. 2, the space will be divided into a cold, lower layer at ambient temperature and a hot upper layer of smoke and hot gases having the temperature T_g, which should reach the equilibrium after approximately 10 minutes time.

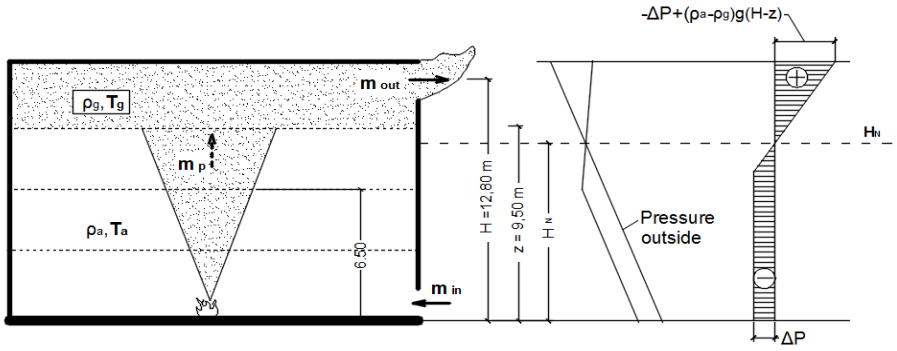

Fig. 2 Atrium energy balance and the pressure profiles

After the smoke layer stabilizes, the volume of the upper layer will remain constant and at a constant temperature T_g. Thus, $dV_g/dt = 0$ and $d\rho_g/dt = 0$.
If the burning rate of the fuel is neglected, the mass balance equation for the atrium takes the form:

$$\dot{m}_{in} = \dot{m}_p = \dot{m}_{out} = \dot{m} \tag{2}$$

where:

$\dot{m}_{in}$ and $\dot{m}_{out}$ are the mass flow rates into and out of the compartment, respectively, and

$\dot{m}_p$ is the plume mass flow of smoke and heat into the upper layer.

The conservation of energy equation is used to express the energy balance for the upper layer. The plume flow rate should be equal with the flow rate of hot gases exiting the compartment plus the heat lost to the compartment boundaries.

$$\dot{Q} = \dot{m}_{out} c_p (T_a - T_g) + \dot{q}_{loss} \tag{3}$$

1.2.1 Smoke layer average temperature

The temperature of the upper layer can be calculated combining the equations (1) and (3), as:

$$T_g = T_a + \frac{\dot{Q}}{\dot{m}_{out} c_p + hA_w} \tag{4}$$

1.3 Pressure difference across the lower openings

The mass flow rate of fresh air into the compartment can be written as a function of the inlet opening area, A_{in}, as:

$$\dot{m}_{in} = C_d \rho_a v_{in} A_{in} = \dot{m} \tag{5}$$

where:

C_d is the discharge coefficient, which accounts for the flow efficiency through an opening. Due to the friction stresses at the corners of a vent, the velocity of the flow is diminished, therefore, considering this effect; the recommended value for C_d is 0.6-0.7, for air [5].

v_{in} is the velocity of the fresh air into the compartment.

From Bernoulli principle, the velocity of the flow into the compartment can be expressed as:

$$v_{in} = \sqrt{\frac{2\Delta P_l}{\rho_a}} \tag{6}$$

Replacing the expression for velocity in equation (6), the pressure difference across the lower openings can be written as:

$$\Delta P_l = \frac{\dot{m}^2}{2\rho_a (C_d A_{in})} \tag{7}$$

1.4 Pressure difference across the upper openings

The pressure difference across the upper is equal to the hydrostatic pressure difference, since the velocity is the same inside and outside. Therefore, taking the height from the opening to the neutral plane, with the notations from Fig. 2, the pressure difference across the upper vents will be written as:

$$\Delta P_u = (\rho_a - \rho_g) g (H - H_N) \tag{8}$$

where: $(H-H_N)$ is the height from the upper vent to the neutral plane.

1.4.1 The total pressure difference across both openings

The total pressure difference across both openings, expressed as a function of densities is:

$$\Delta P = (\rho_a - \rho_g) g (H-z) \tag{9}$$

For convenience, the pressure difference across the upper vent is written as the difference between the total pressure and the pressure difference across the lower vent, from equations (8) and (9):

$$\Delta P_u = (\rho_a - \rho_g) g (H - z) - \Delta P_l \tag{10}$$

1.5 Mass flow rate through the upper openings

The mass flow rate of the smoke leaving the compartment can be written as a function of the outlet opening area, A_{out}, as:

$$\dot{m}_{out} = C_d \rho_g v_{out} A_{out} = \dot{m} \tag{11}$$

From Bernoulli principle, the velocity of the flow out of the compartment can be expressed as:

$$v_{out} = \sqrt{\frac{2\Delta P_u}{\rho_g}} \tag{12}$$

Combining the equations (10) and (11), the mass flow rate through the upper vent becomes:

$$\dot{m}_{out} = C_d A_{out} \sqrt{2\rho_g [-\Delta P_l + (\rho_a - \rho_g) g (H - z)]} \tag{13}$$

1.6 Plume mass flow rate

The plume mass flow rate is estimated using the Zukovski correlation [6]:

$$\dot{m}_l = \dot{m}_p = 0.21 \left(\frac{\rho_a^2 g}{c_p T_a}\right)^{\frac{1}{3}} Q^{\frac{1}{3}} z^{\frac{5}{3}} \tag{14}$$

2 Results

2.1 Smoke layer above the second floor windows

If the ambient temperature is taken as 20°C and the smoke layer is imposed to be above the second floor windows, z = 9.5 m, the plume mass flow rate is $\dot{m} = \dot{m}_p$ = 55.69 kg/s.

The pressure difference across the lower vent results ΔP_l = 53.26 Pa.

Replacing the value for the enclosure area in contact with the smoke, A_w=562 m^2, into equation (4), the average smoke temperature resulted T_g =359.02 K.

From the ideal gas law, the density of the smoke layer can be written as a function of temperature:

$$\rho_g = \frac{353}{T_g} = 0.983 \frac{kg}{m^3} \tag{15}$$

The area of the outlet openings is expressed, from equation (13), as:

$$A_{out} = \frac{\dot{m}_{out}}{C_d \sqrt{2\rho_g[-\Delta P_l + (\rho_a - \rho_g)g(H-z)]}} = 55. \frac{69}{0.6\sqrt{2 \cdot 0.983[-53.26 + (1.2 - 0.983)9.81(12.8 - 9.5)]}} \tag{16}$$

The equation above does not have a natural solution, because the expression under radical, representing the pressure difference across the upper vent, has a negative value. With the actual constraints, as the inlet area, A_{in} = 8.2 m^2 and the smoke layer height z = 9.5 m, it is not possible to reach steady state condition with natural ventilation through the upper openings.

3 Discussions

3.1 The influence of the openings area

The equation (16), above can be solved if the pressure across the upper vent is diminished by increasing the inlet area, or if the smoke layer height is decreased. The neutral plane would descend, remaining closer to the highest vent area.

If the inlet area would be increased, the pressure difference across the lower vents approaches zero and the flow velocity would also decrease. Plotting the inlet area versus outlet area from the equation (16), it can be seen from Fig. 3, that there is a very small variation interval for the inlet in order to keep the outlet area to a feasible range. The outlet vent openings should be evenly spread at the top level and the area of each window should not be greater that $2(H - z)^2$, in order to avoid the plug holing phenomenon [3].

Given these considerations, the optimum solution should lie close to the mean line between the two axes. As the inlet area is limited to the available door openings from the building, estimated as A_{in} = 8.20 m^2, the only variable remains the smoke layer interface.

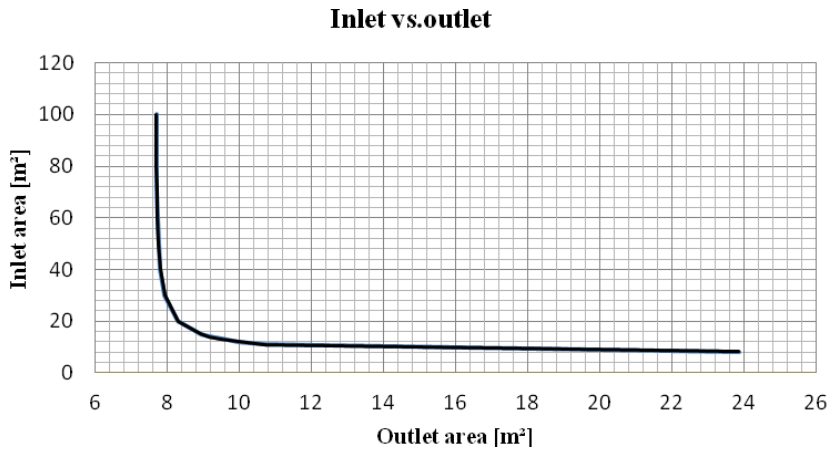

Fig. 3 The variation between the inlet and outlet openings for a steady state flow

Therefore, if the smoke layer is allowed to descend up to 6.5 m, above the first floor windows, the equilibrium in the compartment could be reached for an outlet area of A_{out} = 27, 20 m^2. In this case, the mass flow rate into the atrium would be equal to the mass flow rate out and to the mass plume rate, each of approximately 29.5 kg/s.

3.2 Alternative solutions

With the actual available inlet area, there is not possible to maintain the smoke layer at 9.5 m above the ground floor. Three alternative solutions should be further analysed as costs and safety implications upon the building occupants.

3.2.1 *Mechanical inlet provided at the atrium base*

The inlet area can be supplemented by a number of fans blowing air into the atrium, in case of fire. This will create an overpressure at the lower part of the atrium arresting the smoke layer to descend below a certain height.

3.2.2 *Mechanical extract provided at the top of the atrium*

Knowing the upper layer gas temperature, one can calculate the necessary volume rate for a fan extracting the smoke at the top of the atrium, as:

$$\dot{V}_{out} = \frac{\rho_g}{\dot{m}_{out}} \tag{17}$$

3.2.3 *Lowering the smoke layer height and providing smoke barriers at the second floor balcony*

If the natural ventilation represents the preferred solution and given that a fire occurrence is an accidental phenomenon, smoke screens can be provided along the second floor border towards the atrium space or the balconies can be closed with glass windows. This solution would allow the smoke layer to drop up to 6.5 m and would create the conditions for a steady smoke layer contained above the first floor windows.

3.2.4 *Limiting and controlling the fuel load inside the atrium*

For this particular case, lowering the fire size five times decreases the plume mass flow rate by 40%, but it will still require an additional smoke extraction strategy. Therefore, this preventive method can be used in conjunction with an active control system. Moreover, limiting the fuel load could also decrease the cost associated with high power fans because the fan capacity is proportional with the fire size.

4 Conclusions

Subsequent changes in the original design of a building affects more or less all the systems implemented into the building by the original design. This study has shown how a slight decrease in the inlet area, would require a great increase of the outlet area for a feasible natural ventilation strategy.

References

[1] Milke, J. (2016). Smoke control by mechanical exhaust or natural venting, Chapter 51, SFPE Handbook of Fire Engineering, Fifth Edition, Springer.

[2] Vassart, O. (2008). Dissemination of structural fire safety engineering knowledge (DIFISEK), Part 1: Thermal and mechanical actions, WP1, Final Report EUR 23332 EN, ISBN 978-92-79-08354-9.

[3] NBN S21-208-2. (2010). Fire protection in buildings – Design and calculation of smoke and heat extraction installations – Part 2: Covered car parking buildings, ICS: 13.220.01: 13.220.20, Ontwerp.

[4] Karlsson, B., Quintiere, J. (2000). Enclosure Fire Dynamics, CRC Press, Boca Raton London, New York, Washington DC.

[5] EN 12101-2:2003. Smoke and heat control systems-Part 2: Specification for Natural smoke and heat exhaust ventilators.

[6] Zukovski, E.E. (1995). Properties of fire plume. Combustion Fundamentals of fire, Cox,G.,Ed.,Academic Press, London.

Reinforced Concrete Elements Designed By Alternative Procedure

Fekete-Nagy L.[1], Mosoarca M.[2], Partene E.[3], Diaconu D.[4]

[1] *Politehnica University Timisoara (ROMANIA)*
[2] *Politehnica University Timisoara (ROMANIA)*
[3] *Politehnica University Timisoara (ROMANIA)*
[4] *Politehnica University Timisoara (ROMANIA)*
E-mails: luminita.fekete-nagy@upt.ro, marius.mosoarca@upt.ro, eva.partene@student.upt.ro, dan.diaconu@upt.ro

Abstract

One of the Alternative Design Procedures, worldwide known as the Strut-and-Tie Method come to be an efficient tool, successfully used in reinforced concrete structural element's design. All over the world, researchers have done both theoretical and experimental tests on different type of structural reinforced concrete elements in order to demonstrate that hypothesis. This paper deals with reinforced concrete walls having goals and gives some evidence that the experimental elements designed with Strut-and-Tie Method are capable to develop o good ductility, dissipating an important quantity of seismic energy.

Keywords: alternative, design, reinforced concrete, experimental testing, specimens

1 Introduction

Theoretical and experimental study focused on reinforced concrete walls with goals, research focusing mainly on modelling, numerical analysis and structural compliance of reinforcing making observations on the influence that the position of openings has on the behaviour of diaphragms. This paper presents a case study for the diaphragm wall with goals arranged vertically ordered.

2 Methodology

2.1Designing by Strut-and-Tie Method

2.1.1 Stages for Using Strut-and-Tie Method in Design

As required by this alternative design procedure described in detail in work [1], the tension state in the element has been determined, a selection of models having tensile and compressed bars was done, the so called strut-and-tie model with accuracy for the real state of tension and efforts by determining patterns in bars (compression and stretching) to achieve compliance with its, then for each stretched bar has been determined the appropriate reinforcement area, to support the efforts, taking into account of the plastics characteristics of materials.

First it has to be determined the spout of the loading through element, secondly choose different models of bars, strut-and-ties, to reflect the condition of efforts, then find the efforts from the bars of each model and finally the compliance of the component so as to make account of the specific features.

2.1.2 Specimen for Testing

Diaphragm wall with holes arranged vertically in the middle, the specific SW8 model [3], was requested at the horizontal and vertical forces. Useful load acting on the slab has standardized 200 daN/m^2 value and normal value of own weight is 500 daN/m^2. Behavior analysis under seismic loads in the elastic wall was made of hollow structural design software AXIS VM 5.0 calculating state of efforts, σ_y vertical uniform efforts distribution, the tangential unit efforts τ_{xy} and main efforts distribution. Fig.1 shows the main directions of main efforts distribution in the wall (ground floor and 1st floor) depending on the direction of seismic action [3].

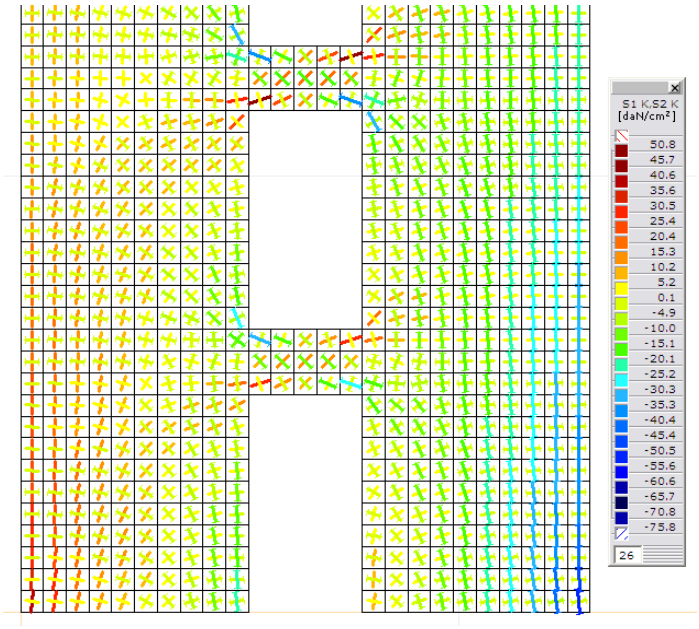

Fig. 1 Distribution of the main unit efforts in SW8 wall specimen with central goals

Analyzing the values of efforts in bars for the wall specimen with central goals SW8 and applying relationships to determine the reinforcement bars corresponding to "ties" bars from model, the orthogonal direction of reinforcement were choose for greater simplicity in execution.

2.2 Experimental Tests

The dimensions of the specimen to be tested have been chosen so that it can be tested in stand trial existing in the hall for tests of our Department. Test items and the experimental stand are presented schematically in Fig. 2. The elements have been fixed in the stand in an upright position and have been requested in the horizontal forces cyclic coherently up to the stage of disposal. The achievement of specimen for testing [3] and their execution was performed to satisfy requirements related to dimensions of experimental stand.

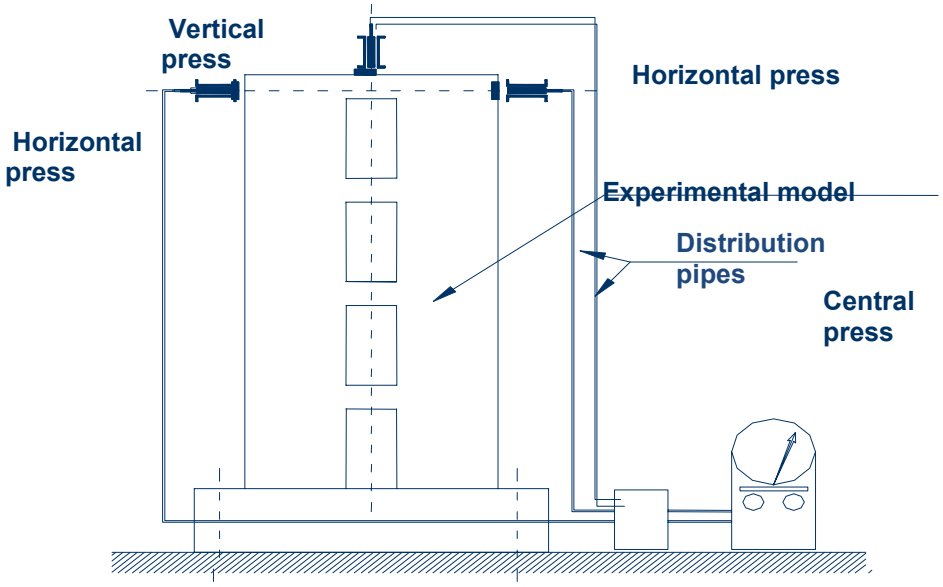

Fig.2 The Testing Experimental Stand – SW8 Model

The SW8 experimental element, reinforced concrete structural wall with door holes located in the middle was requested by the cyclic alternating horizontal forces up to the stage of transfer.

Behavior of experimental models has been observed in various of loading level, and the distribution of cracks at different values of horizontal forces and the failure of SW8 model is shown [3] in Fig. 3.

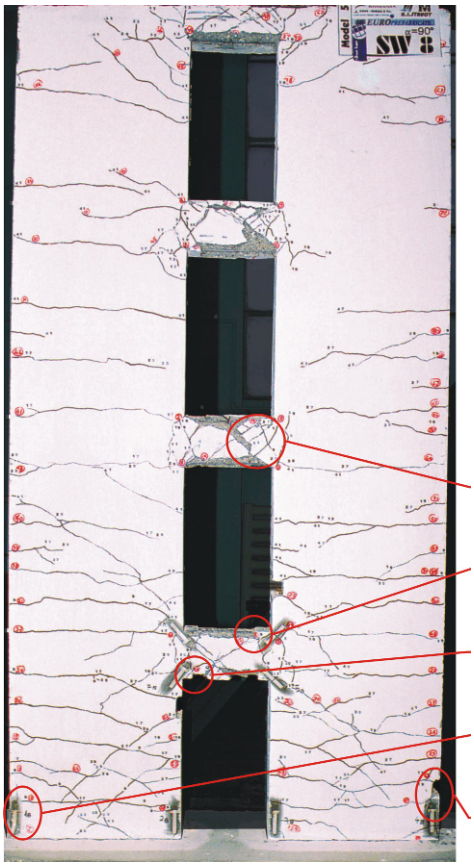

Legend:

1 .Concrete crushing

F= 5 kN

Δ = 7 mm

2. Horizontal reinforcement flow

F= 4 kN

Δ = 2mm

3. Horizontal reinforcement flow

F= 6 kN

Δ = 7mm

4 .Vertical reinforcement flow

F= 6 kN

Δ = 6 mm

5. Vertical reinforcement flow

F= 6 kN

Δ = 6 mm

Fig. 3 Experimental SW8 Model- failure and cracks

2.3 Results

Evaluation of seismic response of experimental models is presented charts suggestive force - displacement (P-Δx) ductility was determined based on which item and calculated the amount of energy dissipated by each experimental model. Because the models with goals of the doors opening have been requested cyclic ratio-bigeminy, these curves shall be presented in the form of ciclograme, as shown in Fig. 4, for the SW8 testing Model.

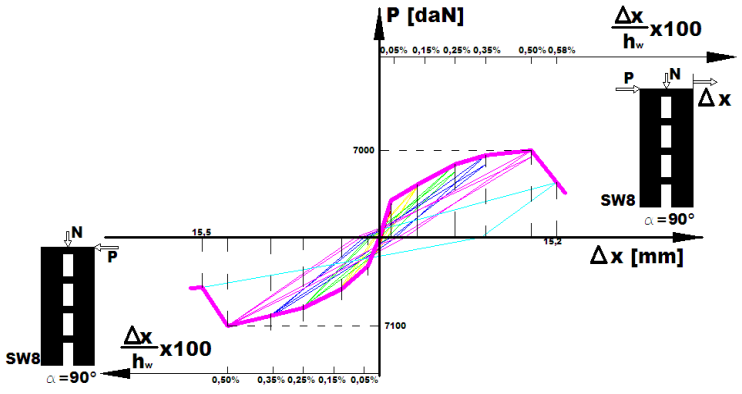

Fig. 4 Experimental SW8 Model- failure and cracks

For the purpose of verification of the results obtained in the experimental path with the theoretical have plotted graphs P-Dx comparative, Fig.5. The experimental results were verified with theoretical results provided by the computer program Biograph [2].

As seen, for the SW8 Model, between the two curves there is a good accordance; differences are given by the different from the seismic request.

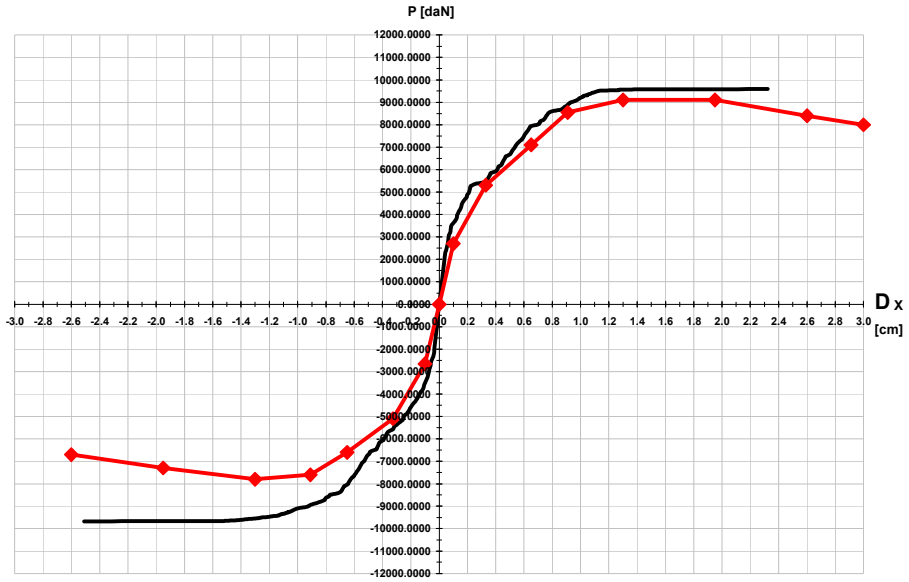

Fig. 5 Plotted graphs P-Dx comparative theoretical-experimental for SW8 Model

Generally, models records a good seismic response, characteristic for well conformed structural walls, deformation is dictated primarily by eccentric compression. Next is shown the force-strain diagram of P-Dx (P-Δx), for SW8 experimental model, goals central diaphragm. Interpretation of curves P - ε indicates that the fittings on order flow valves are different from the walls shifted goals towards those coupled. In conclusion, reinforcement in the absence of special measures stipulated by the regulations shows that hollow walls are not as exposed to delayed brittle disposals as coupled walls.

3 Conclusions

The interpretation of the results of experimental tests carried out and studying the behavior of walls experimental test results are expected and confirmed the results anticipated by theoretical analysis performed to calibrate the experimental models. Also it was verified that the hollow structural walls can be calculated and comply using Strut-and-Tie Method, experimental models designed on the basis of this method is able to develop a good ductility and displacement taking over a significant amount of seismic energy. Therefore, this process may become an alternative to the usual design of reinforced concrete having static or geometrical discontinuities.

References

[1] Fekete-Nagy, L. (2002). Contributii la alcatuirea strucrurilor din beton armat avand discontinuitati statice si geometrice (Contributions to the composition of reinforced concrete structures with static and geometrical discontinuities), PhD. Thesis, May, Timisoara.

[2] Clipii, T., Stoian, V., Fekete-Nagy, L., Mosoarca, M., s.a.(2005) Raport final de cercetare-Metode alternative de Proiectare a Elementelor Structurale din Beton Armat (The final research report - Alternative methods Design of Reinforced Concrete Structural Elements), Contract CNCSIS tip A Cod 489, Tema4, pp. 9-19.

[3] Mosoarca, M. (2004). Contributii la calculul si alcatuirea peretilor structurali din beton armat (Contributions to the calculation and structure of reinforced concrete structural walls), PhD. Thesis, February, Timisoara.

Using EBR CFRP Strips only on Failure Cracks to Retrofit a Reinforced Concrete Wall Panel Subjected to Seismic Actions

Fofiu M.[1], Stoian V.[1]

[1] *"Politehnica" University of Timisoara (ROMANIA)*
E-mails: mihai.fofiu@upt.ro, valeriu.stoian@upt

Abstract

The authors of this paper are presenting an experimental study regarding the influence of a retrofitting procedure on the seismic behaviour of a large Precast Reinforced Concrete Wall Panel (PRCWP), having an initial large window opening that was enlarged into a door opening by removing the parapet. The experimental specimen was subjected to in-plane cyclic loading in order to simulate the shear behaviour and not the flexural one. The lateral loads will be applied in displacement control, while two vertical loads simulating the load of a five-story building will prevent the rocking effect of the test specimen. The measurement will include the lateral force and the drift, up until failure. After the specimen was tested, it will be retrofitted using Externally Bonded Reinforcement (EBR) carbon fibre strips, strips applied on the specimen in the areas where cracking of the concrete was observed during the initial test, then tested again in the same conditions. The primary goals were to restore the specimen's initial load bearing capacity, to determine the effectiveness of the retrofitting procedure, and to obtain information about the shear behaviour of Precast Reinforced Wall Panels. As it will be presented the shear bearing capacity was increased compared to the initial one but the drift level was decreased.

Keywords: experimental test, CFRP, EBR, carbon fibre, seismic action, precast concrete wall, retrofitting

1 Introduction

In this paper the authors investigate the seismic performance of precast RC wall panel with a large door opening weakened by seismic action and retrofitted using Externally Bonded Reinforcement (EBR) carbon fibre strips. The research addresses a common situation in which Precast Reinforced Wall Panels (PRCWP) is weakened by a seismic action and is in need of rehabilitation in order to be safe.

Likewise, other Eastern European countries, Romanian urban areas underwent significant transformation during the second half of the 20th century, regarding the flats housing conditions. A considerable percentage of urban population live in typical low-rise 5-storey high precast reinforced concrete large panels (PRCLP) buildings. Most of these buildings were realized in the period of 1950-2000, totalizing more than 57 000 buildings.

Given the fact that these buildings are old, we need to study the behaviour of their structural element during seismic actions. Similar researches are scarce in the literature. The resisting behaviour of the Reinforced Concrete (RC) structural wall was investigated in the post-damage repair and strengthens case. The retrofitting strategy was chosen after carefully analysing the behaviour of the initial element during the test, all cracks direction and openings were measured, in order to establish the correct effort distribution and to re-establish the load bearing capacity of the element after the retrofitting procedure.

2 Experimental program

2.1 *Experimental specimen*

The element presented in this paper is a PRCWP used in the typical five storey residential buildings from 1970 to 1990 in Romania. In Fig. 1 it is presented the panels distribution for the building with the indicative 770-81, one of many designs used in these buildings [1].

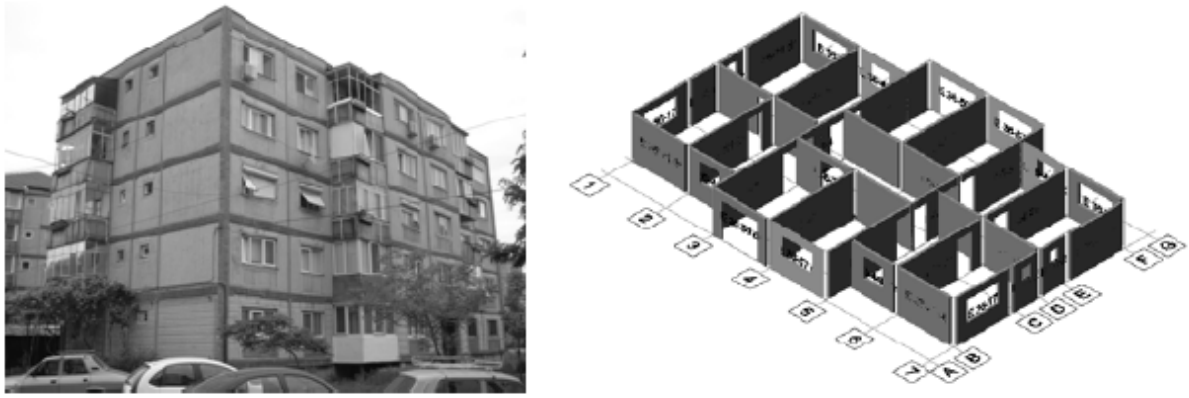

Fig. 1 Project type 770-81

Fig. 2 depicts the reinforcement distribution in the element.

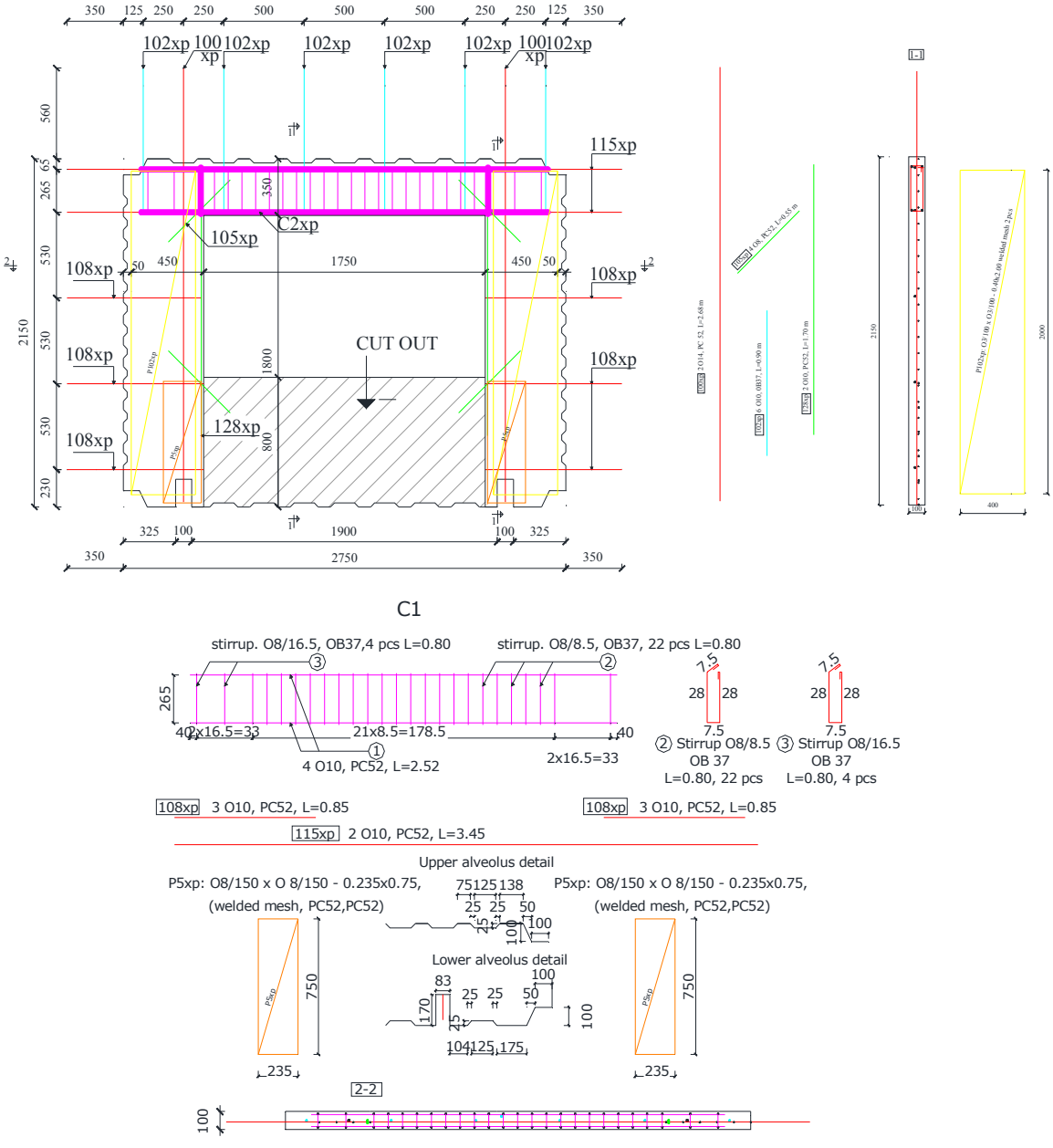

Fig. 2 Reinforcement details for the PRCWP

It can be seen that the top coupling beam is the most reinforced part of the specimen, while in the bottom part, below the window, were the opening was cut and enlarged, there is less reinforcement. The tested specimen had the following dimensions: 2750 mm length, 2150 mm height and 100 mm thickness, while at each end there was a heavily reinforced T shaped boundary element which prevented the out of plane displacement.

All features of the experimental test specimen like: dimensions, reinforcement details and material properties are taken from an existing building. The element had to be scaled down by a factor of 1:1.2 because the laboratory in which the tests were conducted had a limited height and the testing gear peaked at 1000 KN.

2.2 *Experimental procedure*

The test set-up was conceived in such way, that it simulates the seismic behaviour of the tested element. In order to achieve this, we had to reproduce the shear behaviour and not the flexural one. For this, two composite steel-reinforced concrete beams were used as force transmitting system (upper) and foundation (lower) elements. The remaining gap between the tested PRCWP and the beams was filled with high-strength mortar. The stand consists of four reaction frames, two for the vertical (gravitational) forces and two for the in-plane (seismic) forces, which were all induced with four hydraulic jacks. In Fig. 3 the experimental stand can be seen with all its elements, the image is cropped on the symmetry axis of the stand.

The two vertical forces were kept constant at 150 kN and were increased on the horizontally loaded end of the upper beam in order to counter the rocking effect of the element, for each 1 mm of vertical displacement the force was increased by 100 kN. The seismic loading history was comprised of displacement controlled range; this control was defined in terms of constant displacement increments of 0.1% drift ratio (2.15 mm) and two cycles on each displacement level. The subsequent displacement levels, expressed in mm and drift ratio (%), are as follows: ±2.15 mm, ±4.3 mm, ±6.45 mm, ±8.6 mm, etc. and ±0.1%, ±0.2%, ±0.3%, ±0.4% etc., respectively.

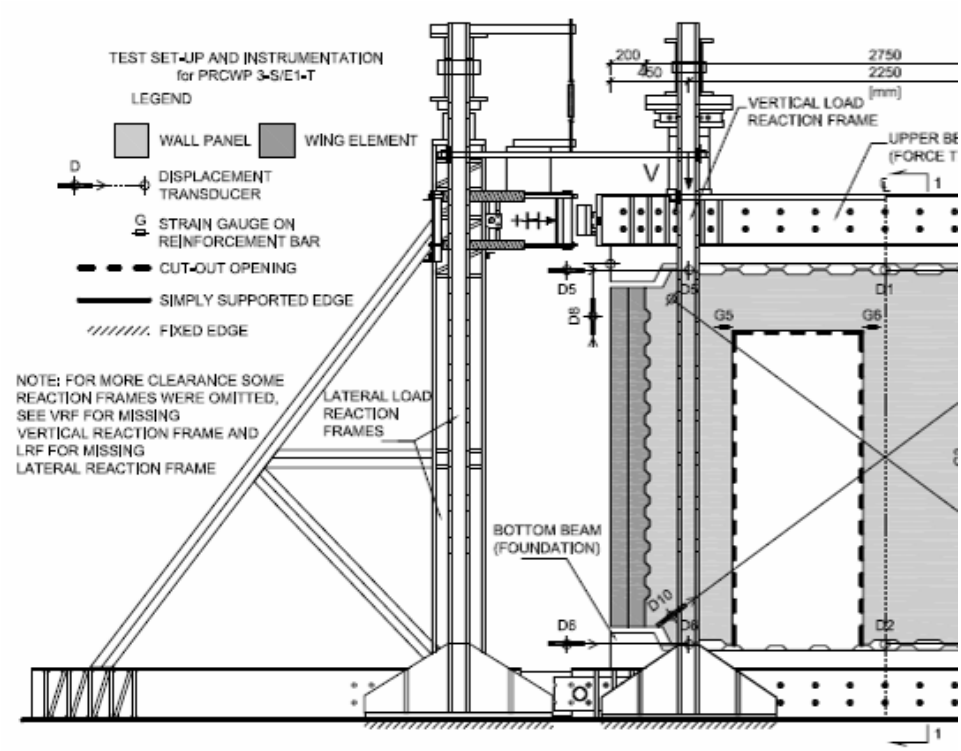

Fig. 3 Experimental stand

The failure criteria was assigned to the displacement level and was considered fulfilled when 20% decrease in the load bearing capacity from one cycle to another was obtained.

3 Strengthening procedure

The principles of the strengthening strategy were based on the behaviour and failure observed during the testing of the unstrengthen specimen. The successful application of FRP to strengthen solid concrete walls has been achieved in several studies [1, 2, 3, 4, 5, 6]. The behaviour pattern noticed was as follows: shear cracking of the piers with diagonal cracks. So, the strengthening strategy was to increase the shear capacity of the wall piers in the cracked areas and to prevent the reopening and further increasing in width of the diagonal cracks.

The retrofitting was performed by means of Carbon Fibre Reinforced Polymers (CFRP) using Externally Bonded Reinforcement (EBR) technique for both increasing the shear strength and to stich the cracks. The first step of the retrofitting procedure was to prepare the concrete surface on the areas were the carbon fibre strips would be placed, by grinding the surface using a rotating diamond disc, in order to remove all prominent imperfections, debris of mortar and irregularities of the surface. Then drilling the holes were the anchorage CFRP mesh would be introduced, and finally removing the dust particles by blowing the surface with compressed air. The second step was to cut the carbon fibre strips and anchorages to the specified dimensions, which were as follow: 30 mm wide and 1.4 mm thick for the carbon strips and 300 mm in length and 100 mm in width for the anchorages. A total of one 2950 mm and 4 600 mm long strips were used for each side of the wall, the sides being symmetrically reinforced. For the anchorage part a total of 11 CFRP anchorages were used. The third step was to insert the anchorages in the previously drilled holes and spread their ends so that the carbon fibre strips would be anchored. The last step was to mix the resin and place the carbon strips in their position on the wall surface. Fig. 4 depicts the strengthened specimen and the designed procedure.

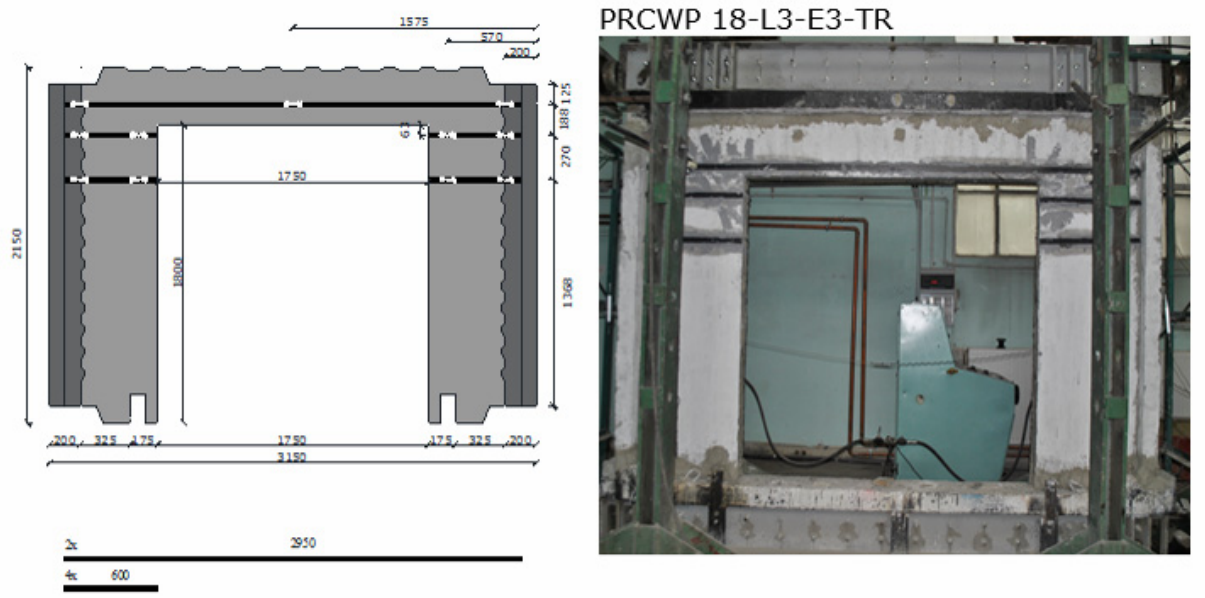

Fig. 4 Strengthening procedurel

4 Behaviour and results

The unstrengthen specimen reached a maximum seismic force of 243 kN at a drift level of 21.5 mm (1.0%) and lost 19 % of its load bearing capacity reaching 197 kN at 32.5 mm (1.50%) drift level. For the retrofitted element, the maximum load bearing capacity was of 285.5 kN at 25.8 mm (1.20%) drift ratio, after reaching its peak value for the seismic force the element lost 27% at its load bearing capacity in the next cycle at a drift level of 27,95 mm (1.30%) reaching a maximum force of 208.5 kN. Fig.5 displays the force displacement diagrams.

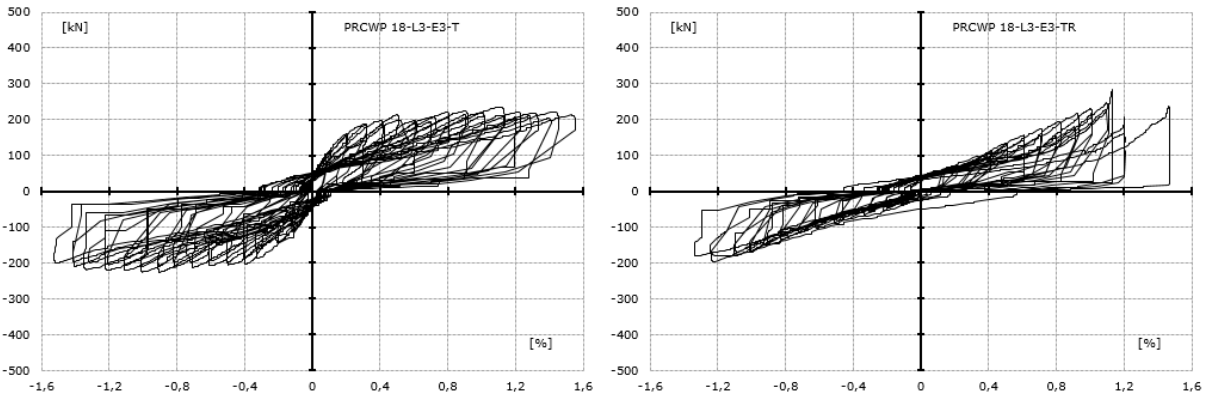

Fig. 5 Force displacement diagrams

The PRCWP had a very predictable ductile behaviour during experimental test, the diagonal cracks that lead to the failure of the unstrengthen element, started to exert tension on the EBR strips. The first noticeable crack width reopening was at the drift level of 1.0% (21.5 mm) when the resin that was holding the strips started to sound as it was trying to cope with the force. The element failed because of the diagonal crack in the left pier reopened and enlarged causing the retrofitting system to debond. The behaviour was characterized by the reopening of the large diagonal crack in the left pier which lead to the unstrengthen specimen failure, concrete crushing at the top edges of the door opening and debonding of the carbon fibre strips. Fig. 6 presents the specimen after the failure criteria was fulfilled, it can be observed the large diagonal crack in the left pier which lead to the failure and the NSM EBR strips that lost the bond with the concrete element.

Fig. 6 Failure details of the specimen

In conclusion, it can be said that the retrofitting procedure was a success, in terms of load bearing capacity, we managed to increase the elements load bearing capacity by 26,3%. However from the diagrams, it can be seen that the retrofitted element had a different behaviour, meaning we did not manage to re-establish the specimens initial seismic response, thus we can say that this approach has its limitations.

References

[1] REFERENCES Demeter I. (2011). Seismic retrofit of precast RC walls by externally bonded CFRP composites. Romania: PhD Thesis, “Politehnica” University of Timisoara.

[2] Antoniades K, Salonikios T, Kappos A. (2005). Tests on seismically damaged reinforced concrete walls repaired and strengthened using fibre-reinforced polymers. Journal of Composites Construction 9.3, pp. 236-246.

[3] Dan D. (2012). Experimental tests on seismically damaged composite steel concrete walls retrofitted with CFRP composites. Engineering Structures 45, pp. 338–348.

[4] Enochsson O, Lundqvist J, Taljsten B, Rusinowski P, Olofsson T. (2007). CFRP strengthened openings in two-way concrete slabs – an experimental and numerical study. Construction and Building Materials 21.4, pp. 810–826.
[5] Florut S-C, Sas G, Popescu C, Stoian V. (2014). Tests on reinforced concrete slabs with cut-out openings strengthened with fibre-reinforced polymers. Composites Part B – Engineering 66, pp. 484–493.
[6] Todut C, Dan D, Stoian V. (2015) Numerical and experimental investigation on seismically damaged reinforced concrete wall panels retrofitted with FRP composites. Composite Structures 119, pp. 648–665.

Practical Use of Steel Fibre Reinforced Concretes for Roads

Iures L.[1], Popa R.[1], Bob C.[1], Chendes R.[1]

[1] *Politehnica University of Timisoara, Construction Faculty (ROMANIA)*
liana.iures@upt.ro, radu@autoeuropa.ro, cbob@mail.dnttm.ro, remus.chendes@gmail.com

Abstract

This study refers to the experimental work of the team for obtaining a sustainable layer for coating of the roads. The paper presents the experimental programme which took into consideration different steel fibre percentage placed into a 5 centimetre thick fibre reinforced concrete that will be suited for coating the roads with heavy traffic conditions. Such a concrete layer was applied since 2014 into the courtyard of the firm SC AutoEuropa SA from Timisoara.

Keywords: steel fibres concretes, new concept in roads coating layers, practical application of steel fibre reinforced concretes.

1 Generalities

The limitation of the cracks into concrete structures, especially in roads concretes slabs; it is one of the main problema in road design. The cracks lead to an early destruction of the road coating, so the reparation of those should be done. Such works usually are expansive and also interrupt partially or totally the traffic on the damaged road. To prevent the appearance of the cracks structural design of the concrete as uncracked section should be made. The use of the steel fibres in concrete can be the solution for avoiding the maintenance costs of the roads coatings.

The rehabilitation of existing structures it is a problem that should take into account, in the first place, the cost effective solution that should be applied. An increase of the load carrying capacity, strength and ductility of the concrete structural element should be connected directly with the sustainability of the chosen rehabilitation solution [1].

The steel fibres reinforced concretes were studied on the international level since the year 1960. The large possibility of using and applying such concretes, makes the researches in this domain to be between the first subjects into the fields of composite materials today. Nowadays researchers continue the experimental works and the theoretical studies on such types of concrete due to their improved properties such us: high tensile and compression strength cracked reduced tendency and so on. In the paper "Corrosion of Steel fibre reinforced concrete from the cracks" by Jean - Luis Granju and Sana Ullah Balouch, published in 2005 [2], it is shown that the fibre addition into concrete leads to a decreasing of its fragile carácter and to an improve in mechanical characteristics.

1.1 *Studied Fibre Reinforced Concretes Compositions*

The tested samples were made of concrete prisms, having the dimensions of 150x150x600 mm. The prisms were filled with simple concrete up to 5 cm to top; the last 5 cm were filled with steel fibre reinforced concrete.

The steel fibre reinforced concrete was made using usual Portland cement CEM I 42.5R, river aggregate (having a maximum diameter of 31 mm) and the steel fibres were added in different quantities (30kg/mc and 60 kg/mc) (see Fig. 1). The FLUX MIX RM 101 additive was used. The fresh concrete was vibrated in moderate way; no special cure for the fresh or hardened concrete was applied (see Fig. 2).

Fig. 1 Steel fibres and aggregates

Fig. 2 Fresh concrete specimens

1.1.1 Fresh steel fibre concrete properties

Fresh steel fibre concrete properties were determined. The volumetric mass, for both compositions was around 2400 kg/mc. The concrete was mechanically mixed. The W/C ratio was 0.44. The moulds were filled with a 5 cm layer of steel fibre reinforced concrete and then the mould it is filled up with plain concrete.

The used superplasticizer has the characteristics as shown in table 1 [3].

Table 1 FLUX MIX RM 101 additive characteristics

Aspect	pH at 20^0C	Density at 20^0C [g/ml]	Chlorines content	Alkaline content
Brown	4.0 - 6.0	1.05 – 1.09	Max. 0.1%	Max. 2.0%

1.1.2 Hardened concrete characteristics

The characteristics of the hardened concrete were determined at 28 days and are presented into Table 2. It can be observed that the bending tensile strength of the tested samples increase with the increasing of steel fibres content into the 5 cm thick layer. The compressive strength for the samples with a 5 cm layer of steel fibre reinforced concrete, has increase by 1.4 – 1.5 compared with the simple concretes one [4].

Table 2 Hardened concrete characteristics

Concrete type	Compression strength at 28 days f_c [N/mm^2]	Bending tensile strength at 28 days f_{ct} [N/mm^2]
Simple concrete	50.12	3.20
30ULC	50.12	3.50
30BLC	54.54	3.97
60ULC	59.43	6.50
60BLC	59.43	6.30

Note: The compression strength was deterimined perpendicular to the pouring direction.
30ULC- 30 kg/m^3 steel fibres in the upper 5 cm layer of the concrete prism;
30ULC- 30 kg/m^3 steel fibres in the bottom 5 cm layer of the concrete prism;
60ULC- 60 kg/m^3 steel fibres in the upper 5 cm layer of the concrete prism;
60ULC- 60 kg/m^3 steel fibres in the bottom 5 cm layer of the concrete prism.

The testes revealed a better behaviour for the samples when subjected to bending tensile force in the case of loading in such a manner that the steel fibre reinforced concrete layer it is situated in the upper part of the tested prism, that is in the compressed zone (see Fig. 3).

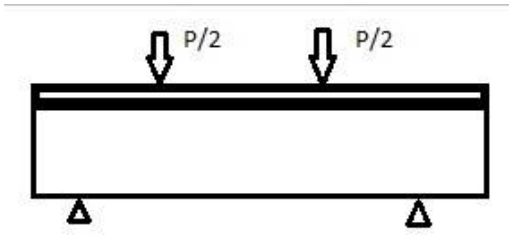

Fig. 3 Upper layer steel fibre reinforced concrete 4 points bending tensile test

2 Practical use of steel fibre reinforced concrete layer

In 2014, the team of the present paper, applied a concrete pavement overlay of 20 cm thickness, reinforced with steel fibres on a portion of the road in the yard of SC AutoEuropa SA Timisoara. For doing this, the old existing concrete was replaced by the new one containing steel fibres, on one side of the road. Another portion of the road was also redone with new simple concrete. This was necessary for the team to be able to compare time behaviour of the two road portions under heavy traffic and to demonstrate the research made in laboratory on specimens (see Fig. 4).

Fig. 4 SC AutoEuropa SA Timisoara, practical use of steel fibre reinforced concrete

Observation of the surface of the two types of concretes was made annually. The simple concrete layer presented, after one winter cracks with an opening of 4 – 5 mm, also some deformation of the surface could be observed. No such defects were observed in the case of the portion made with steel fibres in the concrete. The orientation of the steel fibbers into concrete matrix it is random so they assist in controlling the propagation of micro-cracks and also stops them of widening into major cracks [7].

3 Conclusion

The following conclusions can be made taking into consideration the experimental results:

1. The use of steel fibres into the concrete improves its mechanical characteristics such as: compression and bending tensile strength, crack resistance and so on.
2. The positive effect of steel fibres in concrete for pavement layers it consist of increasing the life cycle as compared to classical concrete pavements [5].
3. The increase in the bending tensile strength of the steel fibre reinforced concrete it is significant when the specimen it is tested having the layer of steel concrete fibres in the upper part, that is, in the compressed zone.

4. By increasing the steel fibre content, the cost of the pavement layer does not increase due to the fact that the layer depth varies according to the design method [6].
5. Durability of steel fibre reinforced pavement used for practical work done by the research team is to be recorded for at least 5 years period in order to establish an accurate result.
6. The orientation of the steel fibbers into concrete matrix it is random so they assist in controlling the propagation of micro-cracks and also stops them of widening into major cracks [7].

References

[1] Ghemis, M. T., Pop, M. (2014). Some Considerations Regarding the Rehabilitation Sustainability of Engineering Works, Journal of Applied Engineering Sciences, ISSN 2247-3769, Vol. 4(17), ISSUE 1/2014, Art. No. 147, pp. 25-28.

[2] Jean - Luis Granju, Sana Ullah Balouch (2005). Corrosion of Steel fibre reinforced concrete from the cracks, Cement and Concrete Research, Volume 35, Issue 3, March 2005, pp. 572 – 577.

[3] FLUX MIX RM 101, Erca Chim Ro, Mosnita Noua, Romania, Technical sheet.

[4] Buchman, I., Badea, C. (2009). The Characteristics of Ultra High Performance Concrete, Proceedings of the 11th WSEAS International Conference on Sustainability in Science Engineering, ISBN: 978-960, pp. 191-195.

[5] Elsaigh, W.A. (2001). Steel Fibres Reinforced Concrete Ground Slabs: A Comparative Evaluation of Plain and Steel Fibre Reinforced Concrete Ground Slabs. Meng (Transport). University of Pretoria: Pretoria, South Africa.

[6] Constantia Achilleos, Diofantos Hadjimitsis et al., Proportioning of Steel Fibre Reinforced Concrete Mixes for Pavement Construction and Their Impact on Environment and Cost, (2011) Journal Sustainability, 3, 965-983, doi 10.3390/su3070965, ISSN 2071-1050.

[7] Ahad, A., Khan, Z.R. and Srivastava, S.D. (2015) Application of Steel Fibre in Increasing the Strength, Life-Period and Reducing Overall Cost of Road Construction (by Minimizing the Thickness of Pavement). World Journal of Engineering and Technology, 3, 240-250.http://dx.doi.org/10.4236/wjet.2015.34025.

Fatigue Failure Probability Evaluation for Truss Structures – MIRA-Fatig Computing Program

Joavină R.[1], Popa M.[2], Ţepeş-Onea Fl.[2]

[1] *Maritime University of Constanta (ROMANIA)*
[2] *Ovidius University of Constanta (ROMANIA)*
E-mails: raduj68@yahoo.com, mpopa@univ-ovidius.ro

Abstract

Truss structures are largely used in various domains of civil engineering. High voltage net pillars, radio TV relays, onshore and offshore drilling and extraction structures are just a few examples. These structures are built as frames of welded elements, with different section types (mostly tubular on offshore structures). These elements nodes support failure mainly due to small welding defects that act as crack initiators and efforts concentrators. Varying loads due cyclical actions, such as wind, waves and currents, causes cyclic structural stress variations and cumulative effect of these stresses cause failure. Since the magnitude of responses in displacements, loads, etc., vary randomly in a group of values, they can be evaluated in the most useful way by probabilistic approximation. This paper is focused on offshore building engineering segment and presents a tool created by the authors to allowed evaluation of the overall annual probability of failure considering the cumulative effect of cyclical events.

Key words: prediction, fatigue curves S-N, fatigue, structural collapse.

1 Introduction

Many structure elements are subjected to cyclic loads that generate a tension history, which can lead to the initiation and propagation of cracks. In these situations for certain load parameters it is important to determine the number of repetitions that would endanger the safety of the structural element. For example, marine structures are continuously subjected to environmental cyclical loads due to waves, wind currents. Offshore structures safety analysis is as important for less severe stages of the sea but with more frequent appearances, as for severe storm conditions.

Therefore it takes two kinds of information on the waves induced loads in the early design study:

- extreme value experienced by structure throughout life, necessary to determine possible structural failure that occurs when a single load exceeds the critical structural strength;
- the frequency of various magnitudes of loads on life, allow to assess possible fatigue collapse, where the repeated loads plays a significant role.

Fatigue is a complex mechanism, characterized by a general reduction of the structural resilience due to repeated loading of a large number of times during the lifetime of the structure. Technical literature appreciate that the metal structural elements can yield at a stress value of approx 50% lower than in static conditions, if this stress is applied a large number of times. Breaking is the result of cracks formation and propagation due to variable tensions. Corrosion effect is also important for promote cracks growth. The manufacturing process affects also the fatigue behavior of connections because the welds are potential sources of stress concentration and cracks. Unlike static strengths, fatigue strengths for a specific load and material type can have a variety of values, depending on many factors.

The soft developed by the paper's authors allows determining the number of repetitions leading to element failure for a wide range of stress variation on the loading cycle. If information regarding the condition described by the number of cycles yearly recorded for different wave heights is available, failure probability can be evaluated.

2 Fatigue analysis using S-N curves

In Romania, to check the structures ultimate limit state there are some regulations in fatigue design codes harmonized with Eurocodes. Thus for steel structures, SREN 1993-1-9 prescribe accounting methods for

fatigue resistance of elements and joints subjected to cyclic actions. In [1] fatigue resistance curves (known in the literature as the curves S-N) are given, expressing the quantitative relationship between the stress domain (algebraic difference between the two extremes of a particular cycle of stress extracted from a tension time history) and number of loading cycles up to fatigue for particular details categories. Details categories are presented as execution details, description and requirements in 10 tables. It is mentioned that fatigue resistances can be apply to structures operated in normal atmospheric conditions with sufficient corrosion protection and regular maintenance program, and seawater corrosion effect is not covered.

The S-N curve is usually based on fatigue tests in the laboratory. For interpretation of S-N curves from fatigue tests, the fatigue failure is defined to have occurred when a fatigue crack has grown through the thickness of the structure or structural component [2].

When using S-N curves for assessing fatigue failure likelihood of a structure is important to consider the validity of the standard. For example, the guidance of Det Norske Veritas (DNV) about fatigue design of offshore steel structure specifies the validity of S-N curves in the air for steel materials with yield strength less than 960 MPa and for steel up to 550 MPa in seawater with cathodic protection or steel with free corrosion, for material temperatures of up to 100°C, to assess fatigue damage in the high cycle region.

As a whole, the design S-N curve is given as:

$$\lg N = \lg b - \mathrm{m} \cdot \Delta\sigma$$

where: N is predicted number of cycles to failure for stress range $\Delta\sigma$; $\Delta\sigma$ - stress range; m is negative inverse slope of S-N curve and lg$b$ s intercept of log N-axis by S-N curve.

The thickness effect is accounted for by multiplication on stress with $\left(t/t_{ref}\right)$, where t_{ref} is reference thickness, t is thickness through which a crack will most likely grow ($t = t_{ref}$ is used for thickness less than t_{ref}) and k is thickness exponent on fatigue strength which is given in standard depending on the category of detail (classified structural detail) and exposure conditions (in air, in seawater with cathodic protection). The reference thickness may have different values in different standards; is equal 25 mm for welded connections other than tubular joints. For tubular joints the reference thickness is 32 mm. In [3], for bolts $t_{ref} = 25$ mm.

There are more types of S-N curves [3]:

- Nominal stress S-N curve with a component stress that can be derived by classical theory such as beam theory.
- Hot spot stress S-N curve with geometric stress created by the considered detail which is treated separately in standards for plated structures and for tubular joints.
- Notch stress S-N curve can be used together with finite element analysis where the local notch is modeled by an equivalent radius.

3 Failure probability evaluation for different the sea states

"The fatigue life may be calculated based on the S-N fatigue approach under the assumption of linear cumulative damage (Palmgren-Miner rule)" [3].

$$\mathrm{D} = \sum \frac{\mathrm{n_i}}{\mathrm{N_i}} \langle 1$$

where: D is accumulated fatigue damage, n_i is number of stress cycles in stress block i, N_i is number of cycles to failure at constant stress range $\Delta\sigma$i.

S-N curves serve as a measure metal fatigue resistance from reversible loads and report the applied stress succession to the number of cycles up to the metal break. Their determination was based on experimental data. Fig. 1 illustrates such curves: BS-F curves by British Welding Institute, AWS-X and modified curves - AWS-x curves by American Society of Welding. It should be noted that curves BS-F are available only for the rank of 10^5 to $2x10^6$ cycles. Their application for higher cycles of fatigue damage is based on extrapolations.

Based on experimental evidence [4] rate of fatigue damage does not diminish at higher cycles as would result from AWS-X original curve. In practical terms, for tubular joints, does not appear a stress value (as limit of endurance) for which failure will not appear independent on how much it would increase the number of cycles. Breaking occurs, very slow, due to the development of an existing defect in the welding or base material.

It is difficult to estimate the fatigue strength of a complex offshore structure, fatigue analysis can be used best to locate areas sensitive to failure and safety checks over the life time of the structure. Sizing structural elements is achieved for field and node areas. Field areas should be designed according to the classic stability

and strength calculation. However, in welded nodes complex states of stress and strain occur, the areas being subject to fatigue - hot spots. Concentrations of tension produced in these points can be up to 20 times higher than nominal stress. The position of these spots depends on the geometrical characteristics of the node and the type of the load.

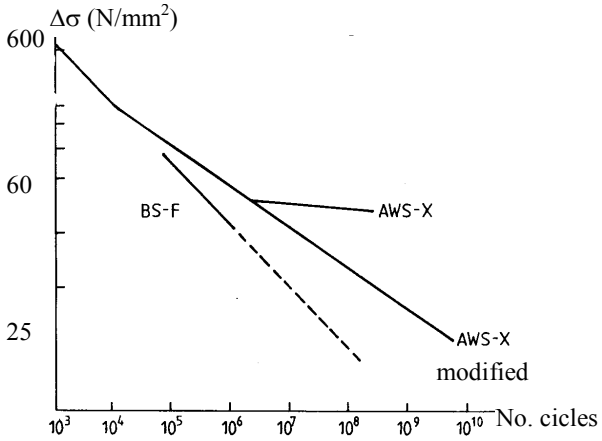

Fig. 1 S-N curves BS-F, AWS-X

Hot spots appear on both the main bar and on the secondary for simple loads being localized depending on the type of load and for the composite loads depending on the node type and weight of each effort (fig. 2). As a detailed assessment of local stress in joints by finite element approximation or experimental, it is expensive and time consuming, these tensions are estimated by multiplying the nominal stress of the element with stress concentration factors (SCF). Semi empiric relationships to estimate the stress concentration factors, are available in the technical literature based on the size and geometry of the joint For example, for K-type joints such relationships are given by Visser , Kuang and Kellog [5].

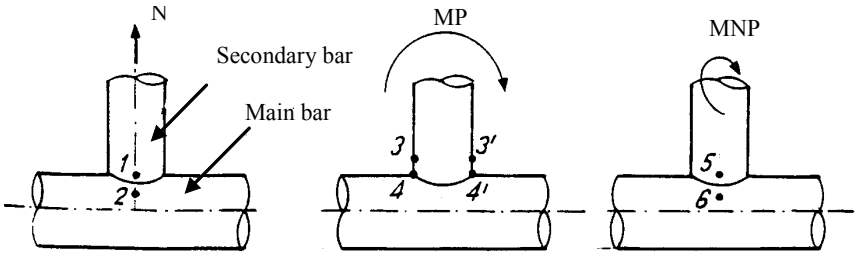

Fig. 2 Examples of hot spots location

4 MIRA – Fatig computing program: presentation, input data, results

Developing a software as a tool for determining the number of cycles of fatigue started with the intention of making the fatigue analysis using S-N curves - AWS type to determine the repetitions number (N) where failure occurs for a stress variation range Δσ. The following relationships are used for curves description, and solving can be done through trial:

$$\lg N = 12{,}29 - 3\lg\Delta\sigma \quad for\ N \le 10^7$$

$$\lg N = 15{,}82 - 5\lg\Delta\sigma \quad for\ N \ge 10^7$$

$$\lg N = 13{,}38 - 0{,}87\lg T - 3\lg\Delta\sigma^* \quad for\ N \le 10^7\ şi\ T \ge 15mm$$

$$\lg N = 17{,}64 - 1{,}45\lg T - 5\lg\Delta\sigma^* \quad for\ N \ge 10^7\ şi\ T \ge 15mm$$

$$\Delta\sigma^* = \Delta\sigma \cdot SCF \cdot \left(\frac{18}{T}\right)^{0,2}$$

The relationship includes the effect of thickness, stress concentration factors, etc. Bar diameters require different S-N curves. It takes into account the influence of the main bar wall thickness by changing the stress amplitude in nodes with wall thickness. Using these relationships (if stress domain Δσ - produced by cyclical actions with known parameters defining a sea state - it is obtained from the structural analysis) make possible the

calculation of the cycles number that would lead to fatigue failure. Based on this value, failure probability can be calculated (fig. 3).

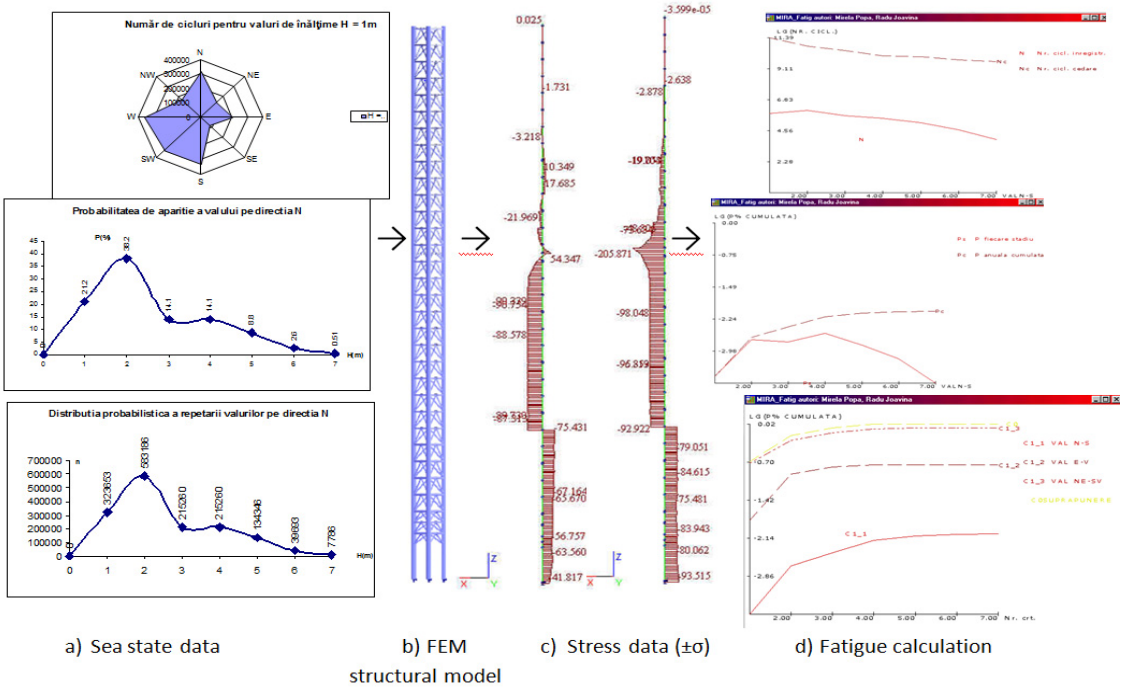

Fig. 3 Steps taken for failure probability evaluation

Source, in Fortan 90 code, is written and compiled using the Lahey developed interface. The input data processed by the program refers to the stress domain Δσ and loading cycles number that leads to a variation of stress value Δσ, and data related to the structural element: wall thickness, stress concentration factor [6] (fig. 4). The input data are read from the keyboard, through dialog windows.

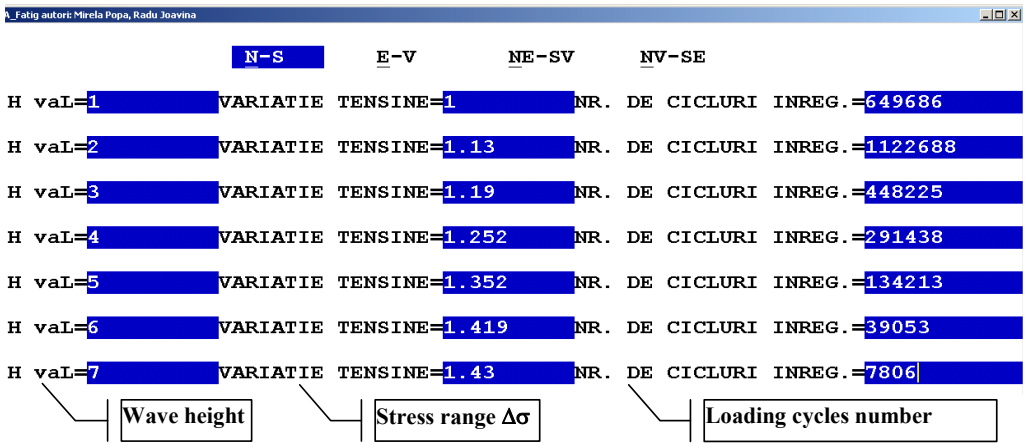

Fig 4. Data input panel

The results are graphically displayed and saved in ASCII files format (fig. 5). Saving in ASCII enables further results processing. Analyzed loads can come from wind, wave, or other dynamic loading. A data set contains data of Δσ stress range and number of loading cycles and can be saved with a name proposed by user. To this name the program adds an extension depending on the nature and direction of the load. The contents of this file is displayed immediately after viewing the graphic representation of the number of cycles recorded compared to the number of cycles to failure, the structural failure probability for each stage of the sea and the cumulated annual failure probability.

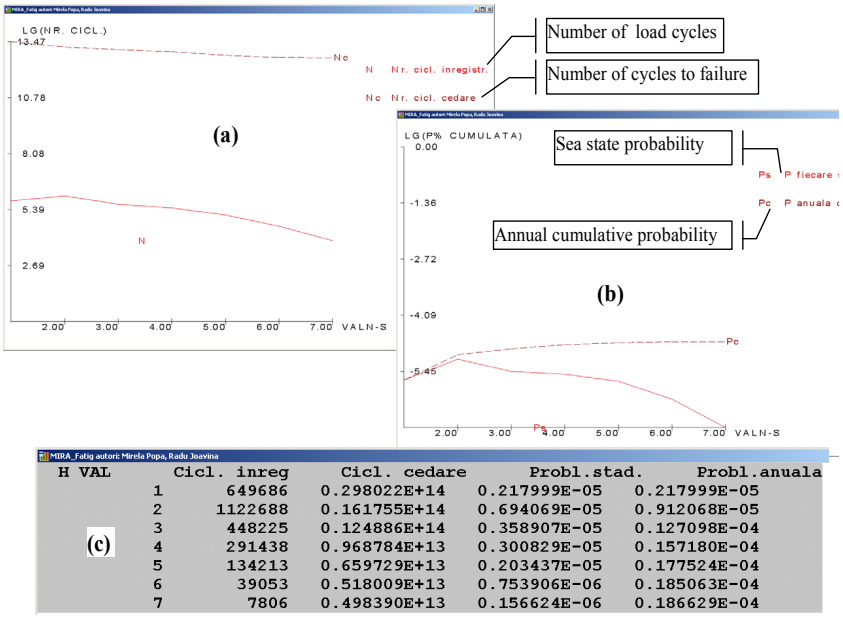

(c)

H VAL	Cicl. inreg	Cicl. cedare	Probl.stad.	Probl.anuala
1	649686	0.298022E+14	0.217999E-05	0.217999E-05
2	1122688	0.161755E+14	0.694069E-05	0.912068E-05
3	448225	0.124886E+14	0.358907E-05	0.127098E-04
4	291438	0.968784E+13	0.300829E-05	0.157180E-04
5	134213	0.659729E+13	0.203437E-05	0.177524E-04
6	39053	0.518009E+13	0.753906E-06	0.185063E-04
7	7806	0.498390E+13	0.156624E-06	0.186629E-04

Fig. 5 Results panel: (a) number of failure cycles and number of loading cycles for each sea state leading to Δσ; (b) failure probability for each sea state sea and the cumulative probability; (c) file containing the results for the data set analyzed according to direction

For example, wave high between 1 and 7 m corresponding to a number of loading cycles for N-S sea state will be introduced as input data (Fig. 4). Separately, for each wave height, the structural analysis (using a 3D FEM model as in Fig. 3b [6]) provide the stress values, use also as input data (Fig. 4). Based on Δσ values (each corresponding to a wave height), program evaluates the number of failure cycles and draw the corresponding Nc curve comparing it with the number of recorded wave cycles (Fig. 5a). It can be easily seen from Fig. 5b and 5c that for the data set studied, the number of failure cycles is significantly higher than the number of loading cycles recorded *lg(NC) >> lg(N)*. Thus the load generated by a wave of 4m (Δσ = 1.25 MPa), failure would occur at a rehearsal of $968784 \cdot 10^4$ cycles, while in a period of 1 year are *291438* repetitions. Failure probability is obtained by reporting the number of loading cycles to the number failure of cycles. Thus for exemplified element, there is a failure probability of $0.3 \cdot 10^{-5}$ for wave loadings of H 4m (curve denoted by Ps), and for all wave heights of 1m to 7m cumulative probability is $0.18 \cdot 10^{-4}$ (curve denoted by Pc). On the horizontal axis the wave heights are listed and on the vertical axis the number of loading cycles in logarithmic scale. If opting for overlapping effects of multiple loads, from the main menu it can be choose "Other loading from the same data set." Overlapping effects operated by selecting "Cumulating for the current data set". Graphical representation thus obtained, also allows failure probability comparison for loads that have been cumulated (Fig. 6).

Failure probabilities for each direction, also the cumulative one, are stored in a file with the data set name and ".dat" extension. C0 graph of Fig. 6 is obtained cumulating failure probabilities calculate for three directions: N-S direction (denoted C1_1 curve), E-W direction (C1-2 curve) and NS-SE direction (C1-4 curve). Predominant effect is seen to be the one given by E-W wave. Taking into account the cumulative effect of waves after directions studied, the probability of failure is of 0.017%. It should be considered that all loads introduced as part of the same set of data are not necessarily cumulated, but only those for which the user responded with "D" to the question "Cumulate the load with others? (Y / N)".

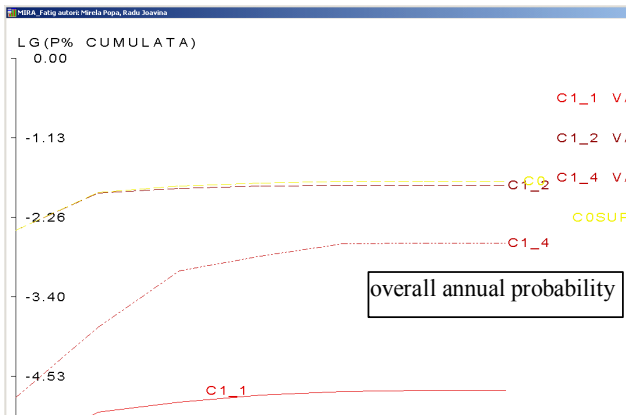

Fig. 6 Failure probability cumulated for 3 directions waves

Also the thickness of the bars or concentration factor for data already entered can be change, or the user can move on to "Other data set".

5 Conclusions

Truss structures design and post design evaluation require a laborious static and dynamic analysis with a solid statistical data base. For offshore structures this evaluation is more restrictive taking in to account the heavy environmental conditions, response analysis involving interaction between hydrodynamics, statistics, geotechnical and structures calculation data. There is considerable uncertainty in determining the stress concentration level and the relationship between stress-fatigue to establish the jacket type welded tubular joints failure. Load values causing failure decreases with increasing of applications number. Thus, the marine structures subject to high number of wave cycles requires a suitable fatigue design.

With a explicit graphical interface, MIRA-Fatig program optimizes the fatigue analysis by giving the user the possibility to choose for local areas of the structure that may be subject to failure the loads that will be applied, numbers of cycles and also the option to cumulate three sets of different loads (sea, wind and other dynamic load) on all cardinal and inter cardinal directions. The program facilitates comparative analysis depending on wall thickness and SCF value. For an already entered data set (field tension and no. of cycles), a reassessment for another bar thickness (other design option or the corrosion effect) and / or other stress concentration factor it can be immediately run. The output data is both graphically and numerically presented.

Note that the analysis is limited to AWS curves type restrictions. A further development of the program might follow in terms of generalization so the user to be able to opt for specific type of S-N curve.

References

[1]. SREN1993-1-9 Eurocode 3: Design of steel structures: Part 1-9: Fatigue (in Romanian).
[2]. Design of Offshore Wind Turbine Structures MAY 2014 DNV-OS-J101.
[3]. Fatigue Design of Offshore Steel Structures OCT. 2011 Recommended Practice DNV-RP-C203.
[4]. Marshall P.W. (1992). *Design of Welded Tubular Connections*, Elsevier.
[5]. Gupta A., Singh R.P. (1986). *Fatigue Behavior of Offshore Structures,* Springer-Verlag, New York.
[6]. Joavina R., Popa M., Vintila D., Slămnoiu G. (2001). *Considerations on Fatigue Phenomenon on Black Sea Offshore Structures of Gloria Type* - in International Symposium of Theoretical and applied Mechanics “Dimitrie I. Mangeron”, Iaşi, 5-6 October.
[7]. Kenny J. P. (1986). *Study on buckling safety factors for offshore structures,* Dept. of Energy, London, England.
[8]. Krempl E. (1998). *Design for Fatigue Resistance,* CISM, Udine, Italy.
[9]. Guide For The Fatigue Assessment Of Offshore Structures, American Bureau of Shipping (2003).
[10]. Ochi, M.K. and Wang, S. (1976). *Behavior of Offshore structures,* New York.
[11]. Vulpe A., Poteraşu F., Cărăuşu A. (1985). *Failure probability and parameter estimation for structures with Weibull -distributed strength. Probabilistic Methods in the Mechanics of Solids and Structures,* Springer-Verlag Berlin-Heidelberg-New York-Tokyo.

Modern Historic Timber Structure Consolidation Technologies – A State of the Art Review

Keller A.[1], Mosoarca M.[1]

[1]*Politehnica University of Timisoara, Faculty of Architecture and Urban Planning, Traian Lalescu str, nr. 2/A, 300223, Timisoara (ROMANIA)*
E-mails: alexandra.keller@upt.ro, marius.mosoarca@upt.ro

Abstract

Timber structures are an important part of the build heritage from all around the world. They present the traditional knowledge of past artisans which makes them unique and valuable. In order to preserve the built timber heritage for future generation, various consolidation and rehabilitation techniques were developed. In recent years timber structure consolidation techniques evolved from simple systems using timber or steel elements which enhance the stability of timber structures to complex systems developed based on the type of structural damage and the general behaviour of the structure. This is why, the paper is evaluating various timber structure consolidation techniques, highlighting their strengths and weaknesses and pointing out what situations they are best suited for.

Keywords: historic roof structures, timber heritage, consolidation, strengthening, new technologies.

Introduction

Timber is one of the oldest materials that human beings have used in construction. Bridges, houses, cathedrals, boats, and even planes, since the end of the 19th century, have been built with timber [1].

Historic timber structures, due to their age, permanent exterior influences and often high degree of deterioration have to be consolidated regularly [2]. Considering the value of historic timber structures and their diversity worldwide, various methods have been developed recently in order to rehabilitate, reinforce and maintain this structure for future generation [3]. Latest academic literature presents a high interest in the development of new advanced and complex materials and technologies suitable for the conservation of heritage structures. The highest interest can be observed concerning the reinforcement of timber elements with fibre reinforced polymers [3].

1 Consolidation technologies

Historic timber structures used to be consolidated using traditional reinforcement materials, like steel [4, 5] or additional timber elements [1, 6]. The main purpose of this intervention was to enhance the mechanical properties of the structure. The development and analysis of historic brick masonry consolidation methods has always been in the attention of researchers [7, 8]. Timber consolidation techniques on the other hand evolved rather in recent years in order to offer an alternative to traditional materials and methods [9] which go beyond the strict strengthening of wooden beams and take the value of the timber heritage into consideration.

Besides the evolution of materials and technologies, an important factor that lead to the development of new consolidation techniques are contemporary conservation philosophies and principles. According to ICOMOS [10] all interventions upon heritage timber structures should be reversible and should not prejudice the value of the structure. This is why a complex assessment of timber structures is of great importance before any consolidation method is chosen [11, 12], in order to clearly determine what materials and techniques and where interventions are absolutely necessary in order to preserve the authenticity of the structure.

Taking this into consideration, contemporary consolidation techniques have a high diversity and go from composite materials, applied locally or globally, rods that are introduced hidden in the interior of timber elements to complex Nano technologies. All of these consolidation techniques strengthen and enhance the flexural stiffness of both timber elements and connection joints.

1.1 *Resins*

Resin timber structure repair is a rather new technology that has a variable applicability from consolidation, structural adhesion to structural gap filling [13]. While the fist two applications are related to fibre reinforced polymers which are connected to the structural element, gap filling is a different approach.

The solution is preserving the authenticity of the historic fabric, introducing the resin in highly decayed gaps of the structural elements (Fig. 1). The decayed areas of structural timber elements are removed and epoxy resin is cast in the resulted gap together with a reinforcing rod in order to raise the bearing capacity of the structure [14].

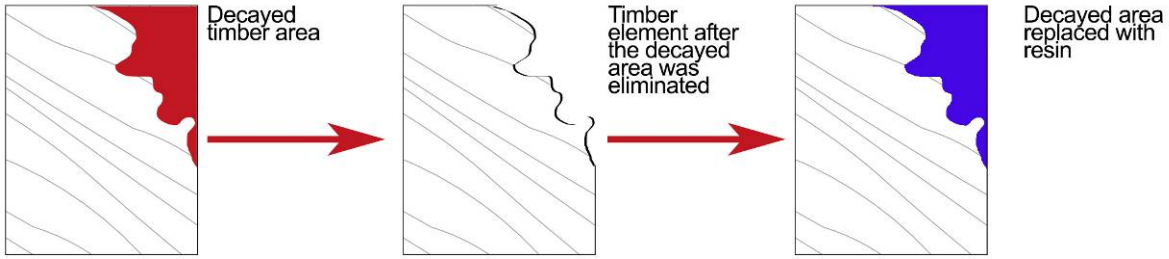

Fig. 1 Consolidation/Repair of historic timber structures using resin

1.2 *Glued-in-rods*

This technique is an adaptation of the traditional steel element consolidation technique [3] and consists of introducing and steel or glass fibre rod into a timber structural element, which is fixed using various adhesives like epoxy or polyurethane [15]. This consolidation method is a very complex and flexible solution since it can be used in the joint area one as well as in the central area of structural elements [16] (Fig. 1.). The main advantage is that the reinforcement is hidden in the interior of the timber element, thus offering an aesthetic consolidation method (Fig. 2).

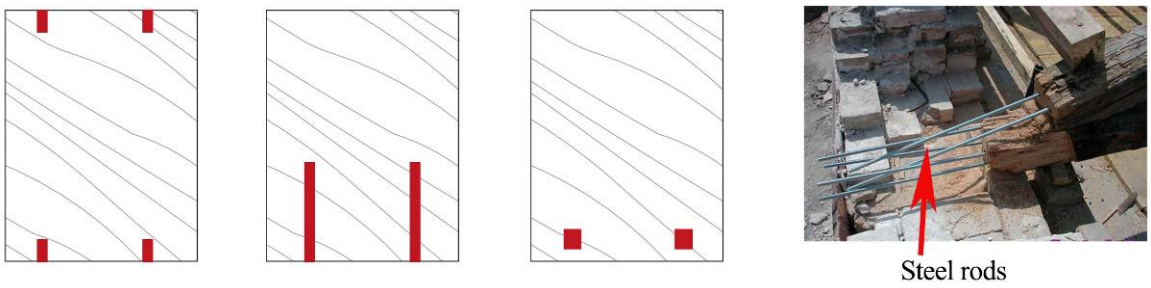

Fig. 2 Position of glued-in-rods in timber elements; glued-in-rod joint consolidation detail [17]

1.3 *Synthetic fibre reinforced polymers*

Fibre reinforced polymers are the most used consolidation materials for timber structures [18, 19] [x, y]. They are composite materials made from various synthetic fibres (glass, carbon, aramid fibres) and an adhesive matrix usually, polymeric resins [9]. Because of the high load bearing capacity and stiffness, the reinforcement materials are usually placed on the bottom part of beam and rafters, thus improving the ultimate bending moment of the elements [20, 21] (Fig. 3).

The main problems of this type of consolidation technique are the adhesives used in order to prevent the sliding of the consolidation material from the structural element. The main purpose of the adhesive is to transfer the load from the timber element to the fibre matrix and to prevent the damaging ore failure of the structural element.

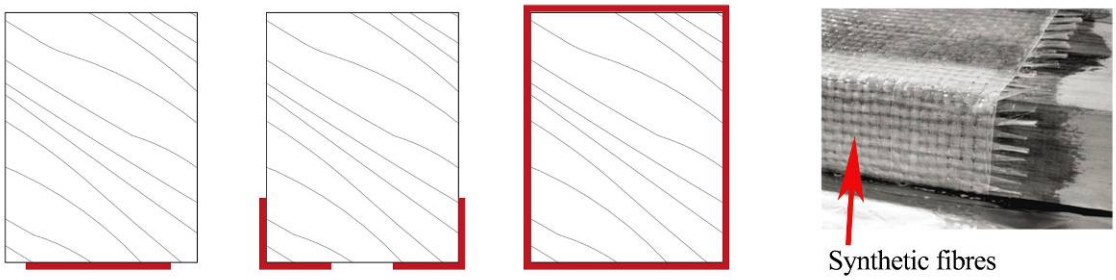

Fig. 3 Position of fibre reinforced polymers on timber elements; Reinforced timber element detail [22]

1.4 *Natural fibre reinforced polymers*

An alternative to synthetic fibre reinforced polymers are reinforced polymers made from natural fabrics, like hemp, flax, basalt or bamboo. This solution is highly contemporaneous since it answers to the current search of ecologic, recyclable, low cost and environmental friendly materials [23].

Natural fibre reinforced polymers are used just like the synthetic type ones, having a slightly reduced load bearing capacity and stiffness [24, 25]. Placed on the bottom part of structural elements, they enhance according to studies the bearing capacity of over 9% [23] (Fig. 4). The main problem of natural fibre reinforced material is the high variability, of both dimension and mechanical properties, of the fibres and their high sensitivity to environmental parameters, like humidity [1].

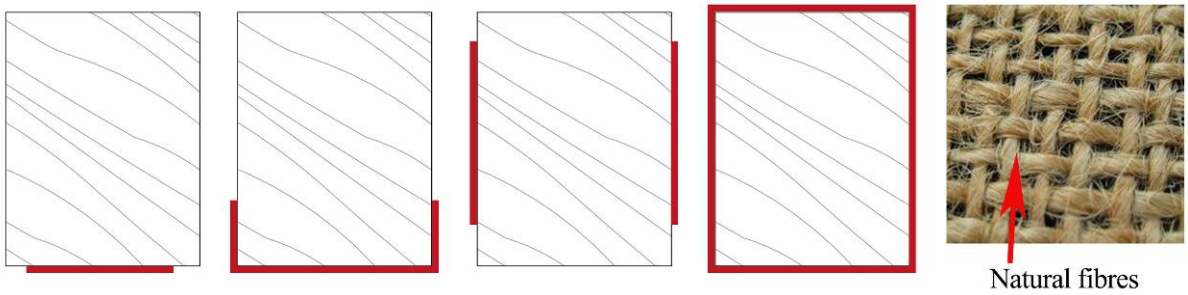

Fig. 4 Position of fibre reinforced polymers on timber elements; natural fibre [26]

1.5 *Nanotechnology*

Nanotechnology is a new approach concerning the consolidation of historic timber structures [27] which got into the attention of researchers stating with the 1990's [28]. It is one of the most promising technologies from both engineering and architectural point of view [29] since it enhances the bearing capacity of the structural elements while not affecting the appearance of the timber structure.

The consolidation method consists of carbon nanotubes immersed in various solvents like ethanol or acetone. The resulted suspension is highly suitable for historic timber elements since the carbon nanotubes will be introduced directly in the wood microstructure [30]. Another used method is introducing the nanotubes in epoxy resin and the applying of this product on the surface of the timber elements. This solution is a rather controversial, taking the mechanical properties difference between the two materials and the load transferring problems of this composite material [29] (Fig. 5).

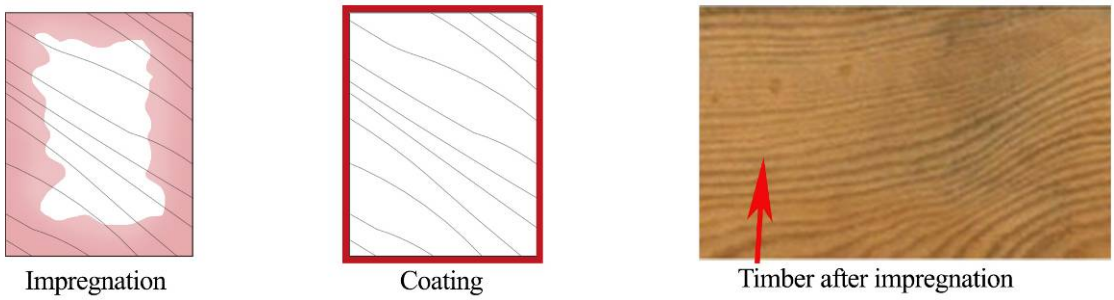

Fig. 5 Position of fibre reinforced polymers on timber elements (Suspension; Coating); Wood fibre after application [27]

2 Consolidation technology synthesis

All the currently used technologies for the consolidation of timber structures were analysed and compared in order to determine which is most suitable for timber heritage structures, enhancing the bearing capacity of the structure while preserving the authenticity of the heritage (Table 1).

Table 1 Analysis of materials used to consolidate historic timber structures

Criteria	Glued in rods	Fiber reinforced polymers	Natural fibres	Nano-technology	Resin
MATERIAL DESCRIPTION					
Used materials	-threaded steel bar -fibres reinforced polymer rod	Glass, Carbon, Aramid	hemp, flax, basalt or bamboo	Carbon nanotubes	Epoxy-Resin
Adhesion material	Epoxy resin	Polymer matrix	Epoxy resin	Solvent/ epoxy resin	
Shape	Bar	Sheet	Sheet	Suspension/Paint	Paste
Typology	Composite	Composite	Composite	Composite	Composite
Material properties	-stiff -high strength -fire resistance	-high strength, -low weight, -corrosion resistant, -electromagnetic neutral	-good mechanical properties -high tensile strength	-high specific resistance - high ductility - permeable to vapour	-high ultimate strength - high strain at failure
Fire resistance	Medium	Low	Low	High	Low
UV resistance	High	Medium (accoring to the chosen resin)	Medium (accoring to the chosen resin)	High	Medium (accoring to the chosen resin)
Humidity resistance	High	High	Medium	High	Hgh
STRUCTURAL IMPROVEMENT					
Recomended used area	Joints	Bottom surface of beams (tension zone)	Bottom surface of beams and rafters (tension zone)	General use	Decayed areas
Structural effect	-decrease of deflection -flexural strengthening	-decrease of deflection -flexural strengthening -crack propagation blockage	-increased bending stiffness -prolonged plastic branch -crack propagation blockage	- significant creep resistance - reduced deformation capacity	- enhancement of local load bearing capacity
STRENGTHS/WEAKNESSES					
Main problem	-occasional insufficient rod anchorage	-expensive	-lower mechanical characteristics -easy influenced by environmental factors	-difference between the mechanical properties of carbon nanotubes and the polymer matrix	-low reversibility
Main advantage	-high aesthtics (invisible intervention)	-no variation of material quality	-ecologic -low price	-very low weight -invisible	- in situ consolidation option

3 Conclusion

In this paper different contemporary consolidation technologies were analysed that are suitable for historic timber structures. While non of the presented consolidation methods are new, all of them are in a continuous evolution in order to be suitable for the special case of historic timber structures: fibres used in reinforced polymers are offering a greater diversity, natural fibres are currently getting in the public attention because of their environmental friendly properties and nanotechnology is stating to be tested on timber in order to identify the effect on the load bearing capacity of the structure.

All this technologies need to be introduced in up-to-date intervention methodologies and in new design codes for heritage buildings with historic value in order enhance their load bearing capacity while preserving their authenticity.

References

[1] André, A. (2006). Fibres for strengthening of timber structures. Luleå University of Technology, Department of Civil and Enviromental Engineering, Division of Structural Engineering, Luleå, Sweden.

[2] Radford, D. W., Van Goethem, D., Gutkowski, R. M., Peterson, M. L. (2002). Composite repair of timber structures. Construction and Building Materials,16(7), pp. 417-425.

[3] Borri, A., Corradi, M. (2011). Strengthening of timber beams with high strength steel cords. Composites Part B: Engineering, 42(6), pp. 1480-1491.

[4] Faggiano, B., Marzo, A., Mazzolani, F. M., Calado, L. M. (2009). Analysis of rectangular‐shaped collar connectors for composite timber‐steel‐concrete floors: Push‐out tests. Journal of Civil Engineering and Management, 15(1), pp. 47-58.

[5] Berindean A. D., Andreica L., Berindean A. C. (2013). Summarized observations upon connections of structural wood members using metallic elements. Journal of Applied Engineering Sciences, 16(1), pp. 13-18.

[6] Prada, M., Tudor, D. (2013). Building rehabilitation course [in Romanian]. Editura Universităţii din Oradea, Oradea, Romania.

[7] Mancia, A., Prada, M., & Ploae, M. (2004). Modern Methods for Rehabilitation and Consolidation of Bricks Buildings. Ovidius University Annals Series: Civil Engineering, 1(6), pp. 187-190.

[8] Cobirzan, N., Dumitras, M., Andreica, L. (2013). Axial deformability of rehabilitated stone masonry walls. Journal of Applied Engineering Sciences, 16(1), pp. 25-30.

[9] Schober, K. U., Harte, A. M., Kliger, R., Jockwer, R., Xu, Q., Chen, J. F. (2015). FRP reinforcement of timber structures. Construction and Building Materials, 97, pp. 106-118.

[10] ICOMOS (1999). Principles for the preservation of historic timber structures. Adopted by ICOMOS at the 12th General Assembly in Mexico, October 1999.

[11] Cruz, H., Yeomans, D., Tsakanika, E., Macchioni, N., Jorissen, A., Touza, M., Mannucci, M., Lourenço, P. B. (2015). Guidelines for on-site assessment of historic timber structures. International Journal of Architectural Heritage, 9(3), pp. 277-289.

[12] Marzo, A. (2006). Methodology for the analysis of complex historical wooden structures. Pollack Periodica, 1(1), pp. 35-52.

[13] Wheeler, A. S., Hutchinson, A. R. (1998). Resin repairs to timber structures. International journal of adhesion and adhesives, 18(1), pp. 1-13.

[14] Cleary, R. (2014). Considering the Use of Epoxies in the Repair of Historic Structural Timber.

[15] Coureau, J. L., Galimard, P., Cointe, A., Lartigau, J., Morel, S. (2016). Resistance-curves and wood variability: Application of glued-in-rod. International Journal of Adhesion and Adhesives, 70, pp. 1-9.

[16] Tlustochowicz, G., Serrano, E., Steiger, R. (2011). State-of-the-art review on timber connections with glued-in steel rods. Materials and structures, 44(5), pp. 997-1020.

[17] Fiorentecnica,. Timber consolidation [in Italian]. Retrieved from http://www.fiorentecnica.it/Betoncinox02.jpg (accessed 01.11.2016).

[18] Harte, A. M., Dietsch, P. (Eds.). (2015). Reinforcement of Timber Structures: A State-of-the-art Report. Shaker Verag, Aachen, Germany.

[19] Plevris, N., Triantafillou, T. C. (1992). FRP-reinforced wood as structural material. Journal of materials in Civil Engineering, 4(3), pp. 300-317

[20] Borri, A., Corradi, M., Grazini, A. (2005). A method for flexural reinforcement of old wood beams with CFRP materials. Composites Part B: Engineering, 36(2), pp. 143-153.

[21] Nowak, T. P., Jasieńko, J., Czepiżak, D. (2013). Experimental tests and numerical analysis of historic bent timber elements reinforced with CFRP strips. Construction and Building Materials, 40, pp. 197-206.
[22] Echavarria, C., Jimenez, L., Ochoa, J. C. (2012). Bamboo-reinforced Glulam beams: An alternative to fiberglass-reinforced glulam beams. Dyna, 79(174), pp. 24-30.
[23] Borri, A., Corradi, M., Speranzini, E. (2013). Reinforcement of wood with natural fibers. Composites Part B: Engineering, 53, pp. 1-8.
[24] Kromer, K. H. (2009). Physical properties of flax fibre for non-textile-use. Research in Agricultural Engineering, 55(2), pp. 52-61.
[25] Lopresto, V., Leone, C., De Iorio, I. (2011). Mechanical characterisation of basalt fibre reinforced plastic. Composites Part B: Engineering, 42(4), pp. 717-723.
[26] Leco. Natural fiber architectural fabric. Retrieved from http://www.archiexpo.com/prod/leco/product-150168-1693595.html (accessed 01.11.2016)
[27] Marzi, T. (2015). Nanostructured materials for protection and reinforcement of timber structures: A review and future challenges. Construction and Building Materials, 97, pp. 119-130.
[28] Fernando, R. H. (2009). Nanocomposite and nanostructured coatings: Recent advancements. Nanotechnology Applications in Coatings, 1008, pp. 2-21.
[29] Bertolini Cestari, C., Invernizzi, S., Marzi, T., & Tulliani, J. M. (2010, June). Nano-technologies/Smart-materials in timber constructions belonging to cultural heritage. In World conference on timber engineering 2010, Proc. of 11th WCTE World Conference on Timber Engineering, Riva del Garda (Italy), pp. 20-24.
[30] Clara, B. C., Invernizzi, S., Marzi, T., & Tulliani, J. M. (2010). Nanotechnologies/ Smart-materials in timber constructions belonging to cultural heritage. World Conference on Timber Engineering, pp. 20-24.

Renovation Solutions for Collective Residential Buildings - Case Study

Măduța C.[1], Brata S.[1], Pescari S.[1], Tănasă C.[1], Stoian V.[1]

[1] *Politehnica University Timisoara, Department of Civil Engineering and Building Services (ROMANIA)*
E-mails: carmen.maduta@student.upt.ro, silviana.brata@upt.ro, simon.pescari@upt.ro, cristina.tanasa@student.upt.ro, valeriu.stoian@upt.ro

Abstract

Building renovation to high energy efficiency standards is a mandatory step in reducing energy consumption and CO_2 emission among residential buildings. The paper presents a study on some proposed solutions for major renovation of a collective residential building located in Timisoara in order to get closer to the nearly zero energy building concept. The solutions effectiveness is presented from three main perspectives: energy efficiency, economic efficiency and positive impact on residents. The proposed solutions successfully manage to combine those three aspects with the advantage of having a high replicability potential.

Keywords: energy efficiency, existing building stock, renovation solutions.

1 Introduction

Being the largest energy consumer in the European Union and having a substantial contribution to greenhouse gas emissions, the building sector is representing the main strategic way for decarbonising Europe. The two main decarbonisation goals proposed for 2050 link two European policies – the energy policy - a 40% to 50% reduction of the buildings energy consumption and – the climate policy - a 90% reduction of greenhouse gas emissions [1] [2] [3]. Achieving these goals is only possible through a joint contribution of each Member State by transposing and implementing the Energy Performance of Buildings and Energy Efficiency Directives into national laws. Besides constructing highly energy efficient new buildings, the EU countries must develop viable and multipliable renovation strategies for the existing buildings [3] [4].

Romania has an important heritage of old buildings, mostly built during 1960 – 1990 and characterized by several shortcomings: low energy performance, thermal discomfort, inadequate architectural aesthetics and very often, poor structural safety. Nationwide, the building sector is responsible for approximately 45% of the total energy consumption. Out of the total residential building stock in urban areas, 72% represents individual housing units located in apartment blocks. The total primary energy consumption of these buildings varies between 150 and 400 kWh/m2/yr [5] [6]. This study is based on the project competition organized by NeZeR "Promotion of smart and integrated NZEB renovation measures in the European renovation market" co-founded by the Intelligent Energy Europe, programme of the European Union, to develop and conceptualize renovation solutions for increasing the energy performance of existing buildings and presents the proposed renovation solutions for an existing residential collective building located in Timisoara, aiming at achieving an energy efficient building [7].

2 Analysed building

2.1 General information

The analysed building (Fig. 1) is a 5 storey collective residential building with an unheated technical basement and a flat roof located in Timisoara, climatic zone II. It was designed and erected during 1968 -1969 based on the legislation at that time; therefore the building has no thermal insulation system. The structure is made of confined masonry walls with RC tie-columns and RC tie-beams and precast concrete slabs. Old wooden framed windows and exterior doors were replaced by residents with PVC framed windows and exterior doors. The apartment block comprises 20 apartments, four on each level, provided with loggias. The existing exterior walls coverings are in poor condition [7].

Fig. 1 Analysed building [7]

The apartment block is connected to the local district heating system through a district heating substation located near the building. The heat transfer medium, namely, the hot water is distributed vertically through columns connected to radiators placed in every heated room. The hot water distribution into the building is made via a network of pipes located in the technical basement, whose thermal insulation is in poor condition. Heat billing is collective for all apartments based on meter readings located in the basement. Domestic hot water and cold water consumption is billed on individual metering [7].

The analysed building was not designed nor equipped with ventilation or cooling system. Out of the total of 20 apartments, 75% were equipped by their residents with split air conditioners [7].

2.2 Geometrical and thermo-technical parameters

2.2.1 Geometrical parameters

The geometrical parameters of the building are listed in Table 1 and Table 2.

Table 1 Envelope elements area [7]

Envelope element	Orientation	Area [m^2]	Total area [m^2]
Exterior walls	N	206.71	813.81
	S	206.71	
	E	199.66	
	V	200.74	
Windows and exterior doors	N	71.34	217.07
	S	71.34	
	E	36.00	
	V	38.39	
Flat roof	Horizontal	311.63	311.63
Floor over unheated basement	Horizontal	307.64	307.64

Table 2 Building geometry parameters [7]

Total envelope area [m^2]	Heated area [m^2]	Heated volume [m^3]	Compactness ratio [m^{-1}]
1 650.15	1 322.17	3 411.20	0.484

2.2.2 Thermal and energetic parameters

Thermal and energetic parameters of the building are listed in Table 3 and Table 4.

Table 3 U- values [7]

Element	U –values [W/m^2K]
Exterior walls	2.165
Windows and exterior doors	2.380
Flat roof	1.020
Floor over unheated basement	2.976

Table 4 Annual energy balance and $C0_2$ emissions before renovation [7]

Energy consumer	Energy consumption [kWh/m^2/year]	Total energy consumption [kWh/m^2/year]	Primary energy consumption [kWh/m^2/year]	$C0_2$ emissions [kg/ m^2/year]
Heating	212.90	290.22	337.92	72.29
Domestic hot water	66.33			
Lighting	10.99			

3 Renovation solution

Major renovation solutions were proposed aimed mainly at reducing the energy consumption of the building. They are described in the following sections, grouped into 2 categories: Solutions targeting the building envelope and solutions targeting the building services. In addition to these, solutions aimed at increasing the well-being and comfort of occupants were also proposed, such as building two new apartments – penthouses- on the 5th floor, creating green areas on the façade and placing an exterior panoramic elevator. The final proposal of the building is shown in figure 2.

Fig. 2 Façades renovation

3.1 Envelope rehabilitation

The proposed renovation solutions described in Table 5 target each envelope element.

Table 5 Envelope rehabilitation solution

Element	Technical renovation solution	Results
Exterior walls	Ventilated façade - 120 mm waterproof glasswool and ceramic tiles as finish coat with green areas insertions using climbing plants on metal gratings;	U-value = 0.298
Flat roof	150 mm polyurethane foam protected with polyurea;	U-value = 0.204
Floor above unheated basement	100 mm polyurethane foam applied by spraying from the bottom up on the underside of the slab and also partially on the basement exterior walls;	U-value = 0.290
Windows and doors	Triple glazing, Low-E, Argon, PVC framed windows and exterior doors equipped with exterior wooden shutters; g = 0.60.	U-value = 0.800

3.2 Equipment modernization

The proposed solutions for building services renovation and modernization target each HVAC component, lightning and domestic hot water system. It is important to mention that when options for the appropriate heating system were analysed, it was decided keeping the current connection to the district heating since the ideal scenario acknowledged by the local heating strategy, in economic terms, is to maintain and renovate the existing district heating system [8]. Nevertheless, for its effectiveness to be high, the whole heating distribution system should be renovated so that the heat loss through it to be insignificant. Also the domestic hot water supply is upheld in the central hot water system.

The proposed technical solutions for all building services are described in table 6.

Table 6 Equipment renovation

Component	Renovation/modernization solution
Heating	Maintaining connection to district heating; Horizontal distribution of heat transfer medium; Resizing the heating system (radiators, pipelines); Thermal insulation of pipes located in the basement; Individual heating consumption metering;
Cooling	Equipping all apartments with individual air condition units;
Ventilation	Equipping all apartments with individual ventilation systems with heat recovery;
Domestic hot water	Maintaining connection to district hot water system; Thermal insulation of pipes located in the basement; Individual hot water consumption metering;
Lightning	Replacing all light bulbs (apartments and common areas) with energy efficient light bulbs;
Renewable energy system	Integrating a PV System on the building's flat roof; 22 PV panels ; Peak power 5.72 kWp; Storage capacity 20.00 kWh; Sized to cover energy demands for apartments + common areas ventilation and lightning; 7195 kWh produced energy from which: 4424 kWh used for ventilation+ lightning, 1280 kWh used for cooling, 1491 kWh delivered to the national electricity grid.

4 Implementation results

4.1 Energy performance

The energy performance of the renovated building was assessed according to Mc001/2007, Romanian methodology for calculating the energy performance of buildings [9]. An important calculation hypothesis is that heat losses through the heating distribution system from central heating and up to the perimeter of our building are not taken into account, because of the difficulty in estimating them.

The ventilation and lighting energy demands are provided by the renewable energy system. Part of the energy excess produced in summer is used for cooling. The lighting energy consumption is including both apartments and common area consumptions. The heating energy consumption result 31.59 kWh/ m^2/year but considering the recovered heat from the exhausted air through the ventilation heat recovery units, the heating energy consumption from fossil fuels could drop up to 10.50 kWh/ m^2/year. The recovered heat (21.09 kWh/ m^2/year) is considered renewable energy for this particular case.

The primary energy conversion factors were considered as specified in methodology, 2.8 for electric energy and 1.1 for natural gas [9]. The energy balance are describe in table 7 and the energy consumption is shown in figure 3.

Table 7 Annual energy balance and $C0_2$ emissions after renovation

Energy consumer	Energy consumption [kWh/m^2/year]		Total energy consumption [kWh/m^2/year]	Primary energy consumption [kWh/m^2/year]	$C0_2$ emissions [kg/ m^2/year]
	Non- renewable energy	Renewable energy			
Heating	10.50	21.09	67.47	83.65	23.00
Cooling	5.54	0.85			
Ventilation	0	1.00			
Domestic hot water	51.44	0			
Lighting	0	2.02			

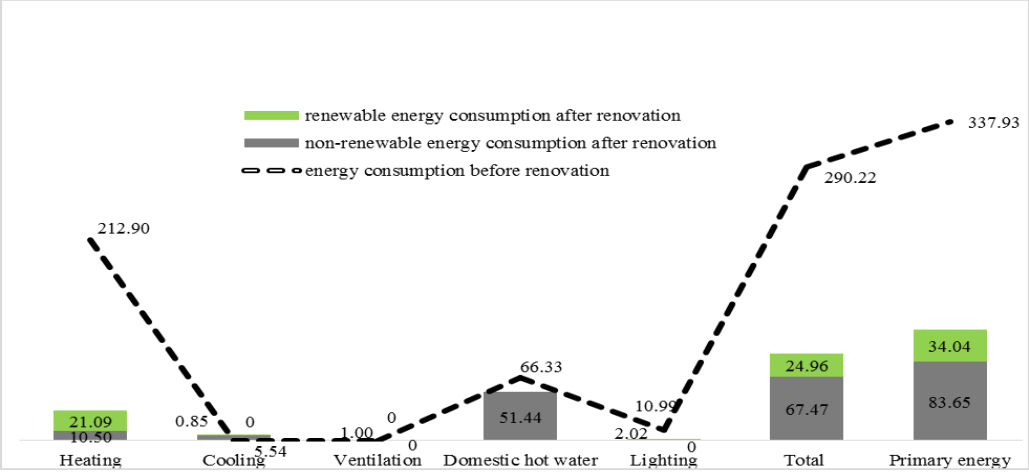

Fig. 3 Energy consumption – comparative chart

4.2 LCC analysis

The life-cycle cost assessment addresses all the potential and relevant costs that occur over the analysis period or life cycle of a building, providing an over overall approach that leads to the choice of the cost-effective solution. The mathematical expression of the life cycle cost applied in this paper is presented in Equation (1):

$$LCC = C_{INV} - \frac{C_{REZ}}{(1+a)^{30}} + \sum_{t=0}^{30} \frac{C^t_{INC} + C^t_M + C^t_E}{(1+a)^t} \quad (1)$$

The life cycle cost components presented in Equation (1) are: C_{INV} is the initial investment, C_{REZ} is the residual value at the end of the analysis period, C_{INC} represent the replacement costs during the period of analysis, C_M is the annual maintenance costs, C_E is the annual cost for energy and a is the real discount rate. For

Romania, according to [10], a rate of 5% in real terms, excluding inflation, is recommended. Also, an escalation rate of 2% is considered or energy prices. A sensitivity analysis will be performed for different values of discount rate of 3%, 5% and 7%. Table 8 presents all the costs considered in the life cycle cost assessment for the three analysed situations.

Table 8 Costs considered in the comparative life-cycle cost analysis

Measure	C_{INV} [€]	C_E [€]	C_M [€]	C_{INC} [€]	C_{REZ} [€]
No renovation measure	0	24 263.10	8 970	0	0
Traditional renovation	67 184	12 708.50	8 970	0	16 890
High energy efficiency renovation	274 477	6 430.06	941	37 600	54 567

Figure 4 presents the graphs with the evolution of the total annual cost for the three building variants during the analysis period of 30 years.

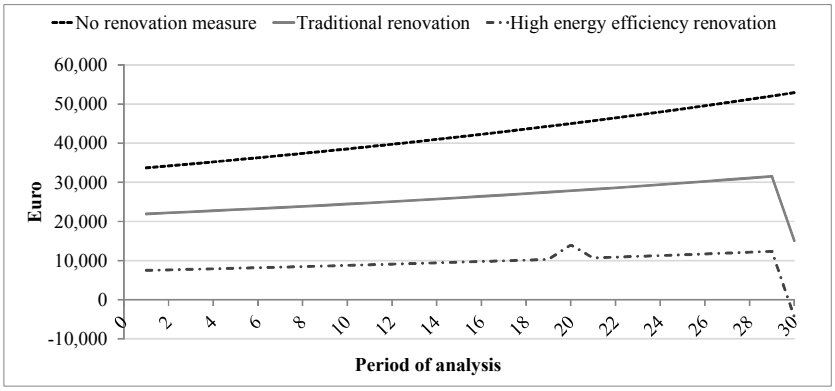

Fig. 4 Annual costs evolution for the period of analysis

Figure 5 presents the results of the sensitivity analysis related to the variation of the discount rate. Due to much lower annual costs, the global cost of the high energy efficiency building renovation solution is less affected by the change of the discount rate compared to the other two variants.

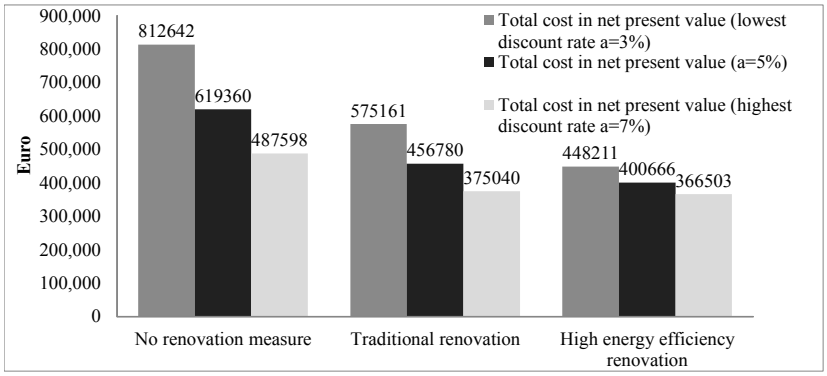

Fig. 5 LCC sensitivity analysis

In the situation of high energy consumption of an old building and forecasts of continuous increase of energy prices, investing in a major renovation using high standards off energy efficiency, proves to have a positive economic impact in the long term, despite additional initial investment. The results of this study show that the sustainable design of buildings (through energy efficiency and renewable energy) is in close touch with saving money in a long-term approach.

4.3 User aspects

Through their high energy efficiency, the proposed solutions have a valuable impact on the residents which are presented in table 9.

Table 9 Impact on residents

Measure	Impact on residents
Envelope thermal rehabilitation	Reducing the risk of condensation, therefore reducing the risk of mould growth; Reducing the risk of low temperatures on the inner surfaces of envelope elements; Avoiding the risk of overheating in summer time; Improving air quality by integrating green areas on the façade;
Building services renovation/ modernization	Improving air quality through controlled ventilation; Possibility of cooling down the living space when required; Lowering the maintenance costs through individual energy consumption metering; Lowering the maintenance costs by integrating renewable energy system.

5 Conclusions

The proposed renovation solutions demonstrate a high efficiency, both in energy and financial terms. At the same time, they have a significant impact in increasing the indoor comfort as well as in the enhancement of the architectural appearance. Specific interventions needed to implement these solutions are not invasive and the technologies and materials required are reachable, so that the solutions could be widely implemented. A shortcoming of the presented case study would be the small amount of renewable energy usage, whereas for a building to be a nearly zero energy buildings, at least 10% of total energy consumption should be provided from renewable energy sources, but the costs for implementing local renewable energy sources are still a financial impediment. National authorities should take measures to make investments in renewable energy technologies more attractive and financially safe. At the same time, policies that enhance the development of energy efficiency of buildings and market uptake of high performance equipment should be a strategic way to promote energy efficient buildings in Romania.

Acknowledgement

This work was supported by a grant of the Romanian National Authority for Scientific Research, CNDI–UEFISCDI; project number PN-II-PT-PCCA-2011-3.2-1214-Contract 74/2012.

References

[1] European Commission (2012). Energy-efficient buildings PPP beyond 2013 - Research and Innovation Roadmap. Document for E2B European Initiative (ECTP), pp. 9-11.
[2] Ramirez-Villegas, R ; Eriksson, O; Olofsson, T. (2016). Assessment of renovation measures for a dwelling area - Impacts on energy efficiency and building certification. Building and Environment, Vol. 97, pp. 26-33.
[3] Pombo, O; Allacker, K; Rivela, B; Neila, J. (2016). Sustainability assessment of energy saving measures: A multi-criteria approach for residential buildings retrofitting-A case study of the Spanish housing stock. Energy and Buildings. Vol. 116, pp. 384-394.
[4] Ferreira, M; Almeida, M; Rodrigues, A. (2015) Improving Buildings Energy Performance - Comparison Between Simple Payback Period And Life Cycle Costs Analysis, Proceedings of Proceedings Of The 2nd International Conference On Energy & Environment: Bringing Together Engineering And Economics, pp.249-256.
[5] Pescari, S; Stoian, V; Tudor, D; Măduța, C. (2015). Energy demands of the existing collective buildings with bearing structure of large precast concrete panels from Timisoara, Journal of Applied Engineering Sciences (JAES), volume 5(18), pp. 75-81.
[6] Ministry of Regional Development and Public Administration, MDRAP (2014), Nearly Zero Energy Buildings (NZEB) Romania, pp. 4-5.
[7] http://www.nezer-project.eu/.
[8] Primaria Municipiului Timisoara, Feasibility study on upgrading the district heating system in Timisoara in order to comply with environmental standards on air emissions and energy efficiency in urban heat supply, www.primariatm.ro.
[9] Mc001-2006, Methodology calculation on energy performance of buildings.
[10] European Commission, Guide to Cost-Benefit Analysis of investment projects.

Advanced Calculation Models in Thermo-Mechanical Analysis

Marginean I.[1], Both I.[1], Dogariu A.[1], Zaharia R.[1]

[1] *Politehnica University Timisoara, Department of Steel Structures and Structural Mechanics (ROMANIA)*
E-mails: ioan.marginean@upt.ro, ioan.both@upt.ro, adrian.dogariu@upt.ro, raul.zaharia@upt.ro

Abstract

The analysis of structures in fire situations is a complex task due to the degradation of the mechanical properties of materials at elevated temperatures and geometrical non-linear effects. Advanced calculation models may be used for the analysis of structures in fire situation. While dedicated software for fire analysis have the necessary setup required for a thermo-mechanical analysis, the general purpose software demands preliminary input and acknowledgment of the entire analysis process. The paper discusses the input parameters for a numerical thermo-mechanical analysis. Theoretical considerations for material properties are presented from the numerical analysis approach and simple examples of structural elements are given to evaluate the input and output for linear elements, shell elements and 3D solid elements in the general purpose software Abaqus.

Keywords: fire design, advanced calculation models, material properties.

Introduction

In the past, the fire resistance of structural elements was determined only by experimental tests. The Eurocodes for fire design [1], [2], [3], [4] allow nowadays the use of either the simple calculation models or the advanced calculation models using computer codes.

Dedicated software, e.g. Safir [5] or Vulcan [6], are commonly used to evaluate the response of structures subjected to elevated temperatures. General purpose software e.g. Abaqus [7] or Ansys [8], also represent an option for a numerical thermo-mechanical analysis. However, these computer codes require a preliminary setup of the working environment through parameters and measurement units.

According to the Eurocodes for fire design, the advanced calculation methods should include a thermal response model for the temperature distribution within structural members and a mechanical response model for the internal forces and displacements of a structure or any part of it.

In order to provide realistic response of structures through advanced models, it is necessary to ensure the validation of these models against relevant test results, according to Section 4.3 of EN 1993-1-2, [3]. The validity of results should be checked for temperature, deformations and fire resistance times.

Several validation models are found in the literature using either general-purpose or dedicated software [9], [10], [11]. Also, a suite of validation examples under the form of benchmark, were collected in Wald et al. [12]. Nevertheless, the verification examples represent a solid support for the numerical analysis of structures subjected to elevated temperatures.

The paper presents a review of the thermo-mechanical analysis in the general purpose software Abaqus. The considerations required for a thermo-mechanical analysis are presented for one-dimensional, two-dimensional and three-dimensional elements. A case study presents the differences between the three approaches.

1 General purpose software

While dedicated software for structural fire analysis has the specific setup for a thermo-mechanical analysis, the general purpose computer codes require the proper definition of the settings of such analysis. In the following, the particular aspects required to perform a thermo-mechanical analysis in the general purpose software Abaqus [7] for one, two and three- diomensional elements are presented. The two options, sequentially coupled thermal-stress analysis and fully coupled thermal stress analysis are presented for shell elements and solid elements, respectively.

1.1 Input

Choosing between Kelvin and Celsius degree scales must be performed in the *Model Attributes* by defining the *Absolute Zero Temperature*. For Celsius degrees the value must be set to -273.15. If radiation heat transfer is considered, the Stefan-Boltzmann constant must be defined as 5.67E-008 [W/m^{2}K^4] for the measurement units kg, N, m, s, ^{o}C. Also all the material properties should consider this unit system for a consistent analysis.

1.1.1 One-dimensional elements

The beam elements defined as wire shaped elements represent a quick solution to determine the capacity of an element subjected to fire. Cross-section shape and material mechanical characteristics must be defined and Abaqus option range from simple shape cross-sections to generalized shape cross-section.

Usually, the analysis is performed in two steps. The mechanical load is defined in the first step and propagated in the second one, and the second step is dedicated to temperature development within the cross-section. For the case of linear elements, both steps are *Static, General*. The time period of the second step should be defined in accordance to the thermal action duration. Regarding the incrementation, a higher number of increments must be defined in order to reach the analysis final stage, since, for instance for unprotected steel elements, the maximum increment size must be limited to 5s according to Section 4.2.5 in EN 1993-1-2 [3]. The temperature increase, correlated to the degradation of mechanical properties, leads, eventually, to the collapse of the element. Also, in order to have a consistent definition of the expansion coefficient variation, a separate *Predefined Field* must be defined for the initial temperature of the structure.

The distinct part of the numerical analysis is the definition of the temperature of the beam elements. For steel elements under standard ISO fire, function of the section factor, the values should be computed using relation 4.25 from EN 1993-1-2. The obtained results are then defined in the second step of the analysis in a tabular form of a *Predefined field*.

The *Beam* family B3 is suitable for such a numerical analysis. For the heat transfer analysis, the finite element must be of *Heat transfer* type, linear DC2D4 or quadratic DC2D8.

1.1.2 Two-dimensional elements

Structural elements, like steel profiles, can be defined using shell elements, due to the slenderness of the cross-section walls. The common practice is to sketch the cross-section shape and extrude the cross-section to the length of the element providing the continuity of the cross-section for the effect of conductivity. If the structural element is constructed by joining several shell elements additional consideration must be defined to consider conductivity between the web and the flange.

The sequentially coupled thermal-stress analysis is presented in the following. The numerical analysis is performed using two separate models, one for the temperature computation and one for the structural response. In the first model the temperatures in the cross-section are determined by defining a *Heat transfer* step while the second model analyses the structural response. Within the first model the convection and radiation are defined according to the following specifications.

The definition of convection heat transfer starts in the *Interactions* module with the *Surface Film Condition*. For the convection heat transfer, the required data are the *Film Coefficient*, *Sink temperature* and *Sink amplitude*. The *Sink amplitude* defines in a tabular form the environmental temperature increase which may be the Standard ISO fire [1]. The thermal actions are obtained by multiplying the sink amplitude with the *sink temperature,* defined as unit. The *Film coefficient* is defined function of the thermal action, for the Standard ISO fire, it is considered to be 25 [W/m^{2}K].

The radiation heat transfer is defined also in the *Interaction* module as *Surface radiation*. The required quantities are the *Emissivity*, the *Ambient temperature* and the *Ambient Temperature Amplitude.* As recommended in the fire design codes the *emissivity* is considered to be 0.7 (for both steel and concrete elements), while the *Ambient Temperature* and *Ambient temperature amplitude* regards the same considerations as for the convection heat transfer. Both heat transfers must be defined on the surfaces exposed to the thermal action, Fig. 1. Of course, the temperature dependent thermal properties i.e. specific heat and conductivity must be defined in accordance with the material type.

If the initial temperature of the element is different from 0^{o}C, it must be defined in the *Initial* step as a predefined field as *Constant through region* variation and the corresponding magnitude. Also, since the temperature increase is time dependent, the step *Time period* must be defined function of the thermal action duration.

As in the case of one-dimensional element, the second model, which analyses the structural response, requires two analysis steps. In the first step, the mechanical load is applied and in the second step the temperature increase is attributed to the finite elements by a temperature *Predefined field*. The definition of temperature is considered *From results or output database file* obtained from the analysis of the first model.

Regarding the analysis steps, the first step, *Static, General,* is independent of time, while the second step, also *Static, General*, must be defined function of the thermal action duration, similar to the *Heat transfer* step in the first model. In order to have the same spatial position of the finite elements in both models, the second model is usually copied and the particular structural considerations e.g. boundary conditions, finite element type, are attributed.

The finite elements are different for each of the presented models. The heat transfer analysis requires a finite element from the DS finite element family, since it incorporates the temperature degree of freedom, usually known in Abaqus as 11 DOF. The second model requires the definition of structural finite elements from the S finite element family e.g. S4, S4R, S8R.

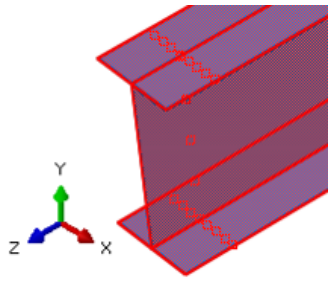

Fig. 1 Thermal action on a shell element

1.1.3 Three-dimensional elements

For complete observations of the element response when subjected to elevated temperatures, 3D finite elements are most recommended. One of the advantages of 3D structural models is that one can define a more refined model by using areas with homogeneous cross-section, Fig. 2a, or with composite cross-section, Fig. 2b, considering more than one material models. The fully coupled thermo-mechanical stress analysis may be defined in a single model as presented in the following.

The model is based on similar principles as the sequentially coupled thermal-stress analysis. A first difference regards the *Step* definition. While the first step remains *Static, General*, the second step must be of *Coupled temp-displacement* type. Within the second step the convection and radiation heat transfers are defined on the exposed faces of the structural element (Fig. 2a), as presented in the heat transfer model of the two-dimensional elements. Since the heat transfer is time dependent, the *coupled temp-displacement* step must be defined with a time period corresponding to the thermal action duration.

Differences arise also for the finite element selection. They must be from the same *Coupled Temperature Displacement* family but are linear 8-node or quadratic 20-node thermally coupled brick, considering both displacement and temperature DOF e.g. C3D8(R)T or C3D20(R)T.

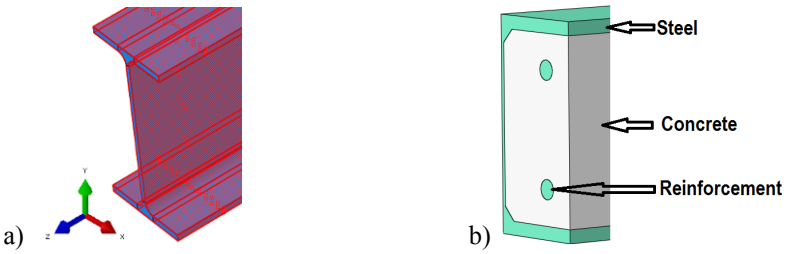

Fig. 2 a) Thermal action on a 3D solid element b) Composite cross-section

1.2 Output

General purpose software offer a wide range of output variables in terms of temperature and deformation, while the resistance times are associated with the failure of elements at the end of an analysis.

Regarding the temperature variables, Abaqus offers the results as nodal temperature NT or temperature in elements TEMP. For all the finite elements, the common variable is NT, but it needs to be mentioned that in the case of gradient definition of temperature, the nodal temperatures for a given section point can be obtained only by using the variable TEMP [7].

The deformations of structural elements are obtained in tabular form for the requested displacements of the nodes (U, UT, UR) but Abaqus offers the deformed shape in a suggestive graphical form when using the symbol filed output variable.

2 Case study

The exemplification of the principles presented above is performed for a simply supported IPE300 steel beam with a span of 6.0 m. The beam is considered fixed in the vertical plane. The material properties are defined according to EN 1993-1-2 [3]. The equivalent mechanical load is considered to be 5kN/m while the thermal action is considered to be the standard ISO 834 fire acting on all sides of the profile.

Fig. 3 - Fig. 5 present the deflection of the beam (a) and the temperature distribution on the cross-section (b) for the one, two and three dimensional finite elements at the same analysis time of 20 min.

For a B31 finite element, the analysis terminated at 23 min, corresponding to a cross-sectional temperature of 760 °C.

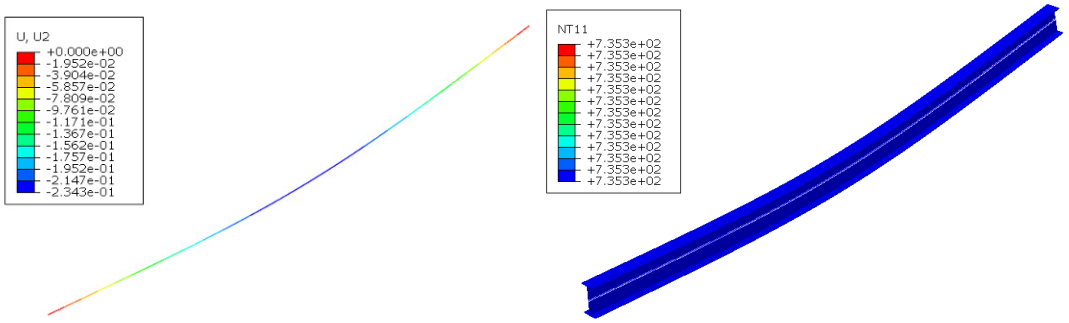

a) b)

Fig. 3 Beam elements a) vertical displacement b) nodal temperature (rendered visualization)

The two-dimensional S4R finite element used for the shell elements lead to an analysis time up to 25 min and temperatures in the cross-section of 793 °C and 759 °C in the web and the flange, respectively.

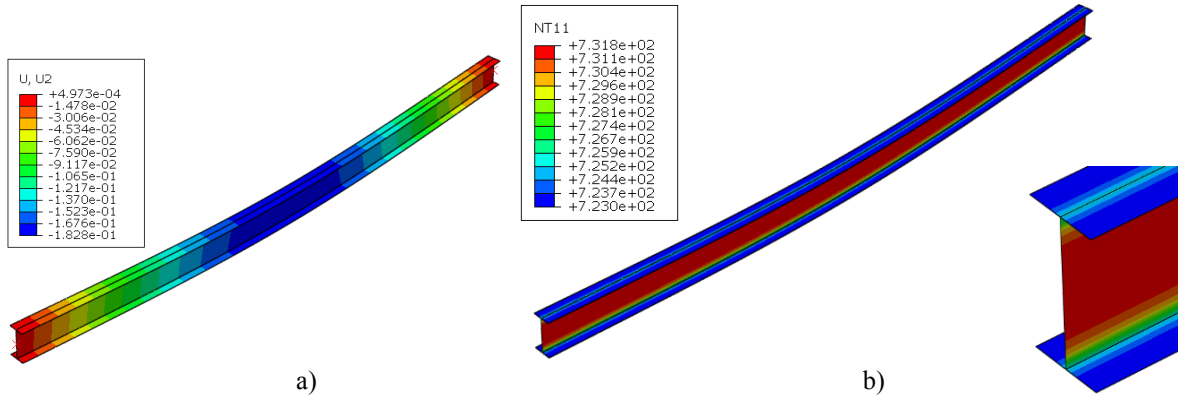

a) b)

Fig. 4 Shell elements a) vertical displacement b) nodal temperature

The analysis of the solid elements, performed using C3D8T finite elements, ended at 26 min with extreme temperatures of 805 °C and 767 °C in the web and flange, respectively.

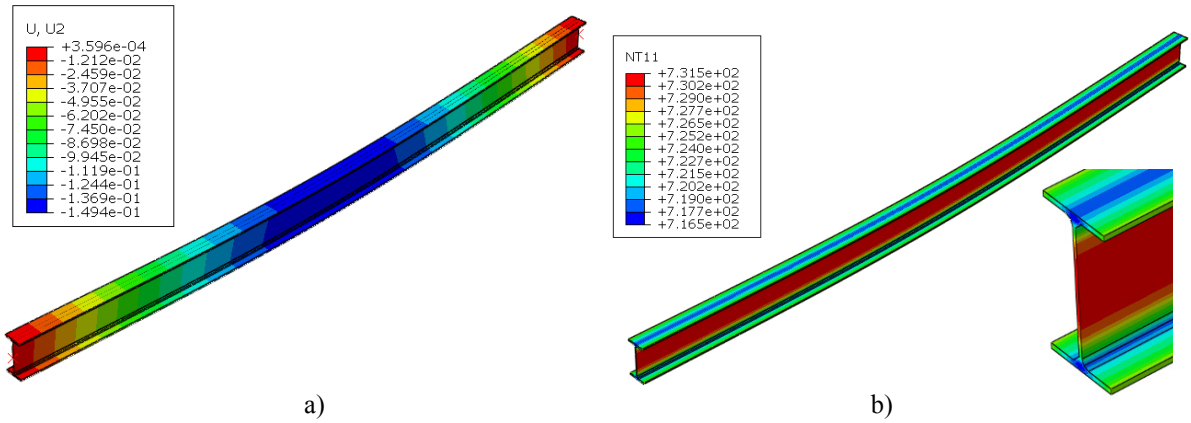

a) b)

Fig. 5 Solid elements a) vertical displacement b) nodal temperature

The temperature mentioned for the flange for the 2D and 3D elements are taken at the mid-distance of the outstand flanges for the last increment of the analysis.

Fig. 6 presents the vertical midspan deflection in time. In Fig. 7 are depicted the standard ISO fire, the temperature development in the beam, the flange of the two-dimensional element and the flange of the three dimensional elements.

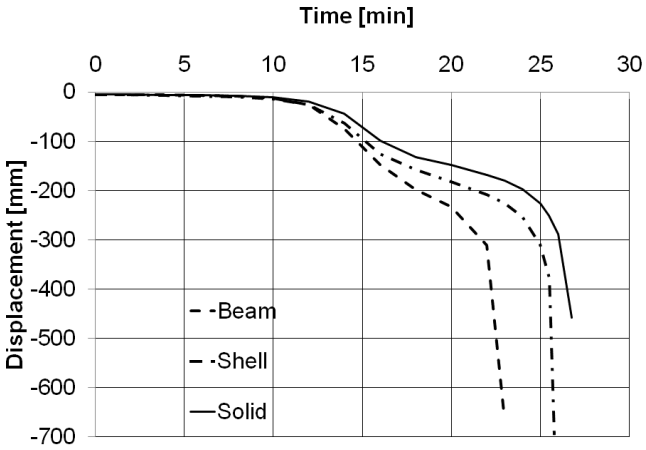

Fig. 6 Midspan vertical displacement

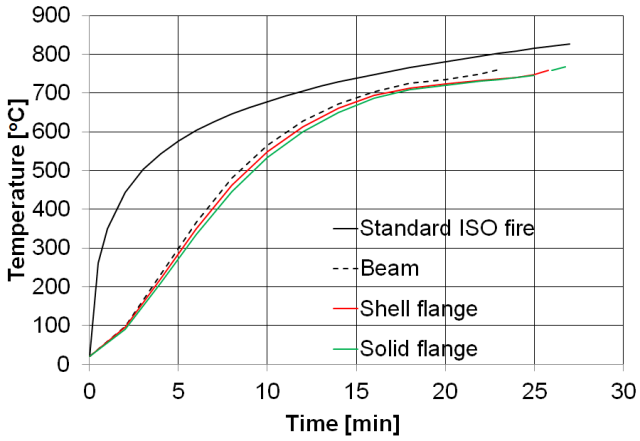

Fig. 7 Nodal temperature

Similar deflection patterns are exhibited by all three finite elements. The difference is observed for the failure time which ranges from 23 min to 26 min. The cause of different failure times is assigned to the temperature distribution over the cross-section. While the temperature for the one-dimensional elements has the same value in the flange and in the web, the two and three-dimensional elements exhibit lower temperatures in the flange, see Fig. 7. The increased fire resistance of the solid elements in comparison to the two-dimensional elements is determined by the fact that the web-to-flange junction in 3D elements is replicated according to the real steel profile. This leads to more bearing capacity and also affects the temperature distribution. In the detail of Fig. 4b it is observed that in case of shell elements the web-to-flange junction has a higher temperature caused by the conductive heat transfer from the more heated web to the flange. In the detail of Fig. 5b, it is observed that in case of solid elements, the coldest part of the cross-section is the web-to-flange junction caused by the massivity of this area, which represents a realistic response.

3 Conclusions

The advanced calculation models are a useful tool in determining the response of structures and structural elements to elevated temperatures. Function of the chosen dimensional element, the output results may be different. Linear elements are not able to be analysed with the corresponding temperature distribution over the cross-section, and therefore, by imposing the highest temperature, the results are conservative. For the shell and solid models, the analysis considers the real temperature distribution over the cross-section and thus the behaviour of the beam is more realistic.

References

[1] C.E.N. (2002). EN 1991-1-2, Eurocode 1: Actions on structures - Part 1-2: General actions - Actions on structures exposed to fire. Brussels.
[2] C.E.N. (2004). EN 1992-1-2, Eurocode 2: Design of concrete structures - Part 1-2: General rules - Structural fire design. Brussels.
[3] C.E.N. (2005). EN 1993-1-2, Eurocode 3: Design of steel structures - Part 1-2: General rules - Structural fire design. Brussels.
[4] C.E.N (2004). EN 1994-1-2, Eurocode 4 - Design of composite steel and concrete structures - Part 1-2: General rules - Structural fire design. Brussels.
[5] Franssen, J-M. (2005). Safir- A thermal/structural program modelling structures under fire. *Engineering Journal* 42(3), pp. 143-158.
[6] Vulcan (2014). http://www.vulcan-solutions.com.
[7] ABAQUS (2011). ABAQUS Documentation 6.11. Providence, RI, USA: Dassault Systèmes.
[8] ANSYS (2008). Ansys Inc. www.ansys.com.
[9] Gillie, M. (2009). Analysis of heated structures: Nature and modelling benchmarks. Fire Safety Journal 44(5), pp. 673-680.
[10] Franssen, J.M., Cooke, G.M.E, Latham D.J. (1995). Numerical simulation of a full scale fire test on a loaded steel framework. Journal of Constructional Steel Research 35(3), pp. 377-408.
[11] Zhao, B., Roosefid, M. (2010). Experimental and numerical investigations of steel and concrete composite floors subjected to ISO fire Condition. Structures in fire (Proceedings of the Sixth International Conference). East Lansing: Destech Publications Inc, pp. 407-416.
[12] Wald, F et al., Eds. (2014). Benchmark studies-Verification of numerical models in fire engineering. Prague: CTU Publishing House.

Assessment of Passive Seismic Protection of Steel Structures

Mathe A.[1], Moldovan I.[2], Catarig A.[3], Chira N.[4]

[1, 2, 3, 4] *Technical University of Cluj-Napoca, Faculty of Civil Engineering, 15 Constantin Daicoviciu Street (ROMANIA)*
E-mails: aliz.mathe@mecon.utcluj.ro, ilinca.lungu@mecon.utcluj.ro, alex.catarig@mecon.utcluj.ro

Abstract

The proposed study presents a simple approach in evaluating the degree of seismic response reduction of steel skeletal type structures equipped with passive seismic protection. The decrease in seismic protection is expressed in terms of reduction in the amplitudes of kinematical parameters associated to seismically induced oscillatory motion of the analyzed structures. This proposed procedure is applicable to other seismic response parameters associated to static and kinematical states of earthquake acted upon steel structures. Assessing parameter for reduction in seismic response via passive seismic protection is associated to the mitigation interval of steel skeletal structures equipped with linear viscous dampers. During this time interval, the picture of vibratory motion is expressed by the length of the interval, the number of vibratory cycles, the amplitudes and their decrease in time and the beginning of the steady state motion. The proposed parameter to assess the effectiveness of seismic passive protection is – in its turn - time variable and synthesizes all the features of the transitory motion. The length of this interval is expressed in number of natural predominant periods of vibrations and its descending tendency expresses the efficiency of seismic protection. Time history type analyses have been carried out on several sets of skeletal steel structures. The structures are analyzed in two situations: without seismic protection (reference structure) and equipped with passive seismic protection. The numerical results of time history analyses are presented and discussed in the terms of the proposed parameter assessing seismic mitigation. The time variation of the proposed parameter is presented graphically for a better and immediate "physical" perception. The effectiveness of the seismic passive protection is discussed in terms of proposed parameter.

Keywords: steel skeletal structures, viscous dampers, time history analysis, mitigation assessment.

1. Introduction

The objective of seismic protection of structures means a reduced seismic response to an input earthquake associated to the location area. Reduction of seismic response may be expressed in various static and kinematical parameters. Structural design based on code provided earthquake loading and the computed seismic response is, usually, expressed in code provided static and kinematical behaviour parameters. Nevertheless, the efficiency of seismic protection is more relevant when it is presented in terms of reduction in the peak values of induced kinematical parameters, mainly in terms of lateral top displacements, as it is the case of a multi-storey structure. Indeed, a dramatic reduction in the top lateral displacements of a skeletal structure induced by a strong earthquake is a symbol of any seismic protection system. Earthquake induced kinematical parameters associated to top structural levels are both, very popular in being connected to seismic protection and, also, very versatile in presenting the level of seismic protectiveness in a comparative manner [1], Chopra [2], Soong [3]. It is important to point out that a passive seismic protection via viscous dampers will result in visible change – ussually decrease - in lateral displacements. From the point of view of seismically induced kinematical parameters (displacements, velocities, accelerations), seismic behaviour of frame type steel structures exhibits three distinct intervals: a first, starting ascending interval during which the seismic induced kinematics increase (in their alternative (positive and negative) values, this interval is associated to rapidly increasing values of lateral displacements directly related to the mechanical inertia of the structure. A second interval is associated to the large values of input accelerogram. During this time interval the structure develops large oscillatory values of its static and kinematical states. The large values of displacements and stresses induce in their turn, damages in skeletal structures: cracks, formation of plastic zones, yielding in tensioned steel, buckling of compressed members, etc. A third, final interval may be related with a reduction in acceleration values down to their complete diminishing. The structure is either saved by dramatic decreases in the values of its static and kinematical states, or collapses.

A seismic efficient protection is achieved if it operates during the second interval by reducing both, its lengths and values of corresponding parameters (displacements, velocities, accelerations). An efficient seismic protection system, fully operating in this interval, will save the structural damages by avoiding the shakedown type behaviour and starting a progressive descending behaviour [7]. The more rapidly is the mitigation interval initiated and the steeper is its form, the more seismically efficient is the protection system. The present contribution focuses on the versatility of the envelop curves that collect the peak values of kinematical parameters to express the efficiency of seismic protection.

The present study deals with computing, assessing and comparing the efficiency of passive seismic protection via viscous elastic dampers from the point of view of this mitigation interval via seismic protection efficiency curves. The study has been conducted on a large set of steel skeletal structures designed for office buildings located in an area of Romania known for its high seismic potential. Out of a larger set of studied structures, a six story five bay frame has been selected and associated to below presented numerical results. The structure is acted upon by Vrancea 1977 Romania recorded earthquake accelerogram (a reference accelerogram) and, also, by a sinusoidal accelerogram. The later has been used in order to prevent mitigation effect associated to the decrease in the values of a natural accelerogram. Both, the Vrancea and the sinusoidal accelerograms are applied on the structure acted upon by dead and live loadings (design code combination) associated to office building serviceability.

A reference seismically unprotected frame and three alternatives (of viscous damping levels) of seismic protection are analysed. The seismic protection consists of nine viscous dampers, placed in the central bay along the entire height of the structure. The three alternatives of seismic protection are approximately equivalent to a general inherent damping level of 10%, 15% and 20% respectively. Performed analyses are of time-history type.

Computed parameters are lateral top displacements with a special focus on the form (length and reduction in values) of the mitigation interval. The graphical representation of the mitigation effect – through seismic protection efficiency curves of seismic protection has been considered more approachable for those interested [8]. A special issue related to the mitigation interval is the amount of reduction in (usually) peak values of computed kinematical parameter. Also, a question arises: when and in what conditions may an oscillatory motion, that is undeniable transitory (due to the transitory feature of the earthquake), may be considered a steady state motion? This question is responsible for introducing - in the present study - a sinusoidal type accelerogram.

By exhibiting an indefinite steady state characteristic, a sinusoidal accelerogram can be associated to a real steady state motion induced into the analysed structure. Under a sinusoidal type action, the mitigation interval and the steady state motion can be clearly defined. A real seismic accelerogram will, only, display a pseudo steady state motion.

2. Analyzed structures

The general and sectional geometry of both, reference (unequipped) frame see Fig. 1 and equipped frames e.g. see Fig. 2 are the same. The cross sections of columns and beams of the reference frame (Fig. 1) have been computed from a loading combination that includes seismic action according to current Romanian design provisions for steel structures. A general stress state of approximately 75% of full (bending) capacity of the frame members is reached and associated to the elements cross sections [9]. The sections of elements, also, observe design provisions with reference to local stability and deformation state. A deep study, of the influence of dampers location in the frame, lead to the present placement: in the central bay along the entire height of the structure (Fig. 2).

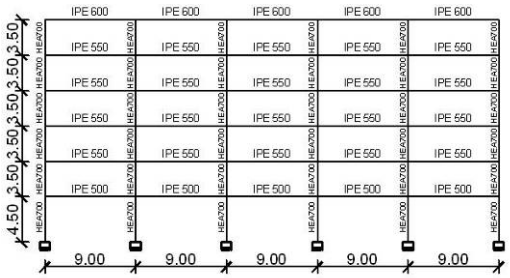

Fig. 1 Reference frame

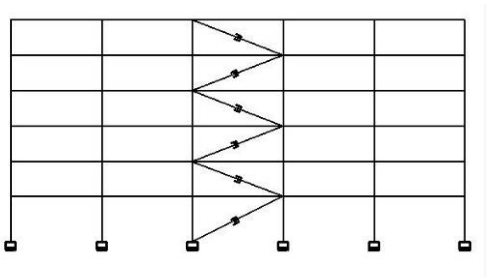

Fig. 2 Frame with viscous dampers

The intensity of sinusoidal accelerogram (Fig. 4) has been fixed at 0.2g, corresponding to the maximum value of recorded Vrancea N-S accelerogram (Fig. 3). Vrancea 1977 earthquake exhibited a 7.2 magnitude on

Richter scale while the maximum predicted magnitude is 7.5 and lasted 50 seconds approximately. By its destructions and casualties, Vrancea 1977 earthquake is considered a reference earthquake in Romania.

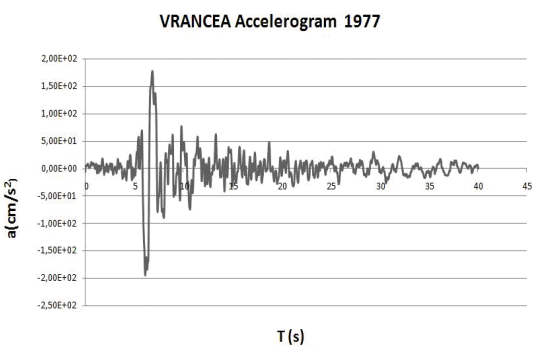

Fig. 3 Vrancea 1977 accelerogram

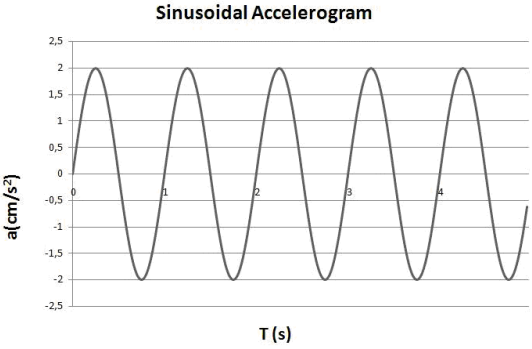

Fig. 4 Sinusoidal accelerogram

Regarding the aspect about global level of damping induced into the structure via viscous dampers, it has been dealt with by using seismic response displacement code spectra for several levels of damping [4]. Induced level of damping has been equated to the damping level of code displacement spectra when producing the same displacements. In this way, a natural (inherent) level of 5% and three artificially induced levels (via viscous dampers) of damping of approximately 10%, 15% and 20% respectively have been taken into account in the performed analyses.

The dampers are of nonlinear viscous type: the damping force is given as $F_a=c*v^{0.15}$ [5]. Here, c is an adaptable damping coefficient (and its values have been computed for each global damping level) and v is velocity of motion and it is implicitly computed.

3. Numerical results

As it has been mentioned, the focus of this contribution is especially on the mitigation interval of lateral top displacements graphically expressed by seismic protection efficiency curves [10]. In the case of recorded Vrancea 1977 accelerogram, as well as in the case of the sinusoidal type accelerogram, the displacements versus time presented diagrams have been extracted from the entire diagram (associated to the real duration of earthquake, approximately 55 seconds), such that "extracted segments" comprise the mitigation intervals. The computed numerical results associated to the three cases of supplemental damping are presented versus the homologous results related to the reference structure.

With the aim of exhibiting the efficiency of seismic protection via viscous dampers and the global level of damping, the seismic protection efficiency curves have been computed as an envelope of peak (positive and negative) values of displacement versus time diagrams. Indeed, the steepness of these envelope curves expresses both, the length (in time) of the mitigation interval and the amount of reduction in the peak values of the kinematical parameters (displacements, in this case).

The steady state motion is considered when the reduction in the displacements values reaches approximately 70% of their maximum values [11]. Presented numerical results refer to displacements variation with time of top lateral displacement in the case of Vrancea earthquake (Fig. 3) for the reference frame and three levels of supplemental damping: 10% (Fig. 5), reference frame and 15% supplemental damping (Fig. 6) and reference frame and 20% supplemental damping (Fig. 7). In the case of sinusoidal accelerogram, similar results are presented: reference frame and 10% supplemental damping (Fig. 8) reference frame and 15% supplemental damping (Fig. 9) and reference frame and 20% supplemental damping (Fig. 10), respectively. Corresponding seismic mitigation curves for above study cases are presented in Fig. 11, Fig. 12 and Fig. 13 – for Vrancea 1977 earthquake and in Fig. 14, Fig. 15 and Fig. 16, respectively – for sinusoidal type excitation.

To exhibit the amount of reduction in the peak values of displacements, the time (horizontal) axis is, also, scaled in terms of fundamental natural period T_1 of analyzed structure. Expressing the seismic mitigation interval in terms of (fundamental) natural period of the structure allows for emphasise of the efficiency of seismic protection (level of supplemental damping) [12]. The proposed seismic protection efficiency curves underline – by their slope - the duration and rapidity of the seismic mitigation in terms of the natural fundamental periods of vibration of analysed structure.

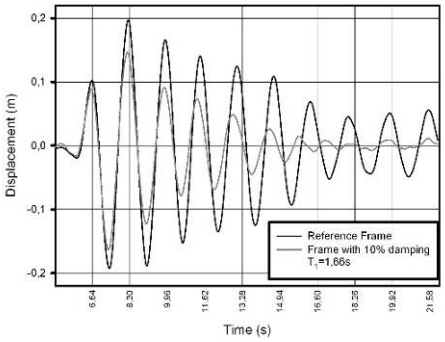

Fig. 5 Displacements - reference frame versus frame with 10% damping (VRANCEA)

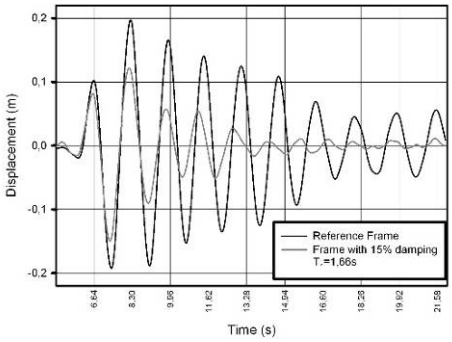

Fig 6 Displacements - reference frame versus frame with 15% damping (VRANCEA)

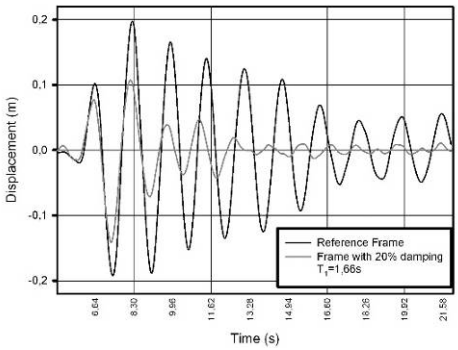

Fig. 7 Displacements - reference frame versus frame with 20% damping (VRANCEA)

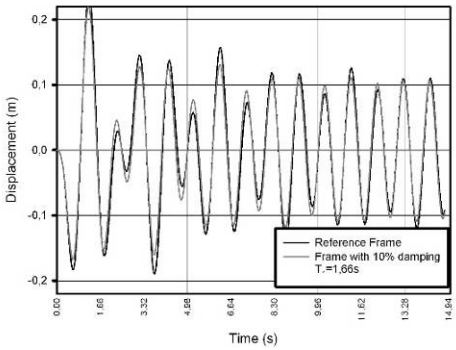

Fig. 8 Displacements - reference frame versus frame with 10% damping (Sinusoidal)

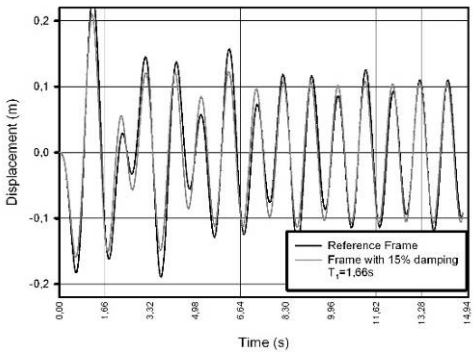

Fig. 9 Displacements - reference frame versus frame with 15% damping (Sinusoidal)

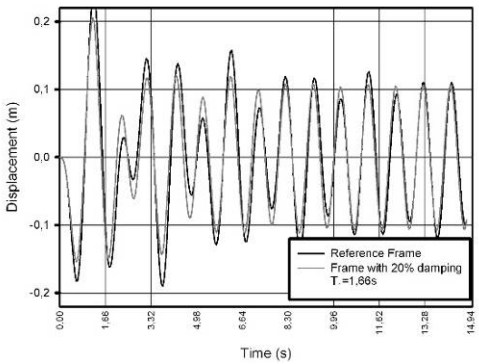

Fig. 10 Displacements - reference frame versus frame with 20% damping (Sinusoidal)

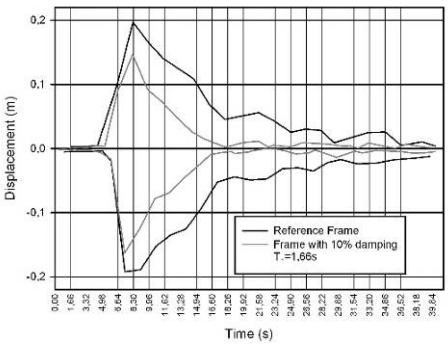

Fig. 11 Displacement mitigation curves – reference frame versus frame with 10% damping (VRANCEA)

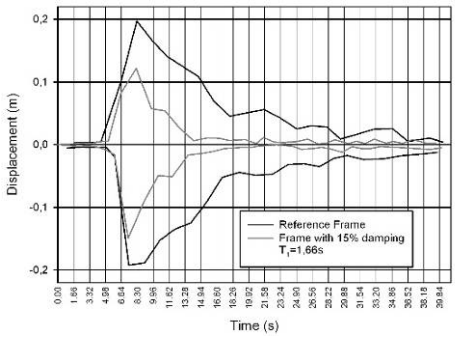

Fig. 12 Displacement mitigation curves - reference frame versus frame with 15% damping (VRANCEA)

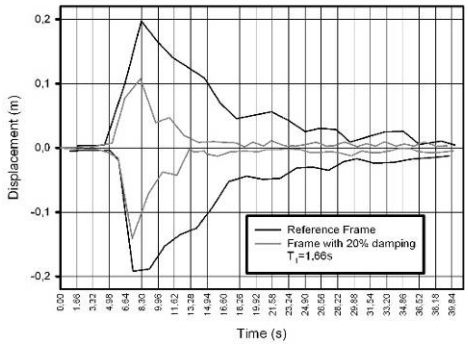

Fig. 13 Displacement mitigation curves – reference frame versus frame with 20% damping (VRANCEA)

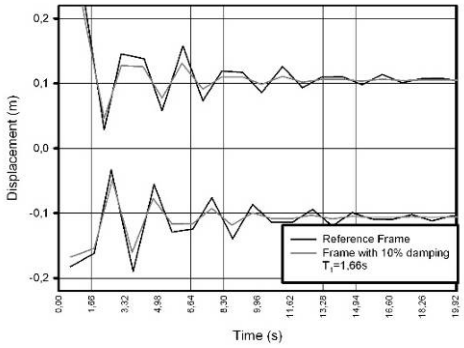

Fig. 14 Displacement mitigation curves - reference frame versus frame with 10% damping (Sinus)

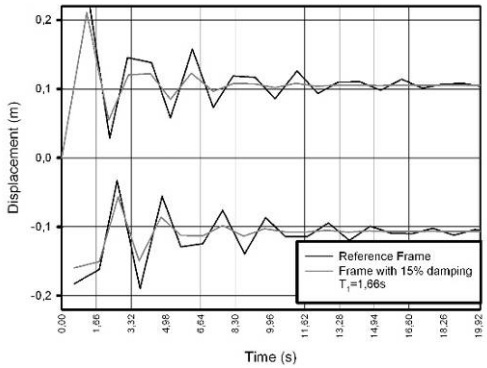

Fig. 15 Displacement mitigation curves – reference frame versus frame with 15% damping (Sinus)

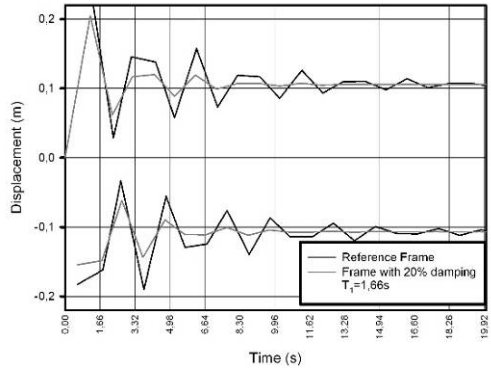

Fig. 16 Displacement mitigation curves - reference frame versus frame with 20% damping (Sinus)

4. Conclusions

Performed analyses and computed results emphasize the versatility and simplicity of proposed analytical tools in assessing the effectiveness of passive seismic protection of multi-story steel structures. The contribution is not focused on the importance of mitigation of seismic response and it does not compare the effectiveness of different passive seismic equipment. Two aspects are referred to in the final conclusions: efficiency of the seismic protection via viscous dampers and, mainly, to the proposed assessment of this effectiveness via mitigation envelope curves. In order to assess the achieved performances of seismically protected structures via supplemental damping, the inherent [6] damping level of 5% is considered as a standard unit of damping level. Therefore, a damping level of 15%, for instance, is referred to as a 3 unit level, while a 20% damping level will be a 4 unit level. Regarding the first aspect – effectiveness of passive protection via viscous damper - it may be concluded that a doubling in the damping level (from standard 5% to a 2 unit level of 10%) results in a reduction in top lateral displacements of 15 %, while a threefold increase in standard damping level induces a decrease of 26 % in lateral top displacements versus standard level. The highest level of damping studied (20%) is equivalent to a reduction of 33% (in the case of Vrancea accelerogram) and of 18%, 27% and 32%, respectively (in the case of sinusoidal excitation). The percentages refer to reductions in the peak values of lateral top displacements [13] [14].

The mitigation envelope curves are, also, very eloquent in terms of the length of the interval expressed in the natural fundamental period. In the case of reference frame, the length of the mitigation interval (starting at $t = 3T_1$ and ending at $t = 10 \cdot T_1$) is reduced from $7 \cdot T_1$ to $4.5 \cdot T_1$ in the case of 10% added damping and Vrancea accelerogram, e.g. see Fig. 11. Similarly, the mitigation curves associated to other levels (15% and 20%) of supplementary damping and sinusoidal type excitation are presented (Fig. 12 - Fig. 16). Time interval of seismically induced vibrations to a multi-story structure may be as important as the magnitude of the seismic action itself. Therefore, the assessment of the decrease in the time interval active vibratory state may become important in the decision process regarding the technical equipment to be installed.

Regarding the proposed mitigation enveloped curves they prove to be a versatile tool of assessing the efficiency of supplemental damping. Their expressing in terms of fundamental natural period of the structure allows a rapid and synthetic evaluation of supplemental damping efficiency. As it has been pointed out, if the structure vibrates at peak values of its kinematical parameters, incipient or even full shakedown type behaviour

is induced [15]. A vibration "stage" along a time interval up to two fundamental periods ($2 \cdot T_1$) may save the structure of shakedown behaviour and, consequently, of remanent plastic deformations. Also, the decrease in the values of associated parameter (top lateral displacements in this study) offers immediate asses of the measure of reductions in these values. The versatility of mitigation envelope curves and their synthetic feature opens the possibility of incorporating them in the set of performance criteria of seismically protected steel structures [16].

References

[1] Constantinou, M.C. and Symans, M.D. (1993). Experimental study of seismic response of buildings with supplemental fluid dampers. Structural design of tall buildings. Vol II,pp. 93-132.

[2] Chopra, A.K. (1995). Dynamics of Structures. Theory and Applications to Earthquake Engineering. Prentice Hall International, Inc.

[3] Soong, T.T. and Dargush G.F. (1997). Passive Energy Dissipation Systems in Structural Engineering. Wiley, Chichester – England.

[4] Constantinou, M.C. (2007). Fluid dampers for applications of energy dissipation and seismic isolation.

[5] Baldo, P., Tomaselli, F. and Pimenta, F. (2004). Loureiro viaduct seismic protection: Testing of non-linear viscous dampers. SEISMICA 2004 Congresso Nacional de Sismologia e Engenharia Sismica, pp. 679-690.

[6] De Silva, C.W. (2007). Vibration Damping, Control, and Design. CRC Press.

[7] Mathe, Aliz, Cătărig, A., Moldovan, I. (2015). Statics and Kinematics of Simirigid Steel Frames under Seismic Action. Journal of Applied Engineering Sciences. Volume 5(18), Issue 2/2015, pp.59-64.

[8] EN 1993-1-1. (2004). Design of steel structures-General rules and rules for buildings. CEN, European Committee for Standardization.

[9] Mathe, Aliz, (2009). Analiza elastică geometric neliniară a structurilor metalice cu conexiuni flexibile. (Nonlinear geometrical elastic analysis of semirigid connections). Phd. Thesis, Technical University, Cluj-Napoca.

[10] Chopra, A.K., Goel, R.K. (2001). A Modal Pushover Analysis Procedure to Estimate Seismic Demands for Buildings: Theory and Preliminary evaluation. Report no. PEER 2001/3, Pacific Earthquake Engineering Research Centre, University of California, Berkeley.

[11] Richard, R.M., Abbott, B.J. (1975). Versatile elastic-plastic stress-strain formula. Journal of the Engineering Mechanics, ASCE, 101(4), pp.511-515.

[12] Pirmoz, A. (2009). Moment–rotation behavior of bolted top–seat angle connections. Journal of Constructional Steel Research 65, pp.973–984.

[13] Citipitioglu, A.M., Haj-Ali, R.M., White, D.W. (2002). Refined 3D Finite Element Modelling of Partially-Restrained Connections Including Slip. Journal of Constructional Steel Research, 58(5-8), pp. 995-1013.

[14] Reynosa, J. M., (2008). Nonlinear elastic-plastic 3d finite element modelling of top and seat angle connections with double web angle. En Eurosteel 2008: 5 European Conference on Steel and Composite Structures, Volume A, Graz, Austria, pp.501-506.

[15] Cătărig, A., Mathe, Aliz, Chira, N., Popa, Anca. (2010). Steel Structures with Semi-Rigid Connections. Analele Universităţii din Oradea, Fascicula Construcţii şi Instalaţii hidroedilitare, (University of Oradea Annals,Journal of Civil engineering and installations ,Vol. XIII-2, pp.21-32.

[16] Cătărig, A., Alexa, P., Kopenetz, L., Mathe, Aliz, Lădar, Ioana. (2009). Geometrically Nonlinear Analysis of Semirigid Steel Structures. International Seminar of IASS Polish Chapter, XV Jubilee LSCE 2009, Warsaw, pp.29-32.

Is a Green Roof an Effective Solution for Reducing Energy Consumption?

Moga L.[1], Munteanu C.[1], Moga I.[1], Babotă F.[1], Tămaş F.[2]

[1] *Technical University of Cluj-Napoca (ROMANIA)*
[2] *Transilvania University of Brasov (ROMANIA)*
E-mail: ligia.moga@ccm.utcluj.ro

Abstract

In order to reduce the high energy consumptions in buildings, passive solutions must be applied. Several types of solutions are given by the green roof technology, through its green roof model identified with the vegetative roof. Literature investigates the impact of a green roof from several aspects, i.e. energy savings, aesthetic appeal, environmental impact and economic feasibility. One of the main positive impacts of a green roof is the reduction of the urban heat island effect that contributes to the global warming. However, many studies that have been conducted, focused on reducing the energy consumptions used for heating or cooling a building having a green roof. The results showed different behaviours and not always the positive expected results. Thus, the objective of this paper is to identify sensitivities to climate variability by quantifying the green roof benefits when used at a passive house building. The paper focuses on the thermal performance of the green roof model based on simulation made with the help of the PHPP program.

Keywords: passive building, cold climate, green roof, thermal insulation, building energy performance.

1 Introduction

Along the years researches have carried out several studies necessary to identify the proper solution for reducing the negative impact that the roof has on the energy performance of the building and also on the environment. It is well known that dark roofs contributes to the Urban Heat Island (UHI) effect, phenomenon which was first observed in the 19th century by Howard [1], many decades before other scientists. In his work he emphasized the way that urban areas have a negative effect on local climate by detecting, describing and analysing the UHI phenomenon. The increased urbanisation also increased the need of new developments that usually are made on the expense of green areas. The result is a shortage of the green areas, an increased temperature and decreased air humidity, as mentioned by Berndtsson [2].

Several studies identified passive strategies to reduce the negative effect of the solar radiation which rises the exterior surface temperature of the roof by 10 to 15oC higher than the surrounding areas due to the high concentration of heat absorbing dark surfaces [3]. The identified solutions for the finishing materials [4-6] are the highly-reflective coatings, i.e. cool roofs, and the vegetative roof, i.e. green roof. However, most of the studies are made only for the summer period of the year. Thus, the choice of using a dark, cool or green roof considering the winter period is more complex and must be analysed relative to the climatic conditions, i.e. solar irradiation and precipitation, and also the aim of implementing one solution versus the other.

In the last years, constructors from Romania understood the benefits of implementing green roofs in buildings. However, the focus of choosing this solution versus a conventional one, i.e. dark roof, was limited to achieving aesthetical benefits and an increased value of the building on the market. This is due to a proper lack of research on the real behaviour of green roofs in predominant cold countries, as is the case of Romania. In this purpose the paper tries to highlight the current available solutions in the green roof industry, the benefits and also the particularities of implementing a green roof technology with respect to energy utilization at a passive building. Some recommendations for future study are also proposed.

2 Methodology

It is well known that buildings account for a significant percent (i.e. around 40%) of the energy consumption with a significant impact on the environment. The very increased energy consumptions are due to the need of ensuring a proper comfort temperature, which usually is felt different from person to person. Thus, the energy consumed by the heating systems will vary along several tenants but will try to fulfil the desired

average temperature around 22°C to 24°C, which is described as being the comfort temperature for Romanian inhabitants. To ensure such comfort values with minimal or reduced costs, a low energy building can be designed, at which several passive solutions can be implemented. An international well-known type of building is the Passive House, which is considered to be more energy efficient that other types of low energy buildings. Thus, the paper is focusing on a passive house building, placed in several climatic zones and considered in three case scenarios: having a conventional roof, having a passive house roof and having a green roof. Comparisons and conclusions are made based on the findings

2.1 *Passive House Concept*

The low energy building can be defined in many ways, but its main characteristic is that it uses much less energy compared to a conventional building, reduces costs and improves occupant comfort and workplace performance. The typical annual energy consumptions for a low energy building, differs from country to country based on their standards and construction practices, e.g. in Germany "Niedrigenergiehaus" an energy consumption for heating ≤50 kWh/m² per year, whereas in Switzerland "MINERGIE" standard energy consumption for heating ≤42 kWh/m² per year. Thus, the passive house represents a superior step in designing energy efficient buildings.

Passive House buildings were built many years before [7] Dr. Wolfgang Feist from Institut für Wohnen und Umwelt (Institute for Housing and the Environment from Germany) and Professor Bo Adamson of Lund University, Sweden, had a conversation regarding the passive house concept in May 1988 [8]. Following, the Passivhaus –Institut was founded in September 1996 in Darmstadt and the Passivhaus standard appeared on the market. Hence, when talking about the passive house the energy consumption for heating must be less than 15 kWh/m² per year [8]. Therefore, a passive house can be defined as an "ultra-low energy building".

The design of a passive house standard is done by using the PHPP-Passive House Planning Package, which is used as a design and verification tool. Its reliability was demonstrated in several international studies that identified only slight adjustments necessary to the results obtained by using PHPP. The basis for the PHPP is an Excel program, thus giving immediate results without significant computing times [9].

2.2 *Green Roof Technology*

Green roof technology is defined as a solution where a vegetated roof, cool roof or even a roof with solar panels is implemented. Typically, a green roof is defined as an ecological solution due to its positive impact on the environment (i.e. ads green space, produces more oxygen, reduces carbon dioxide emission, water runoff) and on its capability of reducing the energy consumption of a building [2, 10-11].

The vegetative roof, usually known on the market as "the green roof", is a technology commonly used in North America, Australia, Japan and Singapore, Germany, Switzerland, and other European countries. Blank et al concluded in [12] that the most research from all the ISI Web of Science identified articles in this field was done in USA (34%), in EU (33%) and in Asia (20%). In latest articles, researchers also outlined that several green roof solutions may not adapt and perform the same around the world. Hence, research is still needed to tailor green roof solutions for different type of climate conditions

A green roof is defined by its four parts, from outer to inner surface, the canopy (the vegetation layer), the porous soil or the growth substrate, the drainage layer with/without aeration and storage water and the support (i.e. the load-bearing slab, vapour barrier, insulation layer, roofing membrane, root barrier) [13]. Nowadays, three types of green roofs are identified, i.e. the intensive, semi-intensive and extensive green roof. The intensive green roof has a soil thickness above 20 cm while the extensive roof has one lower than 15 cm. The thickness of the soil has also a direct influence on the structure of the building and on the roof support system. Thus, extensive green roofs are typical recommended for building retrofitting, needing low maintenance, low capital costs and low weight. The intensive green roofs needs a wide variety of plants, high maintenance and high capital costs and have greater weight. The semi-intensive green roofs imply frequent maintenance and high capital costs. Consequently, the most used solution is the extensive green roof.

As Sailor mentions in his paper [14] one of the most important thermal properties of the soil (i.e. growing media) is its thermal conductivity, specific heat capacity and density. With regards to the heat transfer aspects an important role is also played by the characteristics of the vegetation, i.e. leaf area index, height, albedo, fractional coverage and stomatal resistance [14]. All this characteristics have an effect upon the radiative characteristics, the reflectivity and the transpiration process (i.e. moisture transport).

When looking at the unidirectional heat conduction phenomenon, the variation of the thermal properties of the green roof layers with the moisture content of the soil generates a complex behaviour of such a solution. Thus, when using the thermal properties for the soil the values should be affected by the soil moisture considered/measured for the studied case. As it was observed by Sailor [14], the thermal conductivity varies linear with the soil moisture saturation level. Thus, the thermal conductivity of a saturated soil is usually double

compared to the dry state of the soil, while the specific heat capacity has a 40% higher value for the saturated soil compared to the dry state. Another important aspect is the type of the soil used and its compaction level.

2.3 *The case study*

Several locations are considered for the passive house building, locations characterised by the following H_T heating period [d/yr], G_T heating degree days [k·K·h/yr]: 1st Location: H_T=53 [d/yr], G_t=14 [k·K·h/yr], 2nd Location: H_T=189 [d/yr], G_t=78 [k·K·h /yr], 3rd Location: H_T=237 [d/yr], G_t=97 [k·K·h /yr].

The analysed building has a compact form with two floors (fig 1.). The ground floor is composed of a living room, a dining, a kitchen, a WC, the corridor and the stair case, while the first floor is composed of two bedrooms, a bathroom, a mechanical room, a corridor and the stair case. The free height of both floors is 2.65 m. Although the initial plan is with a cold attic as shown in figure 1, for the studied case the building was considered having a flat terrace roof.

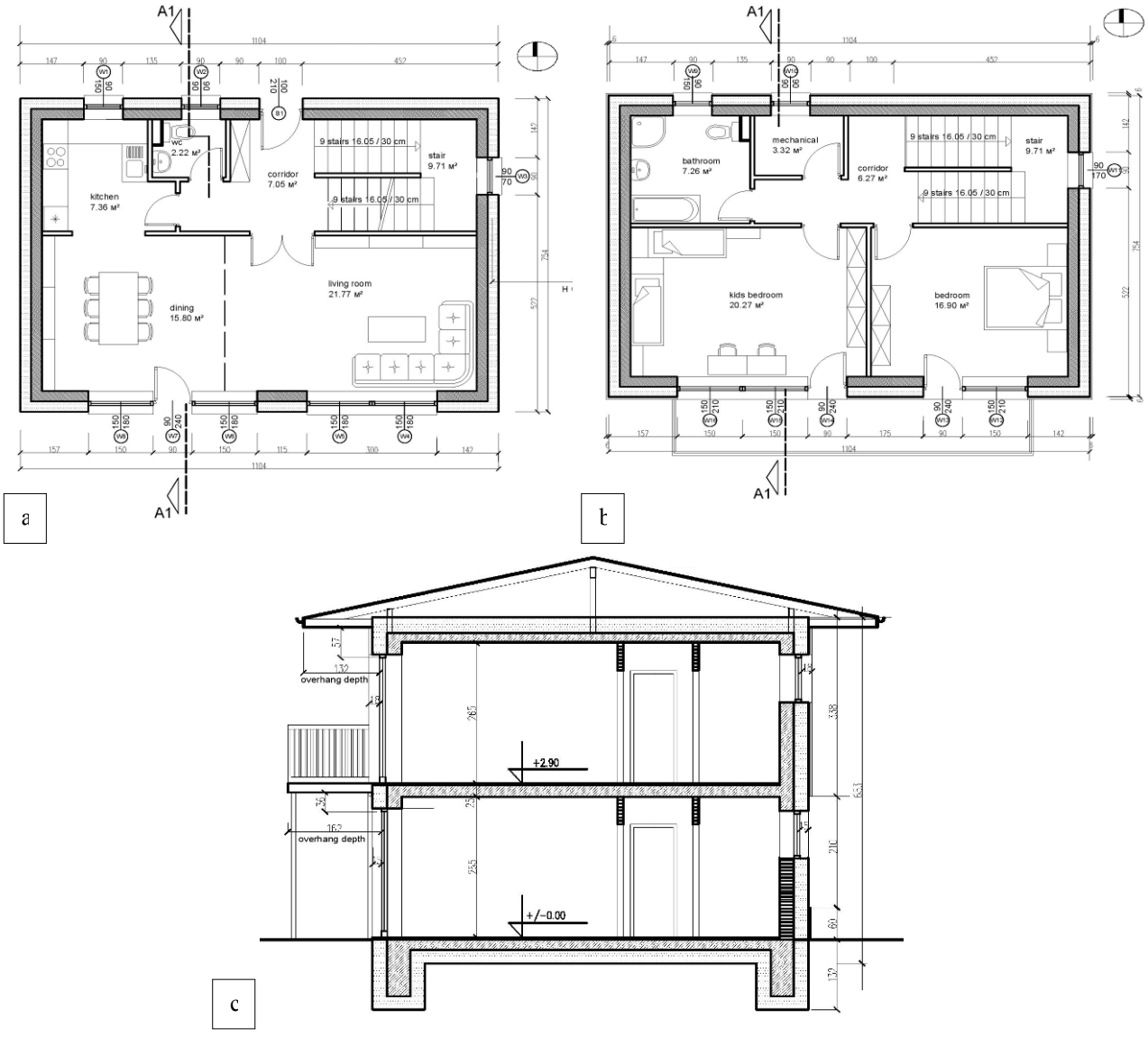

Fig. 1 House plans (a) ground floor (b) first floor (c) building section

The building has a masonry structure made of bricks thermal insulated on the exterior with expanded polystyrene EPS of 25 cm and a flat roof consisting of concrete with exterior insulation XPS of 30 cm. The floor slab is made of concrete with thermal insulated with extruded polystyrene insulation XPS of 25 cm. The windows are double glass solution with air (4-12-4) and an aluminium frame. The main thermo-physical properties are for: a) exterior wall thickness 51.6 cm and thermal transmittance 0.117 [W·m^{-2}·K^{-1}] b) roof

thickness 65.1 cm and thermal transmittance 0.113 [$W \cdot m^{-2} \cdot K^{-1}$]; c) floor slab thickness 46.3 cm and thermal transmittance 0.143 [$W \cdot m^{-2} \cdot K^{-1}$]; d) glass type 4-12-4 and thermal transmittance 0.79 [$W \cdot m^{-2} \cdot K^{-1}$]. All the considered components are designed for the passive house case. To consider the thermal bridges impact the linear thermal transfer coefficient ψ [$W \cdot m^{-1} \cdot K^{-1}$] was considered with respect to the exterior reference dimensions, as stipulated by the PHPP program [9].

Three case scenarios were considered for the roof model: a) conventional detail b.) the passive house initial detail c.) green roof detail. The green roof detail (fig. 2) considered in simulations is an extensive green roof, its system being placed on the existing structural element [15]. For the type of soil it was chosen a composition of 75% expanded shale, 10% compost and 15 % sand with a dry density of 1.25 [$kg \cdot m^{-3}$] and a moisture capacity of 0.22 [g/g] as defined by Sailor [14]. The worst case scenario is considered when the soil is almost saturated at the inferior side and thus the thermal conductivity is around 0.41 [$W \cdot m^{-1} K^{-1}$] (corresponding to a humidity level of 82% [14]) and the vegetative layer is considered humid having a thermal conductivity equal to 0.54 [$W \cdot m^{-1} K^{-1}$]. The vegetative layer is considered uniformly distributed, thus an average thickness of 10 cm is considered in calculation. In order to better understand the thermal behaviour of the green roof detail and its impact on the annual heat demand and passive house criteria, three situations will be considered: the first case as the non-insulated case (c.1), the second case (c.2) thermal insulated with 10 cm, and the third case (c.3) thermal insulated with 30 cm. The thickness of the soil is considered 8 cm. For the (a) case scenario, from the passive house detail (b) the thermal insulation was considered as inexistent.

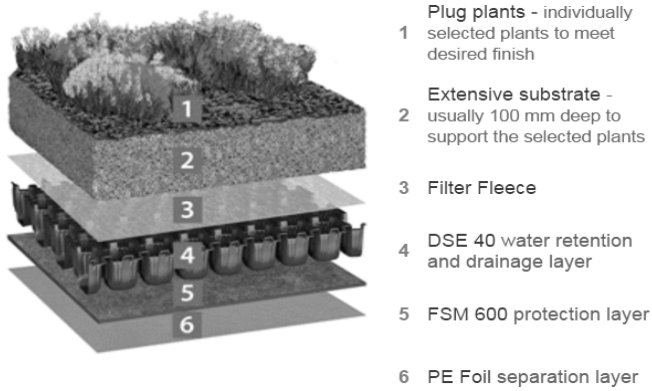

Fig. 2 Extensive green roof detail [15]

The PHPP version 8 is used for analysing the green roof effect on the energy performance of a conventional passive house building. The chosen details for the green roof are the one existing on the market and in literature.

The other inputs refer to:

- the areas of the building envelope elements, resulting the following: the treated floor area of 113,9 m^2, the enclosed volume of 543,6 m^3 and the total area of the envelope of 392.42 m^2, resulting a A/V ratio of 0,72;
- the interior design temperature during winter time is θ_i=20°C and during summer time is θ_i=25°C;
- the cardinal orientation of the building component and the shading characteristics for the glazing surfaces;
- the number of building occupants, which is considered equal to three;
- the ventilation data for summer ventilation;
- the ventilation unit with heat recovery, where a unit with a 84% efficiency is used;
- the ventilation data for ventilation planning of volumetric flows;
- the domestic hot water distribution data and the solar thermal system**;**
- the electricity and auxiliary electricity demand

3 Results

The results obtained for the energy consumption for space heating using the PHPP program are obtained for the specific annual heating demand method. Form the passive house criteria, only the next indicators are emphasized:

- the thermal transmittance U [$W \cdot m^{-2} \cdot K^{-1}$];

- the heat load HL [$W \cdot m^{-2}$];
- the heat demand HD [$k \cdot W \cdot h \cdot m^{-2} \cdot yr$];
- frequency of overheating FO (>25^{o}C)

Looking at the passive house criteria [8] the following should be fulfilled:

- roof detail thickness d [cm];
- thermal transmittance for the roof U≤ 0.15[$W \cdot m^{-2} \cdot K^{-1}$];
- the heat load HL ≤ 0.10 [$W \cdot m^{-2}$];
- the heat demand HD≤ 0.15 [$k \cdot W \cdot h \cdot m^{-2} \cdot yr$];
- excess temperature frequency ≤ 0.10, where >15% catastrophic, 10-15% poor, 5-10% acceptable, 2-5% good, 0-2% excellent;

The values from the simulated cases are synthetized in table 1.

Table 1 Numerical results for the studied case obtained using PHPP

			1st Location			2nd Location			3rd Location		
Analysed details	d	U	HL	HD	FO	HL	HD	FO	HL	HD	FO
a.) conventional	35.1	2.030	16	5	35.7	58	112	10.5	55	156	0
b.) the passive	65.1	0.113	2	0	23	17	16	1.4	17	26	0
c.1) green roof 0	56.1	0.590	5	0	32.1	27	38	3.1	27	56	0
c.2) green roof 10	66.1	0.220	3	0	26.9	19	20	1.4	19	32	0
c.3) green roof 30	86.1	0.097	2	0	22.2	17	15	1.4	17	25	0

The final results obtain with the PHPP program indicate that the thermal insulation is one the most important layer in establishing the thermal performance of the roof and its impact on the building. By comparing the studied cases, an expected result is that of the non-insulated case for the conventional roof (a.) for which all the parameters are the worst ones for all three locations, although that the other elements of the building envelope were design in accordance to the passive house criteria. For the green roof case only the third type of detail (c.3) is the one that is able to fulfil the passive house criteria although that its thermal performance values are not far from the one of the passive house roof detail (b.).

Thus, when using a green roof detail in the design of a passive house situated in a cold dominated location (i.e. the 2nd and the 3rd location), it is necessary to use at least 30 cm of thermal insulation in order to meet the passive house criteria. From the thermal point of view, due to the changing behaviour of the soil thermal characteristics, a green roof does not perform for this type of climate better than a classic passive house detail. In a warm dominated climate (i.e.1st location) the importance of a green roof from the heating demand perspective does not have a greater impact compared to other analysed. For this location the emphasis should be placed on the cooling consumption considering that the excess overheating increased significantly compared to the other two locations.

Another aspect is that of the thermal properties of the soil which for the studied case were considered as mentioned before, with a constant value although that the behaviour can vary along the cold period of the year. Thus, even if the third model of the green roof is used in designing the passive house building, the thermal behaviour of the soil and of the vegetation layer and also the durability of the system components will have a significant influence in maintaining the passive house criteria on a long period of time. The PHPP program should be further developed to be able to model the complex thermal behaviour of a green roof detail.

4 Conclusions

For a further study regarding the real impact that a green roof model has on a building energy and maintenance costs, and also on the environment, investigations should be done considering the installation and operation cost, the environmental impact, the durability of the green roof model, the average solar radiation on the horizontal plane, the average monthly rainfall, and other criteria tailored on the climatic zone where the building is placed. Although results can be positive from the saved energy percentage, it can have a more negative impact on other above mentioned criteria. Thus, when analysing the implementation of a green roof solution, the results answer to the questioned building and not to all other existing buildings. Green roofs do not represent the best solution for some type of buildings and climates.

The PHPP program has several disadvantages, one being that it cannot offer complex simulation for a green roof model. However, the program can still give results similar to existing literature. Options for modelling the green roof behaviour should be implemented in the PHPP program, to allow the user to accurately model and evaluate the implemented roof.

The authors recommend a change in the way that green roof models are perceived, and recommend more research to be addressed in the future. Several questions are still in the air regarding both the energy and

the environmental impact of a green roof model. Also, the involved actors in the construction domain should have access to research results to better perceive that the green roof is not always as "green" as it seems to be. The lack of proper research can lead to an opposite effect with significant economic consequences.

The Romanian Ministry of Environment, Waters and Forests launched the "Casa Verde Plus" program [16] which offers several incentives for using a green roof model in energy retrofitting of existing buildings (i.e. schools, hospitals, and social buildings). The Romanian research on implementing green roof models is still in its developing years. Thus, the implementation of such program comes with a lot of risk, from both economic and sustainability point of view (i.e. energy consumptions, costs, environmental impact).

References

[1] Howard L. (1889.). The Climate of London, I–III, Harvey and Dorton, London.
[2] Berndtsson JC. (2010). Green roof performance towards management of runoff water quantity and quality: a review, Ecological Engineering, vol. 36, pp 351–60.
[3] Liu K, Baskaran B. (2003). Thermal performance of green roofs through field evaluation, In: Proceedings of 1st North American Green Roof Conference: Greening Rooftops for Sustainable Communities, Chicago, The Cardinal Group Toronto.
[4] Akbari H., Konopacki S., Pomerantz M. (1999). Cooling energy savings potential of reflective roofs for residential and commercial buildings in the United States, Energy, vol 24 (5), pp 391–407.
[5] Zinzi M., Agnoli S. (2012). An energy and comfort comparison between passive cooling and mitigation urban heat island techniques for residential buildings in the Mediterranean region, Energy and Buildings, vol. 55, pp 66–76.
[6] Scherba A., Sailor D.J., Rosenstiel T.N., Wamser C.C. (2011). Modelling impacts of roof reflectivity, integrated photovoltaic panels and green roof systems on sensible heat flux into the urban environment, Building and Environment, vol. 46, pp 2542–2551.
[7] Heiduk E. (2009). From low-energy house to the Passive house, International Passive House Summer School for Students.
[8] www.passivhaustagung.de
[9] Pasive House Planning Package PHPP (2013). Version 8.
[10] Morau D., Libelle T., Garde Fo. (2012), Performance evaluation of green roof for thermal protection of buildings in Reunion Island. Energy Procedia, vol 14, pp1008–1016.
[11] Santamouris M., Pavlou C., Doukas P., Mihalakakou G., Synnefa A., Hatzibiros A., et al. (2007). Investigating and analysing the energy and environmental performance of an experimental green roof system installed in a nursery school building in Athens. Greece, Energy, vol. 32, pp 1781–1788.
[12] Blank L., Vasl A., Levy S., Grant G., Kadas G., Dafni A., Blaustein L. (2013). Directions in green roof research: a bibliometric study. Building and Environment, vol.66, pp 23–28.
[13] Rakotondramiarana H. T., Ranaivoarisoa T., Morau D. (2015). Dynamic Simulation of the Green Roofs Impact on Building Energy Performance, Case Study of Antananarivo, Madagascar, Buildings, vol. 5, pp. 497-520.
[14] Sailor D.J., Bass B. (2008), A green roof model for building energy simulation programs, Energy and Buildings, vol.40, pp. 1466–1478.
[15] Bauder (2009). Vegetative roofs. Products catalogue, April Edition.
[16] http://www.afm.ro/casa_verde_plus.php.

Modern Consolidation Solutions for Buildings with Historical Value. Part II: Masonry Structures

Mosoarca M.[1], Apostol I.[1], Stoian V.[2]

[1] *Politehnica University of Timisoara, Faculty of Architecture and Urbanism (ROMANIA)*
[2] *Politehnica University of Timisoara, Faculty of Civil Engineering (ROMANIA)*
E-mails: marius.mosoarca@upt.ro, iasmina.apostol@student.upt.ro, valeriu.stoian@upt.ro

Abstract

In Banat region, in the western part of Romania, there are a great number of historical buildings made of masonry, using brick block, or stone. Nowadays, they present large degradations because of earthquakes, subsidence or negative human interventions during time. That is precisely why they have different bearing capacities and different seismic behaviours.

These are the historical buildings that we are obligated to consolidate, to keep the history alive for the future generations. In this article are presented some consolidation methods with modern materials and innovative technologies, using reversible and natural solutions, applied for two buildings with historical value in Timisoara, Romania.

Keywords: new materials, masonry structure, collapse mechanism, historic building, consolidation methods.

1 Introduction

In Romania, the most used material for civil buildings is the burnt clay brick and lime mortar. In time, the buildings recorded permanent structural changes due earthquakes, settlements of the foundation, negative human interventions due to the need of changing spaces and compartmentations, exterior perturbations, etc. [1].

In Romania, there are two main seismic regions: Vrancea region and Banat region. While the earthquakes recorded in Vrancea region are deep, the Banat region is characterized by shallow earthquakes, so the failure mechanisms are different between the two regions [2].

The failure mechanisms differ also according to the plan shape, the elevation and the construction system of the historic buildings. Therefore, the many diverse types of structures built in Timisoara in the late 19th century and the beginning of the 20th century, such as churches, residential buildings, present specific failure modes, due to the constitutive characteristics of the structural material behaviour when subjected to strong ground motion. Lately, there were studied a lot of modern consolidation methods for masonry structures [3].

Several solutions of intervention, using new materials and technologies which use polymeric composite materials reinforced with carbon, glass or aramid fibres were used with the purpose of increase the bearing capacity of the structure and keep the original stiffness. The modern techniques and materials are very easy to apply, ecological, reversible, in perfect harmony with The Chart of Venice principles and they were partially used on two masonry historic buildings from Timisoara, the buildings Sfantul Gheorghe 2 and 3.

2 Building description

Sfantul Gheorghe Square is one of the oldest squares of the city, and the studied buildings were built at the end of the 19th century, in a shape of a U, with an interior yard, specific for that period [4].

The buildings that are the subject of our case study (Fig 1. a , b), are both presenting a basement, ground level and two stories, have cellular building system, with walls made of brick masonry. Over the basement and the ground floor, the ceiling is made of vaults and arches. The 1st and 2nd floors' ceilings are made of wood beams, with no significant stiffness in horizontal plane. The roof framing is made of wood, with two slopes. The foundations are made of brick masonry [5].

a) 

b) 

Fig. 1 Front view of the studied buildings: a) Sf. Gheorghe 2 building and b) Sf. Gheorghe 3 building

3 Degradation state

The buildings are in an advanced degradation state, mainly due to the external factors that have operated over the structures: settlements, earthquakes and unauthorized interventions on the bearing structure before 1989.

The brick masonries are made with clay and lime mortar of poor quality, being eroded in the areas where there is no plaster. The bricks are in good shape an there haven't been noticed any damages [5].

The cracks on the two buildings are very pronounced at the 1st and 2nd floor, because of seismic actions and differentiated settlements, more pronounced in the neighbouring buildings area. The cracks are also very prominent around the windows and doors areas (Fig. 2). The wood ceilings at the 1st and 2nd floor show damages due to the reducing of the bearing capacity and of the stiffness of the wood beams in time, because of the humidity and of the improper maintenance performed by former owners until 1989. The buildings suffer from the lack of rigid ceilings at the upper floors, the existing wood ceilings being incapable to ensure this role.

a) 

b) 

Fig. 2 a) cracks around the windows and slab, b) cracks in the door

In the longitudinal central wall, there is an important crack that starts from the superior area of the wall, and continues to the basement. Important vertical cracks were find at the nearby building (Sf. Gheorghe 4), in the area of separation between building areas that were built in different times, as we can see in Fig. 3.

a)  b) 

Fig. 3 a), b) Vertical crack in the separation area between buildings built in different ages (Sf. Gheorghe 4)

The damages produced in the basement arches and vaults are due to the irregular settlements of the foundations, producing supplementary horizontal forces into the façade walls. Because of the fact that the interior walls from the transversal direction weren't connected to the façade walls, the last has developed an out-of-plane failure mechanism. The only reason for not getting to the ultimate limit state is because of the ties that were put into the slabs and in the plane of the metal farm of the roof, as we can see in Fig. 4.

a)  b) 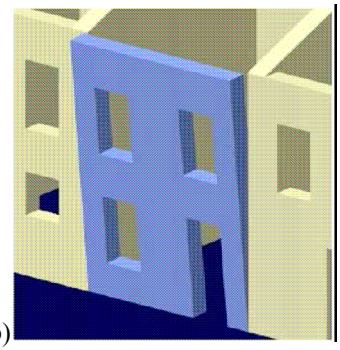

c)   d) 

Fig. 4 a) Vault settlement with damages for Sf. Gheorghe building; b) the out-of-plane failure mechanism; c) transversal walls that are not connected to the façade walls; d) ties on the roof structure

The roof framing is found in good state, there are only some insignificant damages, mainly at the joints. Because of the humidity, the laths are rotten.

4 Consolidation proposal

The past years had revealed an increasing interest for research for identifying and correction of in-plane and out-of-plane collapse mechanism developed by masonry walls [6], [7].

4.1 *Wall consolidation with modern materials*

The walls were consolidated by setting some stainless steel helical joists for sewing the fissures (AISI 304), as we can see in Fig.5 a. A vertical and horizontal glass fibre wired mesh (Rinforzo ARV100) was mounted on top of Geocalce mortar (without cement addition). At last, some vertical metallic profiles were set, for the stiffening of the wall [8] .The wall's bed joints were dug deeply, on the entire length of the sewing joist. After the digging, the wall was fully cleaned. 2/3 of the joint's depth was filled with Geocalce mortar, after which the Steel Helibar 6 was inserted in the joint. The bar was installed with manual pressure. After the bar was inserted, the joint was sealed with the same mortar. A first layer of 2-3 mm of Geocalce mortar was applied. After this layer, the aramidic wired mesh Rinforzo ARV100 was set, and a final layer of 3-5 mm of Geocalce mortar to totally incorporate the reinforcement and to close all the potential wholes [9].

In order to avoid activation of the out-of-plane failure mechanism of exterior walls, were mounted reinforcement grids Kerakoll Rinforzo ARV 100, both on vertical (Fig. 5 b) and horizontal direction. On the interior part of the building, the connections between the transversal walls and the facades walls were assured by mounting reinforcement grids Kerakoll Rinforzo ARV 100 precisely in the area of their connections, as we can see in Fig. 6 a, b, c, d.

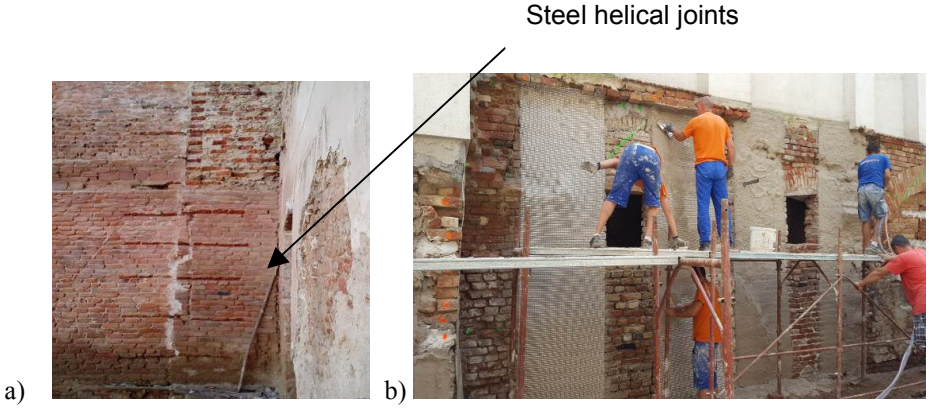

Fig. 5 Consolidation of exterior walls: a) application of the steel helical joints, b) application of the reinforcement grid Kerakoll Rinforzo ARV 100 on the exterior walls

Fig.6 a), b), c), d) The way of putting the reinforcement grids for connecting the façade walls with the interior transversal walls

4.2 *Vault consolidation*

The vaults consolidation has started by setting the wired mesh on the bottom and temporary supporting of the basement vaults. The next step was the mounting of metallic beams, setting the anchors for the vaults and the suspension of the wired mesh on the bottom of the vaults. After the settings of the anchors and suspensions, the next step was to put the reinforced concrete topping, above the vaults from the basement. The last and the most important step was setting the Kerakoll ARV 100 mesh and the rods for the masonry and repeating the actions for the vaults above the ground floor [9]. The reinforcement grid ARV 100 was mounted above the vaults and also on the masonry walls for a height of 100 cm (Fig. 7 a). In order to avoid that the mesh would detach from the vaults or the walls, in the connection area of the vaults and walls were installed perimetral steel rolled profiles, as we can see in Fig. 7 b. The Kerakoll system, compound of the Geocalce mortar, basaltic and stainless steel wired mesh, with a special protective treatment with water-based resin, and basalt fibre reinforced mortar (a mix between basalt fibre wired mesh and mineral mortar, based on pure hydraulic natural lime) was set, laying the mesh uniformly over the entire surface of the vault[10].

a)  b) 

Fig. 7 a), b) Reinforcement of the vaults with Kerakoll Rinforzo ARV 100

5 Conclusions

The main purpose of this article is to present modern and innovative consolidation solutions there were used on two historical buildings in Timisoara, Romania. Considering the fact that in Timisoara, but not only, there are a lot of buildings with masonry structure that are facing problems due to earthquakes, lack of interventions and other, it is important to show solutions that had worked on similar situations.

The new materials that were used for consolidation of the walls and vaults are very easy to apply. They increase the bearing capacity of the buildings, but they don't increase the stiffness of the structure. These materials, based on hydraulic lime solve also the humidity problems that affect the masonry buildings, especially at the basement. At least, the intervention is a reversible one, respecting the Chart of Venice principles.

Because of the obvious advantages of those modern materials and technologies it is necessary to elaborate design methodologies, part of a new design code for calculation the structures of buildings with historical value.

6 Acknowledgments

We would like to thanks to ing. Rares Bradean for all the technical assistance that he offered us during evaluation and structural calculation and during execution.

The researches about the out-of-plane failure mechanism were founding from the European Union's Seventh Framework Programme for research, technological development and demonstration under grant agreement No. 606229 INSYSME.

REFERENCES

[1] Prada, M., Mancia, A., Ploae M. (2004). Modern Methods for Rehabilitation and Consolidation of Brick Buildings, Ovidius University Annals Series: Civil Engineering, Vol. 1, No. 6, p. 1-2.

[2] Cosma, O., Risk evaluation of orthodox churches, using collapse plastic mechanism. Proceedings of the International Conference on RISK MANAGEMENT, ASSESSMENT and MITIGATION.
[3] Narita, A., Mosoarca, M., Modena, C., Da Porto, F., Munari, M., Taffarel, S., Marson, C., Valotto, C., Roverato, M. (2016). Behavior of Historic Buildings in Zones with Moderate Seismic Activity. Case Study: Banat Region, Romania, pp.1-2.
[4] Andreescu, I., Gaivoronschi, V., Mosoarca, M. (2013). The Hidden Gem, Advanced Materials Research, Vol. 778, pp. 880-887.
[5] Gioncu, V., Technical expert's report, unpublished.
[6] Prada, M. (2013). Risk elements in modelling, designing and building-up portant masonry structures, Journal of applied engineering sciences Article Number: 119_VOL. 1(16), issue 1_2013, pp.83-86, ISSN 2247- 3769 ISSN-L 2247- 3769 (Print)e-ISSN:2284-7197.
[7] Partene, E., Fekete-Nagy, L., Stoian, V. (2015). Evaluation of shear capacity for brick masonry walls, Journal of applied engineering sciences vol. 5(18), issue 1/2015 ISSN: 2247-3769 / e-ISSN: 2284-7197 ART.179, pp. 69-74, DOI: 10.1515/jaes-2015-0009.
[8] Kerakoll, The Green Building Company (2016), Guideline for the Consolidation, Structural Reinforcement and Seismic Security with New Green Technologies, pp. 64-65, 74-75.
[9] Mosoarca, M., Design project, unpublished.
[10] Kerakoll, The Green Building Company (2016). Guideline for the Consolidation, Structural Reinforcement and Seismic Security with New Green Technologies, pp. 98-99.

Study on the Acoustic Quality of the "Betania" Church from Cluj-Napoca

Munteanu C.[1], Moga L.[1], Tămaş F.-L.[2], Tămaş-Gavrea D.-R.[1], Suciu M., Babotă F.[1]

[1] *Technical University of Cluj-Napoca (ROMANIA)*
[2] *Transilvania Univeristy of Brasov (ROMANIA)*
E-mails: Constantin.Munteanu@ccm.utcluj.ro, ligia.moga@ccm.utcluj.ro, florin.tamas@unitbv.ro, roxana.tibrea@cif.utcluj.ro, marri.suciu@yahoo.com, Florin.BABOTA@ccm.utcluj.ro

Abstract

This paper concerns the study of the acoustic quality of a church situated in Cluj-Napoca. As the church does not fulfil the acoustic requirements of the norms in Romania, several acoustic rehabilitation solutions were proposed, having in view both aesthetic appearance and economic demands. The research performed by acoustic measurements and through theoretical calculation methods have shown that the solutions proposed considerably improve the noise-related properties of the church. The study showed to be an important concern for the church management and has pointed out to the need of noise-related specialists to perform complex acoustic verifications for such type of buildings both during their design stage and during their service stage.

Keywords: acoustic quality, church, reverberation time, acoustic rehabilitation.

1 Introduction

The present paper concerns a complex research regarding the acoustic quality of the "Betania" Pentecostal Church of Cluj-Napoca (Fig. 1).

Fig. 1 Main façade of the "Betania" Church

The study of the acoustics of churches is relatively limited and only during the last years it became of interest as more and more spacious churches have been erected, to provide better comfort to an increasing number of religious participants. During a religious service, in Pentecostal churches several activities are carried out: the sermon, singing, both vocally and instrumentally, poems reciting and prayer. One of the most significant issues related to church acoustics lies in the design of a proper acoustic environment for musical and speech sounds. "Betania" Church is a newly built church, erected in 2010, in the city of Cluj-Napoca (Fig. 2).

Fig. 2 Inside of the church: a–ground floor view; b-ceiling view; c- balcony view

Its shape is relatively rectangular in plane, with a soil print of 700 m^2, length of 29.0 m, and width of 23.85 m respectively. The church space is divided for use as follows: the basement is dedicated to prayer, the ground floor contains the large room of the church where all the religious programs take place, the first floor has a balcony and rooms for various purposes, such as: locker rooms, office and cashier's room. The large room has a volume of 3750 m^3, accommodating about 680 persons. The interior finishing consists in plastered walls, painted in washable white paint and a surface including the pulpit where the background is painted. The ceiling has a sound insulation system, which is related to the recent construction. The flooring of the ground floor and balcony is made of parquet, the windows are double glazed and with PVC frames. The doors are mainly PVC framed and double glazed. The public seating places are made from wooden tapestry benches.

2 Determination of the reverberation time

2.1 *Determination of the reverberation time by measurements*

To find out this acoustic parameter that is so important for an auditorium and to compare it with the values given in the norm [1] as function of the room volume and destination, we initially found the reverberation time by making acoustic measurements. For this purpose, we used a Bruel & Kjaer acoustic chain, which includes the following components: software type PULSE "FFT&CPB Analysis 7700", installed in a Dell laptop, PULSE Sound&Vibration Analyzer, type 3560, the sound source "OmniPower Sound Source tip 4292" equipped with a tripod, Power Amplifier (300W) type 2716, Microphone type 4189 provided with a tripod, Sound Level Calibrator, tip 4231 (Fig. 3).

Fig. 3 Images of the acoustic measurements: a, b - ground floor; c - balcony

For the purpose of measurement accuracy, the indications in [2] were observed. The reverberation time was found with the interrupted noise approach. In this approach, the decrease curves are found by directly recording the decrease of acoustic pressure level, after the excitation of the room with a wide noise band. The reverberation time represents the time in which the sonorous intensity level diminishes by 60 dB beginning with the moment of source emission stop. The reverberation time was measured in this church with the rooms empty. The source was positioned in the place of the pulpit wherefrom the speaker is supposed to speak. The microphone was placed in 32 points, of which 22 points at the ground floor and 10 points in the balcony, according to the public distribution in the church (Fig. 4). As the church has a perfectly symmetrical structure, the reverberation time was measured in six points along the symmetry axis and 26 points situated on one side of the symmetry axis, but the acoustic calculation was made taking 58 measurement points. The reverberation time was measured and calculated with special software, purposely dedicated by Bruel&Kjaer.

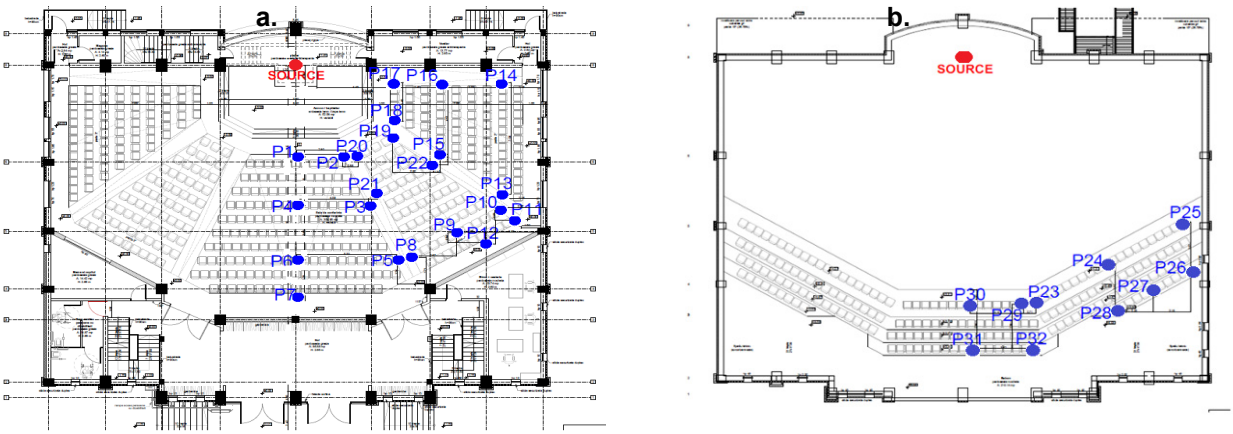

Fig. 4 The sound source and microphone placement: a- ground floor; b- balcony

2.2 Defining the admissible range of the reverberation time

In order to find out whether the reverberation time is included in the admissible range, the indications in the norm [1] are used. An average room reverberation time T_m is chosen function on the sonorous production kind and its volume, as in the diagram from [1], [3]. Function of the church volume, V=3750 m^3 and the line of predominant noise as choral/organ music, the interpolated average reverberation time is T_m=1.72 s. The values of the reverberation time T_f have resulted from the calculations as an average of the 58 points of measurement taken in the church. The values of the ratios T_f/T_m between the measured and calculated reverberation time T_f at the frequencies of 125 Hz, 250 Hz, 500 Hz, 1000 Hz, 2000 Hz and 4000 Hz and the average reverberation time T_m should be included in the requirements for admissible values as in [1]. They are given in the graph from Fig. 5 and show that the values found are not within the admissible range of the reverberation time.

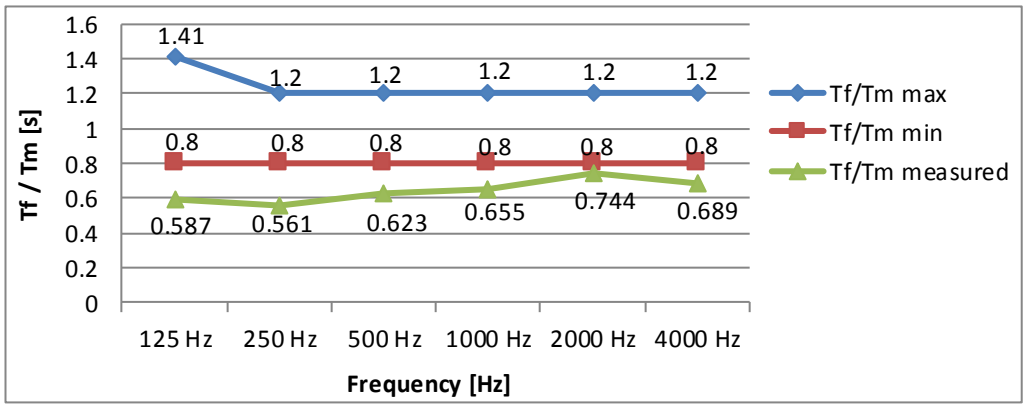

Fig. 5 Comparison of the T_f/T_m ratio to admissible values for the measured reverberation time

2.3. Determination of the reverberation time by calculation

During this stage, a comparison shall be made between the reverberation time values obtained by sound measurements and those found by Sabine's formula. The reverberation time in a room can be calculated according to [4] with the formula:

$$T = 0.163 \frac{V}{A} \quad [s] \qquad (1)$$

where: V is the room volume, in m^3 and A is the equivalent absorption area, in m^2 , calculated with:

$$A = \Sigma \alpha \cdot S + \Sigma a \quad [m^2] \qquad (2)$$

where: S_i represent the interior surfaces of the room with absorption coefficients α_i, while a_j is the unit absorption area of a person or an object. A, in m^2 was calculated with the formula (2) taking into account all the interior surfaces of the church (walls, ceiling, flooring, windows, doors, furniture, benches) with their corresponding absorption coefficients α_i,. The reverberation time T_f, found for each and every frequency provided in [1] was calculated with the formula (1) and the average reverberation time T_m=1.72 s as shown above. The values of the ratio T_f/T_m at every frequency provided in [1] must be contained in the admissible range. The values found by calculation, taking the church as empty, do not range in the admissible values of the reverberation time, as mentioned in [1] and are very similar with what was found by measurements.

3 Proposing solutions to optimise acoustic comfort

During this stage of research, several solutions for improving the church acoustic quality are proposed. As seen from the calculations above, the observations made and the noise measurements performed inside the Betania Church, it is necessary to increase the reverberation time so as to frame ratios T_f/T_m within the admissible limits specified by [1]. The acoustic rehabilitation variants concern Gyptone panels presented in [5]. Gyptone is a gypsum panel, a natural and neuter material with many benefits. During its service and during assembling, no harmful fumes, fibres or particles are emitted against the humans or environment. The Gyptone ceiling panels are very strong and flexible and can be removed for maintenance purposes. The various types of

perforations provide sound absorption and together with no-perforated panels allow for a widely creative ceiling design.

3.1 *Solutions to improve the acoustic quality of the church*

According to [1], it is necessary to check the situation when the room is 50% full and 100% full. As the benches are with tapestry, according to [1], one can take the reverberation time for the empty church as approximately equal to the reverberation time of a fully occupied church. Four solutions to improve the acoustic quality of the church were found and made.

3.1.1 To replace the existing full smooth panels in the ceiling

This acoustic rehabilitation solution consists in replacing the existing full smooth panels in the ceiling with Gyptone Activ'Air Base 31 D2 panels (Fig. 6).

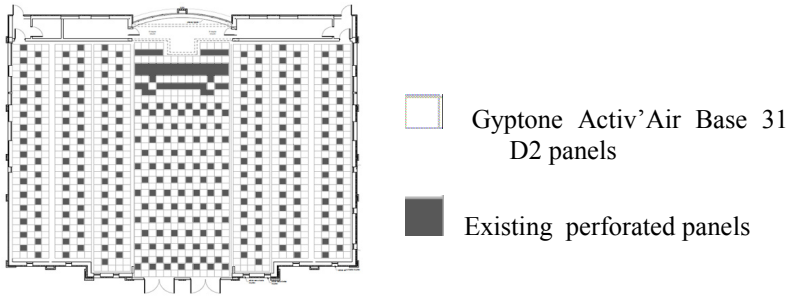

Fig. 6 Proposed acoustic rehabilitation solution

The ceiling Gyptone Activ'Air Base 31 D2 panels are fully uniform and smooth panels, without holes, of sizes 600x600x12.5 mm. The T_f/T_m ratio values for this solution made for the church without the public present range in the limits of [1] (Fig. 7). This solution was also verified for the case of the 50% occupied church. It was found out that T_f/T_m ratios range in the limits provided by [1] (Fig. 8).

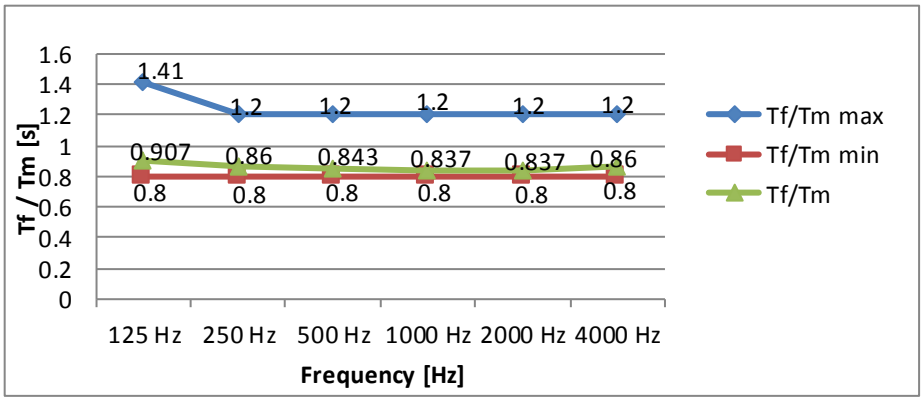

Fig. 7 Comparison of the T_f/T_m ratio to admissible values for the church without the public present

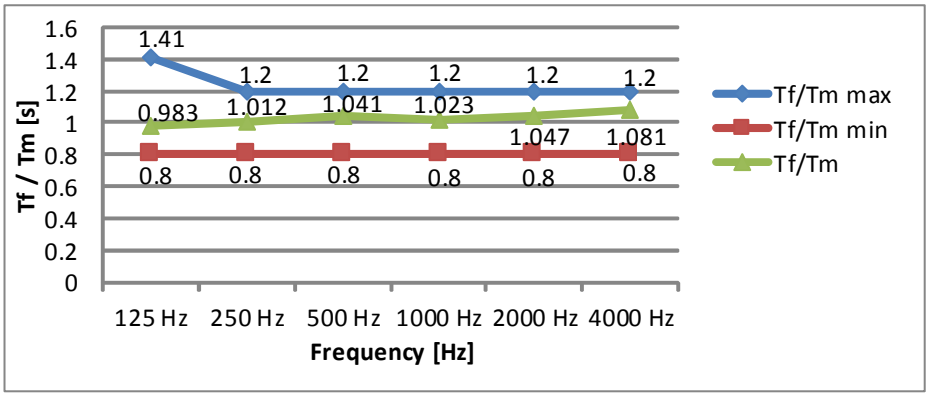

Fig. 8 Comparison of the T_f/T_m ratio to admissible values for the 50% occupied church

3.1.2 To replace the existing perforated panels in the ceiling

This solution consists in replacing the existing perforated panels in the ceiling with Gyptone Activ'Air Quattro 22 D2 panels and to double their surface by replacing several smooth panels. The ceiling Gyptone Activ'Air Quattro 22 D2 model has the dimensions 600x600x12.5 mm and its partial perforations are of 9x9 mm. It was found out that T_f/T_m ratio values made for the church without the public present and for the case of the 50% occupied church range within the limits provided by [1]. In Fig. 9 it is presented the case of the empty church.

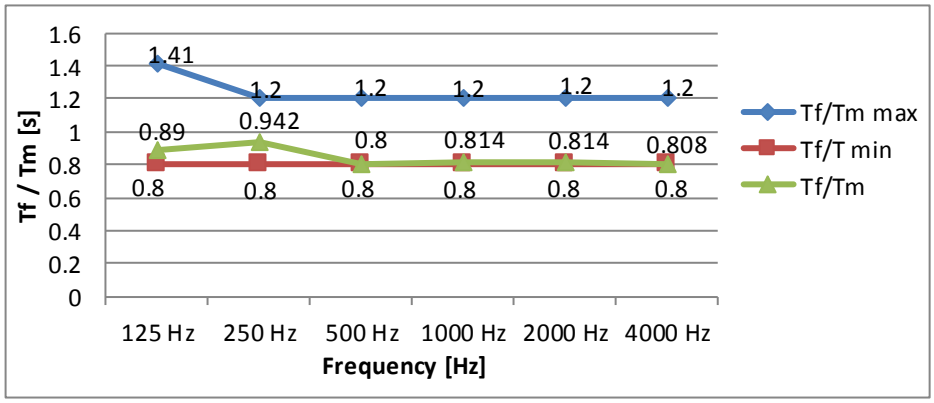

Fig. 9 Comparison of the T_f/T_m ratio to admissible values for the church without the public present

3.1.3 To replace all the panels in the ceiling

This solution consists in replacing all the panels in the ceiling with smooth Gyptone Base 31 D2 panels. It was found out that T_f/T_m ratio values made for the church without the public present (Fig. 10) and for the case of the 50% occupied church range in the limits provided by [1]. In Fig. 10 it is presented the case of the empty church.

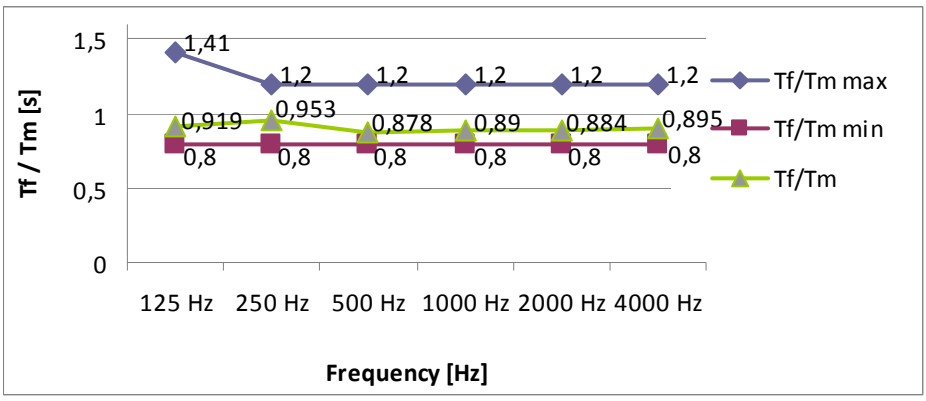

Fig. 10 Comparison of the T_f/T_m ratio to admissible values for the church without the public present

3.1.4 To replace the existing perforated panels with Gyptone Quattro 22 D2 panels, and to replace the existing smooth panels with smooth Gyptone Base 31 D2 panels

The T_f/T_m ratio values for this solution made for the church without the public present range in the limits of [1], but in the case of the 50% occupied church it was found out that T_f/T_m ratios do not range in the limits provided by [1]. It is for this reason that variant 3.1.4 was removed.

3.2 Investment costs analysis

The estimated costs to acoustically rehabilitate the church were made taking into account the price of the new smooth or perforated Gyptone panels and the labour costs for: plastering, washable paints, dismantling and mounting of the Gyptone panels. The total expenses were calculated in Euro (1Euro = 4.50 Lei) and are presented in Fig 11. They are as follows: 8405 Euro for the solution presented at 3.1.1, 11472 Euro for the solution presented at 3.1.2 and 11229 Euro for the solution presented at 3.1.3.

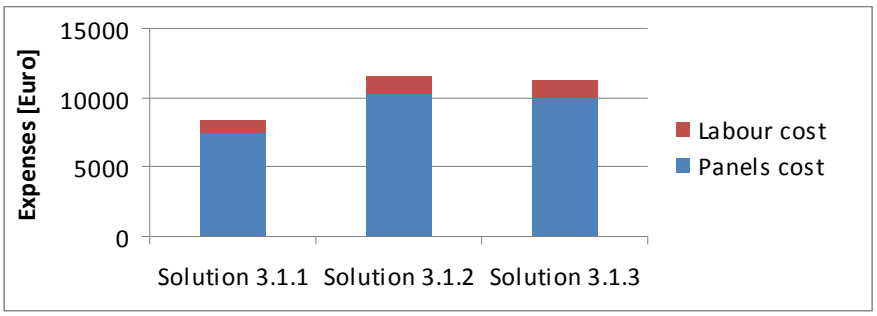

Fig. 11 Total expenses for the acoustic rehabilitation solutions

4 Conclusions

The case study concerns the "Betania" Pentecostal Church and the object of the research was to analyse the reverberation time and to propose solutions to improve the acoustic quality of the church. The first method of determining the reverberation time consisted in using a special acoustic measurement equipment of Bruel&Kjaer type. The results found in more reception points were investigated with the "Pulse" software. It was found that the values of the ratios T_f/T_m between the measured and calculated reverberation time T_f and the average reverberation time T_m are under the minimum necessary limit presented in [1]. The second research method consisted in calculating the reverberation time with the formula presented in [4]. During this process, all the surfaces defining the inner audition volume were measured. The process was laborious if we consider the complexity of the church architecture, the small volume of information on the noise-related features and absorption coefficients α_i of the materials used. Finally, values for the reverberation time were looked for, to be as close to the values obtained with the previous approach (and taken for real). It was quite difficult to decide upon the solutions for rehabilitation, if one takes into account the small values of the reverberation time. It was necessary to find materials with small values of the absorption coefficients α_i to increase the reverberation time so as to make ratios T_f/T_m frame within the admissible limits. In the end, the research results have been satisfactory as after the application of the church acoustic rehabilitation solutions, the new values of the reverberation time lead to ratios T_f/T_m framed among the admissible limits specified by [1]. The most inexpensive rehabilitation solution to improve the acoustic quality of the church is the solution presented at 3.1.1. It is important to perform, as early as the design stage, complex acoustic studies, as in [6], [7], [8], [9], [10], in the case of large size public audition rooms such as the mentioned church, to avoid additional finances to later on bring the buildings to the parameters of design norms. It is also necessary to add to the theoretical studies on the acoustic quality of a church, special "in situ" noise measurements, immediately after the building is erected, with high performance acoustic equipment to have an actual description of the building behaviour. Following such studies, if necessary, acoustic rehabilitation solutions should be made by following the advice of acousticians considering room geometry and the physical properties of all the finishing materials used and proposed for rehabilitation purposes.

References

[1] STAS 9783/0-83, Parameters for the acoustic design and control of public audition rooms.
[2] IS0 3382-1, 2009, Measurement of room acoustic parameters. Part 1: Performance spaces.
[3] Andreica, Horia-A., Munteanu, C. Muresanu, I. Moga, L., M., Tămaş-Gavrea, R. (2009). Construcţii civile (Civil Constructions), pp. 450-462, U. T. Press, ISBN 978-973-662-501-5.
[4] C125-2013, Norms related to the acoustics in construction and in urban zones.
[5] www.placo.fr/var/placo/storage/files/documentation/Guide_Gyptone_2015.
[6] Tamas-Gavrea, R., Munteanu, C. (2010). Elimination of the acoustical defects in auditoriums – treatment solutions, International scientific conference Civil Engineering and Urbanism "CIBv 2010", 12-13 November, Brasov, pp. 325-328, ISSN 1843 – 6617.
[7] Tamas-Gavrea, R., Fernea R., Munteanu, C., Stanca, S., Andreica, L. (2012). Church acoustic rehabilitation-a case study, Bulletin of the Polytechnic Institute of Jassy, Tomme:LVIII (LXII), Fascicle:4/2012, pp. 71-79, ISSN:1224-3884(p), ISSN:2068-4762(e).
[8] www.church-acoustics.com.
[9] www.acoustimac.com/churches.
[10] www.audimutesoundproofing.com/church-acoustics.

Shear Capacity for Masonry Walls Strengthened with FRP Materials

Partene E.[1], Petrus C.[2], Bindean A.[3], Fekete-Nagy L.[4], Stoian V.[5]

[1,2,3] PhD Student, Politehnica University Timisoara, Department of Civil Engineering (ROMANIA)
[4] Lecturer, Politehnica University Timisoara, Department of Civil Engineering (ROMANIA)
[5]Professor, Politehnica University Timisoara, Department of Civil Engineering (ROMANIA)
E-mails: eva.partene@student.upt.ro; cristian.petrus@student.upt.ro, andrei.bindean@student.upt.ro, luminita.fekete-nagy@upt.ro, valeriu.stoian@upt.ro

Abstract

This paper is focused on the experimental program that aims to determine the shear capacity of brick masonry walls, built up using ceramic blocks with vertical hollows. There are three type of walls subjected to cyclic in-plane horizontal loading with constant vertical loads. The purpose is to determine if the strengthened walls using FRP materials are capable to regain their initial shear capacity and furthermore, to determine if the strengthening solution is efficient for this type of walls. Also the three types of walls of unreinforced masonry and reinforced masonry, where tested to see the difference between them and to see if the reinforced concrete has an important influence to the shear capacity of the walls.

Keywords: masonry walls, cyclic in-plane loads, FRP materials, strengthened.

1 Introduction

Masonry structures are a significant portion of the world's heritage buildings and a significant component of the modern residential building stock. Particularly this type of structures is susceptible to damage from seismic horizontal loading [1]. In Romania, many of these structures, located in seismic areas are built without any reference to seismic design rules. Therefore the need for new strengthening technologies is essential [2].

The traditional strengthening methods available today, such as steel plate bonding, steel frame works, welded mesh, shotcrete jacketing, have disadvantages such as adding considerable mass to the structure, are labour intensive, need creating work space and access limitations, and the most important disadvantage is the aesthetics of the building. Therefore the use of fibre reinforced polymers (FRP) has gained much attention. [1]

The advantages of FRP retrofitting solutions are: high strength at low weights, ease of application, requires minor preparation, preserves the material integrity and has high resistance to corrosion over existing conventional techniques [3]. Numerous studies are conducted for the assessment of the behaviour of the masonry walls strengthened using FRP materials, including our experimental program [4].

2 Experimental program

The experimental tests were performed on three types of masonry walls (L x l x b=1500 x 1500 x 250 mm): unreinforced masonry and reinforced masonry with concrete columns on both sides or concrete column in the middle (Fig. 1). The walls were subjected to constant vertical load which was determined assuming the walls were a part of a four storey building. In order to determine the shear capacity of the walls, they were subjected also to horizontal cyclic loads, which were increased using displacement control. The experimental stand was built up having this loading scheme in mind and has the next components: a reaction frame for the vertical loads, a reaction frame for the horizontal loads and a sliding frame for transmitting the horizontal loads to the walls (Fig. 2).

The walls were tested in bear state and then tested again after applying the strengthening solution with FRP materials. In this paper we will focus on the results of the second part of the experimental tests.

The strengthening consists in the application, on both sides of the wall, of a FRP mesh following the two diagonals, where the most of the crack appeared on the walls. The FRP mesh was applied using thixotropic resin.

The strengthening solutions were applied on the damaged structures in order to evaluate the enhancement of the structural response of the masonry walls due to the application of FRP materials [5].

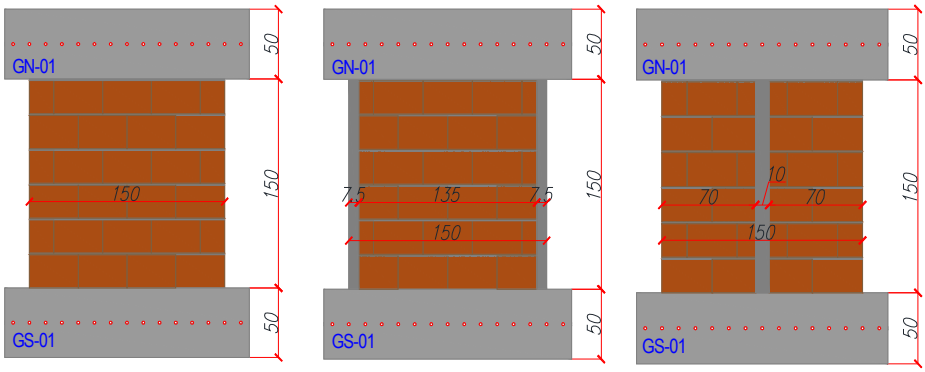

Fig. 1 Wall specimens in bear state (URM, RM1 and RM2)

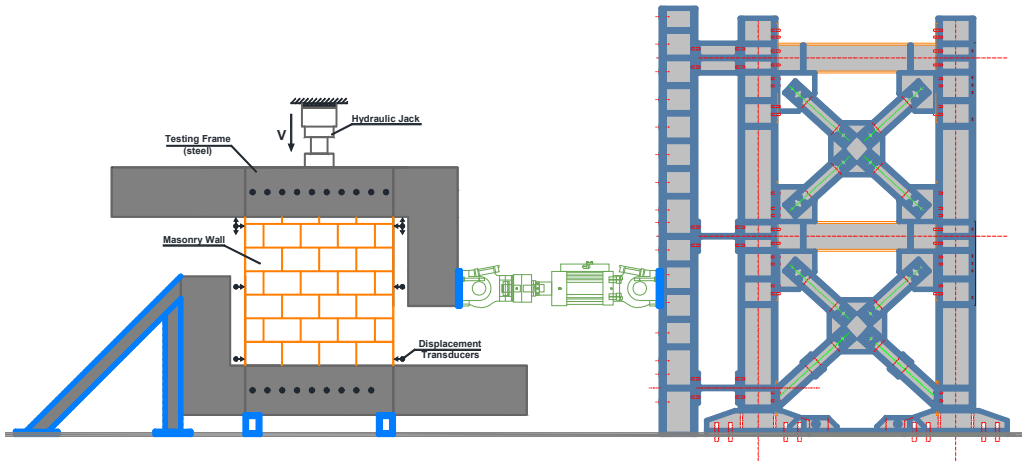

Fig. 2 Experimental stand – loading scheme

3 Experimental results. Conclusions

As mentioned before, the test specimens were subjected to lateral cyclic horizontal loads, while maintaining a constant vertical load. The wall in bear state failed in the classical shear mode with diagonal cracking on both directions, in head and bed joints or in the ceramic blocks. All the specimens had their first cracks in head and bed mortar joints, which lead to an increasement of the horizontal displacements. The tests were performed until the sudden fail along the diagonals of the walls. The strengthened walls had a fragile failure with the splitting of the FRP mesh and the peeling of the blocks. The failure occurred with prediction and it wasn't aggressive (Fig. 3, 4 and 5). [6]

Fig. 3 Failure mode for URM1-C [6]

Fig. 4 Failure mode for RM1-C [6]

Fig. 5 Failure mode for RM2-C [6]

The load-displacement diagrams for the three wall specimen types can be seen in Fig. 6, 7 and 8 [6].

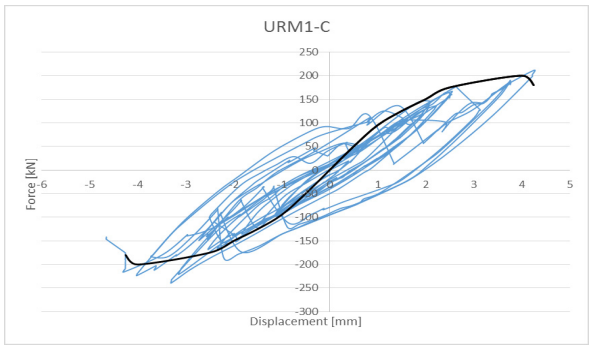

Fig. 6 Force-Displacement diagram for URM-C [6]

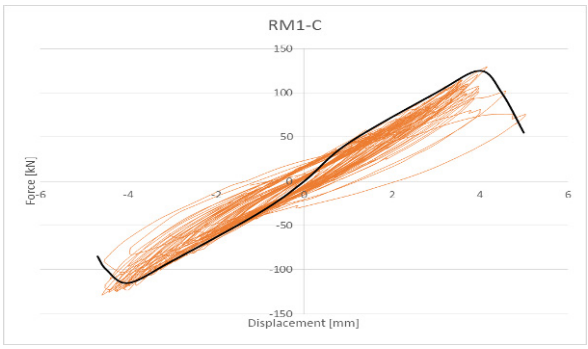

Fig. 7 Force-Displacement diagram for RM1-C [6]

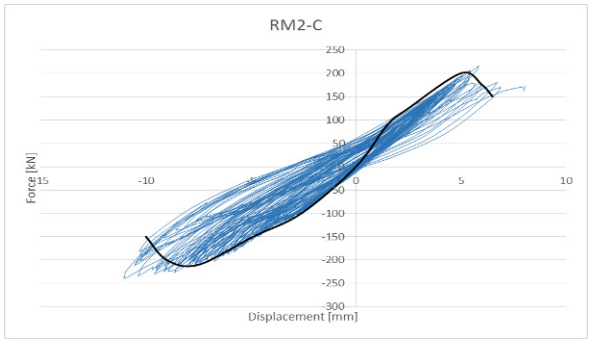

Fig. 8 Force-Displacement diagram for RM2-C [6]

The experimental program was conducted to observe the effectiveness of retrofitting damaged masonry walls, built-up using ceramic blocks with vertical hollows and strengthened using FRP materials.

The following conclusions can be drawn from this experimental study:

- The failure mode for the masonry walls was pure shear failure namely diagonal cracking.
- The displacement capacity of the walls was increased, first due to the reinforcement of masonry and second due to the strengthening of the damaged walls using FRP materials.

- The strengthening of the walls was successful also by restoring the maximum loads of the walls in their initial state and in some cases it was increased (Fig. 9).
- The strengthened walls had greater ability for energy dissipation then the walls in bear state.

The test results show the effectiveness of the FRP mesh used for strengthening masonry walls, by being able to regain the initial wall capacity, before they suffered damage from cyclic in-plane loading which is consistent with seismic loading. By been able to regain the initial capacity, the structure will be able to sustain another horizontal cyclic loading.

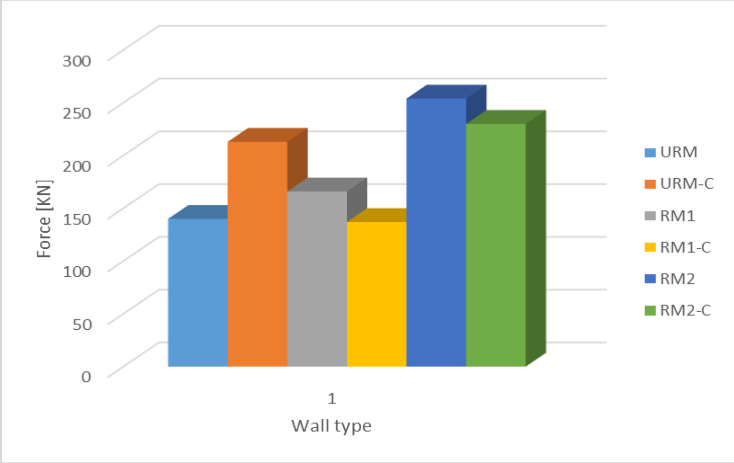

Fig. 9 Maximum horizontal load applied for the experimental tests [6]

Further experimental tests will be performed in our Research Department, in order to obtain more results for different configurations of masonry walls, using different materials and different strengthening methods.

References

[1] Griffith, M., Kashyap, J., Ali, M. (2012). Flexural displacement response of NSM FRP retrofitted masonry walls. Construction and Building Materials.

[2] Dogariu, A. (2009). Seismic retrofitting techniques based on metallic materials of RC and/or masonry buildings. PhD Thesis Volumes.

[3] Elgawady, M., Lestuzzi, P., Abardoux, M. (2006). Shear strength of URM walls retrofitted using FRP. Engineering Structures 26, pp. 1658-1670.

[4] Partene, E., Stoian, V., Bindean, A., Fekete-Nagy, L. (2015). Strengthening of masonry walls using Fiber Reinforced Polymer (FRP) Materials. Key Engineering Materials 660, pp. 198-201.

[5] Cancelliere, I., Imbimbo, M., Sacco, E. (2010). Experimental tests and numerical modelling of reinforced masonry arches. Engineering Structures 32, pp. 776-792.

[6] Partene, E., Bindean, A., Stoian V., Fekete-Nagy, L. (2015). Evaluation of shear capacity for masonry walls strengthened using fibre reinforced polymers. FRPRCS-12 & APFIS-2015.

Effect of Consolidating Materials on the Out of Plane Behaviour of Masonry Infills. A Design Approach

Petruş C.[1], Partene E.[1], Moşoarcă M.[2], Stoian V.[1]

[1] *Politehnica University of Timişoara, Faculty of Civil Engineering (ROMANIA)*
[2] *Politehnica University of Timişoara, Faculty of Architecture and Urban Planning (ROMANIA)*
E-mails: Cristian.petrus@student.upt.ro, eva.partene@student.upt.ro, valeriu.stoian@upt.ro, marius.mosoarca@upt.ro

Abstract

The importance of design for masonry infill walls situated in reinforced concrete frames has been highlighted after the important damages recorded by non-structural elements after the recent earthquakes. To the out of plane failure of masonry infills have been attributed a lot financial and human life loss. In this paper there are presented the results of experimental analysis performed on three types of masonry infill walls: a reference wall, a wall consolidated with a mesh of aramid fibre embedded in a one sided mortar grout, and a wall consolidated with polypropylene strips placed in order to overtake vertical bending. The proposed consolidation solutions are advantageous since they can be applied on the surface of the exterior walls without affecting the ongoing activities inside the building. Based on analytical investigations in correlation with the experimental results, some stiffness reduction factors are proposed for the masonry infills in order to perform fast linear analysis, valuable for structural designers. Analysing a typical reinforced concrete frame building, the validity of these factors was confirmed in terms of seismic forces and displacements occurring in its masonry infill walls.

Keywords: masonry infills, out of plane seismic behaviour, aramid mesh, polypropylene bands.

1 Introduction

A series of drawbacks related to the structural performance and design of masonry infill walls were observed after the recent earthquakes. In plane and out of plane behaviour of these walls impact also the reinforced concrete frame structures in which they are found. Previous earthquakes highlighted the negative effects of using masonry infill walls in framed structures, such as the soft-storey effect or out of plane collapse of the infill and veneer walls. Currently there is a lot of research being performed in order to improve these systems and aim to minimize the structural and non-structural damages occurring in frame buildings with masonry infills in order to limit financial and human losses. The research program "Innovative Systems of Earthquake Resistant Masonry Enclosures in Reinforced Concrete Buildings" aims to complete the lacking code provisions for masonry infill walls [1]. Research related to a one-sided placement of consolidating materials on masonry infill walls indicated an increase of the out of plane bearing capacity of these walls and indicated a clear advantage for infills in buildings situated in seismic zones [2].

2 Experimental testing

2.1 *Test setup*

Three types of infill walls were analysed at real scale using displacement control monitored in the centre of the wall. The tested specimens had a height of H=3.5m, length L=2.65m and width t=0.25m with an H/L ratio of 1.32 and H/t ratio of 14. The specimens were constructed using materials available on the market. By not providing a connection to the columns of the test frame, it was possible to study solely the out-of-plane behaviour coming from bending. The models were constructed simply supported at the bottom part, over a levelling layer of mortar and at the superior part there were provided wooden wedges between the ceramic blocks and the steel test frame. By means of horizontal steel brackets connected by metal rods to the test specimens, a cyclic motion was applied in order to simulate the seismic action. A plan view of the experimental test stand can be seen in Fig. 1a, while Fig. 1b shows the constructed specimen. Nine measurement points were

placed on the surface of the test specimen in order to monitor the out of plane displacement, as it can be seen in Fig. 2a. A cyclic alternant motion with three loading cycles for each step was applied in displacement control, as it can be seen in the loading protocol from Fig. 2b up to a value for the interstory drift of 2.5%. Ceramic blocks with 53% volume of holes with the dimensions of 375x250x238 (length, width, height) were used for the construction of the test specimens. According to the technical sheets provided from the ceramic block producer, the materials had a minimum compressive resistance of 10 N/mm2. For the horizontal joints and mortar pockets of the ceramic blocks, M5 pre-dosed mortar was used, having a compressive resistance of 5 N/mm2. The experimental testing was carried out in displacement control using a differential actuator [3].

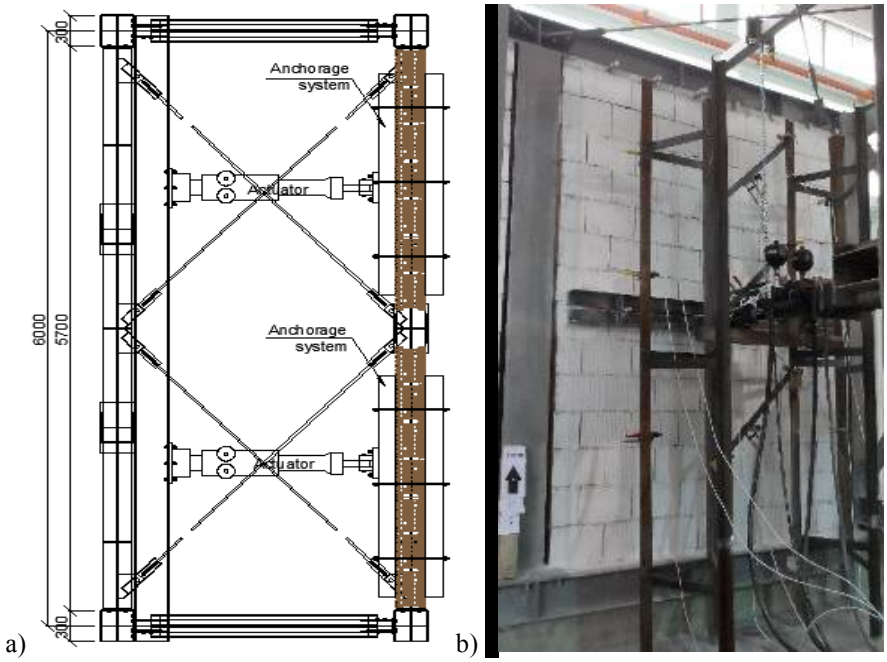

Fig. 1 Test setup for masonry infill wall panels: a) Plan view; b) Test specimen

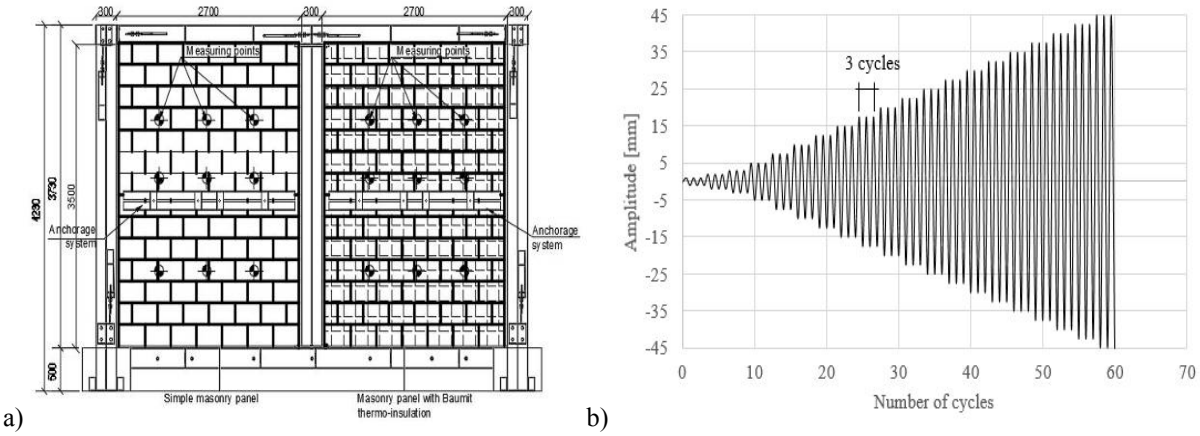

Fig. 2 a) Out-of-plane measuring points of infill panels; b) Loading protocol

2.2 Experimental results

A reference wall (denoted MW1) was constructed without having any consolidating materials, Fig. 3a, just to serve as a comparison standard for the other specimens constructed in the same manner and subjected by the same loading protocol. Using the differential actuator, an out of plane displacement was applied to the wall both in pushing and pulling state, up to a displacement of 45mm corresponding to a 2.5% interstory drift. A maximum force of 56.6 kN was recorder at a displacement of 45 mm, as it can be seen in the graph from Fig. 4a.

First cracks appeared in the middle horizontal joint at a displacement of 10 mm, followed by cracks at the base and top side of the specimen, indicating the formation of an arching mechanism in the infill wall.

A consolidation of MW1 with an exterior one sided reinforced grout with an aramid fibre mesh was applied in order to form the infill specimen denoted MW3. Surface connectors composed by plastic elements inserted in predrilled holes, filled with fluid mortar together with strips of aramid mesh ensured a good transfer of loads from the infill wall to the consolidating materials, Fig 3b.

According to the producer, the tensile resistance of the aramid mesh on the direction of the aramid was 1700 N/mm2, while perpendicular to the aramid, along the glass fibre used to weave the aramid was 1160 N/mm2. An overlap of the mesh of 10cm was applied in order to have a continuous material over the entire surface of the infill specimen subjected to out of plane bending. First cracks appeared at a displacement of 7.5mm in the middle horizontal joint, while at a displacement of 17.5mm at a force of 35.8kN the aramid mesh was broken indicating a drop in load capacity which is observable in the graph from Fig. 4b. Following the failure of the aramid mesh, an increase of the load capacity to 38.5kN of the infill specimen was observed up to 37.5mm when after the 2nd and 3rd loading cycles this capacity dropped significantly. This behaviour suggests two different working stages of the specimen, a composite one when the masonry works together with the aramid mesh up to its failure, and a simple masonry section when the load capacity no longer increases after the capacity of the masonry infill is reached.

Infill test specimen MW4 represents also a one sided consolidation measure using strips of polypropylene bands placed vertically on the surface of the wall in order to overtake vertical bending. The connection of these strips was done by means of mechanical anchors and surface connectors as in the case of MW3, using plastic elements with strips of aramid mesh inserted in predrilled holes which are later filled with fluid mortar. There were used 27 strips of polypropylene bands placed at a distance of 10cm from each other, as it can be seen in Fig. 3c. Strain gauges placed on the bands indicated the presence of tensile force in the material, but the yield limit of 213 N/mm2 as indicated by the producer was not reached, hence no rupture of the bands was observed. The maximum force recorded at a drift of 2.5% was 43.99 kN, as it can be seen in the graph from Fig. 4c.

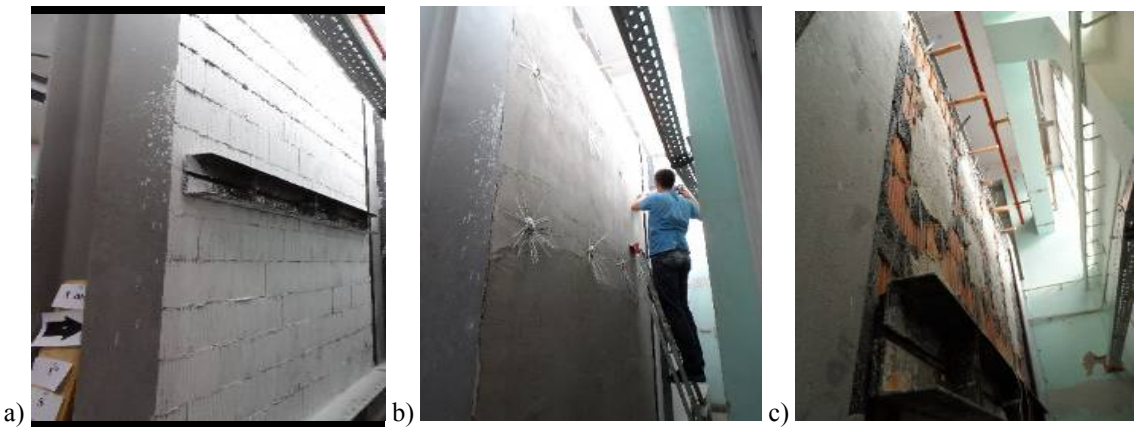

Fig. 3 Infill wall a) MW1; b) MW3; c) MW4

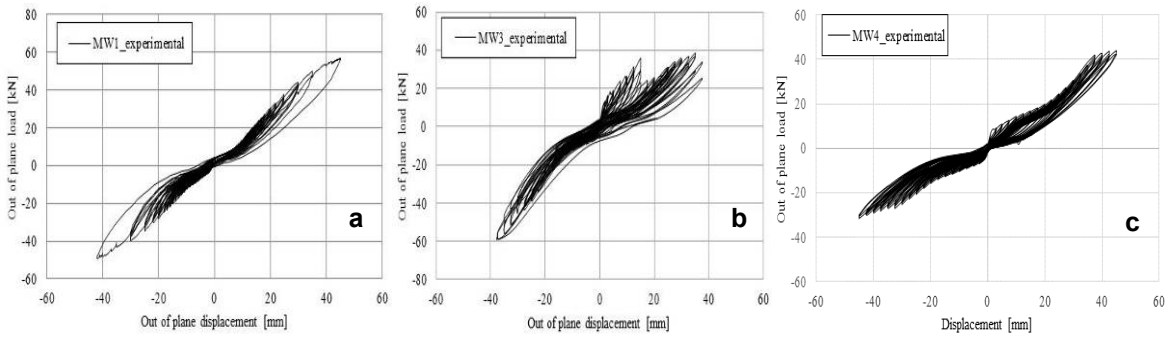

Fig. 4 Force displacement diagram for infill wall a) MW1; b) MW3; c) MW4

3 Analytic evaluation of out of plane resistance

Masonry infills are regarded by the Romanian seismic design code and the Romanian masonry design code as being non-structural elements [4]. These elements proved to have a structural behaviour which can have an effect on the overall structural behaviour of the buildings in which they are placed [5]. Following the formulae given in the Romanian design codes, based on calculations provided by Mosoarca et al. [6], the ultimate force on a meter length of the infill wall which occurs in specimen MW1 can be evaluated at Fu = 21.34 kN. In terms of equivalent pressure, this translates to a value of qu = 12.2 kN/m2. Using the same principles stated in the aforementioned research paper, one can evaluate the ultimate forces for the other two specimens, MW3 and MW4 respectively. For MW3, Fu = 19.50 kN and qu = 11.14 kN/m2, and for MW4 Fu = 16.60 kN and qu = 9.48 kN/m2.

A proposal has been made by Haseltine et al. [7] in order to evaluate the maximum lateral pressure for masonry infill walls in function of the flexural tensile strength fkx = 126 kN/m2 orthogonal to the bed joints in formula (1), in which "a" is a coefficient related to the geometry of the infill panel having a value of 0.081 for the investigated masonry infill specimens and "h" and "t" refer to the height of the specimen and thickness respectively. The maximum lateral pressure determined by Hendry & Kheir [8] on a meter length of masonry panel was evaluated using the compression level σ0 = 28 kN/m2 present in the masonry infill with formula (2). Using the compressive strength of the masonry f'm = 0.538σcb + 0.241σcm McDowell et al. [9] determined the maximum lateral pressure accounting for the arching mechanism with formula (3).

A simple formula was proposed by FEMA 356 [10] for the lateral pressure, depending on the h/t ratio λ2 = 0.03 and using the compressive strength of the masonry taking into consideration the presence of vertical reinforcement, formula (4).For reinforced masonry with vertical bars, Morandi et al. [11] proposes formula (5), in which As is the total cross sectional area of the vertical reinforcement in tension, fy is the yield strength of the reinforcement and the other parameters refer to the geometrical characteristics of the infill panels. Formulas are given in Table 1.

Table 1. Formulation and evaluation of out of plane infill wall resistance

Formula	1 (Haseltine)	2 (Hendry)	3 (McDowell)	4 (FEMA)	5 (Morandi)
Equation	$q_u = \frac{f_{kx}}{6a\left(\frac{h}{t}\right)^2}$	$q_u = 8\frac{\sigma_0}{\left(\frac{h}{t}\right)^2}$	$q_u = \gamma\frac{f'_m}{2\left(\frac{h}{t}\right)^2}$	$q_u = \frac{0.7f'_m\lambda_2}{\left(\frac{h}{t}\right)}$	$q_u = 8\frac{0.9t_w A_s f_y}{\gamma_s h_w^2}$
q_u [kN/m^2]	10.47	1.16	10.24	10.16	11.26

As it can be seen in the previous table, there are some overestimations and underestimations for the tested specimens MW3 and MW4.

This could be explained due to the presence of the reinforcing material which is difficult to have its characteristics and influence evaluated when subjected to out of plane seismic actions. The challenges these formulas present for the fast macro-modelling of the out of plane response of masonry infills have been studied also by Asteris et al. [12].

4 Case study

In order to study the effect of the new proposed systems of masonry infill walls on real buildings, a configuration for a prototype reinforced concrete building was proposed. This chosen building is a 6 storey frame building with three bays of 5.0m and three spans of 5.0m, 2.0m, and 5.0m respectively. The storey height is chosen as 3.0m, giving a total height of the building of 18.0m. A current frame is chosen as the reference frame to be analysed. Various layouts of the masonry infills are presented in Table 2, as the most common types used in typical reinforced concrete frame buildings. A valuable tool for structural designers is given by the interstory drift, which can give pertinent information related to the out of plane solicitations of masonry infills. Fast calculations of this interstory drift can be achieved by performing linear analysis of the given structure under various values of the peak ground acceleration.

Table 2. Different arrangement of masonry infill walls

Type	1	2	3	4	5	6
Masonry infill layout	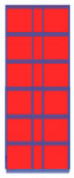	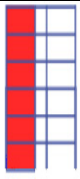	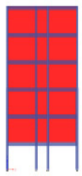	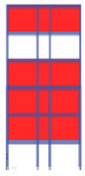	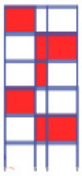	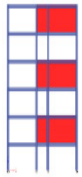

A 3D linear elastic analysis of the structure under seismic actions with different positioning of the infill walls was performed with ETABS software [13] for different types of peak ground acceleration ranging from ag = 0.10g to ag = 0.35g. The study was made for the masonry infill specimens MW1, MW3 and MW4, representing composite walls composed from two materials: masonry and consolidating materials (aramid mesh, polypropylene bands). In order to simplify the analysis and computation process, some assumptions were made for the material characteristics of the masonry infill walls.

For specimen MW1, it was defined a shell section of 250mm thickness, having the stiffness reduced by a factor of 0.5, a density of 8 kN/m3, modulus of elasticity E=800 N/mm2, Poisson's ration υ = 0.092 and compressive strength σ = 10 N/mm2. For specimen MW3, the same characteristics were kept, only modifying the reduction of stiffness from 0.5 to 0.35, and the modulus of elasticity E=1600 N/mm2. Specimen MW4 had the stiffness reduced by a factor of 0.4 and a modulus of elasticity E=1300 N/mm2, while keeping all the other characteristics similar to the first two specimens. The stiffness reduction made for moment and shear solicitations for each type of infill wall corresponds to a 2.5% interstory drift and was obtained by a simplified method. To analyse only the out of plane effect, a gap of 2 cm between the frame columns and the infill masonry walls was considered. The stiffness of the reinforced concrete frame members was reduced by 50% in order not to affect the out of plane behaviour of the infills.

Results obtained from this analysis can be observed in Fig. 5-6 for all masonry infill types MW1, MW3 and MW4, for peak ground accelerations of 0.1g, 0.25g and 0.35g for different layouts of the masonry infills within a reinforced concrete frame building.

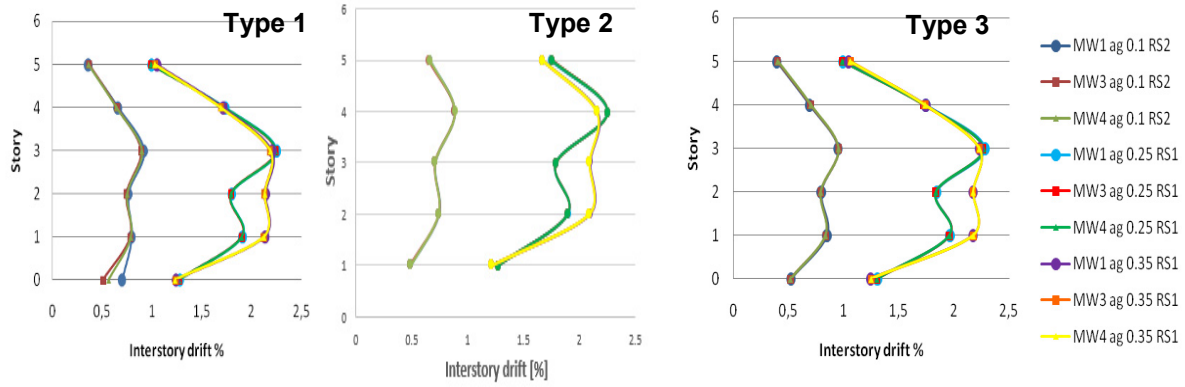

Fig. 5. Variation of interstory drift for MW1, MW3 and MW4 for 0.1g, .25g and 0.35g – Type 1, 2 and 3

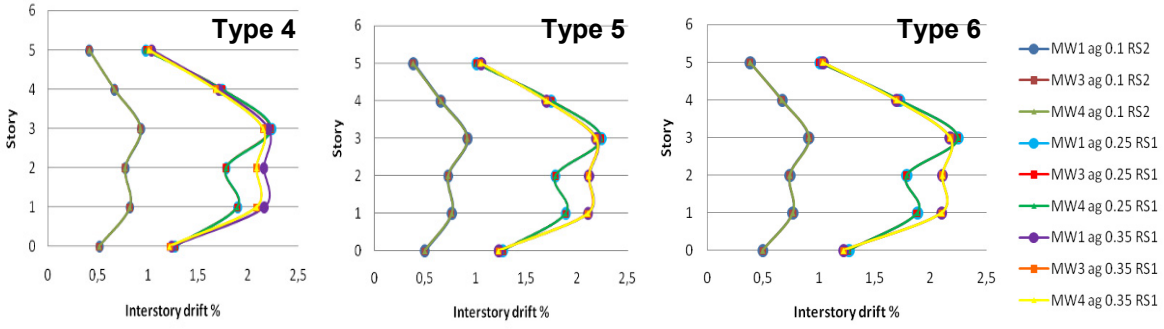

Fig. 6. Variation of interstory drift for MW1, MW3 and MW4 for 0.1g, .25g and 0.35g – Type 4, 5 and 6

As it can be observed in the graphs presented above, the maximum differences occur at the first levels, in the case of low-rise reinforced concrete buildings, highlighting the importance of careful design of such type of infill walls. The infill walls were introduced in the analysis with reduced stiffness determined for ultimate limit state in order to have comparative values of the forces occurring in the infill when compared to the results obtained from experiments from laboratory testing and numerical modelling.

The values of the stiffness reduction of these infills are presented in Table 3, and they represent a quick tool for the structural designers when designing masonry infills in reinforced concrete frame structures. For the analysed masonry specimens, some limit states of the interstory drift were established at 0.3%, 0.5%, 1.0%, 2.0% and at the ultimate 2.5% drift.

These values were based on the capacities of the testing equipment in the laboratory, where it was difficult to obtain values larger than 2.5% drift in alternant direction (push-pull). Evaluating the forces occurring over a unit meter length of the masonry wall, comparative values are presented in Fig. 7 for the analysed specimens MW1, MW3 and MW4.

Table 3. Stiffness reduction for different values of interstory drift

Drift [%]	Model	MW1			MW3			MW4		
		P [kN]	Δ [mm]	Stiff. Red. [%]	P [kN]	Δ [mm]	Stiff. Red. [%]	P [kN]	Δ [mm]	Stiff. Red. [%]
2.5	Bare frame	21.4	45.6	50	19.5	45.4	35	16.6	44.0	40
	Numerical	20.4	45.0	-	-	-	-	17.1	45.0	-
	Experimental	21.4	45.0	-	-	-	-	16.6	45.0	-
2.0	Bare frame	18.8	35.3	57	16.0	35.5	35	13.5	35.8	40
	Numerical	18.4	36.0	-	19.6	36.0	-	15.8	36.0	-
	Experimental	18.8	35.0	-	14.5	35.0	-	14.1	35.0	-
1.0	Bare frame	9.7	17.2	60	10.7	17.4	48	6.7	17.7	40
	Numerical	11.5	18.0	-	14.6	18.0	-	9.5	18.0	-
	Experimental	9.7	17.0	-	9.2	17.5	-	6.8	17.5	-
0.5	Bare frame	5.1	9.9	55	10.0	10.2	55	5.2	10.	55
	Numerical	13.5	9.1	-	10.3	10.0	-	6.1	9.0	-
	Experimental	5.1	10.0	-	10.0	10.0	-	5.2	10.0	-
0.3	Bare frame	2.7	4.9	60	7.2	5.2	60	3.0	5.3	60
	Numerical	3.4	4.5	-	6.1	4.0	-	3.2	4.5	-
	Experimental	2.7	5.0	-	6.0	5.0	-	3.9	5.0	-

Using the proposed values of the stiffness reduction for the masonry infills obtained from the linear analysis, we can compare in terms of force-displacement, the results obtained from experimental and numerical analysis. Observing the graphs presented in Fig. 7, we can observe a good correlation of these values for all the studied masonry infill specimens.

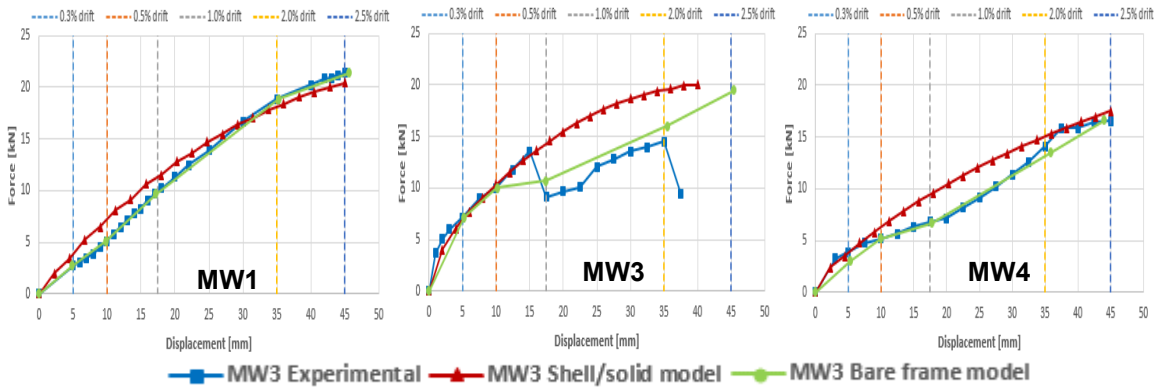

Fig. 7 Force displacement diagram for infill wall panels MW1, MW3 and MW4: experimental, numerical and bare frame model

5 Conclusions

A simplified analysis method for identifying the effect of frame structure on infill walls at out of plane seismic actions in ULS is proposed. This analysis is an easy and quick 3D linear analysis, which can be used by structural designers. Based on the results of experimental analysis, the mode of interaction between the structure and infill walls as well as the damage state of the walls can be determined in function of the value of interstory drift. All the models did not exceed the maximum value of interstory drift of 2.5% so it can be stated that the walls will suffer important deformations and damages at the mid height but will not collapse. The proposed method was verified with the values of loads and horizontal displacements obtained at experimental tests and numerical analyses. In all the studied analytical formulas, the slenderness of the wall (h/t) is a very important factor, which must have correction factors applied in order to account for the reinforcing materials and for the building-infill wall interaction. Further investigations of this parameter must be made in order to obtain calculation methods which can be used by structural designers.

6 Acknowledgement

This project has received funding from the European Union's Seventh Framework Programme for research, technological development and demonstration under grant agreement No 606229. Special thanks also go to the Romanian representatives from Baumit and Kerakoll companies for their material and technical support, and for Eng. Marius Niculescu from H.I. STRUCT design office for his support in the development of this research.

References

[1] da Porto, F. Verlato, N. Guidi, G. Modena, C. (2016). The INSYSME project: Innovative construction systems for earthquake resistant masonry infill walls, 16th International Brick and Block Masonry Conference, Padova, June 26-30, pp. 1173-1178.

[2] Moşoarcă, M. Petruş, C. Stoian, V. Anastasiadis, A. (2016). Behaviour of masonry infills subjected to out of plane seismic actions. Part 2: Experimental testing, 16th International Brick and Block Masonry Conference, Padova, June 26-30. pp. 1293-1299.

[3] Petruş, C. Stoian, V. Moşoarcă, M. Anastasiadis, A. (2015). Reinforced concrete frames with masonry infills. Out of plane experimental investigation. Acta Technica Napocensis: Civil Engineering & Architecture 58(3).

[4] Petrovici, R. (2015). Seismic Design of Structural and Non-Structural Masonry Elements, AICPS Journal Revie 1-2, pp. 102-103.

[5] Petrovici, R. (2013). Design of Buildings for ``Frequent`` Earthquakes, AICPS Journal Review 1-2, pp. 76-77.

[6] Moşoarcă, M. Petruş, C. Stoian, V. Anastasiadis, A. (2016). Behaviour of masonry infills subjected to out of plane seismic actions. Part 1: Theoretical analysis, 16th International Brick and Block Masonry Conference, Padova, June 26-30, pp. 1283-1291.
[7] Haseltine, BA. West, HWH. Tutt, JN. (1977). Design of walls to resist lateral loads, Journal of Structural Engineering, 55(10):422–30.
[8] Hendry, AW. Kheir, AMA. (1976). The lateral strength of certain brickwork panels, Proceedings of the fourth international brick masonry conference, Bruges, Belgium.
[9] McDowell, EL. McKee, KE. Sevin, E. (1956). Discussion of arching action theory of masonry walls, Proceedings of American Society of Civil Engineering, Journal of Structural Division pp. 1067, pp. 27–40.
[10] FEMA 356 – Prestandard and commentary for the seismic rehabilitation of buildings – Federal Emergency Management Agency, November 2000.
[11] Morandi, P. Hak, S. Magenes, G. (2013). Simplified out-of-plane resistance verification for slender clay masonry infills in RC frames, 15th ANIDIS Convention of Seismic Engineering in Italy, Padova, 30 June – 04 July.
[12] Asteris, PG. Cavaleri, L. Di Trapani, F. Tsaris, AK. (2017). Numerical modelling of out-of-plane response of infilled frames: State of the art and future challenges for the equivalent strut macromodels, Engineering Structures, No. 132, pp. 110-122.
[13] ETABS 2015 – Computers & Structures Inc. – User's guide Etabs, Integrated Building Design Software.

Rehabilitation of a (Traditional) Vernacular House in Burzuc Village

Pop Maria T.[1], Lepădatu D.[2]

[1] *University of Oradea, Faculty of Civil Engineering, Cadastre and Architecture, Department of Civil Engineering,, 4 B.St. Delavrancea St., 410085 Oradea* (*ROMANIA*)
[2] *University of Oradea, Faculty of Civil Engineering, Cadastre and Architecture, Department of Cadastre and Architecture,, 4 B.St. Delavrancea St., 410085 Oradea* (*ROMANIA*)
E-mails: pop.maria.ria@gmail.com, danlep58@yahoo.com

Abstract

Rammed earth structures have a long tradition in Romania – i.e., earth was one of the main raw materials used in construction. In the post-war period, for example, earth compensated for the lack of resistant construction materials, especially in rural areas. Today, however, modern construction materials manufactured at industrial scale are increasingly replacing earth.

The use of earth as a construction material has several advantages. These advantages include high ecological value (reusability, environment friendliness), easy handling and a beneficial impact upon human health, as evidenced in time. Moreover, it is a raw material that can be extracted without harming the environment, its processing does not require power consumption, and the preparation work can be performed in-house [1].

This paper presents the rehabilitation (consolidation) solution of a house located at street address no. 178 in the vernacular village of Burzuc. The house was built in approximately 1950; its foundations are made of stone masonry and its structural frame of adobe. The house has deep cracks in the structural wall of the main façade.

Keywords: house, adobe, wall, hypothesis, solution.

1 Summary

Earth-based construction materials remain adequate for a variety of purposes because they entail lower power consumption during the construction works. Because many homes in rural areas have their supporting structure made of earth, their masonry often cracks. Such shortcomings are typically remedied using modern construction materials. While the latter approach does fix the cracks, its overall impact is negative since the bond between the two different types of materials stays unresolved.

Today, houses made of earth (their structures) are no longer up to the construction and design standards and requirements. Hence, the need for consolidation via various means, including construction elements made of earth. When using the latter, one should pay a special attention to bad weather conditions and humidity throughout their construction works and their use thereof.

2 Preamble

In the transition from the rural to the urban house, the novelty lies in the porch – i.e., the porch is enclosed with a glass surface mounted on a grid-like wooden frame, which is called ‘glazing’ (see Fig. 1 for the ground floor survey).

Architect Constantin Joja rightly notes the unfortunate lack of interest of his contemporaries, be they architects or critics, in the Romanian architectural heritage, the whole and true meaning of which he reveals to his readers as follows: "Demolished or hidden in the lateral yards, the authentic urban houses had vanished from the architectural landscape of the street to such an extent that, since 1888, the architects had felt the need to reinsert in the cities a style inspired by rural architecture, and by fortified tower dwellings and churches. The struggle led by Mincu and the Neo-Romanian School, whose results are still valid a century later, today, was a praiseworthy act of heroism. True urban architecture was still not properly understood and analysed. There were too many preconceived opinions which lay heavy thereon and prevented its being re-evaluated: it was deemed to be a "Balcanism", a minor artwork, a weak structure, wood and glass, shingle roof, glazing." [2]

We deem Joja's book and remark important for the current discussion as the house in Burzuc, the subject of this paper, bears an obvious resemblance to the traits noticed by the architect. There are, however, a few differences too, described hereafter.

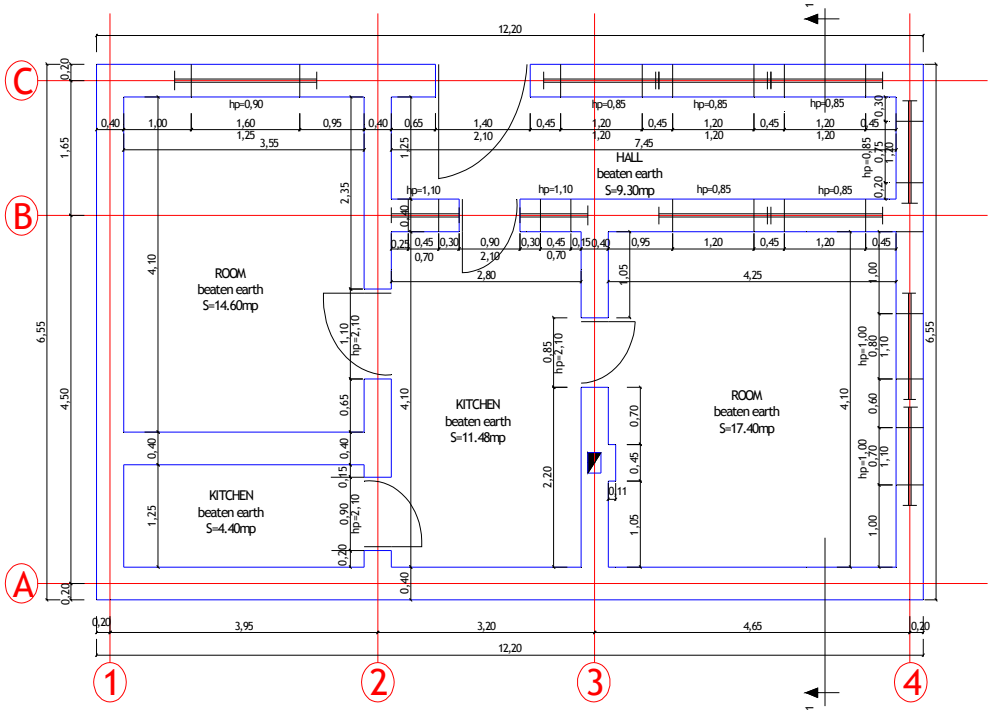

Fig. 1 Ground floor

The house presented in this paper, part of traditional houses stock in the area, is located in the village of Burzuc, Bihor County and has a lifespan of about 65 years. The house was uninhabited for over 10 years and the vegetation around it has expanded widely. Grooves and pipes are damaged and the water runs down the walls. Although the house was placed on a soil predisposed to settlement, the house enjoyed a smart location. It is positioned on top of the hill and the terrain is downhill next to it. The type of terrain on which the house is placed is contractile clay.

Fig. 2 Main façade

In terms of damage there are a few noticeable cracks. The meteoric water, systematically seeping the house wall and washing and infiltrating into its foundations, caused the cracks in the main façade. In dry periods

the foundation clay layer dried while in the rainy times it swelled up (See Fig. 2 below). The other structural walls show no sign of cracking. A further complication is the presence of a fruit tree (plum) placed just 1.0 m away from the wall of the house. Tree roots have penetrated below the foundations and with the contribution of the water dislodged the foundation masonry stone.

The dimensions of the indoor walls are 40.0 cm. Small openings cracks of 0.5 cm are present at the intersections between the structural and compartments walls.

Given the above, the first proposed intervention is to remove the cause of the problem, namely the tree. After cutting the tree, the repair of gutter and pipes should follow.

Next, the house's masonry should be addressed. The masonry, made of adobe, encompasses the full height of elbow rest. Its dimensions are between 2.0cm and 3.0cm for the opening and 1.0cm for height. Hence, for crack filling, we propose the preparation and making use of the following mixture:

8 shares of earth (clay) + 4 shares of sand + 1 share of Portland cement (CEM II)

In dry conditions they will mix with water until reaching the stage of a quasi-solid paste [1] .

The earth (clay) for the works can be taken from the outbuilding located in the courtyard and it can be ground and dried to gain a similar grip as the earth that makes up the house's original structural frame. Formworks should also be made. Hence, sections lacking grip around the cracks should first be cleaned and removed; next, the edges should be wet and the paste prepared should be poured in two layers of 15cm and 18cm, respectively. Finally, these layers shall be compacted with a small hand hummer.

The crack in question is located in the wall of the main façade (see Fig. 3). After the works, the excess material will be removed to obtain a straight wall.

Fig. 3. Crack in the main façade

While addressing the main cracks is an important step, other parts of the house should also receive attention - i.e., the roof. The roof structure of the Burzuc house is made of unsquared wood (see Fig. 4), while the two gables are contained by means of boards. Although the wooden floor above the ground floor has a layer of earth (rammed with chaff and acting as insulation) between its beams, the attic was used for storing food and as a smokehouse. The latter was well ventilated. For a proper insulation, the two gabled roofs should be insulated using cork panels. Furthermore, damaged items of roof structure should be replaced. Since both the hip jack rafter and timber platform are currently missing, struts and new tongues should be mounted to ensure good stiffening. Last but not least, wooden elements of the roof structure must be fireproof.

Fig. 4. The framing of the roof

Having discussed the rehabilitation solution, we now move on to describe the house's main architectural elements.

The Burzuc house's eastern façade (see Fig. 5) is made up of a porch enclosed with three windows with wooden framework fitted with rectangular sheets of transparent glass. The porch covers approximately 60% of the facade surface. A fourth window of the porch is located on the southern facade. This transparent enclosure resembles a horizontal ribbon placed between the adobe earthwork surrounding the porch, and the eaves.

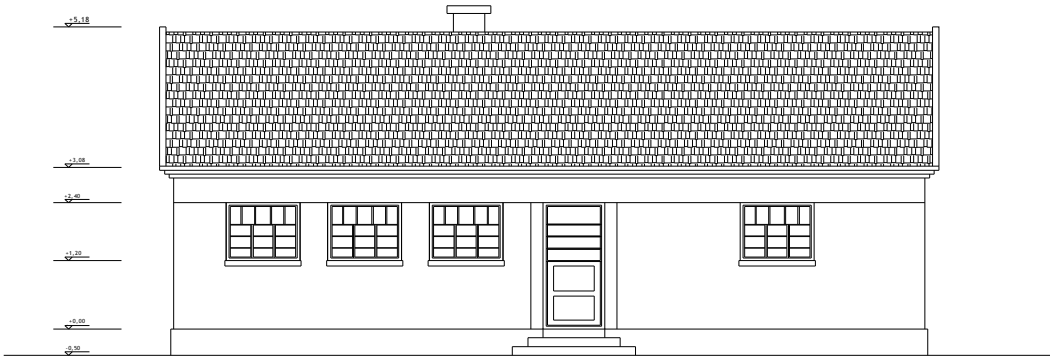

Fig. 5. Eastern façade

In the morning, during wintertime, the greenhouse effect causes the sun radiation to be trapped in the enclosure of the porch and to be stored in the thick earthen walls between the porch and the other rooms; the sun radiation is then slowly transferred to the inner space of the building, contributing to the overall energy balance of the house. This is one of the resemblances to the houses analysed by Joja. The difference, however, lies in the porch orientation. Instead of a southern orientation, which would allow for an efficient solar radiation gain, as in the case of traditional Romanian houses, the porch of the Burzuc house faces eastwards, except for one window on the southern façade (see Fig. 6). This orientation was prescribed by the town-planning requirements of the Bihor area, which called for the short facade to be adjacent to the street frontage.

Following our investigation, we thus come to the following remark: the facades facing southwards and eastwards are fitted with windows, whereas the facades facing northwards and westwards consist of full brickwork. This allows for solar radiation gain and protects from too high or too low temperatures.

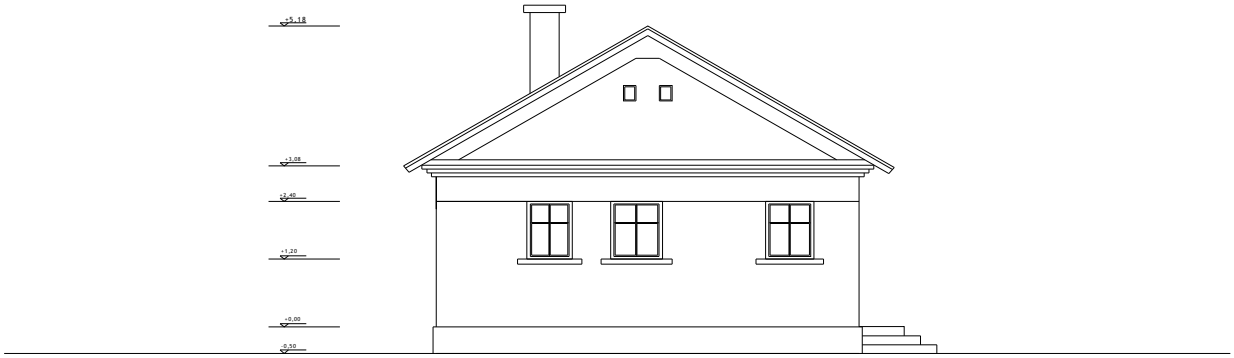

Fig. 6. Southern façade

3 Conclusions

Understanding traditional construction techniques – i.e., their preservation and adaptation to modern standards, is an important lesson to us all. The Burzuc house is just one of many instanced in which tradition can and should be kept by executing repairs with traditional materials.

Our rehabilitation solution envisages the use of traditional materials (among them, earth) and aims to be an alternative to the renovation and rehabilitation techniques for vernacular buildings. The type of house we look at – i.e. having a glass-enclosed porch, and made of wood, glass and adobe, can be seen in some Romanian

villages and cities as early as the 19th century. As such, it has been remarked by prominent architects to the likes of Ion Mincu, Petre Antonescu and Constantin Joja [2].

While carrying out this study, we observed locals who employ the village craftsmen for the consolidation works. The craftsmen's' solutions include concrete, rabitz plastering, and plasters. We deeply encourage this practice and hope that our contribution too will help provide useful solutions to the needs of the community.

Last but not least, the hypothetical solution presented in this paper is available both for old buildings in need of repair as well as for new ones.

References

[1] Dachverband Lehm.(2010).Reguli pentru arhitectura din pământ.(The Ground Rules for Architecture) Arhiterra Publishing House, Bucharest.
[2] Joja,C.(1981). Sensuri şi valori regăsite.(Meanings and Values Found) Eminescu Publishing House. Bucharest, pp.181.
[3] Cardas, M. & co. (1983). Lexicon ilustrat al noţiunilor de sistematizare.(Systematization of the Concepts Illustrated Lexicon).Technical Publishing,Bucharest.
[4] Carmody, J. (1985). Earth Sheltered Housing Design. Van Nostrand Reinhold.
[5] Curinschi, V. G. (1982). Istoria Universală a arhitecturii, vol. II.(Volume II Universal History of Architecture). Technical Publishing Bucharest.
[6] Focsa, V. (1978). Higrotermica şi acustica clădirilor.(Hydrothermal and Acoustic Buildings). Publisher Didactic and Pedagogical Bucharest.
[7] Kaki,H.,Kiffmeyer, D. (2004). Earthbag Building. New Society Publishers, Canada.
[8] Szokolai, S.V., Miklos,Y., Muszaky, F. (1998). Green Design. Budapest.
[9] Gernot, M. (2006).Building with Earth,Design and Technology of a Sustainable Architecture Birkhauser. Publishers for Architecture, Basel.
[10] Bărbulescu, C. (2002). Integrare tehnologică în arhitectura contemporană.(Technological Integration in Contemporary Architecture).Cluj University Press.Cluj Napoca.
[11] Boyer, LI., Grondzyk, W. (1987). Earth Shelter Technology.Texas A&M University Press,College Station, Tx.
[12] Brand, S. (1994). How Buildings Learn. Wiking Penguin.
[13] Bussagli, M. (2003). Understanding architecture, Giunti., Trans. Sauciuc, G., Bucharest, RAO Encyclopedia.
[14] Normativ privind fundarea construcţiilor pe pământuri sensibile la umezire.(Standard on the Founding of Construction on Lands Susceptible to Wetting). Indicativ NP 125. (2010). (Indicative NP 125).

Testing on Concrete Surface Repair with Tri Component Epoxy Resin System

Puskás A.[1], Corbu O.[1], Köllő Sz.A.[1]

[1] *Technical University of Cluj-Napoca (ROMANIA)*
E-mail: attila.puskas@dst.utcluj.ro

Abstract

Reparation and rebuilding of cracked and damaged concrete surfaces represent a real challenge for both the construction companies and the engineers. There are many products and materials developed for solving the above mentioned problems, while others are continuously under developing process, aiming to create more and more durable and sustainable components. Since epoxy based materials are known for their application versatility, use of tri component epoxy resins for concrete surface repair might represent a suitable solution. The paper presents the tests and conclusions on the concrete surface repair using tri component epoxy resin system.

Keywords: tri component, epoxy resin, linkage, resistance.

1.1 Introduction

Need for concrete surface repair increases with the increase of the enhancement of cast concrete surfaces and of the user's needs. Epoxy coating systems are used widespread for their durability also in case of industrial floors. For concrete surface repair a tri component epoxy resin system with low viscosity, fast curing and high resistance to compression is proposed. The epoxy resin system with low viscosity is presumed to have very good adhesion on steel and concrete surfaces. In order to be considered adequate repair solution it must have good compressive strength and also good resistance against oil, fuels and chemicals. Additionally, good resistance against temperatures represents advantages in defining the application areas of the epoxy resin.
In order to evaluate as the possible repair solutions for concrete surfaces tests on a tri component epoxy resin system has been performed, aiming to recover and improve the mechanical resistance of the repaired concrete surfaces. The bond quality between the epoxy resin and the concrete surface has been evaluated.

1.2 Characteristics and advantages of the epoxy based component

The most important characteristics of the tested epoxy resin according to the producer are the followings [1]: liquid, self-levelling, long pot life of 30 minutes, almost no shrinkage, permanent high static strength and resistance to ageing, chemical-resistant, vibration-proof. It is non-porous and does not absorb water or chemicals, and provides excellent carbonation resistance and withstands extreme weather conditions. The technical specifications of the epoxy resin are shown in Table 1. When the material is applied it can be considered completely cured after about 24h at +20°C. The curing time can be reduced by heat treatment: if external heat is supplied for approx. 1-2 hours to the casting resin after solidification the complete curing time is reduced.

Table 1. Technical characteristics of the compound [1]

Basis	Epoxy resin, aluminum filled
Specific Properties	liquid, impact resistant
Density of the mixture	1,5 g/cm³
Processing temperature	+5°C to +40°C
Final hardness	24 h
Mean compressive strength (DIN EN ISO 604)	70 MPa
Strength E Module (DIN EN ISO 527)	4170 MPa
Shrinkage	0,02 %
Color after curing	Grey
Temperature resistance	-40°C to +160°C

The mentioned pot life refers to a preparation of 10 kg materials on +20°C temperature. When mixing a larger amount, the material will cure faster due to the characteristic heat of reaction of epoxy resins. The pot life is extended when the total amount is portioned. Ideally, the processing should take place at room temperature (+20°C). Higher temperatures shorten the pot life and curing time.

1.3 Tests on the epoxy based compound

During the testing process have been analyzed the cooperation of epoxy resin compound with concrete and steel, the compressive strength and the module of elasticity of this solvent. Since the epoxy resin was aimed to be used as a surface repair material, its characteristics have been analyzed according to the standards for the concrete. In the tests the base concrete class has been considered C25/30. Before the application of the epoxy resin on the concrete surfaces to repair the contact surface has to make clean, firm and dry. The surface also has to be free of oil, grease and dust. In this manner the contact surface of the old concrete must be washed down with detergent.

1.3.1 Compressive strength

The compressive strength has been analyzed in accordance with SR EN 12390-3 [4] on concrete cube specimens, which were made with cavities of different depth (or furrows), allowing the introduction and addition of epoxy resin solvent into the pattern with 150x150 mm (Fig. 1) and also a good quality bond between the materials.

Fig. 1 Concrete cube specimens (150x150 mm) with cavities and furrows, prepared for testing

Concrete specimens were demoulded after 24±2 hours, and kept in a pool of water on 20±3 C temperature for 28 days while achieving its characteristic strength. After the 28 days the specimens were dried and placed back into the patterns used during the concrete pouring process. The epoxy based solvent has been introduced into the cavities and furrows, forming a composite specimen of approximatively 150x150 x150 mm. The obtained specimens have been tested for their compressive strength at 24 hours after the epoxy resin has been molded and the special component has been introduced in the prepared pattern. The specimens have been tested to compression applying the compressive force parallel and perpendicular to the adherence (Fig. 2).

Fig. 2 Process of the testing: Concrete cube specimens / Addition of epoxy resin system / Compressive strength determination according to SR EN 12390-3

1.3.2 Modulus of elasticity

The modulus of elasticity for the epoxy resin has been established according to the test standard STAS 5585 – 71 [8]. The dimension of the prismatic test specimen is 100 x 100 x 300 mm, made completely of epoxy resin solvent. The tests have been performed using a servo-hydraulic control console with digital monitoring of all the test data and parameters (Fig. 3).

Fig. 3 Analyzing the module of elasticity of specimens (100 x100 x 300 mm) made of epoxy resin solvent

1.3.3 Tension resistance of the epoxy resin with steel and concrete

In order to evaluate the bond between the different materials two specimens have been prepared. The specimens have been obtained by pouring concrete into a metal non deformable pattern with dimensions: 100 x 100 x 300 mm, completed further by epoxy resin. The concrete length in the specimen has been set at circa two thirds of the length of the metal pattern. Later the rest of the specimen has been filled with the special component. Before the pouring of concrete into the corresponding sector, the anchorage using ribbed reinforcements has been introduced (Fig. 4).

Fig. 4 Pattern (100 x100 x 300 mm) with corresponding partitions and anchorage for concrete

At the end of the free region of the metal patterns the anchorage of has been solved by using a metal plate with welded rebar anchor (Fig. 5).

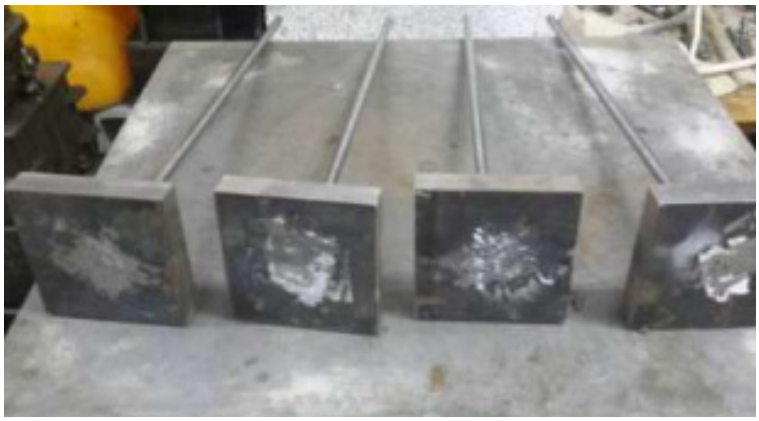

Fig. 5 Metal plates with anchors

After positioning the metal plates with the anchor in the metal pattern the epoxy resin compound has been poured in the remaining area between the metal plate and the concrete specimen. The result formed the composite sample for testing. The sample consisted of concrete, epoxy resin and steel formed two main contact surfaces: between the concrete and epoxy resin and between the epoxy resin and the steel plate at the other end of the specimen (Fig. 6).

Fig. 6 The pattern with the metal plates and concrete specimens before and after the addition of epoxy resin system

The samples` anchorages were placed between the clamping devices of the press (upper and down) aiming to test the tensile strength of the composite specimens (Fig. 7).

Fig. 7 The composite specimen during and after the traction

1.4 Results and conclusions

The results obtained due to the compressive tests on the five samples show clearly the high resistance of the solution (Table 2). The samples tested on compressive strength applying the force parallel with the adhesive plane were knapped completely or partially. In case of specimens I and II the epoxy resin compound showed a plastic deformation causing the partial damage of the composite sample. The results obtained for the specimens loaded perpendicular to the adhesive plane depend on the quantity of compound applied in the cavities and furrows. The more epoxy resin is added to the concrete sample the more high its compressive strength is.

Table 2 Measured compressive strengths on the concrete specimens complementing with epoxy resin material (Fig. 2)

Specimens	I.	II.	III.	IV.	V.
Compressive force [tf]	99	65	88	88	88
Compressive strength [MPa]	44	28.9	39.37	49.18	30.67

The determined values of modulus elasticity on the epoxy resin samples were very close, as it can be remarked from **Table 3**. Compatibility of the determined modulus of elasticity with respect to the mechanical properties of the currently used concrete classes also has to be remarked, while also a durable surface treatment is created.

Table 3 The determined module of elasticity on the specimens made of epoxy resin compound

Specimens	I.	II.
Module of elasticity [GPa]	4.43	4.41

Due to the compressive tests realized on the two concrete – epoxy resin specimens should be establish the existence of a very high and resistant linkage between the epoxy resin compound and the concrete respective the metal plate. In both cases the traction forces applied on the samples provide that the epoxy resin compound ensures the proper resistance, achieving 2.90 N/mm^2 tensile strength in the second case (Table 4).

Table 4 Measured tensile strengths on the concrete specimens complementing with epoxy resin material (Fig. 6)

Specimens	I.	II.
Traction force [tf]	2.05	2.90
Tensile strength [MPa]	2.05	2.90

This value is above the characteristic tensile strength of concrete type C25/30. At 3.00 N/mm^2 should trigger the anchorage steel (type PC) yield, used for the samples.

According to the above mentioned results it can be concluded that the compounds based on composite epoxy resin behave excellent, ensuring a proper bonding of the epoxy resin to the metallic or non-metallic surfaces, including concrete surfaces, confirming results of similar studies performed by others [9][10]. Due to the high mechanical strength and excellent bond between the epoxy resin and the studied surfaces it can be applied for improving and repairing of the concrete surfaces.

Acknowledgement

The writers would like to acknowledge the support and cooperation of the WEICON Romania Company during the tests.

References

[1] Weicon, Chocking Backing Compound, www.weicon.com.
[2] DIN EN ISO 604:2002 Plastics: Determination of compressive properties.
[3] DIN EN ISO 527: Plastics: Strength E Module.
[4] EN 12390-1:2009: Testing hardened concrete – Part 1: Shape, dimensions and other requirements of specimens and moulds.
[5] EN 12390-2:2009: Testing hardened concrete – Part 2: Making and curing specimens for strength tests.
[6] EN 12390-3:2009: Testing hardened concrete – Part 3: Compressive strength of test specimens.
[7] EN 12390-4:2010: Testing hardened concrete – Part 4: Compressive strength – Specification for testing machines.
[8] STAS 5585 – 71: Determination of the modulus of compressibility of concrete.
[9] R. Allahvirdizadeh et al. (2011). Application of polymer concrete in repair of concrete structures: A Literature Review, 4th International Conference on Concrete Repair; Dresden; Germany.
[10] C. A. Issa, P. (2005). Debs Experimental study of epoxy repairing of cracks in concrete, Construction and Building Materials.

Experimental Studies Regarding the Influence of the Connection between Steel and Concrete in Case of Eccentrically Braced Frames

Senila M.[1], Handabut A.[2], Crisan A.[2], Petran I.[1]

[1] *Technical University of Cluj-Napoca (ROMANIA)*
[2] *Politehnica University of Timisoara (ROMANIA)*
E-mail: andreea@sens-group.ro

Abstract

Eccentrically braced frame, both steel and composite, are a very useful solution because it combines the ductility of moment-resisting frames (MRF) and the lateral stiffness of concentrically braced frames (CBF). Also, are used due to architectural reason, because in case of centrically braced frame there are fewer solutions (restrictions). In case of eccentrically braced frame, when the beam is designed in a composite solution concrete-steel, the actual seismic provisions [1, 2] require that in the potentially plastic areas of the beam complete disconnection between the concrete slab and the steel beam. However, the lack of the connection between the concrete slab and the steel beam does not lead to behaviour similar to that one of a steel only beam. The concrete slab has an influence on the behaviour of the plastic hinge in this area.

Keywords: steel, concrete slab, plastic hinge

Introduction

Significant research has been carried out for eccentrically braced frames since the mid-70s starting with pseudo-static tests on a 3-storey structures, scale 1:3 [3,4], followed by a study made on a 5 storey structures, scale 1:3 which has been tested on a vibrating table [5]. Tests on subassemblies formed by link, beam and concrete slab were tested by Kasay and Popov [6] and Ricles and Popov [7]. The eccentrically braced frames (EBF) that were tested showed that the short link frames have a ductile behavior and are stable when subjected to seismic loads are.

In some situations due to the architectural reasons, there are some limitations in the openings of the frames so EBF frames with short links cannot be used. The alternative is the use of frames with long links which deform in bending. Tests were conducted by Engelhardt and Popov [8]. Few tests have been conducted on the behavior of composite beam subjected to cyclic loads. Humar [9] has tested composite steel-concrete beams. The results of the studies showed that if the longitudinal reinforcement is placed in the slab and premature local buckling of the steel section is prevented then the steel-concrete composite sections showed stabile hysteretic loops when subjected to cyclic loading and a good ductility when are subjected to cyclic loading.

37 specimens with 5 different types of cross-sections were tested, all been made by ASTM 1992 steel [10]. The results of the experimental program were intended for large-scale design professionals of EBF links including slenderness limits for the flange, over strength factors and design criteria for links. The results of the experimental program have shown the tested method has an effect on large scale and the inelastic rotations are reached by links. In the PhD thesis [11] the author studied the behavior of the plastic hinges from the composite steel-concrete beams of eccentrically braced frames with short links. The conclusion of the experimental study are that for composite steel concrete beam with short link the simple detachment above the dissipative zone is not enough to assure a pure steel behavior for the beam.

For a comparative analysis between the behavior of eccentrically braced frames with long links with full connection of the composite steel-concrete beam and the ones with a partial composite connection a series of experimental tests were done. Different loading protocol was tried monotonic and cyclic, respectively.

1 Description of Exprimental Program

1.1 *Description of specimens*

The reference building, from which the experimental specimens were extracted, is eccentrically braced frame steel building (EBF). The design was done in accordance with the European provisions. The plastic behavior of dissipative elements was evaluated through static nonlinear analyses, pushover and dynamic nonlinear analyses, time-history. The results obtained led to the conclusion that the dissipative elements fulfill the plastic requirements found it in design norms. The reference structure is a 5 story steel frame building, with 3 spans and 3 bays. Each marginal bay and span has a 6.0m opening, while for the central ones, 4.5 m opening. The eccentrically braced frames are the ones positioned centrally. The height of the first floor is of 3.5m, while for the others is 3.0m, see Fig. 1. The EBF experimental tests were performed considering frame specimens on which three different beam configurations were considered: (i) the simple steel beam; (ii) beam connected with the concrete slab through shear connectors (composite cross-section) on the entire span and (iii) composite beam with connectors suppressed in the potentially plastic region (over the link). Another parameter considered was the loading type: monotonic and cyclic respectively. The behavior factor q=6, who is showing the dissipative capacity of structure, was take for a high dissipative structure (H). In this study only the results obtained for the two composite solutions are presented.

The geometrical characteristics for the sections are: columns are made of HEB260 hot rolled profiles, the beam of EBF bays are HEA200 hot rolled profiles, the exterior beams are HEA260 hot rolled profiles and the braces are HEA180 profiles hot rolled profiles. Note that the structural steel S355 was used for columns and braces and S235 for the beams (both, EBF beams and the exterior beams).

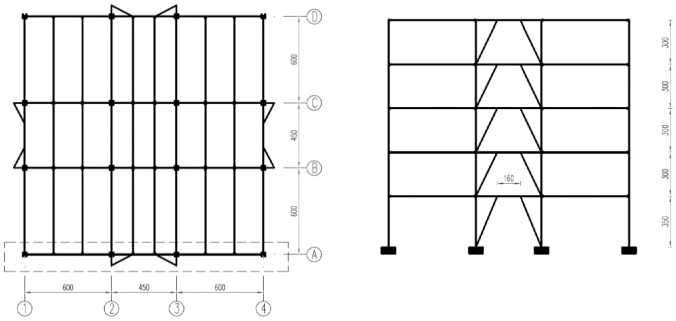

Fig. 1 Plan view of the original structures (left); b) Lateral frame (right)

1.2 Experimental lay-out

The tested BEF specimen is extracted from the reference building presented in the previous chapter. The structural elements and the materials used are the same as in the reference building – HEA 200 for the beam, HEB260 for the columns and HEA180 for the braces, but were adapted specifically to the INCERC laboratory conditions. Unlike in the reference structure, the base of the column is considered to be pinned. The reason was to reduce the force require to form plastic hinges in the composite steel-concrete beam; the response of the structure is not influence by this change. In Fig. 2 the main structural dimensions and test setup are presented. Table 1 describes the EBF specimens which were tested and their configurations.

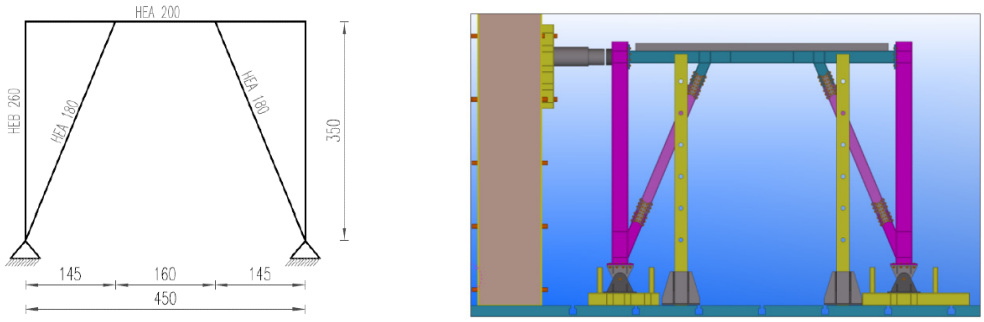

Fig. 2 Frame geometry and sections (left); Test setup (right)

Table 1 Description of the tested EBFs

No of test	Beam type	Loading protocol	Shear studs	Specimen notation
1	Composite	Monotonically	No	EBF_LL_COMP_PM
2	Composite	Cyclic	No	EBF_LL_COMP_PC
3	Composite	Monotonically	Yes	EBF_LL_COMP_TM
4	Composite	Cyclic	Yes	EBF_LL_COMP_TC

The testing procedure for the experimental tests was the the standard ECCS procedure (ECCS 1986) and was used for both monotonic and cyclic tests. The monotonic test was carried out in order to obtain the yield characteristics (yield displacement δy and corresponding force Fy) and those were used for calibration of the cyclic tests. The amplitude for the cyclic tests was increased gradually by considering three cycles for each even multiple of δy.

2 Experimental Results

The experimental program was developed in INCERC laboratory and the main purpose was to determine and evaluate the development of plastic hinges in case of long links of composite steel-concrete beams of eccentrically braced frames. The objective of the study was to find the difference between the behavior of the structure with and without head shear studs on dissipative zones. For eccentrically braced frames with composite beams, the design practice recommends the detachment between the steel beam and the concrete slab in the dissipative area. However, the lack of connection between the concrete slab and the pure steel beam does not lead to a behavior similar to a pure steel beam in the dissipative zone. The presence of the concrete slab has an influence on the behavior of the plastic hinge in that area. In order to measure the rotations at the link extremities displacements transducers were placed on top and bottom flanges, as shown in Fig. 2.

2.1 EBF_LL_COMP_PM – Eccentrically braced frame with composite beam and partial connection, loading protocol - monotonic

For EBF_LL_COMP_PM specimen (Fig. 3) the beam was designed in a composite solution steel-concrete. The connection between the concrete slab and the steel beam was realised with shear stud connector Nelson type, with 19 mm diameter and 90 mm height. Concrete in the slab was C25/30, the reinforcement is PC52 (S500) and 12 mm diameter placed at 150 mm on both directions, the concrete slab has 120 mm thickness. The connection was calculated as a full connection. The shear headed stud was disposed on two rows at 80 mm distance between them. In the dissipative areas, from the limits of the link, the shear headed studs were not lay-out between the steel beam and the concrete slab (on a 480 mm – distance).

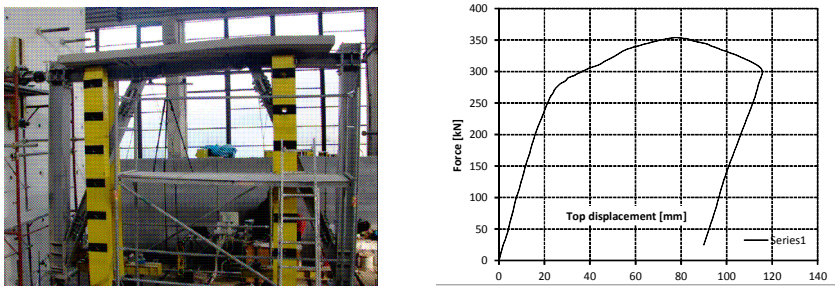

Fig. 3 EBF_LL_COMP_PM during test (left); Force – displacement curve of the steel link (right)

The maximum force during the experiments had a value of 354kN, as it can be seen in Fig. 3. The corresponding displacment for the maximum force is of 80 mm. The maximum displacements had a value of 115 mm for a force of 311 kN. In Fig. 3 is presented force-displacement curve.

2.2 EBF_LL_COMP_PC – Eccentrically braced frame with composite beam and partial connection, loading protocol - cyclic

Completely elastic load cycles were made and after this the ones corresponding to 2ey, 4ey and 6ey yield displacement as in ECCS procedure. The test was stopped after the second cycle corresponding to 8ey displacement after it was noticed that the frame behavior begin to be similar with the behavior of cyclic loaded metal specimen. The maximum force was reached in the first cycle of loading with 4ey displacement and had a

value of 367kN and a global displacement of 55mm. The forces and displacement for each cycle are presented in Fig. 4.

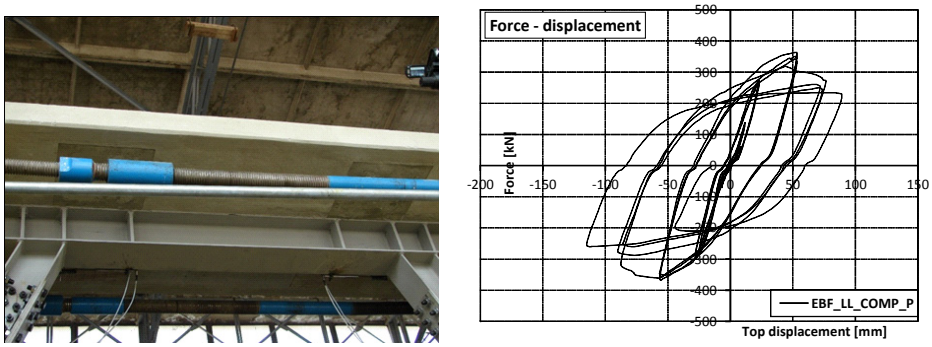

Fig. 4 EBF_LL_COMP_PC during tests (left); Force- displacement curve of steel link (right)

The link rotation meet the acceptance criteria from P100-2013 and the ones from SR EN 1998 (both design codes provide a 20 mrad rotation). Also plastic rotation value has exceeded 24 mrad provided in FEMA 356 for long links (value calculated for HEA200 section, the value is taken as for beams). Overlapping the bending moment – rotation curves are observed for this specimen concrete slab effect on the behavior of the dissipative compression flange beam. The flange in compression develops plastic deformation less then in the free flange from the dissipative zone of the beam (inferior flange has bigger deformations then the superior flange). In Fig. 4 the difference between those deformations can be observed. Top flange of the link has only noticeable deformation after loss of connection between the metal profile and reinforced concrete slab, which led to behavior dissipative area similar to a metal beam, Fig. 5.

Fig. 5 Dissipative behaviour of the beam without connectors on dissipative zones – left and right side of the link

2.3 EBF_LL_COMP_TM – Eccentrically braced frame with composite beam and partial connection, loading protocol - monotonic

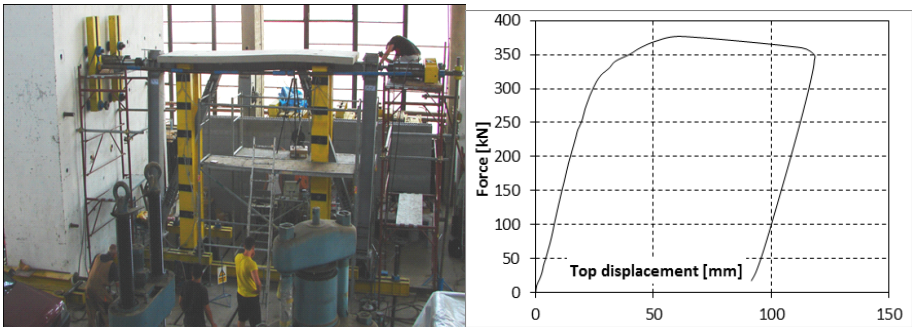

Fig. 6 EBF_LL_COMP_T1 during tests (left); Force – displacement curve of the steel link (right)

The Fig. 6, Fig. 7 show the curve of force - displacement plotted with experimental data obtained by measuring the global displacement of the frame (corrected slip joints at the base of the columns) and force with which it was operated hydraulic press. The maximum force attained during the test was 376 kN at a displacement of 62 mm. The maximum displacement of 118 mm was achieved, displacement whom corresponded to a force of 340 kN.

Fig. 7 Dissipative behaviour of the beam without connectors on dissipative zones – left and right side of the link

2.4 EBF_LL_COMP_TC – Eccentrically braced frame with composite beam and partial connection, loading protocol - cyclic

Hysteretic curves are stable in the cycles carried out until the third cycle corresponding to a displacement 6ey, at which there was a significant increase in displacement (from 86 mm to the second cycle to 104 mm in cycle three) while a less significant decrease in force (from 343 kN to 320 kN second cycle in cycle three). The tested specimen has good ductility in areas located at the ends of the long link dissipative areas. Plastic rotations meet the criteria for acceptance from P100-2013, SR EN 1998 respectively FEMA 356 for long links. Top flange of the link was only noticeable deformation after loss of connection between the metal profile and reinforced concrete, which led to behavior dissipative area similar to a steel only beam.

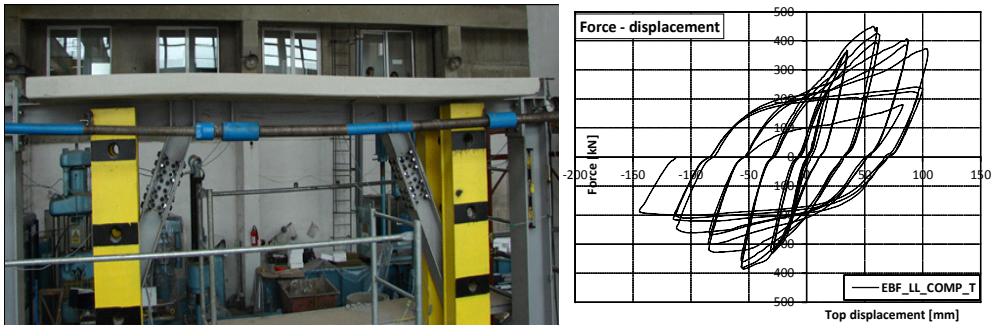

Fig. 8 EBF_LL_COMP_TC during tests (left); Force – displacement curve of the steel link(right)

By overlapping the bending moment – rotation curves presented in the Fig. 8 it is noted that for this specimen also the concrete slab has an influence on the behavior of the compressed flange of the beam from the dissipative area. The curves are plotted from the data obtained from the transducers positioned in the dissipative areas. The compressed flange develops plastic deformations less pronounced that the free flange from the dissipative area. The failure was due to the loss of the connection between the steel beam HEA200 and the reinforced concrete slab, phenomena produced by the failure of the shear headed studs, Fig. 9.

Fig. 9 Dissipative behaviour of the beam without connectors on dissipative zones – left and right side of the link

3 Conclusions

In eccentrically braced frame the dissipative areas are called links and depending on the response (behavior) are different types, in this paper were investigated the long links. The experimental program was made in order to observe the influences of different loading protocols monotonic and cyclic, to study the influence of the concrete slab and also the influence of the connection between the concrete slab and the steel beam (with or without connector on the dissipative area).
The following main conclusions could be drawn from the study:

- Design guideline recommends that for the composite beam of the eccentrically braced frame a full disconnection of the steel beam of the concrete slab. The experimental program revealed that the simple disconnection of the steel beam from the concrete slab in the potential dissipative zones is not sufficient to assure a steel only beam behavior. The behavior observed during the experimental tests is one very similar to a full composite solution.
- In eccentrically braced frames with long links the concrete slab improves the global resistance and stiffness characteristics of the dissipative zone while maintain the ductile character of the solution.
- Considering the stiffness of specimens, the connection over the link elements shows only a small influence, by an increase of stiffness under 10% in comparison to the specimens without connectors over the link. The values of ultimate link rotations exceed 40 mrad for all specimens (with / without connectors, cyclic and monotonic loading respectively), which according to modern seismic norms is considered sufficient to withstand important values of lateral deformations.

Reference

[1] Yurisman, Budiono B. Moestopo M., Suarjana M. (2010), Behavior of Shear Link of WF Section with Diagonal Web Stiffener of Eccentrically Braced Frame (EBF) of Steel Structure, ITB Journal of Engineering Science ISSN 1978-3051 Vol. 42, No. 2, pp. 103-128.
[2] EN 1998-1 EUROCODE 8 (2003): Design of structures for earthquake resistance, Part 1. General rules, seismic actions and rules for buildings, Brussels, CEN, European Committee for Standardisation.
[3] C. W. Roeder și E. Popov (1977), „"Inelastic Behavior of Eccentrically Braced Steel Frames Under Cyclic Loading"," Report No. UCB/EERC-77/18, Earthquake Engineering Research Center, University of California at Berkeley.
[4] D. N. Manheim (1982), „On the Design of Eccentrically Braced Frames," Department of Civil Engineering, University of California at Berkeley.
[5] M.-S. Yang (1982), „"Seismic Behavior of An Eccentrically X-Braced Steel Structure"," Report No. UCB/EERC-82/14, Earthquake Engineering Research Center, University of California at Berkeley.
[6] K. Kasai și E. P. Popov (1986), „A Study of Seismically Resistant Eccentrically Braced Steel Frame Systems," Report No. UCB/EERC-86/01, Earthquake Engineering Research Center,University of California at Berkeley.
[7] K. P. E. Kasai (1986), „General Behavior of WF Steel Shear Links Beams," Journal of Structural Engineering, ASCE, 112 (2), 362-382.
[8] J. M. Ricles, E. Popov (1987), „Experiments On Eccentrically Braced Frames With Composite Floors"," Report No. UCB/EERC-87/06, Earthquake Engineering Research Center, University of California at Berkeley.
[9] J. Humar (1979), „Composite Beams Under Cyclic Loading," Journal of the Structural Division, ASCE, vol. 105, No. ST10, October.
[10] T. Okazakia și M. Engelhardt (2006), „Cyclic loading behaviour of EBF links constructed of ASTM A992 steel," Journal of Constructional Steel Research, vol. 63, pp. 751-765.
[11] G. Danku (2011), „Studiul comportarii articulatiilor plastice in elementele compuse otel-beton supuse la forfecare si/sau incovoiere," Teza de Doctorat (The behavior study of the plastic hinges in steel composite concrete elements subjected to shear and / or bending, PhD Thesis), UPT Timisoara.

Use of Polystyrene Waste in Concrete

Serbanoiu A.A.[1], Barbuta M.[1], Burlacu A.[1], Teodorescu R.[2], Cadere C.[1]

[1] *Gheorghe Asachi" Technical University of Iaşi Faculty of Civil Engineering and Services, 45 Mangeron Blvd., 700050, Iaşi (ROMANIA)*
[2] *University of Agronomical Sciences and Veterinary Medicine in Bucharest, Faculty of Land Improvements and Environmental Engineering, Bucharest (ROMANIA)*
E-mail: barbuta31bmc@yahoo.com

Abstract

The presented research analyzed the possibility of using wastes in obtaining cement concrete. Fly ash and silica fume were used as replacement of cement or addition in concrete. Polystyrene granules of different dosages were used for decreasing the density of concrete. Compressive strength, flexural strength, split tensile strength and density were determined and discussed. The type of addition influenced the mechanical properties, a better influence had silica fume. A high cement dosage improved the compressive strength of concrete with polystyrene granules. The polystyrene granules decreased the mechanical strengths. Good mechanical characteristics were obtained for 10% and 15% content of polystyrene granules.

Keywords: concrete, polystyrene waste, research.

Introduction

In building materials industry new products are obtained from combining different types of wastes. Concrete is a material which can be obtained by mixing varied materials and the tendency today is to obtain concrete with wastes that can replace partially or totally components [1, 2, 3, 4, 5]. Some waste additions can improve the properties of concrete or are used as additions: silica fume [6, 7], fly ash [8, 9], fibers [10, 11], etc. Other types of wastes are used for obtaining lightweight concretes [12, 13, 14, 15]. Wastes of polystyrene are used for obtaining building materials with improved thermal properties [16, 17, 18] in combination or not with other wastes [19, 20]. However concretes with expanded polystyrene foam (EPS) has generally low strengths and because of that is not used for structural elements.

The main purpose of the paper is to present the experimental results obtained on cement concrete with different additions and dosages of polystyrene granules and to analyze their effects on density, compressive strength, flexural strength and split tensile strength.

Experimental Program

1.1 *Materials*

The text included in the sections or subsections must begin one line after the section or subsection title. Do not use hard tabs and limit the use of hard returns to one return at the end of a paragraph. Please, do not number manually the sections and subsections; the template will do it automatically.

The studies were realized on cement concrete having as addition in the mix different dosages of expanded polystyrene granules, silica fume and fly ash [7] [10].

In the case of control concrete of grade C16/20 the mix was prepared with: aggregates type river aggregates in three sorts: sort I, natural sand of 0-4 mm; sort II and III gravel of 4-8 mm and 8-16 mm, respectively. The cement was type CEM I 42.5 R in a dosage of 360 kg/m3. The other mixes were prepared with different dosages of cement, with addition or replacement of cement with fly ash (FA) or silica fume (SUF), with same sorts of aggregates and addition of different dosages of polystyrene granules. The following mixes were studied:

- Mixes type A were prepared with replacement of 10% cement by fly ash; the cement was type CEM II 42.5-ALL [21]; the superplasticizer was type VASCOCRETE-1040, added according producer recommendations. The polystyrene granules were added in dosages of 10% and 20% from the mix volume, Table 1. One mix was prepared with addition of glass fibber near the polystyrene granules (mix A4, Table 1).

• Mixes type B were prepared with a smaller dosage of cement CEM I 42.5-R [21] in comparison with control mix, and 10% addition of silica fume, Table 1. The superplasticizer was type BETOPLAST SUPER PLUS, added according producer indications. The dosage of polystyrene granules varied between 10% and 25%, Table 1.

• Mixes type C were prepared with higher dosages of cement CEM I 42.5 R in comparison with control mix and silica fume addition, only mix C5 was prepared with replacement of 10% cement with silica fume plus an addition of silica fume of 10% from the cement dosage; the superplasticizer was type RHEOBUILD 1000, added according producer indications; the dosage of polystyrene granule was between 10% and 30% from the mix volume, Table 1.

Table 1 The mixes for experimental samples

Sample	Cement Dosage Kg/mc	Aggregate Kg/m^3			Water l/m^3	SUF Kg/m^3	Fly ash Kg/m^3	Polystyrene Granules %	Glass fibers %	fc	fti	ftd
		0-4 mm	4-8 mm*	8-16 mm								
A0 control	360	803	384	559	172	-	-	-	-	45.01	3.05	3.65
A1	360	803	384	559	172		-	10	-	27.92	2.46	2.77
A2	360	803	384	559	172		-	20		8.55	1.43	1.21
A3	324	803	384	559	172		36	20		9.75	1.34	0.70
A4	324	803	384	559	172		36	20	0.25	9.91	1.47	0.95
B1	300	425	390	560	130	30	-	15		27.48	4.46	4.82
B2	300	425	390	560	130	30	-	20		22.5	1.15	1.27
B3	300	425	390	560	130	30	-	25		21.37	3.25	3.34
C1	385	671	430	621	240	38.5	-	10		15.63	2.05	2.32
C2	550	457	359	815	153,3	55		10		31.4	2.5	2.48
C3	550	457	359	815	153,3	55		20		21.7	2.26	1.65
C4	550	457	359	815	153,3	55		30		15.8	1.8	1.15
C5	500	504	408	800	150	60		10		21.94	3.28	2.66

1.2 *Samples*

For determining the mechanical strengths the following samples were poured: cubes of 150 mm sizes, for determining compressive strength (fc), prisms of 100x100x550 mm, for determining flexural strength (fti) and split tensile strength (ftd) [22,23,24]. According to standards the sample were kept in water for 7 days and after that in air at room temperature of ± 200C. The tests were effectuated at 28 days on three samples for each test.

2 Results and discussions

The analysis of density of hardened concrete had shown that the values of these characteristics are situated between 1900 kg/m3 and 2200 kg/m3 for dosages of 15-10% polystyrene and between 1200 kg/m3 and 1900 kg/m3 for polystyrene dosage between 30% and 15%.

The mechanical properties of experimental concrete were analyzed by destructive tests, having in view the influence of polystyrene dosage on compressive strength, flexural strength and split tensile strength, Fig.1. Experimental results on concrete with polystyrene granules are presented in Fig. 2.

Fig. 1 Experimental tests on concrete with polystyrene granules

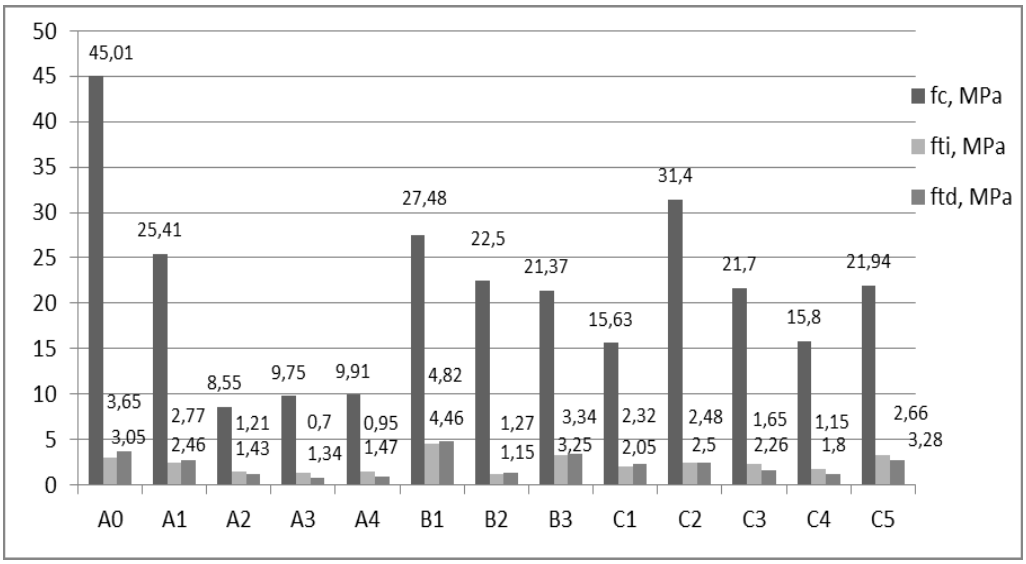

Fig. 2 Experimental results on concrete with polystyrene granules

From experimental results it can observe that all variables influenced the mechanical properties of concrete.

In the case of concrete type A with 10% fly ash replacement of cement, all mechanical strengths decreased in comparison with the control mix. For compressive strength the value decreased with 43.7% in the case of 10% polystyrene granule and with 81.1% in the case of 20% polystyrene. In the case of flexural strength, a decrease between 20.2% for 10% polystyrene and 56.1% for 20% polystyrene was observed. In the case of split tensile strength a decrease between 24.2% and 80.8% was observed. The fibbers addition improved all mechanical strengths in comparison with the mix with the same dosage of polystyrene granules. The maximum values of all mechanical strengths for concrete type A were obtained for 10% addition of polystyrene granules.

In the case of concrete type B with a smaller dosage of cement in comparison with control mix and with addition of SUF, it can observe that only the values of compressive strength had decreased. In the case of compressive strength, a decrease between 39% for 15% polystyrene and 52.5% for 25% polystyrene was observed. In the case of tensile strengths the values had increased, the highest value had been obtained for a dosage of 15 % polystyrene granules (for fti the increase was about 46.2% and for ftd of about 32%). The maximum values of all mechanical strengths for concrete type B were obtained for 15% addition of polystyrene granules.

In the case of concrete type C with a higher dosage of cement in comparison with the control mix and with addition of SUF, it can observe that the values of mechanical strengths are smaller than that of the control mix, only in the case of mix C5 which has an supplementary addition of SUF the value of fti is higher than that of the control mix. In the case of compressive strength, a decrease between 30.2% for 10% polystyrene and 87.1% for 30% polystyrene was observed. In the case of flexural strengths the values had decreased between 18.8% for 10% polystyrene and 41% for 30% polystyrene. In the case of split tensile strength decrease was between 32.1% for 10% polystyrene and 68.5% for 30% polystyrene. The highest value for all mechanical strengths for concrete type C was obtained for a supplementary addition of SUF and 10% addition of polystyrene granules.

The mechanical strengths of concrete prepared with polystyrene granules were generally smaller than that of control mix, smaller with increasing of polystyrene dosage.

With increasing the cement content the compressive strength also increased.

The type of addition also influenced the mechanical strengths: SUF had a better influence than fly ash, especially on the tensile strength in the case of reduced cement dosages.

From all 12 experimental mixes the highest value of compressive strength was obtained for a cement dosage of 550 kg/m3 with 10% SUF addition and with10 % polystyrene granules. For flexural and split strengths the highest value from all 12 mixes was obtained for a cement dosage of 300 kg/m3 with 10% addition of SUF and with15% polystyrene granules (values which are higher than that of the control mix)..

3 Conclusion

In the experimental researches on cement concrete with additions three types of wastes were studied: polystyrene granules, fly ash and silica fume. The fly ash was used as replacement of cement in a dosage of 10% from the cement weight and silica fume was used as addition, in a dosage of 10% from cement weight and replacement of cement, in a dosage of 10% from cement weight. The cement dosage was also varied, from 300 kg/m3 to 550 kg/m3.

The type of addition influenced the mechanical strengths: SUF had a better influence than fly ash, especially on the tensile strength in the case of reduced cement dosages.

The cement dosage had influenced the mechanical strength: with increasing the cement content the compressive strength also increased, but on the tensile strengths there was no influence related to increasing the values, on the contrary it appeared that for smaller cement dosages the tensile strengths were bigger.

The polystyrene dosages influenced the mechanical strengths: with increasing the polystyrene dosage the mechanical strengths decreased in comparison with control mix. The polystyrene granules had decreased the density of cement concrete and increased its elasticity.

References

[1] S. Monosi, M. L. Ruello, D. Sani (2016). Electric arc furnace slag as natural aggregate replacement in concrete production, Cement and Concrete Composites, 66, pp. 66-72.

[2] R. Embong, A. Kusbiantoro, N. Shafiq, M. F. Nuruddin (2016). Strength and microstructural properties of fly ash based geopolymer concrete containing high-calcium and water-absorptive aggregate, Journal of Cleaner Production, 112, pp. 816-822.

[3] Mo Alkaysi, S.El-Tawil, Z. Liu, W. Hansen (2016). Effect of silica powder and cement type on durability of ultra-high performance concrete (UHPC), Cement and Concrete Composites, 66, pp. 47-56.

[4] M. Singh, R. Siddique (2016). Effect of coal bottom as partial replacement of sand on workability and strength properties of concrete, Journal of Cleaner Production, 112, pp. 620-630

[5] C. Shi, Y. Zhang, W. Li, L. Chong, Z. Xie (2016). Performance enhancement of recycled concrete aggregate-A review, Journal of Cleaner Production, 112, pp. 466-472.

[6] E. Ghafari, H. Costa, E. Julio (2015). Statistical mixture design approach for eco-efficient UHPC, Cement and Concrete Composites, 55, pp. 17-25.

[7] M. Barbuta, D.S. Nour. Components compatibility to high strength concrete with silica fume-International Conference VSU 2006 Sofia, Tom I, p.II-46-52-ISBN 13-978-954-331-009-8.

[8] T. Ponikiewski, J. Golaszewski (2013). Influence of high-calcium fly ash on the properties of fresh and hardened self-compacting concrete and high performance self-compacting concrete, Construction and Building Materials 41, pp. 296-302.

[9] Barbuta M., Harja M., Babor D. (2010). Concrete polymer with fly ash. Morphologic analysis based on scanning electron microscopic observations, Revista Romana de Materiale,(Romanian Journal of Materials) vol. 40, nr. 1, pp. 337-345.

[10] Marin E., Barbuta M., Ciobanu L., Cioara I., Ionesi D. S., Dumitras C. (2014). Study regarding the optimization of the mechanical behaviour of glass fiber reinforced concrete, Journal of Optoelectronic and Advanced Materials 16. (11-12):1411-1417.

[11] K. Wille, D. J. Kim, A. Naaman (2011). Strain-hardening UHP-FRC with low fibber content, Materials and Structures 44.3, pp. 35-41.

[12] Y Xu, L. Jiang, J.Xu, Y. Li (2012). Mechanical properties of expended polystyrene lightweight aggregate concrete and brick, Construction and Building Materials 27, pp. 32-38.

[13] A. Laukaitis, R. Zurauskas, J. Keriene (2005). Cement and Concrete composites, 27, pp. 41-47.

[14] A. Prerz - Garcia, a. g. Villora, G. G. Perez (2014). Building's eco-efficiency improvements based on reinforced concrete multilayer structural panels, Energy and Buildings 85, pp. 1-11.

[15] A. Sadrmomtazi, J. Sbhani, M.A. Mirgozar (2013). Modeling compressive strength of EPS lightweight concrete using regression, neural network and ANFIS, Construction and Building Materials 42, pp. 205-216.

[16] A. A. Sayadi, J. V. Tapia, Th. R. Neitzert, G. C. Clifton (2016). Effects of expanded polystyrene (EPS) particles on fire resistance, thermal conductivity and compressive strength of foamed concrete, Construction and Building Materials 112, pp. 716-724.

[17] D.S Babu, K.Ganesh Babu, W Tiong-Huan (2006). Effect of polystyrene aggregate size on strength and moisture migration characteristics of lightweight concrete, Cement and Concrete Composites, 28, pp. 520-527.

[18] A. Chikhi, A. Belhamri, P. Glouannec, A. Magueresse (2016). Experimental study and modelling of hygro-thermal behavior of polystyrene concrete and cement mortar. Application to a multilayered wall, Journal of Building Engineering, 7, pp.183-193.
[19] D.S Babu, K.Ganesh Babu, T. H. Wee (2005). Properties of lightweight expanded polystyrene aggregate concrete containing fly ash, Cement and Concrete Research 35, pp.1218-1223.
[20] M. Lanzon, V. Cnudde, T. De Kock, J. Dewanckele (2015). Microstructural examination and potential application of rendering mortars made of tire rubber and expanded polystyrene wastes, Construction and Building Materials 94, pp. 817-825.
[21] Romanian Standard Association, SR EN 197-1:2011. Cement, Part 1: Composition, specifications and conformity criteria for common cements.
[22] Romanian Standard Association, (2011), SR EN 12390-3:2005. Testing hardened concrete. Part 3: Compressive strength of test specimens.
[23] Romanian Standard Association, (2009), SR EN 12390-5:2005. Testing hardened concrete. Part 5: Flexural strength of test specimens.
[24] Romanian Standard Association, (2005), SR EN 12390-6:2010. Testing hardened concrete. Part 6: Split tensile strength of test specimens.

Multidimensional Descriptive Geometry

Şerbănoiu B.V.[1], Şerbănoiu A.A.[2]

[1] *Faculty of Architecture, G. M. Cantacuzino, Iaşi (ROMANIA)*
[2] *Faculty of Civil Engineering and Building Services, Iaşi (ROMANIA)*
E-mails: bogdan.serbanoiu@tuiasi.ro, serbanoiu.adrian@tuiasi.ro

Abstract

This article proposes the extension of the rules and methods used by the descriptive geometry for the analysis and representation of the abstract complex, multidimensional shapes. The method we propose generalizes the applicability of the conventional methods of tridimensional space folding to spaces with infinity of dimensions.

Keywords: space, multidimensional, descriptive geometry, reference system.

1. Introduction

"This art has two major objectives. The first is to obtain an exact representation on two-dimensional drawings of tridimensional objects that require rigorous definition [...] The second [...] is to deduce from the exact description of bodies, all that necessarily follows from their shape and their respective positions" [1].

1.1 *The space*

Defining the space was one of subjects debated by the great thinkers of the human kind since the oldest times. Philosophically speaking, the notion of space had three major accepted definitions. In the Antiquity and Medieval period, space was perceived as a finite container where all the physical objects and the interactions between them take place (Plato, Socrates) [2]. Starting with the 14th century, there are two different ways of thinking that define the notion of space differently: the substantivalist current which defines space and time as self-standing entities (Isaac Newton) and the relationist current, which identifies space as a projection of our senses, an abstract matrix which we project in the exterior, to understand the objects interaction and the temporality of physical phenomena (Kant) [3].

A mathematically defined space came with the necessity of theoretically representing and analyzing of physical phenomena met in the nature. The first analysis tools were based on the postulates method (Euclid – ca. 300 years b. C), afterwards René Descartes introduces coordinates method (1637) [4], setting the grounds of analytical geometry. An important step in knowing the space is made by mathematician Gaspard Monge (1795) by inventing descriptive geometry, with the help of which the geometrical elements could be represented through projections in a given reference system. In the 19th century, a rupture takes place between mathematically defined space and the physically perceived one, by the introduction of the non-Euclidean hyperbolic geometry of Nikolai Lobachevsky (1829) [5] and Janos Bolyai (1832) [6]. From this moment, mathematics and physics develop separately as two different scientific areas, the mathematic notions evolving at an abstract degree which can no longer find a correspondence with the discoveries in physics. The French mathematician Nicolas Bourbaki named the period between 1795 ("Descriptive geometry", Monge) and 1872 [7], [8], [9] as the golden era of geometry, analytical geometry replacing many of the classical theorems of geometry, reaching a high level of generalization.

Modern mathematics defines the Euclidean space with the help of algebra, invoking terms as vectors, affine space and different degree equations. This way of working with the space assumes wide knowledge's in the field of mathematics, such becoming inaccessible to the wide public whom knowledge limits in general to classic geometry. This paper has at the ground the utilization of the representation rules of space, discovered by Gaspard Monge in descriptive geometry and it proposes their generalization for multidimensional spaces in order to be able to represent the geometrical elements with a higher number of dimensions than those three, specific to physically perceived space. Starting from the idea that the space can be folded, and the space geometry elements can be represented with the help of the relations that establish between its projections, we'll try the generalization of the rules and methods of the descriptive geometry to spaces with more dimensions, transforming it into a tool of actual knowledge, which can keep up the pace with the discoveries from the field.

1.2 *Space Dimensions*

In a mathematically defined space, the space dimensions of an element represent the minimum number of coordinates necessary for its identifications and positioning in the chosen reference system. We can speak about the existence of a space at the moment when we have at least one dimension. The one-dimensional space characterizes through the existence of a landmark and of a direction (vector) alongside which a point or a series of points which form a line can be placed. To represent a space with two dimensions we need to take into account another direction vector different from the initial one, both concurrent in the origin of the reference system. In the Euclidean geometry the two vectors are considered to be perpendicular one from another, the created space having the benefit of a directional isomorphism, the contained phenomena behaving identical in all the directions. The two vectors drawn, become an integrant part of the reference system of the bi-dimensional space and can be named as mono-dimensional spaces. All the contained elements by the bi-dimensional space will be projected and, like this, will have a simultaneous correspondent on the two reference vectors.

To us, the citizens of a tridimensional space, the inferior spaces as number of dimensions become geometrical elements perceptible and identifiable physically as it follows: the space with one dimension manifests under the form of a point or a line, and the bi-dimensional space are perceived as a plan. To define a tridimensional space, we'll need a third vector positioned perpendicular on the other two vectors. Hence, the reference system will be composed from three mono-dimensional subspaces (called axes), and three bi-dimensional subspaces (called projected plans or reference plans), all positioned at a 90 degrees angle one from each other. Starting from this experience, confirmed by the perceived reality, we can generalize the situation and for spaces with a superior number of dimensions; hence it can be observed that a space with any "n" number of dimensions will have a reference system composed from "n" subspaces of inferior dimensions:

$$Un = C_n^{n-1}Sn\text{-}1\ ,\ C_n^{n-2}Sn\text{-}2\ ,\ ....\ ,\ C_n^1S1\ ,\ O \qquad (1)$$

The number of the components of the reference system for a space of "n" dimensions can be computed with the help pf the next formula:

$$NUn = C_n^{n-1}Sn\text{-}1 + C_n^{n-2}Sn\text{-}2 + ... + C_n^1S1 + 1 \qquad (1)$$

where:

- NUn = the number of elements of the reference system,
- Un = the reference system of the space with n dimensions,
- n = the number of dimensions,
- Sn = the space with "n" dimensions,
- O = the origin of the system.

For four dimensional subspaces S4 we'll have the reference system composed by four tridimensional subspaces (S3), four projection plans (S2) and four reference axes (S1) concurrent in O (the origin).

The maximum number of possible space dimensions, in our universe, is five, according to the mathematic model Kaluza-Klein enounced in 1921 by the mathematician Theodor Kaluza [10], [11]. Other mathematic model of recent date reach to count up to 10 space dimensions in the attempt of explaining some phenomena related to quantic physics, but, experimental there couldn't be delivered evidences to support their existence. The field of mathematics allows the existence of a finite number of dimensions through abstraction and generalization of information, but loses the connection with reality, connection delivered by the experimental physics.

1.3 *Projection systems*

The projection system represents an assembly of graphical elements, specific to space dimension of the base on which is designed, and rules that allow the pass from a space with a certain number of dimensions to another with a different number of dimensions and vice-versa.

To design a certain object from a space with n dimensions (Sn) in a space with Sn-1 means to take through different points of the object, line that at the intersection with Sn-1 will determine the projections of these points. The laying out of projection lines is made after a rule characteristic to the type of projection. Points recomposing obtained through their projection in Sn-1 determines the image of the object or his projection on the respective base/support. The space on which the projection is made is called "subspace" or "reference space", and the lines that pass through each point of the object are called projecting lines or projecting rays.

As such, the projection systems structure is characterized by the following defining elements:
- the projection centre (observer), which is the starting point of the projecting lines;
- projecting lines, which pass through each point of the object, projecting that point on the reference space and with the help of whom the image of the object is obtained (projection of the object);
- the projection subspace, base Sn-1 on which the image of the object will be obtained.

Depending on the nature of the observer, two projection systems are known, which are:
- the parallel projection/projecting system (cylindrical);
- the central projection/projecting system (conic).

a) The parallel projection system [12].

To build an image of an object or an assembly of objects using the parallel projection system, we need to take into account the following premises:

1. The projection centre (the observer) stands at an infinite distance by the space in which we want to project.
2. The projecting rays are parallel between them due to the placement of the concurrence point (the observer) at an infinite distance.
3. The projected image of the object remains constant in the reference subspace, no matter his distance from the observer. The object's projection modifies only if the projection subspace changes its orientation or the observer changes the looking direction.

The points that reside in space on the same projecting line will have identical projection on the projection subspace (Sn-1).

The main properties of the parallel projection system:
- The projection of a point will also be a point, no matter the used projection system.
- If the projection ray is parallel with the projection space the point's projection is thrown at infinite.
- The projecting lines are parallel between them.
- Two concurrent lines in space have concurrent projections.
- Two parallel lines in space have parallel projections.
- One parallel projection of an object is not enough to determine the object in space.

b) The central projection system [12].

The central projection system is defined by the following characteristic elements:

1. The projection centre (observer) stands at a finite distance from the projection subspace.
2. The main projection ray passes through the geometrical centre of the object or of the assembly that is projected.
3. The projection lines are concurrent in the projection centre "S" (observer).
4. The projection of the object from space modifies according with the drift of the observer from the projection subspace.

Central projection system properties:
- The projection of a point will also be a point.
- If the projection ray is parallel with the projection space the point's projection is thrown to infinite.
- The projecting lines are concurrent in the observer.
- Two concurrent lines in space have concurrent projections.
- Two parallel lines in space have concurrent projections in the "runaway point".
- One central projection of an object is enough to determine the object in space.

2. Multi axis reference system

The reference system is composed from a set of geometrical elements and rules with the help of whom numerical coordinates can be assigned. The numerical coordinates of a spatial object need to determine in a unique way and enough the position and the dimensions of the respective element. Moving from a reference system to another assume the change of relationships between the coordinates that define the object, however these must keep their characteristic of unique and enough information in the new reference system.

The physical space that we live in can be included in a tri-axis reference system. By assigning numerical coordinated to the object from the physical space, on the basis of the reference system rules, we can find out all the spatial characteristics of the respective object and the spatial phenomenon will multiply with accuracy. Replacing the physical space with the reference system determined the developments of modern mathematics,

where space has become an abstract notion, defined only by the relations between the coordinates, without any connection with the perceptible physical space.

2.1 *Reference system composition*

A reference system that determines a space Sn with n dimensions is composed from a number of subspaces S with inferior number of dimensions. For example, the tridimensional system (Fig. 1) can be expressed through the following relation/equation:

$$U3 = C_3^2 S2 , C_3^1 S1 , O \quad => \quad U3 = 3S2 , 3S1 , O \tag{3}$$

or, replacing with the specific geometric elements:

$$U^3 = (H_{XY}, F_{XZ}, L_{YZ}), (\overline{OX}, \ \overline{OY}, \ \overline{OZ}), O \tag{4}$$

where:

U3 = the tridimensional reference system.

S2, S1 = bi-dimensional, unidimensional subspace.

HXY, FXZ, LYZ = reference plans (horizontal, vertical, lateral).

$\overline{OX}$, $\overline{OY}$, $\overline{OZ}$ = reference axis (abscissa, distance, elevation/height/level).

O = system origin (adimensional space).

The rule that the components elements of a reference system need to meet is that all the subspaces with the same number of dimensions to be perpendicular between them and isomorphs, behaving spatially identical, no matter the orientation.

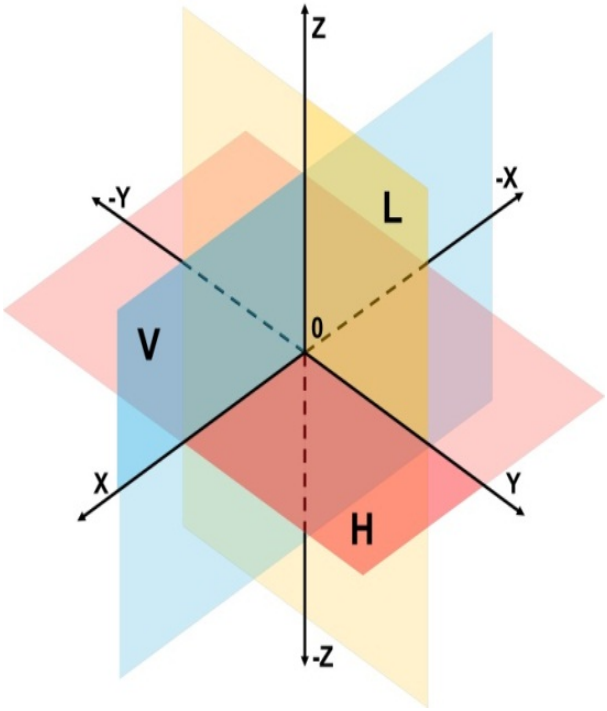

Fig. 1 Tridimensional reference system

The representation of a four dimensional space (Fig. 2) need the introduction of some additional subspaces, as it follows:

$$U4 = C_4^3 S3 , C_4^2 S2 , C_4^1 S1 , O \quad => \quad U4 = 4S3 , 6S2 , 4S1, O \tag{5}$$

or, replacing with the geometric elements we have:

$$U^4 = (S_{XYZ}, S_{YZW}, S_{ZWX}, S_{YZW}), (H_{XY}, F_{XZ}, L_{YZ}, W_{XW}, W_{YW}, W_{ZW}), (\overline{OX}, \overline{OY}, \overline{OZ}, \overline{OW}), O \quad (6)$$

where:

U4 = four dimensional reference system.

S3, S2, S1 = tridimensional, bi-dimensional, unidimensional subspace.

SXYZ … = subspace determined by three axes.

HXY, FXZ, LYZ, WXW… = reference plans (horizontal, vertical, lateral, hyper plan).

$\overline{OX}$, $\overline{OY}$, $\overline{OZ}$, $\overline{OW}$ = reference axis (abscissa, distance, level, time).

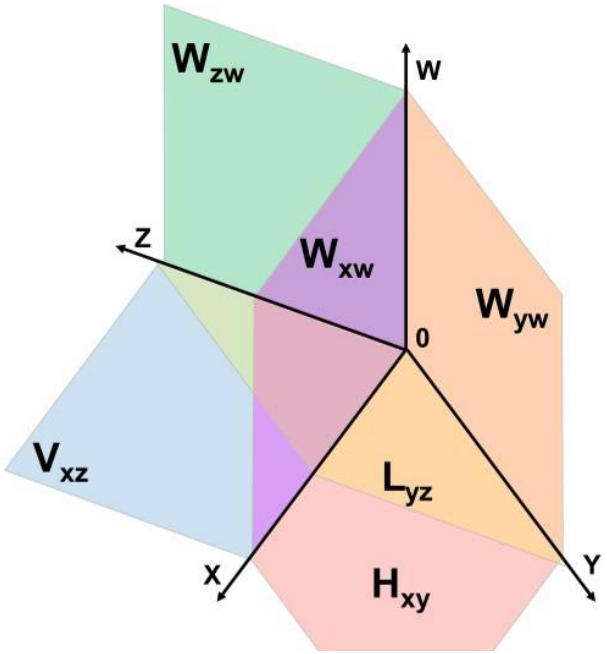

Fig. 2 Four dimensional reference system

A unique geometric object spatially determined with the help of a certain number of dimensions is projected in the same time on all the associated subspaces of that space, the correlation between the coordinated being made simultaneous. The projection represents the method through which the connection between subspace coordinates is made by different number of dimensions.

To graphically represent an object defined by three dimensions in a bi-dimensional space (a plan), we need to roll out the tridimensional space and overlay the object's projections from the reference system U3 over the plan we want to roll out the respective space. The unfolded view of the object is called draught. This graphic procedure was invented by the mathematician Gaspard Monge and it could only be applied for the object defined tridimensional. Through this paper we propose the generalization of this method and to spaces with superior number of dimensions.

2.2 *Four dimensional objects representation*

The representation of the geometric forms with four dimensions can be achieved in two ways: through perspective geometry and through projections or draught. Due to the increase of the number of dimensions, the draught of an object can be of many types depending on the dimensions of the subspace on which the projections are made. For example, an object defined by 4 dimensions will have a draught of rank three (which we'll conventionally note E3) and a draught of rank two – E2. No matter the rank of the draught, it must contain all the necessary information to determine uniquely and enough our four dimensional object in S4 space.

The perspective geometry representation of an object can be of many types, depending on the view direction of the observer and the projection type. The most used way to perspective geometry representation of an object is the parallel perspective geometry, isometric in which the projection is parallel, and the view direction makes an equal angle with each of the axis that define the reference system. Due to particularities of

making this kind of projection, the reference systems that have an even number of dimensions has deficiencies in eloquent representations of the space, due to overlap of the visual marks. That is way, next we'll represent isometric perspective geometry of a space with 4 dimensions in a reference system characteristic to a space with 5 dimensions, from which we extract an axis. The represented object will be deformed on a direction, but the understanding of the space will be enhanced (Fig. 2). We can make an analogy with the representation of a plan in tridimensional isometric perspective geometry where, as in the case of four dimensional spaces, the object will be perceived as deformed on a direction.

2.2.1 Point representation

We'll take as example the four dimensional point, defined by the following coordinates: B (3,6,2,7) where 3 – abscissa, 6 – distance, 2 – level, 7 – time. We need to make known the fact that the term "time" of the measured coordinate on the W axis of the reference system is a conventional name and it's not referring to the physical term of time, this having the same spatial properties as any other axis of the system. We use the term "time" because, traversing the 4th axis, determines the superior level of projection on the tridimensional space, which we perceive as a physical space, form transformations or placement of the projected object, which we associate with the passing of time.

The perspective geometry representation of point B (Fig. 3) has deficiencies due to the impossibility to include a S4 space in a S3 space, so visual aberrations show up, like the intersection between projection plans (WXW) and (LYZ) which, according to the rules of tridimensional geometry, should intersect after a line, but in S4 these are concurrent only in a point (the system's origin).

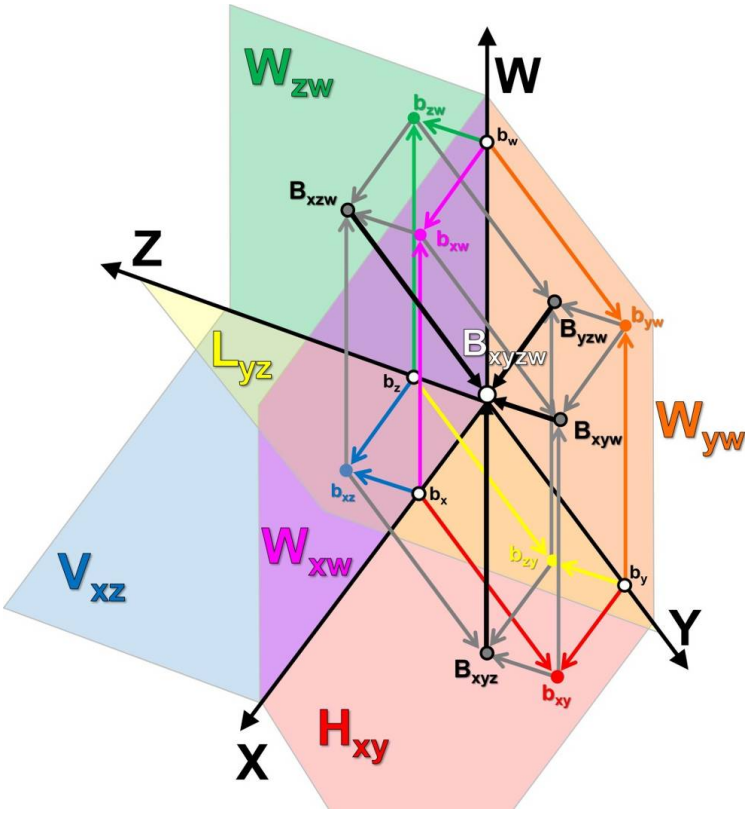

Fig. 3 Isometric perspective geometry of point B(3,6,2,7)

The tridimensional draught of point B is made by rolling out the subspace determined by axis X, Y, Z, in the horizontal projection plan according to the rules of classic descriptive geometry. In the reference system made (Fig. 4), the projection plans respect the geometric rules of the tridimensional space, this being able to be used as a graphical instrument to correctly determine the coordinates of the represented point.

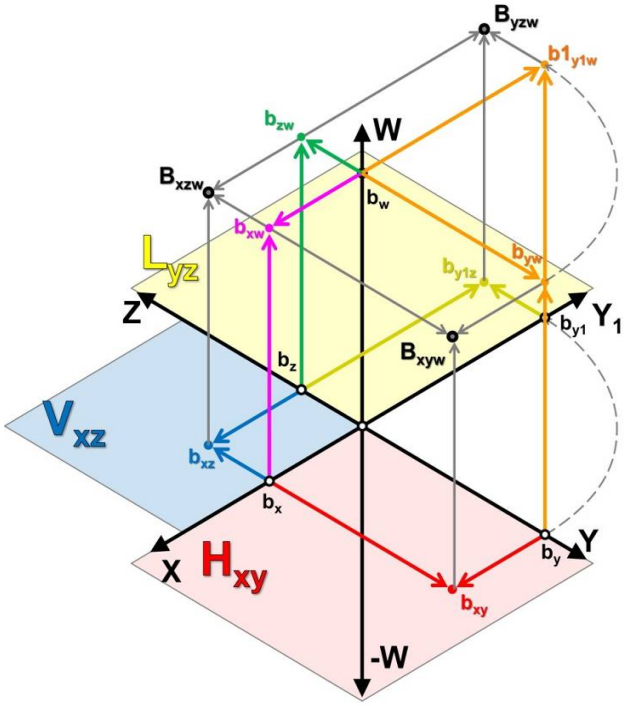

Fig. 4 Tridimensional draught E3 of point B(3,6,2,7)

In the conventional representation above, the subspace SXYZ disappears, being represented just through his projections on the reference plans, and the other tridimensional subspaces overlap in one tridimensional space, governed by the rules of classic geometry. A four dimensional object can have 4 representations on the draught, depending of the tridimensional subspace that is rolled out.

The draught E3 ca be, at its own turn, rolled out into an inferior rank draught (E2) hence making the draught bi-dimensional of point B (Fig. 5). This gives us the possibility to geometrically handle multidimensional object, on the piece o papers plan. This way of representing reduces the graphical complexity of the drawing, assuring in the same time all the information necessary for geometric operations. No matter the number of dimensions that characterize the geometric form, these can be reduced to a conventional representation in two dimensions, the correlations between the reference systems making possible the consecutive passing from a space with a number of dimensions to an inferior one.

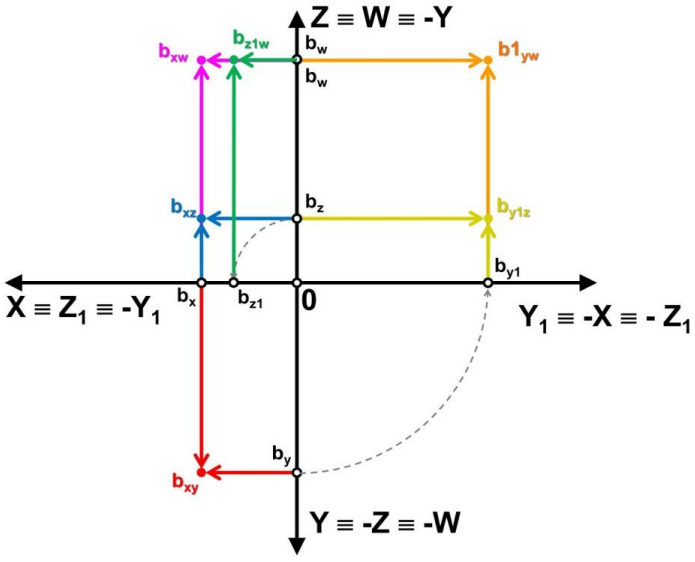

Fig. 5 Bi-dimensional draught E2 of point B(3,6,2,7)

2.2.2 Four dimensional line representation

A line is spatially determined by two points. Next we'll follow the example of the $\overline{AB}$ line determined by the points A(5,2,6,1) and B(3,6,2,7). In the E3 draught (Fig. 6) it can be observed that the line projections can be represented on the S3 subspaces, this rolling out and overlapping on the tridimensional space. We'll note the projection of the points with indexes representing the dimensions which determine the respective subspace; hence AXZW represents point A projection on S3 subspace determined by the $\overline{X}$, $\overline{Z}$,$\overline{W}$ axis. By joining all the projections of the point on the subspace of the same nature, it's obtained the projection of the line on the respective subspace.

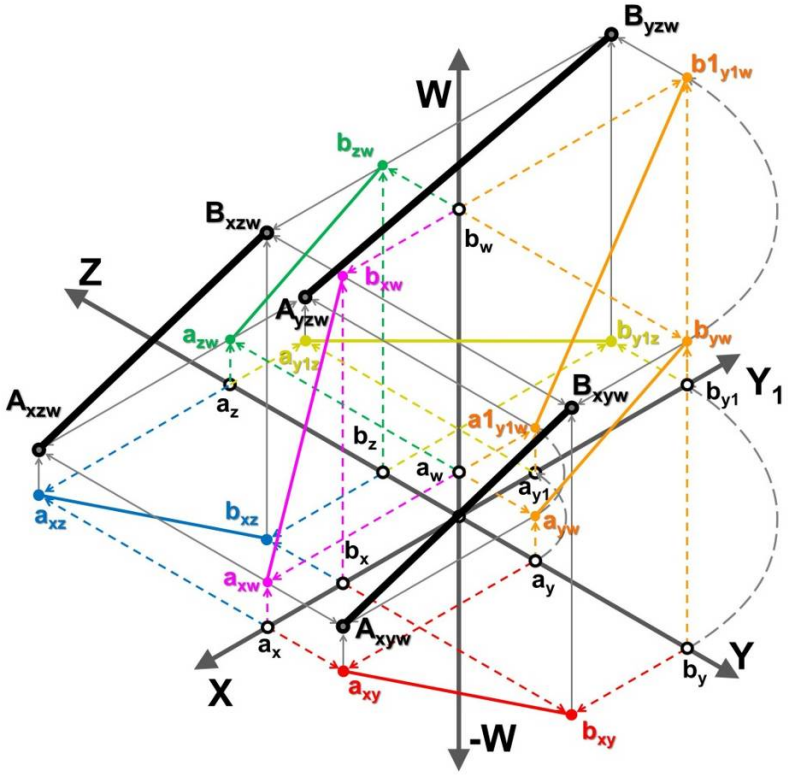

Fig. 6 E3 draught of line $\overline{AB}$

By cutting the plans W(Y, O, W) and W(X, O, W) on the horizontal projection plan, together with line $\overline{AB}$'s projections, we obtain the E3 draught of the line (Fig. 7). The plane representation reduces a lot from the complexity of the drawing and allows the making of geometric operations, like: determining the imprints of the line or of a plan, determining the real size of the elements, the intersection of four dimensional objects, etc.

The postulates characteristic to the tridimensional space remain valid, but they will need to be rephrased such as to also contain the dimensions that have been added. Hence, two lines are parallel if they have all the projections of the same nature parallel between them, but two lines disjoint in the four dimensional space can have the tridimensional projection parallel between them. In mathematics, the problem of postulate generalization from a reference system to another one with a different number of dimensions leads to the apparition of the concept on non-Euclidean space.

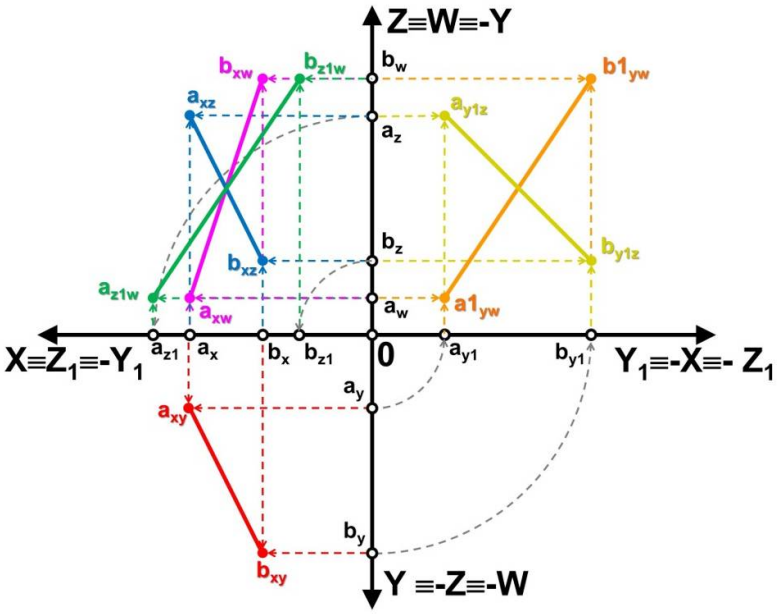

Fig. 7 E3 draught of line $\overline{AB}$

In the case of the object determined by five dimensions, the bi-dimensional draught E2 of the four dimensional space becomes the horizontal plan of the E3 draught, the fifth dimension being represented perpendicularly on it. The process can iterate for n dimensions.

3. Practical applicability

Multidimensional descriptive geometry can have distinct practical appliances from which we'll present a few.

Modern mathematics operates with highly abstract notions and hard to guess at first sight. Descriptive geometry can constitute an educational tool in the graphical exemplification of complex mathematical notions and operations, even offering means of graphical solving of certain problems that belong to the field of mathematics and physics.

The representation in high rank draught can constitute the development base of new modelling tools and graphic analysis, applicable to generative geometry, through movement transfer and metamorphose of objects in time, in tridimensional geometric constructions. The growth of computer processing power allows the visualization and operating with geometrical structures as more as complex they get, and to generate them new methods and tools are necessary.

By introducing the notion of multidimensionality in descriptive geometry it wanted the continuation of graphic procedures described by the mathematician Gaspard Monge, their generalization at complex spaces and the creation of a way of graphic analysis of the geometric forms characterized by more dimensions.

References

[1] Monge, G. (1795a). *Géométrie descriptive. First ed. in Les Séances des écoles normales recueillies par des sténographes et revues par des professeurs*, Paris. Re-edition in Dhombres, J. (ed), 1992: *L'Ecole normale de l'an III, Leçons de mathématiques*, Laplace, Lagrange, Monge. Paris: Dunod, pp. 267-459. This last re-edition has been used as the reference for page numbers.

[2] Plato, *Collected Dialogues* (1961). Edited by Edith Hamilton and Huntington Cairns. Princeton: Princeton University Pressm, ISBN – 0-69109-718-6.

[3] Kant, I., *Critique of Pure Reason* (1965). Translated by Norman Kemp Smith. New York: St. Martin's Press, ISBN – 0-31245-010-9.

[4] Descartes, R. (2001). *Discourse on Method, Optics, Geometry, and Meteorology*. Trans. by Paul J. Oscamp (Revised ed.). Indianapolis, IN: Hackett Publishing. ISBN 0-87220-567-3.

[5] Lobachevsky, N. (1891). *Geometrical investigations on the theory of parallel lines*. G. B. Halsted (tr.). Reprinted in Bonola: NonEuclidean Geometry, 1912. Dover reprint, 1955.

[6] Bolyai, J. (1896). *The science absolute of space: independent of the truth or falsity of Euclid's axiom XI (which can never be decided a priori).* The Neomon, Austin.
[7] Klein, F. (1872). *Vergleichende Betrachtungen über neuere geometrische Forschungen* (*A comparative review of recent researches in geometry*), Mathematische Annalen, 43 (1893) pp. 63–100 (Also: Gesammelte Abh. Vol. 1, Springer, 1921, pp. 460–497).
[8] Klein, F. (2004). Elementary Mathematics from an Advanced Standpoint: Geometry, Dover, New York, ISBN 0-486-43481-8 (translation of *Elementarmathematik vom höheren Standpunkte aus*, Teil II: Geometrie, pub. 1924 by Springer).
[9] Hawkins, Th. (1984). "*The Erlanger Programm of Felix Klein: Reflections on Its Place In the History of Mathematics*", Historia Mathematica 11:442–70.
[10] Kaluza, Th., (1921). "Zum Unitätsproblem in der Physik". Sitzungsber. Preuss. Akad. Wiss. Berlin. (Math. Phys.): 966–972.
[11] Klein, O. (1926). "Quantentheorie und fünfdimensionale Relativitätstheorie". Zeitschrift für Physik A. 37 (12): 895–906.
[12] Șerbănoiu, B. V. (2012). *Reprezentări geometrice: punctul, dreapta și planul* (Geometrical Representations: Point, Line and Plane), Iași, Editura Societății Academice “MATEI-TEIU BOTEZ”, ISBN – 978-606-582-018-0.

The Multi-Criteria Analysis of the Waterproof Rehabilitation Methods of the Buildings' Infrastructure

Tămaş F-L.[1], Moga L.M.[2], Munteanu C.[3], Taus D.[4], Babota F. [5]

[1, 4] *Transylvania University of Brasov, Faculty of Civil Engineering (ROMANIA)*
[2, 3, 5] *Technical University of Cluj-Napoca, Faculty of Civil Engineering (ROMANIA)*
E-mails: florin.tamas@unitbv.ro, ligia.moga@ccm.utcluj.ro, constantin.munteanu@ccm.utcluj.ro, tausdaniel@yahoo.com, florin.babota@ccm.utcluj.ro

Abstract

With a view to adopting an optimal solution for the waterproof rehabilitation of the infrastructure of buildings, we considered necessary a multi-criteria analysis, the more so as the case study is based on a worship object. Thus, the methods based both on the technology of injection and on that of the cut were compared, and the criteria of performance, durability and cost were taken into account. The conclusions of this analysis can be viewed as a starting point to future interventions of this kind.

Keywords: masonry, damp, protective waterproof barrier, injection.

1 Introduction

In the current attempts at eliminating the rising damp in the walls of buildings, we often face the need to choose from the multitude of methods and technologies currently known and promoted by specialized companies. Such an action may prove laborious and time and energy consuming, in the light of the technical and financial implications. The multi-criteria analysis covered three of the most used methods, the case study being an orthodox church.

1.1 *Presentation of the situation*

After the examination of the 'St. Nicholas' Episcopal Cathedral in Gyula, Hungary, several deficiencies that occurred in time were found. The plan of the church is shown in Fig. 1, and some of the issues that were raised are briefly described [1]:

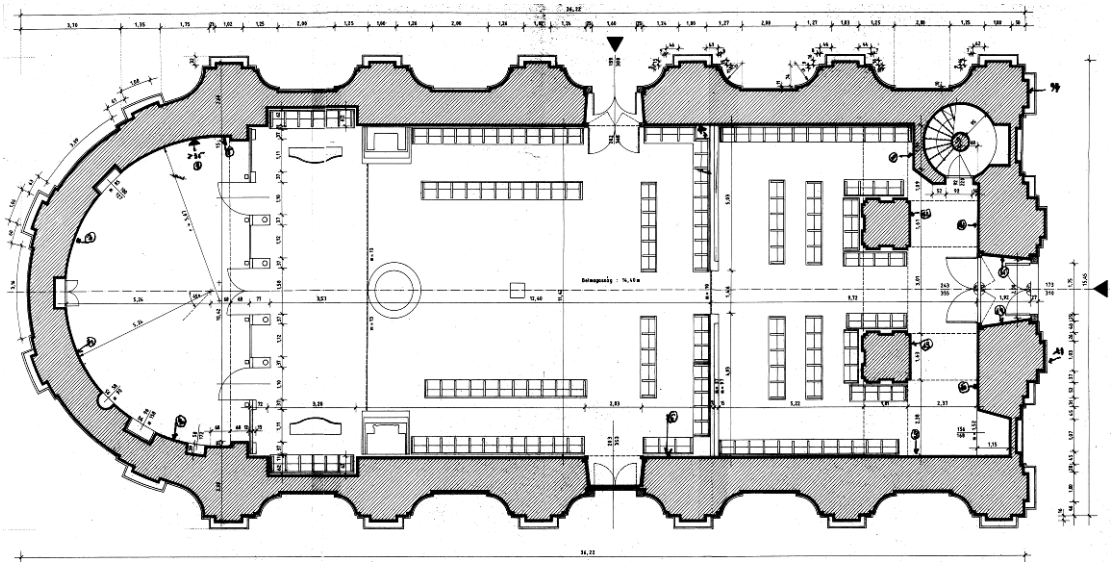

Fig. 1 The plan of the 'St. Nicholas' Episcopal Cathedral in Gyula, Hungary

• variations between 12-35 % of the wall damp, measured in the inside at different elevations relative to the elevation of the finished floor: 20 cm, 50 cm, 1.0 m respectively;

• the occurrence of efflorescence and stains caused by salt degrading the paintings as well;

• especially right at the stone veneer floor joints, the relative humidity had values between 22-28 %;

• the vertical variation of the capillary damp existed to about 2.5 m above the floor level, which could be noticed both from inside and outside.

An image of the church, where one can see the high level of damp is shown in Fig. 2.

Fig. 2 High level of damp on the outside of the church

2 The multi-criteria analysis

From among the methods used for the waterproof rehabilitation of the infrastructure of buildings and acknowledged due to their effectiveness in time Dryzone and DryKit were analyzed, based on the injection technique, and respectively on Comer or the cut method.

Their brief characteristics are listed below as well as the criteria that the study was based on.

2.1 *Characteristics of the DryKit method*

DryKit [2] is a technology suitable for stone or mixed masonry and aims at creating a horizontal chemical barrier to break the rising capillary damp. This is achieved by boring holes in the wall and by injecting solutions with hydrophobic, ecological characteristics – of the type TRE 128 – with reduced drying time.

Depending on the specific conditions to each separate objective, there are two sets of solutions. The first group, A type, contains the compounds TRA 115 and TRX 118, water-based, characterized by a low price cost, environmentally friendly properties, increased penetration capacity and long-term resistance to storage. The second group, B type, contains the solutions TRS 114, TRF 135 and TRE 128, based on solvents. The latter ones are new generation products which do not attack the frescoes; the inhabited buildings can be used the very next day after the intervention.

Judging by what has been mentioned before, the comparative variation of the drying times of the two groups of solutions is shown in Fig. 3.

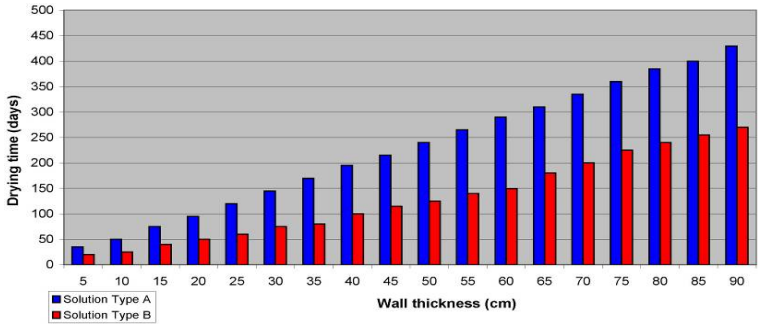

Fig. 3 The variation of the drying times of the solutions in the two groups

2.2 Characteristics of the Dryzone method

Dryzone [3] is a system similar to the previous one, the difference consists in the fact that, for the creation of the horizontal barrier against the capillary damp, it uses substances in the form of a cream, not liquid solutions. It was patented in England and it complies with the provisions BS 6576:2005+A1:2012 Code of practice for diagnosis of rising damp in walls of buildings and installation of chemical dam-proof courses.

For such a system to be competitive, it must meet several criteria referring to the injected substance, by recalling [4]:

- it should be based on water:
- it should provide a stable formula;
- it should have low toxicity;
- the application should be clean, fast and easy;
- it should have no odor and it should be ecologic.

Given the fact that the cream bars are packed in cartridges of 600 ml each [3], the variation of the necessary number for the treatment of the walls with different lengths and thickness is shown in Fig. 4.

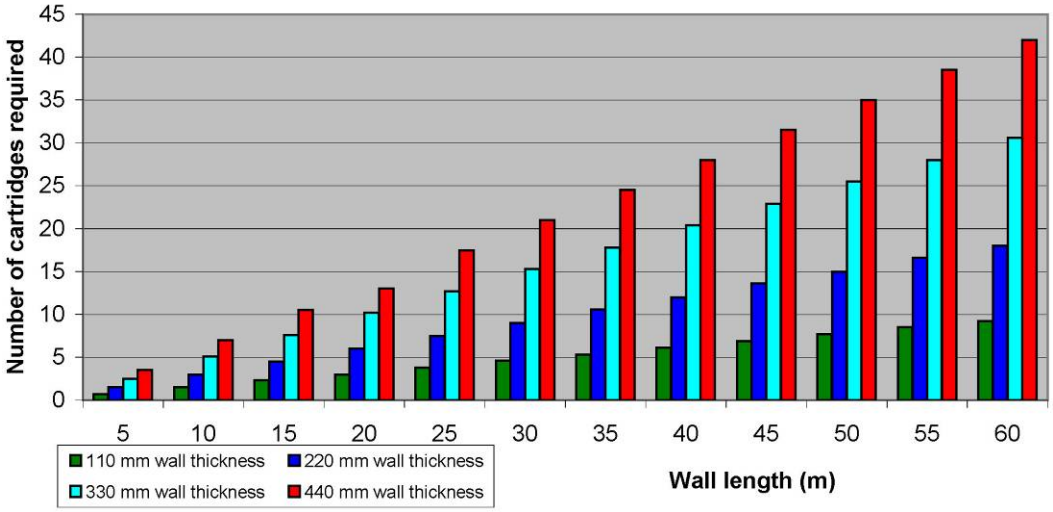

Fig. 4 The variation of the number of bars for different wall lengths and thickness

2.3 Characteristics of the method Comer

The second technological system by which the waterproof rehabilitation measures were implemented in the infrastructure of buildings is based on the principle of the wall cutting.

To this category belongs the Comer method. Basically, this means that in the cut is introduced, firstly, an insulating foil. Then anchorage wedges, made of plastics, are inserted and they have the role to ensure the stability of the wall. They have variable sizes, being shown schematically in Fig. 5, their display being made in concordance with the thickness of the wall [5].

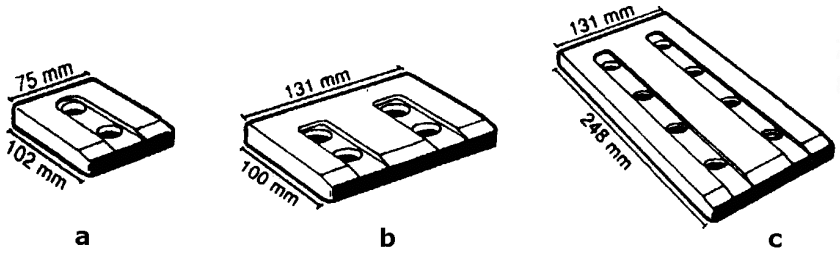

Fig. 5 Anchorage wedges: a - small; b - average; c - big

The whole assembly becomes monolith by injecting grout at a pressure of maximum 2 atm.

In order to optimize this technology different research was carried out by which the variation of the occupancy with anchorage wedges depending on the wall thickness and the percentage of mortar filling, relative to 1 ml wall length could be expressed graphically.

For a wall having a thickness of 44 cm, the display of the wedges in section is done according to Fig. 6.

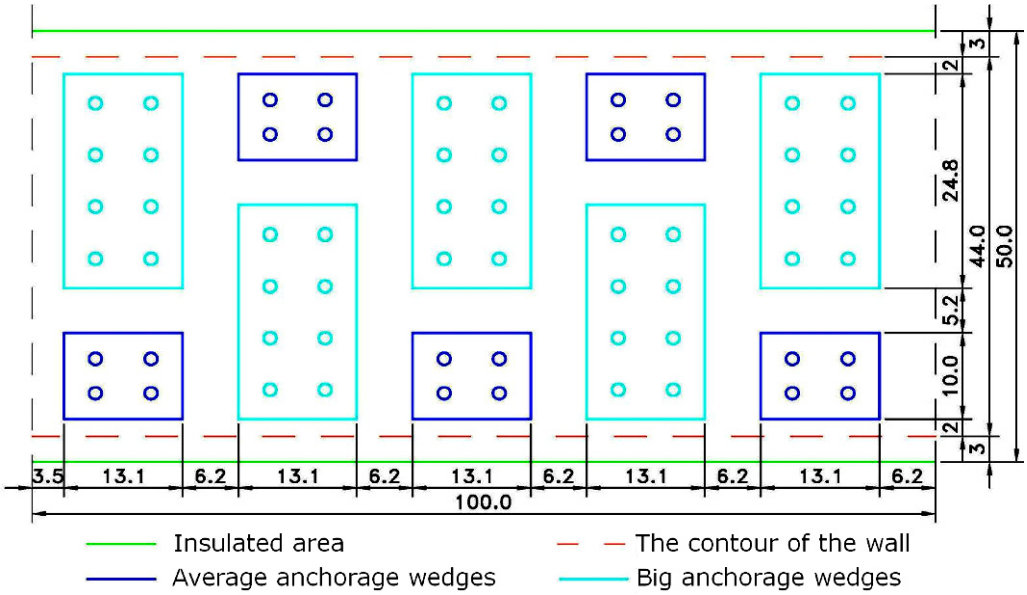

Fig. 6 The display of the anchorage wedges and of the insulating foil for a wall having a thickness of 44 cm

2.4 The analysis criteria

The intervention measures in the sense of the waterproof rehabilitation of the infrastructure of buildings damaged by damp are never singular and they do not simply remove water from walls.

The interventions that were taken into consideration for the multi-criteria analysis were the following:

• the breakage of the capillary action at the level of the walls by one of the methods described above;

• the ventilation of the foundation, on the outside, to the level of the base or up to 1.80 m depth, if it is lower than 2.50 m, as shown in Fig. 7 [1]:

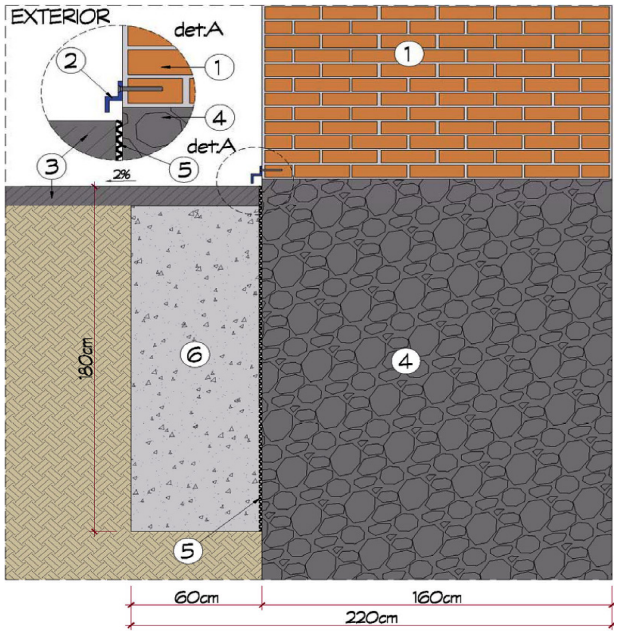

Fig. 7 Ventilation detail of the foundation on the outside

In Fig. 7 the notations are as follows:

1 - exterior masonry wall;

2 - 'Z' protection profile;

3 - concrete pavement;

4 - foundation;

5 - vertical foil waterproofing with neps;

6 - mono-granular gravel filling.

• the ventilation of the foundation and of the floor indoors, to a depth of 80 cm, the breakage of the capillarity beneath it, in the whole Cathedral, by the insertion of a 25 cm thick drainage layer, and the additional endowment of the horizontal waterproofing with neps. This will be interrupted in the area of the ventilation perimeter duct, of about 20 cm thick. These measures are shown in Fig. 8 [1].

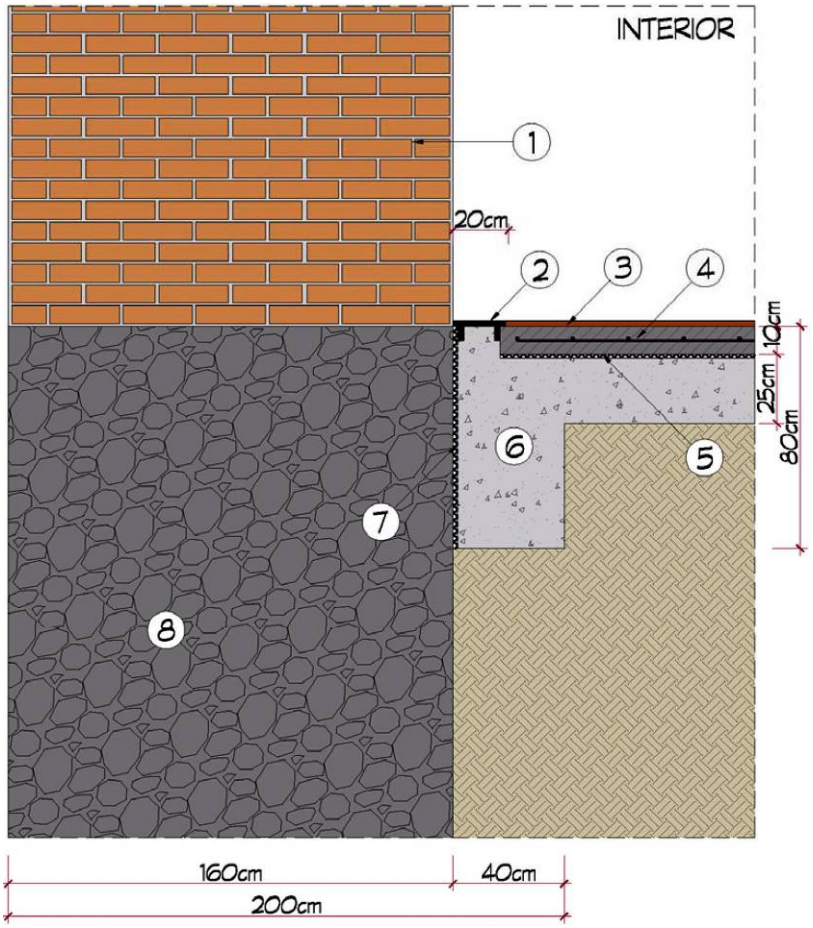

Fig. 8 Ventilation detail of the foundation on the inside

In Fig. 8 the notations are as follows:
1 - exterior masonry wall;
2 - galvanized steel grid;
3 - floor;
4 - lightly reinforced concrete plate;
5 - under-plate horizontal waterproofing, nep foil type;
6 - mono-granular gravel infill;
7 - vertical waterproofing, nep foil type;
8 - foundation.

• the remedial of the rendering in the exfoliated areas;
• the execution of the indoor and outdoor painting with water-based materials and oxides;
• the correct collection of the rainwater.

Taking into consideration the above, the analysis criteria referred to:
• overall quality characteristics;
• the possibility of risks of solution leaks, or the failure to introduce the calculated number of bars;
• the warranty of the work, due to the solving of the problem of rising damp;
• the estimated cost of the intervention;
• the length of the intervention;
• the overall assessment of the investment in the waterproof rehabilitation, comprising the three zones: the exterior of the church, its interior, and the wall, respectively.

3 Conclusions

The multi-criteria analysis conducted after the examination of the 'St. Nicholas' Episcopal Cathedral in Gyula, Hungary, led to the drawing up of some centralizing tables which facilitate the orientation among the three methods that were studied.

At the same time, ratings from 1 to 5 were awarded for a clearer appreciation with a view to the investment decision.

For a 50 cm thick wall, the comparative situation is presented below in Table 1.

Table 1 The comparative situation for a 50 cm thick wall

50 cm thick wall			
Method	DryZone	Comer	DryKit
Solving the problem of the rising damp	10 years	Final	Final
Estimated cost	≈69 euro/ml	≈66 euro/ml	≈140 euro/ml
Intervention type	12 cm Holes	Mechanics	15 cm Holes
Risk of uncontrolled solution leakage	-	-	No
Failure to introduce the number of bars	No	-	-
Quality	4	5	5
Quality -price	4	5	3

References

[1] Streza, T. (2016). From the practical work of removing moisture from the masonry capillary, Book of science house, Cluj-Napoca.
[2] DryKit specifications. www.drykit.it.
[3] DryZone specifications. www.dryzone.eu.
[4] BS 6576:2005+A1:2012, Code of practice for diagnosis of rising damp in walls of buildings and installation of chemical dam-proof courses, BSI 2012.
[5] Comerspa specifications. www.comerspa.com.

Environmental Protection by Construction of the Energy Saving Buildings in Town Satu Mare

Tataru A.C.[1], Tataru D.[1], Stanci A.[2]

[1] *Department of Mechanical and Industrial Engineering and Transports, University of Petrosani, Petrosani, (ROMANIA)*
[2] *Departament of Management, Environmental Engineering and Geology, University of Petrosani, Petrosani, (ROMANIA)*
E-mail: andreeastanci@yahoo.com, dorin.tataru@yahoo.com

Abstract

The concept of ”passive House” has been introduced for the first time in Germany, in the Passive House Institute, subsequently being extended and at higher latitudes and different features climatic from those of Germany, in the south, west and south-west of Europe. In this paper we strive to study at the concept of “passive house” in the Romania. Using the Passive House Planning Package (PHPP) software 2007, we calculate the heating requirements for such a House, depending on the latitude and climate conditions in the locality. For the study were selected a city from Romania placed to 47,47 latitude and 22,52 longitude. To determine the possibility of implementing the concept of the ”passive House” must be determined: required heating, cooling demand and primary energy demand. In order to implement this concept should not exceed maximum limits.

Keywords: passive house, required heating, primary energy, climatic areas.

1 Introduction

One of the most discussed global problems is related to environmental protection. Worldwide, researchers are looking for solutions to reduce the pollution. With these concepts of environmental protection was introduced and passive building concept that means low power consumption house. By reducing energy consumption and reduce pollution to obtain energy.

Passive house concept was first introduced in Germany. Passive building has been defined by Wolfgang Feist, Passive house Institute, as being the building that demand for heating must not be more than 15 kWh/m² year, and total consumption of primary energy should not be more than 120 kWh/m² year. Also, the number of changes of air per hour at a pressure of 50 Pascals should be less than 0.6 h^{-1} [1], [2], [4], [5].

The concept has been extended to other latitudes and climates in southern, western and south-western Europe.

We ask ourselves if this passive building concept also applies to different latitudes than those of Germany. In this paper we propose to study the possibility of implementing the concept of "Passive house" in a city located at different latitudes of Germany, on the Romanian territory.

2 Presenting the concept of "passive house"

"Passive buildings" are categorized as "low energy buildings". The term of "passive house" has its origin in the fact that due to its special construction, the building is less sensitive in terms of thermal comfort to changes of meteorological parameters. The solar energy incident on the outer surface of the building, which penetrates through various mechanisms for transfer, plus the energy generated by the tenant and by the operation of electrical equipment or other, it is normally sufficient for keeping an inner temperature comfortable during the cold season.

Passive buildings are those buildings that provide a comfortable indoor climate in summer and winter, without the need for a conventional heating.

The passive house concept is a peak in energy efficient construction. For the passive house, the need for energy heating is below 15 kW/h/m^2/year.

Passive house is more than a home that saves energy, and passive building concept, is a global concept for building of quality homes, healthy and sustainable.

Most important of the concept of the passive house is the presence of fresh air in every room. It is used for heating - in reasonable quantity, without uncontrolled circulation, without noise and currents.

The idea of "fresh air heating" is only possible in a building very well insulated, tight as passive house. Energy demand for heating should be below 10 W/square meters (habitable sqm) if we want to use air ventilation and heating the building. Passive house supposes performance in terms of: insulation, construction without thermal bridges, air tightness, and ventilation with heat recovery, windows and innovative technique.

For all this to work harmoniously building's energy balance is achieved with specialized PHPP program, developed by the Passive house Institute in Darmstadt [1], [2], [3], [4], [5].

3 Presenting the concept of "passive house"

Satu Mare is a county capital and largest city of Satu Mare County, Romania. It has a population of 102411 habitants in 2011. Satu Mare is located in Satu Mare County, in northwest Romania, on the river Somes, 13 km from the Hungarian border and 27 km from the border with Ukraine. Exact coordinates are latitude 47°47'30, 22°52'30 meridian, altitude 126 meters (Fig. 1) [7].

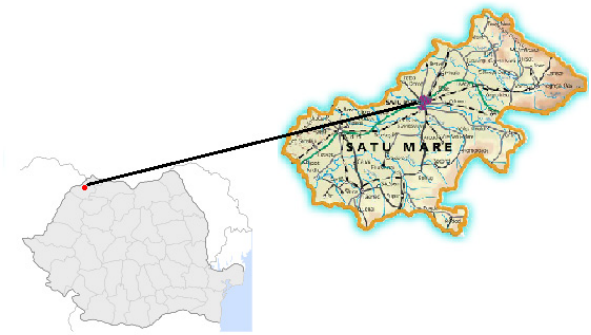

Fig. 1 Location Satu Mare

Satu Mare has a continental climate characterized by warm dry summers and cold winters. Monthly average temperatures maximum values up to 19-20 ° C in the summer and -10 ° C minimum during the winter months (Fig. 2, 3).

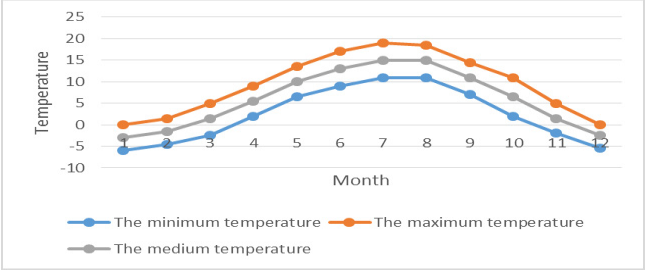

Fig. 2 The monthly temperature for Satu Mare, Romania (°C)

Relative humidity in the study area does not have values that exceed the 71% or less than 47.5%. Relative humidity is lower in summer and higher in winter months (Fig. 3).

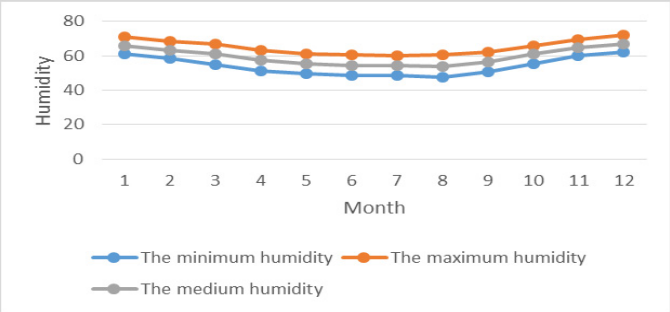

Fig. 3 Monthly relative humidity for Satu Mare, Roumania (%)

4 Evaluation and interpretation of data obtained for the construction of passive houses in the studied area

To interpret climate data as well as possible, we must know very well the types and climatic characteristics of the study area. Determination climate zone was performed using Koppen climate classification system for Europe (Fig. 4) [6].

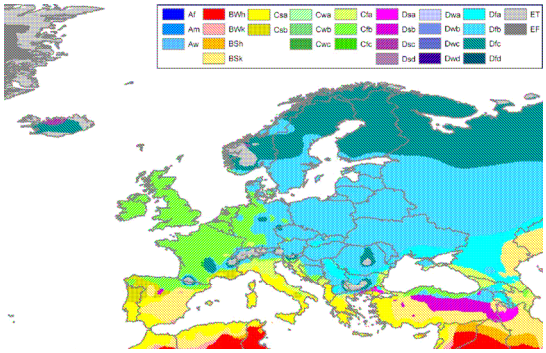

Fig. 4 Europe climate zones according to Koppen [6]

Satu Mare belong Koppen Climate Classification System for Europe of the DFB - Continental wet (hot summers, severe winters moist without dry season).

For this study we processed climatic data (average monthly climatologically database of solar radiation, temperature and relative humidity) for Satu Mare area, taken from the site www.soda-is.com (Fig. 5). (Soda-is) [8].

Climatic date was processed using Fortran Programs, and introduced in the Passive House Planning Package (PHPP) 2007 - the specialized program AMVIC house.

Monthly means of irradiances, temperature and relative humidity

	Irradiance	Irradiance kLy/year	Irradiation	Temp.Min	Temp.Max	Temp.Mean	Rel.Hum.Min	Rel.Hum.Max	Rel.Hum.Mean
01	20	15	173	-8.5	-1.5	-5.0	66.5	77.5	72.0
02	50	38	432	-6.5	1.5	-2.5	64.5	75.5	70.0
03	104	78	899	-4.0	6.0	1.0	60.0	72.5	66.5
04	148	111	1279	2.5	12.5	7.5	57.5	70.0	64.0
05	192	144	1659	9.0	19.0	14.0	55.0	67.5	61.5
06	204	153	1763	13.0	23.0	18.0	54.5	67.0	61.0
07	192	144	1659	15.5	26.0	21.0	54.5	66.5	60.5
08	180	135	1555	15.0	25.0	20.0	53.5	66.5	60.0
09	112	84	968	9.5	20.0	15.0	56.5	68.5	62.5
10	76	57	657	3.5	14.0	9.0	60.5	72.0	66.5
11	34	26	294	-2.0	5.0	1.5	66.5	76.5	71.5
12	18	14	156	-7.5	0.0	-3.5	68.0	77.5	73.0
13	110	83	950	3.5	12.5	8.0	60.0	71.5	66.0

Fig. 5 Climatic data for Satu Mare

Climatic data results after running the FORTRAN program (Fig. 6) and introduced in the climatic data sheet in Passive House Planning Package (PHPP) 2007 program (Fig. 7).

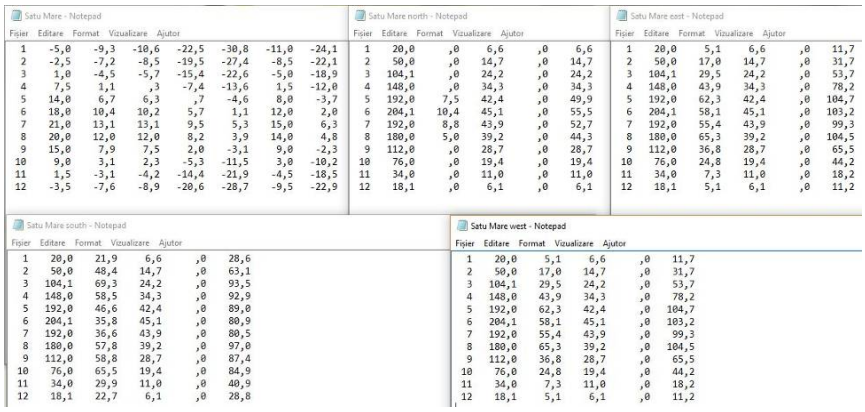

Fig. 6 Climatic data results after running the FORTRAN program

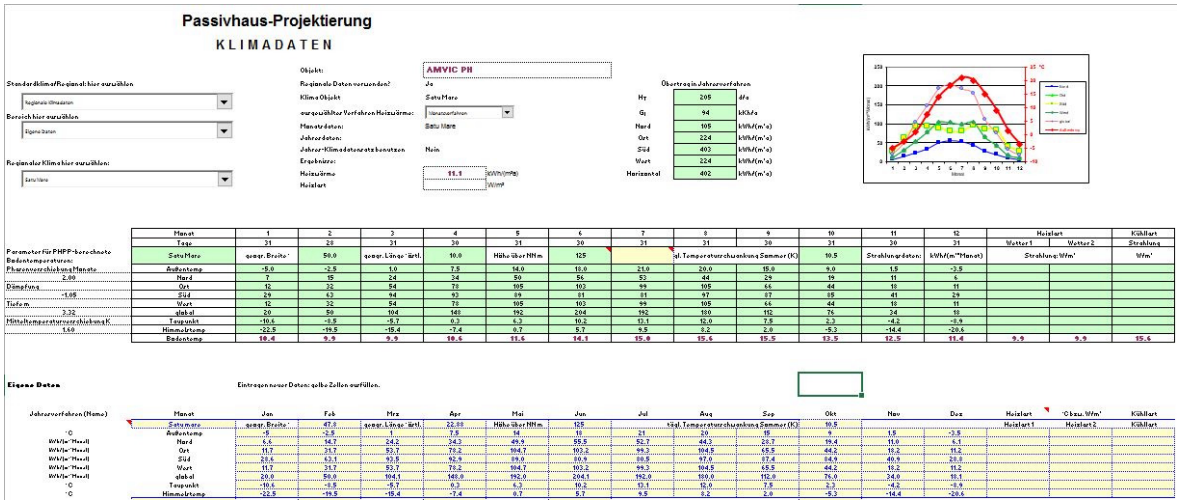

Fig. 7 Introduction of climate data in Passive House Planning Package (PHPP) 2007 program

The analysis was performed after the office building model Amvic (Fig. 8).

Fig. 8 Passive office building AMVIC – Bragadiru

Amvic building is structured as follows: ground floor, three floors and attic. The structure and main functions of the office building Amvic are: on the ground floor there is a large open space, secretarial and department office. In a separate area is a technique room. The first, second and third floor have office space. In the attic there are five apartments Amvic (Fig. 9).

Building envelope and interior divisions are separating elements with high thermal results. They are grouped into inner and outer walls respectively, roof, floor and plate. The outer walls are fitted with triple stratified low-e glazed.

Ground floor plan for office building Amvic

Floors plan for office building Amvic

Attic plan for office building Amvic

Fig.9 Plan for Passive office building AMVIC

After processing climate data and entering them into the computer program Passive House Planning Package (PHPP) 2007, we obtained results for Amvic.

Amvic house is a passive house office with an area of 2086 m^2. Windows from the southern area of 156 m^2, 56,08 m^2 northern, western and eastern 83,21m^2 of 42.35 m^2

Following the analysis made that the office building AMVIC passive heating demand is 11 kWh / m²an. The maximum limit for heating needs of a passive house is 15 kWh / m² year. Total energy consumption is 84 kWh / m²year. The limit on total energy consumption is 120 kWh / m² year (Fig. 10).

Following this analysis, can be seen as passive house concept is viable in this climate zone, falling into a necessary heating less than 15 kWh / m² year.

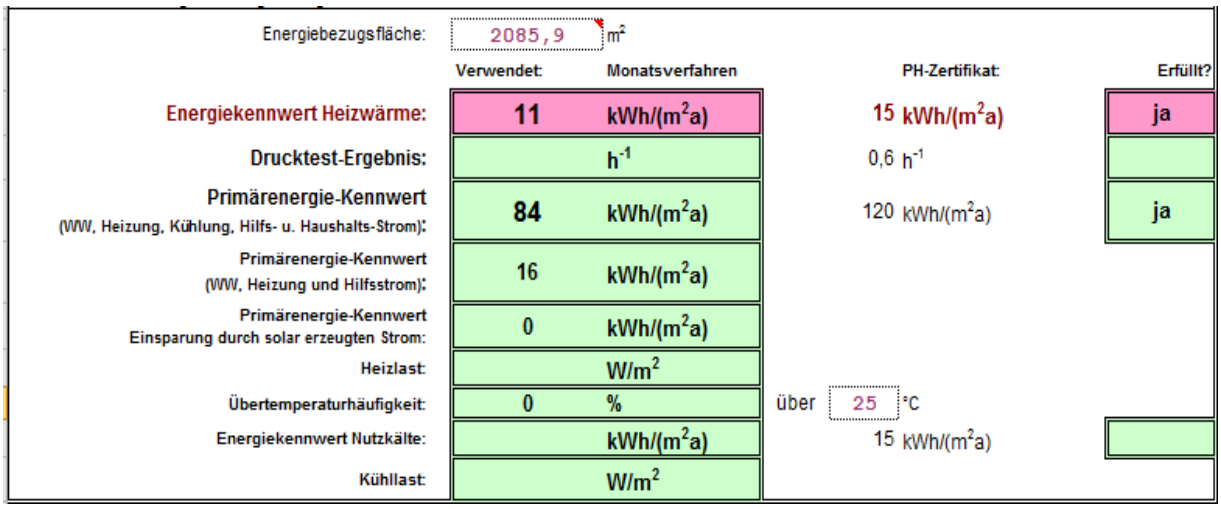

Energiebezugsfläche:	2085,9	m^2		
	Verwendet:	Monatsverfahren	PH-Zertifikat:	Erfüllt?
Energiekennwert Heizwärme:	11	kWh/(m^2a)	15 kWh/(m^2a)	ja
Drucktest-Ergebnis:		h^{-1}	0,6 h^{-1}	
Primärenergie-Kennwert (WW, Heizung, Kühlung, Hilfs- u. Haushalts-Strom):	84	kWh/(m^2a)	120 kWh/(m^2a)	ja
Primärenergie-Kennwert (WW, Heizung und Hilfsstrom):	16	kWh/(m^2a)		
Primärenergie-Kennwert Einsparung durch solar erzeugten Strom:	0	kWh/(m^2a)		
Heizlast:		W/m^2		
Übertemperaturhäufigkeit:	0	%	über 25 °C	
Energiekennwert Nutzkälte:		kWh/(m^2a)	15 kWh/(m^2a)	
Kühllast:		W/m^2		

Fig. 10 Heating requirements and overall energy consumption AMVIC passive office building located in Satu Mare

By implementing the Passive House concept, has been made a significant reduction in energy consumption and also a date and a reduction of pollution. In implementing this concept, we achieve a reduction of pollution with CO^2 by 0,34kg per unused kWh.

5 Conclusions

Passive house concept was first introduced in Germany and represents achieving low energy consumption for buildings.

By reducing the power consumption, was reduced pollution of the environment.

To certify a building as a passive house must meet this demand on heating not more than 15kW/h/m^2/year.

Another criteria is the total energy consumption that should not overpass 120 kWh / m²an.

The study conducted in Satu Mare qualifies a viable realization of buildings to be certified as passive buildings.

By implementing this concept of a reduction of pollution CO^2 for each unused kWh was reduced CO^2 by 0,34kg.

References

[1] Adamson B, (2011). Towards passive houses in cold climates as in Sweden. Division of Energy and Building Design Department of Architecture and Built Environment, Lund University, Faculty of Engineering LTH.

[2] Albert Boqvist, (2010). Passive House Construction, Symbiosis between Construction, Efficiency & Energy Efficiency, Division of Structural Engineering, Lund Institute of Technology, Lund University, Report TVBK-1040, Lund.

[3] Badescu V. (1991). Studies concerning the empirical relationship of cloud shade to point cloudiness (Romania). Theoretical and Applied Climatology 44, 187-200.

[4] Catalin Teodosiu (2008) – Sisteme de instalaţii interioare pentru case pasive adecvate condiţiilor climatice din România.

[5] Energy Saving Potential (2006). The PEP-project is partially supported by the European Commission under the Intelligent Energy Europe Programme, EIE/04/030/S07.39990, May.

[6] http://ru.wikipedia.orghttp://.
[7] http://ru.wikipedia.orghttp://.
[8] www.soda-is.com/eng/services/service_invoke/gui_result.php?InputXML=SoDaParam_1377613126495.xml&ServiceXML=ncep_material.xml.

Cut-out Weakening Investigation on Precast Reinforced Concrete Wall Panels

Todut C.[1], Dan D.[2], Stoian V.[3], Fofiu M.[4]

[1,2,3,4] *Department of Civil Engineering, Politehnica University of Timisoara, Timisoara, Romania*
E-mail: carla.todut@student.upt.ro

Abstract

The current study presents a part of an experimental program developed to study the seismic performance of precast reinforced concrete wall panels with and without openings. The analysed specimen openings implied narrow and wide door openings, small and large window openings, and balcony openings. The investigated cut-out openings were door and balcony cut-outs performed in solid walls, and opening enlargements, from narrow to wide door opening, from small to large window opening, and from window to door opening enlargement. The developed research implied besides the seismic behaviour study and cut-out weakening effect investigation, the determination of other characteristics also, like the energy dissipation, stiffness degradation, strain analysis, numerical modelling, theoretical evaluation using design code provisions and plastic mechanism model. In the present paper, the study is focused on the weakening investigation on two unstrengthened specimens. These two specimens refer to a precast reinforced concrete wall panel (PRCWP) having a large window opening (L3) and tested unstrengthened (T), and a precast reinforced concrete wall panel (PRCWP) having a large window opening (L3), enlarged to a wide door opening (L3/E3) and tested unstrengthened (T).

Keywords: cut-out, reinforced concrete, wall, numerical analysis

Introduction

In order to understand the behaviour of precast reinforced concrete shear wall panels, the authors focused the research on experimental, theoretical and numerical investigation, and searched the latest documentation available in literature with similar research directions. Fintel, author of "Performance of Buildings with Structural Walls in Earthquakes of the Last Thirty Years" [1] and "Shear Walls – an Answer for Seismic Resistance" has investigated on many earthquakes between 1960 and 1990, and reported a good seismic performance of the shear wall buildings. The presence of openings in reinforced concrete walls attracted the interest of several other researchers, such as Mosoarca [3], Guan et al. [4], Wang et al. [5], Hara T. and Doh J. [6], Takehara et al. [7], Fragomeni et al. [8], Demeter [9] and others.

Experimental specimens and test setup

The part of the experimental program presented in this study consists of two 1:1.2 scaled elements of PRCWP (16 and 17), designed and casted according to a Romanian Project Type 770-81 [10], [11]. The reinforcement of the PRCWP (16-L3-T) specimen having a large window opening (L3) contains horizontal rebars, vertical continuity bars, welded wire mesh in the left and right piers, a spatial reinforcement cage in the coupling beam, four inclined bars at the corners of the opening, a vertical bar each side of the opening on its height, and a wire mesh in the parapet. The PRCWP (17-L3/E3-T) specimen having a wide window opening (L3) enlarged to a wide door opening (E3) has the reinforcement corresponding to the large window specimen (16-L3-T), but reduced according to the wider opening dimensions. The specimens were manufactured at the constructional site, whereas the cut-outs were performed at the Reinforced Concrete Laboratory.

1.1 Material properties

Material tests were performed on concrete and steel rebars used for specimens. The results showed the following classes for concrete: C20/25 for PRCWP (16-L3-T) and C16/20 for PRCWP (17-L3/E3-T). The steel reinforcement type used was smooth (OB37) and ribbed (PC52) hot-rolled bars and cold-drawn ribbed welded

fabric (STPB). The properties of the concrete in the web panel specimen are given in Table 1 and the measured steel strengths are given in Table 2.

Table 1 Properties of the concrete in the web panel specimen

Element	No. of samples	$f_{cm,cube}$ (N/mm^2)	f_{ck} (N/mm^2)	Class of concrete
PRCWP (16-L3-T)	3	34,11	23,17	C 20/25
PRCWP (17-EL3-T)	3	26,54	18,31	C 16/20

Table 2 Measured steel strengths

Re-bar type	Production / surface	Φ (mm)	f_y (MPa)	f_t (MPa)	f_t / f_y
OB	hot-rolled / smooth bar	6	400	550	1,38
		8	425	507	1,19
PC	hot rolled / ribbed bar	8	424	553	1,30
		10	450	564	1,25
		14	395	584	1,48
		16	385	613	1,59
STPB	cold-drawn / ribbed wire	4	618	667	1,08

Note: f_y - yield strength of reinforcement; f_t - tensile strength of reinforcement

1.2 Testing methodology and test set-up

The specimens were laterally loaded, reversed cyclic - displacement controlled. The displacement control was set to a drift ratio of 0.1 %, namely 2.15 mm. Two cycles per drift were performed. In addition to the horizontal loading, vertical loads were also applied. These axial loads were composed of a constant part, which was used to simulate the gravity loading condition at the base of the wall specimen, and an alternating part, which was used for restraining the rocking rotation of the elements. The behaviour of the specimens during the experimental tests was monitored by the pressure transducers (P), displacement transducers (D) and strain gauges placed onto the reinforcement bars (G). Detailed data related to the testing methodology was detailed presented in [12].

2 Experimental results

2.1 Force–drift ratio response and observations

The response of the tested specimens is shown in Fig. 1 as load-drift ratio hysteresis loops. A significant reduction in lateral resistance was obtained for the specimen having large opening dimensions (PRCWP 17-L3/E3-T) compared to the one with smaller opening dimension (PRCWP 16-L3-T).

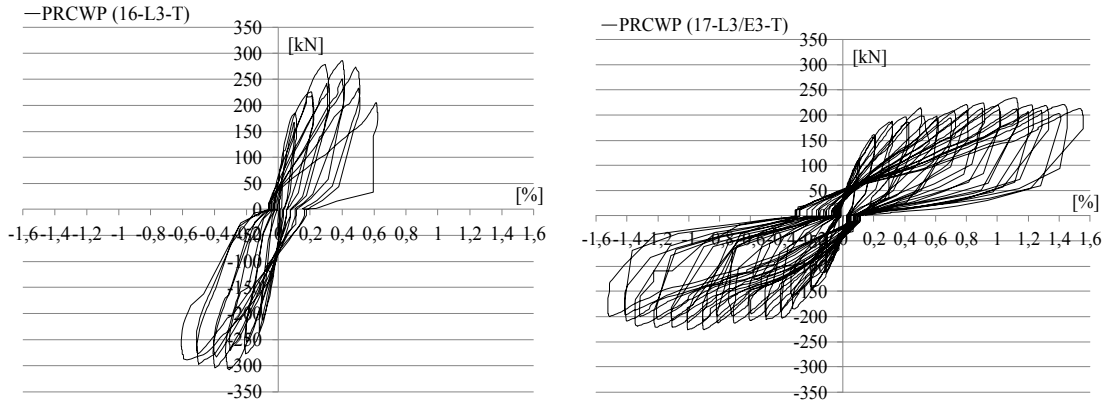

Fig.1 Load–drift ratio hysteresis loops

2.2 Failure details of the specimens

Among the specific failure details that were observed, one can mention a significant number of cracks in all the regions of the panels, inclined cracks in the piers and concrete crushing (Fig. 2). During the experimental test, specimen PRCWP (16-L3-T) developed cracks in all the regions of the wall panel, mostly in

the piers and pier-parapet region. Concrete crushing took place at the bottom corners of panel, and in the wings at the bottom part. Failure of the specimen was attained at a 0.57 % drift ratio. The specimen PRCWP (17-L3/E3-T) exhibited cracks in all the regions of the wall panel, mostly in the pier-spandrel region. Concrete crushing took place at the top left corner of the opening. Failure of the specimen was attained at a 1.57 % drift ratio.

Fig. 2 Failure details of the specimens

2.3 Energy dissipation

The cumulative energy dissipation was obtained by the continuous integration of the load-drift hysteretic response using the iterative equation was presented in detail in [13].

A comparison between the cumulative dissipated energy (CED) per half-cycle versus the drift ratio within each test performed is presented in Fig. 3. One can conclude that a specimen having large opening dimension has a lower contribution in energy dissipation than a specimen with smaller opening dimension. Also, specimens with lager opening dimensions develop an increased deformation capacity with respect to the panels with smaller opening dimensions. For example at 0.6% drift ratio, PRCWP (16-L3-T) dissipated a higher value of energy than PRCWP (17-L3/E3-T).

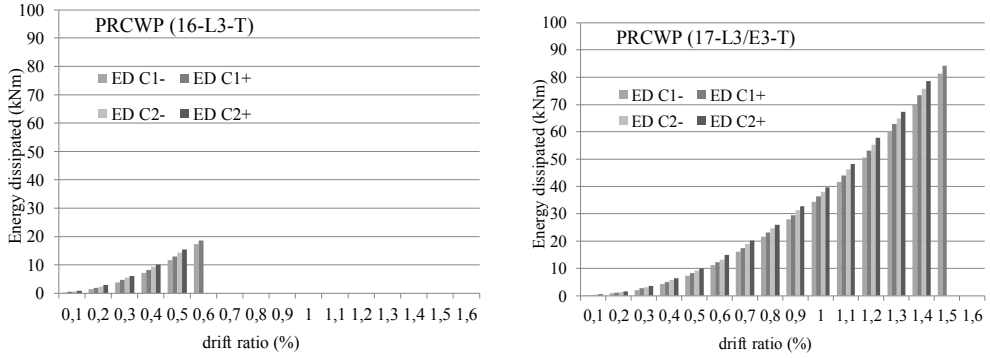

Fig. 3 The cumulative energy dissipation of the specimens

2.4 Stiffness degradation

The stiffness versus drift-ratio diagram is represented in Fig. 4. As we expected, the wall specimen with large opening dimensions (PRCWP 17-L3/E3-T) induced higher reductions in the initial stiffness of the wall compared to a wall with smaller opening dimensions (PRCWP 16-L3-T).

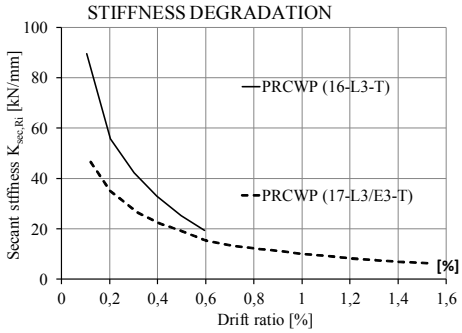

Fig. 4 The stiffness versus drift ratio diagram of the specimens

3 Theoretical and numerical study on the shear resistance of the specimens

The theoretical study on specimens refers in this paper at the evaluation of the shear strength using Eurocode 2 [14] provisions for PRCWP (16-L3-T) and the evaluation of shear strength using the plastic mechanism model for PRCWP (17-L3/E3-T). The numerical study was performed using the Atena 2D software.

3.1 Evaluation of the shear strength using design code provisions and plastic mechanism models

The shear resistance of the member (PRCWP 16-L3-T) was evaluated according to Eurocode 2 [14], section 6, and are presented in Table 3. It can be noticed that the experimental value obtained is significantly higher than the one evaluated using formulas from EC2 [14]. According to Biskinis et al. [15], the shear force which can be sustained by the concrete member, limited by crushing of the compression struts is overestimated in some cases, and for walls designed for high ductility class, VRd,max should be taken as 0.4 of the value determined in other regions than the critical base one. The reduction factor 0.4 seems to be appropriate also for the analysed wall.

Table 3 Shear resistance of the member

ELEMENT	PRCWP (16-L3-T)	
	Pier 1	Pier 2
Reinforcement	ϕ10, ϕ4	ϕ10, ϕ4
A_{sw} [mm^2]	78.5; 12.6	78.5; 12.6
s [mm]	530; 100	530; 100
z [mm]	560	560
f_y [N/mm^2]	450; 618	450; 618
θ [°]	31	23
α_{cw}	1	1
b_w [mm]	100	100
ν_1	0,54	0,54
f_{cm} [N/mm^2]	31	31
$V_{R,s}$ [kN]	134,34	191,00
$V_{R,s}$ (pier 1+2)	325,34	
$V_{R,max}$ [kN]	414,80	337,21
$V_{R,max}$ (pier 1+2)	752,01	
$0.4 \cdot V_{R,max}$ (1+2)	300,80	
$V_{exp,max}$ [kN]	307,5	

Due to the fact that the PRCWP (17-L3/E3-T) specimen has a wide door opening, under external loads, it behaves like a frame. Taking into account the failure mechanism, where four plastic hinges appeared, on the top and bottom of the piers, the corresponding horizontal load could be computed using the scheme shown in Fig. 5.

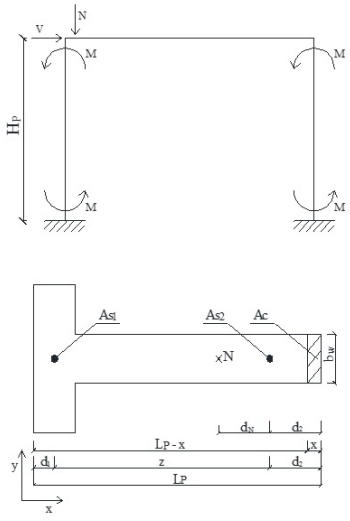

Fig. 5 Plastic mechanism considerations

$M = A_{s1} \cdot f_{y1} \cdot z + N_c \cdot d_N = 47$ kNm

$V_{th} = 4 \cdot M/H_w + N_v \cdot (d_N + d_2) = 182$ kN < 226 kN

3.2 Numerical analysis for the prediction of the shear response

In this study the numerical analysis was performed using the ATENA 2D software [16, 17]. The used material models, FE mesh, loading, boundary conditions and type of analysis is similar with the one presented in detail in [12, 13]. Fig. 6 represents the analytical and experimental load-drift ratio response of the wall specimens. Similar shapes of the experimental curves with those of the numerical models were obtained. The shape and type of cracking of the numerical models under the left-side loading was similar with that observed in the experiment (Fig. 7). The ultimate compressive strain state in the specimen attained is also presented in Fig. 8 (pictures on the right side). The results obtained and presented in this paper indicate that the numerical model is an efficient instrument for analysing the behaviour of precast RC panels of different characteristics.

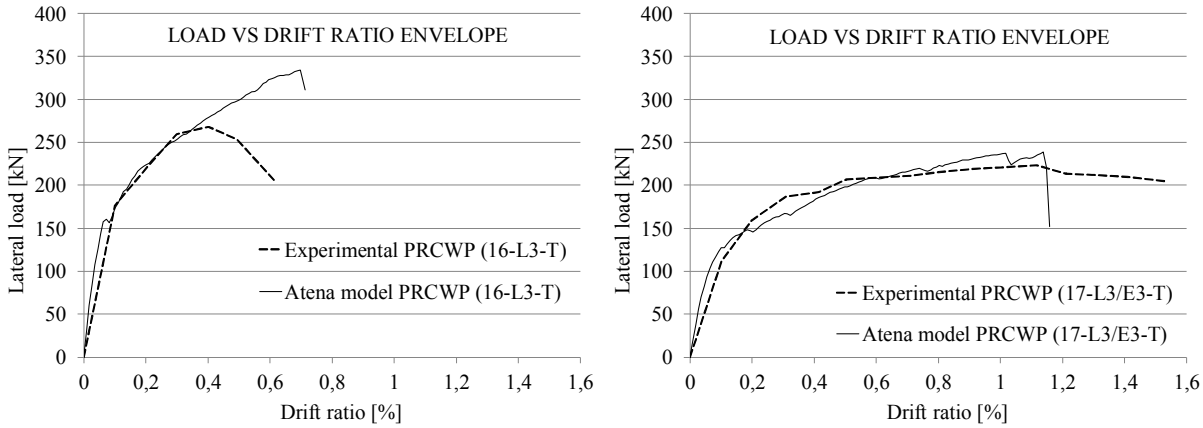

Fig. 6 Experimental versus numerical load-drift ratio curves

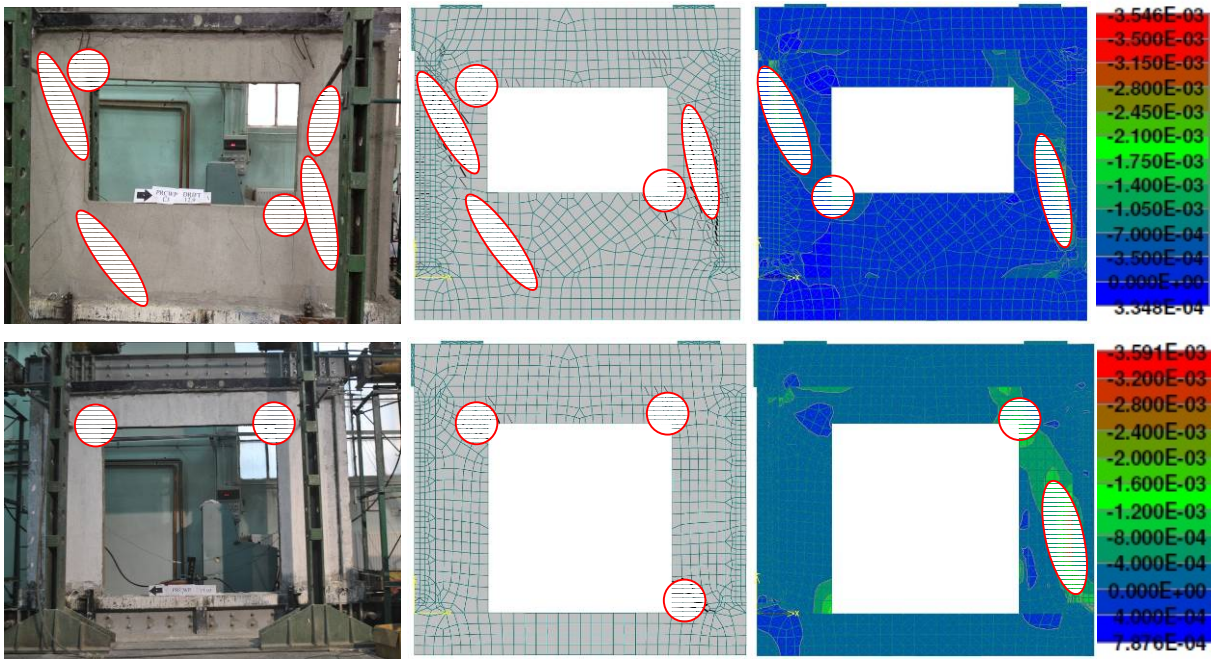

Fig. 7 Experimental versus numerical failure details

4 Conclusion

A number of two, 1:1.2 scaled precast reinforced concrete wall panels were analysed in the current paper. A list of the main conclusions which can be drawn within the limitations of the current research is given below:

- the general behaviour of the specimens consisted in significant cracking, cast-in-place mortar and concrete crushing;
- it can be reported a significant reduction in lateral resistance of the specimen having large opening dimensions (PRCWP 17-L3/E3-T) compared to the one with smaller opening dimension (PRCWP 16-L3-T);
- the wall panel with smaller opening dimension (PRCWP 16-L3-T) was found to dissipate more energy compared to the specimen with larger opening dimension (PRCWP 17-L3/E3-T), where the displacement capacity was higher;
- the wall panel having larger opening dimensions (PRCWP 17-L3/E3-T) developed significant stiffness reduction compared to the specimens having smaller opening dimension (PRCWP 16-L3-T), as we expected.
- the ‘‘0.4’’ reduction factor proposed by Biskinis et al. [28] seems to be more adequate for the prediction of the shear force of DCM walls.
- the model developed using Athena software provided similar behaviour and values with experimental test, so the model could be used for further parameter analysis.

References

[1] Fintel M. (1995). Performance of Buildings with Structural Walls in Earthquakes of the Last Thirty Years. PCI Journal, 40(3), pp. 62–80.
[2] Fintel M. (1991). Shear Walls – An answer for Seismic Resistance? Concrete International, Vol. 13, No. 7, pp. 48–53.
[3] Mosoarca M. (2013). Seismic behavior of reinforced concrete shear walls with regular and staggered openings after the strong earthquakes between 2009 and 2011. Eng Fail Anal; 34:537–65.
[4] Guan H., Cooper C., Lee D. (2010). Ultimate strength analysis of normal and high strength concrete wall panels with varying opening configurations. Eng Struct; 32:1341-55.
[5] Wang J., Sakashita M., Kono S., Tanaka.H, Warashina M. (2008). A macro model for reinforced concrete structural walls having various opening ratios. The 14th World Conference on Earthquake Engineering October 12-17, Beijing, China.
[6] Hara T., Doh J. (2012). Finite element investigation of R/C wall with openings. The 14th International Conference on Computing in Civil and Building Engineering. Moscow, Russia, 27-29 June.
[7] Takehara.M, Motitsuki (1993). Elasto - plastic analysis of framed shear walls with an opening using macro model. Summaries of Technical Papers of Annual Meeting Architectural Institute of Japan, Structures □ 303-304.
[8] Fragomeni S., Doh J. H., Lee D. J. (2012). Behavior of axially loaded concrete wall panels with openings: an experimental study. Adv Struct Eng 2012; 15(8):1345–58.
[9] Demeter I. (2011). Seismic retrofit of precast RC walls by externally bonded CFRP composites. PhD thesis. Politehnica University of Timisoara.
[10] IPCT: Cladiri de locuit P+4 din panouri mari. Proiect 770-81, vol. C: Elemente prefabricate, Bucuresti, Romania; 1982. (IPCT: precast reinforced concrete large panel buildings P+4. Project type 770-81, vol. C: Precast elements, Bucharest, Romania; 1982).
[11] IPCT: Cladiri de locuit P+4 din panourimari. Proiect 770-81, vol. D: Elemente prefabricate – Armari, Bucuresti, Romania; 1982. (IPCT: precast reinforced concrete large panel buildings P+4. Project type 770-81, vol. D: precast elements – reinforcing, Bucharest, Romania; 1982).
[12] C. Toduț, D. Dan, V. Stoian (2014). Theoretical and experimental study on precast reinforced concrete wall panels subjected to shear force. Engineering Structures 80, pp. 323–338.
[13] Todut C. (2015). Seismic strengthening of precast RC panels using FRP composites. PhD thesis. Politehnica University Timisoara.
[14] EN 1992-1-1. Eurocode 2: Design of concrete structures - Part 1-1: General rules and rules for buildings. Brussels: COMITÉ EUROPÉEN DE NORMALISATION; 2004.
[15] Biskinis Dionysis, Roupakias George, Fardis Michael. Degradation of shear strength of reinforced concrete members with inelastic cyclic displacements. ACI Struct J 2004:773–81 [title no. 101-S76].
[16] Ceˇrvenka J, Jendele L. ATENA program documentation. Part 1: theory. Section 2.6; 2011.
[17] Ceˇrvenka J, Jendele L. ATENA program documentation. Part 3–1: example manual. Section 2.10; 2010.

Impacts of Urban Development and Climate Change on Runoff

Tucan L.[1], Bica I.[2]

[1] *University of Architecture and Urban Planning "Ion Mincu" (ROMANIA)*
[2] *Technical University of Civil Engineering of Bucharest (ROMANIA)*
E-mails: laura.tucan@gmail.com, bica@utcb.ro

Abstract

Currently, the impact of urban development and the growth of impervious surfaces on the increase in runoff[1] are not considered fundamental principles in urban planning. A cumulatively high runoff in a very brief time interval could result in the loss of the central sewage system's transport ability and, consequently, in the discharge of rain water (as well as wastewater in the event that there is a combined system for both) and the flooding of urban areas. Moreover, climate change is an international environmental issue and urban development experts should report to it on a mandatory basis in undertaking their activities. The causality relationship between these two components: urban development, climate change and the increase in runoff has been demonstrated in the case study made for the Tineretului Neighborhood in Bucharest, the results of which are provided in this article.

Keywords: runoff, urban development, climate change, sewage system, impervious surfaces.

1 Introduction

In the context of climate change and the recent shifts in the urban environment, urban management and the traditional handling of rainwater must be re-assessed and consolidated, both concerning their current status, as well as their forecast status. The need to advocate this attitude arises from the issues that the city is facing, of which the most severe is the more and more frequent urban flooding, caused on one hand by the growth in impervious surfaces, and, on the other hand, by the changes in rainfall (the increase in rain intensity over very short periods of time) [1].

Therefore, urban planning must reconsider its methodological approach, meaning that, besides reporting to the growth of urban population, it should also report to the medium and long term forecasts on climate change and assess the impact that the increase in impervious surfaces could have on the management of rainwater.

The complexity of issues with which the city is currently faced suggest that there is a necessity for an interdisciplinary approach to the management of rainwater and this must be added as a component that is independent, yet intercorrelated with the other areas of expertise, to the general management of urban settlements.

In order to support this hypothesis, a research was conducted for the Municipality of Bucharest, over a studied surface of 376.53 ha in the Tineretului Neighborhood. In order to identify the effects of urban development - the increase in impervious surface and climate change have on runoff, the first step was to define a point of reference, namely the urban parameters (land occupation with various usage types: asphalt roads, green spaces, buildings etc.) and those relating to rainfall (events of rain) for the year 2013. Based on this data as reference, 3 scenarios of urban and climate evolution were projected for the area [2]:

- Scenario 1: the urban development forecast in the General Urban Plan of Bucharest will be materialized in 2050, and climate change has had an impact which lead to changes in the rain events used as reference;
- Scenario 2: the urban development shall be the same as for the reference point, at the level of 2013, but climate change has had the same impact as in Scenario 1;
- Scenario 3: the urban development is as planned in the General Urban Plan of Bucharest (similar to Scenario 1) and it is estimated that it will materialize in 2050, however climate change is not expected to worsen in relation to the reference year of 2013.

[1] Runoff represents water from rain or snow that flows over the surface of the land area.

2 Methodology

In order to calculate runoff in the case study area, a mathematical model was built for the central sewage system. The objective was to simulate the surface flow of rainwater (the rain-flow model) and the drainage of wastewater and rainwater into the sewage system, so that the effects of runoff on this system may be observed. Mathematical modeling process implied building the model and its calibration.

2.1 *Description of the mathematical model*

2.1.1 Building the mathematical model

The collection system in the studied area is a combined one (it collects both wastewater and rainwater into the same sewage). Their transportation is achieved through service collectors, secondary collectors and the A1 main collector. The A1 collector discharges the water into the A0 main collector and then into the Wastewater main collector of the Municipality of Bucharest (located under Dambovita River). The sewage network is comprised of 1,600 drain holes and 1,650 pipes. The maximum capacity of these drain holes is 4,804.7 m^3. The pipes can be found in 3 types of diameters: 0-70 cm, 71-200 cm and 201-400 cm, and their total volume are of 25,891.1 m3, with a total length of 59.54 km.

Building the mathematical model was a result of building the hydraulic flow model for the collection system and the hydrological model and, implicitly, connecting these models together [3].

The hydraulic model was achieved after collecting the data on the sewage system: data on the drain holes (their number and positioning in stereo 70 coordinates, the grade elevation of the drain holes at ground level, the grade elevation of the drain holes in the underground, the diameter of the drain holes etc.), data on the sewage networks (path and positioning in stereo 70 coordinates, the maximum grade elevation of the sewage network, the minimum grade elevation of the sewage network, length of the sewage network, pipeline types, size of the pipeline elevation etc.) and data of boundary conditions (the output of wastewater in the analyzed area for the dry flow regime, the output upstream of the A0 sewer - Fig. 1 - and the output downstream of the A0 sewer - Fig 2).

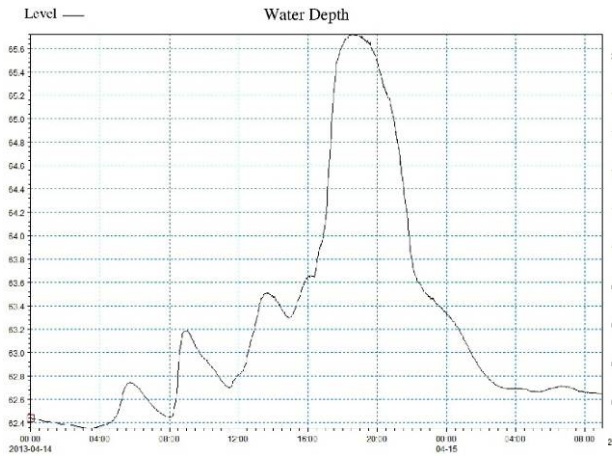

Fig. 1 – Water Depth measured upstream of A0 sewer

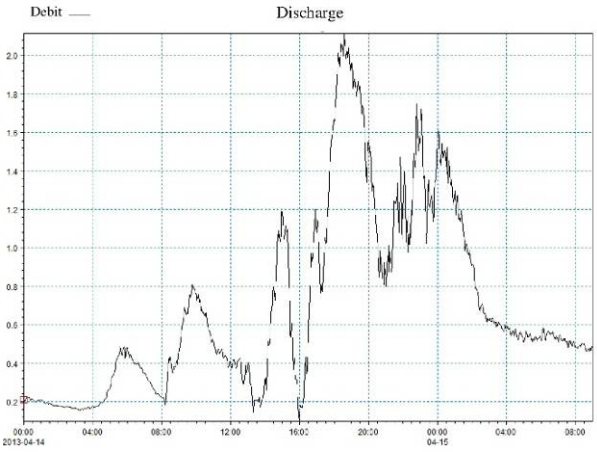

Fig. 2 – Discharge measured downstream of A0 sewer

The building of the hydrological model was performed in several stages. The first stage consisted in subdividing the catchment area into subcatchments, which were used as a reference for distributing the rainwater collected over their surface to the nearest drain hole (every drain hole is allocated with an intake subcatchment, so that the drain hole is located in the centroid of the subcatchment). Their number for the entire analyzed area is of 1634, with varying surfaces, covering between 0.01 ha and 3.08 ha. The average surface of a subcatchment is of 0.23 ha. The overlapping of the sewage system with the resulting subcatchments is provided in Fig. 3.

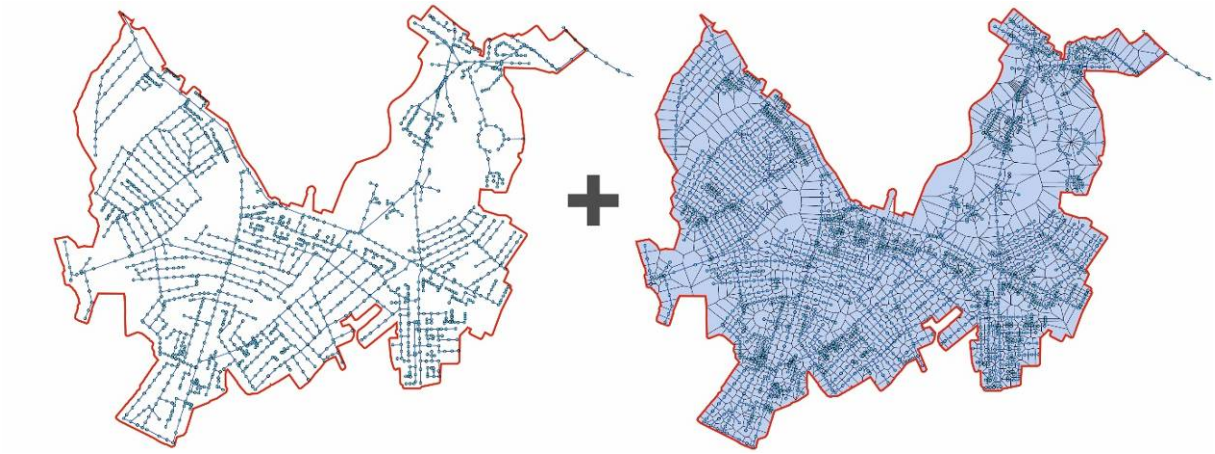

Fig. 3 – Mathematical model of the sewage system and the subcatchment limits resulted

The second stage consisted in the introduction of the time series. Regarding the time series for the year 2013, a rain event specific for this year was considered. On the other hand, when creating the climate projections for 2050, 5 climate change scenarios were used, as rendered for the Municipality of Bucharest under the CLIMSAVE [4][2] project: HADGEM11, CSMK3, CNCM3, MRCGCM, HADCM3, each with 3 associated scenarios for the carbon footprint (SRA1B - average level of CO2 emissions, SRA2 - high level of CO2 emissions and SRB1 - low level of CO2 emissions). The time series for every rain event - existing and projected - can be observed in Fig. 4.

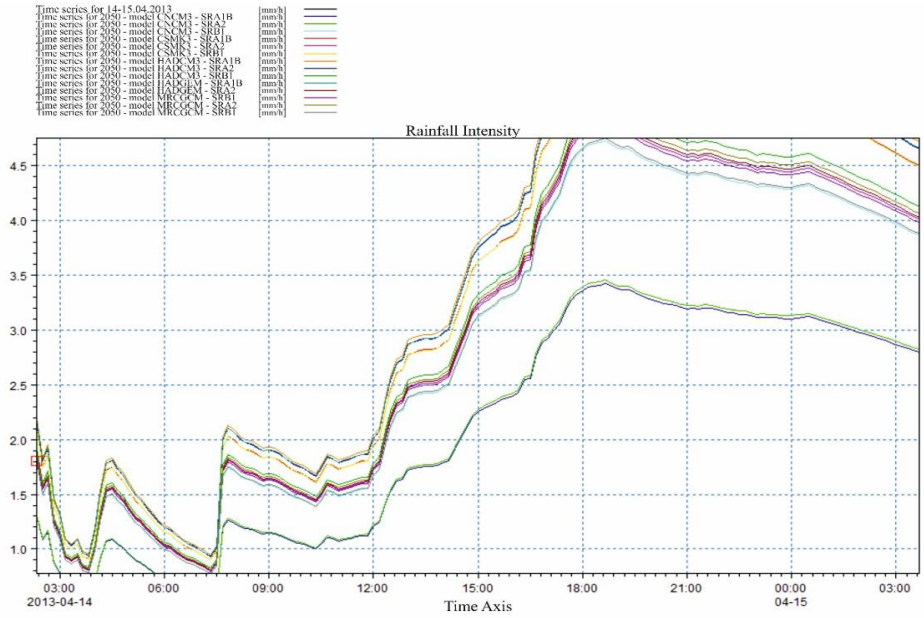

Fig. 4 Rainfall Intensity: time series for 2013 and 2050

The running of the hydrodynamic model was achieved pursuant to connecting the hydraulic model with the hydrological model, which required each drain hole to be connected to the associated subcatchment. As such, the drain hole will take over the volume of water that is flowing from the surface of the land. However, in order to calculate this volume, there was a need for data on the usage of the land, respectively data concerning the drainage coefficient for each type of land usage: buildings, green spaces, asphalt roads etc. By considering these drainage coefficients associated to the land usage types, drainage coefficients were calculated for every subcatchment, as it is shown in Fig. 5 and Fig. 6.

[2] The CLIMSAVE project has resulted in a platform where tests can be run on the impact and vulnerability of, as well as the adaptability to climate change for European territories. In order to meet its purpose, the project needed to reduce the number of climate change models (CGM) which were bound to be used in the assessment of the 3 components by the user of the platform. Therefore, a methodology has been developed to identify the most relevant climate change models for all the countries in Europe.

In order to calculate the volume of rainwater flowing on the surface of the land, the Area-Time hydrograph model was used. For this model, the volume of rainwater which has to be taken over by the central sewage system is determined by the initial losses, the continuous hydrological losses, the area-time curve and the time of concentration. The values considered for these parameters are those defined in the Mike Urban software, specifically: initial losses were assigned the value of 0.0006 m, continuous hydrological losses - 0.90, the Area-Time curve was defined as the TA1 curve - rectangular basin, while the time of concentration was set to 7 minutes.

The flow process of rainwater on the surface of land was simulated in the Mike Urban software at a time step of Δt. In order to calculate the volume of rainwater flowing on the surface of the land, the surface of the catchment area is divided into cells taking up the shape of concentric circles, with the drain hole at the center. The number of cells is equal to:

$$n = \frac{t_c}{\Delta t}$$

where: tc is the time of concentration; Δt is the time step for the simulation.

The rain-flow simulation starts after the depth of the rainwater accumulating at the surface of the land exceeds 0.0006 m, which is the parameter set for "initial losses". Furthermore, the simulation stops when the depth of the rainwater accumulating at the surface of the land drops below the value of 0.0006 m.

For every time step after the rainwater starts to flow, the volume accumulated in a certain cell (the volume of rainwater accumulating on impervious surfaces) is traveling downstream. Therefore, the volume of rainwater at Δt for a specific cell is calculated as a result of adding up the inputs at the upstream point of the cell (the upstream output of rainwater) with the volume of rainwater falling at Δt, multiplied by the surface of the cell, less the discharges at the downstream cell (the downstream output of rainwater). The outputs registered at the last cell located downstream are, in fact, the resulting hydrograph of the surface flows.

Ultimately, the volume of rainwater accumulating on impervious surface, the path of which was detailed in the previous paragraph, is reduced by applying the hydrological parameter "continuous hydrological losses".

2.1.2 Calibrating the mathematical model

The verification of the mathematical model was achieved through the calibration process, which required changing the calculation parameters so that the results obtained by the numeric model are as close to the factual situation as possible. The calibration of the model was performed for a rain event that occurred during September 29 - October 2, 2013. The difference between the outputs of the two rain events was within the 10% range of the value.

2.2 Description of the scenarios

The reference situation, for the year 2013, has given consideration to the following drainage coefficients, depending on the usage of the land [5] (Table 1).

Table 1 – Drainage coefficients used as reference for 2013

Drainage coefficient	Area type
0.90	Buildings with ridged roof
0.70	Buildings with terraced roof
0.30	Lands associated with the buildings
0.10	Parks / Green spaces
0.90	Asphalt roads / Parking lots

The same drainage coefficients were used as reference for Scenario number 2.

On the other hand, for Scenario 1 and Scenario 3, the Land Occupation Percentages projected through the General Urban Plan of Bucharest were used as reference.

The calculation of the drainage coefficients depending on the Land Occupation Percentages was performed as follows:

According to source [6], the drainage coefficient for an urban area is equal to $\frac{1}{F}\Sigma\alpha_i f_i$, where F is the total surface of the catchment, α_i is the drainage coefficient associated to an i type of land usage, while f is the size of the surfaces depending of the usage of the land.

The resulting drainage coefficient is equal to: *drainage coefficient for buildings * building occupation percentage + drainage coefficient for asphalt roads / parking lots * asphalt roads / parking lots occupation percentage + drainage coefficient for parks / green spaces * parks / green spaces occupation percentage* (Table 2).

Table 2 – Drainage coefficients results depending on the Land Occupation Percentages for 2050

Drainage coefficient resulted	Lan Occupation Percentages projected through General Urban Plan of Bucharest [7])	Asphalt roads, parking lots	Parks / Green spaces
0,50	20 %	30 %	30 %
0,58	30 %	30 %	40 %
0,70	45 %	30 %	25 %
0,73	50 %	25 %	25 %
0,74	60 %	20 %	20 %
0,78	70 %	15 %	15 %
0,10	-	-	100 %
0,90	-	100 %	-

For comparison, the resulting drainage coefficients for every subcatchment are provided in Fig. 5 and Fig. 6. Therefore, it can be observed that a materialization of the projections made through the General Urban Plan[3] (up to 2050) would imply a considerable increase in the drainage coefficients by subcatchments.

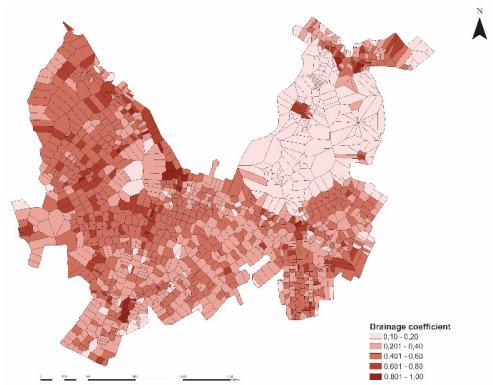

Fig. 5 – Drainage coefficients for 2013

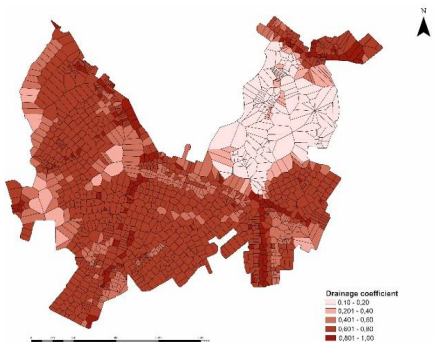

Fig. 6 – Drainage coefficients for 2050

The effects of such projections on the runoff can be seen in section 3, Results.

As mentioned in section 1. Introduction, for every scenario, climate conditions were also considered, specifically the rain events at the level of 2013 and 2050, provided in detail in Fig. 4.

3 Results

After running the mathematical model for the situation deemed as reference - the year 2013, a runoff of 117,083.958 m³ has resulted. The results of the urban development and climate change Scenarios 1, 2 and 3 are provided in Fig. 7.

[3] Projections made through the General Urban Plan of Bucharest suggest a densification of the area and, implicitly, a growth in impervious surfaces

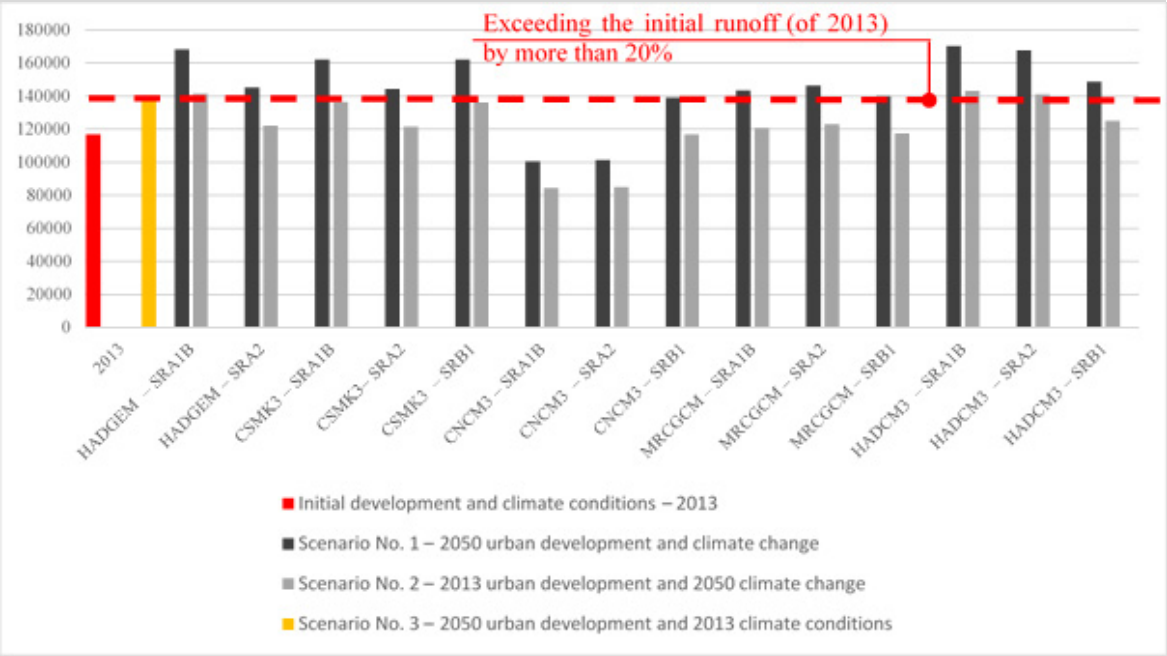

Fig. 7 – The results of Scenarios 1, 2 and 3 provided in relation to the initial urban and climate status – the year 2013

4 Conclusions

As can be noticed in Fig, 7, part of the scenarios lead a significant excess compared to the initially recorded runoff, in the urban and climate conditions of 2013. Therefore, the highest level of excess is recorded for Scenario 1 - a scenario in which the impervious surfaces will increase and, implicitly, so will the coefficients for drainage (urban development scenario for 2050) and climate change HADGEM – SRA1B, CSMK3 – SRA1B, CSMK3 – SRB1, HADCM3 – SRA1B and HADCM3 – SRA2 (climate change scenario for 2050), which will increase the initial runoff by 45.40% The central sewage system taking over such volumes will result in discharges through the drain holes in the area were the A1 collector intersects with the A0 collector.

Considering the projections for the effects that urban development and climate change may have on the studied area, it can be concluded that there is a need to adopt certain technical measures for the de-centralized collection of rainwater (for example Green Infrastructure measures), close to the area in which they manifest, as well as urban planning measures (reducing the building and asphalt roads occupation percentage), in order to reduce future densification of the analyzed area. These measures have to be interrelated, in order to provide an interdisciplinary approach on the process of identifying optimal solutions for urban development and climate change issues.

References

[1] Water Environment Federation and the American Society of Civil Engineers (1998). Urban Runoff Quality Management, WEF Manual of Practice No.23, S.U.A.
[2] Tucan, L. (2015). Research Report No. 2, drafted during the Ph.D. research, UTCB.
[3] Chevereșan, M., Chiru, E., Dinu, C., Dumitru, M., Istrățoiu, A., Mihailovici, Poienariu, T., M., Stancu, M., Zaharia, V., (2015). Guide to good practice for adaptation to climate change in urban areas, Bucharest.
[4] Dubrovsky, M., Harrison, P., Holman, I., Svobodova, E., Trnka, M., (2014). Developing a reduced-form ensemble of climate change scenarios for Europe and its application to selected impact indicators, Springer Science + Business Media Dordrecht, pp. 175.
[5] Bleuzé, P., Pötz, H., (2012). Urban green-blue grids for sustainable and dynamic cities, Coop for life, Delft, pp. 70.
[6] Stănescu, V., (1995). Urban Hydrology, Didactic and Pedagogic Publisher – Bucharest, pp. 60.
[7] Local Council Decision no. 260/2000 for approval of the General Urban Plan of Buharest.

A Numerical Investigation for the Optimisation of the Seismic Response of Steel Eccentrically Braced Frames with Short Dissipative Elements

Vătăman A.[1], Grecea D.[1,2]

[1] *Department of Steel Structures and Structural Mechanics, Politehnica University of Timişoara (ROMANIA)*
[2] *Romanian Academy Timişoara Branch (ROMANIA)*
E-mails: adina.vataman@upt.ro, daniel.grecea@upt.ro

Abstract

The steel Eccentrically Braced Frames (EBF) are recognised as highly dissipative seismic systems due to the formation of plastic hinges in link elements. Based on the ratio between the plastic bending and plastic shear resistances of the link element, and the minimum number of stiffeners present on the link, the normative requirements do not differentiate between minimum/maximum required length of the link nor the increased number of stiffeners. The paper presents the performances of short steel link elements subjected to shear under the form of parametrical study performed using Abaqus FEM software.

An initial FE model is calibrated based on existing experimental tests performed within the CEMSIG laboratory at the Politehnica University of Timişoara. In a second step the numerical analysis investigates three parameters which can affect the behaviour of such systems, whilst remaining in the range of short shear links: (i) the use of compact / slender webs; (ii) the influence of the number of web stiffeners and (iii) the influence of link length, by considering four different lengths. The analyses were performed considering both monotonic and cyclic loading conditions, as well as the composite behaviour of the beam as opposed to the pure steel frame. The results are presented under the forms of V-γ response curves and judged in function of characteristic parameters resulting from these.

Keywords: steel, eccentrically braced frame, finite element.

1 Introduction

The general design of steel frames subjected to seismic loading considers the lateral stiffness criterion, in order to limit the lateral deformations. As Vayas et al. [1] demonstrated, the deformations of non-structural elements is a concern in the serviceability limit state, but in the ultimate limit state conditions the deformations must be limited in order to avoid the second order instabilities. In addition, the ductility of plastic hinges represents an important factor in case of seismic loading, in order to allow the plastic redistribution of forces [2]. A measure of the ductility is the plastic rotation capacity of the member sections.

In case of seismic loading, the steel Eccentrically Braced Frames (EBF) represents structures recognized for their good dissipation capacities. Such systems are characterized in design by high values of the behaviour factor (q greater than 6 in ductility class high case) and consider the input energy dissipated by formation of plastic hinges in the dissipative link elements. In general, these are dissipative beam segments located outside the triangulated beam-column-brace systems and designed to allow the yield in shear or bending. The plastic deformation is mainly dependent on the link element length which can be short (length $e<1.6M_{pl}/V_{pl}$ according to EN 1998-1 [3]), long (length $e>3M_{pl}/V_{pl}$) and intermediate in accordance to the European seismic norm – Eurocode 8.Short links generally present a stiff behaviour and dissipate the plastic energy by shear deformations of the web panel.

As proven by other authors [4], the link element behaviour is very ductile proving high values of distortion of the order 120 to 200 mrad. On the other hand, structural simulations [5] on structures subjected to dynamic incremental analyses with accelerograms have proven that the limiting value proposed by EC8-1, § 6.8.2., of 80 mrad for short links in EBF might be insufficient for structures in high seismicity zones.

Unlike the simple definition of the short link elements offered by EN 1998-1 es < $1.6(M_{pl}/V_{pl})$, studies show that other parameters can influence the capacities of link elements, such as the presence of stiffeners, real length of the element or the slenderness of the profile. The present paper is aimed at investigating the influence of such details on the overall response of EBF with short links.

2 Experimental Background and numerical model calibration

The numerical study that will be presented further is based on a previous experimental research program developed within the "CEMSIG" Research Centre at the Politehnica University of Timisoara. The eccentrically braced frame was initially part of a dual frame (MRF+EBF) structure with five storeys, 3 spans (2 outer spans of 6m and one internal span of 4.5m) and 3 bays (2 outer bays of 6m and one internal bay of 4.5m) designed in a seismic region, according to EN 1993-1-1 [6] and EN 1998-1.

The first story central bay structure was used as a reference testing specimen (EBF-LF-M) with the frame beam a HE200A profile including the dissipative zone (short link). Other element cross sections can be distinguished on Fig. 1.a. The dissipative link element has a length of 300 mm and is classified as a short link element according to EN1998-1 and consequently the characteristic deformation will be in shear. The beam-to-column connections were considered with bolted end-plates resulting in fully resistant connections. The braces were splice connected while the column-base connection was pinned in order to reduce the lateral force needed for the complete development of the plastic hinge. The experimental set-up can be observed in Fig. 1b. Further information on the detailed report can be found elsewhere [4]. As many sections and subsections as you need (e.g. Introduction, Methodology, Results, Conclusions, etc.) and end the paper with the list of references.

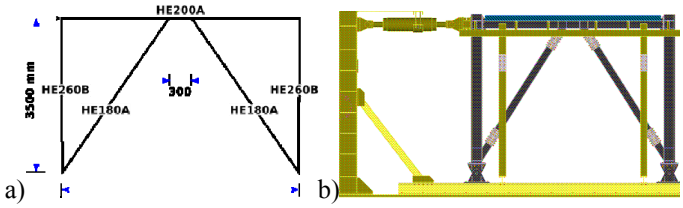

Fig. 1 a) Element profiles; b) Experimental set-up

2.1 Numerical model calibration using monotonic loading procedure

The calibration of the numerical model was based on the experimental specimen previously presented, EBF-LF-M. Both, global geometrical dimensions, cross-sectional properties and general layout were modelled in correspondence to the experimental specimen, with an applied monotonic displacement of 180mm on the top left column, as maximally recorded by the displacement transducer during experimental testing. The assigned material properties correspond to true stress-strain curve for the beam and dissipative link, built from real the material tests performed on coupons.

The finite element model was processed and analysed using computer software ABAQUS 6.11-1 [7] by considering 3D solid frame elements. The analysis procedure used was Dynamic Explicit type with a mesh of hex type elements, considering sweep technique and mixed medial axis and advancing front algorithms. An element size of 6mm was used for the dissipative part of the frame (link element and adjacent beam ends) as shown in Fig. 2a. The frame components, which were expected to remain in the elastic domain, have been assigned larger size elements, ranging from 25mm for columns and column stiffeners, 20mm for beam and beam stiffeners and respectively 15mm for braces.

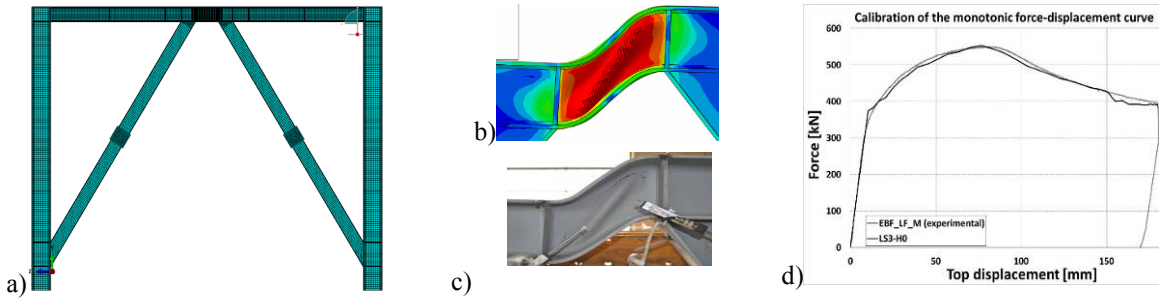

Fig. 2 a) Mesh of the finite element EBF model; b) Link deformed shape- FE Model, c) Link deformed shape-experiment; d) Calibrated numerical result versus experimental force-displacement curve

The initial stiffness of the numerical model was slightly higher than that of the experimental model and since the experimental EBF model had recorded a slip of the bolted connections for braces, this was further integrated in the numerical model by a connection slip using a connector section. The resulting force-displacement curve from the monotonic analysis (denoted as LS3-H0) follows the experimental response EBF-LF-M-DHTL appropriately (Fig. 2d). The deformed shape of the link element can be observed in Fig. 2b) compared to the deformed shape of the experimental specimen, presented in Fig. 2c).

2.2 Parametric study using monotonic loading procedure

After the initial calibration a large parametric study was conducted on 14 numerical models, in three different directions that could influence the global behaviour of the link element: the stiffening of the link, the steel section profile of the link beam and respectively the length of the short link.

2.2.1 Influence of link slenderness

Concerning the cross-sectional parameter, the transition from HE200A profile to IPE240 was made by considering close shear areas of the two profiles, but different web slenderness, computed according to Chapter 6.8 on design and detailing rules for eccentrically braced frames from EN 1998: Part 1.

The elastic behaviour of the two models presents similar characteristics with the main difference present in the post-elastic range: the model with the slender web (IPE profile) showed a slightly smaller maximum resistance, explained by a smaller shear area (Fig. 3b). There was also an important reduction in the distortion corresponding to maximum load; the local instability appeared earlier in case of the slender web. A similar shear hinge formed in both cases was observed, due to web crippling. The stress amplitudes outside the panel were much smaller than those of the internal web itself.

2.2.2 Influence of link web stiffening

The influence of link web stiffening was analysed by considering three different configurations: an initial configuration with no link web stiffening, a second configuration with one intermediate web stiffener placed vertically on the link element and a third configuration considering two intermediate web stiffeners.

The analyses results showed that the behaviour of both HEA and IPE models present an elastic behaviour, initial stiffness and point of plasticisation, which are independent of the number of stiffeners (Fig. 3b). However, in plastic range there are important differences: the ultimate resistance of the specimens and also the post-elastic stiffness (hardening stiffness) increased with the number of stiffeners. All models displayed high distortion capacities, up to 0.4mrad, even though the rotation at maximum load shifts in case of IPE profile from 0.12 to 0.16rad when using one stiffener and respectively 0.25rad in case of using two stiffeners. In case of the HEA models, the same trend can be observed, but with a visible increase of rotation corresponding to the ultimate resistance only for the model with two stiffeners. The failure modes show that in both cases additional stiffeners lead to a division of the original shear panel into multiple panels, with their own web deformation. The initial elastic deformations are shared among the panels, but in the post-elastic range the plasticisation becomes concentrated in one of the panels, the other contributing only partially to the global deformation.

2.2.3 Influence of link length

The third parameter, the link length (for both HEA and IPE) was modified in order to remain within the limits of short link limitations (760 mm). Five different lengths were considered: 300, 400, 500, 600 and 750 mm respectively. The general trend that could be observed in this case is that the link length has little influence on both elastic and post-elastic ranges: the strengths (elastic and ultimate) decrease with the length, but the difference is less than 10%. However, by passing to longer links (750 mm), the web loses its stability earlier, thus having a limited ultimate resistance and ductility. The links with shortest dimensions (300 to 400 mm) are characterized by a global-type shear plastification while the longer link elements (500 to 750 mm) fail by web crippling on sides of the panel, with the other side remaining plain but with high levels of shear stresses (Fig. 3a).

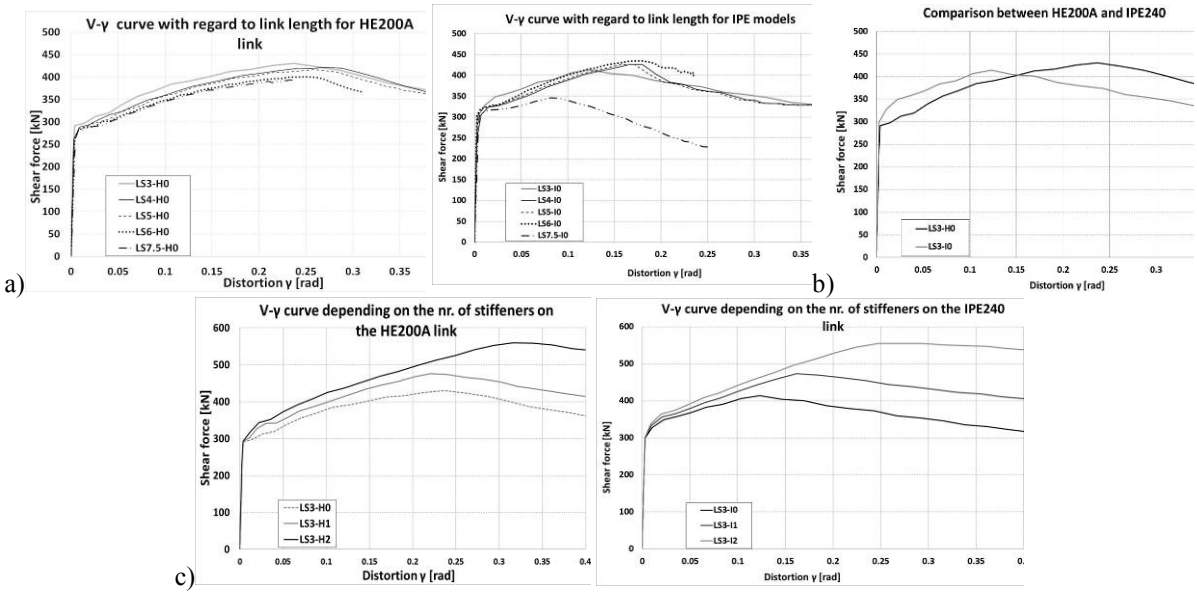

Fig. 3 a) Influence of link length, b) Influence of web slenderness, c) Influence of number of stiffeners

2.3 Numerical model calibration using cyclic loading procedure

After the initial calibration a large parametric study was conducted on 14 numerical models, in three different directions that could influence the global behaviour of the link element: the stiffening of the link, the steel section profile of the link beam and respectively the length of the short link. The same experimental program included a test on a similar pure steel eccentrically braced frame subjected to cyclic loading conditions – specimen EBF-LF-C. The results from this test were used to perform the calibration of the numerical model LS3-H0-C (Fig. 4a). The experimental response of EBF-LF-C specimen showed a ductile behaviour with good dissipation capacity of the link element (values of distortion exceeding 150 mrad). The maximum resistance was of 550 kN (Fig. 4a) with a failure mode by alternate shear buckling of the link web panel in positive and negative cycles followed by tearing of web panel.

In addition to the model geometry, material, frame layout specific cyclic parameters were accounted for. Plastic material properties were assigned in order to provide a combined isotropic and kinematic hardening for beam steel material, including the dissipative link element with a cyclic material model that considered 5 back-stresses in order to model the material behaviour, as suggested by Chaboche [8]. The loading procedure that was used followed the ECCS cyclic loading procedure [9] in experimental testing and was based on finite element application of cyclic loading [10]. The load application point is identical to monotonic simulation – at the top of the frame and applied in displacement control. As in case of monotonic models, the slip in the brace connections was included in analysis, which means considering a rigid body element and a connector that allows for an elastic spring elongation of the braces. Fig. 4a presents the experimental frame top-displacement curves for experimental response (EBF-LF-C curve) and the FE calibration (LS3-H0-C curve).

a)

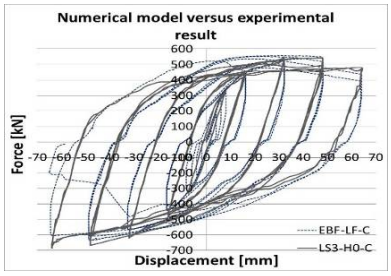

b)

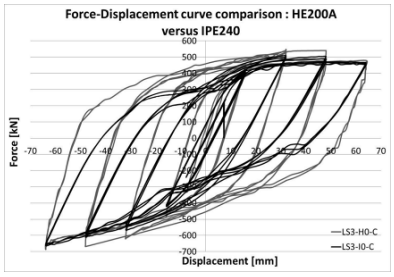

Fig. 4 a) Calibration of the cyclic force-displacement curve; b) Influence of link slenderness

2.4 Parametric study using cyclic loading procedure

2.4.1 Influence of link slenderness

The first parameter that was considered, as in the monotonic case, was the link slenderness. The HE200A profile of the beam (LS3-H0-C) and dissipative element was replaced with an IPE240 steel profile (LS3-I0-C). While the resulting model didn't present a much lower resistance (less than 10% difference), there was a visible decrease in initial stiffness and also post-elastic stiffness, which was to be expected due to the slimmer web panel of the IPE profile (Fig. 4b).

2.4.2 Influence of link web stiffening

The second parameter, the stiffening of the link web, was analyzed using the same three configurations starting from the base model LS3-H0-C without stiffeners on the link, a model with one intermediate vertical stiffener (LS3-H1-C) and respectively a model with two intermediate vertical stiffeners on the link web (LS3-H2-C). The results are presented in Fig. 5b in form of equivalent positive shear force-panel distortion V-γ response curves. The influence of the stiffeners on the response of the link element was important, as they induce improvements in the post-elastic domain. The maximum resistance improved significantly, with more than 10% for each additional stiffener. However, this value is reduced in comparison with monotonic results where the increase was 20%. The distortion capacity in all three cases remained high (over 150mrad).

2.4.3 Influence of link length

Following the parametric study on monotonic FE models, a similar study was performed, taking into consideration the same link lengths of 300/400/500/600 and 750mm. The cyclic results are presented in Fig. 5 in terms of equivalent V-γ envelope curves from positive quadrants (positive shear force, positive distortion).

The main observation that has to be made is that the cyclic behaviour introduces a slight limitation in distortion capacity compared to the monotonic responses (Fig. 5a). However, these values remain higher than the

limit value recognised by EN1998-1 of 80 mrad. For the longer links, the maximum distortion is smaller, similar to the monotonic results. The general trend was that the maximum cyclic resistances were smaller than the ones recorded in monotonic loading, with small differences of up to 5%. This is a clear indicator of the fact, that when subjected to cyclic loading the longer links lead to a drop in maximum cyclic resistance and distortion capacity of the link element, even though the elastic stiffness remained similar for all lengths.

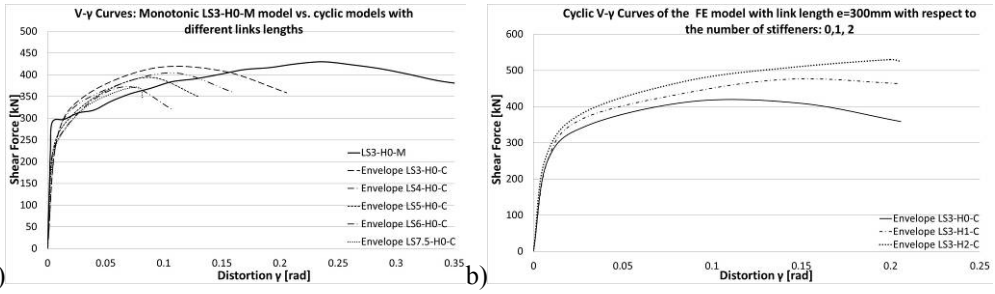

Fig. 5 a) Influence of number of intermediate stiffeners; b) Influence of link length

2.5 Composite eccentrically braced frame - Numerical model calibration

The experimental study presented earlier, also included a cyclic test on a composite EBF with the same geometry of the frame EBF-LF-C, with a full connection between steel beam and reinforced concrete slab provided by headed shear stud connectors, displayed in two rows along the whole length of the beam, including over the link element. A numerical finite element model was developed using the existing calibrated steel model LS3-H0-C.

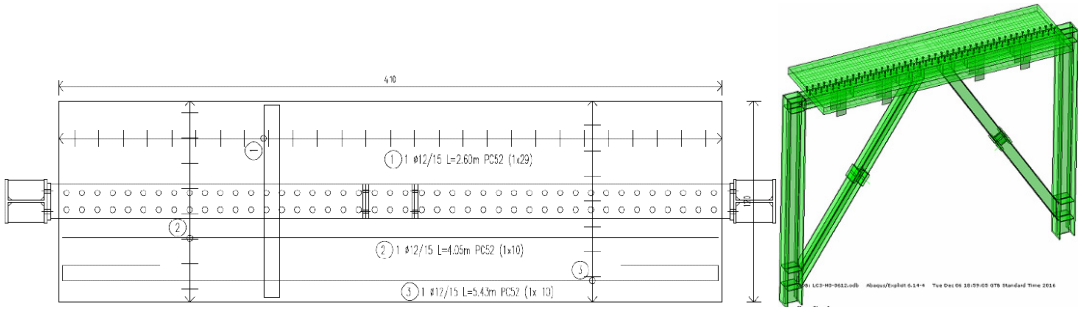

Fig. 6 Geometry of composite beam and composite finite element model

The concrete was modelled using concrete damaged plasticity by applying material properties resulted from experimental tests, while the reinforcement was defined as embedded region in the concrete. The stud connectors were inserted in the concrete slab and in addition to the general contact an additional contact with 0.5 tangential frictions was assigned. The addition of the reinforced concrete resulted into a large increase in additional finite elements and increased the total amount of actual analysis running time by more than 200%.

The resulting force-displacement curve presented an accurate resistance in the first two post-elastic cycles, but an important difference in returning-stiffness. The calibration is on-going and after its completion a parametric study will be performed in order to obtain an optimal disposition of connectors along the beam length and to observe the composite behaviour in the case of different composite beam configurations.

3 Experimental Background and numerical model calibration

In the present paper the seismic performances of steel short link elements, from eccentrically braced frames, were investigated. The finite element analyses were based on two initial calibrations of the results of an experimental test considering an EBF including both monotonic and cyclic loading. The parametric investigation regarded three different parameters: use of a compact/slender web, an increased numbers of intermediate web stiffeners and the variation of the link length. The results were analysed in terms of V-γ response curves and failure modes. The following conclusions could be drawn from the study:

- Both monotonic and cyclic experimental results can be modelled good accuracy using numerical finite element models, only by including the actual experimental conditions, careful definition of testing details and material laws. In the case of cyclic loading the Chaboche material models seems to adequately replicate the cyclic material response;

- The increased number of stiffeners produced similar results in both monotonic and cyclic cases, leading to an improved shear resistance and overall increased ductility, without having an effect on the elastic stiffness;
- The influence of the web slenderness for similar shear link areas is important only in the plastic domain: even with smaller shear area, the compact web (HEA 200 profile) proves a better performance both in ultimate resistance and corresponding distortion;
- The increase in the link length decreases the elastic stiffness of the system significantly with the 300mm links having an almost double stiffness compared to the 750mm ones. There was noted also a decrease in maximum resistance;
- Cyclic loading induces both a reduction in maximum shear resistance (up to 5% in all cases) and distortion capacity of the system (depending on link length – 10% for shorter link lengths and reduced to a third for the longer length);
- The minimum normative requirements for maximum link distortions of 80mrad [3] were satisfied in all monotonic and cyclic analyses cases.

Based on the results offered by the numerical simulations, it can be observed that an optimized response in case of EBFs with short links is given by link elements with lengths closer to upper-bound limit and stiffened. These systems will lead to high post-elastic resistance and ductility as well as will minimise the material strains. Link lengths closer to upper-bound limits and non-stiffened should be avoided. The results of the study should be judged in the context of the initial experimental test. Future investigations should consider other parameters such as the presence of a concrete slab with/without connection over the link or higher link lengths. These parameters can affect the link element performances and in consequence the global performances of EBFs.

References

[1] Vayas, I. (2000). Design of braced frames. Seismic resistant steel structures, Chapter 5, CISM Courses and Lectures, 420, pp. 241-288, Springer Verlag Wien GmbH.
[2] Gioncu, V., Mazzolani, F. (2014). Seismic design of steel structures, CRC Press Taylor and Francis Group.
[3] EN 1998-1 EUROCODE 8 (2003). Design of structures for earthquake resistance. Brussels, CEN, European Committee for Standardisation.
[4] Stratan, A. (1998). Studiul Comportării Clădirilor Multietajate cu Cadre Metalice Duale Amplasate în Zone Seismice (A study of the behaviour of multistorey steel dual frame buildings in seismic areas). PhD thesis, Universitatea Politehnica Timişoara.
[5] Danku, G. (2011). Study of the development of plastic hinges in composite steel-concrete structural members subjected to shear and/or bending. PhD Thesis, Politehnica University of Timisoara, Editura Politehnica, Seria 5, Nr. 72.
[6] EN 1993-1, (2005). Eurocode 3: Design of steel structures. Brussels, CEN, European Committee for Standardisation.
[7] Abaqus 6.11-1. (2011). Dassault Systèmes Simulia Corp.
[8] Chaboche, J.L. (2008). A review of some plasticity and viscoplasticity constitutive theories. International Journal of Plasticity, 24(10), pp. 1642-1693.
[9] European Convention for Constructional Steelwork (1986). ECCS TWS 1.3 N.45/86, Recommended testing procedure for assessing the behaviour of structural steel elements under cyclic loads.
[10] Vulcu, C., Stratan, A., Dubina, D. (2012). Numerical simulation of the cyclic loading for welded beam-to-CFT- column joints of dual-steel frames, Pollack Periodica, Vol.7, No.2, pp. 35-46.

Finite Element Analysis of Surface Subsidence for Establishing the Location of a Gas Pipeline

Vereş I.S.[1], Marian D.P.[2], Fissgus K.G.[3], Ştefan N.[4]

[1,2,3,4] *University of Petroşani (ROMANIA)*
E-mails: veresioel@yahoo.com, dacian_top@yahoo.com, kfissgus@gmail.com, mihacon73@yahoo.com

Abstract

Planning, execution and location of natural gas pipelines must follow certain safety rules so that their integrity is ensured for a longer period of time. Therefore, in areas with mining activity it is required to realize a study on surface stability and hence stability of civilian and industrial objects located in the area of influence of underground mining. This study was conducted using modern methods of calculation, using a program for finite element calculation, CESAR-LCPC.

Keywords: surface stability, underground mining, coal, gas pipeline, FEM, subsidence, displacement.

1 Introduction

The phenomenon of the surface deformation as a result of underground mining is a major problem in most countries with underground mining operations; this problem is a concern of numerous specialists worldwide. Underground mining lead to significant disturbances in the rocks equilibrium from the roof and sometimes bottom floor of the mined coal seam. Finally, under certain conditions, this movement is transmitted to the surface, causing surface damage and damage of the objectives situated in the area of influence.

2 Analysis of surface deformation using the finite element method

2.1 *Generalities*

The principle of the finite elements method is to replace the deformable body (in this case the entire rock massif) through an articulated structure made up of triangular or square elements (for the two-dimensional case). This is a finite element structure that substitutes the real structure.

Numerical modeling of the ground subsidence phenomenon has been developed in recent years using the finite element method, the discrete elements method and other mathematical methods that were used in the design of software such as: CESAR-LCPC, FLAC, Udec, PFC, FLOMEC and other. These applications are important mainly for stability analysis of land and structures from surface and underground, under static loading, seismic, thermal and hydrodynamic loading, etc.

2.2 Finite element analysis regarding the location of natural gas pipelines in the area affected by underground mining

In this paper, to create the calculation model with finite elements was used the 2D design software CESAR-LCPC and CLEO 2D processor [7].

For checking the stability of the area (and hence the future gas pipeline on the designed route) in areas with underground mining activity (mining fields Paroseni and Vulcan) it was used the numerical modeling with finite elements in 2D.

This analysis has been performed through 32 vertical sections (S1 – S32V, fig. 1). These vertical sections have been planned taking into account the direction and tilting of the coal seam, and were placed as far as possible in the center of each mined space (two sections for each panel separately), capturing the maximum influence of the mining of each panel on the surface [6].

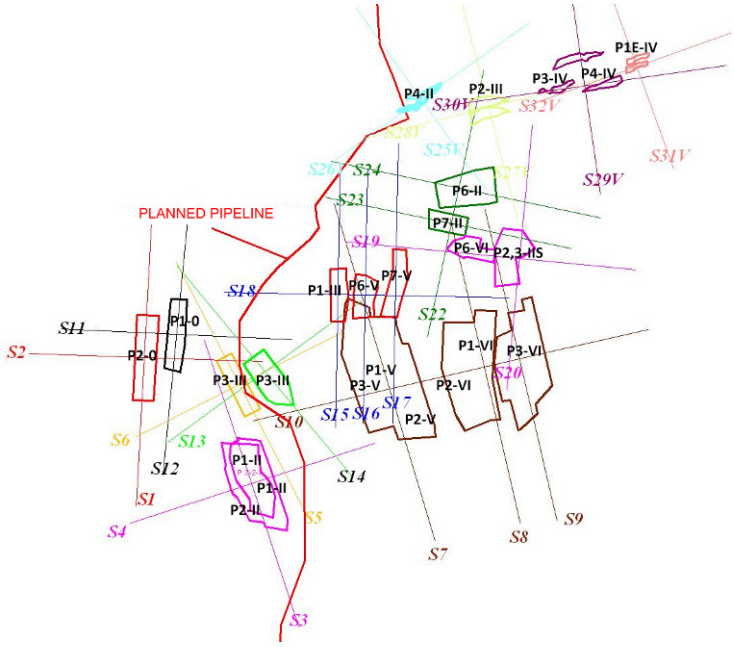

Fig. 1 The choice of vertical sections in relation to the position of the mined spaces

We took account only of the areas extracted from coal seams 3 and 5, (and in this case only recently extracted areas that still have a certain influence on surface) other seams mined in the area over time were not considered in this study because the time elapsed from the termination of mining of such seams is long enough so they do not have a direct influence on the size of surface displacement and deformation.

Calculations made on the numerical models have been carried out in the hypothesis of elastic behavior of the massif, assuming that both surrounding rock layers and extracted coal seams are continuous, homogeneous and isotropic, and the geomechanical characteristics used in the calculations have average values (Table 1).

Table 1 The average values of the rock and coal geomechanical characteristics used in numerical models [1], [5]

Characteristics	Unit	Rocks	Coal
Apparent specific weight, γ_a	kN/m^3	27	14,5
Young modulus of elasticity, E	kN/m^2	5 035 000	1 035 000
Poisson ratio, ν	adim.	0,19	0,13
Compressive strength, σ_c	kN/m^2	43 500	12 500
Tensile strength, σ_t	kN/m^2	4 600	1 000
Cohesion, C	kN/m^2	6 130	1 300
Internal friction angle, φ	^{o}	55	50

Due to the lack of real values of the initial tensions measured on the site, the natural state of tension has been appreciated as one geostatic characterized by vertical $\sigma_v = \gamma \cdot H$ and horizontal $\sigma_h = \frac{\nu}{1-\nu} \cdot \sigma_v$.

2.2.1 Modeling realization

Realization of 2D modeling, assuming plane deformation for each model defined above, required the following steps: a) setting the boundaries of the area of interest and the model mesh; b) determining areas (regions), computing assumptions and geo-mechanical characteristics input; c) setting the boundary conditions; d) setting the initial and loading conditions of the model; e) performing calculations and storing results [2], [3], [4].

For more precise calculations, for each model was considered a distance of 500m from the ends of the model to the edge of the mining space. It were also defined the dimensions of interest area around the underground excavation up to the surface terrain, so as to include the surface of the model where the variation of stresses and strains reaches the maximum values and where there is interest in studying the development of the subsidence phenomenon. Discretization of the model and of each region respectively, was performed by triangular surface finite elements with quadratic interpolation.

To simplify the 2D models were considered two regions with different geomechanical properties, corresponding to the overburden rocks and to the coal seams respectively. The rock characteristics, considered homogeneous and isotropic, are presented as average values in Table 1 and taken into the calculations assuming elastic behavior, have been reduced due to the structural weakness coefficient [2].

Calculations on these numerical models were made in elastic-plastic massif behavior hypothesis of Mohr-Coulomb type.

In terms of the model boundary conditions, it was considered a model with a free upper side and the lower and side blocked (for bottom side vertical movements $v = 0$ and horizontal movements $u \neq 0$, and to the sides $v \neq 0$ and $u = 0$). Fig. 2 shows the finite elements model after the setting of boundary conditions.

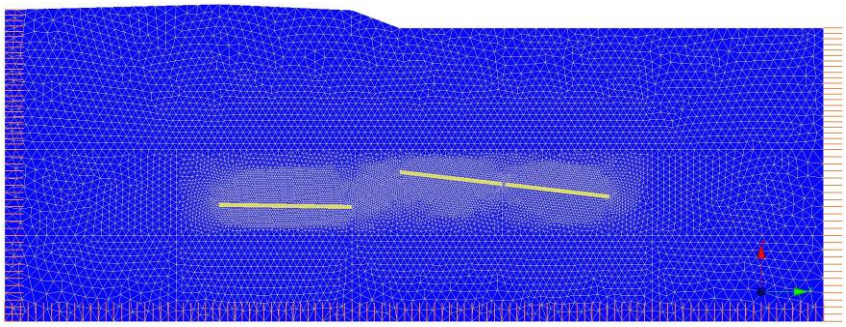

Fig. 2 Setting the boundary conditions for finite elements model (section S10)

Due to the lack of real values of the natural tensions measured in situ, the initial model loading conditions were considered geostatic $[\sigma_o]$, corresponding to an average depth of the mining panels, namely:

- Vertical geostatic tensions $\sigma_{oy} = \rho_s \cdot g \cdot H$
- Horizontal geostatic tension $\sigma_{ox} = \frac{\nu}{1-\nu} \cdot \sigma_{oy} = k_o \cdot \sigma_{oy}$

Tensions induced by the presence of excavations resulting from stope mining of the coal seams were $[\sigma_e]$, respectively the tensions variation represented by horizontal σ_{ex} and vertical σ_{ey}. Finally, the load patterns were performed with the total tensions $[\sigma_T] = [\sigma_o] - [\sigma_e]$ ([3], [4]).

To optimize the accuracy of calculations in order to achieve the required precision of the terrain stability analysis, the calculations were made assuming a total of 60 iterations per increment and a results tolerance of 1%, using for solving the "initial stress method".

2.2.2 Analysis of the results obtained by numerical modeling

After the realization of the calculations by numerical modeling on the presented sections (see Fig. 1), the subsidence values at the ground surface (vertical movement) for each section were extracted. Grouping values resulting from calculations based on every extracted space, the result was one subsidence trough generated for each individual extracted panel. Applying the principle of superposition effects, these partial subsidence troughs were summed resulted a total subsidence trough (Fig. 4).

In Fig. 3 it is presented the longitudinal profile of the subsidence trough on the planned pipeline route between points 5 and 23, in millimeters.

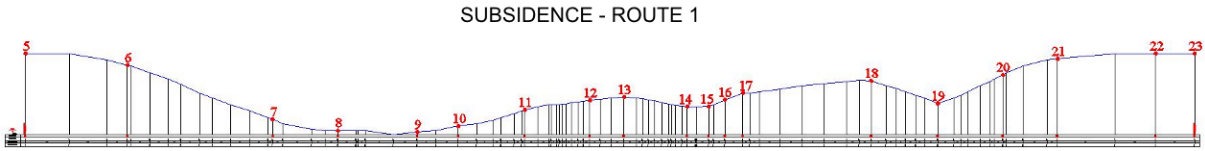

Fig. 3 Subsidence in vertical section along the planned pipeline route

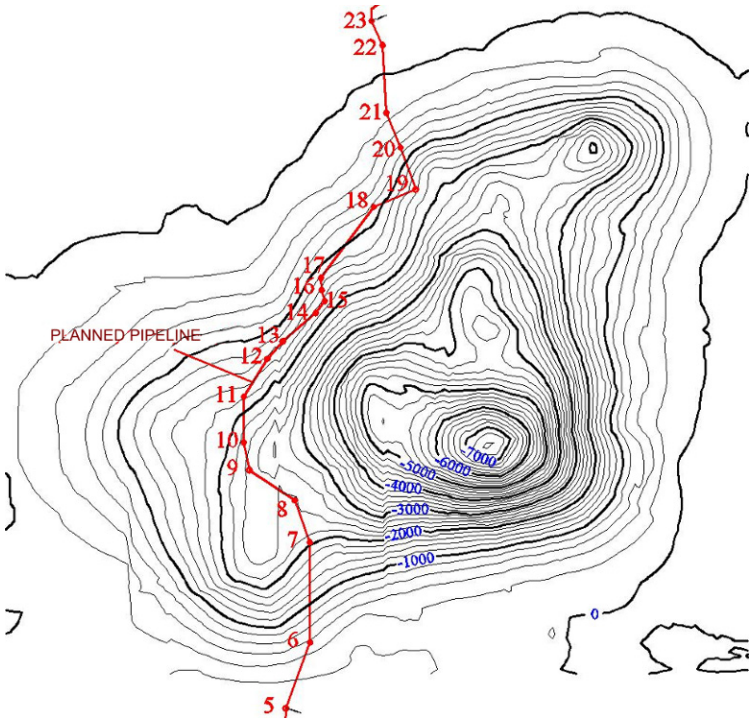

Fig. 4 Subsidence trough resulting in 2D numerical modeling (S in millimeters)

It should be noted that it is considered to be the final subsidence trough, resulting from coal extraction in the current phase (regardless of possible future extraction in the area).

Also, the intermediate stages of development of the subsidence trough are not known, stages that give rise to high traction tensions, respectively compression tensions at the surface, these tensions being more dangerous for the integrity of the objectives at the surface than the final stage of the phenomenon.

Fig. 5 shows the subsidence trough resulting from the finite element analysis, hypsometrical 3D representation.

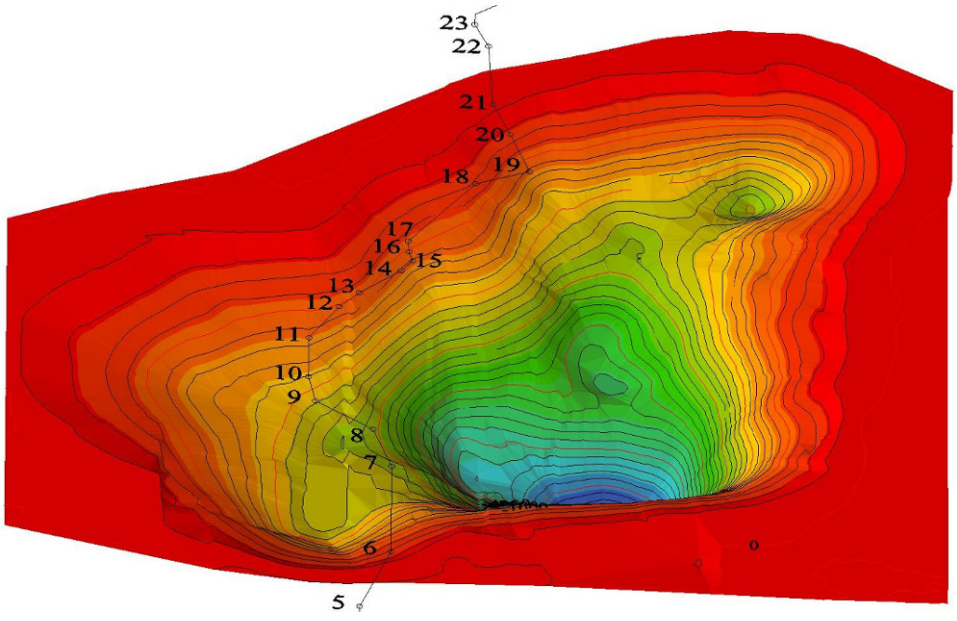

Fig. 5 Subsidence trough – hypsometrical 3D representation

Based on the subsidence, using known relationships were determined the inclinations at the surface due to underground mining. In Fig. 6 are represented curves of equal inclination and the position of the planned pipeline in relation to them. As can be seen, the pipeline passes through areas with major tilts, with values between + 5 mm/m and -5mm/m.

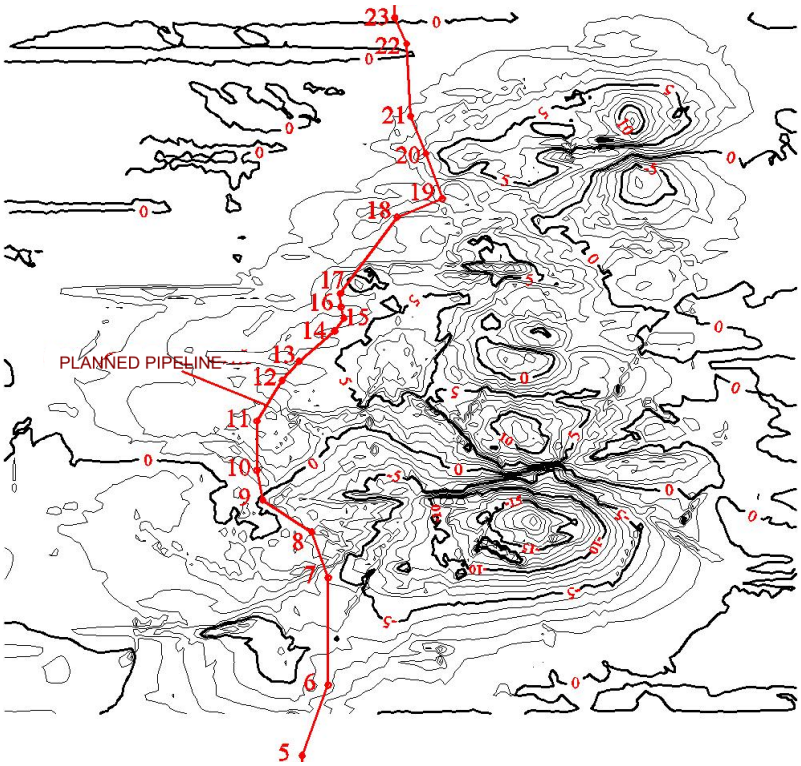

Fig. 6 Curves of equal inclination in pipeline's direction (North-South) resulting from numerical modeling

Fig. 7 shows the tilt profile, results of calculations, on the planned pipeline route between points 5 and 23.

Fig. 7 Tilt in vertical section along the planned pipeline

3 Confirmed results on-site

The results obtained by numerical modeling are confirmed by field observations, on the surface being observed some areas of fissures developed gradually over the past two years (fig. 8 and 9).

Fig. 8 Cracks on the ground in the planned pipeline area, due to stretching deformation

Fig. 9 Deformations of the surface due to underground mining

4 Conclusions

Analyzing the results obtained from 2D finite element numerical modeling, the surface suffers major deformations along the proposed pipeline route and its neighborhood. It should be noted that the deformations resulting from the finite element analysis presented in this paper are considered to be the final stage at the surface, in the current state of underground mining.

Since the underground mining takes place at variable depths on two coal seams (taking into account only the coal seams no. 3 and no. 5 at multiple sites with "empty spaces" of different sizes and in different time periods, it cannot be achieved to forecast the intermediate tension conditions occurring on the surface, generated by each stope mining. These intermediate states of tension (tensile, compression, shearing) can be much more dangerous for the integrity of the objectives at the surface, rather than the final state of deformation of the surface. In conclusion, based on the results of numerical modeling, we can say that the route originally proposed for the natural gas pipeline is not suitable, because it will be affected in the future by underground mining.

Consequently, if with all the inconveniences brought, it will be decided to place the pipeline in this area, we recommend taking additional safety measures to prevent both the deformations emerged on the surface and the tensions generated by these deformations. Also in this case it is appropriate to perform periodic monitoring measurements of the pipeline movement by precision surveying.

References

[1] Hirian, C. (1981). *Mecanica rocilor (Rocks Mechanics)*, Didactical and Pedagogical Publishing House, Bucharest.

[2] Marian, D.P. (2011). *Analiza stabilităţii terenului de la suprafaţă sub influenţa exploatării stratelor de cărbuni cu înclinare mică şi medie din bazinul Văii Jiului (Surface Stability Analysis as Effect of Underground Mining of the Coal Seams with Gentle and Medium Dip from the Jiu Valley Coal Basin),* Ph.D.Thesis, University of Petroşani.

[3] Onica, I. (2001). *Introducere în metode numerice utilizate în analiza stabilităţii excavaţiilor miniere* (*Introduction in the Numerical Methods Used in the Mining Excavations Stability Analysis*), Universitas Publishing House, Petroşani,

[4] Onica, I., Marian, D.P. (2012). *Ground surface subsidence as effect of underground mining of the thick coal seams in the Jiu Valley Basin*, Archives of Mining Sciences, Vol. 57, no. 3, Poland; ISSN: 0860-7001.

[5] Todorescu, A. (1984). *Proprietăţile rocilor* (*Rocks Properties*), Technical Publishing House, Bucharest.

[6] Vereş I.S., ş.a. (2015). *Studiu de cercetare privind amplasarea conductelor de transport gaze naturale în zone cu posibile fenomene de subsidenţă (Research study concerning the location of gas pipelines in areas with possible subsidence phenomena*), Research contract no. 634/09.12.2015, University of Petroşani.

[7] http://www.cesar-lcpc.com/.

Author Index